UNCLASSIFIED

AD 418153

DEFENSE DOCUMENTATION CENTER

FOR

SCIENTIFIC AND TECHNICAL INFORMATION

CAMERON STATION, ALEXANDRIA, VIRGINIA

UNCLASSIFIED

NOTICE: When government or other drawings, specifications or other data are used for any purpose other than in connection with a definitely related government procurement operation, the U. S. Government thereby incurs no responsibility, nor any obligation whatsoever; and the fact that the Government may have formulated, furnished, or in any way supplied the said drawings, specifications, or other data is not to be regarded by implication or otherwise as in any manner licensing the holder or any other person or corporation, or conveying any rights or permission to manufacture, use or sell any patented invention that may in any way be related thereto.

CATALOGED BY DDC
AS AD No. 418153

FTS-9848/1+2+4

64-3

UNEDITED ROUGH DRAFT TRANSLATION

INVESTIGATION OF HEAT RESISTANT ALLOYS

EDITED BY: I. P. Bardin, G. V. Kurdyumov, et. al.

English Pages: 722

DDC
OCT 1 1963
TISIA B

418153

THIS TRANSLATION IS A RENDITION OF THE ORIGINAL FOREIGN TEXT WITHOUT ANY ANALYTICAL OR EDITORIAL COMMENT. STATEMENTS OR THEORIES ADVOCATED OR IMPLIED ARE THOSE OF THE SOURCE AND DO NOT NECESSARILY REFLECT THE POSITION OR OPINION OF THE FOREIGN TECHNOLOGY DIVISION.	PREPARED BY: TRANSLATION DIVISION FOREIGN TECHNOLOGY DIVISION WP-AFB, OHIO.

FTS-9848/1+2+4

AF-WP-O-SEP 63 71

Date 19 June 19 63

P

CATALOGED BY DDC
AS AD No. 418153

FTS-9848/1+2+4

64-3

UNEDITED ROUGH DRAFT TRANSLATION

INVESTIGATION OF HEAT RESISTANT ALLOYS

EDITED BY: I. P. Bardin, G. V. Kurdyumov, et. al.

English Pages: 722

DDC
OCT 1 1963
TISIA B

418153

THIS TRANSLATION IS A RENDITION OF THE ORIGINAL FOREIGN TEXT WITHOUT ANY ANALYTICAL OR EDITORIAL COMMENT. STATEMENTS OR THEORIES ADVOCATED OR IMPLIED ARE THOSE OF THE SOURCE AND DO NOT NECESSARILY REFLECT THE POSITION OR OPINION OF THE FOREIGN TECHNOLOGY DIVISION.	PREPARED BY: TRANSLATION DIVISION FOREIGN TECHNOLOGY DIVISION WP-AFB, OHIO.

FTS-9848/1+2+4

AF-WP-O-SEP 63 71

Date 19 June 19 63

P

Akademiya Nauk SSSR

Institut Metallurgii im. A. A. Baykova
Nauchnyy Sovet Po Probleme Zharoprochnykh Splavov

ISSLEDOVANIYA PO ZHAROPROCHNYM SPLAVAM

Vol. III

Izdatel'stvo Akademii Nauk SSSR

Moskva - 1958

Pages: 1-430

FTS-9848/1+2+4

TABLE OF CONTENTS

PAGE

Changes in Microstructure, Hardness and Electrical Conductivity During Creep in Heat-Resistant Grades of Steel, by V. S. Ivanova and I. A. Oding 1

Certain Problems in the Theory of Heat Resistance, by M. V. Pridantsev..... 15

Certain Problems of Alloying Heat Resistant Pearlitic Steel, by N. T. Gudtsov, I. F. Zudin, and O. A. Bannykh..... 34

The Atomic Mechanism of Aging in Complex Alloys, by I. L. Merkin 54

Concerning the Connection Between Thermodynamic Quantities and the Strength of Alloys at High Temperatures, by M. P. Matveyeva, L. I. Ivanov, and L. N. Bystrov..... 85

The Determination of Thermodynamic Parameters of Chromium and Cobalt Alloys by Measurement of the Pressure of Saturated Chromium Vapors, by Ya. I. Gerasimov, A. M. Yevseyev, and G. V. Pozharskaya..... 94

Concerning the Values of Activation Energy of Certain Processes in Metals, by K. A. Osipov..... 103

A Study of Diffusion in an Iron-Aluminum System Over a Wide Range of Concentration, by S. D. Gertsriken, I. Ya. Dekhtyar, N. P. Plotnikova, L. F. Slastnikova, and T. K. Yatsenko..... 116

Determination of the Parameters of Diffusion and Deformation in Nickel-Chromium Alloys, by I. Ya. Dekhtyar, and V. S. Mikhalenkov 131

Some Results of the Study of Self-Diffusion of Iron and Problems of Heat Resistance, by B. M. Noskov..... 156

Concerning the Connection Between Diffusion and Heat Resistance in Alloys, by A. Ya. Shinyayev..... 168

Diffusion in Nikel-Base Solid Solutions, by Yu. F. Babikova and P. L. Gruzin..... 191

Concerning the Study of the Intercrystallite Diffusion in Metals and Alloys, by V. I. Arkharov, S. M. Klotsman, A. N. Timofeyev, and I. I. Rusakov..... 198

Investigation of the Effect of Mutual Orientation of Crystals on Inter-Crystallite Diffusion and Internal Adsorption, by V. I. Arkharov, and A. A. Pen'tina..... 208

Study of Atomic Interaction in Alloys by X-ray crystal analysis, by V. V. Geychenko, M. A. Krivoglaz, and A. A. Smirnov..... 247

PAGE

Concerning the Theory of Slow Neutron Scattering in Alloys, by V. M. Danilenko, M. A. Krivoglaz, Z. A. Matysina, and A. A. Smirnov..... 263

Calculation of the Absolute Value of the Self-Diffusion Coefficient at Grain Boundaries and the Boundary Widths, by S. Gertsriken, and D. Tsitsiliano..... 280

Investigation of Chromium-Niobium-Vanadium Alloys, by V. N. Svechnikov, Yu. A. Kocherzhinskiy, V. M. Pan, and A. K. Shurin 290

Investigation of Structural Changes in Iron-Nickel Alloys at the $Y - (Y + \alpha)$, by M. I. Zakharova and N. A. Khatanova..... 309

Changes in Fine Crystal Structures During Aging of Nickel and Iron-Nickel-Base Alloys, by V. G. Chernyy..... 319

Dependence of Resistance to Deformation on Temperature and Strain Rate in Copper and Its Alloys, M. A. Bol'shanina, M. B. Makogen, and V. Ye. Panin..... 330

Study of the Behavior of Nickel and Solid Solutions of Titanium in Nickel under High Temperature Conditions and at Low Strain Rates, by V. M. Rozenberg..... 360

Mechanism of Deformation of the Monocrystals of Aluminum of Varied Test Temperatures, by L. I. Vasil'yev, Tsen Lin-Chao and Yang Ta-Yu..... 375

Mechanism of Strengthening and Resoftening, by A. M. Yuferov... 407

$L_{\beta 6}$ and $L_{\gamma s}$ in the Spectra of Copper and Zinc, by M. I. Korsunskiy and I. A. Rumyantsev..... 424

Influence of the Concentration of Components in Iron-Chromium Alloys on the Structure of the Energy Spectrum of the Chromium and Iron Conductivity Zone at High Temperatures, by N. D. Borisov, V. V. Nemoshkal enko, and A. M. Fefer..... 430

Concerning the Theory of Diluted Solid Solutions, by I. B. Borovskiy and K. P. Gurov..... 447

Influence of the Thermal Vibration of Atoms on the Electron Spectrum of Metals and Alloys, by I. B. Borovskiy and G. N. Ronami..... 462

X-Ray Spectroscopic Studies of Ferro-Molybdenum and Ferro-Aluminum Alloys, by S. A. Nemnonov, V. A. Trapeznikov, and K. M. Kolobova..... 470

Migration in Metallic Solid Solutions, by K. P. Romadin..... 491

Possibility of Autoradiographic Detection of the Unevenness in Concentrations of Adsorption Origin, by V. I. Arkharov, V. S. Galishev, S. M. Klotsman, and A. N. Timofeyev..... 498

PAGE

Influence of the Distribution of the Alloying Elements on the Behavior of Alloys at Elevated Temperatures, by M. Ye. Drits, Z. A. Sviderskaya, and E. S. Kadaner..... 511

Influence of Alloying Additions on the Temperature Dependence of the Moduli of Elasticity in Nickel and Nichrome Alloys, by D. G. Polotskiy, T. Ya. Beniyeva, and Z. I. Khodov..... 523

Laws Governing the Mechanical Strength of Materials Obtained by Sintering of Metal Powders, by P. Ya. Pines, A. F. Sirenko, and N. I. Sukhinin..... 549

Certain Problems of the Theory of Thermal Stability, by M. Yu. Bal'shin..... 572

Brittleness of Metals During Creep, by N. Ye. Karskiy..... 584

Concerning the Theory of the Bending Energy of Oxides of Transition Metals, by A. N. Men', and A. N. Orlov..... 616

Electron-Diffraction Study of Phase Changes in Thin Metal and Oxide Films, by D. V. Ignatov..... 630

Apparatus for the Study of the Kinetics of Oxidation in Metals, by P. M. Arzhanyy and N. N. Velichenko..... 643

The Influence of Chromium on Long-Time Strength of Chromium-Molybdenum Steel, by O. A. Bannykh and I. F. Zudin..... 647

Investigation of the Resistance of Plastic Deformation in Alloys of the Nickel-Iron System, by K. A. Osipov and Ye. M. Meroshkina 653

Heat Resistance and Hot Hardness of Alloys of Binary Systems of Nickel with Chromium, Molybdenum, and Tungsten, by I. I. Kornilov, and N. T. Domotenko..... 661

The Role of Nitrogen in High-Temperature Oxidation of Chromium in Air, by V. I. Arkharov, V. N. Konev, I. Sh. Trakhtenberg and S. V. Shumilina..... 675

Investigation of Reactional Diffusion in a Chromium-Nitrogen System, by V. I. Arkharov, V. N. Konev, and A. Z. Men'shikov.. 686

Structure and Properties of Carbon-Nitrided Chromium, by V. N. Konev..... 698

Thermal and Electrical Properties of Copper, Silver, Gold, Aluminum and Alloys with a Copper Base, by V. Ye. Mikryukov... 707

CHANGES IN MICROSTRUCTURE, HARDNESS, AND ELECTRIC CONDUCTIVITY DURING CREEP IN HEAT-RESISTANT GRADES OF STEEL

V. S. Ivanova, I. A. Oding

One of the essential aspects of the problem of heat resistance is the question of the role of inter and intragranular plasticity in metallic creep. But there is not yet any agreement on the importance of either of these forms of plasticity in any particular phase of creep. Some assume that intergranular plasticity plays the most essential part in the first phase of creep, other relate this role to the second (sustained) phase. Finally, there are opinions holding that the processes of inter and intragranular plasticity take place simultaneously in all phases of creep, even the third, and that only the quantitative relations between them may vary with the conditions of the experiment.

At present, the role of inter and intragranular plasticity is under study, mainly for pure metals; it is therefore interesting to trace to what extent such plasticity appears in the creep of heat-resistant grades of steel. For this purpose three grades of austenitic steel and, for comparison, Armco iron (of standard chemical composition) were investigated.

Austenitic steels were investigated in the quenched state

(cooled from 1150° in water), and Armco iron in the normal state (950°). Figure 1 shows a photomicrograph of EI257 steel after creep testing for 58 hours at a temperature of 575°, under a stress of 12 kg/mm². The total deformation amounted to 0.2%. The microsection was photographed using light from an oblique angle, which made it possible to make the intergranular character of the deformation clearly visible. The black shadows on the grain boundaries characterize quite clearly the relative displacement of the grains. This deformation even lends itself to quantitative measurement, for which McLean has developed a method [1].

Using an interference microscope, McLean measured the protrusion of the grains from the surface and conjectured from this quantity what part of the plastic deformation was due to the relative displacement of the grains themselves. Although this method is not very precise, it is, for the time being, the only one existing for the determination of the quantitative contribution of intergranular plasticity to the overall creep deformation. It enables us to establish that intergranular plasticity starts at the very beginning of the creep process and continues through the second and third sections of the creep curve.

However, it is not only through relative displacement of the grains that intergranular plasticity is made apparent. Figure 2 shows a photomicrograph of Armco iron before (a) and after (b) creep testing at a temperature of 450°, under a stress of 13 kg/mm², and with a test duration of 1,200 hours. In this case, intergranular plasticity became apparent through recrystallization. Owing to the displacement of dislocations at the grain boundaries, there was a considerable growth of the grains; this growth also took place at a

lower temperature (400°), though with less efficiency. These data show that under pressure the process of grain growth may take place at lower temperatures than the ordinary recrystallization temperature. Consequently, intergranular plasticity in the process of creep may become apparent through a recrystallization process: the displacement of grain boundaries.

GRAPHIC NOT REPRODUCIBLE

Fig. 1. Microstructure of EI257 steel after creep testing (× 200).

If creep testing is carried out under other condition, for example, under lower stresses, we may observe that, besides causing grain enlargement, creep also causes grain breakdown, while the new

boundaries in Armco iron appear in a very singular way. Figure 3 shows the microstructure of Armco iron after creep testing at a temperature of 400°, under a stress of 6 kg/mm^2, and with a test duration of 1,000 hour. The arrows in this photomicrograph show the new boundaries which have appeared as pointlike formation that are corroded concavities at the spots where the dislocations appear on the surface of the microsection. Later on, these pointlike boundaries become continuous boundaries as a result of the appearance of new dislocations and the reduction of the distances between them.

GRAPHIC NOT REPRODUCIBLE

Fig. 2. Microstructure of Armco steel (× 200).

Thus, we may state that in creep two processes take place in opposite directions: one, connected with the enlargement of the grains, is a process of recrystallization by the mechanism of plasticity, while the other, involving breakdown of the grains,

is a polygonization process. Depending on the relative efficiencies of the two processes, it is possible to give the metal a smaller or larger grain at the end of the test.

According to our observations, the polygonization process becomes most effectively apparent at lower temperatures and under lower stresses. It is still impossible, however, to draw a sharp line between the conditions for grain growth or breakdown during creep.

During the testing of EI432 steel, we succeeded in bringing to light the following aspect of intergranular plasticity as well (Fig. 4). There were a great number of twins in the initial structure (a). During the creep process they gradually disappeared (b), so that after 1,000 hr of testing there were no twins at all left in the structure, but signs of recrystallization did appear (c). Consequently, plastic deformation in creep may take place not only through twinning, but also through its disappearance. So far, the details of mechanism plasticity remain unclear.

Thus, intergranular plasticity during creep of heat-resistant grades of steel shows up quite clearly.

It is considerably more difficult to expose the intragranular processes taking place during creep in these steels.

With small creep deformation (0.2 to 0.3% and sometimes more) it is impossible to observe the shear lines inside the grains by means of an ordinary optical microscope. The question then arises whether plastic deformation takes place in the grains themselves during the process. At the present time, there is a hypothetical concept--the so-called "fine slip" (homogene Gleitung) which has been interpreted as local slip with a low degree of displacement on the

given slip plane. The nature of this slip has been barely investigated so far.

The mechanics and nature of shear processes that result in slip lines visible in an ordinary metallographic microscope have been comparatively well studied. It has been established that this type of slip is accompanied by changes in the microhardness, electric conductivity, and other physical characteristics of the metal.

We investigated the changes in microhardness and electric conductivity after creep testing for a certain time,* for the purpose of studying these characteristics during creep and for verifying the fundamental assumptions of the dislocation theory of creep, which has been promulgated by one of the authors [2]. The measurements of microhardness and electric conductivity were carried out at room temperature. The basic postulate of the dislocation theory of creep was that the rate of creep is proportional to the number of the dislocations at a given instant of time t:

$$v_p = Aw_o (1 + \alpha t)^m,$$

where A, α, w_o and m are coefficients that depend on the nature of the metal and the conditions of the experiment.

Changes in the dislocation density (i.e., the number of dislocations per unit of volume of the metal) must, of course, result in changes in the microhardness and electric conductivity. If

---

* The experimental part of the work was carried out by L. K. Gordiyenko on a device developed by him.

GRAPHIC NOT REPRODUCIBLE

Fig. 3. Microstructure of Armoco iron after creep testing.

the dislocation density increases during the creep process, the rate of creep must increase; in this case the hardness increases and the electric conductivity decreases; the reverse is also possible. However, while investigating this problem with a metal that is supersaturated solid solution, we must also take other factors into account, namely: during the first stage of aging, such a solution will increase its hardness but, at the same time, the rate of creep must decline; in the second stage, during the coagulation of the secondary phases, the hardness of the metal must decrease whereas the rate of creep must increase. Moreover, the first stage of aging must result in the decline of the electric conductivity, while coagulation leads to increase in electric conductivity.

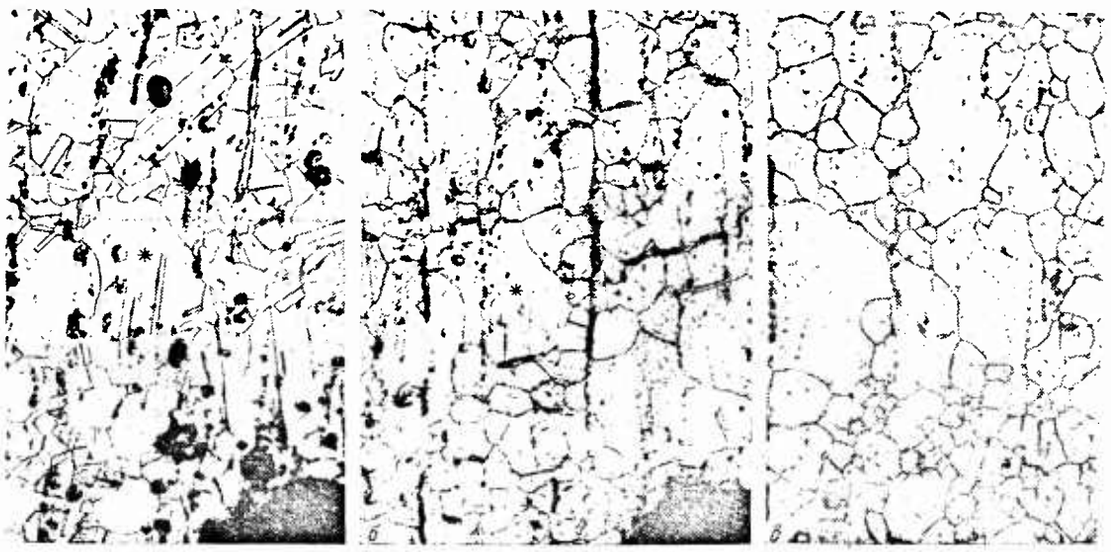

Fig. 4. Microstructure of EI432 steel (× 200). T - 600°; σ = 20 kg/mm².

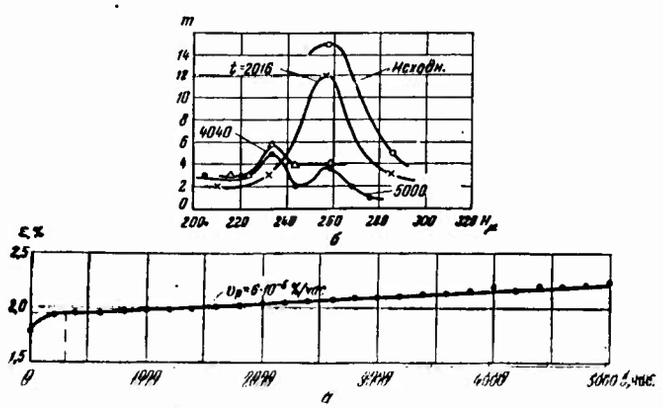

Fig. 5. Curves showing creep (a) and changes in microhardness (b) for EI257 steel.

Let us consider to what extent all this corresponds to the experimental data. Figure 5 shows the creep curve of EI257 steel obtained from testing at a temperature of 575° uder a stress of 15 kg/mm^2. This curve reflects a slowly vanishing cross section. The same figure shows curves characterizing the changes in microhardness of the metal during creep. The microhardness was measured on twenty grains, and the results of these measurements were expressed in curves of recurrence. It is easy to see that with the increase of the testing time, a decline in hardness takes place together with a decline in the rate of creep, which fits in well with the dislocation theory.

Figure 6 shows the creep curve as a function of its increase in rate for EI395 steel tested at a temperature of 575° and under a stress of 25 kg/mm^2.

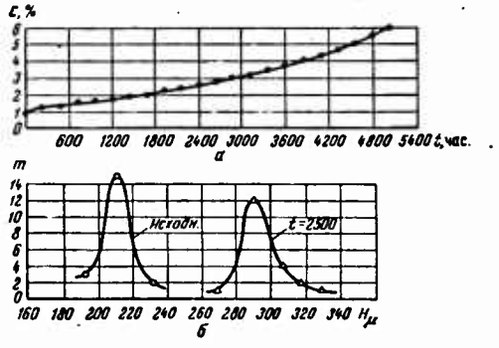

Fig. 6. Curves showing creep (a) and changes in microhardness (b) for EI395 steel.

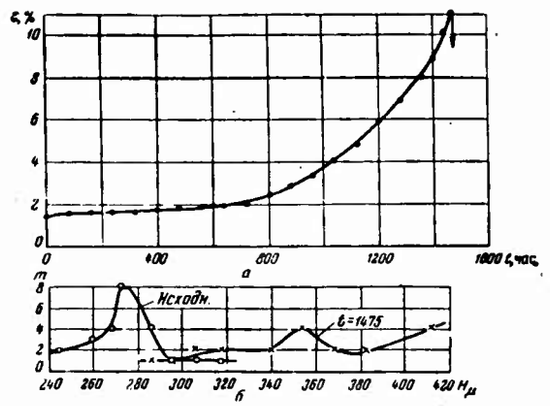

Fig. 7. Curves showing creep (a) and changes in microhardness (b) for EI432 steel.

According to the above-mentioned theory, the increase in rate of creep should be accompanied by an increase in dislocation density and, consequently, by an increase in the hardness of the metal. As is seen from Figure 6, hardness-distribution curves of the metal before and after testing for 2,500 hr show a very clear increase in hardness, which again confirms the above-mentioned dislocation theory.

Figure 7 shows the creep curve of EI 432 steel, tested at 600° under a stress of 25 kg/mm^2. In the given instance, and increase in the rate of creep is accompanied by a considerable increase in microhardness. The distribution curve becomes diffuse and extends toward the higher hardness values.

Very interesting test results are given in Figure 8 for EI395 steel, tested for creep at a temperature of 575° under a stress of 22 kg/mm^2. As is known, this steel is characterized by a great

tendency toward aging. In the first section, approximately up to 4,000 hr, the creep curve tends to vanish, while hardness increases, as is clear from the curve of recurrence. After the aging has terminated the dislocation processes, which cause considerable resoftening, become of marked importance. These processes are also accompanied by fading creep (see Fig. 8, section from 5,000 to 8,000 hr). Thereafter the process of accelerated creep begins; this results in a marked increase in microhardness. Consequently, the fundamental assumptions of the above-mentioned theory are also reflected in this very complex case.

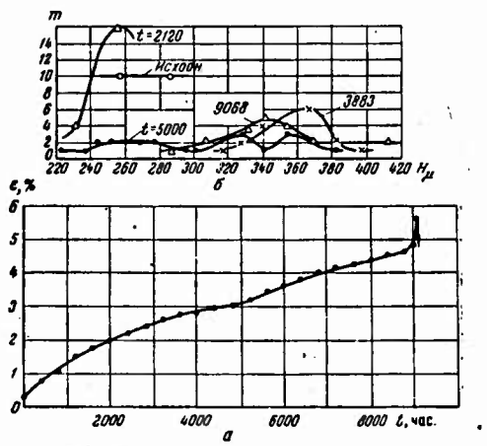

Fig. 8. Curves showing creep (a) and changes in microhardness (b) of EI 395 steel.

We can obtain an analogous pattern by measuring the electric conductivity. Figure 9 gives the creep curve of EI432 steel tested at a temperature of 600° under a stress of 20 kg/mm^2; it also gives the curve showing changes in electric conductivity. Up to 500 hr, creep proceeded at a decreasing (or uniform) rate. The dislocation

density declined while electric conductivity increased. Creep then began to appear at a rate increasing with time (the so-called third stage), which, according to our theory, was caused by the increase in dislocation density. This increase was reflected in the marked decline of the electric-conductivity curves.

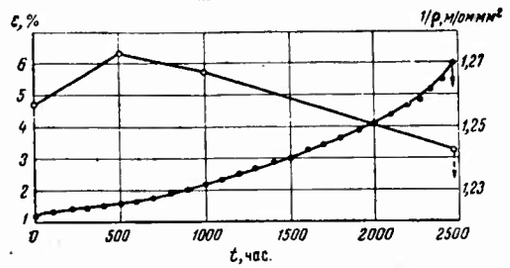

Fig. 9. Changes in electric conductivity of EI432 steel during creep.

The increase in electric conductivity in the first section of the creep curves can also be seen in Figure 10 which shows curves of electric conductivity and creep for the same steel tested at a temperature of 600° under a stress of 22 kg/mm². A higher stress reduced the section of fading creep and from the beginning of the portion of accelerated creep, electric conductivity again began to decline.

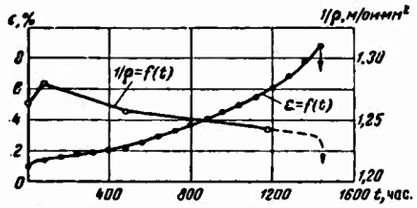

Fig. 10. Variations in electric conductivity of EI432 steel during creep.

Conclusions

1. Creep occurs at all stages as a result of intergranular as well as intragranular plasticity. Intergranular plasticity may become apparent by simple relative displacement of the grains with their protrusion on the surface of the microsection or by recrystallization and polygonization processes, or else through a special mechanism resulting in the disappearance of twins. The quantitative determination of intergranular plasticity is so far possible only in the case of relative displacement of the grains.

2. The measurement of microhardness and electric conductivity of test pieces subjected to creep showed that the processes of intragranular plasticity play a very effective part during creep.

3. The data obtained on the changes in electric conductivity and microhardness of test pieces during the process of creep agree very well with the dislocation theory of creep in metals.

REFERENCES

1. MCLEAN, D. Journ. Inst. Metals, v. 1, 1952.

2. ODING, I. A. Research on Heat-Resistant Alloys, Vol. 2, Acad. Sci. USSR, Press, 1957.

CERTAIN PROBLEMS IN THE THEORY OF HEAT RESISTANCE

M. V. Pridantsev

Heat resistance, i.e., the resistance of a material to small plastic deformation, is determined by many factors, among which, in the case of metals, we should mention the following: the energy level of the interatomic bond; the strength of this bond in the crystal lattice, an indication of which is given by such constants (for metals) as the melting point, the heat of sublimation, the characteristic temperature, the parameters of self-diffusion, the recrystallization temperature, etc.; structural factors, by which we mean--in the case of metals (not alloys)--the sizes of the grains and blocks and the state of their boundaries, the degrees of imperfection of the crystal lattice, the number and density of dislocations and impurities at the grain boundaries.

The same factors are characteristic of steels and alloys with relatively stable solid solutions, in addition to the following: the diffusion parameters of the solute atoms of the alloying elements and admixtures, the thermal stability of the carbide phase and the structural stability in relation to the redistribution of the alloying elements between the solid solution and the carbide phase, and the growth and distribution of the latter.

The heat resistance of steels and alloys with unstable solutions and those which are aging is determined by the same factors described above as well as by the bond energies in chemical compounds(intermetallic compounds, carbides, nitrides) and the related temperatures of formation and coagulation of the strengthening phases coexisting with the solid solution; by the temperature of dissociation of the phases and their solutions; and also by additional structural factors among which are the quantity and distribution of the strengthening phases, the eventual formation of new phases (for example, α and σ phases) and other structual changes, i.e., the degree of stability of the structure in time at working temperatures.

At present time, we lack sufficient experimental data on the bond strengths in the crystal lattice or on the very interesting constants related to them. Hence, it is not clear as yet to what extent they play a determining role in the heat resistance of steels and alloys. All known experimental data show that for the majority of the heat-resistant steels and alloys in use (comparing the same base), the structural factors and the role of the grain boundaries are decisive, i.e., they substantially increase the heat-resistant properties. It is definitely established that a certain part and, when the base is chosen, the determining part is played by the bond strengths in the crystal lattice of the solid solution and also in the strengthening phase.

For metals at temperatures above the recrystallization temperature, at which there is a rapid return of the properties of a deformed metal (above 0.45 t_m), we observed close agreement between the activation energy for creep and such constants as the activation

energy for self-diffusion and the melting point. We also noticed a connection between the activation energy for creep in a metal and the atomic number.

Research [1] shows the direct relationship between the activation energy for self-diffusion and the activation energy for creep in certain metals: these quantities proved to be almost equal. It follows, therefore, that the factors conditioning the rate of self-diffusion are also the factors controlling the rate of metallic creep under the given temperature conditions. The relationship obtained in this study, between the activation energy for creep and the activation energy for self-diffusion for zinc, lead, aluminum, copper, gold, and iron, is given in Figure 1.

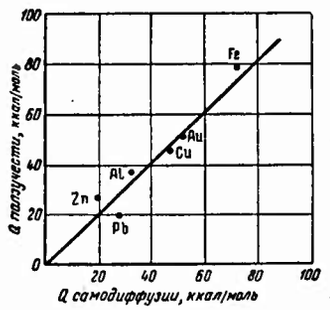

Fig. 1. Relationship between the activation energy for creep and the activation energy for diffusion.

In the same work, the authors make the assumption that the activation energy for creep in metals at temperatures above 0.45 t_m is a periodic function of the atomic number. The authors draw this conclusion from data on the activation energies for creep and the activation energies for self-diffusion for a series of metals with respect to their atomic numbers. These data show that alkali and

alkali-earth metals have the lowest activation energies for creep, whereas elements located in the middle of each period have the highest activation energies for creep and self-diffusion.

However, the influence of the structural factor on the activation energy for creep is not taken into account in this periodic law. It also follows from this law that all metals having higher melting points have higher activation energies for creep. It is known that temperatures below 0.45 t_m these laws do not apply to metals since, during the deformation process of creep, particularly if there is an increased rate and considerable deformation, structural changes in the metal take place in time; these changes, in turn, change the values of the constants related to creep. With relatively pure metals, a structural factor begins to operate at these temperatures. This factor varies with time in its influence on the creep process, i.e., with increased deformation.

With heat-resistant steels and alloys of pearlitic as well as austenitic types, we do not observe such conformity with the law either at temperatures slightly below 0.45 t_m, or even at higher temperatures, since the influence of the structural factor is manifested in both cases and is most considerable in the case of steels and alloys. The literature contains ample data on the influence of the structure of steel (using the word structure in a broad sense) on creep, long-time strength, and plasticity under protracted stress, which confirm these assumptions.

In this connection, the more interesting constants of heat-resistant materials related to creep processes should be studied not only for the materials in the original state but also after various test durations, in order to establish laws for the variations

of constants of various groups of steels and alloys and to take the structural factor into account. It is particularly necessary to study the constants (for example, bond strengths, parameters of diffusion, self-diffusion, etc.) at actual working temperatures of the metals.

Many researchers represent creep as a complex process consisting of two alternating processes--the strengthening of the metal as a result of deformation, and resoftening--taking place in time under prescribed conditions of stress and temperature. Depending on the temperature at which creep occurs--below or above the recrystallization temperature--resoftening is considered the result of recovery relaxation. This interpretation is quite probable and is admissible under the test temperature conditions at which these processes can take place. The role of these processes becomes particularly obvious in the investigation of creep in lead and alloys at temperatures above the recrystallization temperatures.

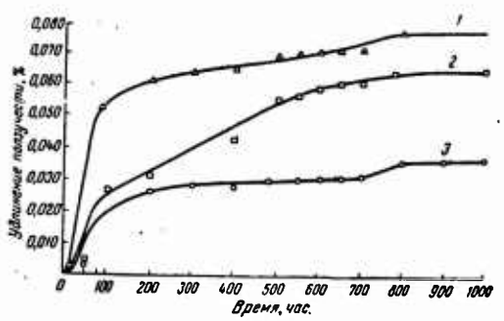

Fig. 2. Creep curves of St 70 wire, with a periodic section. 1) Cold-drawing; 2) cold-drawing tempering, 225° 6 hr; 3) cold-drawing and tempering 450° and 10 sec.

When applied to many steels and alloys, this concept is contrary to the experimental facts, which show that the phenomenon of creep is observed not only at temperatures considerably above the recrystallization or recovery temperature but also at normal temperatures at which these processes practically never take place. The recrystallization temperature and the temperature limits for recovery are not fixed for a given metal or alloy; they depend also on the duration of the temperature influence on the metal.

It is often assumed that creep in carbon and alloyed pearlitic and austenitic steels and alloys begins only at a certain temperature. It is known however, that the yield point and proportional limit, determined not only at increased temperatives (considerably lower than the recrystallization temperature) but also at normal temperatures, depend on the rate of elastic deformation, i.e., on the rate of increase of stress during static testing and on the accuracy of the determination. The processes of creep and relaxation are also observed at normal temperatures. From experience in the use and investigation of highly resistant wire used for ferroconcrete and for piano wire, we know of processes of creep and recovery which take place in time at normal temperatures and under stress below the yield point, and where the proportional limit is determined from static experiments. For example, the work of I. A. Yukhvets, carried out at the TsNIIChM*, has shown that a cold-drawn wire made of steel 70, with a periodic section and nominal diameter of 4 mm, exhibited marked creep when tested for a period of 1,000 hr, both without

* Central Scientific Research Institute of Ferrous Metallurgy

subsequent tempering and after tempering (225 and 450°), under a tension amounting to 70% of the tensile strength. The lowest rate of creep was observed in wire subjected to tempering at 450°, and the highest in a cold-drawn wire (Fig. 2).

TABLE 2

$\overline{\sigma_B}$ and σ_S (kg/mm^2) of Wire made of Steel 70 (~ 0.7% C and ~ 0.4% Mo), Nominal d = 4 mm. Before and After Creep Testing at Normal Temperature and Stress σ = 70% of σ_B.

State of wire during test	σ_B	$\sigma_{0.1}$	$\sigma_{0.01}$	$\sigma_{0.005}$
Cold-drawn before creep testing	172.0	128.4	80.5	72.3
Same, but after creep testing at σ = 120 kg/mm^2 for 1,000 hr	172.0	142.0	113.0	101.0
Cold-drawn and tempered at 225° for 6 hr before creep testing	173.8	153.3	128.8	124.0
The same, but after creep testing at σ = 121 kg/mm^2 for 1,000 hr	174.0	149.5	124.5	118.5
Cold-drawn and tempered at 450° for 10 sec before creep testing	164.0	144.0	124.5	120.3
The same, but after creep testing at σ = 115 kg/mm^2 for 1,000 hr	167.0	138.5	120.0	116.5

Table 1 shows the tensile strength and yield point ($\sigma_{0.1}$, $\sigma_{0.01}$ and $\sigma_{0.005}$) of a wire made of steel 70 (with a periodic section and a nominal diameter of 4 mm) in a cold-drawn state with and without subsequent tempering at the given temperatures, determined before as well as after creep testing at normal temperature for 1,000 hr. The data in this table show that after 1,000 hr of testing under a stress

σ = 70% of σ_B, the yield point of cold-drawn wire increases considerably as a result of aging, while this phenomenon is not observed with tempered wire. As can be seen from a comparison of the data given in Fig. 2 and Table 1, creep takes place in tempered wire at stresses somewhat below the original yield point of the wire.

Figure 3 shows as a function of stress, the creep curves of cold-drawn and tempered wire made of steel 70 with a diameter of 4 mm, and having in the initial state (before testing) tensile strength σ_B = 173 kg/mm^2; it is clear from these curves that the low rate of creep is apparent at relatively low stresses (40 to 60% of σ_B), and that the lower the stress the lower the rate of creep.

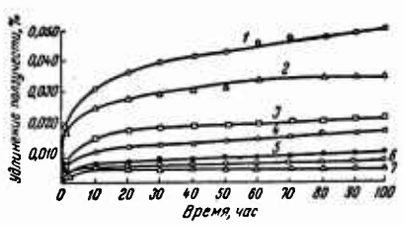

Fig. 3. Influence of stress on creep at room temperature in a cold-drawn, tempered wire made of St; σ_m in % of σ_B : 1) 80 2) 70; 3) 60; 4) 50; 5) 40; 6) 30; 7) 20.

Figure 4 shows the creep curves of a 65G wire made of manganese steel after oil-hardening from 880° and tempering at 450 to 500° for 10 to 15 sec, and also after cold-drawings. Cold-drawn wire with d = 4 mm had a tensile strength σ_B = 137 kg/mm^2 and a yield point $\sigma_{0.01}$ = 69.2 kg/mm^2, and hardened and tempered wire with

d = 4.2 mm had σ_B = 144.4 kg/mm² and $\sigma_{0.01}$ = 89. 1 kg/mm².

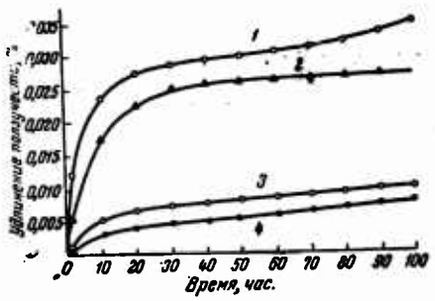

Fig. 4. Creep curve of wire made of St 65 G. σ_m in % of σ_B: 1) 70, cold drawn, d = 4 mm, hardening plus tempering; 2) 70, d = 4.2 mm; 3) 60, d = 5 mm; 4) 60, d = 4.2 mm.

The presence of a relaxation process in various metals at room temperature was shown by T. I. Volkova [2] in tests over a period of 50,000 hr with copper, Armco iron, and carbon steel (0.2 to 1.0% C). These results indicate, convincingly enough, a relaxation of stress with time at room temperature. The absolute value of the drop in stress during the test (40,000 to 50,000 hr) for all the investigated materials amounted to about 17 to 18% for copper, 2.5 to 3% for annealed low-carbon iron, and from 3.2 to 0.6% for carbon steels annealed to produce laminated and granular pearlite (at initial stresses: for Cu = 25 to 42%; for Armco iron, 52 to 79% and for steel, 34 to 92% of $\sigma_{0.2}$. Analogous data on stress relaxation at room temperature were obtained by I. A. Oding and Ye. N. Volosatova [3] for a series of austenitic grades of steel.

The quoted data on creep and stress relaxation at normal temperatures show that in this instance a definite role is played by the

processes of aging, which, under such conditions, may take place in time in the investigated metals. Moreover, these data show that the mechanism of creep is not connected with the processes of re-softening due to recovery and recrystallization.

Under field conditions where heat resistant steels undergo prolonged service, we are interested in those stresses which cause a small over-all plastic deformation, and creep rates of the order of $1 \cdot 10^{-5}\%$ per hour, i.e., essentially stresses causing a transition from elastic to plastic deformation.

The decrease in elastic properties with time (not counting the first stage of creep) i.e., the occurrence of plastic deformation at a constant low rate or "fading" rate, should be considered from the point of order of what causes the fundamental act of plastic deformation with time, and not thought of as cold-hardening and re-softening as a result of recovery of recrystallization, which are consequences of plastic deformation and not causes of the latter.

At increased temperatures, the prolonged action of stress results in greater plastic deformation than at normal temperatures since the thermal oscillations of the atoms are increased and the diffusion processes are facilitated.

The movement of dislocations, under stress in the course of time, and the shear resulting from these dislocation movements enable us to explain the reduced strength of metals and alloys as used, and, obviously, the mechanism of creep as well.

The movement of dislocation depends both on the magnitude of the stresses and on time, as well as on temperature; movement of dislocation is facilitated by increases in these factors. In contrast to their ideal counterparts crystals and grains, contain

structural imperfections (defects). Such imperfections primarily include vacant spaces, dislocated and foreign atoms in the crystal lattice, irregularities in the arrangement of the atoms under the influence of dislocated foreign atoms, impurities and phases, grain and block boundaries, and phase and dislocation boundaries inside the grains as well as at the grain boundaries.

Dislocations are considered to be linear imperfections which can move under the influence of stresses through the crystal lattice and cause plastic deformation inside the grains or at the grain boundaries. The stress necessary for the movement of the dislocations is several orders of magnitude lower than the stress required for shear of one atomic plane with respect to another in an ideal lattice; this also explains the low strength of the grains under shearing in real polycrystalline metals and alloys.

Dislocations, like all other imperfections, are surrounded by fields of elastic stresses which, interacting mutually, become unstable in energy. The stresses causing movement of the dislocations, (and, consequently, plastic deformation) must be sufficient to push the dislocation through the opposing fields of stress of other dislocations. Thus, additional dislocations (as well as other imperfections) originating as a result of alloying, heat treatment, or cold plastic deformation, strengthen the grain. On the other hand, in all instances where the dislocation density in the grains declines, the remaining dislocations move more easily at lower stresses, causing a decline in strength.

The stability of the structure with time at high temperatures is of great importance for the correct determination of the extrapolated values of the limits of strength and creep, and for the normal

operation of heat-resistant materials. On the other hand, the instability of the structure does not enable us to determine correctly the values of the limits of long-time strength and creep extrapolated from data obtained with shorter test durations.

The structural changes taking place in time at high temperatures are related to phenomena of great importance in theory and practice such as the inflection of the logarithmic curve of long-time strength, the decline in plasticity under prolonged rupture, and the lowering of the creep limit.

The length of time preceding fracture, τ, is related to the actual stress σ by the equation $\tau = B \cdot \sigma^{-n}$ which is expressed by a straight line in logarithmic coordinates. However, as experiments have shown, by this means does this dependence always remain linear throughout the test. For some steels, the straight line has a downward inflection in the logarithmic diagram. This inflection is usually explained by a variation in the character of the fracture of the metal, and by the transition from intracrystallitic to intercrystallitic fracture. The location of the point of inflection on the logarithmic straight line is different for various steels and temperatures, but for each of them the time prior to the inflection decreases as the test temperature increases.

The physical basis for the inflection of the logarithmic curve of long-time strength of some structurally unstable steels lies in an unfavorable change in structure resulting from diffusion processes taking place in time at certain temperatures for each steel. The inflection of the curve, or more correctly the change in the slope of the curve of long-time strength, plotted against the logarithmic coordinates stress verses time to fracture is possible when the de-

crease in stress is not proportional to the increase in time to fracture of the test pieces, i.e., when the duration of the test at a prescribed temperature is predominant in influence, compared with the stress, on the process of deformation and fracture of the steel. This phenomenon is possible in a case when, owing to diffusion processes, the following changes take place in the steel:

1. Increase of creep rate and faster transition to the third stage, owing to a decline in the heat resistance of the solid solution (grains). The latter occurs as a result of a considerable decrease in concentration of the strengthening elements in the solid solution during the test because of their redistribution through the solid solution and the carbide phase and their absorption by the carbides, or because of the resoftening of the solid solution as a result of coagulation of the strengthening phases or the formation of new phases (α and σ phases). If, at the same time, no considerable unfavorable changes in the grain boundaries are observed, viscous intercrystallitic fracture will take place.

The example of pearlitic boiler steels, which have been used for a long time as tubes for superheating steam in high-pressure steam boilers, shows to what degree the concentration of strengthening components in the solid solution may decrease as a result of their transition in time to the carbide phase. A great reduction in the molybdenum content in the solid solution is observed with 15M and 12MKh steels when, by additional alloying with vanadium and niobium, the decrease in molybdenum content in the solid solution is considerably less. The same can be said of vanadium as a strengthening element.

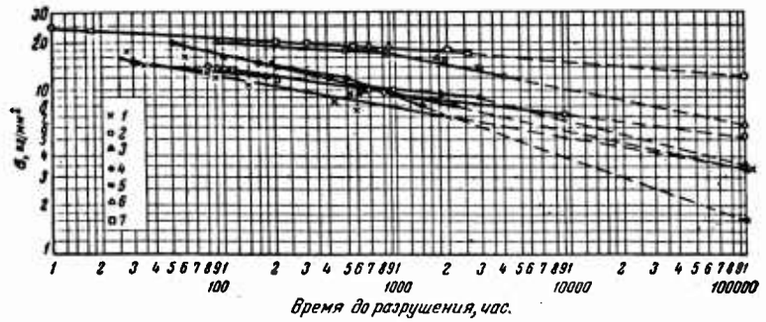

Fig. 5. Logarithmic curves of long-time strength for various austenitic steels at 700°. 1) 1Kh18N9T; 2) EI257; 3) Kh23N13; 4) Kh23N18; 5) EI69; 6) EI572; 7) EI434.

2. Fracture of steel depending on the relationship between the strength of the grains and their boundaries. At a lower relative grain strength, plastic deformation under prolonged rupture occurs predominantly in the grains themselves and the test pieces undergo considerable elongation and viscous rupture. At a greater relative grain strength, when the deformation takes place chiefly on the grain boundaries, the fracture of the steel is brittle and intercrystallitic. In steels and alloys with a greatly strenghtened solid solutions, fracture is always intercrystallitic with slight residual deformation, i.e., relatively brittle. The considerable change in the relative strengths of grains and their boundaries in the direction of a decrease of intergranular strength as a result of the change of state of the boundary zones at the time of precepitations of the phases, the formation of unfavorable stresses on the grain boundaries at the time of the precipitation of phases with different volumes or as a result of corrosion on the grain boundaries

on the surface of the test piece under the influence of an external medium, these factors, either separately or jointly, may cause an acceleration of the creep process, particulary at the third stage, and may also cause fracture. Such fracture is intergranular in character and has, in the majority of cases, a low plasticity. The absolute and relative duration of the third stage of creep, which depends on the susceptibility of the steel to viscous or brittle fracture in plastic deformation, and to the formation and development of cracks over fairly long period, also influences the shape of the logarithmic curve. The less the tendency of the steel toward plastic deformation at the third stage and, consequently, the shorter the third stage of creep, the more likely an inflection in the logarithmic curve of long-time strength.

We should mention that the duration of the third stage (as well as the second) depends, moreover, on the structure of the metal and its changes in time. The less stable the structure of the metal during the prolonged action of temperature, the greater the probability of variation in the slope of the logarithmic curve "stress verses time to failure", and the higher the temperature, the shorter the time before the appearance of the inflection. The duration and test temperature at which the inflection occurs thus depend on the composition and initial structure of the steel. The most probable and most frequently observed phenomenon of inflection of the logarithmic curve results from structural changes caused by coagulation and changes of disposition of the carbide phase, by the precipitation of new phases (α and σ phases) and by the impoverishment of the solid solution of strengthening elements through partial transition of the latter to the carbide phase. With metals of a more stable

structure, no inflection of the logarithmic curve is observed as a rule.

Figure 5 shows the logarithmic curves of long-time strength for the steels 1Kh18N9T, EI257, EI69, Kh23N13, Kh23N18, EI434, and EI572 at a temperature of 700°. The chemical composition of these grades of steel is given in Table 2.

By comparing these curves we see that the inflection of the logarithmic curves is observed in EI69 steel, differing from EI257 steel only in higher carbon content; in Kh23N13 steel, differing from Kh23N18 steel in the presence of the α phase from which the σ phase precipitates; and in EI434 and EI572 steel, which have increased carbon content.

The structural instability caused by long heating and the related variations in the properties of heat-resistant materials are also very important in the choice of a material for long service at high temperatures. For service under such conditions, it is in a number of instances more advisable to use materials that are structurally more stable: in test of short duration, the values for the limit of long-time strength are lower, while over long periods of testing these materials are better than some heat-resistant aging alloys which attain greater long-time strength over a short period of testing due to the intermetallic strengthening phase.

TABLE 2

Chemical Composition of Austenitic Steel, Logarithmic Curves for which are Given in Figure 5.

Марка стали	Содержание элементов, %								
	C	Si	Mn	Cr	Ni	Mo	W	Nb	Ti
1Х18Н9Т	≤0,12	≤1,0	≤1,5	17,0 / 20,0	9,0 / 11,0	—	—	—	До 0,8 (0,02 C)·5
ЭИ257	≤0,15	≤0,8	≤0,7	13,0 / 15,0	13,0 / 15,0	0,45 / 0,60	2,0 / 2,75	—	—
ЭИ69	0,40 / 0,50	≤0,8	≤0,7	13,0 / 15,0	13,0 / 15,0	0,25 / 0,40	2,0 / 2,75	—	—
Х23Н18	≤0,20	≤1,0	≤2,0	22,0 / 25,0	17,0 / 20,0	—	—	—	—
Х23Н13	≤0,20	≤1,0	≤2,0	22,0 / 25,0	12,0 / 15,0	—	—	—	—
ЭИ572	0,28 / 0,35	0,3 / 0,8	0,75 / 1,50	18,0 / 20,0	8,0 / 10,0	1,0 / 1,5	1,0 / 1,5	0,2 / 0,5	0,2 / 0,5
ЭИ434	0,32 / 0,42	0,5 / 1,2	0,5 / 1,2	12,0 / 14,0	11,5 / 13,5	1,8 / 2,4	2,5 / 3,5	1,0 / 1,5	0,06 / 0,15
									9—11 Co 0,05—0,1 V

The advantage of alloys that are structurally more stable for long-term service is clear from a comparison of the austenitic steel EI726 (Kh14N18 with 2.4% W, 1% Nb, and 0.007% B) with an alloy having a nickel base EI437 (Kh20N80 with 2.5% Ti) whose logarithmic curves of longOtime strength are given in Figure 6. As is clear from the figure, the long-time strength of the EI437 alloy is greater by 100 to 200 hr than in EI726 steel, although over long period of testing the limits of long-time strength is considerably higher in EI726 steel; the longer the test period, the higher the long-time strenth becomes. The heat resistance of the EI437 alloy for a long period of testing can be greatly increased by strengthening

the solid solution through the addition of molybdenum (the latter even strengthens the grain boundarie, alloy EI445R).

Fig. 6. Logarithmic curves of long-time strength for various metals at 700°. 1) EI445R; 2) EI726; 3) EI437; 4) EI695.

In the evaluation and selection of a material for long-term service, we encounter requirements for increases not only in the limits for creep and for long-time strength but also in the yield point. Such requirements for heat-resistant steels intended for running and nozzle blades of turbines and tubes for superheating and conducting steam in boiler installations are unjustified. It is well known that the yield point of steel can only be increased by increasing its carbon content and the quantity of the strengthening carbide phase. This method, while increasing the yield point, leads to a decrease in the resistance of the structure and, as it has been shown above, to a low limit of long-time strength. All steels possessing a more stable structure have a low yield point, which, under operation temperatures, approaches the long-time strength. However, such steels are undoubtedly superior in the fundamental heat-resistant properties. Hence the choice of a steel for a long period of service at high temperatures must be made above

all on the basis of its heat-resistant characteristics (limits of creep and long-time strength) and the degree of resistance of the structure to the prolonged action of temperature and stress. The demand for an increased yield point of heat-resistant steels is only justified in the case of their use as disks and rotors of turbines, where the temperature of the metal does not exceed 300 to 400° in the sections of these parts under the greatest stress. In this case however, it would be more correct to determine the limits of creep and long-time strength at a temperature of 200 to 400° and to base ones calculations on these characteristics and not on the yield point, which, moreover, is usually determined as $\sigma_{0.2}$, i.e., with insufficient accuracy.

REFERENCES

1. SHERBY, R. L.; ORR, and I. E. DORN. J. Metals, Vol. 6, Nr. 1, Sect. 1, 1954.

2. VOLKOVA, T. E. "Problems of Metallography of Boiler-Turbine Materials" (Problemy metallovedeniga kotloturbinnykh materialov), Bk. 71, State Sci. Tech. Press Machine Lit. (Mashgiz), Centr. Sci. Res. Inst. Techn. and Mach. (TsNIITMASh), 1955.

3. ODING, I. A. and VOLOSATOVA, E. N. Proc. Acad. Sci. USSR (DAN SSSR), Nr. 4, 1954.

CERTAIN PROBLEMS OF ALLOYING HEAT-RESISTANT PEARLITIC STEEL

N. T. Gudtsov,* I. F. Zudin, and O. A. Bannykh

Increasing the heat resistance of pearlitic steel by rational alloying is a problem of great practical importance. We should keep in mind that the threshold of 550 to 570°, which at the present time represents the temperature range within which pearlitic steel can be used in power engineering, may be increased by 30 to 50° in the very near future.

The development of the principles of alloying heat resistant pearlitic steel should help us to find compositions of steel with qualitites which fit the requirements of industry and which, at the same time do not contain either elements, of little effect in increasing heat resistance or elements that are of limited availability.

At comparatively low temperatures, when the processes of spheroidization and coagulation of carbides take place very slowly, high creep resistance can be obtained by thermal treatment of the steel to obtain finely dispersed lamellar carbides. In practice, however, it is difficult to check the processes of coagulation and spheroidization of the carbides sufficiently to obtain a steel that will remain

---

* deceased

stable in structure for many thousands of hours at a temperature above 550°.

As has been shown by Mirkin and Solonouts [1], after service at 510° for 15,000 hr, the pearlite-ferrite structure of steel with 0.5% Mo undergoes sharp changes-- inplace of the lamina of the carbide phase, there appear large carbides of a granular shape, located mainly on the grain boundaries.

The addition to the steel of such elements as chromium, molybdenum, vanadium, and tungsten reduces the coagulation rate of the carbides. Bokshteyn [2] considers that tungsten checks the coagulation rate of the carbides to a very great degree. If the influence of the elements is compared in atomic percentages.

The sharp change in creep resistance in the steel during service may occur as a result of spheroidization and coagulation of the carbides; for practical use at temperatures above 550° it is therefore necessary to apply heat treatment to the steel to stabilize the structure. The normal structure of steel intended for service at temperatures above 500° consists of grains of ferrite and carbide of granular shape. The size of the ferrite grains is 3 to 5 on the standard 8-mark scale, and that of the carbide particles is more than $2 \cdot 10^{-4}$ mm, i.e., carbide particles are visible under an ordinary microscope. This structure is obtained after annealing or normalizing with tempering at a temperature approximately 80 to 100° above the service temperature, i.e., not lower than 650°.

The decisive part in the change in heat resistance, if a stable structure is to be obtained is played by the composition of the α solid solution. The basic principles which must be observed to ensure the high heat resistance of pearlitic steel for boiler con-

struction were formulated in the works of Pridantsev and Lanska. They are as follows:

The carbon in the steel must be converted into stable carbides by powerful carbide-forming elements. This is necessary to prevent redistribution when the steel is in service of the alloying elements among the carbide phase and the α solid solution.

An alloying element must be added to the α solid solution to increase the heat resistance.

Taking these concepts as fundamental, and combining the results of experiments with the equilibrium diagrams of the "iron--carbon--alloying elements" system, we can determine the appropriate intervals for alloying with a particular element and also complexes of elements which will ensure high heat resistance in steel alloys.

Practice has shown that molybdenum, tungsten, vanadium, chromium, niobium, and titanium have the greatest effect on high-temperature resistance.

Molybdenum sharply increases heat resistance (at a temperature above 500°) basically through the α solid solution. The addition of niobium and titanium makes it possible to convert the carbon into special carbides and to strengthen by driving out other elements in the steel into it. There are various data for tungsten, vanadium, and chromium.

For example, in a relatively early survey, Grun[3] found that molybdenum and vanadium should increase the heat resistance of low-carbon steel most effectively at temperatures of 400 to 500°. Similar conclusions were also drawn by Holtmann [4]. Tamman [5] established that tungsten and molybdenum were about equally effective in alloying of heat-resistant steel if their influence is com-

pared in atomic percentages; this does not accord with Grun's data. Smith [6] considered tungsten to be as effective as molybdenum.

In general, the influence of tungsten has been investigated considerably less than that of molybdenum. Powers [7] points out that because of its high cost relative to molybdenum, tungsten has not been widely used in heat-resistant steel; as a result, little research has been devoted to its influence on heat resistance, and there are hardly any actual data on its effectiveness.

The question of the influence of a particular element becomes clearer if we examine separately its effect on heat resistance through the carbide phase and through the α solid solution. This can be done either by studying the distribution of the alloying element between the carbide phase and the solid solution or by studying the properties of carbon-free alloys of iron with alloying elements.

M. M. Steinberg [8] obtained interesting data on the influence of alloying elements (W, Nb, Mo, Cr, Ti, Al and Ni in concentrations not exceeding 2%) on the process of change in hardness with time in tempering cold-hardened iron. Having considered the process of resoftening in time at tempering temperatures of 550, 600, and 650°, the author concludes that tungsten checks the process of resoftening and recrystallization most effectively. Niobium and molybdenum are also fairly effective. The higher the temperature tempering, the higher the relative efficiency of tungsten. In chromium, titanium, aluminum, and nickel alloys, the process of resoftening is very little retarded as compared with pure iron. The author considers that the elements which should impart heat resistance to steel are the very ones which check the process of softening and move the "threshold" of ferrite crystallization upward on the temperature scale.

It is interesting to note that according to Steinberg's data tungsten alters the ferrite lattice more than molybdenum, titanium, vanadium, aluminum, chromium, and manganese.

While considering the influence of tungsten and molybdenum as well as of W + Mo on the heat resistance of steel with 0.1 to 0.2% C, Powers [7] found that the two elements were equally effective (Fig. 1). The curves in the figure refer to values of the Larson-Miller parameter T (20 + log τ; T is temperature in degrees Rankine, τ is the time in hours); 32, 36, and 39 which are respectively, the tensile strength during testing for a short period and the tensile strength for 1,000 and 100,000 hr at 593° (1100°F). The use of the empirical parameter makes it more difficult to judge quantitatively the influence of the elements, however, the tendency toward change in long-time strength with the change in the steel composition is clear enough.

We made a comparison of the influence of vanadium, chromium, molybdenum, and tungsten on the heat resistance of iron alloyed according to the scheme given in Table 1.

The total atomic percentage of the alloying elements, determining the degree to which the α solid solution is alloyed, was the same for all melts. The melts were carried out with electrolytic iron and pure metals, each melt weighing 2.5 kg. After being forged into a disk of 10 mm diameter, the metal was annealed at a temperature of 830 $\pm$ 10°, and it assumed a structure consisting of ferrite grains of equiaxial shape. After annealing, the billets, 10 mm in diameter, were made into samples of 4 mm, and tested on a Kornilov-Prokhanov, centrifuge. The test was carried out at a temperature of 600° under a stress of 9.5 kg/mm^2 for 115 hr, after which the stress was in-

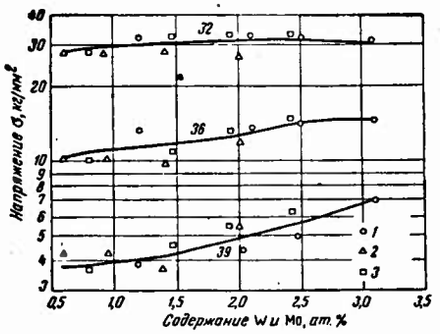

Fig. 1. The effect of W, Mo, and W + Mo, on the heat resistance of steel (test temperature 593°). 32) brief; 36) 1000 hrs; 39) 100,000 hrs. 1) Mo; 2) W; 3) Mo + W.

creased to 15 kg/mm² for 2 hr. The results of the tests (average of two samples) are given in Table 2.

TABLE 1

№ плавки	Содержание элементов, %			
	V	Cr	Mo	W
T-66	—	—	—	—
T-67	0,82	—	—	—
T-68	—	0,84	—	—
T-71	0,41	0,42	—	—
T-72	0,41	—	0,77	—
T-73	0,41	—	—	1,48
T-74	—	0,42	0,77	—
T-75	—	0,42	—	1,48
T-76	—	—	0,77	1,48
T-77	0,27	0,28	0,51	—
T-78	0,27	0,28	—	0,99
T-79	0,27	—	0,51	0,99
T-80	—	0,28	0,51	0,99
T-81	0,20	0,21	0,38	0,74

TABLE 2

№ плавки	Элементы	σ = 9,5 кг/мм²		σ = 15 кг/мм²
		5 час.	100 час.	2 часа
T-66	Fe	70	Снят	—
T-67	Fe + V	60	»	—
T-68	Fe + Cr	70	»	—
T-71	Fe + Cr + V	60	»	—
T-72	Fe + V + Mo	9	12	38
T-73	Fe + V + W	11	Снят	—
T-74	Fe + Cr + Mo	5	8	30
T-75	Fe + Cr + W	2	4	8
T-76	Fe + Mo + W	3	6	20
T-77	Fe + V + Cr + Mo	3	6	8
T-78	Fe + V + Cr + W	7	Снят	—
T-79	Fe + V + Mo + W	4	7	11
T-80	Fe + Cr + Mo + W	5	11	24
T-81	Fe + V + Cr + Mo + W	6	Снят	—

As we see, the alloying of α iron with chromium and vanadium does not increase resistance to a bending load. Comparatively high values of the curvature reading, indicating lower heat resistance, were obtained with the combinations iron-vanadium-tungsten and iron-chromium-vanadium-tungsten; these high values are possibly connected with the strong oxidation of the samples during the test. The highest degree of heat resistance, characterized by a small curvature reading, was obtained with the iron-chromium-tungsten alloy. It therefore follows that tungsten in certain combinations (for example, with chromium) increase heat resistance at 600° through the α solid solution at least as much as does molybdenum. The slight effectiveness of alloying steel with tungsten--for example, 2.5% Cr-Mo--is due mainly to the fact that in order to obtain a relatively high concentration of tungsten in the α solid solution of the given steel, 4.5% tungsten must be added. It is well known that tungsten has a stronger tendency to form carbides than chromium and molybdenum, and in order to combine only 0.1% C into the carbide W_2C about 3.2% W is needed. But if we add an element such as niobium to steel in sufficient quantity for the carbon to combine completely into niobium carbide in which the solubility of tungsten is slight [9], the effictiveness of the addition of tungsten is beyond doubt. The influence of tungsten on heat resistance of three steel melt containing niobium in sufficient quantity for complete combination of the carbon into the special carbide is clearly shown.

Tests with a centrifuge at 600° and with a stress of 25 kg/mm^2 for 120 hr resulted in the appearance of a curvature reading of 22 mm for steel containing no tungsten (1), 15 mm for steel containing

1.5% W (2) and 7 mm for steel with 3% W (3) (Fig. 2).

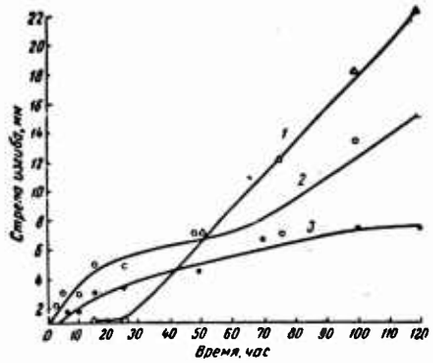

Fig. 2. Dependence of curvature reading on time, for steel containing tungsten. 1) 0; 2) 1.5% 3) 3%.

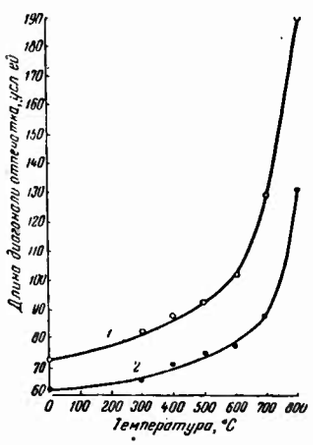

Fig. 3. Temperature dependence of the length of the diagonal of indentation for steel containing tungsten. 1) 0; 2) 3%.

The study of the dependence of hot hardness on temperature in a vacuum showed that while steel which did not contain tungsten (T-25) (1) sharply decreased in hardness at temperatures above 600°, steel with 3% W (T-27) (2) maintained a fairly high degree of hardness up to 700° (Fig. 3). After annealing, steel samples of the same melt were subjected to 20% deformation by upset forging. This increased hardness by 8 to 9 R_B units. Subsequent tempering resulted in the reestablishment of the initial hardness in the case of steel from the T-25 melt (without tungsten) for 2 hr at 700° and 60 hr at 650°. Steel from the T-27 melt (3% W) decreased in hardness down to its initial value after 80 hr at 700°, but this phenomenon was not observed after 320 hr at 650°.

Creep tests on steel with different tungsten contensts show that the tungsten sharply reduces the rate of creep at 610°. The addition of vanadium to steel containing tungsten and niobium (Nb/C = 10/1) results in an increase in the rate of creep. Obviously, the vanadium-tungsten combination is undesirable in α solid solutions. After creep testing for 500 hr at a temperature of 610° and under a stress of 9 kg/mm², steel from the T-26 melt (1.5% W) produced an elongation of 0.259%, and that from the T-27 melt (3.0% W) produced an elongation of 0.137%. The steel from the T-29 melt (1.5% W plus 0.5% V) underwent an elongation of 0.487% and that from the T-64 melt (1.5% W plus 1.0% V) underwent 1.520% elongation.

If molybdenum and tungsten affect the heat resistance of pearlitic steel through the α solid solution, then by using the diagram of equilibrium we may determine the concentrations of these elements which cause a sharp change in heat resistance. Obviously, the addition of tungsten or molybdenum in quantities not resulting in

the formation of special carbides of these elements will be effective in altering the heat resistance since the solubility of these elements in cementite is limited.

Let us consider steel alloyed with molybdenum. We know that molybdenum is the most effective element for increasing the heat resistance of steel. We also know that the sharpest increase in creep resistance is ensured by the addition of molybdenum in quantities of 0.5 to 1%, but that an increase in the molybdenum content to 1.5 to 2% results in relatively little increase in creep resistance. For practical purposes, the alloying of pearlitic steel with molybdenum in quantities in excess of 2% is hardly worth while, and most research is limited to the study of the influence of molybdenum within the limits of a concentration of 0.0 to 2.0%.

However, as was shown by Powers [7], an increase in the content of molybdenum in steel above 4% results in a very sharp increase of heat resistance. The author examined four compositions of steel with a molybdenum contents ranging from 1.9 to 5.2%. The steel was hardened at 1150° in oil and tempered at 690 to 720° for 1 hr. According to Bokshteyn's data [2] the tempering of steel containing molybdenum for 1 hr at a temperature of 700° leads to a nearly balanced molybdenum content in the carbide phase and in the α solid solution. With composition No. 1 (1.9% Mo), a Larson-Miller criterion of 39 corresponds to a stress of 4 kg/mm^2, which is equivalent to the limit of long-time strength for 100,000 hr at 593°; with steel composition Nr. 2 (3.4% Mo) it is 4.2 kg/mm^2; with steel composition Nr. 3 (3.9% Mo) it is 4.9 kg/mm^2, and with steel composition Nr. 4 (5.2% Mo) it is 6.8 kg/mm^2.

Thus, we may assume that in heat-resistant steel containing

0.1 to 0.2% carbon, molybdenum is effective in altering heat resistance for concentrations up to 1.0%, but is not very effective in the interval 1 to(3.5-4)%; it is again effective when the content is more than 4%, at least up to 5.2%.

Let us examine the iron angle of the equilibrium diagram of the iron-molybdenum-carbon system [10] (Fig. 4).

An increase in the molybdenum content to about 0.7% does not result in the appearance of carbides other than $(Fe, Mo)_3C$. We should point out that a carbide of type $Me_{23}C_6$ may form in steel containing 0.49% Mo and 0.22% C at a temperature of 510° after service for 15,000 hr under a stress of 4.5 kg/mm² [1].

Molybdenum concentrations of 0.7 to (2.7 - 3.8)% corresponds to a zone where two carbides exist simultaneous: $(Fe, Mo)_3C$ and $(Fe, Mo)_6C$. The solubility of molybdenum is greater in the carbide $(Fe, Mo)_6C$ than in the carbide of the cement type. The authors give a different formula for this carbide. I. Ye. Kontorovich [11] gives the formula Fe_3Mo_3C, and E. Beyn [10] gives the formula $Fe_7Mo_5C_2$. According to data from other research, the second carbide that forms in the steel alloyed with molybdenum is not the carbide $(Fe, Mo)_6C$ but Mo_2C [12].

In all these formulas at least two atoms of molybdenum correspond to one atom of carbon in the carbide, i.e., the molybdenum content in the carbide exceeds the carbon content in weight by a factor of 15. Consequently, in order to combine all the carbon into a special molybdenum carbide we need about 1.5% Mo with 0.1% C, and about 3% Mo with 0.2% C (taking the carbide Mo_2C).

According to the equilibrium diagram, at 0.1% C, the boundary dividing the zones $\alpha + (Fe, Mo)_3C + (Fe, Mo)_6C$ and $\alpha + (Fe, Mo)_6C$ is

located at 2.2% Mo.

Considering that at a point on this boundary all the carbon is combined into a special carbide in which two atoms of molybdenum correspond to each atom of carbon, we obtain a molybdenum content in the α solid solution equal to 2.2 minus 1.5 = 0.7% Mo.

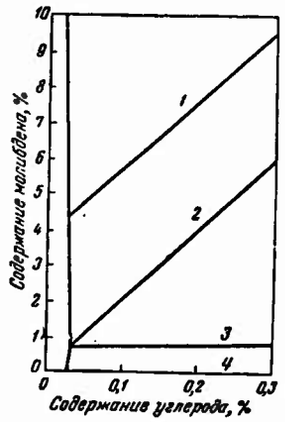

Fig. 4. Iron angle of the equilibrium diagram of the iron-molybdenum-carbon system.
1) - α + $(FeMo)_3$ + $(Fe_3Mo)_6C$;
2) - α + $(Fe, Mo)_6C$;
3) - α + $(FeMo)_3C$ + $(Fe, Mo)_6C$;
4) - α + $(Fe, Mo)_3C$

If the steel contains 0.2% C, the boundary of these zones is at 3.8% Mo. Then, knowing that 3.0% Mo is needed to form the carbide, we obtain in the α solid solution 3.8 minus 3.0 = 0.8% Mo.

V. A. Delle [13] indicates that the solubility of molybdenum in cementite does not exceed 2 to 3% atom%, or 5% by weight.

Consequently, if we add to steel a quantity of molybdenum that does not result in the formation of a carbide of a special type, where the carbon content does not exceed 0.2% the smaller part of the molybdenum goes into the carbide, and the greater part remains in

α solid solution. N. E. Karskiy [14] furnished convincing proof of this fact.

In steel a molybdenum content resulting in the formation of a special carbide should cause the appearance of an inflection on the curve of "molybdenum verses creep resistance (long-time strength)." In concentrations corresponding to the increase of up to 100% in quantity of the special carbide, the majority of the molybdenum atoms go into the carbide phase, and the molybdenum concentration in the α solid solution does not increase in proportion with the increase of the molybdenum content in the steel. All the molybdenum added in excess of the amount necessary to combine the carbon into a special carbide goes into the α solid solution, effectively influencing the heat resistance of the steel.

In chromium-molybdenum or chromium-tungsten steels, the heat resistance must also be connected with the state of the carbide phase and the distribution of molybdenum or tungsten between the α solid solution and the carbides.

Let us examine the influence of chromium on the heat resistance of steel containing 0.5% Mo. As shown in practice, in steel containing 0.1 to 0.2% C and 0.5% Mo, variation of the chromium content from 0 to 15% (i.e., the range within which the transition $\alpha \rightarrow \gamma$ can take place) cause many changes in the value of the creep resistance (long-time strength). When increasing the chromium content from 0 to 1.25 to 2.25%, heat resistance increases markedly. Above 2.25% Cr there is a concentration range within which heat resistance declines and reaches a minimum at 3 to 3.5% Cr. Further increase in chromium content, to approximately 7 to 9% at first, causes a slow increase in creep resistance and then a somewhat more

effective increase of heat resistance. A comparison of this dependence with equilibrium diagram of the iron-chromium-carbon system [10](Fig. 5) shows that the heat resistance increases in the zone α + $(Fe, Cr)_3C$, declines in the zone α + $(Fe, Cr)_3C$ + $(Fe, Cr)_7C_3$, and reaches a minimum approximately at the boundary of the zones α + $(Fe, Cr)_3C$ + $(Fe, Cr)_7C_3$ and α + $(Fe, Cr)_7C_3$. In the zone α + $(Fe, Cr)_7C_3$ there is a small increase in heat resistance.

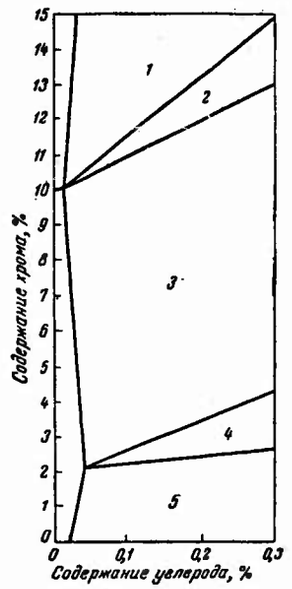

Fig. 5. Iron angle of the equilibrium diagram of the iron-chromium-carbon system.
1) - α + $(Cr, Fe)_{23}C_6$;
2) - α + $(Fe, Cr)_7C_3$ + $(Cr, Fe)_{23}C_6$;
3) - α + $(Fe, Cr)_7C_3$;
4) - α + $(FeCr)_3C$ + $(Fe, Cr)_7C_3$;
5) - α + $(Fe, Cr)_3C$

We give below the results of long-time strength tests for seven melts of chromium-molybdenum steel, in which the chromium content was varied from 0 to 7.33%; the data was taken from a collection

entitled " The elevated-temperature properties of chromium-molybdenum steel" compiled by W. F. Simmons and H. C. Cross[15].

The chemical compositions of the melt are given in Table 3.

All the melts, which were oxidized by ferrosilicon and aluminum, were made in an electric-arc furnace and weighed 10 to 30 tons.

The forged metal was annealed at 840° (except melt No. 2 and No. 7, which were given different heat treatment: No. 2 was heated to 925° soaked for 1.5 hr, cooled in air to 700°, soaked for 1.5 hr and cooled in the furnace; No. 7 was normalized from 950° and tempered at 700°).

After the heat treatment, the microstructure of the steel showed an equilibrium between the ferrite grains and carbides of granular shape.

The size of the grains according to the McQuaid-Enn method and the Brinell hardness appear in Table 4.

TABLE 3

№ плавки	Содержание элементов, %						
	C	Mn	Si	P	S	Mo	Cr
1	0,13	0,49	0,25	0,011	0,010	0,52	—
2	0,13	0,47	0,14	—	—	0,55	0,40
3	0,10	0,36	0,25	0,011	0,014	0,55	0,97
4	0,17	0,42	0,72	0,010	0,017	0,54	1,24
5	0,11	0,45	0,42	0,012	0,015	0,50	2,08
6	0,10	0,45	0,18	0,011	0,013	0,55	5,09
7	0,11	0,43	0,92	0,010	0,011	0,59	7,33

TABLE 4

№ плавки	Размер верна по Мак-Квед-Эну	Твердость H_B	№ плавки	Размер верна по Мак-Квед-Эну	Твердость H_B
1	6—8	121	5	6—8	131
2	6—7	118	6	6—8	146
3	6—8	137	7	4—6	174
4	4—5	149			

We see that steel hardness is basically determined by the silicon content; however, the concentration of chromium also affects hardness slightly increasing it. The difference in the silicon content observed in the melt examined cannot substantially change the heat resistance of the steel, although it sharply changes its properties at room temperature. A variation in the silicon content from 0.1 to 1.0% in chromium-molybdenum steel slightly lowers the heat resistance; however, the influence of silicon is considerably weaker than the influence of chromium and molybdenum, particularly at temperatures above 550° [16]. Annealing at 840° ensures an almost balanced chromium and molybdenum concentration in the carbides and the solid solution.

The values for the limit of long-time strength at temperatures of 538 and 593° are given in Fig. 6, which shows a clearly defined maximum in the magnitude of the limit of long-time strength given a chromium content of 0.97% (melt No. 3) and 1.24% (melt No. 4). The maximum appears most accentuated at a test temperature of 538° and is weaker at 593°. It is impossible to explain the presence of the maximum by a variation in the grain size of steel No. 4, since steel No. 3, which has a grain that does not differ from that of the other melts, also has abnormally high values for the limit of long-time strength, particularly at 538°.

As we know, chromium has little effect on the heat resistance of steel; it is therefore difficult to assume that the sharp change in heat resistance within the range of chromium concentrations of 1.5 to 3.5% is connected with the degree to which chromium is alloyed in the α solid solution. Obviously, the change in heat resistance is connected with the variation of the molybdenum content in the α

solid solution. If chromium, in quantities that do not result in formation of a carbide other than cementite, is added to steel that contains 0.5% Mo, some of the molybdenum atoms must be displaced by the chromium from the carbide phase into the solid solution, and the heat resistance increases as a result of the enrichment of the α solid solution by molybdenum.

The addition of chromium in quantities sufficient for the formation of the carbide $(Fe, Cr)_7C_3$ results in a change in the ratio of the balanced chromium and molybdenum concentrations in the carbides. As has been shown by research [17], in the iron-chromium-tungsten-carbon system, even small additions of tungsten to chromium steel with a composition corresponding to the range of existence of the carbide $(Fe, Cr)_7C_3$ cause the appearance of a carbide of the type $Me_{23}C_6$ with a high tungsten content (~ 20%). Obviously, a pattern of this kind must also be observed with molybdenum. There must therefore be a chromium concentration range within which the carbides of types $(Fe, Cr)_7C_3$ and $(Mo, Cr, Fe)_{23}C_6$ exist simultaneously. The more carbide $(Fe, Cr)_7C_3$ forming in the iron-chromium-carbon system, the more carbide $(Mo, Cr, Fe)_{23}C_6$ with a relatively high molybdenum content there will be in the iron-molybdenum-chromium-carbon system, and the less molybdenum there will remain in the α solid solution.

A maximum concentration of molybdenum in the carbide phase will have obviously been attained when there is 100% $(Fe, Cr)_7C_3$ in the iron-chromium-carbon system. A further increase of the chromium content in the $(Fe, Cr)_7C_3$ zone may lead to an enrichment of the α solid solution with chromium and the displacement of a certain quantity of molybdenum from the carbides into the α solid solution.

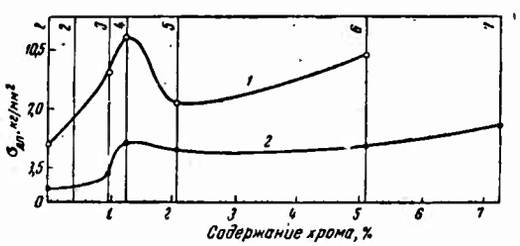

Fig. 6. Prolonged strength for 100,000 hours vs. amount of chromium and steel with 0.5% Mo and 0.1% C at 538° (1) and 593° (2).

The alloying of steel with molybdenum or tungsten with a chromium concentration corresponding to the zones $\alpha + (Fe, Cr)_3C +$ $+ (Fe, Cr)_7C_3$ and $\alpha + (Fe, Cr)_7C_3$ obviously prevents a high concentration of these elements in the α solid solution since they go into the $Me_{23}C_6$ type carbide. This led to the opinion that a 3 to 7% Cr base in chromium-molybdenum steels was of no long-term value in research into steel with high creep resistance. However, if niobium, titanium, or vanadium are added to steel in quantities sufficient for the carbon to combine into special carbides with there elements, it is possible to influence effectively the heat resistance of steel with 3 to 7% Cr by varying the molybdenum or tungsten concentration in the α solid solution.

Conclusions

1. At elevated temperatures, tungsten and molybdenum strengthen the α solid solution most effectively. Comparison of their influence in atomic percentages on heat resistance at temperatures of 550 to 600° shows that tungsten increases heat resistance almost as effectively as does molybdenum.

2. The alloying of steel with tungsten or molybdenum without the addition of elements combining with the carbon into special carbides, in which tungsten and molybdenum are only slightly soluble, can only be effective within a range of concentration which does not result in the formation of carbides other than cementite. An increase in the tungsten or molybdenum content in the concentration range corresponding in the equilibrium diagram to a zone in which the two carbides exist simultaneously--one of the cementite type and the other a special one--does not substantially change heat resistance.

An increase in content of the alloying element above the concentration necessary for the carbon to combine completely into a special carbide leads to an increase in heat resistance.

3. Chromium and vanadium are elements that do not effectively increase the heat resistance of steel through the α solid solution.

4. The variation in heat resistance of chromium-molybdenum steel, in the given variation in the chromium content, may be related to variation in the molybdenum concentration in the α solid solution.

REFERENCES

1. MIRKIN, I. L. and SOLONOUTS, M. I. Metallurgy and Metal Treatment (Metallurgiya i Obrabotka Metallov) No. 2, 1957.

2. BOKSHTEYN, S. Z. Structure and Mechanical Properties of Alloyed Steel (Struktura i Mekhanicheskine Svoystva Legirovannoy Stali) Metallurgizdat, 1954. St. Sc. Pub. House for Lit. on Ferr. and Non-Ferr. Met.

3. GRÜN, P. Arch. Eisenhüttenwesen. 8, 1934.

4. HOLTMANN, W. Mitteilungen Kohle-und Eisenforschung, 3, 1941.

5. TAMMAN, G. Z. Metallkunde, 28, 1936.

6. SMITH, G. W. Properties of Metals at High Temperatures, McGraw-Hill Book Co., 1950.

7. POWERS, A. E. J. Metals, Oct. 8, Nr. 10, Sect. II, 1956.

8. SHTEYNBERG, M. M. Struktura i Mechanicheskiye Svoystva Legirovannogo Ferrita. Problemy Metallovedeniya i Termicheskoy Obrabotki (Structure and Mechanical Properties of Alloyed Ferrite. Problems of Metallurgy and Heat Treatment), (UFAN)(Ural Branch, Acad. Sci. USSR) Mashgiz (State Sci. Tech. Press for Machine Literature), 1956.

9. UMANSKIY, Ya. S. Karbiby Tverdykh Splavov (Carbides of Hard Alloys), Metallurgizdat, 1947.

10. BEYN, E. Vliyaniye Legiruyushchikh Elementov Na Svoystva Stali (Influence of Alloying Elements on Steel Properties), Metallurgizdat, 1945.

11. KONTOROVICH, I. Ye. Termicheskaya Obrabotka Stali i Chuguna (Thermal Treatment of Steel and Pig Iron), Metallurgizdat, 1950.

12. LASHKO, N. F. and TSEYTLIN, V. Z. Vliyaniye Sostava i Vzaimodeystviya Faz Na Soprotivleniye Relaksatsii Perlitnoy Stali (Influence of the Composition and Interaction of Phases on Resistance to Relaxation of Pearlitic Steel), TsNIITMASh (Central Sci. Research Inst. for Tech. and Mach.), book 71, 1955.

13. DELLE, V. A. Legirovannaya Konstruktsionnaya Stal ' (Alloying of Construction Steel), Metallurgizdat, 1953.

14. KARSKIY, N. Ye. "Metallovedeniye i Obrabotka Metallov" ("Metallurgy and Treatment of Metals"), Nr. 3, 1957.

15. SIMMONS, W. F. and CROSS, H. C. The Elevated-Temperature Properties of Chromium-Molybdenum Steel, ASTM, Spec. Techn. publication, Nr. 151, 1953.

16. SALLI. Polzuchest' Metallov i Zharoprochnyye Splavy (Creep in Metals and Heat-Resistant Alloys), Oborongiz (State Press of the Defense Industry), 1953.

17. KEHSIN, Kuo. J. Iron and Steel Inst., 185, p. 3, 1957.

CONCERNING THE ATOMIC MECHANISM OF AGING IN COMPLEX ALLOYS

I. L. Mirkin

Research into steels and alloys able to operate under considerable stress at high temperatures without suffering any large deformation (through creep) and without breaking down over a long period of time is an important task in modern science and technology. Progress in this direction determines to a consideralbe degree the possibility of progress in building new power installations and engines for transportation and improving their operation parameters, efficiency factor, speed, and length of service.

The research of the last few years has shown that one of the principal problems in producing new heat-resistant alloys intended for very long service is that of obtaining the greatest possible structural stability of the alloy and preventing, or decreasing and retarding as much as possible, resoftening and embrittlement during the period of operation. It has been established that the formation and growth of new-phase crystallites, which are precipitated from the solid solution when the alloy is subjected to high temperature and stress for a long time, are fundamental to these processes. The appearance of new crystallites of the excess phase and the variations in their dispersion and conjugation with the matrix sharply

influence the strength characteristics not only directly but also through a substantial impoverishment of the basic solid solution of the alloying elements. It is the latter fact which often plays a decisive part in the resoftening of alloys at later stages. Hence, an analysis of the laws and mechanisms of these processes and the exposure of the fundamental factors determining their kinetics is extremely important.

It is particularly essential here to determine the relative part played by each factor in this complex process and to determine at least approximately the extent to which each component factor contributes to the resulting rate at which the process proceeds.

A deeper and clearer understanding of these problems and an accurate evaluation of the role of each will help us in our scientific search for new alloys that have greater resistance to resoftening and embrittlement and that are therefore most suitable for very long service at high temperatures.

Most modern heat-resistant steels and alloys have multiple components; during their service excess-phase crystallites originate and grow in them from the basic supersaturated and supercooled solid solution.

Even in those cases where the basic stage of this precipitation has already been completed as a result of previous heat treatment, structural changes do not cease during service: coagulation of the phases present in excess takes place, i.e., the dissolution of some crystallites and the growth of others, sometimes accompanied by a change in their composition. There is frequently a phase transition of the precipitated crystallites and the formation of crystallites of a new and more stable phase as well.* Thus, nucleation of the

* However, the contemporary theory of crystallization indicates that the growth of a crystallite is a step-by-step, multistage sedimentation of two-dimensional nuclei on the faces of a three-dimensional nucleus or crystallite. Consequently, here also the formation of a nucleus is fundamental to the process.

new phase is one of the fundamental and most important of all the structural changes in the alloy in service.

The rate at which the crystallites of the excess phase originate and grow depends on many factors: the degree of supersaturation and supercooling of the basic solution; the work involved in the formation of an effective nucleus, determined by its size and surface tension; the change in elastic energy; the diffusion mobility of the atoms in the lattice; etc.

During the formation of a new phase that differs substantially from the mother liquid in chemical composition, the most important part is played by fluctuations in concentration, as has been shown in the research [1, 2]. Nucleation must be preceded by the formation of a fluctuation zone, which, being enriched with one component and impoverished of others, must attain (or approach) the composition of the new phase, and this change must definitely take place in a lattice volume equal to the volume of the equilibrium (effective) nucleus. The formation of such fluctuations depends on the difference in concentration between the initial and the new phase and on the size of the equilibrium nucleus.

With the increase in difference between the compositions of the initial and the new phase and with the increase in size of the equilibrium nucleus the number of atoms of a given element; also increase these must, in the given instance, either collect in the given zone or leave it, and therefore both the probability that similar fluctuations will occur and the number of such fluctuations per unit of volume of the alloy decrease sharply.

The rate of formation of fluctuations, i.e., the number of zones of a given magnitude and composition forming in 1 cm^3 of alloy in

1 sec, also depends on the thermal mobility of the atoms, as has been established by research [2], and varies in proportion to the diffusion coefficient.

By generalizing all the previous calculations concerned with the fluctuation of carbon concentration in austenite, which take into account both the degree to which the given zone is enriched in or impoverished of carbon and the dimensions (volume) of the zones with the prescribed variations in composition, we constructed the free-space fluctuation diagram given in Fig. 1, taking as a model the fluctuations of carbon atoms in a simple carbon steel of eutectoid composition.

On this diagram are plotted: the carbon concentration in the fluctuation zone (expressed in atomic percentages) on the x axis; the size (voluem) of the fluctuation zone, which can be expressed as a linear dimension either by the number of elementary cells of the lattice, by the number of iron atoms, or by the normal (non-deviated) average number of carbon atoms contained in that zone before the formation of a fluctuation, on the y axis; the number of fluctuation zones of a given size and given degree of enrichment (impoverishment) in unit volume of the alloy (in 1 cm^3), expressed a logarithmic-alloy, on the z axis.

The diagrams constructed in the research [1, 2] are like flat sections of this generalized space diagram of fluctuations.

The necessary calculations were made according to the formula

$$N_f = N_0 P_j^{(c)} = N_0 \frac{c^j l^{-c}}{j!}, \qquad (1)$$

in which

N_f is the number of fluctuation zones of a given size and given

degree of deviation from the average composition in unit volume (1 cm^3) of the alloy;

N_o is the total number of zones of given size (with any composition of the alloy per 1 cm^3;

$P_j^{(\epsilon)}$ is the probability of fluctuation formation consisting in the deviation of the number of atoms in the given zone from their normal (i.e., arithmetical average) number ϵ to a random number j.

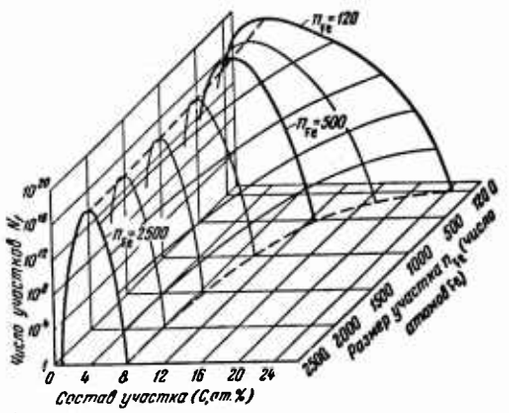

Fig. 1. Space diagram of carbon fluctuation in austenite (steel 0.8% C), the number of fluctuation zones N_f depending on their composition and size.

A detailed account of the system of calculations developed by us, its conditions for use, the assumptions adopted and the factors left out was published in [1] and is not given here. A detailed analysis showed that although these calculations are approximate, their experimental verification for the case in which austenite is converted into pearlitie conformed closely enough with the results of a direct test [2].

If we divide the whole volume of austenite in the steel into zones each containing 12 cells (48 metal atoms), then, calculation shows, the probability of a fluctuation accretion of carbon in the cells to a "cementite" concentration (16 atoms of carbon instead of the normal 2) is $P_{16}^2 = 4.2 \cdot 10^{-10}$, and the number of fluctuations is $N_f = 7.5 \cdot 10^{11}$.

Let us consider the conditions of the fluctuation theory of the behavior of alloyed steel as compared to carbon steel. Let us take a steel containing 2% chromium. In an annealed or high-tempered state it contains, as we know [4], an alloyed chromium carbide with a lattice of the cementite type but containing 16 to 23[chromium. Thus, in this instance, for the formation of carbide, a fluctuation accretion of not only carbon but also chromium must take place, at the same time, in the same zone of the solid solution. However, according to probability theory, the probability of the coincidence of two events is equal to the product of the probabilities of occurence of each of them (we do not take into account their interrelation). Near the point of equilibrium or at sufficiently high temperatures, a nearly stable carbide is formed during the transformation. Consequently, the number of chromium-carbide fluctuation nuclei may be expressed by the formula

$$N_f(\mathrm{C} + \mathrm{Cr}) = N_0 P_{i_1}^{(e_1)}(\mathrm{Cr})\, P_{i_2}^{(e_2)}(\mathrm{C}). \qquad (2)$$

It is easy to calculate that the following two facts must coincide in time and space in the zone of the initial solid solution of the same size (48 metal atoms) in order to make the formation of the carbide $(Fe, C)_3C$ possible (see diagram in Fig. 2):

the accretion of carbon atoms from 2 to 16;

the accretion of chromium atoms from 1 to 8.

The probability of the first fact was calculated above:

$P_{(c)} = 4.2 \cdot 10^{-10}$.

The probability of the second fact is easy to calculate:

$P_{(8)}^{Cr} = 9.1 \cdot 10^{-6}$.

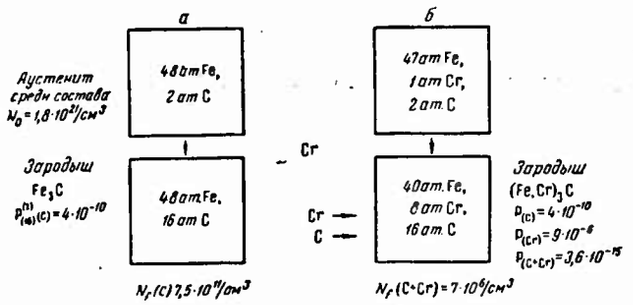

Fig. 2. Diagram of formation of cementite nuclei Fe_3C in nonalloyed and alloyed steel containing 0.8% C (a) and 0.8% C + 2% Cr (b).

As we see, fluctuations of chromium have small probability, and this must very sharply reduce the total probability of alloyed cementite formation and the number fluctuating nuclei of this carbide compared to simple cementite. Actually,

$$N_1(C + Cr) = N_0 P(C) P(Cr) = 1{,}77 \cdot 10^{21} \times 4{,}23 \cdot 10^{-10} \times 9{,}10 \cdot 10^{-6} = 6{,}9 \cdot 10^{5}.$$

As we see, the probability of nucleation in alloyed cementite and the number of fluctuation nuclei are only about 100,000 that in nonalloyed cementite. In the case of larger nuclei, this difference becomes still greater; for example, in zones 72 metal atoms in size it amounts to 7 orders of magnitude. This dependence is shown in a generalized manner in Fig. 2 and 3, which bring out the degree to which the number of fluctuations is lower in alloyed chromium cemen-

tite compared to simple carbide iron. Moreover the theory of fluctuation proves that the simple cementite nuclei of the greatest size which may only form once as a result of fluctuation, are much larger than alloyed ones (116 metal atoms as against 76). Without therefore, considering the other factors, we may expect the nuclei of chromium cementite to precipitate under more pronounced conditions of supercooling or supersaturation and in considerably smaller numbers. Obviously, the rate of growth of the precipitating crystallites, which consists of a gradual deposit of two-dimensional nuclei on the faces of three-dimensional nuclei, must also, though for the same fluctuation causes, sharply decrease in alloyed cementite; this is well confirmed by tests.

We should point out that in alloying, the thermal mobility of the atoms also influences the kinetics of precipitation of the new phase. As was established earlier [2], the rate of fluctuation formation (r. f. f.)--i.e., the number of fluctuations forming per unit volume of the alloy in unit time --is directly proportional to the coefficient of diffusion D and for a fluctuation zone of $\underline{h}$ cm is expressed by the following formula:

$$\text{c.o.}\Phi = n_f = \frac{8(\epsilon+j)^2}{\pi h^2} N_f D. \qquad (3)$$

Zener [5] established that the rate of crystal growth is also proportional to the coefficient of diffusion D, and B. Ya. Pines [6] established this more precisely. However, as shown by experiment [4], the diffusion coefficient of carbon D_C decreases when 2% chromium is added to the steel; for example, in the case of diffusion in ferrite at 700° it decreases from $6.6 \cdot 10^{-6}$ to $4.5 \cdot 10^{-6}$ cm^2/sec, i.e., by a factor of 4 [7]. This cannot substantially affect our

conclusions. Considerably more important is the fact that for the formation of alloyed cementite and accumulation of chromium atoms is necessary in the given zone of the solid solution, i.e., a further displacement of metal atoms whose mobility, as we know, is much lower than that of the carbon atoms. We were not able to find published data on our type of steel suitable for direct comparison. Such data can be approximated by taking data obtained S. D. Gertsriken [8] on the diffusion coefficient of chromium in an iron alloy containing 8% chromium--at 1010° $D_{Cr} = 6.16 \cdot 10^{-8}$-- and for the diffusion of carbon at 1000° from data obtained by M. Ye. Blanter [7] (see above)--$D_C = 2.5 \cdot 10^{-7}$, i.e., greater by a factor of 20. According to other data, this difference is still greater and may reach a factor of 40. In the presence of carbon, however, the diffusion of metal is considerably accelerated. By analyzing all these data, we may draw the following conclusion.

The alloying of steel causes a decrease in the precipitation of the alloyed carbide as a result of the decrease in the probability of fluctuation as well as in the mobility of the atoms, particularly the metal atoms; not only is the fluctuation factor not secondary, it is decidedly more important and more strongly affects the retardation of the precipitation of carbide in alloying than does a decrease in thermal mobility.

Indeed, as shown above, the decrease in the probability of formation of the necessary fluctuation in alloying caused a decline in the number of nuclei by 5 to 7 orders of magnitude, and a decline in diffusion mobility by only 0 to 2 orders of magnitude.

These are the results of an analysis of the mechanism of the

influence of alloying on the precipitation of the excess phase and, consequently, on the structural resoftening and aging of alloys in precipitation of carbides of the cementite type. As we see, the most important factor in this problem is the sharp decline in the probability of a fluctuating accumulation until the composition corresponds to the new phase;this is a result of the complex composition of the new phase; and the necessity for the displacement of atoms of several elements (C, Cr) at the same moment and in the microzone of the nucleation lattice of the new phase with a new composition.

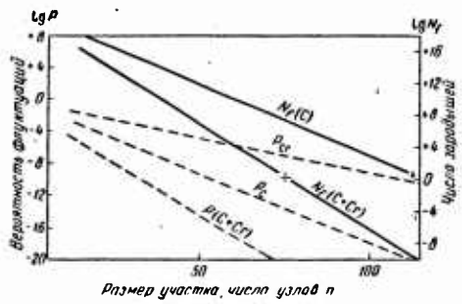

Fig. 3. Diagram of fluctuation during the formation of carbide $(Fe, Cr)_3C$ (steel 0.8% C + 2% Cr).

This conclusion differs substantially from the prevailing opinion that the change in the kinetics of structure transformation in alloying is mainly based on variations in the diffusion mobility of the atoms in the lattice. A quantitative analysis shows that this opinion is not well founded and that the reduced probability of fluctuations in concentration is at least as important as the decline in diffusion mobility of the atoms in the alloying of steel. We run the risk that this conclusion as to the importance of the fluctuation

probability is limited and is valid only for chromium-cementite formation.

In order to resolve this problem, let us examine the process of precipitation of phases other than cementite. Let us analyze the case of precipitation from chromium steel of a trigonal carbide of the type $(Cr, Fe)_7C_3$, which is known to precipitate at a sufficiently high temperature or near the point of equilibrium even at relative low chromium concentrations.

As we know, this carbide contains over 40% chromium and about 9% carbon by weight. To make the analysis clearer, let us make the calculation for steel containing 0.4% carbon and 2% chromium (by weight). Let us calculate the probability of formation, in a given zone, of various degrees of enrichment in carbon and chromium due to fluctuations leading to the composition of a trigonal carbide (Fig. 4; Table 1).

The calculation shows that in this case the concentration of carbon and chromium in the fluctuation zone must increase in nearly equal and (at the same time) very large amounts--by a factor greater than 20. It is clear that phenomena of this kind have very low probability of occurrence, and it is completely impossible to produce them in a large volume of 50 or 100 lattice points. Even the formation due to fluctuations of a zone of 20 lattice points with the necessary chromium enrichment has a probability of the order of 10^{-10}; and the simultaneous enrichment of the same zone with carbon and chromium has a probability of 10^{-20}. Consequently, the number of such fluctuations per cm^3 of chromium steel, $N_j(C + Cr) = N_o (Cr) P (C) = = \sim 10^1$, amounts to only several order of ten, and it is only the smaller zones which are found in a great number.

TABLE 1

Fluctuations for the Formation of Trigonal Carbide in Chromium Steel (0.4% C + 2% Cr)

	Размер участка (число металлических атомов-узлов)	Состав участка		
		C	Cr	Fe
Исходный твердый раствор нормального среднего состава	100	2	2	96
Флуктуационный участок (состав равен составу тригонального карбида 9% C, 39% Cr)	100	43	43	57
Твердый раствор нормального состава	50	1	1	49
Обогащенный флуктуационный участок	50	22	22	38
Твердый раствор нормального состава	10	0,2	0,2	9,6
Обогащенный флуктуационный участок	10	4,3	4,3	6

Key:

A) Initial solid solution of normal average composition

B) Fluctuation zone (composition equal to the composition of trigonal carbide 9% C, 39% Cr)

C) Solid solution of normal composition

D) Enriched fluctuation zone

E) Solid solution of normal composition

F) Enriched fluctuation zone

Thus it is only under the most favorable conditions and, moreover, extremely slowly, that the trigonal carbide can precipitate directly from a solid solution in chromium steel with a low chromium content. In the majority of cases, a carbide of the cementite type with a chromium content close to the average composition of the steel will be precipitated at first, and this will be converted into

a carbide of the trigonal type gradually and only after a long period of time, during which the chromium content is increased; this is confirmed by direct testing.

The extent of the role of enrichment probability is apparent in this case, from the fact that a carbide of the cementite type without chromium enrichment (see Fig. 4) produces without accretions 10^{17} per cm^3 with 20 points and a maximum fluctuation of about 120 adjacent points--not 20, as occurs with a trigonal carbide.*

Thus, fluctuation of concentrations plays an extremely important part in the problem of formation of stable and intermediate phases during the transition. This part becomes much greater still when a sharp change of concentration is necessary for the formation of the new phase, not only in one but in two components--in carbon and chromium at the same time, as in precipitation of a trigonal or cubic ($Cr_{23}C_6$) carbide in chromium steel.

To sum up the results, Table 2 and Fig. 5 show a comparison of the curves of the number of fluctuations N_f per cm^3 of steel as a function of the size of the fluctuation nucleus $\underline{n}$ (number of points)

---

* In a less distinct form, but based on the same principle it is possible, in many cases, to explain the primary formation of enriched cementite carbide, since it may contain up to 20 to 25% Cr, while trigonal carbide showed contain as much as 40% and often even 70% Cr in its composition. This also explains why trigonal carbide forms more easily in steel that contains a higher percentage of chromium.

for various cases of precipitation of carbide from austenite. Curve 1 shows the precipitation of cementite Fe_3C in carbon or chromium steel (but without change in the carbide composition with respect to chromium) as compared to the initial solid solution; in this case, the maximum size of the section n_{max}, in which the concentration may increase up to the composition of cementite attains 116 adjacent lattice points, and for a size of $\underline{n} = 16$, we obtain $N_f = 10^{18}/cm^3$. Curve 2 shows the precipitation of chromium cementite $(Fe, Cr)_3C$, containing about 16% chromium in a steel (0.4%C) with 2% Cr and gives $n_{max} = 76$ points; at n = 16 points, the number of nuclei is $N_f = 10^{16}$ cm^3. Larger nuclei are found in considerably smaller numbers than nuclei of simple cementite Fe_3C; for example, at n = 60,

$$N_f(Fe_3C) = 10^{10}\ см^3;\ а\ N_f(Fe,Cr)_3C = 10^4\ см^3;$$

Curve 4 for the precipitation of trigonal chromium carbide $(Cr, Fe)_7C_3$-- containing about 40% Cr--in the same steel--containing 2% Cr--indicates a sharp decrease in the size of the maximum nucleus up to $n_{max} = 22$ points and indicates a still sharper decrease in the number of nuclei with n = 16, up to $N_f = 10^5/cm^3$.

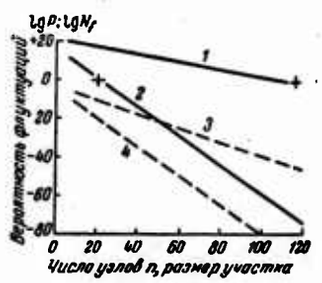

Fig. 4. Diagram of fluctuations in the formation of carbide $(Cr, Fe)_2C_3$ (steel 0.4% C + 2% Cr): 1) N_f (Fe_3C); 2) N_f $[(Cr, Fe)_7C_3]$; 3) PCr $[Cr, Fe)_{23}C_3]$; 4) $P(C + Cr)$ $[Cr, Fe)_7C_3]$.

TABLE 2

Number and Size of Fluctuation Nuclei of Various Phases

Сталь (содержание элементов, %)	Выделяющаяся фаза	Число зародышей N_f, см^3	Размер зародыша n узлов решетки	n узлов. Максимальный размер зародыша при $N_f = 1$ см^3
		Карбиды		
0,8C	Fe_3C	$1 \cdot 10^{16}$	16	116 узлов
0,4C + 2Cr	$(Fe, Cr)_3C$	$1 \cdot 10^{16}$	16	76
0,4C + 6,7Cr	$(Cr, Fe)_7C_3$	$3 \cdot 10^{10}$	16	34
0,4C + 2Cr	$(Cr, Fe)_7C_3$	$1 \cdot 10^{5}$	16	22
		Интерметаллиды		
18Cr+8Ni (скорость зарождения)	σ	$2 \cdot 10^{11}$	400	1 000
	σ	10^{14} см^2/сек	500 узлов	
18Cr + 8Ni + 3,6Mo (скорость зарождения)	σ	$1 \cdot 10^{6}$	400	500
	σ	10^{8} см^2/сек	500	
75Ni + 20Cr + 2,5 Ti + +0,6Al	α′	$3 \cdot 10^{11}$	500	
		$6 \cdot 10^{8}$	100	120

Curve 3 shows the precipitation of the same trigonal chromium carbide, but from a salt* of high chromium content (6.7% Cr) and not 2% as in the previous case. In this steel we may obtain larger nuclei (n_{max} = 34 points) and we may obtain them in greater quantitie (for example, with n = 16, $N_f = 3 \cdot 10^{10}/cm^3$) than in steel with a low chromium content. The results obtained demonstrate clearly that the fluctuation theory explains the appearance of intermediate phases and carbide transformation when the alloyed steel is kept at a high temperature for extended periods. However, we should mention that even the isolated three-dimensional nucleus of 8 elementary cells contains 63 metal atoms when the lattice is face-

* Translators note: As in original. This should probably read steel.

centered if we also take into account all the atoms forming its surface. We can hardly assume that the nucleus of the new phase has a cube edge length of less than two lattice constants. Nevertheless, as shown by the curves of Figure 5 and by the above-mentioned examples, in a series of cases--for example in the case of the formation of a trigonal carbide--even a nucleus of the size (63 metal atoms) will hardly ever form, and the direct and nonincubated (i.e., without a very long formation period) precipitation of the trigonal carbide from the solid solution (particularly favorable conditions excepted) will therefore fail to take place in the majority of cases. An indirect confirmation of this conclusion is furnished by results from the research [12], according to which a trigonal carbide was found in steel containing 2% Cr only after several hours, and in steel with 6.7% Cr after several seconds of soaking at 650°.

The process is considerably facilitated when the new phase is grown on the face of an already existing crystal without loss of coherence. A two-dimensional, one-layer nuclei of the same linear size (2 constants X 2 constants) contains only 13 atoms in the lattice of a face-centered cube, while it contains 25 atoms when the size is 3 constants X 3 constants. This does not exceed the number of atoms in maximum fluctuation (see Table 2). Consequently, elementary carbide-crystal growths or their formation on a ready-made base may occur in great numbers not only in the case of chromium cementite but also with trigonal carbide. Moreover, this possibility is realized even in steel with a low chromium content.

Let us consider the problem of the precipitation of crystallites of intermetallic compounds in alloys. The question of the probability of the formation of concentration fluctuations is of paramount

importance not only in the case of the precipitation of carbides, but also in intermetallic compounds. We know, for example, that in austenitic chrome-nickel types of steel σ phases may form causing hardening and embrittlement of the steel in varying degrees, depending on the conditions of heat treatment aging, and service at high temperatures. Research [10] has shown that with a steel containing 0.06% C, 8 to 14% Ni, 18% Cr, and 3.5% Mo, a σ phase precipitates. This has a composition of 28% Cr, 4% Ni, and 12% Mo.

Calculation according to the theory of concentration fluctuations shows the relative role of the probability of accumulation of atoms of certain elements in the production of a concentration corresponding to the new σ phase. In this case, we should take into account not only the need for accumulation of an increased number of chromium atoms in the zone of the future σ phase but also the departure of some of the nickel atoms from that zone (Fig. 6). The role played by the components which do not enter into the new phase but which sometimes exert a strong effect on the probability and rate of its formation and growth must be particularly emphasized, since no importance has previously been attributed to this factor; nevertheless, in some alloys--for example, those with a high nickel content--this role is very great in the formation of an α' phase and it also explains, to a considerable extent, the increased heat resistance and durability of those alloys (containing tungsten, molybdenum, and niobium) which seldom enter into the composition of the α' phase. Calculation according to the theory of fluctuations shows clearly that in a chrome-nickel steel the factor of chromium accumulation and the factor of nickel impoverishment have a commensurate magnitude during the formation of the σ phase. For example,

in a zone 500 atoms in size the necessary enrichment with chromium has a probability $P_{Cr} = 6.4 \cdot 10^{-7}$, and the nickel impoverishment $P_{Ni} = 5 \cdot 10^{-5}$. As a result, the number of fluctuation nuclei of a σ phase 500 atoms in size in chrome-nickel steel amounts to:

$$N_{\sigma}(\mathrm{Cr}+\mathrm{Ni}) = N_0 P_{\mathrm{Cr}} P_{\mathrm{Ni}} = 1{,}7 \cdot 10^{20} \cdot 6{,}4 \cdot 10^{-7} \cdot 5 \cdot 10^{-5} = 5{,}4 \cdot 10^{9}/\mathrm{см}^3.$$

A series of similar calculations, generalized in the diagram (Fig. 7), shows that the maximum size of the σ phase nucleus of normal composition able to originate directly from the homogeneous solid solution (austenite) in a simple chrome-nickel steel as a result of concentration fluctuations without forming intermediate transitory phases is about 1,000 atoms. Numerous smaller zones originate, reaching an order of 10^6 zones per cm^3 of steel, and attaining 700 atoms in size. However, if we further alloy the steel with molybdenum, the situation changes quite substantially.*

---

* We do not examine here the variations in the diagram of state, temperature, and concentration corresponding to the equilibrium the degree of supersaturation, or other thermodynamic factors affecting the steel's tendency toward precipitation of the σ phase when molybdenum is added to it. Because of these factors, the real quantity of the σ phase formed may substantially change with the addition of molybdenum to the steel, but this will happen for reasons completely different from the kinetic problem under consideration.

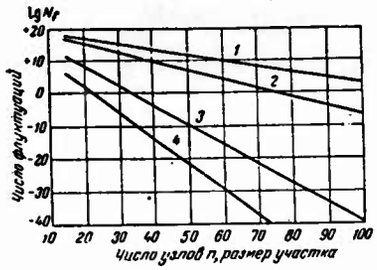

Fig. 5. Comparison of the number and size of fluctuation nuclei of various types of carbides.

Actually, in this case the formula for the number of fluctuations is:

$$N_{f\sigma}(\mathrm{Cr} + \mathrm{Ni} + \mathrm{Mo}) = N_0 P_{\mathrm{Cr}} P_{\mathrm{Ni}} P_{\mathrm{Mo}},$$

i.e., an additional multiplier P_{Mo} appears in the equation, indicating the probability of an increase in the concentration of molybdenum from 3.5% in the solid solution to 12: in the σ phase. By transforming these numbers into atomic percentages, we calculated that for a zone of 500 atoms the probability for such an accumulation of molybdenum amounts to $P_{Mo} = 4.6 \cdot 10^{-10}$; i.e., it is almost as difficult to effect this accumulation of molybdenum atoms as simultaneously to accumulate chromium in the given zone and displace nickel from it. On the strength of this, the number of fluctuations of the σ phase declines disastrously when molybdenum is introduced; it decreases by a factor of 10^9:

$$N_{f\sigma}(\mathrm{Cr} + \mathrm{Ni} + \mathrm{Mo}) = 2{,}5/\mathrm{см}^3,$$

and the maximum size of a possible fluctuation nucleus decreases sharply: in steel without molybdenum it amounts to about 1,000 atoms, and in the presence of molybdenum it amounts to not more than 500 (see Fig. 7).

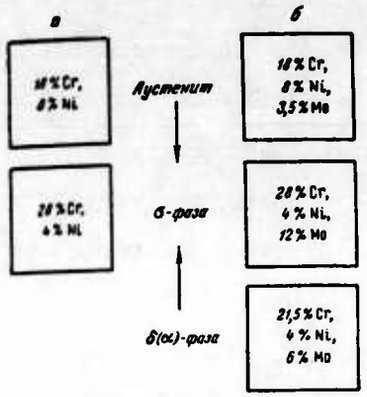

Fig. 6. Diagram of formation of σ phase nuclei in steel containing 18% Cr + 8 % Ni a) and 18% Cr + 8% Ni + 3.5% Mo b)

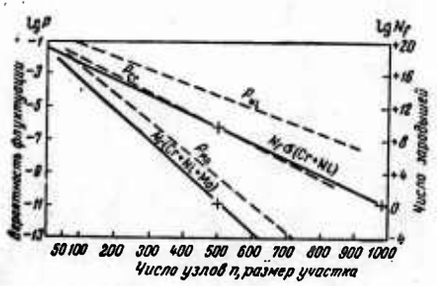

Fig. 7. Diagram of fluctuations during the formation of a σ phase in steel containing 18% Cr + 8% Ni and 18% Cr + 8% Ni + 3.5% Mo.

The analysis we made shows that an additional alloying with a new element sharply retards the resoftening process, owing to the fact that the growth of crystals and strengthening phases is made difficult as a result of the extremely sharp decrease in the probability that the prescribed fluctuation variation in concentration of the given zone will take place in respect to many components at the same time. Thus, the fluctuation theory may explain the phenomenon frequently observed in tests: less resoftening of the alloy over a long period of service and an improvement--partially dependent on this in its heat-resistant properties when its composition becomes more complex, and it is, in addition, efficiently alloyed with new components. The latter fact is so intrinsically apparent that some researchers even connect the degree of the alloys heat resistance with the number of components forming it; in fact, they consider this to be the main criterion. So simplified an interpretation is, of course, incorrect. But analysis on the basis of the fluctuation theory clears the way for a scientific treatment of this question.

Proceeding from the fluctuation theory, we should point out that the precipitation of the σ phase from the α or Δ solution must take place much more readily than from the γ solution. Indeed, we can reckon from the data obtained from research [10] that the nickel concentration hardly changes during the α--σ transition (it decreases by half during the γ--σ reaction), whereas the chromium and particularly the molybdenum concentrations increase to a considerably lesser degree than during the γ--σ transition in the same alloy (see Fig. 5). We should add that diffusion in the α solution also takes place faster than in austenite. Therefore, both the probability and rate of formation of the necessary fluctuations increase considerably during

the α-σ reaction.

The result is a considerably faster precipitation of the σ phase from the α or Δ solution than from austenite. This fact has been frequently observed in experiments.

The question of variations in the degree of structural conformity between the lattices of the solid solution and the precipitating phase in alloying and transition from the γ--σ reaction to the α--σ reaction calls for special investigation.

Let us consider the question of the thermal mobility of the atoms in the lattice. As has been established by research [2], the rate of fluctuation formation, i.e., the number of fluctuation zones nuclei of a prescribed composition and size originating per unit volume of the alloy in unit time, is directly proportional to the diffusion coefficient. The rate of crystal growth has the same dependence on diffusion. It is well known that the diffusion coefficient varies substantially in the case of additional alloying. Let us try to determine the role of thermal mobility of the atoms in this problem. At the present stage of our knowledge, an accurate solution of this problem is hardly possible since it is very difficult strictly quantitatively to allow for the variations of mobility of the atoms of each element participating in the concentration variations of mobility of the atoms of each element participating in the concentration variations during the formation of the new phase, and there are no experimental data on record for the diffusion coefficient of each element for alloys having the composition in which we are interested. We therefore restrict ourselves to an approximate evaluation of the role of the diffusion factor, on the basis of available data published over the last few years [8, 11, 12]. An

analysis of these data shows that although the coefficients of diffusion of the atoms of various alloying elements in steel and the coefficient of self-diffusion of iron are considerably different, they are quantities of the same order. Thus, the diffusion coefficients of chromium and tungsten in iron at 750° are $0.5 \cdot 10^{-12}$ and $2 \cdot 10^{-12}$, respectively, and the coefficient of self-diffusion of iron is $2.8 \cdot 10^{-12}$ cm^2/sec; at 850°, the respective quantities are 19, 34, and $47 \cdot 10^{-12}$ cm^2/sec.. Consequently, the rates of diffusion of the separate metallic components of the steel differ by the factors of 2 to 5. It can also be shown that when the effective diffusion coefficient is determined, each of the components enters into the equation with its own statistical weight, which reduces the difference between them still more. Thus, in calculations with an accuracy of up to half an order, we may safely use the value of the effective diffusion coefficient, or the quantity D, for one of the metallic components (for example, for iron atoms), thus characterizing the thermal mobility of all the atoms of the given alloy.

The second assumption which should be adopted for an approximate calculation, in view of the absence of data for an alloy corresponding exactly to our composition, is that the additional alloying of two alloys of the same type with a given element produces in each the same change in diffusion. We find this to be roughly the case for the self-diffusion of iron when it is alloyed with chromium, if we compare the data for iron + chromium alloys with iron + nickel + chromium alloys. The diffusion coefficient of iron in austenitic nickel steel at 1000° decreases from $0.8 \cdot 10^{-11}$ if 3.5% Mo is added to the steel (i.e., by a factor of about 5 [12]).

This difference increases with the fall in temperatare. Let us use the dependence of diffusion on temperature that was established for these alloys [12], and let us calculate the value D_{Fe} at 723°, since we have no data from direct tests at this temperature. We then find that by the addition of 1.8% Mo the diffusion coefficient at 723° decreases by a factor of $1 \cdot 10^2$, and with the addition of 4.5% Mo, by a factor of $2.5 \cdot 10^3$. Thus, in our steel the addition of 3.5% Mo must reduce the rate of formation of phase nuclei through retarding diffusion by a factor of less than 10^3 and through decreasing the fluctuation probability by a factor of 10^4 to 10^9, depending on the size of the nucleus, as has been shown above.

We tried to determine the rate of precipitation of the σ phase, taking the diffusion rate into account and approximately calculating n_f (the number of fluctuation zones forming in 1 cm^3 of steel in 1 second) using the formula (3) quoted above. As we know, the rates of nucleation and growth of the crystallites of the precipitating phase depend on that quantity. It was found that the rate of formation of "σ fluctuations" sharply decreases: a) with an increase in the size of the σ phase nucleus; b) with an increase in complexity of its composition; and c) with the temperature decrease of the process.

Thus, for example, in steel containing 18% Cr and 8% Ni (without molybdenum) and at a temperature of about 700° C, taking the effective diffusion coefficient $D = 10^{-15}$ cm^2/sec, the " σ fluctuations" that are less than 1,000 adjoining points in size form at a tremendous rate; millions of nuclei form in 1 cm^3 per second when the size is 1000 points; this number becomes small only when the size increased to 1400. In steel of the same composition but additionally alloyed

with molybdenum, the rate of precipitation is much lower and the possible zones are considerably smaller. Thus, with 3.5% Mo (assuming $D_{eff} = 10^{-17}$ cm^2/sec) about 10^3 cm^3/sec " σ fluctuations" 500 atoms in size, are formed, while this number amounts to 10^{14} cm^3/sec in steel without molybdenum. Hardly any σ phase zones of more than 600 atoms originate in steel containing molybdenum (the rate falls below 1 nucleus per cm^3 per sec). Thus, the analysis we made shows that the additional alloying of a complex alloy with a new component may sharply reduce the rate of formation of nuclei new-phase as well as the rate of their growth, both as a result of the decrease in the probability of concentration fluctuations and of the decline in the thermal mobility of the atoms. The first factor, is however, considerably more influential and, in some instances (for example, with large nuclei) is even dominant. A similar calculation confirmed the validity of this conclusion also for the formation of carbides of various types.

This concept substantially differs from the widespread opinion that additional alloying retards phase transition mainly by increasing the bond strengths within the lattice and by reducing the thermal mobility of the atoms in it. Without denying this hypothesis, we must point out that the factor of probability of fluctuation of state has a still greater influence in this direction. At the same time we should remember that other important factors in alloying--changes in the difference between the free energies and the work of nucleus formation (i.e., between the surface tension and the size of the equilibrium nucleus) have not been calculable so far in the case of alloys of a complex composition.

Let us now analyze, on the basis of the fluctuation theory, the

process of precipitation of the strengthening phases in nonferrous heat-resistant alloys. Let us take as an example an alloy of the "nimonik" type, which has a nickel base, is strengthened with titanium and a small quantity of aluminum, and which, during aging, precipitates an α' phase of the type $Ni_3(Ti, Al)$ with a face-centered cubic lattice. Data on the chemical composition of this alloy and its precipitation phase are given in the work of G. V. Kurdyumov and N. T. Travina [13]. These data, converted into atomic percentages, are given in Table 3. Disregarding a small quantity of titanium carbide (less than 0.02% C in the alloy), we shall assume that after hardening we have a homogeneous solid solution. We see that for the formation of an α' phase nucleus, the number of titanium atoms in the given zone of the solid solution, which contains 100 adjoining points, has to increase from 3 in the initial solution to 16 in the fluctuation nucleus as a result of fluctuations in concentration (i.e., by a factor of more than 5. Furthermore, enrichment in aluminum is necessary at the same time (4 atoms instead of 1) although to a lesser degree. Finally, a simultaneous and, moreover greater impoverishment of chromium is essential in the given zone there were 23 chromium atoms, in the initial solution but only 2 showed remain in the nucleus.

Let us determine the probability for each of these conditions. We will make an approximate calculation using the Poisson equation, which in essence, does not take into account the interactions of the different atoms and the statistical correlation of displacements. However, as has been shown in the investigations made by B. N. Finkel'shteyn and B. Ya. Lyubov, taking this correlation into account only introduces a small correction in the result; this

correction usually does not exceed 10 to 20%, as compared to the method proposed by us [2] and makes the calculation much more complicated.

TABLE 3

	Elements			
	Cr	Ti	Al	Ni
Composition of alloy, wt. %	20.15	2.48	0.6	base
Composition of alloy, atom %	23.2	2.85	1.23	base
Composition of precipitating phase during aging (700° - 16 hours), wt. %	2.0	14.0	2.0	base
Atom %	2.14	16.25	4.1	base

As we see, two fluctuation processes have the lowest probability: the enrichment in titanium and the impoverishment of chromium. The latter was not normally taken into account, although it proved to be extremely essential and no less important in its role than the enrichment in titanium. In this connection, we must mention another important conclusion, which is significant in principle. In the study of these alloys we are primarily concerned with the role of the component which is fundamental in the formation of the new phase (titanium, for example). Calculation shows, that however, those components not directly contained in the new phase may play and important part and strongly influence the kinetics of precipitations and growth of crystals of the new phase, since the probability of their leaving the given zone is sometimes of the same order of magnitude as that of the fundamental new-phase components entering this zone. It is clearly this fact, not taken into account in the

theory, that partially explains the great influence of tungsten, molybdenum and other alloying additions that do not accumulate in the new phase (α') but greatly affect the kinetics of its precipitation and growth. The increase in heat-resistant properties of such complex alloys can also be partially explained by this calculations. The probability of nucleation of the new phase decreases particularly sharply since, as has been shown above, it is necessary for this purpose to have a simultaneous change in concentration of many components in the same zone of the solid solution.

Thus, the formation of a nucleus of the α' phase in a zone with 100 adjoining points has an effective probability P (α') equal to:

$$P(\alpha') = P(\mathrm{Cr})\,P(\mathrm{Ti})\,P(\mathrm{Al}) = 2{,}27\cdot10^{-8}\cdot1{,}65\cdot10^{-8}\cdot1{,}53\cdot10^{-2} = 6{,}84\cdot10^{-18}.$$

Application. According to the data obtained by R. B. Golubtsova and L. A. Mashkovich (DAN USSR, 106, 1956)* if this alloy ages for a long period at 800°, the α' phase contains more chromium (2.5 to 8% by weight), considerably more aluminum (3.6 to 14.6%) and as much titanium (11 to 14%). Therefore, P (Cr) will be greater, and P (Al) considerably less than the values calculated by us. However, the overall total quantities P (α') and N_f (α') do not change as sharply since they are a product of P (Cr) P (Al) P (Ti).

We may then calculate how large a number of fluctuation nuclei of the α' phase of various sizes N_f (α') can exist in a unit volume of the alloy

$$N_f(\alpha') = N_0 P(\alpha')(\mathrm{Cr} + \mathrm{Ti} + \mathrm{Al}).$$

N_o is the total number of zones of a given size of any composi-

* [Proceedings of the Academy of Sciences of the USSR].

tion and it can be determined since we know the lattice constant of the alloy in a hardened state from research [13], d_o = 3.562 A. Consequently, the number of elementary lattice cells in 1 cm^3 of alloy N_{cell} is

$$N = \frac{1}{(3{,}562 \cdot 10^{-8})^3} = 2{,}214 \cdot 10^{22} \text{ см}^3.$$

Taking into account that there are 4 atoms per cell in a face-centered cubic lattice, we find that the total number of zones 100 atoms in size in 1 cm^3 of alloy amounts to

$$N_0(100) = \frac{N_{яч}\,4}{100} = \frac{N_{яч}}{25} = \frac{2{,}214 \cdot 10^{22}}{25} = 8{,}86 \cdot 10^{20}/\text{см}^3.$$

Let us now calculate N_f (α')--the number of fluctuation nuclei of the α' phase, 100 atoms in size:

$$N_f(\alpha') = N_0(100)\,P(\alpha') = 8{,}86 \cdot 10^{20} \cdot 6{,}84 \cdot 10^{-18} = 606 \cdot 10^3/\text{см}^3.$$

Thus, the analysis shows that the fluctuation zones which in composition approximate the α' phase in a "nimonik" type of alloy are small in size. If we make similar calculations for zones of a different size, the results obtained can be expressed in the form of the diagram (Fig. 8). As this diagram shows, the maximum size of a phase nucleus able to originate spontaneously as a result of concentration fluctuation in an alloy of the "nimonik" type is very small, viz.: 120 atoms. But such zones do occur, even if they are very rare. Only smaller fluctuations are present in larger quantities. Thus, for example, there are 10^8 zones of 75 adjoining lattice points per cm^3 of alloys. This predetermines the necessity for higher supersaturation and supercooling of the solid solution for the precipitation of a crystal of the new phase, or the possibility of it forming only on a ready-made base or under some other favorable conditions.

The independent existence of a three-dimensional nucleus of a

very small size is hardly possible. In practise, one would therefore expect zones to form that do not attain the composition Ni_3 (Al, Ti) but are nearer to that of the initial solid solution and grow under conditions of a coherent bond with the fundamental lattice. In this case, the input of work for the formation of a separation boundary (surface energy) decreases considerably and even approaches zero, while the nucleus assumes a two-dimensional character.

Experimental data from an x-ray structural analysis confirms the theoretical conclusions given above. In particular, the formation of a cubic α' phase of the Ni_3Al type, as an intermediate phase even when there is a small quantity of aluminum in the alloy and the absence of direct precipitation of a hexagonal phase of the Ni_3Ti type during the early stages of aging are sufficiently covered by theory.

REFERENCES

1. MIRKIN, I. L. Problemy teoreticheskogo metallovedeniya (Problems of Theoretical Metallurgy), M., 1938.

2. MIRKIN, I. L. Struktura i svoystva metallov (Structure and Properties of Metals and Alloys), M., 1941.

3. MIRKIN, I. L. and SOLONOUTS, M. I. Change in Structure and Properties of Pipe Steels During Operation. Metallurgy and Metal Treatment, Metallovedeniye i obrabotka metallov, Nr. 2, 1957.

4. BOKSHTEYN, S. Z. Struktura i mekhanicheskiye svoystva legirovannoy stali (Structure and Mechanical Properties of Alloyed Steel), M. 1954.

5. ZENER, Metals Technology, 13, Nr. 1, 1946.

6. PINES, B. Ya. K voprosu o skorosti kristallizatsii (Concerning the Rate of Crystallization), ZhETF, Journ. of Exp. and Tech. Phys., 18, Nr. 29, 1948.

7. BLANTER, M. Ye. Fizicheskiye osnovy khimikotermicheskoy obrabotki (Physical Bases of Chemico-Thermal Treatment M., 1949.

8. GERTSRIKEN, S. D. and DEKHTYAR, I. Ya. Problemy metallovedeniye i fiziki metallov (Problem of Metallurgy and Metal Physics, Kiev, 1950.
9. MIRKIN, I. L. and BLANTER, M. Ye. Ravnovesnoye sostoyanie splavov zhelezo uglerod-khom (State of Equilibrium of Iron-Carbon-Chromium Alloys. "Metallurg" ("Metallurgist"), No. 8, 1940.

10. VACHER, BECHFOLD. S. Res. Nat. Bureah of Standards, 53, Nr. 2, 1954.

11. GRUZIN, P. L. a.o. Problems of Metallurgy and Physics of Metals, Coll. 4. Metallurgizdat, 1955.

12. BOKSHTEYN, a.o. (Diffusion in Iron-Nickel Alloys) Diffuziya v zhelezonikelevykh splavakh. Izv. AN SSSR, OTN. No. 12, 1955.

13. KURDYUMOV, G. V. and TRAVINA, N. T. Problemy metallovedeniya i fizhiki metallov, cb. 4. Metallurgizdat, 1955.

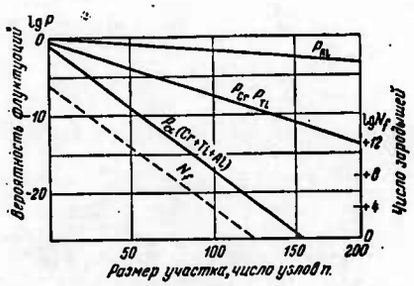

Fig. 8. Diagram of the formation of fluctuations with the formation of the α-phase in a nimonik-type nickel-base alloy.

CONCERNING THE RELATIONSHIP BETWEEN THERMODYNAMIC MAGNITUDES AND THE STRENGTH OF ALLOYS AT HIGH TEMPERATURES

M. P. Matveyeva, L. I. Ivanov, and L. N. Bystrov

Study of the behavior of alloys under stress at elevated temperatures had led to the necessity for studying the relationship between the strength of alloys and the strength of their interatomic bond. As we know, the energy of the interatomic bond is characterized by such physical factors as heat of sublimation, melting point, activation energy in diffusion and self-diffusion, etc. Furthermore, the values indicating the nature of the interaction between homogeneous and heterogeneous atoms in an alloy play a great part in the study of alloys.

In our opinion, the strength of the interatomic bond is characterized, first of all, by the heat of evaporation, although it should also be borne in mind that the heat of sublimation is a value which is structurally almost imperceptible and is averaged out for a certain volume of the material; as for the nature of the interaction of like and unlike atoms, the thermodynamic activity of the component is a very perceptible factor.

It should be mentioned that until now no sufficiently reliable methods have existed for measuring the partial values of thermodynamic factors for alloy components at elevated temperatures, particularly

in the solid state. The use of radioactive isotopes as indicators has not only made it possible to improve the old methods, but also to develop a series of methods which are new in principle and based on the study of isotopic exchange. As a consequence, thermodynamic data for a number of solid solutions of binary alloys have recently been published.

The aim of the present work was to obtain data characterizing the variation in the heat of sublimation of one of the components of a ternary alloy and to relate these data to the strength of alloys at high temperatures.

In our investigations we used the method of so-called unilateral isotopic exchange developed at the Institute of Metallurgy of the Academy of Sciences of the USSR, using the device shown in Fig. 1. In the working area of the device (a high-temperature vacuum furnace are simultaneously placed 10 pairs of samples (of like or unlike compositions) enclosed in small corundum ("korundiz") cups (7). Two test samples of the same chemical composition are placed in each cup: one is small and radioactive (9), and the other large and nonradioactive, serving as the target (8). The corundum cups, ground for close fitting, are set up in a column, placed in a special container made of sheet molybdenum, and put into a molybdenum heater. The heater and the electrodes supplying current are covered with a copper hood which has a small receptacle on one side for activated carbon. A sufficiently high vacuum ($1 \cdot 10^{-6}$ mm hg) is created in the system by pumps (types RVN-20 and TsVL-100) a trap cooled by liquid nitrogen and the activated carbon.

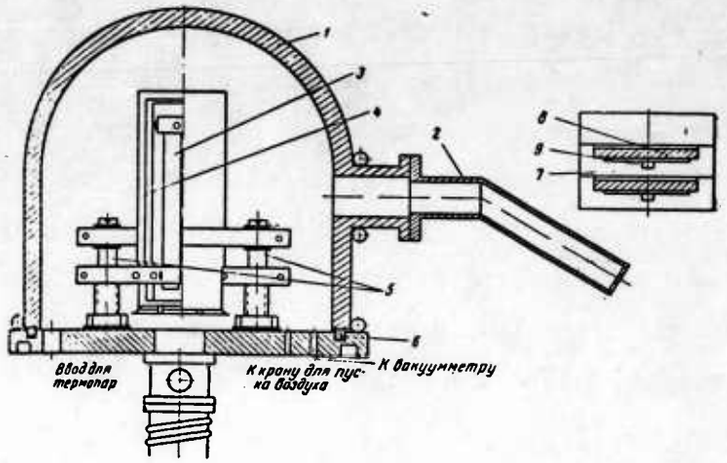

Fig. 1. Diagram of the device for isotopic exchange: 1) copper hood; 2) receptacle for activated carbon; 3) molybdenum heater; 4) shields; 5) electrodes; 6) rubber seal; 7) ceramic cup; 8) target; 9) sample containing radioactive isotope.

Next, the samples are heated to the prescribed temperature at which the soaking appropriate for the conditions of the test is to be carried out. The temperature is controlled by means of three platinum and platinumrhodium thermocouples with the aid of a PPTN-1 potentiometer. The accuracy of the temperature measurement is $\pm$ 1.5°. By successive annealing at the same temperature and by measuring each time the radioactivity of the sample that was not radioactive at the beginning of the test, we obtain data for calculating the rate of evaporation and vapor tension.

The samples are in the shape of disks 1 mm thick and 16 and 4 mm in diameter. The surface of the larger sample is made highly corrugated so that its area will be increased. The samples are made by

fusing alloys of the same chemical composition, the radioactive isotope being added to the smaller sample either directly during the melting or by irradiation with thermal neutrons.

For the investigation we selected alloys of the ternary system chromium-molybdenum-iron, which were in the plane of two cross-sections and had constant chromium contents of 55 and 65% (Fig. 2).

At a temperature of 1150°, the selected alloys are in the zone of the homogeneous solid solution α and in the two-phase zone α + σ. We should point out that at higher test temperatures the alloy containing 10% Mo and 55% Cr is on the very boundary of the zone α + σ.

Electrolytic chromium, electrolytic iron approximately 99.9% pure, and 99% pure molybdenum were used as starting materials. The alloys were made in high-frequency induction furnace in a helium atmosphere.

The radioactive isotope Cr^{51} was obtained from the stable isotope Cr^{50} by direct irradiation of the samples with thermal neutrons in an atomic reactor. At the same time it is possible to obtain simultaneously the radioactive isotopes Fe^{55} and Fe^{59} and several short-lived molybdenum isotopes, among which is Mo^{99}, which has a short half-life of 67 hours, along with the radioactive isotope Cr^{51}. The radioactive isotope Fe^{55} has only K-capture, which results in the emission of x-rays that do not register if glass or metal counter tubes (STS-6) are used.

Thirty or forty days after irradiation there is practically no radioactive molybdenum left in the alloys.

When the alloy iron content is high, the formation of the radioactive isotope Fe^{59} will be very small, in view of the fact that

the effective cross section for neutron capture by the stable isotope Cr^{50} is 30.5 times as large as the effective cross section for Fe^{58} capture, while the percentage of Cr^{50} in natural chromium is 13 times that of Fe^{58}.

The test were carried out at a temperature of 1150-1250°. Fig. 3 shows the variation in the heat of sublimation as a function of the molybdenum content in alloys containing 65% (1) and 55% (2) chromium. As is clear from Fig. 3, in alloys containing 65% chromium the heat of sublimation rises with the increase in molybdenum content. Alloys containing 55% chromium have a maximum heat sublimation when the molybdenum content is about 20%.

If it is assumed that the ionization energy of the chromium atoms depends only slightly on the iron and molybdenum concentration, then the increase in the heat of sublimation indicates that these alloys may have a tendency toward the formation of a stronger bond between the heterogeneous atoms of which they are composed.

Consequently, proceeding from the thermodynamic data, we may assume that alloys containing 65% Cr will be stronger if the molybdenum content is over 15%. Apparently there is a higher value in these alloys for the bond energy between the atoms of chromium, molybdenum and iron. Among the alloys containing 55% Cr, those lying in the formation zone of the σ phase will be the strongest. Since these are two-phase alloys, however, the views expressed earlier regarding binary solid solutions may not apply to them.

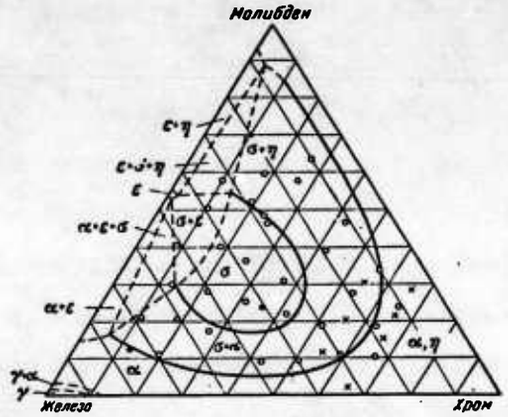

Fig. 2. Isothermal cross section of the system chromium-molybdenum-iron at 1100°.

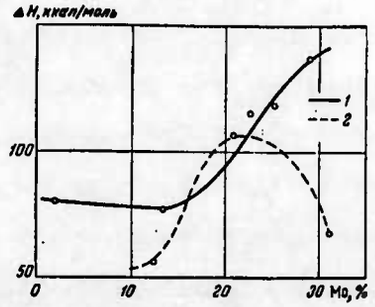

Fig. 3. Variation in heat of sublimation Δ H, depending on the iron and molybdenum content.

In order to verify this assumption, we determined the mechanical strength of the alloys at a temperature of 1150° by following two methods: With 65% Cr by the centrifugal-bending method.

With 55% Cr by a method of torsion in a vacuum at high tempera-

ture with the use of a special device.

The tests by the first method were carried out under a load of 0.5 kg/mm^2 for 20 hours. The results of these tests confirm the above assumption.

The higher heat-of-sublimation values correspond to the alloys with a lower bending deflection, and, as shown by analysis of the values of thermodynamic activity, this increase tends to be exponential.

As we have already stated, a special device (Fig. 4) was used for the mechanical testing of the alloy containing 55% Cr; the operating principle of this device involves twisting the sample under a torque that increases linearly with time.

The sample, which is cylindrical in shape and has a diameter of 4 mm and a length of 15mm with square tips, is inserted in molybdenum clamps and placed in a microfurnace made of sheet tantalum. One of the clamps (9) is fixed to the tip (4) which is free to move forward along guiding rails; the second clamp is connected to the tip (8), which has a free torsional movement. The sample is charged on the "hourglass" principle by means of fine lead powder pouring out through an orifice in the load bin (1) into the charge container (3), which is joined to a large pulley (14) by a flexible cable passing over a small pulley (13).

The torque-arm in the given case is 4 cm long, which ensures a maximum torque of M = 7 kg/cm, the weight of the powder being 1.7. The rate of charging P_o = 100g/min. The device permits a maximum torque angle of $\alpha = 225°$. The maximum tangential stress is $\tau_{max} = 1094$ kg/cm^2, and the maximum relative torque angle α_{max} =

= 150 deg/cm.

The microfurnace is connected by means of the current feeders (12) to the water-cooled copper electrodes, which are insulated and fixed to a steel plate. Power is supplied from the secondary winding of a 3kw, 220 v. step-down transformer. The heating is regulated by an auto-transformer, TNN-45 and the temperature is controlled by a platinum and platinum-rhodium alloy thermocouple fixed to the surface of the microfurnace heater. To reduce heat lossed due to radiation and to reduce heating of the glass hood, the microfurnace is protected by special shields.

Fig. 5 shows the relationship between the time required to attain a 10° angle of twist and the molybdenum and iron content in alloys containing 55% Cr. The results obtained confirm the assumption that alloys in which a σ phase forms have greater strength.

Thus the heat of sublimation and the thermodynamic activity of chromium have been experimentally determined in a number of alloys of an iron-chromium molybdenum system. The hypothesis has been put forward that the alloys most resistant at high temperature are those in which the heat of sublimation of chromium has a higher value while the value of thermodynamic activity is at a minimum, indicating a tendency toward the formation of preferential bonds between heterogeneous atoms.

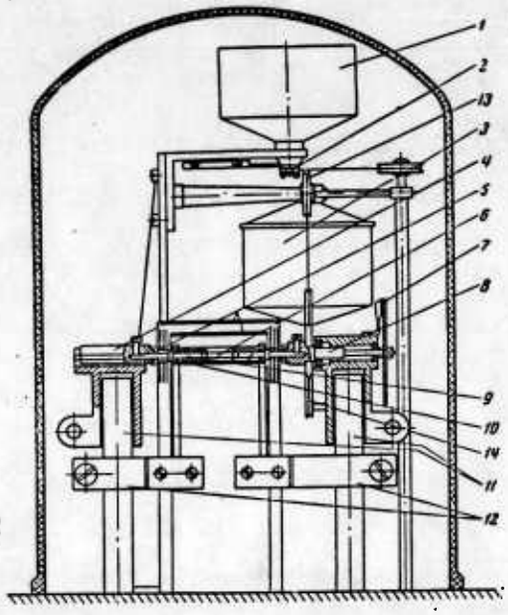

Fig. 4. Diagram of device for torsion testing of samples at high temperature in vacuum. 1) charge bin; 2) charge vent; 3) load container; 4) tip which is free to move forward; 5) shields; 6) sample; 7) dial; 8) tip with torsional freedom; 9) clamps; 10) heater; 11) electrodes; 12) current feeders; 13) small pulley; 14) large pulley.

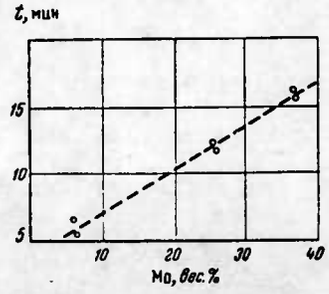

Fig. 5. Plotting of the time required to attain a torque angle of 10°.

DETERMINATION OF THE THERMODYNAMIC PARAMETERS OF CHROMIUM AND COBALT BY MEASUREMENT OF THE SATURATED VAPOR PRESSURE OF CHROMIUM

Ya. I. Gerasimov, A. M. Yevseyev, and G. V. Pozharskaya

Measurement of saturated vapor pressures is widely used to determine the thermodynamic functions of melts of liquid metals. For the study of the thermodynamics of alloys in the solid state this method, as well as the electromotive force method, is less frequently employed.

Nevertheless, the method of measuring saturated vapor pressure is convenient and may give reliable results with most metals if the evaporation is of single and not of associated atoms. When measuring the saturated vapor pressure over solid alloys, we must take into account the loss of volatile components from the surface layer of the alloy during the evaporation process. In order to reduce the influence of the phenomenon, which is apt to distort the results, we must use alloys with a well-developed surface; this excludes use of the Langmuir method, which is applicable in the case of liquid alloys [1].

The most accurate and convenient methods in dealing with low pressure vapors, which are a characteristic of most metals in solid form, are those of Langmuir and Knudsen. We chose Knudsen's method.

In the Knudsen method, the rate of evaporation depends on the saturated vapor pressure and the area of the effusion orifice. In order to create the saturated vapor in the Knudsen chamber, the surface of the evaporating substance has to be many times greater than the area of the effusion orifice. For this purpose the alloy we used in the Knudsen chamber was in the form of fine shavings.

Measurement of the saturated vapor pressure of chromium in chromium-cobalt alloys was effected with the device shown in Fig. 1. The effusion chamber (1) is a metallic cylinder into which a cup and an effusion diaphragm with an orifice are placed. It is fixed to a quartz tube in the center of the device. A platinum and platinum-rhodium alloy thermocouple (2), the junction of which is fixed to the bottom of the cup in the chamber, passes along the inside of the tube. A quartz cap (3) is placed over the chamber, and the chromium, after evaporation effected by the inductor code (4), precipitates onto the cap. When the evaporation is complete, the cap is weighed and the chromium removed with hot, concentrated acid. The quantity of chromium is determined from the difference in weight of the cap with and without the deposit, as well as by colorimetric analysis of the chromium solution. In the case of a cobalt-chromium system, the effusion chamber is made of tantalum.

The effusion chamber is heated by a high-frequency electromagnetic field. As a source of high-frequency energy for out tests, we used an MVP-1 apparatus made by the "Platinopribor" factory. The heating of the chamber was controlled by means of a photorelay; as a measuring device we used a platinum and platinum-rhodium thermocouple, the electromotive force of which was measured simultaneously by a PPTN-1 low-resistance potentiometer. During the

entire text, the temperature was kept constant to within 2°. Occasional deviations caused by voltage fluctuation in the circuit did not exceed 4°.

After determination of the quantity of chromium evaporating over a certain period of time, we calculated the saturated vapor pressure of chromium according to the equation

$$P = \frac{\Delta G}{S \tau K} \sqrt{\frac{2\pi RT}{M}}, \qquad (1)$$

Where P is the saturated vapor pressure;

ΔG is the quantity of evaporated substance in grams;

τ is the time of exposure in hours;

S is the area of the effusion orifice, in mm;

K is the Clausing* coefficient; and

M is the molecular weight.

The area of the effusion aperture varied within the limits of $4 \cdot 10^{-3}$ to $1 \cdot 10^{-3}$ cm^2, and the time of exposure τ from 2 to 6 hours; the thickness of the effusion diaphragm was 0.08mm. The measurements of the chromium vapor pressure in the cobalt-chromium system were made within the temperature range 1,227 to 1,297°. Six alloys were tested altogether. With alloys of the same composition, from 3 to 5 values for the chromium vapor were measured at various temperatures.

Electrolytic chromium with a purity of 99.7% by weight and

---

* Translator's note: The transliterated form of this name is "Klyauzing".

cobalt with a purity of 99.0% by weight were used in making the alloys.

The experimental results were processed according to the equation

$$\lg P = -\frac{A}{T} + B. \qquad (2)$$

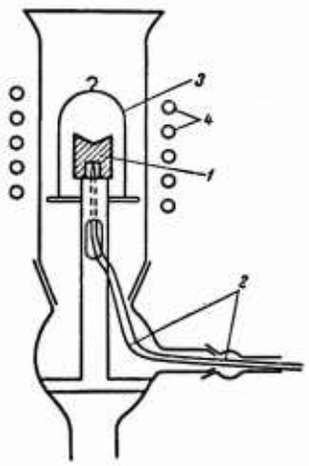

Fig. 1. Diagram of device for the measurement of the saturated vapor pressure of chromium in cobalt-chromium alloys.

The experimental data coincide closely with the lines log P- $\frac{1}{T}$ within the temperature range 1,227 to 1,297°. Discrepancies between the calculated and the experimental values of P did not exceed 5%. The cobalt vapor pressure within the given temperature range in alloys enriched with chromium is insignificant, i.e., of an order of $1 \cdot 10^{-5}$ mm Hg and the pressure of pure cobalt is of the order of

$1 \cdot 10^{-4}$ mm Hg.

The cobalt-chromium system (2) contains a compound Co_2Cr_3, based on which is a solid solution with a small range of homogeneity. At a temperature near 1297° this compound decomposes. We therefore restricted ourselves in calculating the thermodynamic functions to data for the range 1227 to 1277° in order to maintain uniformity in the results.

From Eq. (2) we calculated the saturated vapor pressure of chromium for alloys of various chromium concentrations at 1500, 1525 and 1550° K. The activity of chromium is determined by the ratio

$$a_i = \frac{P}{P_0},$$

where P_0 is the chromium vapor pressure in a pure state at a given temperature;

P is the chromium vapor pressure over the alloy at the same temperature.

Table 1 gives the experimental results of determining the activity of chromium and the rounded-off values of this activity. We have also calculated the values for the partial free energy of combination for chromium in cobalt-chromium alloys at T = 1525° K (Fig. 3), according to the formula

$$\Delta\mu_{Cr} = RT \ln a = RT \ln \frac{P}{P_0}. \qquad (3)$$

Fig. 2 gives experimental data which basically corresponds to the structural diagram of a cobalt-chromium system. The result of calculation of the partial molar heat of combination of chromium obtained from the equation

$$\overline{\Delta H}_{Cr} = -4{,}5756\, T_1 T_2 \frac{\lg a_2 - \lg a_1}{T_2 - T_1}, \qquad (4)$$

are given in Fig. 3. Here, the partial molar entropies of combination are calculated from the equation

$$-\frac{\Delta(\Delta\mu)}{\Delta T}\overline{\Delta S}_{Cr} = -4{,}5756\frac{T_2 \lg a_2 - T_1 \lg a_1}{T_2 - T_1}. \qquad (5)$$

To calculate the integral quantities we used the Duhem-Margules equation:

$$\Delta H_{см} = N_{Co}\int_0^{N_{Cr}} \overline{\Delta H}_{Cr} d\,\frac{N_{Cr}}{N_{Co}};$$

$$\Delta Z_{см} = N_{Co}\int_0^{N_{Cr}} \Delta\mu_{Cr} d\frac{N_{Cr}}{N_{Co}}.$$

TABLE 1

Сглаженные опытные данные для активностей хрома $a = \frac{P}{P_0}$

N_{Cr}	T равна (°K)			N_{Cr}	T равна (°K)		
	1500°	1525°	1550°		1500°	1525°	1550°
0,1000	0,1125	0,1060	0,0990	0,6000	0,3725	0,3800	0,3875
0,2000	0,2263	0,2135	0,2019	0,6052	0,3784	0,3885	0,3987
0,2741	0,3030	0,2907	0,2791	0,7000	0,4050	0,4150	0,4350
0,3000	0,3160	0,3075	0,2980	0,8000	0,4175	0,4325	0,4500
0,3541	0,3360	0,3216	0,3188	0,8835	0,4590	0,4810	0,5037
0,4000	0,3300	0,3250	0,3200	0,9000	0,7188	0,7379	0,7563
0,5000	0,3300	0,3250	0,3200	1,0000	1,0000	1,0000	1,0000
0,5610	0,3291	0,3260	0,3232				

By graphic integration we found the integral heat values and integral free energies of formation of cobalt-chromium alloys at a temperature of 1525°K. The results of these calculations are given in Fig. 4.

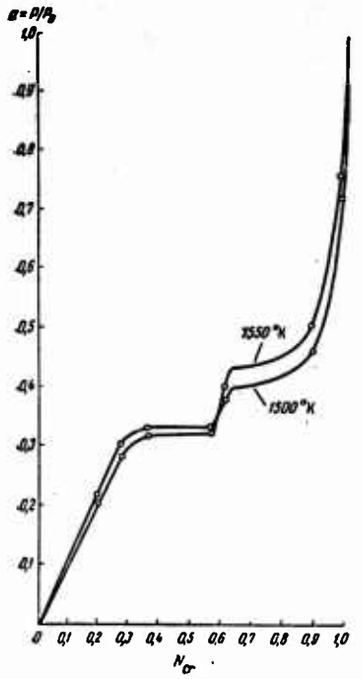

Fig. 2. Activity of chromium in a cobalt-chromium system.

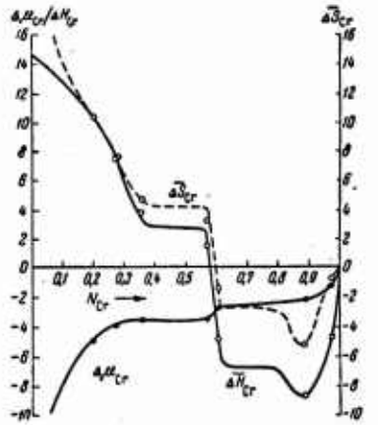

Fig. 3. Partial thermodynamic functions of chromium in a cobalt-chromium system.

The cobalt-chromium system in a solid state in the chromium-rich zone produces large negative deviations of activity from the Raoult Law, and small positive deviations in the cobalt-rich zone. In the zone of the solid solution based on Co_2Cr_3 (0.56 - 0.62 mole fractions of chromium) a sharp decline in activity takes place, and the partial heat of diffusion of chromium changes its sign from negative to positive. It is clear from the data on the integral heats of formation of cobalt-chromium alloys that the formation of Co_2Cr_3 is accompanied by heat absorption. The heat effect of the formation of the compound Co_2Cr_3 is equal to + 3,100 large cal.

The maximum loss of energy during the formation of cobalt-chromium alloys is sustained by alloys containing 0.85 to 0.95 mole fractions of chromium, i.e., by the zone of the solid solution of cobalt in chromium. This phase is marked by greater interatomic bond strength for Co-Cr, as can be concluded from the curves for the heat of formation of the alloys (see Fig. 4).

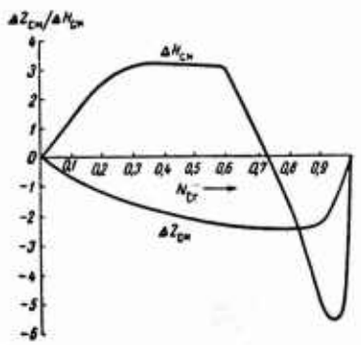

Fig. 4. Free energy and heat of alloy formation in a cobalt-chromium system.

REFERENCES

1. LYUBIMOV, A. P. and GRANOVSKAYA. Primeniye radioaktivnykh isotopov v metallurgii (Use of Radioactive Isotopes in Metallurgy), Coll. XXXV, Moscow, 1955.

2. KHANSEN, M. Struktury binarnykh splavov (Structures of Binary Alloys), Gostekhteorizdat (State Press for Technical and Theoretical Literature), Moscow Leningrad, 1941.

CONCERNING THE VALUES OF ACTIVATION ENERGY OF CERTAIN PROCESSES IN METALS

K. A.. Osipov

Research [1] shows that the values for the activation energy of self-diffusion in solid metals obtained from experimental measurement of the coefficients of self-diffusion conform to the relation

$$\Delta H = nq, \tag{1}$$

where n is the number of atoms in the activated group;

q is the activation energy for one atom in a group of n atoms in gram-atoms.

The magnitude q was obtained from the Gibbs free-energy values which the metal possesses at various temperatures, on the assumption that in an activated state a certain group of atoms may be compared to their state at the moment before melting or at the temperature of fusion, when the crystal lattice loses its thermodynamic stability and can pass into a liquid state. Calculated in gram-atoms, the magnitude q has the value

$$q = -T_S\left[\frac{H_{T_S} - H_{298}}{T_S - 298}(6{,}7 - \ln T_S) - S_{298}\right], \tag{2}$$

Where T_S is the temperature of fusion, °K;

H_{TS} is the heat content (per gram-atom) of the solid metal at the melting point;

H_{298} is the heat content (per gram-atom) at the standard temperature of 298.16°K; and

S_{298} is the entropy (per gram-atom) at standard temperature.

The analysis of some experimental data, given below, prompts the author to make the assumption that activation-energy values for the most diverse phenomena involving the displacement of atoms and vacancies in solid metals (diffusion, recovery and recrystallization, plastic deformation and failure, shear planes, and displacement of dislocations), may be expressed by Eq. (1). The activated state of each of these phenomena is essentially the same; it corresponds to the state where the crystal lattice loses its thermodynamic stability and is able to pass into a liquid state in local structures; the magnitude changes little in the same metal and represents a kind of connecting link as it were between the most diverse phenomena, showing that the activation in them is essentially the same. The wide range of activation energy values obtained from experimental measurements of the rates of various phenomena is caused mainly by a difference in the values of the quantity n, i.e., a difference in the size of the activated groups of atoms, and the quantity n may vary from 1 to considerably higher values, depending on the phenomenon under investigation and the conditions under which it occurs. In Eq. (1), the quantity n is the most sensitive to changes in external conditions.

Given this approach to the varied phenomena occurring in metals,

there is no need to consider whether the question there has anything in common in the mechanism of these phenomena, for example in self-diffusion and high-temperature creep, or self-diffusion and displacement of dislocations, etc. Instead, our efforts should be directed toward clarification of the conditions leading to a change in the relation (1), more specifically to a change in the number n since the specific features of a particular phenomenon depend on it.

To substantiate our assumption, let us examine some theoretical aspects and the experimental data.

According to calculation, the quantity q is a constituent part of the difference $\Delta G_T^{T_S}$ in the Gibbs free-energy factor, for pressure at a constant temperature, i.e., the quantity $\left(\frac{\partial G}{\partial P}\right)_T$, calculated per gram-atom, is equal to the volume of the latter and consequently is a rather small quantity in typical metals, we may disregard the variation of the Gibbs free energy factor and hence that of the quantity q with the variation within rather large limits of the pressure.

It is difficult to solve the problem of the dependence of q on the magnitude of uniaxial tensile or compressive stresses applied to the specimen or on the degree of its plastic deformation, since we do not know of any theoretical investigations into the variability of the Gibbs free-energy factor with the above-mentioned factors. It may be considered, however, that the quantity q will not be subject to substantial changes in these cases either since the structures of the local break-up of the crystal lattice caused by the applied stresses and various degrees of plastic deformation will be surrounded by an elastic medium, interaction with which will subject them to hydrostatic pressure.

For the time being, therefore, until a more thorough analysis is made, we will consider the quantity q as approximate to the boundary values of the activation energy of diverse processes connected with the displacement of atoms and vacant sites; we assume that it should not vary substantially in the case of wide variation in the state of the crystal lattice in its local structures.

The proximity of the quantity q to the boundary value of the activation energy and its low sensitivity to changes in the state of the lattice are confirmed by a series of experimental data. In particular, it can be stated that even in a liquid state near the melting point the activation energy of self-diffusion has a value which is very close to the quantity q. For example, in the case of sodium the quantity q calculated according to Eq. (2) amounts to 2,545 cal/g-atom, while the activation energy of self-diffusion in liquid sodium near the melting point is equal to 2,580 cal/g-atom (2). On the basis of experimental measurement of the viscosity in the liquid state (3) the value of the activation heat of the self-diffusion of liquid aluminum can be estimated at approximately 6,100 cal/g-atom; this value is near the value of q = 7186 cal/g-atom, calculated for aluminum according to Eq. (2).

Let us also mention the very interesting fact that the values of q calculated from Eq. (2) agree closely with those of the activation energy of the process of low-temperature recovery of electrical conductivity, which was studied in a number of pure metals when subjected to various actions, such as irradiation with deuterons, mechanical cold-hardening at low temperatures, and rapid cooling from high to low temperatures. Thus in copper (~ 99.99%), after irradiation at a temperature of 180° with deuterons having an energy

of 12 mev (4), after mechanical cold hardening at the temperature of liquid helium (5), and also after hardening from high to low temperatures (6) and (7), the process of return of electrical conductivity at temperatures of 30° and higher takes place with an activation energy of approximately 15,688 cal/g-atom. A similar value for the activation energy of return was obtained for silver irradiated with deuterons (8). This value coincides for all practical purposes with the value q = 15.415 cal/g-atom for copper and q = 15.933 cal/g-atom for silver, obtained by us from Eq. (2). In aluminum (99.995%), rapidly cooled from a temperature of 504°, the process of return of electrical conductivity (9) takes place with an activation energy equal to 6921 cal/g-atom, which is near the value q = 7186 cal/g-atom.

The theory of dislocation claims that a displacement of substance is necessary for the movement of the dislocation in a plane perpendicular to the slip plane. It is assumed that this is effected by a diffusion of vacancies or dislocated atoms near the nucleus of the dislocation. The publication [10] contains a calculation of the activation energy necessary for this displacement of dislocations, and in the case of aluminum, values of 7,844 to 9228 cal/g-atom were obtained for various directions in the lattice, which are close to the value q = 7186 cal/g-atom obtained by us.

Shepard and Dorn [11] studied experimentally the process of generation and expansion of the slip bands in aluminum containing 1.89% in its solution magnesium. Creep testing under stress below the yield point was carried out at temperatures of 78 and 114°K. The authors came to the conclusion that the generation and expansion of slip bands are related to the de-blocking of the dislocations

retained by the salute atoms. They considered that the basis of this process of deblocking of the dislocations as well as the process of origination and expansion of the slip bands, is, some kind of heat process with an experimentally determined activation energy equal to 6000 to 6800 cal/g-atom. This value also differs little from that of q calculated for aluminum. It is possible that the agreement also would be close even if magnesium were absent in the aluminum solution.

The above-mentioned data re in accord with our assumption that the quantity q may be considered to be approximate to the boundary value of the activation energy of various phenomena.

By taking the quantity q for the minimum initial value of activation energy corresponding to one activated atom, and using the relation (1), it becomes possible to obtain wide variety of values for activation energy in the experimental study of the most diverse phenomena.

In the case of self-diffusion in metals with a face-centered cubic lattice, we have the relation $\Delta H = 3q$. From this relation, we derive for aluminum $\Delta H = 3 \cdot 7186 = 21{,}558$ cal/g-atom. This theoretical value of the activation energy of self-diffusion in aluminum agrees closely with the value ($21{,}000 \pm 2000$ cal/g-atom) which was obtained from measurements at temperatures of 15 to 440° by means of the magnetic resonance method (12). We do not beleive that this agreement is accidental; it rather convinces us rather that the activation energy of self-diffusion in solid aluminum is in effect near the value of 21,588 cal/g-atom calculated by us, as apposed to the value 33 to 36 kcal/g-atom, generally accepted for aluminum.

In the case of creep, the activation energy depends on the magnitude of the stresses applied to the sample, as becomes apparent when the stresses are varied within wide limits. In this connection, the form of the dependence and the initial and final values of the activation energy are of interest to the theory. The available experimental data and the theoretical investigations so far carried out do not enable us to formulate definite answers to all these questions.

As regards to the initial values of the activation energy of creep, which are generally accepted as zero values of the applied stresses and are obtained by extrapolation, most of the researchers claim that for pure metals these values are near the values of the activation energy of self-diffusion or even coincide with them. This gave rise to the belief in the similarity or even identity of the mechanisms of creep and self-diffusion. S. N. Zhurkov and others [13], however have obtained for a series of metals (Zn, Al, Ni, Pt) initial values for the activation energy of creep which are considerably higher and closer to the values of the heat of sublimation.

In spite of the contradictary nature of these experimental data, they can be reconciled by our own idea of the applicability of the relation (1) to the most diverse phenomena. With pure aluminum, for example, various authors have obtained the following initial values for the activation energy of creep: 14.1 [14]; 27.6 [15]; 32.2 [16]; 36.0 kcal/g-atom [17]. S. N. Zhurkov obtained a value of 53.0 kcal/g-atom. The discrepancy in these results may be caused by the fact that the degree of purity of the aluminum and the experimental conditions differred with various researchers. In spite of this, they can all be expressed by the relation (1) with differing

values for n, but with close values to that of q.

As regards to the form of the functional dependence of the activation energy of high-temperature creep on the tensile stresses applied to the test piece, it has been impossible so far to come to any definite conclusion on the basis of available experimental data. Many experiments carried out with a number of pure metals have shown that the activation energy of creep decreases with an increase in the applied stresses. But for molybdenum the dependence was found to be completely the inverse [18]. Thus, for molybdenum (99.95% pure) melted in the electric arc, the values of the activation energy of creep studied at temperatures of 870 to 1095° and at constant effective stresses varying between 10.5 and 21 kg/mm^2, increase in direct proportion to the applied stress. The initial value of the activation energy of creep, obtained by extrapolation with respect to the zero stress applied, amounts to 73 kcal/g-atom and is considerably lower than the activation energy of self-diffusion of molybdenum (104-120 kcal/g-atom; under a stress of 10.5 and 21 kg/mm^2, the activation energy of creep obtained is equal to 78 and 89 kcal/g-atom, respectively.

It is difficult at present to explain this peculiarity in the functional dependence on stress of the activation energy of creep in the case of molybdenum. Possibly this is a case of aging as a result of precipitation under stress of small quantities of admixtures dissolved in the molybdenum. It is not out of the question, however, that a similar law will also be established for other high-melting metals as well, or that it has basic significance; the cause may be the influence of strain-hardening in metals with high elastic constants. We may then conclude that as an effect of the stresses

applied the quantity n in Eq. (1) can both increase and decrease, depending entirely on the state of the material and the conditions under which it deforms. An increase in the number n will indicate that with an increase in stress and consequently in the deformation rate ever larger units are drawn into the process of simultaneous activation and that the primary activation extends to ever larger elementary structures.

S. N. Zhukov et al. obtained for a number of metals (Zn, Al, Ni, Pt) and alloys the following empirical dependence of the activation energy of creep (and of failure) ΔH on the applied stresses σ:

$$\sigma: \Delta H = \Delta H_0 - \gamma\sigma$$

Where ΔH_0 is the initial value of the activation energy; and

γ is a constant coefficient [13].

It results from this function that the activation energy of creep (and of failure) decreases in direct proportion to the applied stress and at higher stress values may equal zero.

Let us point out, however, that the dependence of the activation energy of creep on the applied stresses, as indicated by S. N. Zhurkov et al. was not observed in the experiments carried out by Carreker [19], although he made a very careful investigation of creep in platinum under a wide variety of conditions. Carreker made tests with annealed platinum wire (diameter 0.38 mm; purity 99.98%) in the temperature range 78 to 1550°K. Elongation was effected under a constant tension of 0.63 to 28 kg/mm^2 and a deformation rate of 10^{-1} to 10^{-6} min^{-1}; the degree of deformation amounted to from 0.001-0.1. At temperatures of 300 to 1200 °K the elongation was done in an atmosphere of purified dry nitrogen and above 1200°K, in air.

Fig. 1 shows Carreker's data for the dependence of the activation energy of creep in platinum on the degree of deformation (0.005 to 0.03) and on the magnitude of the stresses applied (0.7 to 7.0 kg/mm^2) at temperatures of 450 to 1550°K. It is seen from this graph that the initial value of the activation energy of creep may be taken as equal to 68 - 78 kcal/g-atom, which is considerably lower than that of the sublimation energy of platinum (~ 127 kcal/g-atom); there is no linear dependence on stresses. With an increase in the stress the dependence of the activation energy on the deformation and stress decreases and tends to become a boundary value. With a deformation of 0.1 to 0.03, at which we were able to determine the activation energy with the greatest accuracy, and under a stress of 7 kg/mm^2, the value of the activation energy amounts to 25.9 to 28.6 kcal/g-atom and is apparently already very close to the boundary value. Let us point out that with platinum the quantity q which we calculated from Eq. (2) amounted to 34 kcal/g-atom, which is but little different from the value of the activation energy of creep (25.9 to 28.6 kcal/g-atom. This small discrepancy may indicate that the quantity q is a slightly decreasing function of the elongation stresses.

The investigation of creep in pure aluminum (99.996%) in experiments made by Sherby, Lytton, and Dorn [20] with cyclic variations in temperature during the process, is of great interest. Studying creep in aluminum in the temperature range 77 to 880°K and at constant tensile stress values (0.3 to 15.33 kg/mm^2), the researchers established the following very important facts:

The dependence on time of creep deformation remains the same at very low temperatures (77°K) as well as at high temperatures;

The activation energy of creep is a complex function of temperature.

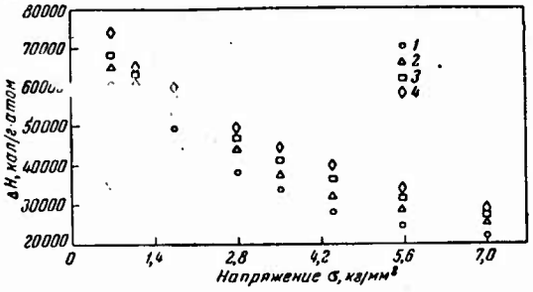

Fig. 1. Activation energy for plastic flow of platinum (99.98%) as a function of stress at various degress of deformation: 1) 0.005; 2) 0.010; 3) 0.020 4) 0.030.

Fig. 2 shows diegramatically the dependence of the activation energy of creep in aluminum on the test temperature according to data obtained by the authors in [20].

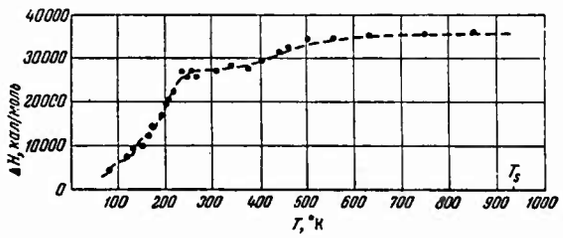

Fig. 2. Activation energy of creep in pure aluminum (99.996%) as a function of the absolute temperature.

The graph given in Fig. 1 shows two regions corresponding to temperature ranges of 880 - 500°K and 357 - 250°K with constant activation energy values wqual to 35,500 and 27,500 cal/g-atom respectively; at other temperatures, the activation energy has

varying values.

In accordance with the established temperature-dependence of the activation energy of creep in aluminum, the authors of [20] came to the conclusion that in the various temperature ranges creep may be due to different mechanisms, each having its own activation energy value.

According to the idea we are elaborating, the experimental data shown in Fig. 2 may be interpreted in a different way than that in [20].

The fact that dependence on time of creep deformation does not vary qualitatively with the temperature suggests that the process of activation of the elementary act of creep is in essence qualitatively the same at all temperatures. Its essence, as pointed out above, is loss of thermodynamic stability by the lattice in local structures. Accordingly, the entire graph in Fig. 2 may be described by the same relation [1], in which the quantity n is a decreasing function of the temperature, and the quantity q a slightly varying quantity near the limit value of activation energy.

Let us note that when applied to the data shown in Fig. 2 the relation (1) gives us the following values for the quantity ΔH: for the plateau of the graph in the temperature range 880 - 500°K, $n = \frac{35\,500}{q} \sim 5$; and for that in the temperature range 375 - 250°K, $n = \frac{27\,500}{q} \sim 4$. These values which proximate whole numbers for the value n may indicate that the same mechanism of creep operates in the given temperature ranges, but with different number of the activated units. In other temperature ranges, the values of n are not whole numbers but fractions, which may be due to the microscopic inhomogeneity, of the process of creep.

We believe that if it were possible to establish the activation energy of creep in small local structures with a homogeneous energy state n in the relation (1) would always be a whole number.

In our opinion, the low-temperature sections of the graph in Fig. 2 can be brought up to the plateu with a constant value for the activation energy of creep, close to the quantity q for aluminum.

REFERENCES

1. OSIPOV, K. A. (Fusion and Self-diffusion in Solid Metals) These lectures held at the 11th scientific and technical session on heat-resistant, thermally stable and metallo-ceramic materials. Plavleniye i samodiffuziya v tverdykh metallakh Tezisy dokladov na XI nauchno-tekhnicheskoy sessii po zharoprochnym, teploustoychivym i metallokeramicheskim materialam. Pub. by Acad. Sci. USSR, Moscow, 1957, Bull. Acad. Sci., Dept of Tech. Sci. Nr. 7. 1957.

2. NACHTRIEB, N. H. and HANDLER, G. S. Handler, Acta Metallurg, 2, Nr. 6, 1954.

3. YAO, T. P. and KONDIC, V. J. Inst. of Metals, 81, p. 1, September, 1953.

4. OVERHAUSER, A. W. Phys. Rev., 90, Nr. 3, Second Ser., May 1953.

5. EGGLESTON, J. Appl Phys., 23, 1952.

6. KAUFFMAN, J. W. and KOEHLER, J. S. Phys. Rev., 88, 1952.

7. MANINTVELD, J. A. Nature, 169, 1952.

8. COTTRELL, A. H. Effects of Neutron Irradiation on Metals and Alloys, Metall. Rev, Published by the Institute of Metals, Vol. I, P. 4, 1956.

9. PANSERI,; GATTO, F.; and FEDERIGHI, T. Acta Metallurg., 5, Nr. 1, 1957.

10. SEEGER, A. Report of the Conference of Defects in Crystalline Solids, Published by the Physical Soc., London, 1955.

11. SHEPARD, L. A. and DORN, J. E. J. of Metals, Sec. 2, Vol. 8, Nr. 10, 1956.

12. SEYMOUR, E. F. W. Proc. Phys. Soc. A 66, London, 1953.

13. ZHURKOV, S. N. and SANFIROVA, G. P. Svyaz' mezhud prochnost'yu i polzuchest'yu metallov i splavov. Tezisy dokladov na XI nauchno-tekhnicheskoy sessii po zharoprochnum, teploustoychivym splavam i metallokeramicheskim materialam (Connection Between the Strength and Creep of Metals and Alloys. These of lectures given at the 11th scientific and technical session on corrosion and heat-resistant alloys metallo-ceramic materials. Publ. Acad. of Sci. USSR, Moscow, 1957.

14. DUSHMAN, S.; DUNBAR, L. W.; and HUTHSTEINER, H. J. Appl. Phys., 15, Nr. 2, 1944.

15. UNDERWOOD, E. E. and MARSH, L. L. J. Metals, Sec 2, Vol. 8 Nr. 5, 1956.

16. HUANG, H. J.; SHERBY, O. D.; and DORN, J. E. J. Metals, Sec 2, Vol. 8 Nr. 10, 1956.

17. WEERTMAN, J. J. Mechanics and Physics of Solids, 4, Nr. 4, 1956,

18. PUGH, J. W. Trans. Am. Soc. for Metals, 47, 1955.

19. CARREKER, R. P. J. Appl. Phys., 21, Nr. 12, 1950.

20. SHERBY, O. D.; LYTTON, J. L.; and DORN, J. E. Acta Metallurg 5, Nr. 4, 1957.

A STUDY OF DIFFUSION IN AN IRON-ALUMINUM SYSTEM WITHIN A WIDE RANGE OF CONCENTRATIONS

S. D. Gertsriken, I. Ya. Dekhtyar, N. P. Plotnikov,
L. F. Slastnikova, and T. K. Yatsenko

A study of the processes of diffusion in alloys based on elements of the iron group is of scientific and practical interest. As a result of the complex interaction of the d and S electron in the formation of alloys based on these elements the nature of the atomic interaction changes substantially. The sum total of the characteristics of alloys obtained by various methods enables us to visualize more specifically the nature of atomic interaction and its variation over a wide range of concentrations.

The aim of this work is to define the connection between the diffusion parameters and the magnitudes characterizing the interatomic bonds.

Preparation of Alloys and Specimens

Alloys of concentrations varying from 3.47 to 52.2 atom % Al were prepared for the study of diffusion in an iron-aluminum system. All the alloys were melted in a high-frequency vacuum furnace with an Armco iron base containing 0.07% C (by weight) and pure Al. The composition of the alloys according to the data furnished by chemical

analysis is given in Table 1.

TABLE 1

	№ сплава								
	1	2	3	4	5	6	7	8	9
Al, ат.%	3,47	7,95	13,5	20,6	23,6	35,5	42,0	47,3	52,2
Al, вес.%	1,75	4,1	7,2	11,2	13,2	21,0	26,0	30,0	34,5

Within the range between room temperature and 1200° are a one-phase solid solution with an α lattice. The alloys were homogenized in quartz ampules for 50 hours at 1150-1200°. Alloys with a lower aluminum content (up to 20 atom percent) were forged into rods and cut into specimens. The alloys with high aluminum content did not forge well because they were found to be brittle. Therefore the specimens were cut directly from the ingots.

Method Used in the Experiment

The radioactive isotopes Co^{60} and Fe^{59} were used to determine the diffusion coefficients of cobalt and iron. The values of the diffusion coefficients were found by the method of removing layers and measuring the integral activity [1], and were calculated from the equation

$$D = \frac{1}{4 \cdot t \lg \alpha}. \qquad (1)$$

As is known, an essentail requirement for the applicability of this method is the plating of the specimen, with a thin, radioactive

layer of the metal whose diffusion is being studied. The thickness of the plating must be considerably less than the depth of penetration of the diffusing element. In the given instance, all these requirements were met; the thickness of the plating was 0.5 - 1 micron, and the depth of diffusion 200 - 700 microns.

A radioactive layer of cobalt was applied electrolytically to one of the flat surfaces of the specimen (approximately 1 cm^2); the plating was effected in a tank containing a solution of cobalt chloride in water, with a current density of ~ 0.6 amp/cm^2.

Diffusion annealing of the specimens was done in an atomsphere of argon. The test pieces were powdered with aluminum oxide to prevent sintering and were placed in a porcelain boat to avoid any possible effect of differences in temperature within the furnace. During the annealing of the boat the test pieces used for the study of the diffusion coefficient of cobalt, were made into a compact pile and wrapped in nickel foil. The temperature was measured by a platinum and platinumrhodium thermocouple and controlled and registered by an EPD-17 recording instrument to within $\pm$ 2°.

After diffusion annealing for a certain time at a given temperature, the distribution of activity in depth was measured with a B-2 unit, using a γ counter. The layers were removed with abrasive paper and the thickness of each layer was found by weighing it on micro-analytical scales ($\Delta h = \frac{h_o}{P_o} \Delta P$). The coefficients were usually found by averaging two values. Errors in calculating the diffusion coefficient sometimes reached 50%.

The x-ray method was also used for the study of mutual diffusion in the under reference. A layer of nonradioactive iron with about 5 microns thick was applied electrolytically to the surface of the

plane-parallel test piece. The iron plating, subsequent diffusion annealing, and removal of the layers were effected in the same manner as in the study of diffusion, using radioactive isotopes. The distribution of concentration in the diffusion layer was determined from variation in the lattice parameter of the alloy. According to data published in scientific literature [2], and on the basis of our own measurements, a linear dependence of the lattice parameters on the concentration of aluminum is only observed is solutions ranging upwards of 20 atom percent of the latter.

The exposure was made with chromium radiation in RKD-17 chambers, using a variation of the assumetrical method for precision measurement of the lattice parameter. Here, the flat test piece is fastened by the Preston method, and the exposure is made asymmetrically, which makes it possible to determine the effective radius of the chamber from the picture. Calculation was made from the line (211).

Results of the Experiments

Study of the Diffusion of Iron in Iron-Aluminum Alloys. The diffusion of iron was investigated in alloys containing 1.7, 4, 7, 13, and 34.5% Al by weight. The results of the measurements of the diffusion coefficients are given in Table 2. It follows from these results that the diffusion coefficients of iron in an iron-aluminum system, increase gradually with the concentration of aluminum.

Fig. 1 shows the temperature dependence of the diffusion coefficients.

In many instances, the low-temperature point (900°) does not come on the straight line connecting the high-temperature points. Possibly the influence of the grain boundaries begins to show at

this temperature.

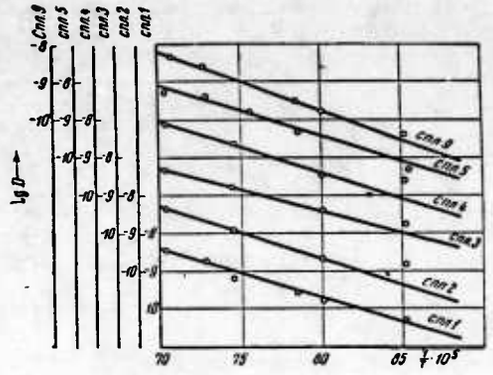

Fig. 1. Temperature-dependence of the diffusion coefficient of iron in an iron-aluminum alloy.

From the data on temperature dependence given above we obtain the following results for the activation energy and the pre-exponential multipliers D_o in the diffusion of iron in an iron-aluminum alloy (see Table 3).

Investigation of the Diffusion of Cobalt in Iron-Aluminum Alloys. The diffusion coefficients of cobalt in iron-aluminum alloys were calculated for Al content by weight of 1.7; 4; 7; 11; 13; 21; 26; 30; 34.5%. The resulting figures are quoted in Table 4. No apparent dependence of the diffusion coefficient on concentration was found.

Fig. 2 shows the temperature dependence of the diffusion coefficients of cobalt. The data obtained on the activation energy and the pre-exponential terms are given in Table 5.

The figures quoted in Table 5 indicate that the activation energy of diffusion of cobalt rises with an increase in the aluminum concentration, particularly in the zone of high concentrations.

TABLE 2

Value of the Diffusion Coefficients of Iron at Various Temperatures (in cm^2/sec)

Al, вес.%	Al, ат.%	Температура, °C			Температура, °C			
		1150	1100	1070	1050	1000	975	900
1,75	3,47	$2,8 \cdot 10^{-9}$	$18 \cdot 10^{-9}$	$0,6 \cdot 10^{-9}$	—	$2,5 \cdot 10^{-10}$	$1,5 \cdot 10^{-10}$	$4,8 \cdot 10^{-11}$
4,2	7,95	$4,3 \cdot 10^{-9}$	—	$1,2 \cdot 10^{-9}$	—	—	$2 \cdot 10^{-10}$	$1,6 \cdot 10^{-10}$
7,1	13,5	$4,4 \cdot 10^{-9}$	—	$1,6 \cdot 10^{-9}$	—	—	$3,6 \cdot 10^{-10}$	$1,6 \cdot 10^{-10}$
11,1	20,6	$7,3 \cdot 10^{-9}$	—	$2,4 \cdot 10^{-9}$	$1,5 \cdot 10^{-9}$	—	$3,5 \cdot 10^{-10}$	$2,4 \cdot 10^{-10}$
13,2	23,6	$5 \cdot 10^{-9}$	$4 \cdot 10^{-9}$	—	—	$4,8 \cdot 10^{-10}$	—	$5 \cdot 10^{-11}$
34,5	52,2	$4,2 \cdot 10^{-9}$	$2,4 \cdot 10^{-9}$	—	—	$3 \cdot 10^{-10}$	$1,6 \cdot 10^{-10}$	$4,5 \cdot 10^{-11}$

TABLE 3

Value of Q and D_o for Iron Diffusion

Al, ат.%	Al, вес.%	Q, ккал/г·атом	D_o, см²/сек
3,47	1,75	59,0	3,2
7,95	4,1	60,0	4,5
13,2	7,2	52,0	0,4
20,6	11,2	63,0	32,0
23,6	13,2	62,5	27,0
52,2	34,5	66,0	60,0

TABLE 4

Value of Diffusion Coefficients of Cobalt at Various Temperatures (in cm^2/sec)

Al, вес.%	Al, ат.%	Температура, °С					
		1150	1100	1050	1000	975	900
1,7	3,47	$6,7\cdot10^{-10}$	$3,7\cdot10^{-10}$	$1,7\cdot10^{-10}$	—	$5,5\cdot10^{-11}$	—
4,2	7,95	$6,4\cdot10^{-9}$	$2,8\cdot10^{-9}$	—	—	$2,7\cdot10^{-10}$	$1,3\cdot10^{-10}$
7,2	13,5	$6,7\cdot10^{-9}$	$4,0\cdot10^{-9}$	—	$4,0\cdot10^{-10}$	$4,6\cdot10^{-10}$	—
11,2	20,6	—	$8,6\cdot10^{-9}$	$4,6\cdot10^{-9}$	$1,7\cdot10^{-9}$	$8,5\cdot10^{-10}$	$1,7\cdot10^{-10}$
13,2	23,6	$1,8\cdot10^{-10}$	$9,5\cdot10^{-9}$	$4,10\cdot10^{-9}$	$1,6\cdot10^{-9}$	—	$3,7\cdot10^{-10}$
21,0	35,5	$1,1\cdot10^{-8}$	$5,6\cdot10^{-9}$	$1,8\cdot10^{-9}$	$6,8\cdot10^{-10}$	—	$1,9\cdot10^{-10}$
26,0	42,0	$7,7\cdot10^{-9}$	—	$1,1\cdot19^{-9}$	$3,5\cdot10^{-10}$	$2,5\cdot10^{-10}$	$1,4\cdot10^{-10}$
30,1	47,3	$7,4\cdot10^{-9}$	$2,4\cdot10^{-9}$	—	—	$1,5\cdot10^{-10}$	$1,8\cdot10^{-11}$
34,5	52,2	$1,1\cdot10^{-8}$	$3,2\cdot10^{-9}$	$1,2\cdot10^{-10}$	$6,0\cdot10^{-10}$	—	$4,8\cdot10^{-11}$

D_o increases continuously with an increase in the percentage content of aluminum and is considerably greater than one.

Investigation of Mutual Diffusion in Iron-aluminum Alloys. To determine the distribution in depth of the aluminum concentration in the specimen, a calibrating curve of the dependence of the lattice parameter on the aluminum concentration was first obtained (Table 6 Fig. 3).

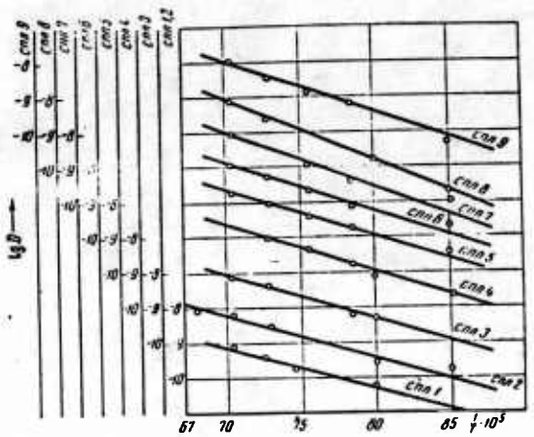

Fig. 2. Temperature dependence of the diffusion coefficient of cobalt.

TABLE 5

The Value of Q and D_0 for the Diffusion of Cobalt in an Iron-Aluminum Alloy

Al, вес.%	Al, ат.%	Q, ккал/г-атом	D_0 см²/сек
1,7	3,47	53,0	0,1
4,2	7,95	56,0	1,9
7,2	13,5	58,5	6,8
11,2	20,6	60,0	22
13,2	23,6	60,0	27
21,0	35,5	67,0	210
26,0	42,0	71,0	580
30,1	47,3	79,0	6300
34,5	52,2	67,0	148

The parameter was calculated from the line (211); the corresponding φ angle 78° for iron and 74°54' for the alloy containing 20% Al. The lattice parameter is determined to the fourth decimal.

TABLE 6

Variation in the Lattice Parameter According to Aluminum Concentration

№ сплава	ат. % Al	Параметр решетки, Å
0	железо армко	2,8612
1	3,47	2,8689
2	7,95	2,8779
3	13,49	2,8890
4	20,6	2,9008

TABLE 7

Value of the Coefficient of Mutual Diffusion in Iron-Aluminum Alloys (in cm^2/sec)

№ сплава	Температура, °С				
	1200	1150	1080	980	900
2	$1,9 \cdot 10^{-6}$	—	$4,17 \cdot 10^{-8}$	$1,9 \cdot 10^{-9}$	$3,8 \cdot 10^{-9}$
3	$2,38 \cdot 10^{-6}$	—	$5,7 \cdot 10^{-8}$	$3,28 \cdot 10^{-9}$	$4,37 \cdot 10^{-9}$
4	—	$1,47 \cdot 10^{-7}$	$6,07 \cdot 10^{-8}$	$3,38 \cdot 10^{-9}$	—

A variation in the aluminum content by 1% corresponds to a variation in the lattice parameter by 0.0018 Å, from which it was possible to determine the variation in the aluminum concentration as 0.3 atom percent. Mutual diffusion was investigated in alloys Nos. 2, 3 and 4, in which there was a linear dependence of the lattice parameter on composition (Fig. 2). The diffusion annealing was carried out at temperatures of 900, 980, 1080, 1150, and 1200°.

The diffusion coefficients D at various temperatures were calculated by plotting the dependence of the logarithm of iron concentration in the layer on the square of its depth from the equation

$$D = \frac{1}{4t \cdot \operatorname{tg} \alpha},$$

Where t is the time of annealing; and

α is the angle of slope of the curve.

The depth of the layer was reckoned from the surface coated with iron. Due to the considerable thickness of the iron coating (~ 5 microns) the dependence of ln C on X^2 at distances of 20 microns differed greatly from the linear dependence and was only approximately linear at greater depths. The diffusion coefficients D established by us are therefore of the nature of an estimate. All diffusion coefficients calculated are given in Table 7.

The relatively elevated values of the diffusion coefficients at 900° should perhaps be attributed to the presence of boundary diffusion at that temperature. It is noteworthy that there is a tendency towards an increase in the diffusion coefficient with an increase in the percentage content of aluminum. This prevented us from estimating the activation energy from the temperature rate of the diffusion coefficient with a sufficient degree of accuracy. The activation energy was evaluated by the following means. Fig. 4 shows the concentration distribution in depth of the components in the alloy at two different temperatures: T_1 and T_2. For a known concentration C_1 we may write:

$$\ln C_1 = A - \frac{x_1^2}{4D_1 t_1} \quad \text{при } T = T_1$$

$$\ln C_2 = A - \frac{x_2^2}{4D_2 t_2} \quad \text{при } T = T_2$$

from which

$$\frac{x_1^2}{x_2^2} = \frac{D_2 t_2}{D_1 t_1}, \qquad (2)$$

substituting

$$D_1 = D_0 e^{-\frac{E}{RT_1}}, \qquad D_2 = D_0 e^{-\frac{E}{RT_2}},$$

results in

$$\frac{D_2}{D_1} = e^{\frac{E}{R}\left(\frac{1}{T_2} - \frac{1}{T_1}\right)}. \qquad (3)$$

From the Eqs. (2) and (3) we obtain

$$\frac{x_1^2}{x_2^2} = \frac{t_1}{t_2} e^{\frac{E}{R}\left(\frac{1}{T_2} - \frac{1}{T_1}\right)}. \qquad (4)$$

Equality (4) is used to compute the activation energy of diffusion Q at a given concentration C_1. Hence, it also possible in this way to find the concentration-dependence of the activation energy of diffusion. We evaluated Q in this way for an alloy containing 7.95% Al (Table 8). The corresponding concentration curves are given in Fig. 4. We could not make a similar evaluation in other instances.

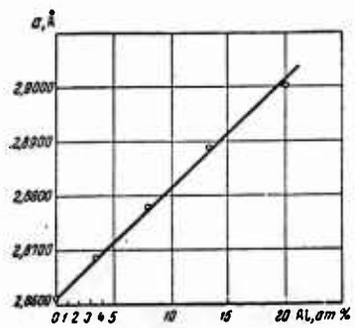

Fig. 3. Calibrated graph

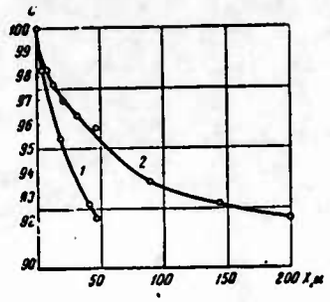

Fig. 4. Distribution of the concentration of components in depth at two different temperatures in an iron-aluminum alloy. 1) T_1 = 1000°, t_1 — 484° C; 2) T_2 = 1100°, t_2 484°C.

TABLE 8

Value of Q in Iron-Aluminum Alloys

Al, ат. %	Q, ккал/г·ат
4	68
5	71
6	71
7	78

A comparison of the results obtained in the study of mutual diffusion in iron-aluminum alloys with the phenomenon of self-diffusion of iron in the said alloys enables us to conclude that in the first instance both the diffusion coefficients and the activation energy have somewhat higher values.

The dependence of the activation energy of diffusion on the aluminum concentration can be understood if we proceed from the idea that this energy is connected with the interaction of the atoms

and that this interaction may be characterized by the "fill" factor of the electronic d-states [4]:

$$q = \frac{d_0 - m}{d_0}, \qquad (5)$$

Where d_0 is the number of d-vacancies per atom of alloy in the gaseous state;

$m = d_{sol}$ the number of d-vacancies per atom of alloy in the solid state.

The latter number may be obtained by measuring the magnetic moment per atom of alloy [5], and d_0 is known from spectroscopic data and is equal to 4 for iron. Table 9 gives the "fill" factors calculated in this way.

TABLE 9

Al, at. %	d_{TB}	d_0	q
0	2,22	4,0	0,45
10	2,00	3,6	0,44
20	1,71	3,2	0,47
25	1,51	3,0	0,50
30	1,17	2,8	0,58
40	0,61	2,4	0,75
50	0,04	2,0	0,98
52	0,04	1,92	0,98

It is clear from Table 9 that in a zone ranging up to about 25 atom %, the magnitude q varies little but rises sharply with a further increase in its content. Fig. 5 exhibits a similar pattern for the dependence of the activation energy of cobalt diffusion in the alloys under consideration on the aluminum concentration. Up to 25 atom % Al we observe a slight increase in the activation energy

but it increases appreciably in higher concentrations. As regards to the diffusion of iron, the activation energy was found to vary little in the zone of aluminum concentrations up to 25 atom % just as in the case of cobalt diffusion.

It is important to note that for an aluminum concentration near the limit of solubility in the α phase the activation energy of cobalt diffusion decreases sharply. If we consider an alloy containing 52.2 atom % (with up to 0.07% carbon in the charge iron) as the saturation limit, then the decline in the activation energy of the diffusion of cobalt with respect to the quantity Q, obtained by extrapolation of the curve of the dependence Q = f up to $\Delta Q \approx 90 - 67 = 23$ kcal/mole. This considerable decrease in the activation energy could be explained by the presence of a higher concentration of vacancies, apparently structural in origin, in the alloy containing 52 atom %. If this assumption is right, then the diffusion coefficient in the said alloy, just as in the case of the corresponding cobalt-aluminum alloys [7], is determined in effect merely by the diffusion rate of the vacancies. This assumption is to a certain extent is borne out by the fact that the coefficient for the alloy containing 52 atom % is almost double that of the alloy containing 48 atom % Al.

However, further study, possibly by other methods will be required to verify this assumption.

A comparison of the data on the diffusion of cobalt and iron in the alloys under investigation (see Tables 2 and 4) leads us to conclude that the diffusion parameters of iron and cobalt are proximates.

REFERENCES

1. GRUZIN, P. L. Problemy metallovedeniya i fiziki metallov. TsNIIChM, In-ta metallovedeniya i fiziki metallov. [Problems of Physical Metallurgy and the Physics of Metals] Sb. Nauchnykh rabot. [Coll. of Scientific Papers of the Centr. Sc. Res. Inst. Ferr. Met., Inst. of Metallography and Physics of Metals], Nr. 3, 1952.

2. UMANSKIY, L. S; FINKEL'SHTEYN, B. N.; BLANTER, M. Ye.; KISHKIN, S. T.; FASTOV, N. S.; and GORELIK, S. S. Fizicheskoye metallovedeniye. [Physical Metallurgy] Metallurgizdat [State Sc. Press for Lit. on Ferr. and Non-ferr. Met], 1955.

3. GERTSRIKEN, S. D. and DEKHTYAR, I. Ya. Informatsionnoye pis'mo. No. 3, [Informative Letter Nr. 3] Acad. Sci. Ukr. SSR, Inst. of Physics of Metals.

4. DEKHTYAR, I. Ya. DAN SSSR [Reports of the Acad. Sci. USSR], 85, Nr. 3. 1952.

5. BOZORT, P. M. Ferromagnetizm. [Ferromagnetism] GITTL [State Press for Tech. and Theor. Lit.], Moscow, 1956.

6. GERTSRIKEN, S. D. and DEKHTYAR, Ya. I. Fizika metallov i metallovedeniye. [The Physics of Metals and Physical Metallurgy] [Sb. nauchn. rabot Laboratorii metallofiziki] Coll. of Sci. Stud. of the Laboratory for the Physics of Metals], Nr. 7, Acad. Sci. Press, Ukr. SSR, 1956.

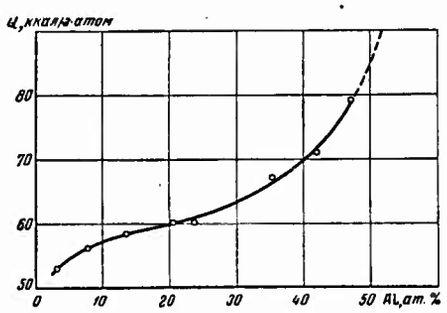

Fig. 5. Cobalt diffusion in an iron-aluminum alloy.

DETERMINATION OF THE PARAMETERS OF DIFFUSION AND DEFORMATION IN NICKEL-CHROMIUM ALLOYS

I. Ya. Dekhtyar and V. S. Mikhalenkov

The mobility of atoms in a crystal lattice is a determining factor in the heat resistance of metals. This is explained by the fact that atomic mobility is involved in the mechanism of creep and causes the metal to change or retain its structure.

The mobility of atoms in a crystal lattice depends directly on the character and magnitude of the forces of the interatomic bond, which are described by the sum total of the following physical quantities:

Sublimation energy;

Melting point;

Activation energy of self-diffusion and diffusion;

Characteristic temperature;

Modulus of elasticity, its temperature coefficient, etc.

Although it is impossible, in view of the structural sensitivity of the strength characteristics, to establish a clearly defined relationship between resistance to plastic deformation, failure, and the magnitudes describing the forces of the interatomic bonds, we may nevertheless speak of a certain tendency toward increased strength as the binding forces in the crystal increase.

There are indications that the mobility of the atoms in the lattice and over the boundaries is related to the problem of plastic deformation at elevated temperatures. It is therefore worthwhile to investigate the diffusion parameters of atomic mobility in a crystal lattice and to find the link (if any) between the diffusion parameters and plastic deformation, in order to clarify the connection between the mechanism of plastic deformation at high temperatures and displacements of the atoms by diffusion and the part played in this by defects of various kinds in the crystal structure.

Material and Methods

The alloys under investigation were made in a vacuum induction furnace from nickel and chromium of high purity produced electrolytically. The composition of the alloys is given in Table 1.

For the purpose of homogenization, were subjected to forging and annealing at a temperature of 1200° for 75 hours in order to obtain a uniform structure.

TABLE 1

№ сплава	Cr, вес. %	Cr, ат. %	№ сплава	Cr, вес. %	Cr, ат. %
1	3,83	4,51	4	14,23	15,79
2	7,88	8,79	5	20,25	22,03
3	12,02	13,3	6	24,99	25,11

The diffusion parameters of the alloys were investigated by means of radioactive isotopes. Isotope Co^{60} was used as a radioactive indicator. Selection of this isotope was conditioned by the

aim of the investigation, which was to determine the diffusion parameters of the basic component of the alloy; so far, our country has not produced any radioactive nickel isotope suitable for the investigation; an article [1] however, appeared recently in the foreign press, dealing with the study of the self-diffusion of nickel by means of the radioactive isotope Ni^{63}.

The data on the diffusion of cobalt in a nickel-chromium alloy are probably different from the true diffusion rates of the basic components; they however, are quite suitable for describing the atomic interactions, particularly the concentration-dependence, especially since cobalt and nickel are closely related in their physical and chemical properties as elements of the same periodic group and are absolutely soluble in each other.

Radioactive cobalt has been used many times for the investigation of atomic mobility in nickel alloys. The diffusion coefficients of cobalt in nickel-aluminum alloys were determined in research [2], and the results showed that for the study of the laws of diffusion in these alloys it is advisable to use the radioactive isotope Co^{60}, which is most suitable for this purpose instead of the nickel isotope.

In investigating the diffusion parameters we used the absorption method, by which the correlation of β activities of the side of the test piece covered with the radioactive isotope is determined by the equation

$$\frac{I_{0.t}}{I_{0.0}} = e^{\mu^2 Dt}\left[1 - er/\mu\sqrt{Dt}\right], \qquad (1)$$

Where $I_{0.0}$ and $I_{0.t}$ are the β activities of the surface of the test piece before and after annealing for time t;

D is the diffusion coefficient of the given component in the alloy;

μ is the absorption coefficient of the given radiation in the alloy.

The use of this formula presupposes an infinitely thin layer of radioactive isotope on the surface of the test piece. In our case the radioactive indicator was applied to the test piece electrolytically and the thickness of the layer amounted to about 1 micron. A part from β rays with an energy of 0.31 Mev, the isotope Co^{60} radiates γ rays components with an energy of 1.17 and 1.33 mev. The γ radiation was eliminated by means of an aluminum shield and was deducted from the total activity. From the γ activity we were able to ascertain the state of preservation of the coating. If part of the radioactive coating evaporated, the γ activity of the test piece changed after annealing and we then had to make the necessary correction. In such a case, we shall have the ratio $\frac{I_\beta}{I_{\beta_o}} \quad \frac{I_{\gamma_o}}{I_\gamma}$ in the left hand term of Eq. (1). However, such cases seldom occurred in our experiments, since the test pieces were annealed in an atmosphere of argon.

Using the available tables, we derived from the ratio $\frac{I_{o.t}}{I_{o.o}}$ the quantity $x^2 = \mu^2 Dt$, from which $D = \frac{x^2}{\mu^2 t}$.

The use of the absorption method requires knowing the absorption coefficient of radioactive radiation in the given material. This is the chief disadvantage of the method and it shows up particularly in a case when the β radiation of the radioactive indicator is not monochromatic. This is not the case with Co^{60}.

The absorption coefficients of β radiation of Co^{60} in the components were calculated on the basis of the known absorption coefficient of β rays of cobalt in cobalt (μ_{Co} = 518 cm^{-1}) by equation

$$\mu_M = \frac{\rho_{Ni}}{\rho_{Co}}\mu_{Co} \quad \text{and} \quad \mu_{Cr} = \frac{\rho_{Cr}}{\rho_{Co}}\mu_{Co},$$

Where ρNi, ρCo and ρCr are the densities of nickel, cobalt, and chromium respectively. The absorption coefficients in an alloy being subject to the rule of addition were found from the correlation

$$\mu_{спл} = \mu_{Ni} C_{Ni} + \mu_{Cr} C_{Cr}, \qquad (2)$$

Where C_{Ni} and C_{Cr} are the atomic concentrations of nickel and chromium respectively. The absorption coefficients for the alloys under investigation are given in Table 2.

TABLE 2

	№ сплава					
	1	2	3	4	5	6
$\mu_{спл}$, $см^{-1}$	519,3	510,1	506,5	503,3	497,7	493,1

Experimental Data

The diffusion coefficients of nickel-chromium alloys were determined in the temperature range 1050, 1100, 1150, 1200, and 1250°, at which all the alloys were a homogeneous solid solution with a cubic face-centered lattice [3]. The results obtained are shown in

Table 3.

Each coefficient is an average of two test pieces. The average error in calculating the diffusion coefficient was 15 to 20%. The points plotted on the graph log D — 1/T are for each alloy on the straight line (Fig. 1) and from the latter we can determine by the formula $D = D_0 e^{-E_a/RT}$ the pre-exponential term D_0 and the activation energy E_a of cobalt diffusion in the alloys in question. The calculated parameters E_a and D_0 are given in Table 4.

TABLE 3

№ сплава	Содержание Кробальта ат. %	D, см²/сутки					
		1000°	1050°	1100°	1150°	1200°	1250°
1	4,51	$1,22 \cdot 10^{-7}$	—	$5,89 \cdot 10^{-7}$	$1,22 \cdot 10^{-6}$	$3,02 \cdot 10^{-6}$	$5,82 \cdot 10^{-6}$
2	8,79	$8,07 \cdot 10^{-8}$	$2,22 \cdot 10^{-7}$	$4,92 \cdot 10^{-7}$	$1,02 \cdot 10^{-6}$	$2,52 \cdot 10^{-6}$	—
4	15,79	—	$2,37 \cdot 10^{-7}$	$8,9 \cdot 10^{-7}$	$2,2 \cdot 10^{-6}$	$5,42 \cdot 10^{-6}$	$1,66 \cdot 10^{-5}$
5	22,03	—	$1,59 \cdot 10^{-7}$	$3,69 \cdot 10^{-7}$	$9,6 \cdot 10^{-7}$	$1,92 \cdot 10^{-6}$	$8,3 \cdot 10^{-6}$
6	25,11	—	$2,15 \cdot 10^{-7}$	$4,45 \cdot 10^{-7}$	$8,72 \cdot 10^{-7}$	$1,89 \cdot 10^{-6}$	$5,27 \cdot 10^{-6}$

TABLE 4

№ сплава	Cr, % ат.	q	D_0, см²/сек	E_a, ккал/моль
1	4,51	0,8	0,045	61,6
2	8,79	0,88	0,206	67,0
4	15,79	0,97	94,1	82,0
5	22,03	—	0,567	70,0
6	25,11	—	0,054	63,4

The concentration-dependence of the diffusion coefficients is difficult to detect since they vary only slightly from one alloy to another, although the alloy containing 15.79 atom% Cr has greater atomic mobility at all the temperatures investigated (see Table 3). The concentration-dependence of the pre-exponential term and of the activation energy of diffusion are very clearly marked, however.

Analysis of Results

The basis of all existing heat-resistant alloys are metals of the transition group. This is because a metal with an incomplete electron d shell is able to accept electrons from a precipitate, which increases the forces of interatomic reaction owing to the additional electronic bonds created. This situation continues to exist until all the vacancies in the incomplete electron d shell are filled. The extent to which d vacancies are filled is conveniently characterized [4] by the fill factor

$$q = \frac{d_0 - d_H}{d_0}, \qquad (3)$$

when d_0 is the number of unpaired d electrons per atom in the gaseous state, and d_H is the number of unpaired d electrons per atom in the solid state.

The activation energy of diffusion, which expresses the magnitude of the forces of interatomic reaction is liable to increase together with the fill factor, reaching the maximum at $q \approx 1$, i.e., when all the d vacancies are filled. After that, any increase in the electron concentration will increase the kinetic energy of the electrons in the system, which leads to a decline in the energy of

the interatomic reaction and, consequently, of the activation energy also. The qualitative connection between the activation energy of diffusion and the fill factor was established for many alloys in which either one or several components are elements of the transition group. For example, during the study of diffusion of cobalt in nickel-magnese [4] cobalt-aluminum, cobalt-iron and cobalt- chromium [5] alloys, a parallel change in the activation energy of diffusion and the fill factor up to q = 1 was observed.

With nickel-chromium alloys, the additional electronic bonds which occur during the filling of the electron d shells are particularly strong since both alloyed metals are elements of the transition group and have incomplete d status.

The fill factor q was calculated according to the formula (3) for each of the alloys investigated. The number of unpaired d-electrons in the gaseous state d_o, which is subject to the rule of addition, was calculated for each alloy from the junction

$$d_o = d_{o_{Ni}} C_{Ni} + d_{o_{Cr}} C_{Cr},$$

where C_{Ni} and C_{Cr} are the atomic concentrations in the alloy of nickel and chromium, respectively. Sprectroscopic data show that in the gaseous state nickel and chromium have 2 and 5 unpaired d-electrons per atom respectively, i.e., $d_{oNi} = 2$, $d_{oCr} = 5$.

The number of unpaired electrons per atom in the solid state for each alloy was taken from published data [6]. The values of the fill factor q are given for each alloy in Table 4; it is clear from the table that the activation energy of diffusion increases together with the increase of q in the alloy containing 15.79 atom% in which the electron d orbits are completely filled. The subsequent

sharp decrease in activation energy is due to the fact that the potential bond energy does not vary whereas the kinetic energy of the electrons increases with the electron concentration.

It follows that the concentration-dependence of the activation energy of diffusion of cobalt in nickel-chromium alloys (Fig. 2) obtained agrees well with the theoretical premises regarding the character of the interatomic reaction in alloys.

As the theory shows, we can estimate the temperature coefficient of the modulus of elasticity in alloys from the concentration-dependence of the activation energy of diffusion.

Accordingly [7], the pre-exponentail term D_o is theoretically expressed by the formula

$$D_0 = \gamma a^2 \nu e^{\Delta S/R}. \qquad (4)$$

Where a is the lattice parameter

ν is the activation energy;

ΔS is the activation entropy; and

γ is a coefficient equal to one in the case of "hole" diffusion in body-centered and face-centered cubic lattices.

The activation entropy, according to Zener, is expressed by the formula

$$\Delta S \approx \beta \frac{E_a}{T_s}, \qquad (5)$$

Where E_a is the activation energy of diffusion,

T_s is the temperature of fusion;

$$\beta = -\frac{d\left(\frac{\mu}{\mu_0}\right)}{d\left(\frac{T}{T_s}\right)}; \qquad (6)$$

μ is the modulus of elasticity at a given temperature;

μ_o is the modulus of elasticity at 0°.

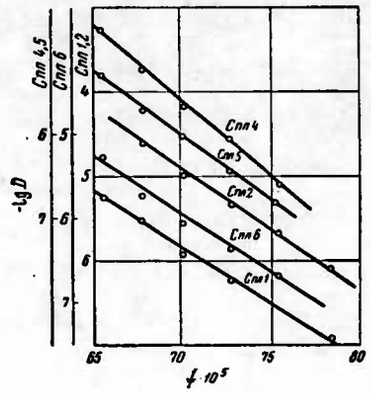

Fig. 1. Dependence of log $\underline{D}$ on $\frac{1}{T} \cdot 10^5$

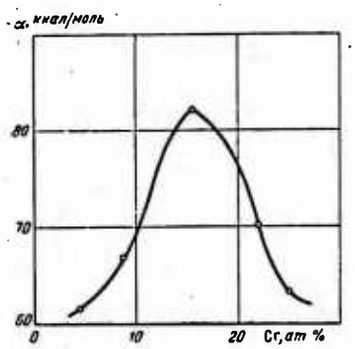

Fig. 2. Dependence of E_a on the chromium content.

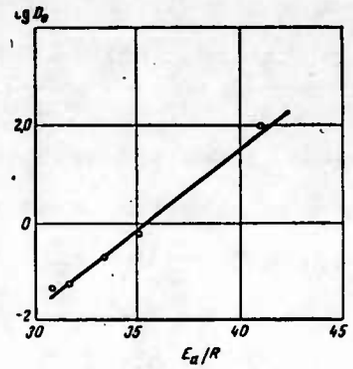

Fig. 3. Dependence of log D_0 on E_a/R.

Substitution of the expressions (5) and (6) in the Eq. (4)

$$D_0 = \gamma a^2 \nu e^{\frac{\beta}{T_S} \cdot \frac{E_a}{R}}.$$

Taking $\frac{\beta}{T_S} = \beta_1$ we obtain

$$D_0 = \gamma a^2 \nu e^{\beta_1 \frac{E_a}{R}}, \qquad (7)$$

Where $\beta_1 = \frac{1}{\mu_0} \frac{d\mu}{dT}$ is the temperature coefficient of the modulus of elasticity.

Hence by plotting log D_0 against $\frac{E_a}{R}$, for various concentration, we obtain the temperature coefficient β_1 of the modulus of elasticity as a tangent of the angle of slope of the straight line.

This dependence is given in Fig. 3, and it is clear from the graph that the points fall satisfactorily along a straight line. The temperature coefficient of the modulus of elasticity calculated from the graph is $8.55 \cdot 10^{-4}$ degree $^{-1}$.

This indirect method of determining the temperature coefficient of the modulus of elasticity cannot compete with direct methods for

the following reasons:

The accuracy in calculating the diffusion parameters is lower than that attained in determining the modulus of elasticity;

The temperature coefficient of the modulus of elasticity that can be obtained is an average both for the alloy concentrations and the temperature range, under consideration since we have to base our calculations on a graph in which each point is obtained within the temperature range under investigation, while the calculated line is plotted for alloys with different concentrations. However, if it is taken into account that the variation in the temperature coefficient of the modulus of elasticity with a concentration within a one-phase composition is small, as in the variation in the temperature range 200 to 250° in which the diffusion parameters are usually calculated, the suggested method of determining this temperature coefficient is quate suitable for a rough estimate.

Influence of the Deformation Rate on the Diffusion Rate

Method of investigation. In order to study the influence of the deformation rate on the diffusion rate we designed and built a vacuum unit for the diffusion annealing of test pieces under load. The operating principle of the unit was as follows: during annealing a mechanical axial load of constant magnitude was applied to the diffusion surface of the test pieces. The diffusion coefficients were determined by the absorption method, using the radioactive isotope Co^{60}.

The test pieces consisted of small cylinders 1.5 mm deep and from 7.5 to 12 mm in diameter to ensure various pressures at the

same load. It is essential for the test pieces to be strictly plane-parallel, or else the load would be distributed unevenly over the surfaces.

The deformation rate was determined from the equation*

$$\dot{e} = \frac{e}{t},$$

Where t is the time of annealing;

e is the average deformation of the test piece during the time of annealing, equal to

$$e = 2 \ln \frac{d}{d_0},$$

and where d_0 and d are the diameters of the test piece before and after annealing, respectively.

The diameters were measured with a micrometer at several points and the mean used for calculation. The relative error did not exceed 0.2% since the area of the test pieces varied during annealing as a result of deformation under the axial load, the method of calculating the ratio of β activities in the test piece before and after annealing was somewhat modified.

Since the solid angles at which the aperture of the end-type counter is visible, are not equal the ratio of β activities of test pieces of different size obtained from sectors of those pieces at a different distance from the axis of the counter will differ from the true value.

The following equation may be used [8] for the ratio of activities of two test pieces of different diameter, with allowance for the fact that they are not pointed in shape.

$$\frac{A_1}{A_0} = \frac{I_1}{I_0} \frac{R_1^2 \int_0^{R_0} K(r) r\,dr}{R_0^2 \int_0^{R_1} K(r) r\,dr}.$$

* At short deformation times the quantity ė hardly depends on t.

Here: $\frac{A_1}{A_0}$ is the true ratio of β activities of test pieces with radii R_1 and R_0;

$\frac{I_1}{I_0}$ is the measured ratio of their activities.

The quantity $\int_0^{R_1} K(r) r\, dr$ is the area of the graph $K(r)r - r$, limited by the curve, the axis of the abscissae and the ordinary $r = R_1$. The quantity $\int_0^{R_0} K(r) r dr$ is found by analogy. The function $K(r) = \frac{n(r)}{n(0)}$ is the ratio of activity of a pointed source, placed on a stage at a distance r from the axis of the counter to the activity of the same source placed on its axis.

In order to plot the graph $K(r)r - r$, the following experiment was made. The β activity of a pointed source in about 1 mm^2 area was measured according to the distance from the axis of the counter. The distance r from the axis was varied from 0 to 15 mm. The quantity $\varphi(r) = \frac{n(r)}{n(0)}$ was then calculated and plotted on the graph $K(r)r - r$.

The results of the experiment for the two distances from the aperture of the counter h_1 and h_2, at which the measurements of the activities of the test pieces were taken, are shown in Fig. 4.

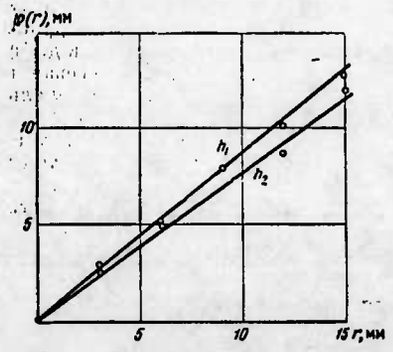

Fig. 4. Dependence of $\varphi(r)$ on r.

However, Eq. (8) gives the correction for the ratio of activities, for the non-pointed nature of the test pieces. We ourselves had to make a correction for the same sample which changed in size through deformation. For this to be done it is necessary to measure the activity per unit of surface.

Taking these corrections into account, we calculated the true activity from the equation

$$A = IR^2 \frac{1}{\pi R^2 \int_0^R K(r)\, r dr} = I \frac{1}{\pi \int_0^R K(r) r dr}.$$

Then, the true ratio of β activities is

$$\frac{A_1}{A_0} = \frac{I_1}{I_0} \cdot \frac{\int_0^{R_0} K(r)\, r dr}{\int_0^{R_1} K(r)\, r dr}. \qquad (9)$$

The unit used for investigating diffusion rates under load is shown in Fig. 5. The unit is mounted on a metal base and covered with a glass vacuum bell jar (1). The furnace (2) stands on a thermal insulating support (3). A force plug, which is constructed as part of the cover (4) attached to the metal base, fits into the working space from above. The load (5) is increased 15 fold by means of the lever (6) and is applied to the test pieces through the rod (7). A bellows (8) serves as packing between the rod and the support. For purposes of insulation the test pieces are separated from the force plug and the movable rod by small quartz cylinders 20 mm in length. Two pieces of different diameters are placed in the furnace at the same time in order to obtain different pressures. To ensure that the applied load acts over the

whole area of both test pieces, the latter are separated by a molybdenum washer 2 mm thick. Washers are also inserted between the test pieces and the quartz cylinders.

Since the faces of the test pieces coated with a radioactive isotope were in close contact with the molybdenum washers, the atoms of the radioactive isotope might have diffused into the washers as well as into the test pieces, which would have affected the results of the absorption method of measuring. In order to eliminate this possibility completely, even though it might only have been slight because of the low diffusion rate of molybdenum, thin tempered mica foil was inserted between the test pieces and the molybdenum washers; the foil also had another purpose which is described below.

The test pieces, which had been subjected to diffusion annealing, underwent axial compression. Nevertheless, owing to friction between the faces of each test piece and the washer, hydrostatic in addition to unidirectional pressure must have occurred. This hydrostatic pressure will obviously be greatest at the faces and will decline towards the center of the test piece. This distribution of load could have resulted in the formation of convex side surfaces on the test piece. The presence of hydrostatic pressure in addition to unidirectional pressure should have reduced the effect of the latter, since there is reason to assume that with respect to the rate of diffusion they act in opposite directions. In general axial compression will in fact produce a state of complex stress.

The mica foil located between the washers and the test pieces reduced if not completely eliminated, the effect of hydrostatic pressure by acting as a lubricant. The use of the foil as well as the thinness of the test pieces reduced if not completely eliminated

any convesity of the test pieces in our experiments.

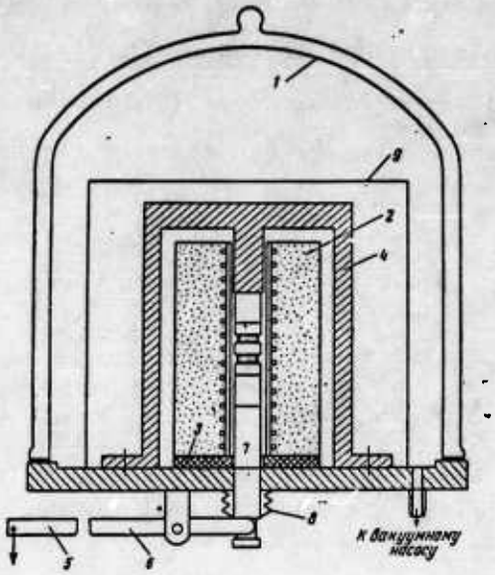

Fig. 5. Schematic representation of device for studying diffusion rates under load.

The temperature in the combustion space of the furnace was measured by means of a thermocouple, the hot junction of which was placed close to the test pieces. The annealing temperature was controlled with in $\pm$ 2°. The base was cooled by running water. The bell jar was shielded from the heat of the furnace by the cylinder (9) and was, in addition, cooled from the outside.

Results of the Measurements

A study was made of the diffusion rates under load of the same alloys for which the diffusion coefficients under normal conditions were being determined. The investigations were carried out at a temperature of 1000 and 1100°. The load applied to the

specimens amounted to 200 kg. The pressure on the test pieces was varied from 1.8 to 4.5 kg/mm^2, depending on their dimensions. The results of the measurements are shown in Fig. 6 and 7.

In all cases the diffusion coefficient increased with the increase in deformation rate $\dot{e}$, revealing a linear dependence on $\dot{e}^2$.

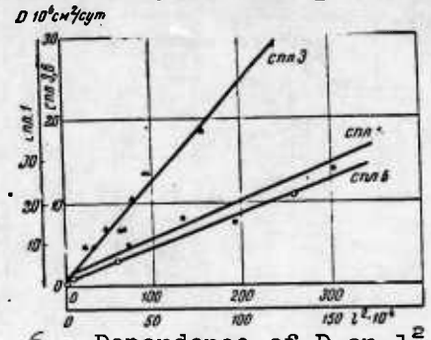

Fig. 6. Dependence of $\underline{D}$ on $\underline{l}^2$.

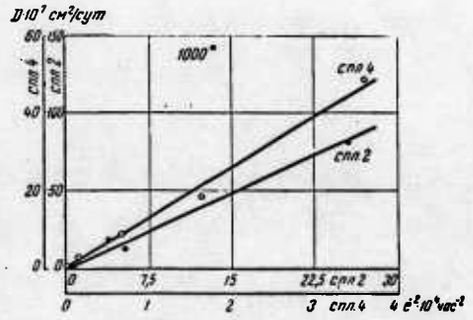

Fig. 7. Dependence of $\underline{D}$ on $\dot{e}^2$.

Table 5 shows the results of the measurements of the diffusion coefficients in relation to the deformation rate in alloys containing 13.3 atom % Cr.

TABLE 5

$\dot{\varepsilon}$, час$^{-1}$	0,033	0,04	0,048	0,057	0,0575	0,062	0,089	0,108
$D_\varepsilon \cdot 10^{-6}$ см^2/сут	4,75	4,8	6,97	6,7	6,8	10,4	18,15	28,6

Analysis of Results

The influence of deformation on the diffusion rate can be considered from the viewpoint of acquiring a clearer idea of the diffusion mechanism, or from that of elucidating the mechanism of plastic deformation at high temperatures. Although the influence of stress on the diffusion rate has been known for a long time, it is only the development of new methods for investigating diffusion by the use of radioactive isotopes that enables us at the present time to raise the question of quantative laws.

The influence of hydrostatic pressure on the self-diffusion rate of sodium was studied[9]. It resulted that hydrostatic pressure (~ 80 kg/mm^2) appreciably reduces the self-diffusion coefficient about 10 times at 60° and increases the activation energy (by about 15%). This has made it possible to hypothesize a model of diffusion called "relaxed vacancies". Instead of the mechanism of diffusion through the movement of individual vacancies, the author suggests consideration of the formation and movement of a disordered zone of atoms (12-16 atoms) relaxing around a vacancy. Here the activation energy of self-diffusion is equal to about 16.5 L, L being the latent heat of fusion. An increase in activation energy is apparently caused by a higher melting point under hydrostatic pressure. As to the influence of unidirectional pressure on the diffusion rate, it has been shown [10] on the basis of the self-diffusion of iron at 890° that the self-diffusion coefficient is approximately a linear

function of the deformation rate. However, the authors were unable to interpret the progression which they had obtained of the dependence of the diffusion coefficient on the deformation rate. One of us [11] has made an attempt to explain this result, basing himself on the assumption that deformation at high temperature causes an increase in the concentration of foci of disordered zones of atoms or vacancies according to a law governing the eventual failure of the metal [12]. But this assumption [11] of an increase in the concentration of vacancies has not been related to the deformation mechanism itself. The aim of the present work, however, was to draw certain conclusions concerning the mechanism of deformation at high temperatures from the effect of deformation on the diffusion rate.

For a qualitative interpretation of this influence we should rely on our concepts regarding the development of vacancies in dislocations. In so doing, we are adopting the following dislocation model of high-temperature deformation. It is assumed that deformation is determined by the movement and interaction of dislocations. The dislocations brought into movement by stress flock together when they collide with an natural obstacle. The stresses occurring in the close-packed group incite the Frank-Read sources in the other slip systems to form dislocations. When non-parallel dislocation lines intersect, dislocation protrusions and related vacancies occur. In addition to this, the dislocations may also serve as outlets for the vacancies.

At high temperatures the vacancies must diffuse into the outlets of a different type in such a manner that an approximately equalized number of vacancies becomes established. However, porosity

in the diffusion zone as a result of the Kirkendall effect shows that there may be considerable deviation from the concentration equilibrium of the vacancies. This indicates that the dislocations cannot establish this concentration with any great ease. In this connection we may assume the presence (during high-temperature deformation) of excess vacancy concentration, apparently a product of the diformation rate ($\dot{e}$), which causes an increase in the diffusion rate.

Let $D\sigma$ denote the diffusion coefficient under a certain effective stress σ, and ΔC the excess concentration of vacancies. Then,

$$D_\sigma = D + \Delta D = D + \Delta C D_v, \tag{10}$$

where Dv is the diffusion coefficient of the vacancies.

In accordance with the above and in order to explain the results obtained, let us assume that $\Delta C \backsim \dot{e}^2$. Furthermore, ΔC must also depend on the average number of protrusion per unit length of the dislocations inducing the vacancies (n_j).

We may then assume that*

$$\Delta C = K n_j \dot{e}^2, \tag{11}$$

where K. is the coefficient of proportionality.

The number of dislocation protrusions n_j is connected with the dislocation density N_d [13] in the following way:

---

* In other cases, the vacancy-generation rate is proportional to the deformation rate.

$$n_j = fLN_d, \tag{12}$$

where f is the number of dislocation protrusions capable of generating vacancies:

L is the average half-distance covered by the dislocation from the source to the barrier.

The diffusion coefficient of vacancies D_V can be found, according to [13], from the relation

$$D_v T^* = mb^2, \tag{13}$$

where m is the average number of vacancy jumps from the source to the outlet;

b is Burger's vector; and

T* is the average life span of a vacant site on the standard course, determined from the expression

$$T^* = m\tau_0 e^{\epsilon S/KT}, \tag{14}$$

where τ_0 is the oscillation period of the atoms;

ϵS is the height of the activation barrier;

$\tau_0 e^{\epsilon S}/KT$ is the normal length of the sedentary life of the vacancy until its exchange with an adjoining atom.

From Eqs. (10), (11), (12), (13) and (14) we obtain:

$$D_a = D + \frac{KfLN_d b^2 e^{-\epsilon S/KT}}{\tau_0} \dot{e}^2. \tag{15}$$

An analysis of Eq. (15) shows that the rate of increase in the mobility of atoms following deformation at high temperatures may be described by the coefficient

$$P = \frac{dD_a}{d\dot{\varepsilon}} = \frac{2K\beta LN_d b^2 e^{-\varepsilon S/KT}}{\tau_0}\dot{\varepsilon}. \qquad (16)$$

It follows from Eq. (16) that at a given temperature and at a constant deformation rate the metal's ability to soften is determined by the dislocation density, the quantity L of the mean free path of the dislocation, and the height of the activation barrier, which in turn depends on the interatomic bond strength.

We should point out that, given our assumption, our analysis has only a qualitative character.

The softening coefficients in high temperature deformation can be compared from experimental data. With alloys Nos. 1 - 3 and 6 at 1100°, and at a deformation rate of 0.17 hours^{-1} (Fig. 6), they equal $1.26 \cdot 10^{-5}$cm^{-2}, $5.3 \cdot 10^{-5}$cm^2, and $1.13 \cdot 10^{-5}$cm^2, respectively; under the stated conditions, softening is greatest in alloy No. 3.

Further investigation is necessary to verify all the conclusions which can be drawn on the basis of the approximate method proposed. In particular, we should investigate the temperature-dependence determined by Eqs. (15) and (16). Nevertheless, it apparently seems safe to assume that the diffusion coefficients by themselves cannot fully describe the resistance of a metal to deformation at elevated temperatures. This can best be judged from the sum total of the diffusion coefficients and the manner in which they vary with changes in the deformation rate.

Conclusions

1. The parameters obtained for the diffusion of cobalt in nickel-chromium alloys with a chromium concentration of 4 to 25 atom % enabled us to establish the fact that the dependence of the

activation energy of diffusion on the chromium concentration agrees with theoretical speculation as to the character of the atomic interaction in alloys based on elements of the transition group. The activation energy of diffusion increases with the increase in chromium concentration and attains maximum values at ~ 15 atom % Cr, at which the vacant sites of the electron d shells are filled to the maximum extent; after which, it declines.

2. From the data on diffusion we estimated the average temperature coefficient of the modulus of elasticity for the investigated alloys $8.55 \cdot 10^{-4}$ degree^{-1}.

3. We designed a device and developed a method for the study of diffusion parameters during plastic deformation at high temperatures.

4. It was discovered that the diffusion coefficients rise with an increase in the deformation rate $\dot{e}$ proportionally to $\dot{e}^2$. We suggested a tentative explanation of this effect, according to which the increase in the diffusion coefficient under plastic deformation is ascribed to the development of an excess number of vacancies during the movement of the dislocations.

5. An expression was found for the coefficient of softening of a material at high temperature under load.

6. The hypothesis was advanced that the resistance of metals to deformation at high temperatures cannot be fully explained by the diffusion coefficient when obtained under normal conditions. For this to be alone, one has to take into account the variation in the diffusion coefficient arising from variation of the deformation rate.

REFERENCES

1. BERGESS, H. and SMOLUCHOWSKY, R. J. Appl. Phys., 26, No. 4 1955.

2. BERKOWITZ, A.; JAMOT, F.; and NIX, F. Phys. Rev., 95, 1185, 1954.

3. Metals Handbook. ASM. Clevland, 1948.

4. DEKHTYAR, I. Ya. DAN SSSR, [Reports of Acad. Sci. USSR], 85, No. 3, 1952.

5. GERTSRIKEN, S. D. and DEKHTYAR, I. Ya. Paper Read at the International Conference on the Peaceful Use of Atomic Energy, Vol. 15. Geneva, 1955.

6. BOZORT, P. M. Ferromagnetism. GITTL, 1956.

7. ZENER, C. Imprefections in Nearly Perfect Crystals, 289, No. 9. 1952.

8. RAYSKIY, S. M. and SMIRNOV, V. G. Fizicheskiye osnovy metoda radioaktivnych indikatorov. (Physical bases of the Method of Radioactive Indicators), GITTL, M., 1956.

9. NACHTRIEB, N. H. and HANDLER, G. Acta met., No. 6. 1954.

10. BUFFINGTON, F. and COHEN, M. J. Metals, 4, No. 8. 1952.

11. DEKHTYAR, I. Ya. Voprozy fizike metallov i metallovedeniya (Problems of Physics of Metals and of Metallography), Coll. of Scientific Works IMF. Acad. Sci. USSR, No. 7. 1956.

12. DEKHTYAR, I. Ya. and OSIPOV, K. A. Reports of Acad. Sci. SSSR, 104, No. 2, 1955.

13. SEITZ, F. Advances in Phys. 1, 1952; Acta Met., 1, 1953.

SOME RESULTS OF A STUDY OF THE SELF-DIFFUSION OF IRON AND PROBLEMS OF HEAT RESISTANCE

B. M. Noskov

The activation energy of self-diffusion is a function of the bond energy of the crystal lattice. Hence data on self-diffusion made it possible to evaluate the interatomic bonds in metals and the properties of metals which depend on these bonds. Specifically the activation energy of self-diffusion can be considered as one of the physical characteristics of heat resistance in alloys.

A definite relationship between the bond energy and the activation energy of diffusion has been established so far only in the case of self-diffusion where $\frac{E_a}{E_{bee}} = 0.67$ for a face-centered lattice and $\frac{E_a}{E_{bee}} = 0.85$ for a body-centered lattice.

There is no such quantitative relationship for inhomogeneous diffusion. However, since inhomogeneous diffusion is related to the self-diffusion of the atoms of the solvent, the data on it do, at least indirectly express the magnitude of the interatomic bonds in the region of the diffusing solute atom.

It will be shown below that the alloying elements equally influence the self-diffusion of iron and the diffusion of cobalt. Consequently, data on inhomogeneous diffusion may also be used to discover the qualitative influence of the alloy components on the

strength of atomic interaction.

It has been established that the diffusion process is very easily affected by the composition of the diffusion medium. The presence of very small quantities of foreign atoms may greatly change the diffusion characteristics. We may expect the influence of an alloy component to be determined not only by its quantitative content but also by the elements themselves which compose the alloy. Since today's heat-resistant alloys are usually multicomponent systems, the study of the influence of the alloying components on the self-diffusion constants is particularly important.

Besides the composition of the alloy structure also greatly influences the diffusion constants since the inhomogeneity of the diffusion process arising from the difference in diffusion with in the body of the grain and in the boundary layer determines the high sensitivity of this process. The connection between the alloy's composition, the diffusion-activation energy and its heat-resistance may only be considered under structurally identical conditions.

A study of the influence of the composition of alloys and their structure on the diffusion process was made at the Gor'kiy State University.

The influence of manganese, chromium, nickel, vanadium and carbon on the self-diffusion and diffusion of iron and cobalt in certain alloys with an iron cobalt base was investigated and the results of the work are shown in Fig. 1-5.

We can see from Fig. 1 that an increase ranging up to 4% in the manganese content, the alloy leads to a constant increase of the diffusion-activation energy but a further increase (up to 8%) results in a decline. Nevertheless with 8% Mn it is still higher than in

pure iron. The variation in activation energy with a greater manganese content is exactly similar to self-diffusion of iron and the diffusion of cobalt, both in body-centered and intercrystalline structures.

A study of the influence of chromium on diffusion in cobalt-chromium alloys has shown that increasing the chromium content up to 7% leads to a rise in the activation energy and self-diffusion of cobalt and the diffusion of iron. A comparison of these results with the data provided by P. L. Gruzin [1] on the influence of chromium on self-diffusion in iron shows the complete similarity of the influence of chromium in both iron-chromium and cobalt-chromium alloys. Chromium has a similar influence on the diffusion of cobalt in an iron-nickel-chromium alloy as well.

An increase in the nickel content of a cobalt-nickel alloy up to 4% leads to an increase in cobalt's activation energy of self-diffusion but a further increase in the nickel concentration causes it to diminish; when the nickel content is 30%, the activation energy is even less than the activation energy of self-diffusion in pure cobalt. Nickel has the same in the diffusion effect of iron in cobalt-nickel alloys.

We also studied the influence of carbon concentration on the diffusion of cobalt in iron-carbon and iron-nickel-carbon alloys. A comparison of the results with the data obtained by P. L. Gruzin, Yu. V. Kornev, and G. V. Kurdyumov [2] and with the work of P. L. Gruzin and Yu. V. Kuznetsov [3] on the influence of carbon on the self-diffusion of iron in these alloys shows that a higher carbon content leads in every case to a decrease in activation energy and a certain addition of carbon produces an approximately equal decrease

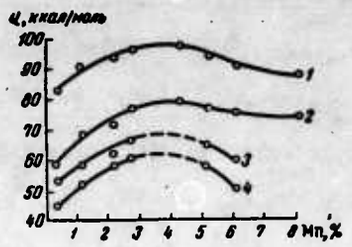

Fig. 1. Dependence of E_a on manganese concentration in an iron-manganese alloy. 1) body; 2) intercrystallitic self-diffusion of iron; 3) body; 4) intercrystallitic diffusion of cobalt.

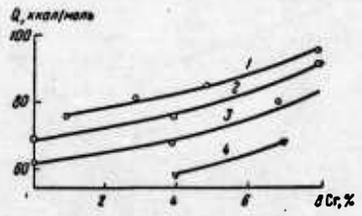

Fig. 2. Dependence of E_a on chromium concentration. Diffusion: 1) Co in a Fe-Ni alloy; 2) Fe in a Fe-Cr alloy; 3) Co, 4) Fe in a Co-Cr alloy.

in the activation energy in each instance.

A study of the influence of small additions of vanadium on the self-diffusion of iron showed that an addition of 2.13 atom % V reduces the activation energy of self-diffusion to 63,000 cal/mole. According to data obtained by V. A. Il'ina and V. K. Kritskayo [4], an addition of 2.3 atom % leads to a decrease in the bond strength and an increase in dynamic distortions of the crystal lattice, corresponding to the decrease in the activation energy of self-diffusion which we have observed.

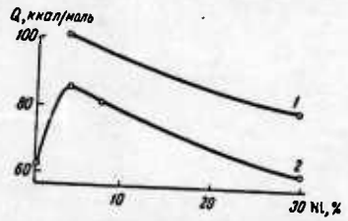

Fig. 3. Dependence of E_a on nickel concentration. Diffusion in a Co-Ni alloy: 1) Fe, 2) Co.

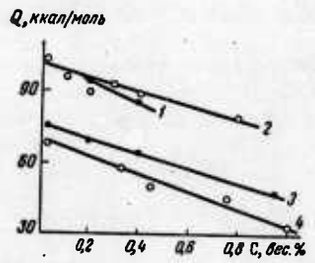

Fig. 4. Dependence of E_a on carbon concentration. Diffusion of Co in the alloys: 1) Fe-Ni-C; 2) Fe-C; self-diffusion of Fe in the alloys: 3) Fe-Ni-C [3]: 4) Fe-C [2].

As we can see from Figs. 1-5, the influence of the alloying elements both on self-diffusion and on diffusion is the same. The curves of concentration-dependence of the activation energy are parallel to each other. This enables us to use the data on the inhomogeneous diffusion of atoms related because of their chemical nature for qualitative evaluation of the influence of the alloy components.

We should, however, point out that although in some systems (Fe-Mn, Co-Cr) inhomogeneous diffusion proceeds in conjunction with a lower activation energy as compared with self-diffusion, in other systems (Co-Ni, Fe-C, Fe-Ni-C) the reverse occurs. This indicates a difference in the nature of the interaction of two or three different atoms and shows that not only is the overall quantity of alloying elements important, in alloying, but also their number and nature.

Investigation shows that additions of manganese and chromium increases the heat resistance of iron and its alloys, while additions of vanadium and carbon have an unfavorable effect. But this conclusion is valid only for alloys with the same structure.

A study of the influence of the structure of alloys on self-diffusion has shown that the martensitic transformation, which produces a great number of internal separation planes, increases the self-diffusion coefficient by influencing diffusion over grain boundaries. This leads to the formation of a break in the straight line showing the dependence of log $\underline{D}$ on $\frac{1}{T}$. P. L. Gruzin, Ye. V. Kuznetsov, and G. V. Kurdyumov [5] have established that alloys which retain their austenitic structure when cooled to room temperature do not produce such a break, and that the latter is only

observed in specimens cooled to a point below that of the martensitic transition. Since the diffusion tests were carried out at considerably higher temperatures than that required for the transformation of martensite back into austenite, it followed that the lattice distortions along the former boundaries of the martensite crystals and blocks are retained to a considerable degree in the austenite grains and only disappear after a period of time. The existence of such intragrain slip boundaries ensures accelerated diffusion paths in addition to the normal grain boundaries, and gives rise to increased coefficients in the low-temperature zone, since a certain average ("apparent") coefficient (the result of simultaneous body and intercrystallitic diffusion is measured). Gradual destruction of the traces of these intragranular slip planes brings the measured diffusion coefficient nearer to the coefficient of homogeneous body diffusion. It does not make a difference here whether the number of bands decreases gradually or whether the crystal lattice is gradually restored along all the bands, both cause a decrease in the diffusion coefficients.

In collaboration with Ye. V. Kuznetsov, G. V. Shcherbetinskiy, G. K. Borisov, and Ye. I. Shevin we investigated the influence of the intragranular separation boundaries on diffusion, testing the following alloys: iron-nickel-carbon (24% Ni, 0.9% C); iron-nickel-carbon (19.85% Ni, 0.95% C); and iron-nickel-chromium (25% Ni, 5% Cr).

All these alloys retain their austenitic structure when cooled to room temperature. To ensure a martensitic structure, the specimens were soaked 30 - 40 minutes at the temperature of liquid oxygen (-183°). Some of the specimens which had undergone martensite transformation were reheated, which restored the austenite. The

heating took place at various temperatures (for a prescribed time) and at a different time (at a stipulated temperature).

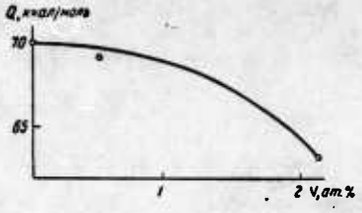

Fig. 5. Dependence of E_a on vanadium concentration in an iron-vanadium alloy.

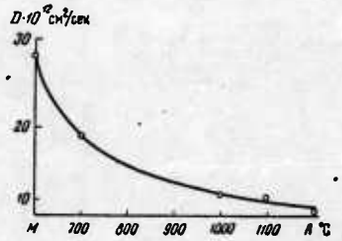

Fig. 6. Dependence of D on temperature of preliminary heating for 1 hour. Alloy containing 24% Ni, diffusion at 950°, duration of diffusion 170 hours.

The coefficients of self-diffusion were determined with the aid of radioactive isotope Fe^{59} by the integral-residual method [6] and by the absorption "ratios method" [7]. The results of the measurements show that the "apparent" diffusion coefficient for martensite specimens is in all cases higher than for the austenities which had not undergone the martensite transformation. The restoration of the austenitic structure after a heating for one hour leads to a drop in

the diffusion coefficient; the higher the temperature of the one-hour heating that restores the austenite (Fig. 6), the steeper the drop.

The greater the decrease in the diffusion coefficient, the longer is the heating time to restore the austenite at a prescribed temperature (Fig. 7). Consequently, if the martensite specimens are not heated long enough at a temperature above the transition of martensite to austenite, not all the traces of martensitic transformation are entirely eliminated. An identical value for the coefficient of self-diffusion and, consequently, the elimination to an equal degree of the traces of martensitic transformation are obtained under the following conditions:

При температуре, °С	Сплав железо — никель — углерод за часы нагрева	Сплав железо — никель — хром за часы нагрева
800	100	—
900	20	36
250	8	16
1000	4	9
1050	—	4,5
1000	1	2

The elimination of the traces of preliminary martensitic transformation is an activated process, described by the equation

$$\tau = \tau_0 e^{Q/RT},$$

in which τ is the time necessary for the elimination of the traces of martensitic transformation.

The activation energy of this process (Fig. 8) is equal to 45,000 cal/mole for the iron-nickel-carbon alloy, and 44,000 cal/mole

for the iron-nickel-chromium.

The elimination of the traces of martensite transformation appears to us as a diffusion process taking place in the zones of the former slip planes. Consequently, the activation energy of this process must be close to the activation energy of diffusion on the grain boundaries. Certain indirect considerations enable us to assume this closeness. According to other data, the activation energy of intercrystalline self-diffusion in iron is 75-80% of the activation energy of body self-diffusion [8]. In iron-nickel-carbon alloys the activation energy of intragranular self-diffusion amounts to 58,000 kcal/mole [3]. If we assume that the same correlation holds for the activation energies of intra-and intercrystalline self-diffusion in this alloy, then the quantity Q = 45,000 kcal/mole is very close to the assumed energy value for diffusion on the grain boundaries.

If the process of regularizing the crystal lattice of austenite, which involves elimination of the traces of martensitic transformation, is a diffusion process and takes place with an activation energy close to that of intercrystalline diffusion, then we feel that the following conclusion may be drawn.

A long period of distortion in the crystal lattice in the zone where traces of former martensite slip planes exist gives rise to a state of high diffusion permeability for the duration of these traces in austenite obtained through this transformation of martensite. Self-diffusion in such a medium must take place with a lower activation energy, which means lower heat-resistant properties in the alloy. If the alloy serves under conditions of rapidly fluctuating temperatures falling below the point of martensitic transformation, at high temperatures (900-800), it will in practice retain the disordered

crystal lattice caused by the traces of former martensitic transformations during the whole period of service, provided that the time between the alternation of high and low temperatures is less than 20 - 100 hours, respectively. An alloy of this kind will have a high diffusion permeability and a low activation energy of self-diffusion while in service and, consequently, lower heat resistance. Hence, alloy which do not undergo such structural transformations in the given temperature interval are preferable for use under conditions of alternating high and low temperatures.

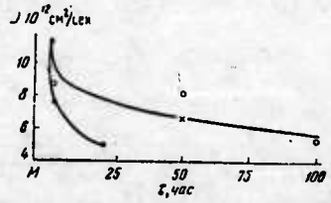

Fig. 7. Dependence of D on the preheating time at constant temperature.

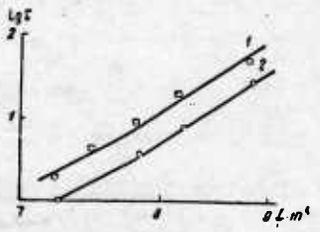

Fig. 8. Dependence of log τ on $\frac{1}{T}$ for an iron-nickel-chromium alloy (1) and an iron-nickel-carbon alloy (2).

REFERENCES

1. GRUZIN, P. L. DAN SSSR, [Reports of Acad. Sc. USSR]100, 1955.

2. GRUZIN, P. L.; KORNEV, Yu. V.; and KURDYUMOV, G. V. DAN SSSR, 80, 1951.

3. GRUZIN, P. L. and KUZNETSOV, Ye. V. DAN SSSR, 93, 1953.

4. IL'INA, V. A. and KRITSKAYA, V. K. DAN SSSR, 100, 1955.

5. GRUZIN, P. L.; KUZNETSOV, Ye. V.; and KURDYUMOV, G. V. DAN SSSR, 93, 1953.

6. GRUZIN, P. L. DAN SSSR, 86, 1952.

7. GRUZIN, P. L. and LITVIN, D. F. DAN SSSR, 94, 1954.

8. GRUZIN, P. L.; NOSKOV, B. M.; and SHIRIKOV, V. I. DAN SSR, 99, 1954.

CONCERNING THE CONNECTION BETWEEN DIFFUSION AND HEAT RESISTANCE IN ALLOYS

A. Ya. Shinyayev

Great attention is being given at present to the study of diffusion in heat-resistant alloys. This research is being conducted for the reason that diffusion processes exert a great influence on the most important characteristics of alloys and particularly on their heat resistance [1, 2]. In this connection the study of diffusion in nickel alloys is now assuming very great significance.

Nickel alloys have been carefully investigated from the viewpoint of improving their mechanical properties by means of alloying. A study of the heat resistance of these alloys made by Prof. I. M. Kornilov and others has shown that heat resistance is considerably increased by adding nickel, titanium, chromium, tungsten, aluminum, and other elements [3] to the solid solution. The high heat-resistance of alloys based on nickel corresponds to the transition zone from solid solutions to heterophase alloys and can only be attained by the simultaneous addition of several (five, seven or nine) elements to the nickel solid solution. The maximum heat-resistance increases stepwise during the transition from binary to ternary, quaternary, and more complex alloys.

We formulated the problem of making a systematic study of diffusion in nickel alloys of those systems which are the most important from the viewpoint of heat resistance. For our investigation we took the binary nickel-titanium, the ternary nickel-titanium-chromium and the quinary nickel-titanium-chromium-tungsten-aluminum systems. The above-mentioned systems had already been carefully studied from the viewpoint of heat resistance [5-8] and data for a wide temperature interval had been obtained. It was therefore of great interest to investigate diffusion in the said system in order to establish the connection between diffusion and heat resistance.

We should point out that the investigation of diffusion in multicomponent alloys, for example, alloys of the quinary system nickel-titanium-chromium-tungsten-aluminum, is a new and very complex problem. In general, the study has been concerned with the concentration-dependence of the diffusion coefficient of the atoms of the alloy base, which however cannot show the actual change in atomic interaction in the given system. This is explained by the fact that in the study of diffusion in complex systems there is always some uncertainty as to the data obtained on atomic interaction, occurring as a result of the concentration-dependence of the diffusion coefficient. But in cases where the concentration-dependence is more sharply defined than the change in atomic interaction, we may obtain an entirely distorted picture of this change in alloys when investigating diffusion. In order to compare the data on diffusion and heat resistance, we should study diffusion in such a way that the experimental data we obtain represent the true change in atomic interaction when passing from one alloy of any given system to another.

A considerable variation in the percentage of nickel content (the base) and of the other components of the alloy occurred in the alloys of the systems mentioned. In order to avoid the influence of differences in the concentration of the components on the diffusion characteristics, we chose as a diffusing substance an element that was not directly part of the reference alloy. The diffusion coefficient of the element in question had to be equal to or higher than that of any of the components of the alloy. This is because of the fact that the softening of the crystal lattice of the alloy may be caused at high temperatures by the most mobile component--which diffuses easily.

The above-mentioned requirements are fully met by iron. It is not directly a component of the alloy under study and, furthermore, it can be traced by the radio-active isotope Fe^{59}.

Research [9] has shown that the addition of such high-melting admixtures as molybdenum, nicobium, titanium, and vanadium to the matrix of the iron-nickel alloy reduces the value of the self-diffusion coefficient of iron and increases the activation energy of the process. As has also been shown by P. L. Gruzin [10], chromium sharply increases the self-diffusion energy and reduces the self-diffusion coefficient of iron.

In view of the fact that metals similar to iron and nickel have many physical properties in common, we were able to assume that the addition of titanium, chromium, and other elements into the nickel-base solid solution must have the same effect as in the case of iron. A convincing argument in support of this assumption is provided by the study of atomic interaction in nickel alloys made by G. V. Kurdyumov and N. T. Travina [11]. They showed that the

value of the mean square deviation of the atoms from the state of equilibrium increases when chromium, titanium, and aluminum are added to the nickel matrix. The greatest decrease in the mean square deviation was observed when these elements were added simultaneously. It follows from this that by measuring the diffusion rate of iron in nickel alloys we may obtain the diffusion coefficient, which characterizes by its magnitude the upper level of the diffusion coefficients of the alloy components.

Since the original elements (nickel and chromium) contained small admixtures of iron (up to 0.13%), neither the addition of less than 0.5 mg per 2 cm^2 of radioactive iron to the given alloy now the diffusion of these radioactive atoms could affect to any extent the properties of the alloys under investigation.

In accordance with our task, which was to compare the diffusion characteristics of alloys with their heat resistance, we chose the zones of the above-mentioned systems in which maximum heat resistance is found.

The experiments on diffusion and heat resistance were carried out with specimens identical in structure and compositon, for which purpose we used the same starting materials. The alloys were melted in a high-frequency furnace under a slag of Al_2O_3, MgO, and Cao in the ratio of 48:7:45. As starting material, we used 99.8% pure electrolytic nickel 98.5% pure metallic titanium, 99.05% pure alumothermic chromium, 99.95% pure tungsten and 99.8% pure electrolytic aluminum.

The melted ingots were subjected to exactly the same annealing conditions as were established in the tests for heat resistance. This made it possible to avoid the influence of structure on the

alloy characteristics.

Investigation of the microstructure showed our data coincided closely with the data obtained by others [5-8].

The diffusion coefficients were measured by the method we proposed in an earlier study [12] based on the use of electrolytic polishing to remove thin layers from the specimen. Disks 15 mm in diameter and 2-3 mm thick were made from the ingots for use in this method.

An electrolytic bath containing a solution of radioactive iron and ammonium oxalate was used to deposit a thin layer of radioactive iron Fe^{59} on one of the polished surfaces of the disk. After diffusion annealing at a constant temperature by electrolytic polishing, thin layers (8-10 microns) were removed from the specimen. The intensity of the radioactive radiation from the electrolyte in which the electrolytic polishing took place and the specific activity of the radioactive iron in each layer removed were determined by direct measurement. The error of measurement of the diffusion coefficient by this method was 5-8%.

Diffusion in a Nickel-Titanium System

Titanium is one of the most important alloying elements for heat-resistant alloys. Its addition to nickel alloys improves many of their mechanical properties and, as shown by experimental data, results in considerably greater resistance to deformation at high temperatures.

It follows from the phase diagram of the nickel-titanium system [13] that the solubility of titanium in nickel within the temperature interval 800-1200° is 8-11% by weight. When the titanium content

rises above the limit of solubility at a given temperature, a phase forms in the alloys, based on the compound Ni_3Ti. The chemical compound Ni_3Ti has a hexagonal lattice, while the solid solution of titanium in nickel has a face-centered cubic lattice.

The investigation of heat resistance in alloys of the nickel-titanium system [5] has shown that at 800° the composition-heat resistance curve reaches a clearly defined maximum which relates to the zone in which the nickel solid solution is saturated with titanium and corresponds to alloys containing 8-10% Ti by weight.

We chose alloys of the nickel-titanium system relative to the zone of maximum heat resistance for our study of diffusion. The titanium content in these alloys was 4, 6, 8, 10.6 and 14% by weight.

The investigation has shown that in alloys with a titanium content of up to 8% in weight inclusive, the solid solution had a large-grain polyhedral structure and that alloys containing 10.6 and 14% by weight had a clearly defined two-phase structure. The largest polyhedrons in the solid solution had a diameter of 3-4 mm.

The study of diffusion was made out at 950, 960, 1050, 1093, and 1247°. The diffusion coefficients of iron in nickel-titanium alloys at these temperatures are shown in Table 1.

Fig. 1 shows graphically the variation of the diffusion coefficients $\underline{D}$ when the titanium content in the alloy is increased. As we see, the value of $\underline{D}$ decreases with the increase in titanium and attains a minimum at 950° in an alloy containing 8% Ti by weight.

If there is a further increase in titanium in the alloys, $\underline{D}$ increases. If the temperature increases the minimum value of $\underline{D}$ is observed in alloys containing a small quantity of titanium. At 1093° the minimum of $\underline{D}$ corresponds to 6% Ti by weight, and at higher tem-

peratures it is entirely displaced into the zone of dilute solid solutions.

TABLE 1

Diffusion Coefficients D, the Pre-exponential Multiplier D_0 and the Activation energy E of Iron Diffusion in Alloys of the Nickel-Titanium System

Титан, вес. %	$D \cdot 10^{11}$ см²/сек					Энергия активации диффузии E, кал/г-атом	Значение предэкспоненц. множителя D_0, см²/сек
	950°	960°	1050°	1095°	1245°		
4	0,31			3,2	49,9	62,8	1,55
6	0,21	0,31	1,75	2,9	52	68,6	3,9
8	0,12	0,16	1,44	3,0	51,3	73,1	$1,6 \cdot 10^1$
10,6	0,2			4,5	71,1	71,2	6,8
14	0,125			3,0	45,2	73,0	$1,5 \cdot 10^1$

The values of the activation energy E and the pre-exponential multiplier D_0 of the diffusion process, were calculated from the values of the diffusion coefficients given in Table 1, and are given in the same Table.

The data obtained on diffusion in alloys of the nickel-titanium system make it possible to draw the conclusion that the addition of titanium to the nickel solid solution increases the forces of atomic interaction in the crystal lattice of the alloy. These forces attain a maximum at temperatures of 950-1000° in the saturated solid-solution zone.

In inhomogeneous alloys where there are coagulated phase for-

mations based on Ni_3Ti, the value of the bonds decreases, but if there is a great deal of the Ni_3Ti excess phase the forces of atomic interaction again increases.

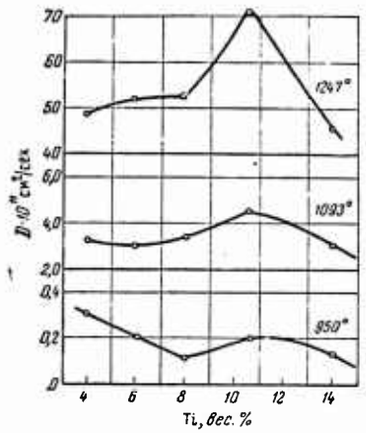

Fig. 1. Iron diffusion coefficients in alloys of the nickel-titanium system, depending on the titanium content at various temperatures.

Diffusion in a Nickel-Chromium-Titanium System

The ternary system nickel-titanium-chromium was investigated [5, 6] and various parallel sections of this system were studied. Microstructural x-ray and other investigations of alloys with differing titanium contents showed that the solubility of titanium at temperatures up to 800° varies little and amounts to about 2.2% by weight; at a temperature above 900° it increases considerably.

A careful study of the heat resistance of alloys of this system with a constant chromium content (20% by weight) was made [5]. It follows from the results that the zone of maximum heat resistance varies in a complex way according to temperature. At low temperatures

the greatest heat-resistant alloys correspond to saturation zones with precipitation of the second phase in the form of finely dispersed inclusions. At elevated temperatures from 500 to 750° the zone of maximum heat resistance is displaced towards alloys with a lower titanium content, but at a temperature 750-800° it shifts to alloys with a higher titanium content. In the case of a further increase in temperature (above 1000°), the zone of maximum heat resistance is displaced monotonieally toward unsaturated solid solutions.

We undertook the study of diffusion in a wide temperature range in order to compare the data obtained with existing data on heat resistance in these alloys. This enabled us to discover the nature of the temperature-dependence of the curve of maximum heat resistance from the viewpoint of diffusion processes.

We chose alloys with a constant 20% chromium content for our investigation of diffusion. The titanium content amounted to 1, 2.5, 3.4, 5, and 7 % by weight. The alloys were subjected to thermal treatment under the following conditions at 1200° for 6 hours, at 1150° for 18 hours, and at 800° for 24 hours (with air cooling).

Examination of the microstructure of these alloys showed that polyhedrons were observed in the solid solution with a titanium content of up to 3.4% by weight. Alloys with a titanium content of 5 and 7% by weight contained an excess phase in the form of elongated thin laminae. The grain size in these alloys was somewhat smaller than in the nickel-titanium system, although the structure remained large-grain to a high degree, the largest grain diameter was 2-3mm).

The results of our measurement of the iron diffusion coefficients in alloys of the nickel-chromium-titanium system at 960, 995, 1010,

1218, and 1265° are shown in Table 2. The duration of diffusion annealing at these temperatures varied from 300 to 4 hours accordingly.

On the basis of the experimental data shown in Table 2, we plotted the curves of the variation in the diffusion coefficient according to the composition of the alloy at the experimental temperatures. Fig. 2 as we see there, minima are observable on the curves. At temperatures of 995 - 1050°, the minimum value relates to the alloys containing 3.4% Ti by weight; at a higher temperature it shifts towards alloys with a lower titanium content, and at 1218 -1250° it shifts to the zone of unsaturated solid solutions with a titanium content of about 1%.

TABLE 2

Iron Diffusion Coefficient Activation Energy and the Pre-exponential Multiplier in Alloys of the Nickel-Chromium-Titanium System

Титан, вес. %	$D \cdot 10^{11}$ см²/сек						Энергия активации диффузии E, кал/г-атом	Значение предэкспоненциального множителя D_0 см²/сек
	960°	995°	1016°	1050°	1218°	1256°		
1		0,33	0,29	1,4	15,3	25,4	65,8	0,6
2,5		0,17	0,26	0,64	26,3	38,8	80,0	$1,16 \cdot 10^1$
3,4	0,06	0,14	0,2	0,42	20,9	35,2	84,0	$4,45 \cdot 10^2$
5		0,25	0,29	1,18	37,0	51,8	82,6	$4,4 \cdot 10^2$
7		0,20	0,29	0,69	—	34,7	78,2	$6,4 \cdot 10^1$

We should point out that the alloys of the nickel-titanium chromium system are less oxidation-resistant than those of the nickel-titanium system. Reliable data on the diffusion coefficient were only obtained when diffusion annealing took place under the following conditions. The specimens of the alloys were sealed into double quartz tubes under a vacuum of 10^{-3} - 10^{-4} mm Hg; with small strips of titanium between the tubes (Fig. 3). This was to avoid oxidation of the surface of the specimens and to ensure that the experimental conditions could easily be reproduced.

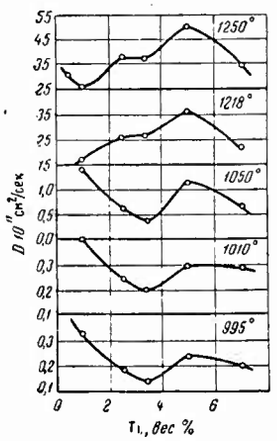

Fig. 2. Dependence of diffusion coefficient in alloys of the nickel-chromium-titanium system on the titanium content at various temperatures.

As shown by investigation of the thickness of the oxide layer which forms after diffusion annealing, the greatest oxidation occurred in the case of the alloy containing 3.4% Ti; alloys containing 2.5 and 5% Ti by weight oxidized to a lesser degree, and with a content of 1 and 7% Ti in weight there was no oxidation at all for all practical purposes.

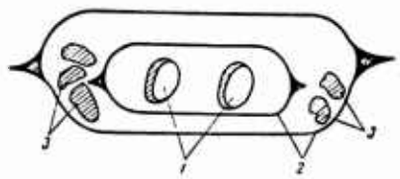

Fig. 3. Cross section of ampule with specimens for diffusion annealing. 1) specimens; 2) quartz ampules; 3) titanium.

The value of the activation energy of the diffusion process and of the pre-exponential multiplier calculated from the results of measurements of the diffusion coefficient, are shown in Table 2. It follows from this Table that the maximum value of the activation energy and the pre-exponential multiplier corresponds to the alloy containing 3.4% Ti. In the case of a lower titanium content E and D_0 decrease sharply, and in case of higher contents, they decrease, though to a lesser degree than in solid-solution alloys.

Diffusion in the System Nickel-Chromium-Tungsten-Aluminum-Titanium

The studies of heat resistance and other properties of the system nickel-chromium-tungsten-aluminum-titanium, described in [8], showed that the heat resistance of alloys of this system is considerably higher than of that of the nickel-titanium and nickel-chromium-titanium systems, although the melting point is lower. Consequently, it was of interest to measure the diffusion coefficients of iron in this system. It has been shown [8] that the solubility of titanium in this quinary system is lower than in alloys of the

nickel-chromium-titanium and the nickel-titanium systems and is about 1% at temperatures up to 1100°. At higher temperatures, the solubility of titanium sharply increases. At temperatures of about 600°, the most highly heat-resistant alloys correspond to the zone of supersaturated solid solutions with the precipitation of a finely dispersed phase. When the temperature is increases up to 750°, the zone of maximum heat resistance is shifted to alloys with a lower titanium content. However, at higher temperatures (850 -950°), the temperature dependence curve of alloys with maximum heat resistance changes direction and shifts towards alloys with a higher titanium content. After passing through the inflection, the zone of alloys with maximum heat resistance shifted regularily toward unsaturated solid solutions with a further increase of temperature (1000-1250°).

Specimens corresponding in composition to the alloys used for the study of heat resistance in [8] were made for the study of diffusion in the given system. In all alloys there was a constant content of the following elements: 20% chromium, 6% tungsten, and 4.5% aluminum. The titanium content varied with the matrix and amounted to 0, 0.5, 1, 2, 3, 5, 7, 6, and 9% by weight. The alloys underwent heat treatment at 1200° for 4 hours.

The investigations showed that in alloys with a titanium content up to 3% had a solid-solution structure with a considerably smaller grain size (of the order of 300-400 microns) than in the case of nickel-titanium and nickel-chromium-titanium systems. In the case of a titanium content of 3% and more in the given quinary system we observed precipitation of an intermetallic phase based on Ni_3Al on the boundaries and in the body of the grains; with a further increase in titanium content, the excess phase precipitated in even larger

quantities.

The investigation of diffusion was made at temperatures of 955, 1060, 1165, and 1250°. No oxidation of the specimens surface was observed at these temperatures during diffusion annealing, the duration of which varied from 400 to 4 hours respectively.

The results of the investigation of the diffusion of iron in alloys of the nickel-titanium-chromium-tungsten-aluminum system are shown in Table 3.

Figure 4 shows a graph of the variation of the value D with the percentage of titanium in the alloys of the quinary system at various temperatures. As we see, the curves have clear-cut minima, at which D is 80-100% lower than in the neighboring (with respect to the minium) alloys. If we take into account that this variation in the quantity D in alloys corresponds to a variation in the temperature of diffusion annealing of 50°, we can conclude that the observed variations of D by 80-100% may indicate considerable variations in the forces of atomic interaction in alloys with a different titanium content.

It also follows from Fig. 4 that the position of the minimum diffusion coefficient in the alloys of the system under investigation has a clearly defined temperature-dependence. In the range of the investigated temperatures (955-1250°), the minimum diffusion coefficients regularly shift from heterophase alloys to the unsaturated solid-solution zone as the temperature increases.

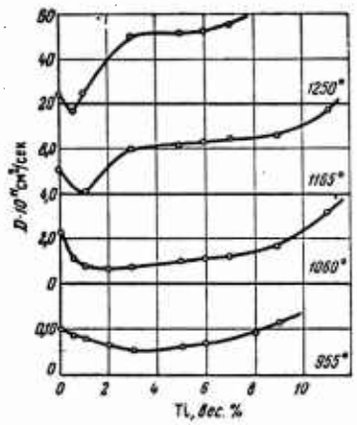

Fig. 4. Iron diffusion coefficients in alloys of the nickel-chromium-tungsten-aluminum-titanium system, according to the titanium content at various temperatures.

TABLE 3

Diffusion Coefficients, Activation Energy of Diffusion and the Pre-exponential Multiplier in Alloys of the Nickel-Chromium-Tungsten-Aluminum-Titanium System

Титан, вес. %	$D \cdot 10^{11}$ см²/сек				Энергия активации диффузии E, ккал/г-атом	Значение предэкспоненциального множителя D_0, см²/сек
	955°	1060°	1165°	1250°		
0	0,098	2,3	6,2	29,1	71,8	3,2
0,5	0,082	1,03	—	19,7	69,7	2,0
1	0,08	0,78	4,0	21,0	70,4	2,2
2	0,072	0,63	—	33	76,1	$3,2 \cdot 10^1$
3	0,047	0,7	8,2	51,5	87,6	$1,7 \cdot 10^3$
5	0,065	0,97	8,3	52,6	85,5	$1 \cdot 10^2$
7	0,052	1,14	5,9	55,3	80	$1,6 \cdot 10^2$
9	0,13	1,6	8,1	Оплавился	76,3	$5,7 \cdot 10^1$

On the basis of measuring the diffusion coefficients we calculated the values of the activation energy of the diffusion process

E and of the pre-exponential multiplier D_o, which are also shown in Table 3. It follows from this Table that the diffusion characteristics of E and D_o increase with an increase in titanium content in the alloys, and attain a maximum when the Ti content is about 3% by weight. In the case of a further increase in titanium, the values of E and D_o decrease.

Our investigation of the dependence of iron diffusion on titanium content in the nickel-titanium, nickel-chromium-titanium and nickel-chromium-tungsten-aluminum-titanium system shows that the curves of the dependence of the diffusion coefficient on the composition of the alloy have features that are characteristic for all systems. At comparatively low temperatures (900-1000°) we observe clearly defined minima in the zone of transition from solid solutions to heterophase alloys on the curves of the variation of D according to the titanium content. When the temperature increases, the minimum point on this curve shifts towards the unsaturated solid solution.

For example, in the nickel-titanium system at temperatures of 950 and 1093°, the minimum value of D corresponds to alloys with a titanium content of 8 and 6%. In the nickel-chromium-titanium system at 995, 1010, and 1050°, the minimum value of D corresponds to alloys containing 3.4% Ti and at temperatures of 1218 and 1250° to alloys with 1%.

In the system nickel-titanium-chromium-tungsten-aluminum, at the investigation temperatures of 955, 1060, 1165, and 1250°, the minimum value of D corresponds to alloys with a titanium content of 3, 2, 1, and 0.5% respectively.

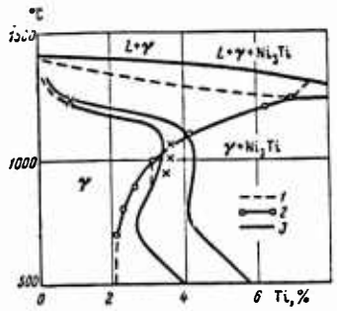

Fig. 5. Position of minima of the diffusion coefficient with respect to zone of maximum heat-resistance in alloys of the nickel-chromium-titanium system (curves 3) at the experimental temperatures. 1), 2) boundaries of solubility of titanium.

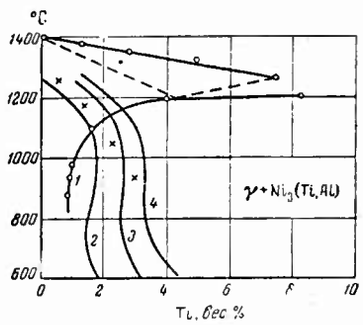

Fig. 6. Position of the minima of the diffusion coefficient with respect to zone of maximum heat-resistance in alloys of the nickel-chromium-tungsten-aluminum-titanium system (curves 2 and 4) at various temperatures. 1) boundary of solubility of titanium; 3) alloys with maximum heat resistance at corresponding temperatures.

If we compare the minimum values of D for the same alloys with the values at the corresponding temperatures of maximum heat

resistance, we notice that for all three systems these characteristics coincide, within the limits of accuracy of the experiment. Alloys containing 8-10.8% Ti possess maximum heat resistance at 800°. The minimum value of D at a temperature of 950° corresponds to the alloy containing 8% Ti (5).

The crosses in Fig. 5, which is taken from the research described in [6], indicate those alloys of the nickel-chromium-titanium system for which a minimum value of D eas obtained at the corresponding experimental temperatures. The zone of maximum heat resistance of the alloys of the system under consideration depending on temperature is also indicated by this Figure.

A comparison of the minimum values of the diffusion coefficient with the values of maximum heat resistance for a given temperature in the system nickel-chromium-tungsten-aluminum-titanium is given in Fig. 6.

As we see from Figs. 5 and 6, the crosses fall well with in the zones of maximum heat resistance of the alloys. It follows that the most heat-resistant alloys in the systems studied are those in which a minimum diffusion coefficient is observed. It also follows from the graphs that the minimum value of D and the zone of maximum heat resistance have the same temperature-dependence. We may conclude from this that in the systems studied the shifting of the zone of maximum heat resistance at temperatures above 950° is chiefly determined by the diffusion processes.

The study we made enables us to present a theoretical explanation of the temperature-dependence of the zone of the most highly heat-resistant alloys. The experimental data cited above show that in the alloys studied the diffusion process may be observed without the

application of stress, beginning at 850° in the nickel-titanium system at 900° in the nickel-chromium-titanium system, and at 950° in the nickel-tungsten-aluminum-titanium system.

This means that it is only at these temperatures that diffusion processes can begin to play a substantial part in the alloys of these systems in an unstressed state.

In the case of a state of stress, when the values of the coefficients may increase considerably, the diffusion processes affect the state of strength of the crystal lattice in the alloy at a lower temperature.

If we consider heat resistance at temperatures at which the diffusion coefficients have negligible values (in our systems 500-700°) and cannot play any part in the weakening of the crystal lattice, even under stress, then the magnitude of the interatomic forces (chemical composition) and the alloy structure will be of decisive importance. Since the influence of such an essential factor as diffusion is excluded at low temperatures, this fact should also affect the form of the composition and heat-resistant curves. Indeed, as it has been established in [8], in the study of heat resistance in the nickel-titanium-chromium-tungsten-aluminum system at 600°, the composition and heat-resistance curve is found to have a poorly defined maximum, whereas at temperatures of 800, 900, 1000°, when the diffusion mechanism comes into operation, a clearly outlined maximum is observed on the curves of the heat resistance which is dependent on the composition of the alloy. It is characteristic that at high temperatures the zone of maximum heat resistance is considerably narrower than at low temperatures.

An analysis of the curves of the temperature-dependence of the

zone of maximum heat resistance given in Figs 5 and 6 shows that the inflection divides them into two parts essentially different from the viewpoint of diffusion. One of these relates to the high-temperature zone in which the variation of heat resistance is wholly determined by diffusion, and the other part corresponds to the low-temperature zone in which diffusion plays no role. In the zone of the inflection, the role of diffusion is limited to a certain degree.

This makes it possible to conclude that the inflection of the curves for temperature-dependence of the zone of maximum heat resistance is a result of the diffusion factor of softening of the crystal lattice of the alloy. This conclusion enables us to give a single explanation for the whole run of the temperature-dependence curve, of the zone of maximum heat resistance, shown in Figs. 5 and 6. Indeed, at low temperatures (in nickel alloys up to 700°) heat resistance is determined by the strength of the interatomic bond and by the alloy structure. As shown by numerous experiments, heterophase alloys have maximum heat resistance at these temperatures.

It is well known that when the temperature increases the coagulation of precipitations is accelerated, resulting in a decline in heat resistance. Therefore the zone of the most highly heat-resistant allous shifts toward alloys containing a smaller quantity of titanium (the structural factor has substantial influence here). At a certain temperature, the diffusion displacements of atoms becomes noticeable, and heat resistance in the given chemical composition is determined by both structural and diffusion factors. The zone of the most highly heat-resistant alloys corresponds to heterophase alloys in which a minimum value for the diffusion coefficient and a maximum value for its activation energy are observed (temperature range 700 - 1100°).

As shown by investigation, at such temperatures the maximum value of the diffusion coefficient corresponds to alloys with a higher titanium content, and this explains the fact established by the experiment of I. I. Kornilov and others that the zone of heat-resistant alloys displaces towards a higher titanium content at temperatures of 700 - 1100° (See Figs. 5 and 6). At a higher temperature the fundamental cause of the weakening of crystal lattice is the diffusion processes. The diffusion coefficients are very high at these temperatures. As follows from our data on the measurement of diffusion coefficients and their comparison with data on heat resistance (see Figs. 5 and 6) the shift of the zone of highest heat-resistant alloys towards dilute solid solution beginning at a temperature of 1100° is wholly determined by diffusion. It follows from this that heat-resistant nickel alloys belong to the temperature interval 700-800°, which corresponds to the start of the inflection of the curves of maximum heat resistance depending on the alloy's composition and temperature. A very low diffusion rate ($\sim 10^{-15}$ cm^2/sec) is characteristic of this temperature interval. Above this temperature, a zone of alloys with limited heat resistance extends along the whole course of the curve (800 - 1100° for nickel alloys). At these temperatures, the alloys resist strain only for a limited time. Alloys corresponding to the temperature interval above 1100°, where the diffusion rate is high, become rapidly deformed under stress.

The study of the factor limiting the use of heat-resistant alloys at high temperatures is of great practical importance. On the basis of what has been described above, we may conclude that one of the most important of these factors is the development of diffusion, which leads to a decrease in the strength of the crystal lattice and weakening of the bonds between individual crystals. Hence, the study

of diffusion processes in an alloy to which admixtures are added in various concentrations can be of very great importance in the search for heat-resistant alloys suitable for use at high temperatures.

Since the development of diffusion in heat-resistant alloys (resulting in a decline in the crystal-lattice strength and the weakening of the bonds between the individual crystallites of the alloy) is the factor limiting the use of heat-resistant alloys at high temperatures, it might be thoroughly advisable to choose chemical compounds as a base for these alloys. As has been shown [14], there is a clear- cut minimum diffusion coefficient and a maximum activation energy in chemical compounds.

Chemical compounds, however, are characterized by greater brittleness. If it were possible therefore, to find a compound with good plastic properties, we could obtain an alloy based on it which would be greater in heat-resistance than any other combination of the given alloy components. Consequently, through modifying the alloy with this base by adding different quantities of admixtures and by measuring the level of the diffusion coefficients, it would be possible, taking the structure into account to find the right composition for an alloy which will have a minimum diffusion coefficient and, therefore, maximum heat resistance at the prescribed temperature.

REFERENCES

1. KURDYUMOV, G. V. Primeneniye izotopov v tekhnike, biologii, biokhimii i sel'skom khozyaystve. Konferentsiya v Zheneve. (The Use of Isotopes in Technology, Biology, Biochemistry, and Agriculture, Geneva Conference, Acad. Sci. USSR. 1955.

2. DEKHTYAR, I. Ya. Problemy fiziki metallov i metallovedeniya. (Problems of the Physics of Metals and Physical Metallurgy) Urals Branch of Acad. Sci., USSR Nr. 6.

3. KORNILOV, I. I. Reports of Acad. Sci., USSR. 106, 1956.

4. KORNILOV, I. I. Bull. Acad. SCi., USSR. (Tech. Sci. Dept). No. 1, 1956.

5. PRYAKHINA, L. I. Diss. Moscow, 1956.

6. KORNILOV, I. I. and KOSMODEM'YANSKIY, V. V. Bull. Acad. Sci., USSR (Tech. Sci. Dept). Nr. 2, 1955.

7. KORNILOV, I. I. and PRYAKHINA, L. I. Bull. Acad. Sci., USSR (Tech. Sci. Dept.) Nr. 7, 1956.

8. KORNILOV, I. I. and TITOV, F. M. Bull. Acad. Sci.,USSR (Tech. Sci. Dept) No. 10, 1956.

9. BOKSHTEYN, S. Z.; KAZAKOVA, V. A.; and MIRSKIY, L. M. Bull. Acad. Sci. USSR (Tech. Sci. Dept). No. 12, 1955.

10. GRUZIN, P. L. Reports of Acad. Sci., USSR. 100, 1955.

11. KURDYUMOV, G. V. and TRAVINA, N. T. Idem, 99, 1954.

12. NEYMAN, M. B. and SHINYAYEV, A. Ya. Idem, 96, 1954.

13. WALLBAUM, H. Arch. f. Eisenhüttenwesen, 14, 1941.

14. NEYMAN, M. B. and SHINYAYEV, A. Ya. Reports of Acad. Sci., USSR, 103, 1955.

DIFFUSION IN NICKEL-BASE SOLID SOLUTIONS

Yu. F. Babikova and P. L. Gruzin

Nickel is used as a base for several brands of heat-resistant alloys [1]. A characteristic feature of these alloys is that they are used in a hardened form, which is achieved by precipitation hardening. The preservation of the alloys in hardened form at high temperatures is determined to a considerable degree by the diffusion rate of the elements making up the base of the alloy and embodied in the hardening phase. At elevated temperatures, the more stable alloys will be those in which the diffusion of the basic elements proceeds slowly. In spite of this, however, diffusion in nickel-base solid solutions has not been studied up until now. Scientific literature contains only a few publications on this subject [2, 3, 4, 6].

In the present work we give data on the study of the diffusion of chromium in solid nickel-chromium solutions alloyed with titanium (see Table 1).

The compositions were chosen which ensured that at temperatures above 1000° the alloys were in the homogeneous solid-solution zone. The alloys were melted in a vacuum high-frequency furnace. The radioactive isotope Cr^{51} was used in the experiments for the study

of diffusion. The diffusion coefficients were determined by measuring the integral radioactivity of what remained of the specimen after layers were removed [5]. The results of the calculation of the mean values of the diffusion coefficients for the alloys are given in Table 2 and for one of the alloys, in Fig. 1. Table 3 gives the diffusion parameters of chromium for the alloys studied and also the self-diffusion parameters for nickel and the diffusion parameters of chromium for nichrome [2, and 3].

TABLE 1

Chemical Analysis of the Alloys

№ сплава	Содержание элементов, %							
	Ni	Cr	Ti	Al	Fe	Co	Cu	Si
1	Основа	10,15	2,69	0,18	0,35	0,50	0,05	0,12
2	»	9,60	3,70	0,12	0,31	0,45	0,05	0,16
3	»	10,00	4,80	0,10	0,31	0,45	0,06	0,10
4	»	18,82	3,12	0,10	0,37	0,50	Сл.	Сл.
5	»	28,42	3,00	0,20	0,30	0,80	»	»

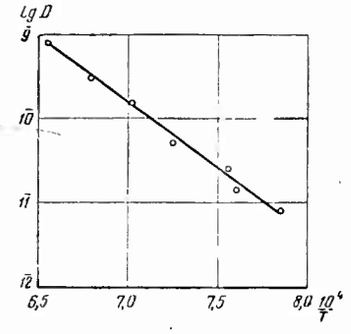

Fig. 1. Temperature-dependence of the diffusion coefficients of chromium for the alloy nickel-chromium (10%)-titanium (2.7%)

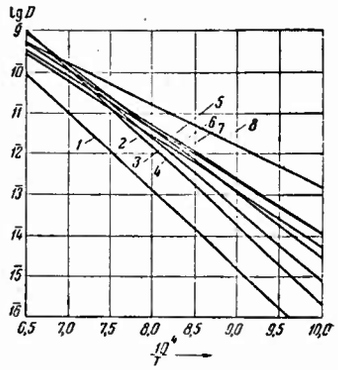

Fig. 2. Comparative graph of the temperature-dependence of diffusion coefficients.
1) self-diffusion of Cr; diffusion of chromium in the alloys: 2) Ni-Cr (28%) - Ti (3%); 3) Ni-Cr (19%) - T i (3%); 4) Ni (10%) - Cr (2.7%); 5) Ni-Cr (10%) - Ti (3.7%); 6) Ni-Cr (10%) - Ti (4.8%); 7) self-diffusion of Ni; 8) Cr in Ni.

TABLE 2

Mean Values of the Diffusion Coefficients of Chromium for Nickel-Chromium-Titanium Alloys

№ сплава	T, °C	D, см²·сек⁻¹	№ сплава	T, °C	D, см²·сек⁻¹
1	1250	$8 \cdot 10^{-10}$	3	1100	$4{,}0 \cdot 10^{-11}$
То же	1200	$3{,}1 \cdot 10^{-10}$	То же	1040	$1{,}3 \cdot 10^{-11}$
»	1150	$1{,}5 \cdot 10^{-10}$	»	1000	$8{,}6 \cdot 10^{-12}$
»	1100	$5{,}3 \cdot 10^{-11}$	4	1260	$1{,}0 \cdot 10^{-9}$
»	1050	$2{,}5 \cdot 10^{-11}$	То же	1200	$3{,}1 \cdot 10^{-10}$
»	1040	$1{,}3 \cdot 10^{-11}$	»	1150	$1{,}4 \cdot 10^{-10}$
»	1000	$8{,}5 \cdot 10^{-12}$	»	1100	$4{,}7 \cdot 10^{-11}$
2	1250	$4{,}4 \cdot 10^{-10}$	»	1050	$1{,}6 \cdot 10^{-11}$
То же	1200	$2{,}2 \cdot 10^{-10}$	»	1000	$9{,}1 \cdot 10^{-12}$
»	1150	$1{,}3 \cdot 10^{-10}$	5	1250	$9{,}1 \cdot 10^{-10}$
»	1100	$3{,}4 \cdot 10^{-11}$	То же	1200	$2{,}4 \cdot 10^{-10}$
»	1040	$1{,}8 \cdot 10^{-11}$	»	1150	$9{,}2 \cdot 10^{-10}$
3	1250	$3{,}0 \cdot 10^{-10}$	»	1100	$3{,}6 \cdot 10^{-11}$
То же	1200	$2{,}3 \cdot 10^{-10}$	»	1040	$1{,}1 \cdot 10^{-11}$
»	1150	$1{,}6 \cdot 10^{-10}$	»	1000	$7{,}6 \cdot 10^{-12}$

Our findings show that the addition of up to 30% chromium and up to 5% titanium to nickel results in a noticeable slowdown of the diffusion of chromium, compared with pure nickel; this is greatest in the alloy containing 28% chromium (Fig. 2).

TABLE 3

Diffusion Parameters for the Alloys

Наименование материала	D_0, см²·сек⁻¹	Q, ккал/г ат	Примечание
Никель	1,27	66,8	Самодиффузия по данным работы [3]
Никель	$4 \cdot 10^{-3}$	48,0	Диффузия хрома по данным работы [20]
Никель — хром (20%)	10^{-1}	58	То же
Никель — хром (20%) — титан (2,5%)	2	66,0	»
Никель — хром (19%) — титан (3%)	$3 \cdot 10^{2}$	81,0	Диффузия хрома по данным наст. раб.
Никель — хром (28%) — титан (3%)	10^{3}	85,0	То же
Никель — хром (10%) — титан (2,7)	20	75,0	»
Никель — хром (10%) — титан (3,7)	1	64,0	»
Никель — хром (10%) — титан (4,8%)	0,1	62,0	»
Хром		85,0	Самодиффузия по данным работы [4]

It follows that with an increase of the chromium content in nickel there is an increase of the chromium's activation energy of diffusion and a decrease in the diffusion coefficients. It is interesting to note that the diffusion parameter Q for the alloy containing 28% chromium and 3% titanium has approximately the same value as that for pure chromium. Alloys with nickel-chromium (10-28%)-titanium (3%) composition and pure chromium have close diffusion characteristics with respect to the chromium. This means that the alloys of the said compositions and chromium are proximates in their levels of interatomic bond strength.

The addition of titanium has a peculiar effect on the diffusion characteristics of nickel-chromium alloys. When the titanium content in the alloy is increased up to 3%, a deceleration of diffusion and an increase in activation energy are observed. An increase of titanium content in alloys of nickel-chromium (10%) up to 4.8% appreciably reduces the activation energy of diffusion of chromium and accelerates the diffusion of its atoms. This enables us to conclude that in fairly low concentrations (5%) titanium has a complex effect on the diffusion of chromium. It is possible that this effect is due to peculiarities in the structural change of the alloys under study when heated to high temperatures.

A comparsion of the diffusion characteristics of chromium in the alloys with the self-diffusion parameters of nickel is of note worthy. It shows that at high temperatures the self-diffusion of nickel and the diffusion of chromium in alloys of nickel-chromium (10-30%)-titanium (3%) occur with approximately the same intensity (Fig. 2). The given alloys are examples of the fact that the diffusion of the atoms of one of the alloying elements can proceed at almost the same rate as self-diffusion in the base metal of the alloy. From data contained in scientific literature it is known that the reverse also occurs. In nickel-chromium alloys the atomic bonds are strengthened, which apparently is responsible for the fact observed. Hence one of the basic functions of chromium in nickel-base heat-resistant alloys is to form a nickel-base solid solution while maintaining the levels of diffusion coefficients inherent in it. However, the alloying of nickel with chromium also brings about a change in the actual recrystallization process [4]. This establishes the preconditions for an increase in the recrystallization tempera-

ture of the alloy (as compared with pure nickel) and, consequently, an increase in the temperature of intensive softening. The addition of titanium and aluminum to the nickel-chromium solid solutions is chiefly necessary to create the conditions necessary for precipitation hardening, which is used to obtain alloys of special structural form characterized by great strength. The softening rate of unalloyed and alloyed solid nickel-chromium solutions at high temperatures should, apparently be about the same. Of course, in studying such a complex problem, one has to take into account many other aspects of the behavior of the alloy that are not directly connected with diffusion.

It is known that heat-resistant nickel-chromium alloys markedly soften at temperatures of 750-800°. According to our data, the self-diffusion coefficients of nickel and the diffusion coefficients of chromium in nickel-chromium alloys have values close to 10^{-13} cm^2 · sec^{-1} [7]. We can therefore consider that in the case of nickel-chromium heat-resistant alloys under deformation the threshold level of the diffusion mobility of intensive softening has this value. The postulate of the threshold level of the diffusion mobility of recovery in nickel-chromium alloys accords with the results obtained in studying the relation between diffusion and recrystallication processes in pure metals and solid solutions [4]. It should be considered that the effect of diffusion on heat-resistance is as yet far from clear. One of the basic problems in this field should be the study of intragranular and boundary diffusions in solid solutions and the latter's recovery.

Conclusions

The diffusion of chromium in nickel-chromium alloys (10-28%) was studied and it was found that the self-diffusion coefficients of nickel and the diffusion coefficients of chromium for these alloys have approximately the same values in high temperature zones. It was shown that intensive recovery in nickel-chromium alloys takes place at a diffusion level of the order of $10^{-13} cm^2 \cdot sec^{-1}$. The diffusion level of solid solutions corresponding to the diffusion coefficients of the basic elements of the given magnitude may be tentatively called the threshold level of the diffusion mobility of intensive recovery in heat-resistant alloys, intended for short-time service at high temperatures. This enables us to make a rough estimate of the potential level of heat resistance of solid solutions from data obtained from the calculation of diffusion coefficients.

References

1. BOCHVAR, A. A. Science of Metals. Metallurgizdat, 1956, (St. Sc. Press Lit. Ferr and Non Ferr. Met).

2. GRUZIN, P. L. and FEDOROV, G. B. DAN USSR, (Reports of Acad. Sci. USSR), 105, No. 2, 1955.

3. HOFFMAN, R. E.; PIKUS, F. W.; and WARD, R. A. J. Metals, 8, S. 2, No. 5, 1956.

4. GRUZIN, P. L. and TYUTYUNNIK, A. D. Physics of Metals and Metallurgy (Fizika metallov i metallovedenie) Vol. 3, ed. 1, 1956.

5. GRUZIN, P. L. DAN USSR, 86, Nr. 2, 1956 (Rep. Acad. Sci. USSR).

6. SWALIN, R. A. and MARTIN, A. J. Metals, 8, S, 2, Nr. 5, 1956.

7. GRUZIN, P. L.; KURDYUMOV, G. V.; TYUTYUNNIK, A. D.; and ENTIN, F. I. Issledovanie po zharoprochnym splavam (Research on Heat-resistant alloys) Vol. II Acad. Sci. USSR, 1957.

A STUDY OF INTERGRANULAR DIFFUSION IN METALS AND ALLOYS

V. I. Arkharov, C. M. Klotsman, A. N. Timofeyev, I. I. Rusakov

During recent years a large number of papers have appeared on the study of intergranular diffusion [1-5]. Some of them are devoted to the quantitative study of intergranular diffusion, others to its qualitative study.

Until recently, quantitative studies of intergranular diffusion through intercrystalline transition zones is much greater than in the grain, the isoconcentration surface of the diffusion zone forms "protrusions" along the grain boundaries. The shape of these protrusions (the angle between the isoconcentration periphery and the grain boundary at their intersection) is definitely determined by the relation of the coefficients of intra- and intercrystalline diffusion. The variation in the concentration of the diffusing substance with the depth of diffusion likewise depends on the coefficients of intra- and intercrystalline diffusion.

This being so, plotting of the concentration curve or the quantitative measurement of the protrusions on the diffusion front makes it possible to determine the parameters of predominantly intercrystalline diffusion.

Qualitative studies of intercrystalline diffusion [1, 2, 3]

were made by comparing the lengths of the protrusions on the diffusion front, which can be determined in various ways.

In the research done by the Smoluchowski [3, 4] the dependence of intercrystalline diffusion on the boundary structure was studied by microstructural and radioautographic methods, and conclusions regarding the varying diffusion penetrability of the separate boundaries were drawn on the basis of a comparison of the lengths of the protrusions. This qualitative approach is possible if the length of the protrusion is determined solely by intercrystalline diffusion.

In general, as Fisher's theoretcial analysis shows, the length of a protrusion on the diffusion front depends on the ratio of the coefficients of intra- and intercrystalline diffusion. If there were no penetration of the diffusing compound from the intercrystalline transitional zones into the grain, the diffusion zone, restricted to regions of 100-1000 A [7], could not be determined at all.

Accordingly, qualitative studies of intercrystalline diffusion based on comparisons of the length of the protrusions on the diffusion front can lead to sound conclusions provided that in the cases compared the resorption of the diffusing material into the grain does not change either through variation in the mean coefficient of intragranular diffusion or through the latter's anisotropy.

In our research [1, 8, 11], the influence of small admixtures on the diffusion of the third element in the solvent was studied microstructurally. In studying the effect of the addition of small quantities of antimony on the diffusion of silver in polycrystalline copper, it was found that antimony accelerates the intragranular diffusion of silver and that the length of the protrusions on the diffusion front in copper alloyed with 0.4% silver is of an order

greater than in pure copper [8]. In none of these studies, however, was it taken into account that the determinability of the protrusion on the diffusion front depends on the relation of the coefficients of intra-and intercrystalline diffusion. To determine the effect of small additions of antimony upon the parameters of intercrystalline diffusion of silver in copper, we made a radiometric study of the diffusion of silver in polycrystalline copper in an alloy of copper and 0.4% antimony.

Specimens of pure copper and of copper alloyed with 0.4% antimony were forged and then underwent recrystallization annealing at 900° for 5 to 7 hours. Some of the specimens were subjected to an additional heat treatment for 100 hours at 650°. This treatment was intended to enrich the intercrystalline transtion zones of the alloy by the horophyle addition of antimony. Next the specimens were coated with radioactive silver Ag^{110} by means of vacuum dispersion. They were then assembled in pairs, with the radioactive surfaces in contact, and placed in a quartz tube evacuated down to 10^{-2} mm Hg. The tube containing the specimens was placed in a preheated oven. The diffusion-annealing temperautre was 650° and was maintained to within $\pm$ 3°. This temperature was selected so that the distribution of antimony resulting from previous annealings would not be changed.

The distribution of radioactive silver in the specimens was determined by layer analysis using the integral-residual method [9]. The accuracy of measurement was 1-3% for the activity and 10% for the thickness of the specimen. On the basis of the experimental data we derived the dependence of the logarithm of the specific activity upon the depth of penetration [6].

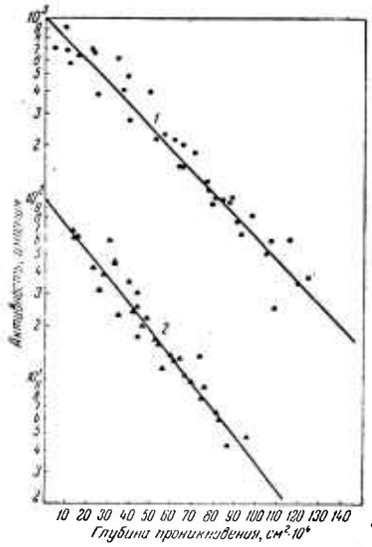

Figure 1. Graph showing the dependence of the logarithm of activity on the depth of penetration in the diffusion of silver.
1) into polycrystalline copper,
2) into a polycrystalline alloy of copper with 0.4% antimony.

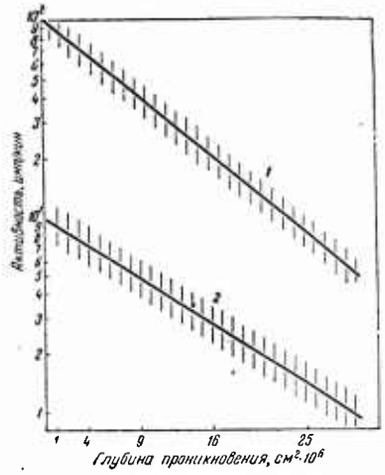

Fig. 2. Graph shows the dependence of the logarithm of activity on the square of the depth of penetration in the diffusion of silver.

1) into single crystals of copper;
2) into singlecrystals of copper alloyed with 0.4% antimony.

The tangent of the angle of slope of the straight line so derived was found from the experimental data by the method of least squares.

The relation between the coefficients of inter- and intracrystalline diffusion was determined by the formula

$$\operatorname{tg}^2\alpha' = 0{,}21\,\frac{D^{1/2}}{\sqrt{t}\,aD_{гр}},$$

where $\operatorname{tg}\alpha'$ is the tangent of the angle of slope of the linear dependence of the logarithm of the specific activity x;

D is the coefficient of intragranular diffusion;

a is the active half-width of the intercrystalline zone;

D_{bound} is the coefficient of diffusion in the intercrystalline zone;

t is the length of diffusion time.

The coefficient of intercrystalline diffusion was determined from measurements of single crystals of copper and a copper alloy with 0.4% antimony, using the formula

$$\operatorname{tg}\alpha'' = -\frac{1}{4Dt},$$

where tanα" is the tangent of the angle of slope of the linear dependence of the logarithm of the specific activity on the square of the depth of penetration;

D is the coefficient of intragranular diffusion;

t is the length of diffusion time.

The obtained dependence of the specific activity logarithm on the depth of penetration is given in Figs. 1 and 2, and the values of the diffusion coefficients in Table 1.

TABLE 1

Материал	$\operatorname{tg}\alpha \cdot 10^{-4}$	D, см²/сек	$\alpha D_{гр}$, см³/сек	$D_{гр}$
Поликристаллическая медь	1,23	—	$8{,}42 \cdot 10^{-14}$	$8{,}42 \cdot 10^{-8}$
Поликристаллический сплав медь + 0,4% сурьмы	1,47	—	$6{,}92 \cdot 10^{-14}$	$6{,}92 \cdot 10^{-8}$
Монокристалл меди	—4,72	$6{,}4 \cdot 10^{-12}$		
Монокристалл сплава медь + 0,4% сурьмы	—4,52	$8{,}8 \cdot 10^{-12}$		

Radiometric measurements show that the coefficient of intragranular diffusion of silver in single crystals of a copper alloy with 0.4% antimony is slightly higher than in single crystals of pure copper. The coefficients of intercrystalline diffusion of silver, calculated according to Fisher's method provided that the width of the zone does not change and is of the order of 10^{-6} [7, 10], are also different, the intercrystalline diffusion coefficient being greater in copper than in the alloy.

The variation in the intercrystalline diffusion coefficient is evidence of the enrichment of the intercrystalline transition zones with antimony. The adsorption of antimony in the intercrystalline zones, resulting in a reduction in the excess energy of the latter, probably produces changes in the bond strengths locally within the zone and in its geometric structure in such a way that the diffusion penetrability of the zone, calculated by Fisher's method is lessened. This dependence cannot be taken to apply generally to all systems, since no idea whatever can be formed of the mechanism of the influence of horophyle additives upon the structure of the zone and upon local changes in the bond strengths with in it.

Our measurements make it possible to explain from a single viewpoint the microstructural and radiometric studies of the diffusion of silver in polycrystalline copper and in a copper alloy with 0.4% antimony. As can be seen from Fig. 1, at equal depths, the total quantity of diffused material in pure copper is greater than in the alloys. At first sight, this contradicts the pattern obtained by metallography. However, on the basis of Fisher's method of calculation, it can be shown that the protrusions on the diffusion front in the alloy will have a greater width and a lower concentration of diffusing material than the protrusions in pure copper at equal

distance from the external source of diffusion. In fact, a higher coefficient of intragranular diffusion in the alloy will lead to greater resorption of the diffusing element from the intercrystalline zone, i.e., to the appearance of a wider protrusion of the diffusion zone in the alloy than in pure copper. Since the angle between the boundary and the isoconcentration periphery at their intersection is small (about one degree), even a slight increase in the width of the protrusion of the diffusion zone will lead to this protrusion being found in metallographic examination at a greater depth than the corresponding protrusions in pure copper. The lower diffusion penetrability in the intercrystalline zones will cause the concentration of the diffusing silver at equal distances from the source of diffusion to be weaker in the alloy than in pure copper.

The conclusions stated above are derived from measurements made according to Fisher's method. However, the model on which Fisher's calculation is based is quite crude. In this model the complex structure of the transition zone, which is characterized by continuous change in the distortions from the central part toward the edges, is replaced by a narrow band with a diffusion penetrability that is sharply altered, as compared with the thickness of the crystallite. Future systematic study of the real structure of the intercrystalline zone in the model used for calculating intercrystalline diffusion may possibly lead to a more complex pattern of the changes in the diffusion penetrability of the intercrystalline zone, namely, a sharp increase in penetrability in the central part and a decrease at the sides. From the point of view of the diffusion penetrability of the intercrystalline zone, such a pattern would signify a reduction in its effective half-width. It is conceivable that such changes actually

occur in our case. However, Fisher's calculation does not enable us to determine separately the effective half-width of the intercrystalline zone and the true diffusion coefficient with in it. Hence our conclusion regarding the decrease in penetrability in the copper alloy with 0.4% antimony, as compared with pure copper, is valid within the same approximation as the model for Fisher's calculation.

Finally, Fisher's calculation makes it possible to only determine the relation between the intercrystalline and the intragranular diffusion coefficients. Independent measurements of volume diffusion in single crystals may perhaps bring to light characteristics differing from those of polycrystals. Indeed, inasmuch as the distribution of the horophyle element in the adsorption zone is characterized by a continuous gradient, diffusion of the material from the intercrystalline zone into the body of the crystal adjacent to the zone will proceed in the material with an appreciably higher concentration of the horophyle element. This is certain to lead to a situation where the intragranular diffusion coefficient measured in a polycrystal will differ from the corresponding coefficient for a single crystal of the alloy. This implies that the data derived from Fisher's calculation described the effect of horophyle additives in an alloy on intercrystalline diffusion in a rather crude and approximate way.

A calculation [10] based on Fisher's model has recently appeared, however, which makes it possible to calculate separately the intragranular diffusion coefficient and the product aD_{bound} from measurements made on a single specimen.

The calculation made by S. D. Gertskriken and D. Tsitsiliano apparently enables us to determine separately the effective half-

width of the inter-crystalline transition zone and the intercrystalline diffusion coefficient. However, this calculation is also based on Fisher's model, and moreover the influence of intragranular diffusion on the distribution of the concentration in the protrusion on the diffusion front is not taken into account.

It follows from the above that the study of intercrystalline diffusion in alloys, and especially the problem of internal adsorption, requires first of all a method of calculation which will allow separate determination of the intra- and intercrystalline diffusion coefficients and the effective width of the intercrystalline zone. For a higher degree of accuracy it will be necessary to take into account the possibility of the existence of a number of diffusion coefficients in a cross section of the zone. As a first approximation, a model can be found for this (as in Fisher's method) by selecting zones with different diffusion coefficients. This system of calculation will not only enable us to determine the effect of additives on intercrystalline diffusion but also to draw some conclusions regarding the structure of intercrystalline zones and the effect of internal adsorption on this structure.

References

1. ARKHAROV, V. I. and GOLDSHTEYN, T. YU. Papers of IFM UFAN SSSR, No. 2, 1950.

2. BOCKSTEIN, S. Z.; GUDKOVA, T. I.; KISHKIN, S. T.; and MOROZ, L. M. "Zav. laboratoria" ("Factory Laboratory"), No. 4, 1955.

3. SMOLUCHOWSKI, R. and ACHTER, M. R. J. Appl. Phys., 22, 1951.

4. COULING, L. and SMOLUCHOWSKI, R. Phys. Rev., 91, I, 1953.

5. HOFFMAN, R. and TURNBULL, D. J. App l. Phys., 22, 1951.

6. FICHER, J. C. (FISHER). J. Appl. Phys., 22, 1951.

7. ARKHAROV, V. I. and SKORNYAKOV, N. N. DAN USSR, 89, No. 5, 1953 Reports Acad. Sci. USSR).

8. ARKHAROV, V. I. and PENTINA, A. A. Article in this collection, page 119. Stat'ya v nastoyashchem sbornike.

9. GRUZIN, P. L. Problemy metallovedeniya i fiziki metallov, Problems of metallurgy and metal physics. Collection No. 3, Moscow, 1953.

10. BORISOV, V. T.; GOLIKOV, V. M.; and LIUBOV, B. Ya. Izv. AN USSR, OTN, Bull. Acad. Sci. USSR, Tech. Sci. Dept., No. 10, 1956.

11. ARKHAROV, V. I.; IVANOVSKAYA, C. I.; and SKORNYAKOV, N. N. Works of Inst. Phys. Met., Ural Branch of Acad. Sci. USSR, No. 16, 1955, Trudy IFM UFAN USSR.

A STUDY OF THE EFFECT OF THE MUTUAL ORIENTATION OF CRYSTALS ON INTERCRYSTALLINE DIFFUSION AND INTERNAL ADSORPTION

V. I. Arkharov and A. A. Pentina

In polycrystalline bodies the most sharply defined structural inhomogeneity is found in intercrystalline boundaries. This inhomogeneity depends upon the disorientation of the grains.

More and more attention is being paid of late to the problem of the effect of granular disorientation on the properties of solid bodies. This includes determination of the mechanism of the effect of granular disorientation upon the energy of the transition zones, mechanical properties, diffusion in polycrystalline bodies, adsorption phenomena, corrosion and a number of other properties of polycrystals, as well as the phenomena taking place in them which are of importance in regard to the heat and corrosion resistance of the material.

The present study seeks to determine the effect of the mutual orientation of crystals upon intercrystal line diffusion in pure metal and also in the same metal when it contains a horophyle additive. It was carried out in order to develop further existing ideas on the effect of internal adsorption with respect to differences in the distribution of a horophyle additive along crystallographically

distinct intercrystalline boundaries.

In earlier research into the problem of intercrystalline internal adsorption this effect was, in essence, either studied qualitatively from the metallographic pattern of frontal diffusion of the indicator component into the alloy containing the horophyle admixture, or else study was made of the averaged effect by measurement of the parameter of the crystal lattice of the alloy with variation of the grain size. In the present work, specific concrete boundaries linking a pair of crystallites of a definite orientation were investigated.

The character of distortions in the intercrystalline abutments depends on the mutual orientation of the crystalline grains, and hence also the excess energy, the binding forces, and the activation energy. These features determine intercrystalline diffusion in pure metals. With the presence in metals and alloys of horophyle additives, often deliberately added, internal adsorption caused by excess energy occurs on the intercrystalline abutments. The aim of this study was to determine the quantitative effect of disorientation of adjacent crystal grains on the degree of irregularity in the concentration distribution of the horophyle admixture.

Structural Inhomogeneities and Their Effect on Physical Properties

In pure metals and in one-phase or heterophase alloys, there are always present in practice, structural inhomogeneities varying in form and origin:

Intercrystalline bonds in polycrystals, which may be bonds of crystals of one phase if the system is one-phase or bonds of crystals of different phases in the case of a heterophase system;

Free outer surface of the crystal (layer of polyatomic thickness);

Interblock bondings in the macro- and micromosaic;

intertwin bondings;

Zones of slip under plastic deformation, as well as elastically distorted zones in the bonding of sectors of the lattice that have undergone ordered phase transitor with zones of the initial phase;

Periphery of "pretransition" formations at the dissociation supersaturated solid solutions;

Agglomeration of dislocations, making up zones of elastic stresses, and individual dislocations;

Agglomerations of foreign atoms, and individual foreign atoms in the lattice of the solid solution;

Agglomeration of vacancies, and individual vacancies in the crystal lattice.

These structural imperfections are characterized from the crystallo-geometrical standpoint by a disturbance of the regular periodic arrangement of the various atoms and, from the physical viewpoint, by a divergence from the minimal potential energy of interaction of the atoms (i.e, by excess energy, depending on the type of structural inhomogeneity.

Any deviation from the ideal crystalline structure in the metals and alloys studied affects their structurally-sensitive physical properties (strength, plasticity, coefficient of diffusion, recrystallization, and others) and is the cause of divergence betweeen theoretically calculated values for these properties and values obtained experimentally.

The existence of structural inhomogeneities in true crystalline metals and alloys in some combinations of components (solvent and

additive) can also show up in the internal-adsorption capacity [1]. This capacity is linked with the redistribution of foreign atoms in the body of the phase, which causes uneven concentration in it, while at the same time the foreign atoms localize themselves primarily in the deformed portions of the lattice. The stimulus for this adsorption is the ability of foreign atoms to reduce the excess energy of structural inhomogeneities.

In accordance with the wide range of variance in the scale of structural inhomogeneities encountered in real crystalline bodies, the phenomenon of internal adsorption can occur over a similarly varied area ranging from the coarsest heterogeneities of the intergrain bondings (intergranular internal adsorption) type to micro-atomic distortions of the lattice (adsorption at dislocations, for example).

The phenomemon of internal adsorption in the processes of diffusion and plastic deformation plays a large role [2]; hence, the study of this effect and its influence on many properties is important for a detailed elaboration of the theory of heat-resistant materials.

Effect of the Mutual Orientation of Crystals on the Amount of Excess Energy in Intercrystalline Transition Zones and on Intergranular Diffusion

Much attention has been paid in recent years to the study of the dependence of boundary energy and intercrystalline diffusion on the angle of disorientation of the crystals forming the boundary, with a view to determining the effect of grain boundaries upon the structurally-sensitive physical properties, especially the plastic qualities, of polycrystalline materials.

Study of the profile of the valley formed along the grain boundary on the surface of polished specimens during annealing in vacuum or in an inert atmosphere has been of great importance in the attempt to resolve these problems. This research leads to the conclusion that the dihedral angle formed by the lateral planes of the valley* can serve as a measure of the excess surface energy connected with the boundary. It varies in accordance with the relative orientation of the grains forming the boundary.

Research on the dependence of the surface energy of grain boundaries on the disorientation of adjacent grains has been stimulated by the work of Smith [3], in which he showed that in α -brass, brought to a state of equilibrium by annealing, the boundaries of three grains form unequal angles in relation to each other at their abutments. From this Smith concluded that the excess energies at the various boundaries were also unequal. Further studies have been carried out by many workers using different methods, and all the data obtained are in qualitative agreement.

The most extensive research has dealt with the measurement of the angle of the boundary valley formed by the effect of thermal etching of the bicrystal as a result of the equilibrium achieved by the migration of atoms from the boundary along the surface. When the bicrystals of the reference material are annealed, there forms an equilibrium configuration, as shown in Fig. 1 where: γ is the angle of the boundary valley, E_A and E_B are free energies of the

---

* This dihedral angle, or the plane angle measuring it, is called the "angle of the boundary valley".

outer surfaces of crystals A and B, and E_{AB} is the surface energy of the boundary arising from the condition of equilibrium:

$$\frac{E_{AB}}{\sin\gamma} = \frac{E_A}{\sin\alpha} = \frac{E_B}{\sin\beta}. \qquad (1)$$

Assuming that $E_A = E_B = E_S$, (the free surface energy does not depend on the relative orientation of the crystals, the condition of equilibrium will become

$$E_{AB} = 2E_S \cos {}^1/_2\gamma. \qquad (2)$$

Knowing the angle of the boundary valley and the free surface energy, it is possible to measure the absolute energy of the grain boundaries. If, however, the free surface energy is not known, then the equilibrium relation (1) makes it possible to calculate the relative energies of the boundaries in relation to the mutual orientation of the grains.

The research experiments were performed on specimens in which the mutual orientation of adjacent grains differed by the angle of relative rotation of planes of the same crystallographic nature around a common axis. In this case no asymmetry of the valley was observed. These facts served as a basis for the assumption, made in the experiments of the non-dependence of free surface energy on the disorientation of adjacent crystals.

Greenough and King [4] were the first not only to determine qualitatively the effect of the dependence of the angle of the boundary valley (and therefore the excess boundary energy) on the angle of disorientation of adjacent crystals, as was done previously [5 and 8], but also to evaluate this effect quantitatively on bicrystals of silver grown according to Chalmer's method of controlled

hardening [9]. Annealing was performed either in vacuum or in nitrogen (which does not dissolve in silver) [10] at 900° for 19 hours. A subsequent increase in annealing time did not change the angle of the boundary valley. The disorientation of the crystals varied from 0 to 50° and was determined by the Laue method with an accuracy of $\pm$ 2°. The results obtained determine the dependence of the relative surface energy (E_{AB}/E_S) on the disorientation of the crystals ($\Delta\theta$). Beginning with zero the excess energy increases to a definite reproduceable maximum for $\Delta\theta$ between 30 and 40°; while a further increase in the angle of disorientation leads to a decrease in excess energy. The typical relation of E_{AB}/E_S to $\Delta\theta$ is shown in Fig. 2.

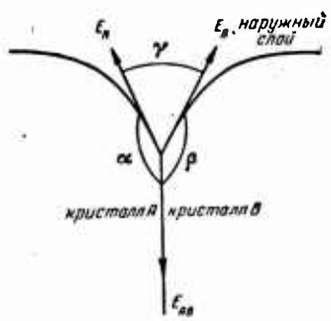

Fig. 1. Condition for the formation of a valley along the grain boundary under thermal etching.

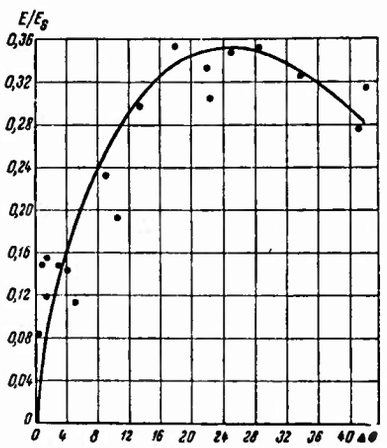

Fig. 2. Dependence of the relative boundary energy on the mutual orientation of adjacent crystals. (Reproduced from [4]).

In the research carried out by the second group the variation in boundary energy with the relative orientation of the grains was studied by a different method, for which "tricrystals" were grown with a different relative orientation in adjacent crystals. In the annealing process three grains are linked together at one point on the outer surface at definite angles which are formed at equilibrium. These angles depend on the relation of the energies of the three boundaries. This instance is shown schematically in Fig. 3.

The equilibrium ratio is analogous to formula (1):

$$\frac{E_1}{\sin\psi_1} = \frac{E_2}{\sin\psi_2} = \frac{E_3}{\sin\psi_3}. \qquad (3)$$

When the angles formed by the intercrystalline boundaries on the surface of the tricrystal in a state of equilibrium are known, it is possible to determine the relative energies of the grain boundaries and their relation $\Delta\theta$.

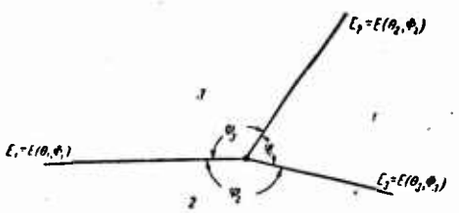

Fig. 3. Equilibrium configuration of the boundaries of a "tricrystal" (in plane projection).

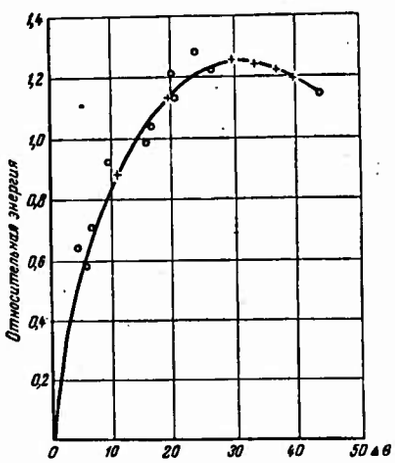

Fig. 4. Dependence of the relative boundary energy on the angle of disorientation of adjacent crystals for iron alloyed with 3% Si.

Dann and others [11, 12] carried out experiments of this kind on iron alloyed with 3% Si, and Aust and Chalmers [13] did so on lead and tin. The results are qualitatively in agreement. The excess energy of the boundary rises with the increase in the angle of disorientation. The results of [11 and 12] are given in Fig. 4.

Read and Shockley [14] and Van der Merwe [15], representing the boundary of grains of shlghtly different orientation as a series of linear dislocations, deduced the theoretical relation of the dependence of boundary energy on $\Delta\theta$.

$$E = E_0 \Delta\theta (A - \ln \Delta\theta), \qquad (4)$$

where E_0 and A are constants.

Experimental values satisfactorily coincide with the curve plotted from the given formula. This justifies the conclusion that the boundary formed by crystals with slight disorientation can definitely be represented as a series of dislocations.

On the basis of experimental data and approximate theoretical calculations the general conclusion can be drawn that the excess energy of the intercrystalline transition zones depends on the relative orientation of the crystals.

The Smoluchowski group has devoted its work to study of the dependence of preferred inter-crystalline diffusion on the relative orientation of crystals. Achter and Smoluchowski [16, 18] investigated the dependence of the boundary diffusion of silver into polycrystalline copper on the disorientation of the copper grains. For convenience in interpreting the results, textured columnar copper was chosen in which almost all grains had the same direction [100] to the outer surface; the disorientation is determined by one

degree of freedom and the angle of rotation of the other cubic axis in the outer plane. The experiment was conducted in such a way that it was possible to compare the depth of penetration of the diffusing silver along grain boundaries of columnar copper in the columar direction [100]. Metallographic methods were employed for this. Diffusion annealing was carried out at temperatures between 673 and 725°. The results of the study show that for nagles of disorientation between the grains greater than 20° and smaller than 70° diffusion along the grain boundaries is greater than intragranular diffusion and reaches its maximum at an angle of about 45°. If the angle of disorientation between the grains is smaller than 20° or greater than 70°, no preferred intergranular diffusion is observed.

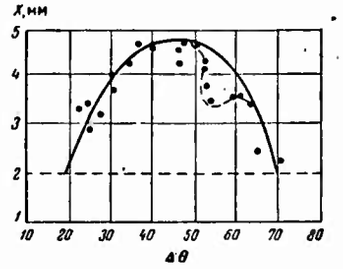

Fig. 5 Dependence of the depth of penetration (X) of silver into polycrystalline copper on the angle of disorientation Δθ of the crystals.

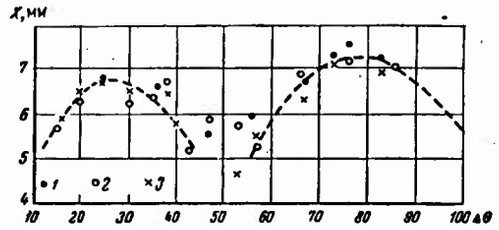

Fig. 6. Effect of disorientation of adjacent crystals on the depth of penetration in diffusion of Fe^{55} into ferrosilicon. 1) and 2) 769°; 3) 810°.

The dependence of the depth of penetration of silver in polycrystalline copper on Δθ according to the results of these experiments is shown in Fig. 5.

Flanagan and Smoluchowski [19] investigated the diffusion of

zinc into columnar copper in the same manner. The results of this work confirm the effect of the angle of disorientation of adjacent crystals on intercrystalline diffusion with a maximumat about 45°.

Couling and Smoluchowski [20] later confirmed the results obtained by Achter and Smoluchowski using radioactive silver as the diffusing element, by radioautographic methods.

Haynes and Smoluchowski [21] performed experiments on self-diffusion along grain boundaries in ferrosilicon by means of radio-autographic and radiometric procedures. This metal was chosen for its body-centered cubic lattice and was expected to have different diffusion characteristics compared to boundary diffusion into a metal with a face-centered (close-packed) lattice. Specimens were so textured that the plane (110) of all grains was parallel to the outer surface coated with Fe^{55}. Grain disorientation varied in the region $5° < \Delta\theta > 86°$. The results of the experiments showed the absence of observable boundary diffusion for angles of disorientation less than 10° and an increase in the depth of penetration (b) along the grain boundaries up to 86°. The graph of the dependence of b on $\Delta\theta$, given in Fig. 6, has a wide minimum in the area of 50° and two indeterminate maxima, one in the region 25-39°, the other around 76°.

The results of the research [16-21] enable us to conclude that with a change in the angle of disorientation of adjacent crystals, the character of the dislocations of the grain boundaries (or, more correctly, of the intercrystalline transition zones) also changes; this is shown in the changes in intercrystalline diffusion with the change of $\Delta\theta$.

Formulation of the Task and Choice of Material for the Investigation

Heretofore, the phenomenon on internal adsorption in the case of intercrystalline boundary contacts has only been studied qualitatively. It is of great importance for further work to connect available experimental data on the effect of internal adsorption with the various factors suitable for quantitative evaluation, such as diffusion characteristics and particularly diffusion coefficients, whose value, it seems will depend not only on the character of structural inhomogeneities in the polycrystalline material but also on the changes which occur in them due to internal adsorption. A no less important factor is the crystallographic orientation of adjacent crystals, which changes the character of the most sharply defined structural inhomogeneities, called intercrystalline abutment, on which the effect of internal adsorption is most evident.

The purpose of the present investigation was to study the effect of this factor on intercrystalline diffusion and irregularity of distribution of the horophyle additive in the intercrystalline bonding zones of differently oriented crystals. For this, we determined the quantitative dependence of the rate of intercrystalline diffusion of the indicator component from the outside into the reference (material which can be determined metallographically) on the disorientation of the crystals abutment along the oundary along which diffusion was being observed.

The base material chosen was 99.99% pure copper, and the horophyle additive was 99.97% pure antimony (the antimony content of the alloy was 0.25%). Silver was the indicating component, the interior adsorption of antimony in copper, diffusing from the outside.

The choice of these three elements was based on the following considerations. The assumption that antimony is a horophyle in re-

lation to copper(aside from the relation of the values for surface tension in liquid form) is confirmed by the following series of experimental data:

1. V. I. Arkharov and Gol'dshteyn, T. Yu. [22] discovered a sharp difference in the metallographic patterns of the diffusion of silver into pure copper and into copper containing 0.35% Sb. Although in the first case, an even and continuous diffusion front is observed in which there are no great differences in the body of the grain and on its borders, in the latter case a sharply defined boundary effect was observed; the diffusion of silver along the grain boundaries in the alloy of copper with 0.35% antimony forms protrusions on the front which far outstrip the continuous diffusion front throughout the grain.

2. In his work S. A. Nemnonov [23] on the determination of the effect of small additions of antimony on the diffusion rate of zinc into polycrystalline brass, observed an acceleration which is a function of the size of the grain; this can be explained by the horophyle nature of antimony.

3. McLean [24] and Hopkin [25] investigated intercrystalline brittleness in copper-antimony alloys with a small antimony content (the former, at low annealing temperatures; the latter at both low and high temperatures). This effect can also be explained by the intercrystalline internal adsorption of antimony in copper without referring to the earlier papers of Arkharov, Gol'dshteyn, and Nemnonov (both authors)call this phenomenon somewhat inaccurately, "segreagation without precipitation".

4. V. I. Arkharov and others [26, 27] found that the alloy of copper with 0.2% antimony has a greater lattice parameter in a coarse-

grained condition than in a fine-grained state and that the variation in the lattice parameter according to grain size is reversible. These results confirm radiographically the horophyle nature of antimony in relation to copper.

Silver was chosen as an indicator of the internal adsorption of antimony in copper on the grounds that the diffusion rate of silver in a copper-antimony alloy with a large concentration of antimony (2%-5%) is considerably greater than in pure copper, as was shown by V. I. Arkharov and T. Yu. Gol'dshteyn [22]. In a copper-antimony alloy with a small antimony concentration, therefore, silver should diffuse more intensively through intercrystalline transition zones, since the antimony content of the latter is greater than in the body of the grain.

The study was made with specimens of pure copper and copper with 0.25% antimony.

Experimental Procedure

Growing a Coarse Grain

It was essential for our study to have coarse-grained specimens with grain diameters of 2 mm or more, since they were to be later used to determine the crystallographic orientation of each grain individually. Moreover it was necessary that the grains in the polycrystalline specimens have a preferred orientation. This condition is essential for the following reason. Generally speaking, the difference in orientation of neighboring crystals is determined by three degrees of freedom (one grain can be rotated in relation to another around three mutually perpendicular axes. This is very inconvenient in

experimental research on intercrystalline abutment, since it complicates the comparison of individual results and their overall interpretation. The grains of the coarse-grain specimens therefore, should have some kind of axial or structured texture so as to limit the number of orientational variations.

Bearing these conditions in mind, we adopted the following procedure for growing coarse grains in polycrystalline copper and in the polycrystalline alloy of copper with 0.25% antimony. Ingots of pure copper and of copper alloyed with 0.25% antimony were cast from copper and antimony of the required purity. These were then forged into rods 5 x 20 mm and annealed in a vacuum at 800° for stress-relief. The rods were cut and rolled with a certain degree of deformation to ensure that the specimens acquired the texture of the rolling.

The rolled specimens of the copper alloy with 0.25% antimony and of the pure copper were annealed for recrystallization. This thermomechanical treatment ensured a coarse grain with a recrystallization texture imparted by the texture of the rolling and characterized by a plane (101) parallel to the plane of rolling for all grains in the specimen. The stipulation that the difference in the orientation of the crystals be determined by one degree of freedom was thereby met. The grain boundaries were approximately perpendicular to the surface of the specimen and completely penetrated the thin slabs.

Certain difficulties were encountered here which are apparently typical in growing a grain by recrystallization in specimens that are not made of pure metal, since recrystallization in metals containing even small quantities of impurities (much less than the solubility limit) is often greatly inhibited. This makes it difficult to produce the

grain by subjecting it to critical deformation and subsequent annealing. The same effect was also observed in the copper alloy with 0.25% antimony under investigation.

Pure copper (without antimony) recrystallized well. After a 5% deformation by rolling and subsequent annealing at 850°, the specimens acquired a coarse grain with the requisite diameter for later study. This method of growing coarse grains was found unsuitable for the copper-antimony alloy. In order to find the optimum conditions for growing a coarse grain the specimens were subjected, according to the general rule to various relative deformations (from 0.3 to 99%), and various annealing temperatures were used (from 600 to 1000°) with varying soaking periods (from 1 to 20 hours). However, none of these numerous variations in experimental conditions enabled us to grow a sufficiently coarse grain. This can be explained as follows. V. I. Arkharov and others [22, 26, and 27] determined the horophyle nature of antimony in relation to copper. In the present instance antimony, enriches the periphery of the growing grain during annealing because of its adsorptive capacity.
A consequence of the enrichment of the grain boundaries with antimony is a reduction of the "surface energy" on the grain boundaries (or, rather, of the excess energy of the intercrystalline transition zones). Since the movement of the boundaries during recrystallization depends on this excess energy, it is clear that with a horophyle additive in the alloy, which reduces the energy, the movement of boundaries during recrystallization will be lessened. This difficulty in growing a coarse grain in the copper-antimony alloy was overcome by the following heat treatment. An 80 to 90% deformation was produced in the reference copper 0.25% antimony alloy by rolling. The specimen

was then heated at a fairly fast rate (200°/minute) in an inert atmosphere from room temperature to 1000° and annealed at this temperature. This treatment was used in the belief that in such a short time the antimony would not be able to diffuse to the grain boundaries and would not affect the displacement of these boundaries during the growth of the grains. Experiments confirmed this assumption; the grain grew well. It was possible by this method to obtain grains 4 to 10 mm in diameter.

Later, as a result of our determination of the texture of the specimens which had recrystallized after rolling and orienting of adjacent grains it was found in them, that with large angle of disorientation ($\Delta\theta > 70°$) in neighboring grains the texture is less perfect in reference to the parallelism of face (101) with respect to the outer surface; in such grains this face forms an angle of 16-20° with the outer surface of the specimen. This makes it difficult to compare measurements of the effect of bonding such grains with data for less disoriented grains where the face (101) is nearly parallel to the outside surface (with a dispersion angle in the texture no greater than 8°). To eliminate this difficulty, besides the copper serving as the base of the copper alloys with 0.25% antimony, electolytic copper (oriented so that the plane (101) in its grains would lie parallel to the outer surface, as in the rolled specimens was also used in the experiments, but because of the axial character of the orientation of electrolytic copper, it was possible to increase the range of the angles of disorientation $\Delta\theta$ to 90° without increasing the texture dispersion angle, which did not exceed 8°.

In a series of experiments with electrolytic copper, a solid solution of copper-antimony was obtained by annealing copper specimens

(2-3 mm thick) in evacuated quartz ampules, together with a metered portion of antimony, at 800° for 200 hours. The concentration of antimony in the copper which was checked by chemical analysis, was therby brought up to 0.2-0.3%, throughout the specimen.

Preparation of Specimens for Diffusion Annealing

In order to determine the effect of grain disorientation on intercrystalline diffusion, experiments were performed on the diffusion of an indicator metal (silver of high purity) into pure copper and into a solid solution of copper with 0.25% antimony, respectively. For the subsequent diffusion annealing the specimens were prepared in the following manner.

One method was by compression of the alternating thin slabs; here the silver diffused from the thin silver slabs into the copper slabs. For this, the silver slabs and the coarse-grained specimens of pure copper (obtained by both recrystallization and electrolysis, in various series of experiments) were placed on top of each other, alternately, forming a number of layers consisting of a silver slab 0.2-0.5 mm thick, a copper slab 0.2-0.4 mm thick, another thin silver slab, and so on. The last layer was always of silver.

This set of layers was placed in an iron clamp to ensure good contact between layers. Iron clamps were chosen so that during the lengthy diffusion annealing the complete mutual insolubility of silver and iron would preclude diffusion of the iron into the silver, eliminating any possible effect of the iron on the diffusion of silver into the pure copper (or into the copper-antimony alloy in similar experiments). After diffusion annealing the set was removed from the clamps, easily this being a proof of the absence of iron diffusion

in the specimens studied.

The small deformation due to the pressure of the clamps did not spoil the previously prepared coarse grains, had no effect on their orientation, nor changed the grain shape or size in the subsequent diffusion annealing. This deformation was apparently much smaller than the critical deformation required for recrystallization.

This method of preparing the specimens prior to diffusion annealing was employed both for the recrystallized specimens of the copper alloy with 0.25% antimony and for the solid solution of copper with 0.25% antimony, formed as a result of vacuum saturation of electrolytic copper with antimony. However, in both cases the specimens were given additional thermomechanical treatment prior to assembly into sets of laters, the primary purpose of which was to create an adsorption effect in the specimens containing the horophyl additive, as well as to eliminate a possible surface effect. For this, the specimens of the selected composition were annealed at 700° for 200 hours in vacuum or charcoal. After annealing, they were cooled in water and layers 0.1 mm thick were then removed from both sides with fine emery cloth, after which the sides were polished. The specimens were afterwards lightly etched with a 50% solution of H_2O_2 to remove the layer strained by the mechanical treatment, and were made up into a set, as was done for the copper specimens: the first layer was silver, the second layer copper-antimony, the third layer was silver, etc.

Other methods were also used to ensure the best possible contact between the slab surface in preparing specimens for diffusion annealing. Copper or copper-antimony specimens, previously treated to produce the absorption effect, were coated with silver either

by electrodeposition or by vacuum condensation of silver vapor.

Before being plated with silver, the specimens were thoroughly cleaned by pickling in an aqueous solution of hydrogen peroxide, beofre and after which they were washed with alcohol.

The electrodeposition of silver was carried out in a bath of the following composition (grams/liter):

Silver chloride (AgCl)	39
Potassium cyanide (KCN)	65
Potassium carbonate (K_2CO_3)	38

The current density was 0.3 amp/dm^2 and the temperature of the bath was 20°; the anode was made of silver of high purity.

Some of the experiments were likewise carried out in a bath of different composition [28] (with a current density of 1.2 amp/dm^2 at a temperature of 70°):

Silver chloride (AgCl)	40
Potassium ferricyanide ($K_4Fe(CN)_6 \cdot 3H_2O$)	200
Potassium carbonate (K_2CO_3)	20

As a result of the experiments it was ascertained that electrodeposition of silver is better than vacuum plating for two reasons. First, the deposit produced electrolytically has a better bond with the basic metal; second, it is easy to get compact and uniform fine crystalline deposits of great thickness by electrodeposition.

The subsequent preparation of a set of specimens silver-plated in this way is the same as in the first method.

Diffusion Annealing

To bring about diffusion of silver from the outside into the copper and copper-antimony slabs, the latter were annealed at 650°

This temperature was chosen for two reasons.

It must be remembered that the intercrystallite transition zones in the copper-antimony alloy form a ternary solid solution when silver is diffused into them, with a melting point lower than that of the binary solid solutions of copper-antimony, copper-silver and silver-antimony within the concentration range under study. During the investigation it was determined that at this temperature there is no danger of the grain boundaries fusing. It would have been possible to choose a higher temperature for our experiments on the diffusion of silver into pure copper, but then the correlation of the results with similar experiments on copper-antimony alloys would have presented certain difficulties.

The given temperature is sufficiently high to ensure apprecaible diffusion activity by the silver.

Diffusion annealing were performed in different experiments either in vacuum (10^{-3} - 10^{-4} mm Hg) or in charcoal powder. The duration of the annealing was 600 hours. This length of time permitted bertter observation of the diffusion of silver into copper-antimony alloys with 0.25% antimony or especially into pure copper. In the latter case the maximum depth of penetration into pure copper after annealing for 600 hours at 650° was about 50 microns. For shorter annealing periods the effect of irregular intercrystalline diffusion in copper was not sufficiently clear and was difficult to measure.

Metallographic Study

Examination of the results of the diffusion of silver in the specimen slabs of pure copper or of copper alloyed with 0.25% antimony was made after the diffusion annealing. For this, the sample was removed from the iron clamps and subjected to layer-by-layer grinding with fine emery cloth in such a manner that the plane of the layer being removed was perpendicular to the direction of diffusion. This method of grinding was started at the surface forming the outer layer of silver diffusing into the interior of the specimen under study. The thickness of each layer removed was 5 microns. The thickness of the specimen before and after the removal of each layer was measured by means of a microscope with an ocular micrometer.

After the removal of each layer of material from the specimen, a section was prepared on the exposed surface by a well-known method [29] and the polished surface was etched. An etchant was chosen (ammonium persulfate 15 grams; ammonium hydroxide 6cc; distilled water 79cc) which would differentiate the base material (copper or copper-antimony alloy) and the solid solution formed as a result of the diffusion of silver in various ways (with sufficient contrast).

In a number of cases, instead of removing layers with fine emery cloth and subsequently polishing and etching the exposed surface, the specimens were subjected to electropolishing and electro-etching. In the first instance the electrolyte was orthophosphoric acid (specific gravity 1.48). The conditions of electropolishing were current density 2.5 - 3.0 amp/dm^2, voltage 1.1-1.8 volts, temperature of bath 15-20°. The cathode was electrolytic copper in the form of a thin slab 4 mm thick. The electropolishing lasted 10-15 minutes.

The electroetching of the specimen was performed in a bath of the following composition: iron sulfate, 30 grams; sodium hydroxide, 4 grams; sulfuric acid (specific gravity 1.84), 100cc; distilled water, 1,900cc; current density when the bath was operating, 0.5 amp/dm^2 the voltage, 8-10 volts; temperature of the bath, 40-50°. The cathode was a slab of electrolytic copper 2mm thick.

After electroetching for 10 seconds (which corresponds to the removal of a layer 5 microns thick) the specimens were ready for metallographic investigation. This treatment was applied to specimens made from thin copper or copper-antimony plates (0.2-0.5mm) coated with silver (electrolytically or by vapor condensation in vacuum) before diffusion annealing. It is difficult to make metallographic specimens in the usual manner on the surface of such plates.

The etched surface of the specimens was viewed through a microscope with varying degrees of magnification (x3-380). Low magnification was used to observe the sharply defined diffusion zone at intermediate stages of the examination while the progress of the continuous and boundary diffusion was being followed. High magnification was used to determine the beginning and end of the zones of body or intergranular diffusion.

By measuring the thickness of the layers of material which had been systematically removed and then tracing the metallographic pattern of the exposed surface, it was possible to determine separately the depth of penetration of the diffusing substance due to intragranular diffusion (measured according to the depth of total diffusion in a direction perpendicular to the outer surface) and the depth of penetration of silver along various individaul grain boundaries

which characterizes boundary diffusion. Knowing the characteristics of the depth of the intergranular penetration for different grain orientations, it is possible to clarify the effect of the disorientation of adjacent grains on intercrystalline diffusion.

Determination of Grain Orientation

There are many radiographic methods, described in detail in [30], for determining the preferred orientation of the grains of a polycrystalline aggregate.

In our investigation, Laue's back-reflection method was employed, with the construction of the standard polar diagrams [31, 32]. This method is simpler than others, and with some experience it enables the preferred orientation of the grains to be determined fails quickly. The difference in orientation between neighboring crystals is determined by the angle between like crystallographic directions in them. To make the calculation easier and quicker, Sachs screens were used, recalculated for the distance between the specimen and the film in our camera. Determination of grain orientation was further speeded by construction of the Greninger diagram, with allowance for the diameter of the camera being used (distance from specimen to film).

It was found by this method that there is a recrystallization pattern in the thin slabs as shown by the fact that the plane (101) of all grains is parallel to the outer surface of the specimen (or to the rolling plane). The specimens of electrolytic copper required for the investigation were selected so that the crystallographic plane (101) of the majority of the grains would be parallel to the

outer surface of the specimen. The angle of dispersion of the orientation in both instances, was not greater than 8°.

The accuracy in determining the disorientation of $\Delta\theta$ of adjacent crystals (which varied over a wide range from 0° to 90°) by this method with all stages being carried out with great care was $\pm$ 2°.

Experimental Procedure and Results Obtained

Results of the Metallographic Study

The depth of penetration of silver into the body of the grain as well as along the grain abutments was assessed by removing consecutive layers of the material of the specimen, the plane of the removed layer (the thickness of which was 5 microns) being perpendicular to the direction of diffusion. After the removal of each layer a metallographic examination was made of the exposed surface.

After annealing, there is a solid layer of silver (residual) on the starting surface of the specimen. As a result of subsequent grinding, a layer in which there is total diffusion of silver in the alloy (or pure metal) is exposed with no distinction between grain body and intercrystalline transition zones. After several layers are removed, the zone of total diffusion ends and the zone of intercrystalline diffusion is seen. The depth at which the zone of total diffusion ends is identified as the depth of penetration of silver into the body of the grains, and this characterizes its intragranular diffusion.

With the removal of subsequent layers, "gaps" appeared in the sections of the micro-ground surface (made on the surface of the specimen after removal of the layer) corresponding to the centers of the grain fields, while the sections on which the diffusion of silver

occurred at this depth formed a kind of "network" of wide bands aligned along the grain boundaries. At the beginning (at lesser depths from the outer surface this "network" was unbroken and delineated all the boundaries. Further removal of layers led to a narrowing of the bands forming the network, even to the point of disappearance along some boundaries (intercrystalline abutments); i.e., the diffusion of silver along grain boundaries ceased to be observable. The distance between the layers in which the beginning and the end of the intercrystalline diffusion of the indicator (silver), shown metallographically, were observed identified the depth of its penetration along each grain boundary. The depth of this penetration characterized intercrystalline diffusion; it was determined twice for each boundary, since subsequent removal of layers exposed, first, zones entirely unaffected by the diffusion and, later, a zone of diffusion along the same intercrystalline borders on the other side of the specimen (it must be kept in mind that the grains grew right through the test piece). Here the sequence of zones formed by the diffusion of silver was in reverse order to the sequence of the initial observations.

The experiments showed that practically identical depths of penetration were obtained on both sides of the specimens, as regards each specific boundary as well as the body of each grain (for all grains, regardless of their orientation, the depth of penetration into the body in each specimen was the same; in the case of diffusion in pure copper it was 15 ± 5 microns, and in the case of diffusion in the alloy of copper with 0.25% antimony it was 25 ± 5 microns).

Although 15 series of experiments were performed, and in each series a set of 3-4 composite sets of slabs copper alloyed with 0.25% antimony (or, similarly, of pure copper) interlaid with silver

strips were used.

In generalizing on the metallographic data, it can be said that as a result of the diffusion annealing the silver chosen as an indicator of internal adsorption in the copper-antimony alloy diffused in both the alloy and the pure copper and formed a diffusion zone with an uneven front. This diffusion front is characterized, apart from the continuous more or less even zone permeating the body of the grain, by the formations of protrusions on the front along the intercrystalline transition zones, which are unequal in their degree of extension along the various joint-bonds because of the different orientation of the grains with respect to each other. The result of the diffusion of silver into the alloy of copper with 0.25% antimony, for example, is shown schematically in Fig. 7.

It was revealed by the investigation that the depth of penetration selected as being characteristic of intragranular and intercrystalline diffusion differs substantially in the cases of silver diffusion into pure copper and into the selected alloy which were compared. It is characteristic that the protrusions of the diffusion front along intergranular boundaries do not greatly exceed the total diffusion front (the maximum depth of penetration along certain abutments did not exceed the solid diffusion front by more than three times) in the diffusion of silver into pure copper. For the diffusion of silver into the copper-antimony alloy, however, the intercrystalline diffusion revealed metallographically far exceeds the intragranular diffusion front (maximum depth of penetration along individual boundaries exceeded the solid diffusion front by more than 14 times).

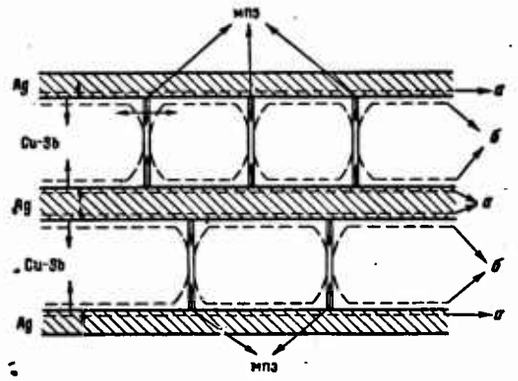

Fig. 7. Schematic representation of the diffusion of silver into copper alloyed with 0.25% antimony

The shaded sector represents the silver layer; the unshaded sector the specimen (plate of the alloy of Cu + 0.25% Sb.) Layer of solid solution formed as a result of diffusion: a) Ag in Cu, b) Ag in the alloy Cu-sb; M_{itz} intercrystalline transitional zone.

Dependence of Intercrystalline Orientation of the Penetration Depth of the Diffusing Substance Along Intercrystalline Boundaries

The results of the measurements of penetration depth (b) along the various bond-contacts and of the disorientation ($\Delta\theta$) of the adjacent crystals that form them were plotted in the form of curves showing the dependence of b on $\Delta\theta$. Fifteen curves showing this relationship were plotted for the diffusion of silver into pure copper or into copper-antimony alloys. The depth of penetration is slight for small disorientations of the grains and reaches a maximum at a certain degree of disorientation. This relationship is not

monotonic but complex in character, since the curve shows maxima and minima characterizing intercrystalline diffusion.

Dependence of b on $\Delta\theta$ for the diffusion of silver into a pure solvent (Cu). Figure 8 shows a composite curve obtained from many series of experiments representing the dependence of b on $\Delta\theta$ for pure copper used as the base for the copper-antimony alloys from which the specimens were rolled and Fig. 9 gives the same for electrolytic copper.

Since intragranular diffusion is a diffusion of silver through the undistorted lattice of the grain body, it may be considered equivalent to boundary diffusion between crystals with zero disorientation

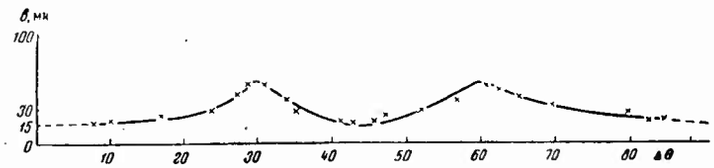

Fig. 8. Composite curve of the dependence of the depth of penetration of silver(β) into recrystallized copper on the relative orientation of adjacent crystals ($\Delta\theta$). Temperature of diffusion annealing (T) 650°; length of diffusion annealing (t), 600 hours.

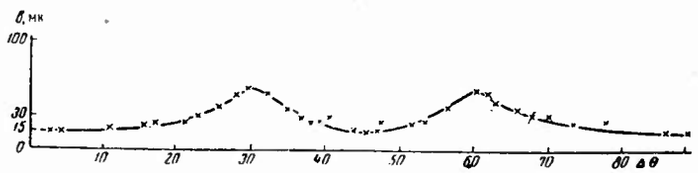

Fig. 9. Composite curve of the dependence β on $\Delta\theta$ (in degrees) in the diffusion of silver into electrolytic copper T = 650°; t = 600 hours

The characteristic of intragranular diffusion b, determined by the metallographic pattern of continuous diffusion, is therefore plotted on the graphs of the dependence of the depths of silver penetration due to boundary diffusion on the disorientation of grains at the point of zero-disorientation on the ordinate (b). The depth of penetration of silver into the body of grains of pure copper was 15 microns.

It is seen from Figs. 8 and 9 that the curve showing the dependence of the depth of penetration of silver along the grain borders in pure copper specimens on the disorientation of the grains has a maximum value b $\simeq$ 50 microns for two disorientation angles ($\Delta\theta$), 30 and 60°, and a minimum value b $\simeq$ 15 microns for $\Delta\theta$ = 45°. For other disorientation angles between neighboring cyrstals intermediate values were obtained for b.

This definite dependence of the depth of penetration of silver along intergranular boundaries of copper on the disorientation of the grains forming these couplings is similar to the findings of Smoluchowski and others [16-18] in samples of columnar polycrystalline copper. The difference in the texture of the copper under investigation and the copper chosen by Smoluchowski affected the nature of the dependence of b on $\Delta\theta$. In the studies made by Smoluchowski and others [17-19] the texture is characterized by the direction [100] along the direction of diffusion (which was the columnar direction), whereas in our case this direction was (101).

The difference in the dependence of b on $\Delta\theta$ found by us and in the studies of Achter and Smoluchowski [16-18] consists of the following. In the studies made by the latter the maximum value for

the depth of penetration of silver was obtained when $\Delta\theta = 45°$, i.e., the periodicity in the dependence of b on $\Delta\theta$ was observed through 90°, evidently because the direction (100) is an axis of symmetry of the fourth order. In our experiments on pure copper (Figs. 8 and 9) we obtained two maxima, when $\Delta\theta = 30$ and 60°, and a minimum, $\Delta\theta = 45°$. The periodicity in the dependence of b on $\Delta\theta$ was observed through 180° in this case, due to the fact that direction [101] is an axis of symmetry of the second order.

Dependence of b on Δ in diffusion of silver into a solid solution of copper with 0.25% antimony. Figs. 10 and 11 show composite curves of the dependence of the depth of penetration of silver (b) on $\Delta\theta$, obtained by investigating intercrystalline diffusion in samples of a copper-antimony alloy, produced by electrolysis and properly rolled. As in the case of pure copper, the value plotted at zero abscissa is the value of b obtained from measurement of the depth of penetration of silver in the body of the grains in the selected specimens. It was 25 microns.

From Figs. 10 and 11 it is seen that the intercrystalline diffusion of silver in the alloy of copper with 0.25% antimony proceeds with considerably greater intensity as compared to intragranular diffusion in the same alloy and very definitely depends on the relative orientation of adjacent grains. The curve of the dependence on disorientation of the penetration depth of silver along grain boundaries has two maxima: 350 and 260 microns at $\Delta\theta$ = 35 and 75°, and a minimum (b $\simeq$ 30 microns) at $\Delta\theta$ =56°. At other disorientation angles between neighboring grains the depth of penetration of silver has intermediate values, varying in a regular manner within the limits of 25 and 350 microns.

A comparison of data obtained on intercrystalline diffusion of silver into the alloy of copper with 0.25% antimony and into pure copper reveals the following:

The values for the penetration depth of silver along intercrystalline boundaries of the alloy are substantially higher in comparison with the corresponding values for pure copper. This increase is especially great for the maxima of $\underline{b} \sim 350$ microns for the alloy, and 50 microns for copper.

The locations of the maxima and minima on the $\Delta\theta$ scale <u>do not</u> for the copper antimony alloy and for pure copper <u>coincide</u> in the first case the maxima are observed at $\Delta\theta = 35$ and 75°, in the second at 30 and 60°, while the minima are observed at $\Delta\theta = 56$ and 45° respectively. These locations were repeatedly obtained in a series of experiments using different specimens and specimens of varying types produced by(melting and rolling as well as electrolysis).

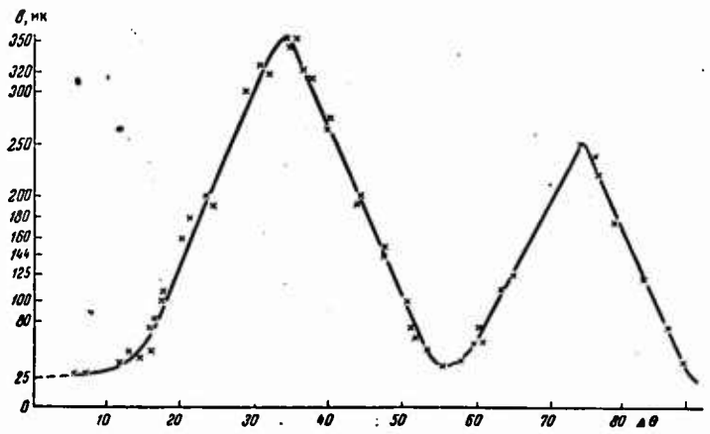

Fig. 10. Composite curve of the dependence of β on $\Delta\theta$ in the diffusion of silver into the alloy of Cu with 0.25% Sb, the coarse grain of which was obtained in the specimens by recrystallization

T = 650°; t = 600 hours

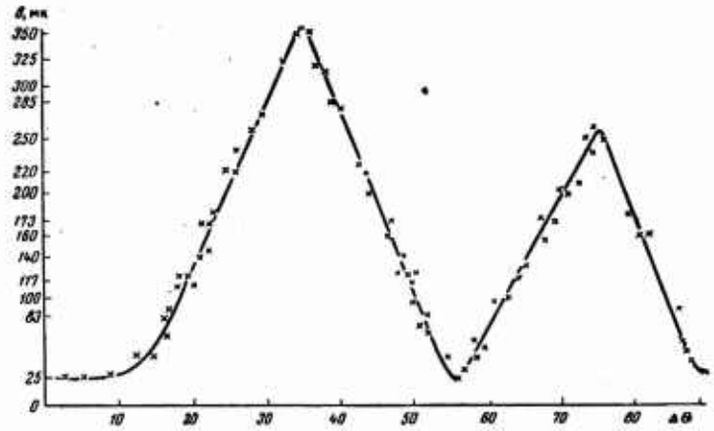

Fig. 11. Composite curve of the dependence of β on $\Delta\theta$ for the diffusion of silver into the solid solution Cu with 0.25% Sb. The copper being electrolytic copper.

$t = 650°$, $t = 600$ hours

Analysis of Results and Conclusions

During the last 20 to 25 years it has been determined by a great number of experiments that diffusion occurs more rapidly along the boundaries of grains than through their body.

This fact was first established indirectly through determination of the coefficients of diffusion or self-diffusion. It was found that the values of the diffusion coefficients for the same materials studied are not identical unless the grain size of these materials is the same and that, namely the diffusion coefficient usually increases with a reduction in grain size. This fact has been confirmed more obviously by recent research (beginning in 1951) carried out

by radioautographic methods. The combining of the theoretical approach with experimental data, best exemplified by Fisher [33], has made it possible to conclude that the activation energy of boundary diffusion is substantially less than the activation energy of intragranular diffusion.

The data of our investigation relate in particular to a series of experiments to determine the orientational dependence of intercrystalline diffusion as observed by metallographically methods, and they show a definite dependence of the intercrystalline diffusion of silver into pure copper or into a solid solution on the mutual orientation of adjacent crystals (Figs 8-11).

This effect, in relation to diffusion into pure copper may be explained as follows. The distortion of the boundary crystal structure varies with a change in the degree of disorientation of adjacent crystals and governs the variation in the excess energy of atomic interaction in the intercrystalline zone as compared to the body of the grain, which has a regular crystalline structure. It is therefore natural that the character of the distortions in the zone of transition from the crystal lattice of one grain to the lattice of another has an effect on the interatomic bonds with in it, which facilitates the elementary act of diffusion. In other words, diffusion along intercrystalline face planes will be facilitated to a greater or lesser degree, according to the disorientation of the adjacent crystals.

Our experiments determined that for grain disorientation of 0 to 10° and from 82°30' to 90° and also in the interval between 41°30' and 47°15' the intercrystalline diffusion of silver as shown metallographically is not significantly greater by comparison with

intergranular diffusion. Apparently, with these crystal grain rotations the distortions are not great, and the intercrystalline couplings can easily be represented with the aid of the dislocation model. At other angles of disorientation the number of dislocations should increase; interaction between dislocations now appears and the boundary structure can no longer be represented by such a simple model. A more convenient model is the one based on the concept of a "two-dimensional nonius" [1].

On the basis of what has been stated above and the experimental data obtained (Figs. 8, 9), it is possible to draw the following two conclusions in regard to intercrystalline diffusion of silver into pure copper.

The distortion of the crystal structure of the intercrystallite zone, which reduces its bonds in comparison with the undistorted crystal structure in the interior of adjacent crystals, govern the acceleration of the diffusion of silver along the boundaries, as compared to the grain body (maximum depth of penetration b for the intercrystallite coupling is more than three times the volume value of b). The degree of distortion of the crystal structure of the intercrystalline zones, varies with cahnges in the disorientation of adjacent grains, which also affects the quantity of the excess energy of intercrystalline zones, and consequently of Q boundary. Hence, for different mutual orientations of the crystals the degree of intensification of intercrystalline diffusion as compared to intragranular diffusion (as a function of the magnitude of the excess energy and binding forces in the intercrystalline coupling will be unequal. The result of this is the irregular character of the diffusion of silver along crystallographically different abutments

in the copper specimens.

The results obtained from the study of the intercrystalline diffusion of silver into the copper alloy with 0.25% antimony may be explained as follows. The internal adsorption effect is contingent on the presence of excess energy in the intercrystalline zone [1, 2]. It has been determined that the quantity of the excess energy depends on the disorientation of the grains forming the transition zone [3-15] and, therefore, on the disorientation of adjacent grains also conditions the quantity of horophyle additive absorbed in the intercrystalline zone coupling them, i.e., The degree of distortion of the intercrystalline transition zone must have an effect on the irregular character of internal adsorption.

The selected alloy contains the horophyle additive, antimony, the adsorption capacity of which has been shown by research [22-27], and also in the present work on the observed effect of antimony on the recrystallization of the copper alloy with 0.25% antimony on the boundaries of differently oriented grains in the copper-antimony alloy, became apparent in our work, through the unevenness of the increase of the intercrystalline diffusion of silver as shown metallographically, into the copper-antimony alloy, compared with pure copper. At the same time it is known [22] that with the increase in antimony content of the copper-antimony alloy the diffusion rate of silver into this alloy increases. It can be assumed in this connection that the diffusion of silver through various intercrystalline bond contacts will depend on the quantity of adsorbed antimony in them.

On the basis of the above and of the results obtained (Figs. 10 and 11) the following conclusions can be drawn with regard to

the intercrystalline diffusion of silver into the copper-antimony alloy.

1. The effect of disorientation of adjacent crystals on the degree of unevenness of the intercrystalline diffusion as shown metallographically is indicative of the unevenness of the distribution of the antimony concentration along the abutting zones of grains with different orientations with respect to each other.

2. The unevenness of diffusion of silver into the copper alloy with 0.25% antimony as compared to pure copper is much more sharply defined. This is because the unevenness of the diffusion of silver into pure copper is governed only by the differences in the quantity of excess energy in the intercrystalline abutments with different degrees of grain disorientation. In the case of the alloy of copper with 0.25% antimony, however, the unevenness of the diffusion of silver also increases because of the adsorption capacity of antimony, the content of which along the intercrystalline abutments is increased as compared to the body of the grain.

3. The nature of the distortions in the intercrystalline zones which causes a certain acceleration of the diffusion of silver in them compared to the body of the grain, apparently differs in the case of pure copper from similar distortions observed in the copper-antimony alloy, since in the latter case a large amount of antimony enters the intercrystalline zones through adsorption. The change in the nature of the distortions in the intercrystalline zones with a given grain disorientation, which this brings about, is evidently the reason for the shift of the maxima and minima on the curves $b = f\Delta\theta$ for the diffusion of silver into the alloy of copper with 0.25% antimony, compared with diffusion in pure copper.

These conclusions appear to us most likely to be true, but for a final answer to the question further research is essential, and, first of all, similar experimental data must be obtained for other alloys.

REFERENCES

1. ARKHAROV, V. I. Tr. IFM UFAN, (Papers of IFM of Ural Branch of Acad Sci. USSR) Nr. 8, 1946; Nr. 16, 1955.

2. ARKHAROV, V. I. Tr. IFM UFAN, Nr. 12, 1949.

3. SMITH, C. S. Trans. AIME, 175, 1948.

4. GREENOUGH, A. P. and KING, R. J. Inst. Met., 79, 1951.

5. SHUTTLEWORTH, R ; KING, R.; and CHALMERS, B. Nature, 158, 1946.

6. FORSYTH, P.; METCALF, G.; KING, R.; and CHALMERS, B. Nature, 158, 1946.

7. CHALMERS, B.; KING, R.; and SHUTTLEWORTH, R. Proc. Roy. Soc., 193A, 1948.

8. SHUTTLEWORTH, R. Metallurgia, 38, 1948.

9. CHALMERS, B. Proc. Roy. Soc., 162A, 1937.

10. STEACIE, E. and JOHNSON, F. Proc. Roy. Soc., 112A, 1926.

11. DUNN, C. G. and LIONETTI, F. Trans. Amer. Inst. Min. Met. Eng., 185, 1949.

12. DUNN, C. G.; DANIELS, F. W.; and BOLTON, M. J. J. of Met., 188, 1950.

13. AUST, K. T. and CHALMERS, B. Proc. Roy. Soc., 201A, 1950.

14. READ, W. T. and SHOCKLEY, W. Phys. Rev., 78, 1950.

15. VAN DER MERWE, J. H. Proc. Phys. Soc., 63 A 1950.

16. ACHTER, M. R. and SMOLUCHOWSKI, R. Phys. Rev., 76, 1949.

17. ACHTER, M. R. and SMOLUCHOWSKI, R. Phys. Rev., 83, 1951.

18. ACHTER, M. R. and SMOLUCHOWSKI, R. J. Appl. Phys., 23, 1952.

19. FLANAGAN, M. R. and SMOLUCHOWSKI, R. J. Appl. Phys., 23, 1952.

20. COULING, S. and SMOLUCHOWSKI, R. J. Appl. Phys., 25, 1954.

21. HAYNES, C. W. and SMOLUCHOWSKI, R. Acta Metallurgica, 3, 1955.

22. ARKHAROV, V. I. and GOLDSHTEYN, T. Yu. Tr. IFM UFAN, Nr. 11, 1950.

23. NEMNONOV, S. A. Tr. IFM UFAN, Nr. 11, 1950.

24. MCLEAN, D. J. Inst. Met., 81, 1952.

25. HOPKIN, L. M. T. J. Inst. Met., 84, 1955.

26. ARKHAROV, V. I. and SKORNYAKOV, N. N. Tr. IFM UFAN, Nr. 16, 1955.

27. ARKHAROV, V. I. and VANGENGEYM, S. D. Issledovaniya po zharoprochnym splavam (Investigations of Heat Resistant Alloys) Vol. II. Acad. Sci. USSR 1957.

28. SEMERYUK, V. I. Zhurn. Prikl. Khim (Journ. Appl. Chem) 28, Nr. 11, 1955.

29. LEVIN, E. E. Mikroskopicheskoye issledovanie metallov (Miscroscopic Study of Metals) Mashgiz, 1955. St. Sc. Tech. Press. Lit. on Mach.)

30. "X-ray diffraction by polycrystalline Materials". The Institute of Physics. London, 1955.

31. ZHDANOV, G. S. and UMANSKY, Ya. S. Rentgenografia metallov (Metal Radiography), Part II, 1938.

32. GRENINGER, A. B. Trans. AIME, 117, 1935, 122, 1936.

33. FISHER, J. C. J. Appl. Phys., 22, 1951.

34. SMOLUCHOWSKI, R. Phys. Rev., 87, 1952.

STUDY OF ATOMIC INTERACTION IN ALLOYS BY ANALYSIS OF X-RAY SCATTERING FROM THE CRYSTAL LATTICE

V. V. Geychenko, M. A. Krivoglaz, A. A. Smirnov

The propagation of various types of waves by a crystal lattice may be utilized to determine the atomic interaction constant in lloys since these constants enable us to estimate, to a certain extent, the strength of the crystal lattice. The present study with this end in view deals with the diffuse scattering of x-rays by alloys of various kinds. The formulas derived are also applicable to the study of radiation of other types of waves (electrons, neutrons*).

The theory only takes into account diffuse scattering involving the irregular alternation of different kinds of atoms at the points of the crystal lattice, and in the case under consideration the

---

* Certain other peculiarities exist in the scattering of slow neutrons which have been studied in the paper "Concerning the Theory of Slow-neutron Scattering in Alloys" included in the present collection.

static geometric distortions of the lattice are slight; i.e., in the calculations the lattice is held to be geometrically ideal. Also, scattering due to the thermal vibration of atoms is not considered here.

The present paper gives the results of investigations on the basis of which formulas were derived relating the atomic interaction constants to the diffuse background intensity.

Diffuse Scattering in Substitutional Alloys

Let us examine a substitional-type alloy with any number of components which, in a disordered state, has a Bravais lattice, any composition, and long-range order. In calculating the background intensity we shall allow for correlation in the substitution of atoms of a different kind in the points of the crystal lattice in all coordination spheres.

As is well known, the intensity I_{bg} of the diffuse scattering of x-rays by the crystal lattice of the alloy of the given type, expressed in electronic units, can be written as follows:

$$I_{\Phi} = \sum_{s,\, s'=1}^{N_0} \sum_{\kappa,\, \kappa'=1}^{\mu} (f_{s\kappa} - \bar{f}_{\kappa})\,(f^{*}_{s'\kappa'} - \bar{f}^{*}_{\kappa'})\, e^{i\vec{q}(\vec{R}_{s\kappa} - \vec{R}_{s'\kappa'})}, \qquad (1)$$

where N_0 is the number of elementary cells in the crystals;

μ is the number of points in the elementary cell of the ordered alloy;

$f_{s\kappa}$ is the scattering factor of the atom replacing point κ in cell number s;

$\vec{q} = \vec{k\kappa'} - \vec{k}$ is the difference between the wave vector of the scattered and incident waves;

$\vec{R}_{s\kappa}$ is the vector drawn from the first point of the first cell to point number κ of the s cell.

The line over $f\kappa$ and $j^*\kappa'$ denotes the averaging of these quantities for all points of the given type.

Formula (1) may be expressed in another form by the method set forth in [1]. As a result we obtain for I_{bg} the formula

$$I_{bg} = S_1 + S_2, \tag{2}$$

where:

$$S_1 = N_0 \sum_{\substack{\alpha,\ \alpha'=1 \\ (\alpha<\alpha')}}^{\zeta} \Delta_{\alpha\alpha'} \sum_{L=1}^{Q} \lambda_L p_\alpha^L p_{\alpha'}^L; \tag{3}$$

$$S_2 = -\frac{N_0}{2} \sum_{\substack{\alpha,\ \alpha'=1 \\ (\alpha\leq\alpha')}}^{\zeta} \Delta_{\alpha\alpha'} \sum_{L=1}^{Q} \sum_{\kappa_L=1}^{\lambda_L} \sum_{l=1}^{\infty} \sum_{L'=1}^{Q} [\varepsilon_{\alpha\alpha'}^{LL'}(\rho_l) + \varepsilon_{\alpha'\alpha}^{LL'}(\rho_l)] \sum_{m_{lL'}=1}^{z_{lL'}} \cos \vec{q}\vec{\rho}_{m_{lL'}} \tag{4}$$

here α and α' are the type of atom;

ζ is the number of components in the alloy;

L, L' is the number of the type of point (L, L = 1,. . .,Q);

κ_L is the number of the point of type L in the elementary cell ($\kappa_L = 1, \ldots, \lambda_L$);

p_α^L is the a priori replacement probability of a point of type L by an atom of type α;

$\underline{l}$ is the number of the coordination sphere of radius $\rho_{\underline{l}}$, described around point of type L number κ_L;

$\vec{\rho}m_{lL'}$ is the vector extended from the central point to point number $m_{lL'}$ (of the type L' in the lth coordination sphere);

$z_{lL'}$ is the number of points of type L' in the lth coordination sphere;

$$\Delta_{\alpha\alpha'} = |f_\alpha - f_{\alpha'}|^2; \tag{5}$$

$\epsilon_{\alpha\alpha}^{LL'}(\rho_1)$ is the correlation parameter determined by the formula

$$\epsilon_{\alpha\alpha'}^{LL'}(\rho_l) = p_{\alpha\alpha'}^{LL'}(\rho_l) - p_{\alpha}^{L} p_{\alpha'}^{L'}. \tag{6}$$

In this expression $P_{\alpha\alpha}^{LL'}$ denotes the probability that atom α is at a point of type L, while atom α' is situated at a point of type L', at distance ρ_1 away from it.

In a case where the correlation in the alloy is insignificant and its parameters may be considered equal to zero, $S_2 = 0$ and the intensity of diffuse scattering is equal to S_1. If, however, the correlation is essential, S_2 must also be considered. Here the correlation parameters (or their combinations) may in some cases be determined from analysis of the intensity distribution of the background. For instance, in the case of binary ordered alloys A-B, certain combinations of the correlation parameters may be found by Fourier analysis of the intensity I_{bg}, in the same way as in [2] for disordered alloys.

Let us resolve vector $\vec{q}$ into the vectors of the Bravais reciprocal lattice of an unordered alloy: $\vec{b}_1$, $\vec{b}_2$, $\vec{b}_3$:

$$\vec{q} = 2\pi(x\vec{b}_1 + y\vec{b}_2 + z\vec{b}_3), \tag{7}$$

and vector $\vec{\rho}m_{1L'}$ into vectors $\vec{a}_1$, $\vec{a}_2$, $\vec{a}_3$ of the Bravais lattice of an unordered alloy:

$$\vec{\rho}_{m_{lL'}} = \nu_{1m_{lL'}}\vec{a}_1 + \nu_{2m_{lL'}}\vec{a}_2 + \nu_{3m_{lL'}}\vec{a}_3. \tag{8}$$

In formula (7) x, y, z are certain continuous variables, and in formula (8) $\nu_1 m_{1L'}$, $\nu_2 m_{1L'}$, $\nu_3 m_{1L'}$ are whole numbers.

Then, for binary alloys, in which $\epsilon_{AB}^{LL'} = \epsilon_{AB}^{L'L}$, expression (4) may be written as

$$\frac{S_2}{N_0 \Delta_{AB}} = -\sum_{L=1}^{Q} \sum_{\kappa_L=1}^{\lambda_L} \sum_{l=1}^{\infty} \sum_{L'=1}^{Q} \epsilon_{AB}^{LL'}(\rho_l) \sum_{m_{lL'}=1}^{z_{lL'}} \exp\left[2\pi i \left(x\nu_{1m_{lL'}} + y\nu_{2m_{lL'}} + z\nu_{3m_{lL'}}\right)\right]. \qquad (9)$$

From this

$$\sum_{L=1}^{Q} \sum_{\kappa_L=1}^{\lambda_L} \epsilon_{AB}^{LL'}(\rho_l) = -\frac{1}{N_0} \int_0^1 \int_0^1 \int_0^1 \frac{I_\Phi(x, y, z)}{\Delta_{AB}} \exp\left[-2\pi i \left(x\nu_{1m_{lL'}} + y\nu_{2m_{lL'}} + z\nu_{3m_{lL'}}\right)\right] dx\, dy\, dz, \qquad (10)$$

where S_2 in formula (9) may be replaced by $I_{bg} = S_1 + S_2$, since $\frac{S_1}{\Delta_{AB}}$ does not depend on x, y, z, and after integration is equal to zero. For binary unordered alloys, the combination of the quantities $\epsilon_{AB}^{LL'}(\rho_1)$, cannot be obtained this way, but it the correlation parameters are $\epsilon_{AB}(\rho_1)$:

$$\epsilon_{AB}(\rho_l) = -\frac{1}{N} \int_0^1 \int_0^1 \int_0^1 \frac{I_\Phi(x, y, z)}{\Delta_{AB}} \exp\left[-2\pi i \left(x\nu_{1m_l} + y\nu_{2m_l} + z\nu_{3m_l}\right)\right] dx\, dy\, dz, \qquad (11)$$

where $N = N_0 \mu$ is the total number of atoms in the crystal.

Knowledge of the correlation parameters makes it possible to determine the short-range order in the alloy, i.e., to determine the distribution of atoms of any kind near an atom of a given kind, and thereby to assess the micro- heterogeneities of the composition of the alloy. On the other hand, it may be possible in certain cases, using the statistical order-disorder theory, to relate the correlation parameters to the energies of atomic interaction (ordering or disordering energies). For instance, for an unordered binary alloy at sufficiently high temperatures, Kirkwood's theory gives us the following form for $\epsilon_{AB}(\rho_1)$:

$$\epsilon_{AB}(\rho_1) = c_A^2 c_B^2 \frac{w_1}{kT}, \qquad (12)$$

where: c_A and c_B are the relative atomic concentrations of the components A and B;

w_1 is the ordering energy (or disordering energy) for the first coordination sphere;

k is the Boltzmann constant;

T is the absolute annealing temperature of the alloy.

Equations (11) and (12) make it possible to determine the magnitude w_1 characterizing the atomic interaction in the alloy.

Diffuse Scattering in Interstitial Alloys

Let us examine interstitial alloys, in which the lattice points and interstices form a single Bravais lattice. If relatively small atoms* become embedded in the interstices of an alloy of this kind, the resultant alloy can be treated as a substitutional alloy, the points of which (being the points and interstices of the interstitial alloy in question) have been replaced by various other atoms and vacancies. Hence, formulas (2) - (4) may be applied to these instertitial alloys. Keeping the notation $\alpha(\alpha = 1,\ldots,\xi)$ for the type of atoms at the points, and denoting by $\beta(\beta = 1,\ldots,\xi)$ the type of atoms (including the vacancies) in the interstices, we obtain the following expressions for S_1 and S_2:

---

* The embedded atoms should not distort the lattice to a point where an additional background, brought about by the distortion, substantially changes the distribution of the diffuse-scattering intensity.

$$S_1 = N_0 \Big(\sum_{\substack{\alpha,\alpha'=1 \\ (\alpha<\alpha')}}^{\xi} \Delta_{\alpha\alpha'} \sum_{L_\gamma=1}^{Q_\gamma} \lambda_{L_\gamma} p_\alpha^{L_\gamma} p_{\alpha'}^{L_\gamma} + \sum_{\substack{\beta,\beta'=1 \\ (\beta<\beta')}} \Delta_{\beta\beta'} \sum_{L_M=1}^{Q_M} \lambda_{L_M} p_\beta^{L_M} p_{\beta'}^{L_M} \Big), \tag{13}$$

$$S_2 = -\frac{N_0}{2} \Big\{ \sum_{\substack{\alpha,\alpha'=1 \\ (\alpha=\alpha')}}^{\xi} \Delta_{\alpha\alpha'} \sum_{L_\gamma=1}^{Q_\gamma} \sum_{\kappa_{L_\gamma}=1}^{\lambda_{L_\gamma}} \sum_{l=1}^{\infty} \sum_{L'_\gamma=1}^{Q_\gamma} [\varepsilon_{\alpha\alpha}^{L_\gamma L'_\gamma}(\rho_l) + \varepsilon_{\alpha\alpha'}^{L_\gamma L'_\gamma}(\rho_l)] \sum_{m_{lL'_\gamma}=1}^{z_{lL'_\gamma}} \cos \vec{q}\vec{\rho}_{m_{lL'_\gamma}} +$$

$$+ \sum_{\alpha=1}^{\xi} \sum_{\beta=1}^{\xi} \Delta_{\alpha\beta} \Big[\sum_{L_\gamma=1}^{Q_\gamma} \sum_{\kappa_{L_\gamma}=1}^{\lambda_{L_\gamma}} \sum_{l'=1}^{\infty} \sum_{L'_M=1}^{Q_M} \varepsilon_{\alpha\beta}^{L_\gamma L'_M}(\rho_{l'}) \sum_{m_{l'L'_M}=1}^{z_{l'l''_M}} \cos \vec{q}\vec{\rho}_{m_{l'L'_M}} +$$

$$+ \sum_{L_M=1}^{Q_M} \sum_{\kappa_{L_M}=1}^{\lambda_{L_M}} \sum_{l''=1}^{\infty} \sum_{L'_\gamma=1}^{Q_\gamma} \varepsilon_{\beta\alpha}^{L_M L'_\gamma}(\rho_{l''}) \sum_{m_{l''L'_\gamma}=1}^{z_{l''L'_\gamma}} \cos \vec{q}\vec{\rho}_{m_{l''L'_\gamma}} \Big] +$$

$$+ \sum_{\substack{\beta,\beta'=1 \\ (\beta<\beta')}}^{\xi} \Delta_{\beta\beta'} \sum_{L_M=1}^{Q_M} \sum_{\kappa_{L_M}=1}^{\lambda_{L_M}} \sum_{l'''=1}^{\infty} \sum_{L'_M=1}^{Q_M} [\varepsilon_{\beta\beta'}^{L_M L'_M}(\rho_{l'''}) +$$

$$+ \varepsilon_{\beta'\beta}^{L_M L'_M}(\rho_{l'''})] \sum_{m_{l'''L'_M}=1}^{z_{l'''L'_M}} \cos \vec{q}\vec{\rho}_{m_{l'''L'_M}} \Big\}. \tag{14}$$

Here, the indices y and m indicate that the quantities denoted by them refer to the corresponding lattice points and interstices; l and l" denote the number of the coordination spheres made up of lattice points, projected around the point and interstice, respectively, and l' and l" are the number of the spheres consisting of interstices projected around the point and interstice, respectively.

Let us examine the specific case of a disordered alloy having atoms of two kinds A and B on the points forming a face-centered cubic lattice, and atoms C and holes (denoted by D) in the interstices. Let the concentration with respect to atom C be small. In this case the last term in Eq. (14), which expresses part of the background intensity dependent on the correlation between interstices, may be disregarded. We shall take into account the fact that the embedded atoms usually have greater mobility than the atoms at the lattice points. Hence correlation at the lattice points is

established by prolonged annealing at a high temperature, while for correlation between lattice points and interstices a relatively lower temperature and a comparatively shorter time are needed. Thus it is possible to prepare an interstitial alloy and produce correlation between the lattice points and interstices without disturbing the correlation between the lattice points which exist in the binary alloy A-B. This makes it possible experimentally to exclude the part of the background depending on correlation at the lattice points. The quantity S_1 may here be calculated and taken into account.

For the part of the background I'_{bg} remaining in Eq. (14), conditioned by the correlation between lattice points and interstices in alloys of the type in question, bearing in mind that $\epsilon_{AC} = \epsilon_{BD} = \epsilon_{BC} = \epsilon_{AD}$ we arrive at the expression

$$I'_{\phi} = 4N_0 [(f_A - f_B) f_C^* + (f_A^* - f_B^*) f_C] \sum_{n=1}^{\infty} \epsilon_{AC}(\rho_n) \sum_{m_n=1}^{z_n} \cos \vec{q}\vec{\rho}_{m_n}. \qquad (15)$$

Here: f_A, f_B, f_C are the scattering factors of atoms A, B, and C;

n is the number of the coordination sphere drawn around a lattice point through the interstices, or around an interstice through the points (which for the given structure is the same);

$\vec{\rho}_{m_n}$ is the radius-vector determining the location of the m_nth point (or interstice) in the nth coordination sphere;

z_n is the coordination number for the nth coordination sphere.

Applying Fourier analysis to the quantity

$$F(x, y, z) = \frac{I'_{\phi}}{4N_0 [(f_A - f_B) f_C^* + (f_A^* - f_B^*) f_C]}, \qquad (16)$$

it is possible to obtain the following expression for the correlation parameter $\epsilon_{AC}(\rho n)$:

$$\epsilon_{AC}(\rho_n) = \int_0^1\int_0^1\int_0^1 F(x, y, z) \exp[-2\pi i (xv_{1m_n} + yv_{2m_n} + zv_{3m_n})]\, dx\, dy\, dz. \qquad (17)$$

The quantities $\epsilon_{AC}(\rho n)$ make it possible to determine which atoms (A or B) will be predominantly surrounded by atoms C.

The relationship of the correlation parameter $\epsilon_{AC}(\rho_1)$ to the interaction energies v_{AC} and v_{BC} of the neighboring atoms AC and BC has been determined in a paper, as yet unpublished,

$$\epsilon_{AC}(\rho_1) = \frac{e^{\frac{v_{AC}-v_{BC}}{RT}} - 1}{c_A e^{\frac{v_{AC}-v_{BC}}{RT}} + c_B} c_A c_B c_C, \qquad (18)$$

where c_A and c_B are the ratios of the number of atoms A and B to the number of lattice points, and c_C is the ratio of the number of atoms C to the number of interstices.

Knowing I'_{bg}, equations (16), (17), and (18) make it possible to find the quantity $v_{AC}-v_{BC}$ and, in particular, to determine with which atoms on the lattice points the C atoms interact most strongly.

It should be noted that the determination of $\epsilon_{AC}(\rho n)$ by Eq. (17) can best be applied to alloys, the interstices of which are interspersed with hydrogen atoms, which causes relatively slight distortion of the crystal lattice. It is clear that in this case slow neutrons should be used instead of x-rays, the diffuse scattering intensity of these neutrons (which is related to correlation) being determined by equations of the same type.

Investigation of Diffuse Scattering of X-rays in Substitutional Alloys by the Method Fluctuations

In the above method of investigating x-ray scattering we have discussed secondary waves scattered by individual atoms of the alloy and the scattering intensity has been defined as the result of interference of these secondary waves under conditions of a given distribution of atoms. Using this method, it is possible to express the intensity of the true reflections through the concentration of the alloy components and the long-range order parameters and the diffuse scattering intensity through the concentration, the long-range order parameters, and the correlations. The derived equations also make it possible to determine the long-range order parameters (the p_{α}^{L} probabilities, for instance) and the correlation parameters, using the distribution of the scattering intensity, determined experimentally. It is of interest, however, to determine as well the dependence of the scattering intensity on the temperature (and the composition of the alloy), as well as on the constants characterizing atomic interactions in the alloy. To study these relationships, it is much more convenient to use another method which was introduced by Einstein [3] in the problem of the dispersion of light and then applied to a study of the intensity of x-ray diffuse scattering near true reflections [4]. In this method the diffuse scattering intensity in alloys is expressed through Fourier components of the parameters characterizing concentrations of the alloy components and the long-range-order parameters. Since the mean values of the square of the fluctuations depend intrinsically on the interaction energies of the atoms of the alloy and on the temperature, the diffuse scattering intensity can also be expressed through these quantities.

In [4] the calculation was made without a specific atomic model

of the alloy, using the thermodynamic theory of second-order phase transitions. In order to relate the scattering intensity to the atomic interaction constants, one of the authors made the calculation for binary and ternary substitutional alloys, using a specific atomic model. The results of the calculation for binary alloys are given below.

The intensity of the diffuse scattering of monochromatic radiation by single crystals was determined, and, as above, the background associated with the geometric (static and thermal) distortions of the lattice and with Compton scattering was not considered. The model taken is the conventional statistical model of an alloy, in which the energy of the crystal is represented as the sum of interaction energies of different pairs of atoms. In the calculation the interaction, as well as the correlation of the atomic pairs with any distance between the atoms, is taken into account.

As a result, the following equation was derived for the intensity of x-ray diffuse scattering by a disordered alloy A-B with a Bravais crystal lattice of conventional structure:

$$I_\phi = N|f_A - f_B|^2 \frac{1}{X_0 + \sum_{l=1}^{\infty} X_l \sum_{m_l=1}^{z_l} \cos \vec{q}\vec{\rho}_{m_l}}, \qquad (19)$$

where I_{bg} is the scattering intensity expressed in electronic units;

z_l is the coordination number of the l th coordination sphere;

m_l is the numbering of lattice points in this sphere;

$\vec{\rho}_{m_l}$ is the vector drawn from the central point to point number m_l of the l th coordination sphere.

The quantities X_0 and X_l are expressed by the second derivatives of the thermodynamic potential of the concentrations p_{Aj} of A atoms in the different sub-lattices n_0 (numbered with the index j), into

which the crystal lattice of the alloy is divided:

$$X_0 = \frac{n_0}{NkT}\frac{\partial^2 \Phi}{\partial p_{A1}^2}; \quad X_l = \frac{n_0}{NkT}\frac{\partial^2 \Phi}{\partial p_{A1}\partial p_{Am_l}}. \tag{20}$$

The division into these sub-lattices is done in such a way that each atom only interacts with one point of the foreign sub-lattice and does not interact with atoms at the points of the same sub-lattice.

p_{A1} is the concentration of A atoms at the points of the sub-lattice containing the central atoms, and A_{Am_e} is the concentration of A atoms at the points of the sub-lattice containing the atom at point number m_1 of the 1 the coordination sphere.

The quantities X_o and X_1 may be determined by Eq. (20) if the expression for the thermodynamic potential as a function of the variables p_{Aj} is known. A simple approximation for bg may be obtained at high temperatures. Then

$$X_0 = \frac{1}{c_A(1-c_A)}, \quad X_l = \frac{w_l}{kT}, \tag{21}$$

where w_1 is the ordering energy for the 1 th coordination sphere

$$w_l = 2v_{AB}(\rho_l) - v_{AA}(\rho_l) - v_{BB}(\rho_l), \quad \text{where}$$
$$v_{AA}(\rho_l),\ v_{AB}(\rho_l) \text{ и } v_{BB}(\rho_l) -$$

with the opposite sign, are the interaction energies of the atomic pairs AA, AB, and BB, located at distance ρ_1 equal to the radius of the 1 th coordination sphere.

The approximation used for expressing the thermodynamic potential is applicable if, for all 1 $|w_1| \ll kT$. In the case of arbitrary temperatures it is possible to obtain an expression for bg and therefore for X_o and X_1, if the concentration of one of the alloy components is sufficiently small ($C_A \ll 1$). In this case

$$X_0 = \frac{1}{c_A(1-c_A)}, \quad X_l = 1 - e^{-\frac{w_l}{kT}}. \tag{22}$$

Equation (19) for the diffuse-scattering intensity is also valid for ordered alloys of stoichiometric AB Composition in which lattice points of the first type are surrounded by points of the first and second types, in the same way as the points of the second type are surrounded by points of the first and second types (crystals of β-brass, Au, Cu types, etc.). In this case, for almost completely ordered alloys ($1-\eta \ll 1$, η is the degree of long-range order)

$$X_0 = \frac{4}{1-\eta^2}, \tag{23}$$

$$X_l = 1 - l^{-\frac{w_l}{kT}}, \tag{24}$$

if the l th coordination sphere around the point of the first type consists of points of the first type and

$$X_l = l^{\frac{w_l}{kT}} - 1, \tag{25}$$

if the l th coordination sphere consists of points of the second type. Here, we assume that points of different types corresponding to one and the same ρ_l belong to different coordination spheres.

From Eqs. (19), (21), and (22) it follows that the background distribution tends towards a monotonic background, both when there is a rise in temperature and when the concentration of one of the components of the alloy tends towards zero (when the solution becomes ideal or weak)

$$I_\Phi = N|f_A - f_B|^2 C_A(1-C_A). \tag{26}$$

At sufficiently low temperatures, since $1-\eta$ decreases faster than the factors $e^{\frac{wl}{kT}} - 1$ (or $e^{-\frac{wl}{kT}} - 1$) increase, the background

intensity, in accordance with Eqs. (19) and (23) — (25), tends to the expression [5]:

$$I_\Phi = \frac{1}{4} N |f_A - f_B|^2 (1 - \eta^2), \tag{27}$$

i.e., disappears when $\eta \to 1$.

From the above equations it follows that if the interaction with atoms of the first coordination sphere alone is essential ($w_1 = w$, $w_l = 0$ when $l \neq 1$), then, for the ordered solution ($w > 0$), the maxima of the background intensity of the type under consideration will lie near super lattice reflections and the minima near those of the lattice. In disintegrating alloys ($w < 0$), on the contrary, the maxima of background intensity lie near the lattice reflections.

With the aid of Eq. (19) and the equations for X_0 and X_1 it is possible to study the dependence of the diffuse-scattering intensity of x-rays on the annealing temperature composition of the alloy and degree of long-range order, and energies w_l. These equations are applicable in those ranges of temperatures and compositions where the correlation is slight. Near the temperature of phase transition, the correlation becomes substantial. In this case, if the interaction with atoms of the first coordination sphere alone is essential, the scattering intensity may be expressed as

$$I_\Phi = N |f_A - f_B|^2 \frac{1}{a_1 + a_2 \sum_{m_1=1}^{z_1} \cos \vec{q}\vec{\rho}_{m_1}}. \tag{28}$$

Here z_1 is the coordination number of the first coordination sphere, and for unordered alloys with a body-centered cubic lattice

$$\begin{aligned} a_1 &= \frac{1}{\varphi} + 8\varphi \left(\frac{w}{kT}\right)^2 - 8\varphi(1 - 4\varphi)\left(\frac{w}{kT}\right)^3 - \varphi\left[-\frac{2}{3}(7 - 72\varphi + 180\varphi^2) + \right. \\ &\quad \left. + 48\varphi(1 - 6\varphi)\right]\left(\frac{w}{kT}\right)^4 + \ldots, \\ a_2 &= \frac{w}{kT} - \frac{1}{2}(1 - 4\varphi)\left(\frac{w}{kT}\right)^2 + \frac{1}{6}(1 - 6\varphi)\left(\frac{w}{kT}\right)^3 + \\ &\quad + (1 - 4\varphi)\left[\frac{1}{24}(1 - 12\varphi)^2 + 11\varphi^2\right]\left(\frac{w}{kT}\right)^4 + \ldots, \end{aligned} \tag{29}$$

where $\varphi = c_A (1 - C_A)$.

For disordered alloys with a face-centered cubic lattice

$$a_1 = \frac{1}{\varphi} + 12\varphi\left(\frac{w}{kT}\right)^2 - 12\varphi\left(\frac{w}{kT}\right)^3 + \ldots,$$
$$a_2 = \frac{w}{kT} - \frac{1}{2}(1 - 4\varphi)\left(\frac{w}{kT}\right)^2 + \frac{1}{6}(1 + 12\varphi - 60\varphi^2)^2\left(\frac{w}{kT}\right)^3 + \ldots \quad (30)$$

If the transition to the ordered state is a second-order phase transition, then near the transition temperature T_0, the diffuse scattering near the super-lattice reflections becomes unusually large. For alloys with a face-centered cubic lattice, in this case

$$I_\Phi = N|f_A - f_B|^2 \beta \frac{1}{\frac{T - T_0}{T_0} + \gamma q'^2}. \quad (31)$$

Here $\vec{Q}'$ is the complement of vector $\vec{q}$ to the vector at which the superlattice reflection under discussion occurs.

$$\beta = \frac{1}{4}\left[1 + \frac{1}{z_1} + \frac{5}{3}\frac{1}{z_1^2} + \frac{39}{z_1^3} + \ldots\right],$$
$$\gamma = \frac{1}{6}\left[1 + \frac{2}{z_1} + \frac{14}{3}\frac{1}{z_1^2} + \frac{68}{3}\frac{1}{z_1^3} + \ldots\right]\rho_1^2, \quad (32)$$

where ρ_1 is the distance between neighboring atoms.

From Eq. (31) it is evident that if $q' \ll 1$, then near the ordering temperature the diffuse-scattering intensity does indeed increase sharply.

The quantities X_1 in Eq. (19) can be determined if the distribution of the background intensity for various $\vec{q}$ in the experiments is known. For this purpose a Fourier transform of the expression $\frac{N|f_A - f_B|^2}{I_{bg}}$. should be made.

As a result, we obtain

$$X_0 = \frac{1}{8\pi^3}\int_0^{2\pi}\int_0^{2\pi}\int_0^{2\pi} \frac{N|f_A - f_B|^2}{I_\Phi} dk_1 dk_2 dk_3, \quad (33)$$

$$X_l = \frac{1}{8\pi^3}\int_0^{2\pi}\int_0^{2\pi}\int_0^{2\pi} \frac{N|f_A - f_B|^2}{I_\Phi} \cos\left(\sum_{i=1}^{3} \nu_{im_l} k_i\right) dk_1 dk_2 dk_3. \qquad (34)$$

Here ν_{im_l} are as above, the resolution ratios (8) of vector $\vec{\rho}_{m_l}$, corresponding to any lattice point of the l th coordination sphere, resolved into the basic vectors $\vec{a}_i$ of the crystal lattice. The quantities R_i are the resolution ratios of vector $\vec{q}$ resolved into the basic vectors $\vec{b}_i$ of the reciprocal lattice

$$\vec{q} = \sum_{i=1}^{3} R_i \vec{b}_i. \qquad (35)$$

When using Eq. (34) it should be borne in mind that other aspects of the diffuse scattering, not discussed here (related to thermal vibrations, geometric distortions etc.), have been excluded and do not enter into I_{bg}.

Thus, with the aid of Eqs. (34), (21), (22), (24), and (25), and experimental values for the background intensity of various crystal orientations and various angles of scattering (various q; i.e., various R_i) it is possible to calculate the ordering (or disordering) energies for various coordination spheres. This calculation can be performed in the case of alloys which are at a sufficiently high temperature and in which the concentration of one of the components is low, or in alloys which are in an almost completely ordered state.

REFERENCES

1. DANILENKO, V. M.; KRIVOGLAZ, M. A.; MATYSINA, Z. A.; and SMIRNOV, A. A. Article in the Present Collection, page 150.

2. COWLEY, J. M. J. Appl. Phys., 21, 1950.

3. EINSTEIN, A. Ann. d. Phys., 33, 12, 1910.

4. LANDAU, L. D.. ZhETF, Journ. Exp. Theor. Phys, 7, 1937.

5. LIFSHITZ, I. M. ZhETF, 8, 1938.

CONCERNING THE THEORY OF SLOW-NEUTRON SCATTERING IN ALLOYS

V. M. Danilenko, M. A. Krivoglaz, Z. A. Matysina, and A. S. Smirnov

The formulation of a theory to determine the scattering intensity of slow neutrons in alloys as a function of their composition, degree of long-range order, and correlation parameters between the filling of lattice points by unlike atoms (i.e., in effect, the annealing temperature) makes it possible to study the distribution of atoms at the lattice points of the alloy. Inhomogeneities in the distribution of atoms in the lattice effect many of the properties of alloys of practical importance and, specifically, their heat resistance. It is therefore of interest to develop the theory of slow-neutron scattering in alloys more generally than has been done heretofore [1-4], and to use the results in this study. The development of a method of this kind is especially important for alloys consisting of atoms with close atomic numbers (this category includes heat-resistant alloys) where x-ray structure analysis in ineffective, whereas an analytical method based on slow-neutron scattering may be successful.

The present paper gives an account of the work of the authors in which they deduce formulas for both the probability of neutron scattering associated with the disturbance of the regular alternation

of atoms of various kinds at the crystal lattice points and for magnetic dispersion. The general case of a multicomponent alloy which in an ordered state has any number of lattice-point types is the one considered, and the correlation between the filling of lattice points by atoms in all coordination spheres is taken into account. The scattering associated with the thermal or static distortions of the crystal lattice is not considered.

The general equation we derived makes it possible to clarify a series of problems in each individual case such as the effect of an impurity in a binary alloy on the neutron-scattering intensity, the effect of high-temperature annealing resulting in a short-range order, or the effect of the presence of isotopes on neutron scattering, and so forth. Individual cases of neutron scattering by binary alloys, as well as by alloys containing a third element and which have body-centered and face-centered cubic lattices, were investigated in detail, and correlation is taken into account. The angular distribution of neutron-scattering intensity for single crystals and polycrystals in alloys of this structure was studied.

Along with nuclear scattering, the magnetic scattering of neutrons by atomic electron shells becomes substantial in a number of cases; hence the utilization of nuclear scattering to study inhomogeneities makes it essential to be able to separate magnetic scattering. The paper considered the magnetic scattering of thermal neutrons near the Curie point of a ferromagnetic substance at small angles, as well as at angles corresponding to the Bragg reflection, is dealt with here, and the dependence of the diameter of the neutron scattering on the angle of scattering, annealing temperature, neutron wave length, alloy composition, and the distribution of

scattered neutrons as to energies are also studied.

Deriving a General Formula for the Probability of Nuclear Scattering of Slow Neutrons by Alloys

Let us consider the case of a multicomponent, ordered alloy of any composition with any number of lattice-point types which in a disordered state has any type of Bravais lattice.

We shall limit ourselves to the case where the magnetic neutron scattering by electrons, as well as their capture by the nuclei, is not substantial, and shall ignore these effects. The probability of elastic slow-neutron scattering by the crystal lattice within the solid angle $d\Omega$ in a unit of time may then be expressed as [1]:

$$dW = \frac{mkd\Omega}{4\pi^2\hbar^3\tau}\left\{\left|\sum_{s=1}^{N_0}\sum_{n=1}^{\mu} A_{s\kappa} e^{iqR_{s\kappa}}\right|^2 + \frac{1}{4}\sum_{s=1}^{N_0}\sum_{\kappa=1}^{\mu} B_{s\kappa}^2 j_{s\kappa}(j_{s\kappa}+1)\right\}. \qquad (1)$$

Here: m is the mass of the neutron;

$q = \frac{p' - p}{\hbar} = k' - k$ where p' and p are the impulses of the scattered and incident neutrons,

τ is the body of the crystal;

$A_{s\kappa}$ and $B_{s\kappa}$ are constants characterizing the interaction between the neutron and the nucleus located at point number κ of the sth elementary cell; these constants differ both for atoms of different elements as well as for the isotopes of each element;

$j_{s\kappa}$ is the quantum number of the momentum of the nucleus located on lattice-point number $s\kappa$;

$R_{s\kappa}$ is the vector of the position of lattice point $s\kappa$.

N_0 is the number of elementary cells in the crystal;

μ is the number of lattice points in the elementary cell.

Using $\tilde{A}_{s\kappa}$ to denote the mean value of $A_{s\kappa}$ and taking out the

probability of diffuse scattering dW_{bg} alone from Eq. (1) we obtain:

$$dW_{\Phi}=\frac{mkd\Omega}{4\pi^2\hbar^2\tau}\left\{\sum_{s,s'=1}^{N_0}\sum_{\kappa,\kappa'=1}^{\mu}(\tilde{A}_{s\kappa}-\bar{\bar{A}}_{s\kappa})(\tilde{A}_{s'\kappa'}-\bar{\bar{A}}_{\kappa'})\,e^{iq(R_{s\kappa}-R_{s'\kappa'})}+\right.$$
$$\left.+\sum_{s=1}^{N_0}\sum_{\kappa=1}^{\mu}(A_{s\kappa}-\tilde{A}_{s\kappa})^2+\frac{1}{4}\sum_{s=1}^{N_0}\sum_{\kappa=1}^{\mu}B_{s\kappa}^2 j_{s\kappa}(j_{s\kappa}+1)\right\}, \qquad (2)$$

where $\bar{\bar{A}}_{s\kappa}$ is the mean value of $\tilde{A}_{s\kappa}$ for all lattice points number κ. The last two terms of Eq. (2) give the neutron diffuse-scattering due to the presence of isotopes of the metals of the alloy and the scattering intensity spin direction of nuclei and neutrons. They can be easily expressed through the relative atomic concentrations of elements in the alloy c_α. Denoting these terms by V, we find

$$V=N\sum_{\alpha=1}^{\xi}c_\alpha\sum_{\substack{\beta,\beta'\\(\beta<\beta')}}c_\beta^\alpha c_{\beta'}^\alpha(A_\beta^\alpha-A_{\beta'}^\alpha)^2+$$
$$+\frac{1}{4}N\sum_{\alpha=1}^{\xi}c_\alpha\sum_{\beta}c_\beta^\alpha(B_\beta^\alpha)^2 j_\beta^\alpha(j_\beta^\alpha+1), \qquad (3)$$

where $N=\mu N_0$ is the number of atoms in the alloy;

ξ is the number of chemical elements forming the crystal;

c_β^α is the relative atomic concentration of isotope β

$\alpha/\sum_\beta c_\beta^\alpha$ (1);

A_β^α, B_β^α and j_β^α are possible values of quantities $A_{s\kappa}$, $B_{s\kappa}$, and $j_{s\kappa}$ corresponding to the replacement of lattice point $s\kappa$ by the isotope β or element α.

Let us compute the first of Eq. (2), for which we shall divide it into two parts corresponding to the diagonal and nondiagonal members of the sum under consideration. The term comprising the diagonal members may be easily expressed by a priori probabilities

of the occupation of the lattice points by atoms of various kinds. Denoting this term by S_1, and the probability of a substitution of lattice points of the L type by atoms of the α type by p_α^L, and carrying out the transformation by a method similar to the one used in [5], we find

$$S_1 = \sum_{s=1}^{N_0} \sum_{\kappa=1}^{\mu} (\tilde{A}_{s\kappa} - \bar{\tilde{A}}_\kappa)^2 = N_0 \sum_{L=1}^{Q} \lambda_L \sum_{\substack{\alpha,\alpha'=1 \\ (\alpha<\alpha')}}^{\xi} p_\alpha^L p_{\alpha'}^L \Delta_{\alpha\alpha'}, \tag{4}$$

where

$$\Delta_{\alpha\alpha'} = (\tilde{A}_\alpha - \tilde{A}_{\alpha'})^2; \tag{5}$$

$\tilde{A}_\alpha$ is equal to the value of $\tilde{A}_{s\kappa}$ corresponding to the case when an atom of type α is found at lattice point $s\kappa$;

γ_L is the number of lattice points of type L in the elementary cell; Q is the number of types of lattice points. The quantity $\Delta_{\alpha\alpha'}$ does not depend on the type of lattice point L.

The second part S_2 of the first term of formula (2), comprising the nondiagonal members of the sum can also be computed [5] if the correlation parameters $\epsilon_{\alpha\alpha'}^{LL'}(\rho)$ determined by the interrelation

$$\varepsilon_{\alpha\alpha'}^{LL'}(\rho) = p_{\alpha\alpha'}^{LL'}(\rho) - p_\alpha^L p_{\alpha'}^{L'}, \tag{6}$$

are brought into the discussion where $p_{\alpha\alpha'}^{LL'}(\rho)$ is the probability that atom α is situated at a lattice point of type L and atom α' is at lattice point L' at a distance of ρ.

For crystal lattices in which each point is a center of symmetry of the crystal, we find

$$\begin{aligned} S_2 &= \sum_{s,s'=1}^{N_0} \sum_{\kappa,\kappa'=1}^{\mu} (\tilde{A}_{s\kappa} - \tilde{A}_\kappa)(\tilde{A}_{s'\kappa'} - \bar{\tilde{A}}_{\kappa'}) e^{iq(R_{s\kappa} - R_{s'\kappa'})} = \\ &= -\frac{N_0}{2} \sum_{L=1}^{Q} \sum_{\kappa_L=1}^{\lambda_L} \sum_{s} \cos q\rho \sum_{\substack{\alpha,\alpha'=1 \\ (\alpha<\alpha')}}^{\xi} [\varepsilon_{\alpha\alpha'}^{LL'}(\rho) + \varepsilon_{\alpha'\alpha}^{LL'}(\rho)] \Delta_{\alpha\alpha'} \end{aligned} \tag{7}$$

The primes in s, s' and κ, κ' by the signs of summation signify that the summation is carried out on condition that the lattice point characterized by sκ does not coincide with lattice point s'κ'. The sum (7) may be expressed otherwise in a more convenient manner, by substituting for the summation over ρ, the summation over lattice points of a specific type in each coordination sphere, over the types of lattice point and over the coordination spheres:

$$S_2 = -\frac{N_0}{2} \sum_{\substack{\alpha,\alpha'=1 \\ (\alpha<\alpha')}}^{\xi} \Delta_{\alpha\alpha'} \sum_{L=1}^{Q} \sum_{\kappa_L=1}^{\lambda_L} \sum_{l=1}^{\infty} \sum_{L'=1}^{Q} [\varepsilon_{\alpha\alpha'}^{LL'}(\rho_l) + \varepsilon_{\alpha\alpha'}^{LL'}(\rho)] \sum_{m_{lL'}=1}^{z_{lL'}} \cos q\rho_{m_{lL'}}, \tag{8}$$

where ρ_l is the radius of the l the coordination sphere;

$\rho m_{lL'}$ is the vector drawn from a lattice point of type L of the number κ_L to lattice point number $m_{lL'}$ of type L' of the l th coordination sphere;

$z_{lL'}$ is the number of lattice points of type L' in the l th coordination sphere drawn around a lattice point of type L, number κ_L of any one elementary cell.

The sum found (8) characterises the neutron-scattering which is related to the correlation between the filling of crystal lattice points by atoms of different types. If however, the correlation is not substantial and the correlation parameters can be held equal to zero, sum (8) no longer applies, and the probability of neutron scattering is determined solely by the quantity $S_1 + V$. When correlation is taken into account, the parameters $\epsilon_{\alpha\alpha'}^{LL'}(\rho l)$ can either be calculated by the statistical theory or can be considered as empirical constants which are determined by the background intensity of the neutrons or of some other type of wave. Knowledge of the correlation parameters makes it possible to determine the

probability of encountering atoms of various kinds near an atom of a given kind, i.e., the short-range order in the alloy.

Eq. (8) provides the correlation part of the neutron-scattering intensity in single crystals. Let us write the expression for the back-ground intensity appearing in polycrystals when neutrons are scattered. To do this it is necessary to average the expression for $S = S_1 + S_2$ in all orientations of the crystals. The averaging does not affect the expression for S_1. Substituting the mean values $S_2 \cos q\rho m_{1L'}$ in respect to all possible angles between the vectors q and $\rho m_{1L'}$ in expression S_2, we obtain

$$S_2 = \frac{N_0}{2} \sum_{\substack{\alpha\alpha'=1 \\ (\alpha<\alpha')}}^{\xi} \Delta\alpha\alpha' \sum_{L=1}^{Q} \sum_{L=1}^{\lambda_L} \sum_{l=1}^{\infty} \sum_{L'=1}^{Q} Z_{lL'} \cdot \cdot [\varepsilon_{\alpha\alpha'}^{LL'}(\rho_e) + \varepsilon_{\alpha'\alpha}^{LL'}(\rho_e)] \frac{\sin q_{m_{lL'}}}{q\rho_{m_{lL'}}}. \quad (9)$$

Wherein, the modulus of vector $\underline{q}$ is equal to:

$$q = \frac{4\pi}{\lambda} \sin\theta,$$

where 2θ is the angle of neutron scattering with the wavelength λ.

Study of the Dependence of Slow-Neutron Scattering Intensity on the Alloy Composition, on Long-Range-Order Parameters, Correlation Parameters, and also on the Angle of Scattering in Particular Cases

The probability of slow-neutron diffuse scattering (proportional to the scattering intensity) is expressed, as has been shown, by the equation

$$W_{cp} = C(S_1 + S_2 + V), \quad (10)$$

where W_{av} is the probability of neutron scattering per unit of solid angle per unit of time;

C is the proportionality factor non-dependent upon the composition and nature of the atomic arrangement at the lattice points.

S_1, S_2, and V are determined accordingly by Eqs. (4) and (8) or (9) and (3).

Individual cases of binary and ternary alloys are considered below.

Binary Alloys

We shall assume that for binary alloys in Eqs. (10), (4), (8), (9), and (3) $\zeta = 2$; $\alpha, \alpha' = A, B$. Let us also consider the case in which the crystal lattice has two kinds of points; i.e., $Q = 2$. Expressions for S_1, S_2 and V will then take the following form:

$$S_1 = N_0 \Delta_{AB} (\lambda_1 p_A^{(1)} p_B^{(1)} + \lambda_2 p_A^{(2)} p_B^{(2)}), \tag{11}$$

$$S_2 = -N_0 \Delta_{AB} \sum_{L=1}^{2} \sum_{\times L=1}^{\lambda L} \sum_{l=1}^{\infty} \sum_{L'=1}^{2} \varepsilon_{AB}^{LL'}(\rho_l) \sum_{m_{lL'}=1}^{z_{lL'}} \cos q\rho_{m_{lL'}} \tag{12}$$

for single crystals, and

$$S_2 = -N_0 \Delta_{AB} \sum_{L=1}^{2} \sum_{\times L=1}^{\lambda_L} \sum_{l=1}^{\infty} \sum_{L'=1}^{2} z_{lL'} \varepsilon_{AB}^{LL'}(\rho_l) \frac{\sin q\rho_{m_{lL'}}}{q\rho_{m_{lL'}}} \tag{13}$$

for polycrystals,

$$V = N\Big[C_A\Big(\sum_{\substack{\beta,\beta' \\ (\beta<\beta')}} c_\beta^A c_{\beta'}^A \Delta_{\beta\beta'}^A + \sum_\beta c_\beta^A \Delta_\beta^A\Big) + C_B\Big(\sum_{\substack{\beta,\beta' \\ (\beta<\beta')}} c_\beta^\beta c_{\beta'}^\beta \Delta_{\beta\beta'}^\beta + \sum_\beta c_\beta^\beta \Delta_\beta^\beta\Big)\Big], \tag{14}$$

in which we denote

$$\Delta_{\beta\beta'}^\alpha = (A_\beta^\alpha - A_{\beta'}^\alpha)^2 \tag{15}$$

and

$$\Delta_\beta^\alpha = \frac{1}{4}\left(B\ {}^{\alpha}_{\beta}\right)^2 \int_\beta^\alpha \left(\int_\beta^\alpha + 1\right). \tag{16}$$

Equation (14) indicates the appearance of a part of the background which is in linear dependence on the concentration of the alloy components; the background caused by the isotope content may be considerable if the constituent isotope atoms greatly differ in the diameters of their neutron scattering.

Let us proceed to examine Eqs. (11), (12), and (13).

Background Intensity of Scattered Slow Neutrons, Disregarding Correlation. If the correlation of the filling of lattice points with atoms of an alloy can be disregarded, the background intensity of scattered slow neutrons for S_1 and V will be determined solely by expressions (11) and (14) and will depend on the composition of the alloy and the degree of long-range order [4]. To find this dependence we must substitute the values λ_1 and λ_2 for each specific structure and express the probabilities of occupation of lattice points by atoms using the alloy-component concentrations and the long-range order parameter [6]. This dependence (V excluded) in the case of neutron scattering is the same as in establishing the residual electrical resistance of binary alloys [6], disregarding correlation. Physical conclusions regarding the dependence of background intensity on concentration as well as on the degree to which the alloy is ordered will remain unchanged.

Background Intensity of Scattered Slow Neutrons with Correlation.

If the correlation in the alloy is considerable, the expression for S_2 should also be considered in calculating W_{av}. The dependence of W_{av} (after deduction of V) on composition, long-range-order parameters, and correlation parameters will here be the same as in the problem of the residual electrical resistivity of alloys [7]. In the case of disordered alloys, when all crystal lattice points are

equivalent, S_2 is

$$S_2 = -N\Delta_{AB}\sum_{l=1}^{\infty}\epsilon_{AB}(\rho_l)\sum_{m_l=1}^{z_l}\cos q\rho_{m_l}. \qquad (17)$$

Taking into account the correlation in the first coordination sphere alone, and using the expression for $\epsilon_{AB}(\rho 1)$ obtained for high temperatures in the statistical theory, we obtain

$$S_2 = -N\Delta_{AB}c_A^2c_B^2\frac{w}{kT}\sum_{m_1=1}^{z_1}\cos q\rho_{m_1}, \qquad (18)$$

where W is the ordering energy of the alloy;

k is the Boltzmann constnat;

T is the absolute annealing temperature of the alloy.

Here, in the case of the scattering of very slow neutrons ($q\rho m_1 \ll 1$) at high temperatures, the correlation correction will invariably diminish the background intensity in alloys undergoing ordering ($w > 0$), and increase it in those undergoing disintegration ($w < 0$).

It is interesting to ascertain the angular distribution of background intensity. The correlation part of this intensity, which is significant for high-temperature-annealed alloys, will depend on the direction of the neutron scattering and the orientation of the crystals. It will in the case of polycrystals be a rapidly attenuating oscillating function of the scattering angle, with the following form, (keeping only the correlation of the first coordination sphere in mind)

$$S_2 = -16N_0\Delta_{AB}\epsilon_{AB}^{12}\frac{\sin q\rho_1}{q\rho_1} \qquad (19)$$

for a body-centered cubic lattice, and

$$S_2 = -24N_0\Delta_{AB}(\epsilon_{AB}^{12} + \epsilon_{AB}^{22})\frac{\sin q\rho_1}{q\rho_1} \qquad (20)$$

for a face-centered cubic lattice.

Allowance for the correlation in the following coordination spheres can greatly affect the angular distribution of background intensity. Thus for alloys with a body-centered cubic lattice, with correlation in the first and second coordination spheres considered, S_2 takes the following form:

$$S_2 = -N_0\Delta_{AB}\left[2z_1\varepsilon_{AB}^{12}(\rho_1)\frac{\sin q\rho_1}{q\rho_1} + z_2\left(\varepsilon_{AB}^{'}(\rho_2) + \varepsilon_{AB}^{22}(\rho_2)\right)\frac{\sin q\rho_2}{q\rho_2}\right]. \qquad (21)$$

In the case of single crystals, calculating $\sum_{m_1=1}^{z_1} \cos q\rho_{m_1}$ for each structure (with correlation in the first coordination sphere), we obtain the functions S_2 for alloys with body-centered cubic and and face-centered cubic lattices respectively:

$$S_2 = -16N_0\Delta_{AB}\varepsilon_{AB}^{12}\cos\frac{qa_1}{2}\cos\frac{qa_2}{2}\cos\frac{qa_3}{2}, \qquad (22)$$

$$S_2 = -8N_0\Delta_{AB}(\varepsilon_{AB}^{12} + \varepsilon_{AB}^{22})\left(\cos\frac{qa_1}{2}\cos\frac{qa_2}{2} + \right.$$
$$\left. + \cos\frac{qa_1}{2}\cos\frac{qa_3}{2} + \cos\frac{qa_2}{2}\cos\frac{qa_3}{2}\right), \qquad (23)$$

where a_1, a_2, and a_3 are the basic vectors of the lattices in question.

Ternary Alloys

Let us consider ternary alloys with two kinds of lattice points. Assuming that in our general formulas (4), (8), (9), and (3) α, α' = = A, B, C and Q = 2, we obtain for the corresponding expressions for S_1, S_2 and V in a ternary alloy

$$S_1 = N_0\Delta_{AB}(\lambda_1 p_A^{(1)}p_B^{(1)} + \lambda_2 p_A^{(2)}p_B^{(2)}) + N_0\Delta_{AC}(\lambda_1 p_A^{(1)}p_C^{(1)} + \lambda_2 p_A^{(2)}p_C^{(2)}) +$$
$$+ N_0\Delta_{BC}(\lambda_1 p_B' p_C' + \lambda_2 p_B^{(2)}p_C^{(2)}). \qquad (24)$$

In the case of scattering by a single crystal

$$S_2 = -\frac{N_0}{2}\sum_{L=1}^{2}\sum_{x_L=1}^{\lambda_L}\sum_{l=1}^{\infty}\sum_{L'=1}^{2}\{\Delta_{AB}[\varepsilon_{AB}^{LL'}(\rho_l)+\varepsilon_{BA}^{LL'}(\rho_l)]+ \\ +\Delta_{AC}[\varepsilon_{AC}^{LL'}(\rho_l)+\varepsilon_{CA}^{LL'}(\rho_l)]+\Delta_{BC}[\varepsilon_{BC}^{LL'}(\rho_l)+\varepsilon_{BC}^{LL'}(\rho_l)]\}\cdot\sum_{m_{LL'}=1}^{z_{lL'}}\cos q\rho_{m_{lL'}}. \tag{25}$$

In the case of scattering by a polycrystal

$$S_2 = -\frac{N_0}{2}\sum_{L=1}^{2}\sum_{x_L=1}^{\lambda_L}\sum_{l=1}^{\infty}\sum_{L'=1}^{2}\{\Delta_{AB}[\varepsilon_{AB}^{LL'}(\rho_e)+\varepsilon_{BA}^{LL'}(\rho_e)]+ \\ +\Delta_{AC}[\varepsilon_{AC}^{LL'}(\rho_l)+\varepsilon_{CA}^{LL'}(\rho_l)]+\Delta_{BC}[\varepsilon_{BC}^{LL'}(\rho_l)+\varepsilon_{CB}^{LL'}(\rho_l)]\}\cdot z_{lL'}\frac{\sin q\rho_{m_{lL'}}}{q\rho_{m_{lL'}}} \tag{26}$$

and

$$V = N\Big\{c_A\Big(\sum_{\substack{\beta,\beta'\\(\beta<\beta')}}c_\beta^A c_{\beta'}^A\Delta_{\beta\beta'}^A+\sum_\beta c_\beta^A\Delta_\beta^A\Big)+c_B\Big(\sum_{\substack{\beta,\beta'\\(\beta<\beta')}}c_\beta^B c_{\beta'}^B\Delta_{\beta\beta'}^B+\sum_\beta c_\beta^B\Delta_\beta^B\Big)+ \\ +c_C\Big(\sum_{\substack{\beta,\beta'\\(\beta<\beta')}}c_\beta^C c_{\beta'}^C\Delta_{\beta\beta'}^C+\sum_\beta c_\beta^C\Delta_\beta^C\Big)\Big\}. \tag{27}$$

The expression for V does not depend on the structure of the investigated alloy. The first two terms of Eq. (27) correspond to the background intensity of scattered neutrons, which is connected with chaotic spreading of isotopes and also with the dependence of the energy of interaction between neutrons and nuclei on the direction of nuclear and neutron spins in the binary alloy AB. The third term appears with the addition of the third component C to the alloy; it produces a supplementary background which may be considerable if the isotopes of the admixture greatly differ in the diameters of their scattering.

If the alloy is not ordered and there is no correlation, then the background intensity is determined by the sum S_1 and V, where S_1 takes the form

$$S_1 = A_1 c_A c_B + (A_2 c_A + A_3 c_B) c_C. \tag{28}$$

Hence, it can be seen that when the values of c_c are small, the increase in background intensity undergoes a linear change with the concentration of the third element C, and the proportionality factor is in linear dependence on the concentration of the basic alloy components A and B.

In a binary alloy undergoing ordering, the correlation in the first coordination sphere always reduces the intensity of neutron scattering, and the correlation, if taken into account, may greatly affect the background intensity. The third element admixture can be such as to make the correlation parameters $\epsilon_{AC}^{LL'}(\rho_e)$ and $\epsilon_{BC}^{LL'}(\rho_e)$ negative. Then the addition of the third element C as is evident from Eq. (25), will decrease the role of correlation.

The angular distribution of the background intensity of scattered neutrons, both for single crystals as well as for polycrystals in the case of ternary alloys, remains the same as in the binary alloys of the same structure. However the addition of a third element to a binary alloy can greatly influence (in one direction or an other) the correlation part of background intensity in conformity with Eqs. (25) and (26).

Magnetic Scattering of Neutrons in the Circuit of the Curie Point of Ferromagnetic Materials

Experiments carried out on the scattering of heat neutrons by ferromagnetic materials [9, 10] have shown that magnetic scattering becomes extremely active at temperatures near the Curie temperature. A qualitative explanation of this phenomenom was put forward by Van Hove [10] and V. L. Ginsburg [11] who linked the observed

scattering with fluctuations of the magnetic moment in the vicinity of the Curie point. The easiest way to make a quantitative calculation of the anomalous magnetic scattering is to proceed from the thermodynamic theory of second-order phase transitions rather than to use an atomic model of the ferromagnetic material. The results of such a calculation [12] are given below.

To ascertain the differential diameter of magnetic scattering of monochromatic unpolarized neutrons $\frac{d^2\sigma}{dEd\Omega}$ by a single crystal, calculated per solid unit angle and per energy unit, the following expression was used

$$\frac{d^2\sigma}{dEd\Omega} = \frac{A}{2\pi\hbar}\tau^2\frac{k'}{k}\sum_{i,j=1}^{3}\left(\delta_{ij}-\frac{q_iq_j}{q^2}\right)\int_{-\infty}^{\infty}\mathfrak{M}_{iq}^{(0)}\mathfrak{M}_{jq}^{*}(t)\,e^{i\omega t}dt. \qquad (29)$$

Here i and j are the number of the Cartesian coordinates;

δ_{ij} — δ— is the symbol; $A = \frac{2\pi l^2\gamma^2}{c^2\hbar^2}$;

γ is the magnetic moment of the neutron in nuclear magnetons ($\gamma = 1.91$);

$\omega = \frac{\Delta E}{\hbar}$, where ΔE is the decrease in neutron energy during scattering;

$\mathfrak{M}_{iq}(t)$ is the Fourier component of the j th constituent of the magnetic moment $\mathfrak{M}_{iq}(t)$ at the time t.

Diffuse magnetic neutron scattering is determined by fluctuations of the magnetic moment. The mean square values and mean product value of the Fourier component of the fluctuations in the magnetic-moment constituents were calculated by means of the thermodynamic of theory fluctuations. Use was made of the expansion of the thermodynamic potential by degrees of magnetization, obtained from the thermodynamic theory of second-order phase transitions. As a

result we find that pure cubic ferromagnetic metals at temperatures somewhat above the Curie point, in the absence of a magnetic field, the intensity of diffuse monochromatic neutron scattering in the vicinity of regular reflections or at small-angle scattering is determined by the equation

$$\frac{d^2\sigma}{dEd\Omega} = \frac{2A}{\pi\hbar}\tau|f_n|^2 kT \frac{1}{a(T-T_0)+\alpha q_n^2}\cdot\frac{a(T-T_0)(\gamma_1+\gamma_2 q_n^2)}{a^2(T-T_0)^2(\gamma_1+\gamma_2 q_n^2)^2+\omega^2}\frac{k'}{k}. \qquad (30)$$

Here f_n is the magnetic scattering factor, corresponding to the considered regular reflection;

q_n is the complement of vector $\underline{q}$ up to the value at which the n th regular reflection occurs (at small scattering angles ($q_n = q$, $f_n = 1$);

T_0 is the Curie point;

is a constant, connected with the magnetic susceptibility at $T > T_0$ by the simple relation $a(T-T_0) = \frac{1}{\kappa}$;

α, γ_1 and γ_2 are constants.

It can be seen from Eq. (30) that in the vicinity of the Curie point the average change in neutron energy at scattering is very small (in proportional to $T-T_0$), and depends essentially on the scattering angle. In order to find the integral of the scattering diameter $\frac{d\sigma}{d\Omega}$ per unit solid angle, we could integrate (30) over the energy, taking ω alone to be dependent on E. Then, at $T > T_0$,

$$\frac{d\sigma}{d\Omega} = 2A\tau|f_n|^2\frac{kT}{a(T-T_0)+\alpha q_n^2}. \qquad (31)$$

Thus, at small q_n (i.e., at small scattering angles or in the vicinity of directions of regular reflection) an extremely intensive diffuse scattering sharply dependent on temperature should be observed with the maxima of this scattering located at $q_n = 0$.

Since at small scattering angles

$$q_n^2 = q^2 = \left(\frac{4\pi}{\lambda}\right)^2 \sin^2\theta, \qquad (32)$$

here, with small $T-T_0$, a sharp increase in $\frac{d\sigma}{d\Omega}$ as the wave length λ and the scattering angle decrease should also be observed.

In a more general case, in the presence of an external magnetic field directed along one of the cubic axis (axis oZ), and with a magnetization parallel to the field, the scattering intensity is determined by the equation

$$\frac{d\sigma}{d\Omega} = A\tau |f_n|^2 kT \left(\frac{1+\vartheta_Z^2}{\frac{1}{\chi_\perp} + aq_n^2} + \frac{1+\vartheta_Z^2}{\frac{1}{\chi_\parallel} + aq_n^2} \right). \qquad (33)$$

Here: $\chi_\parallel$ is the magnetic susceptibility along axis oZ;

$\chi_\perp$ is the magnetic susceptibility along axis oX (or oZ);

ϑ_Z is the cosine of the angle between vector $\underline{q}$ and axis oZ.

In this case, scattering and anisotropy becomes apparent, even at small scattering angles. Equation (33) is valid at $T > T_0$ as well as at $T < T_0$. Since at $T = T_0$ $\frac{1}{\chi_\parallel} = \frac{1}{\chi_\perp} = 0$, of diffuse scattering intensity for a given qn assumes its maximum value at $T = T_0$ and linearly decreases from this value both in the case of temperature, increase and decrease. A temperature dependence of this kind has been observed experimentally [8, 9].

In disordered ferromagnetic alloys, fluctuations of the magnetic moment and concentrations c_A atoms of any type A, generally speaking are not statistically independent, and in computing the fluctuation probabilities deflections of magnetization M and of the composition from equilibrium values should both be considered. Consequently, instead of Formula (33), we obtain a more complicated expression for

the intensity of diffuse scattering

$$\frac{d\sigma}{d\Omega} = A\tau|\bar{f}_n|^2 kT\left(\frac{1+\vartheta_Z^2}{\frac{1}{\chi_\perp}+\alpha q_n^2}+\frac{1-\vartheta_Z^2}{\frac{1}{\chi_\parallel}-a^2\left(\frac{dT_0}{dC_A}\right)^2 M^2\Big/\frac{d^2\Phi_0}{dC_A^2}+\alpha q_n^2}\right), \qquad (34)$$

where: $\bar{f}_n$ is the mean atomic magnetic scattering factor in the alloy;

Φ_0 is the thermodynamic potential of the alloy at $T > T_0$.

From Eqs. (33) and (34) we see that in an alloy the magnetic scattering intensity is greater (at the same $\chi_\parallel$, $\chi_\perp$, α, and $\bar{f}_n$) than in a monocomponent crystal. At temperatures higher than the Curie point, when there is no magnetic field, Eqs. (31) and (34) coincide.

REFERENCES

1. POMERANCHUK, I. ZhETF (Journal. Exp. Theor. Phys.), 8, 1938.

2. AKHNEZER, A. and POMERANCHUK, I. Some Problems of the Nuclear Theory (Nekotoryye voprosy teorii yadra), GITL (St. Press Theor. Tech. Lit.), Moscow-Leningrad, 1948.

3. SMIRNOV, A. A. and VONSOVSKIY, S. V. Journ. of Phys., 5, 1941.

4. SMIRNOV, A. A. and PADOUCHEV, B. V. ZhETF, 21, 1951.

5. DANILENKO, V. M. et al. Physics of Metals and Metallurgy (Fiziki metallov i metallovedeniye), AN SSSR (Acad. Sci. of UkSSR).

6. SMIRNOV, A. A. ZhETF, 17, 1947.

7. KRIVOGLAZ, M. A. and MATYSINA, Z. A. ZhETF, 28, 1955.

8. PALEVSKY, N. and HUGNES, D. J. Phys. Rev., 92, 1953.

9. REYNOLDS, A. W. and RISTE, T. Phys. Rev., 95, 1954.

10. VAN HOVE, L. Phys. Rev., 93, 1954.

11. GINZBURG, V. L. DAN SSSR, (Reports of Acad. Sci. USSR). 105, 1955.

12. KRIVOGLAZ, M. A. DAN SSSR.

CALCULATING THE ABSOLUTE VALUE OF THE SELF-DIFFUSION COEFFICIENT AT GRAIN BOUNDARIES AND OF THE BOUNDARY WIDTH

S. Gertsriken and D. Tsitsiliano

At elevated temperatures the mobility of atoms in a solid body determines a number of its physical properties. The study of the mobility of atoms at grain boundaries is of special interest. In [1] method was suggested for the calculation of the diffusion factor at the boundaries D_{bound} by the following equation

$$\frac{aD_{гр}}{D} = \frac{0{,}21}{\sqrt{Dt}\,\mathrm{tg}^2\,\beta}, \qquad (1)$$

where a is the boundary width taken as equal to $5 \cdot 10^{-8}$ cm;

D is the body diffusion coefficient (in a grain);

t is the diffusion time;

$\tan\beta$ is determined from a graph of log C vs. X (C is the concentration at a depth X).

Study [2] provides a criterion for the applicability of the Fisher Method and notes that the coefficient 0.21 in Eq. (1) should be replaced by 0.37. Neither of these methods makes it possible to determine D_{bound} since a is unknown.

Study [3] considers the final problem of diffusion, for the calculation of which tables of the following function are given:

$$v(\lambda,\nu)=\frac{1}{\lambda}\left\{ierfc\,\nu\lambda+\sum_{n=1}^{\infty}ierfc\,(2n+\nu)\lambda+ierfc\,(2n-\nu)\lambda\right\},$$

where $\lambda = \frac{1}{2\ Dt}$;

$\underline{l}$ is the thickness of the entire specimen;

$\underline{t}$ is the diffusion time;

$\underline{n}$ is the thickness of the layer from which diffusion occurs;

$$ierfc\,L=\frac{1}{\sqrt{\pi}}e^{-J^2}-LerfcL;$$
$$erfc\,L=1-erfL;$$
$$erf\,L=\frac{2}{\sqrt{\pi}}\int_0^J e^{-J^2}dL.$$

If Q_o is the total quantity of diffusing substance and Q the quantity of the diffusate after the diffusion time $\underline{t}$, then between the planes X = x and X = 1 the relationship is as follows:

$$2\frac{Q}{Q_0}\frac{h}{l}=2\frac{N}{N_0}\frac{h}{l}=v\left(\lambda,\frac{x_1-h}{l}\right)-v\left(\lambda,\frac{x_1+h}{l}\right). \qquad (2)$$

If labeled atoms are used, we take N and N_o instead of Q and Q_o (N_o is the initial intensity of the specimen's, radioactive radiation and N is the same after removal of the layers). The intragranularself-diffusion in silver was investigated by this method [4]. If for any reason Q_o or N_o are unknown, λ can be found in the following manner [5]:

$$2\frac{Q_1}{Q_0}\frac{h}{l}=\frac{2N_1}{N_0}\frac{h}{l}=v\left(\lambda,\frac{x_1-h}{l}\right)-v\left(\lambda,\frac{x_1+h}{l}\right)=\varphi_1;$$
$$2\frac{Q_2}{Q_0}\frac{h}{l}=\frac{2N_2}{N_0}\frac{h}{l}=v\left(\lambda,\frac{x_2-h}{l}\right)-v\left(\lambda,\frac{x_2+h}{l}\right)=\varphi_2;$$
$$\frac{N_1}{N_2}=\frac{\varphi_1}{\varphi_2}. \qquad (3)$$

Knowing N_1, N_2, x_1, X_2, 1 and h, a value for λ should be selected which will make $\frac{\varphi_1}{2} = \frac{\varphi_1}{2}$. Then, knowing λ, we find D.

It has been shown by research [6] that this method may be used to determine D_{bound} and the boundary width. It is known that at very high temperatures D_{bound} is several orders larger than D_{grain}; the lower the temperature, the more this ratio increases. At comparatively low diffusion temperatures (300 to 400° for self-diffusion of Ag), it is easily shown by Eq. (2) that due to intragranular diffusion, Q_1 and Q_2 or, accordingly, N_1 and N_2, even at small X values, are practically zero; the whole effect in this case is determined by diffusion inside the boundaries, and Q_1, Q_2, Q_o and N_1, N_2 and N_o will relate to the boundaries. Formula (3) will take therefore the following form:

$$\frac{2Q_{1rp}}{Q_{orp}}\frac{h}{l}=\frac{2N_{1rp}}{N_{orp}}\frac{h}{l}=v\left(\lambda_{rp},\frac{x_1-h}{l}\right)-v\left(\lambda_{rp},\frac{x_1+h}{l}\right)=\varphi_1,$$

$$\frac{2Q_{2rp}}{Q_{orp}}\frac{h}{l}=\frac{2N_{2rp}}{N_{orp}}\frac{h}{l}=v\left(\lambda_{rp},\frac{x_2-h}{l}\right)-v\left(\lambda_{rp},\frac{x_2+h}{l}\right)=\varphi_2,$$

$$\frac{N_{1rp}}{N_{2rp}}=\frac{\varphi_1}{\varphi_2}. \qquad (4)$$

When x_1, x_2, l, N_{1bound} and N_{2bound} are known, we determine [4] first λ_{bound} and then D_{bound}. Here the boundary width is not taken into account, and the value D_{bound} is no longer relative.

Having determined D_{bound} it is possible to determine N_{bound} from the formula

$$\frac{2N_{1rp}}{N_{orp}}\frac{h}{l}=v\left(\lambda_{rp},\frac{x_1-h}{l}\right)-v\left(\lambda_{rp},\frac{x_1+h}{l}\right), \qquad (5)$$

in which all values are known. Knowing N_{obound} it is possible to evaluate the boundary width. Assuming that $Q_{o_{bound}}$ only relates to the radioactive material which lies above the boundaries, it is possible to determine equation

$$\frac{Q_{0\,rp}}{Q_0} = \frac{N_{0\,rp}}{N_0} = \frac{2a}{b}, \qquad (6)$$

where b is the grain size and $N_{0\ bound}$ is the initial intensity from the boundaries.

Methods Used in the Experiment

Foil 20 microns thick was rolled from 99.99% pure silver. Next, some of the foil was annealed at 850° for 24 hours and some at 550° for 32 hours. In the first instance the average grain size was 20 microns, and in the second, 10 microns. The pieces of foil were then electrolytically plated with radioactive silver Ag^{110} (thickness of plating 0.25 to 0.5 microns) at a current density of 3 ma/cm^2 in a bath of the following composition: 100 g NaCN and 30 g AgCN per liter of water, plus several granules of radioactive silver. The anode was a silver plate. The active layer was formed on one side of the specimen, leaving a margin of about 1.5 mm. After diffusion, this margin was cut off. The diffusion annealing was carried out in vacuum.

One or two specimens, 10 and 20 microns thick, were used for each temperature point. They were sprinkled with Al_2O_3, jointed in pairs with their active sides facing and placed in a small nickel envelope. After diffusion annealing, the overall intensity decreased somewhat through evaporation and also for mechanical reasons. The temperature, determined by a chrome-alumel thermocouple, was regulated to $\pm$ 2°.

Thin layers were removed electrolytically. The composition of the electrolyte was the same as for plating (without the radioactive Ag). If the electrolyte is one quarter diluted with water, the

polishing at a current density of 10 to 15 ma/cm^2 is improved. The thickness of the removed layer just as the thickness of the plating, was determined with a microanalytical balance.

While the layers were being removed, the reverse side of the specimen was protected by a coating of vaseline. Special experiments proved that the radioactive layer (on the specimen which had not undergone diffusion annealing) can be removed uniformly by electrolysis. The removal of the layers after diffusion annealing was carried out in the following sequence.

In order to avoid the possible effect of intragranular diffusion, a 1 to 3 micron layer is removed from the side covered with labeled atoms, during which the intensity decreases from many thousands to 10 to 200 pulses/min;

A layer of several tenths of a micron is removed from the reverse side of the specimen to remove any labeled atoms which might have penetrated to this side through condensation or for other reasons; the intensity decreases to several score pulses per minute.

Another thin layer is removed from the reverse side. The intensity remains practically the same as in the previous operation; this shows that the pulses detected in the second operation are not caused by the isotopes passing through the boundaries into the specimen.

Layers from 0.5 to 1 micron are then removed consecutively from the face. Here, the intensity gradually decreases, and combinations of these values of N_{bound} enable us to determine λ_{bound}.

The radiation intensity was measured by an AMM-12 glass counter. The investigated specimen, contained in a paper envelope, was held in position in the testing area of the counter tube by means of

rubber rings. This ensured that the geometrical conditions remained the same and that, in addition, the radiation given off the specimen was used to its maximum. To keep the statistical error low the counting was carried out for 1 to 2 hours.

Analysis of the Experimental Data

Let us take an example from our analysis of the results of the experiments. The diffusion annealing of the specimen was carried out at 375° for 4 hours. When the margins of the specimen had been cut off, the pulses were 25,550 per minute, without any correction for the "dead time" (h = 0.38, l = 20, grain size b = 10 μ). A layer of 2.9 μ (N = 159 pulses/min) was taken from the active side, then a layer of 1.1 μ (N = 84 pulses/min) and another layer of 1.5 μ (N = 84 pulses/min) from the reverse side. The results of the consecutive removal of the layers are shown in Table 1.

Table 1

x_1, мк	N_{pp}, имп/мин	x, мк	$N_{гр}$, имп/мин
2,9	84	5,6	55
4,0	72	6,7	46
4,8	64	8,0	34

We then calculated D_{bound}

$$\nu = \frac{x_1 - h}{l} = \frac{4 - 0{,}38}{20} = 0{,}181;$$

$$\nu = \frac{x_1 + h}{l} = \frac{4 + 0{,}38}{20} = 0{,}219;$$

$$\nu = \frac{x_2 - h}{l} = \frac{6{,}7 - 0{,}38}{20} = 0{,}316;$$

$$\nu = \frac{x_2 + h}{l} = \frac{6{,}7 + 0{,}38}{20} = 0{,}354.$$

Let us assume $\lambda = 1.8$; then, for data ν in Table 1 we find:

$$\nu_1 = (1{,}8;\ 0{,}181) - \nu_1(1{,}8;\ 0{,}219) = 0{,}16521 - 0{,}14203 = 0{,}02318 = \varphi_1;$$
$$\nu_2 = (1{,}8;\ 0{,}316) - \nu_2(1{,}8;\ 0{,}354) = 0{,}09382 - 0{,}07878 = 0{,}01504 = \varphi_2;$$
$$\frac{\varphi_1}{\varphi_2} = \frac{0{,}02318}{0{,}01504} = 1{,}54, \qquad \frac{N_{1гр}}{N_{2гр}} = \frac{72}{46} = 1{,}565$$

Let us assume $\lambda = 2$. Then, similarly, we find for $\lambda = 2$ from Table 1 $\frac{\varphi_1}{\varphi_2} = 1.66$. Consequently, the true value of λ lies between 1.8 and 2. At $\lambda = 1.84$

$$\frac{\varphi_1}{\varphi_2} = 1{,}565 = \frac{N_{1гр}}{N_{2гр}}, \qquad \text{т. е. искомая } \lambda = 1{,}84.$$

Since in our example there are six values for depth x and N_{bound}, by combing the data in Table 2 we obtain 15 values for λ which, within the limits of experimental error, should coincide

TABLE 2

x, мк	λ	x, мк	λ
2,9—4	1,84	4,0—8,0	1,89
2,9—4,8	1,80	4,8—5,6	2,10
2,9—5,6	1,89	4,8—6,7	1,87
2,9—6,7	1,84	4,8—8,0	1,91
2,9—8	1,89	5,6—6,7	1,70
4,0—4,8	1,80	5,6—8,0	1,88
4,0—5,6	1,91	6,7—8,0	1,95
4,0—6,7	1,84		

$$\lambda_{ср} = 1{,}87 \pm 0{,}06;$$
$$D_{ср} = (1{,}98 \pm 0{,}13) \cdot 10^{-11}\ \text{см}^2/\text{сек}.$$

Now, knowing λ_{av}, by a reversal of this operation we are able to determine $N_{o\ bound}$ since all other quantities of Eq. (4) are known, except $N_{o\ bound}$:

$$\frac{2,84}{N_{0\,гр}} \cdot \frac{0,38}{20} = v(1,87;\ 0,181) - v(1,87;\ 0,219) = 0,1549 - 0,13216 = 0,227.$$

Hence $N_{o\ bound}$ = 120 pulses/min.

From Table 2 we can also find the values $N_{o\ bound}$ = 120, 120, 122, 119, 122 and 116. The mean value is $N_{o\ bound}$ = 120 pulses/min. Using Eq. (6)

$$\frac{N_{0\,гр}}{N_0} = \frac{2a}{\delta}, \text{ найдем}$$

$$a = \frac{120 \cdot 1,10^{-3}}{27550 \cdot 2} = 2,2 \cdot 10^{-6} \text{ см}.$$

All measurement data are summarized in Table 3.

Having plotted log D_{bound} against $\frac{1}{T}$, we obtain the activation energy of self-diffusion along the boundaries of silver, which is 20.3 kcal/g-atom. From our data for boundary self-diffusion we obtain the following equation:

$$D_{гр} = 1,5 \cdot 10^{-4} \exp\left(-\frac{20300}{RT}\right) \text{ см}^2/\text{сек}.$$

There are reasons to believe that the measurement of D_{bound} and a can also be carried out on massive specimens; in this case

$$\frac{2N_{1\,гр}\,h}{N_{0\,гр}} = \frac{1}{\lambda}\left[ierfc(x_1 - h)\lambda - ierfc(x_1 + h)\lambda\right];$$

$$\lambda = \frac{1}{2\sqrt{Dt}}.$$

It is interesting to note that for the boundary self-diffusion of silver, as investigated by the Fisher method [7], it has been obtained that

$$D_{гр} = 2,5 \cdot 10^{-2} \cdot \exp\left(-\frac{20\,200}{RT}\right) \text{ см}^2/\text{сек}.$$

TABLE 3

Температура, °C	b, мк	$\bar{N}_0$*	N_0	$N_{0гр}$	$a \cdot 10^8$	$D_{гр} \cdot 10^{11}$	$D_{гр} \cdot 10^{11}$, см³/сек
275	10	31 250	34 300	166	2,4	0,126	
275	10	28 720	31 400	180	2,9	0,094	0,116±0,014
275	10	30 100	32 900	168	2,7	0,127	
300	10	28 500	31 100	156	2,5	0,192	
300	10	29 680	32 400	154	2,4	0,214	0,194±0,013
300	20	27 900	31 400	154	4,8	0,177	
327	10	13 200	13 600	99	3,6	0,48	
327	10	14 500	15 150	105	3,5	0,56	0,52 ±0,04
350	10	25 000	26 900	104	1,9	0,94	
350	10	26 800	29 000	111	1,9	1,14	
350	20	28 100	30 500	98	3,2	1,14	1,13 ±0,09
350	20	23 450	25 100	91	3,6	1,29	
375	10	25 550	27 550	120	2,2	1,98	
375	20	26 240	28 350	116	4,1	1,60	1,79 ±0,19

* $\bar{N}_0$ means the initial number of pulses per minute disregarding the "dead" time, while N_0 takes it into account.

Thus the activation energy, practically speaking, coincides with the energy discovered by us, and the pre-exponential members differ mainly because in the Fisher method a is arbitrarily taken as $5 \cdot 10^{-8}$ cm, whereas the true value of a is considerably larger:

$$\frac{a_{ист}}{a_{Фиш.}} = \frac{a_{ист}}{5 \cdot 10^{-8}} \cong \frac{2{,}5 \cdot 10^{-2}}{1{,}5 \cdot 10^{-4}}; \quad a_{ист} \cong 8{,}3 \cdot 10^{-6} \text{ см}.$$

Consequently the boundary width a is approximately two orders greater than that assumed by Fisher and by those who used his method to investigate boundary diffusion. It should be noted that in the studies made by V. I. Arkharov and his collaborators, in particular [8], the boundary width estimated from measurement of the cahnges in the lattice parameter for different grain sizes in lead containing small admixtures was 350-900 A.

Conclusions

Self-diffusion along the boundaries of grains of silver was investigated by a method proposed by one of the authors, and absolute diffusion factors were determined, i.e., without any arbitrary assumptions regarding the boundary widths as was done previously.

The coefficients of the self-diffusion of silver along the boundaries conform to the relationship

$$D_{гр} = 1{,}5 \cdot 10^{-4} \exp\left(-\frac{20\,300}{RT}\right).$$

The boundary width in silver was also evaluated and was shown to be several hundred A, not 5 A as previously assumed.

REFERENCES

1. FISHER, J. S. J. Appl. Phys., 22, 1951.

2. BORISOV, V. T. and GOLIKOV, B. Ya. Fizika Metallov i Metallovedeniye (Physics of Metals and Metallurgy), 1, 2, 1955.

3. GERTSRIKEN, S. D. and LOZOVIK, B. G. Voprosy fiziki metallov i metallovedeniye (Problems of Metal Physics and Metallurgy) AN SSSR, Acad. Sci. USSR, Kiev, 1956.

4. GERTSRIKEN, S. D. and TSITSILIANO, D. D. Physics of Metal and Metallurgy, AN SSSR, Acad. Sci. USSR, 1957.

5. GERTSRIKEN, S. D. Information Letter No. 5, IMF, AN USSSR Kieve, 1956.

6. GERTSRIKEN, S. D. Scientific Information KDU, No. 2, Kiev, 1957.

7. HOFMANN, R. F. and TURNBULL, D. Atom movements, ASM, 1951.

8. ARKHAROV, V. I. and SKORNYAKOV, N. N. Papers of Urals Branch of Acad. Sci., No. 16, 1956.

STUDY OF CHROMIUM-NIOBIUM-VANADIUM ALLOYS

V. N. Svechnikov, Yu. A. Kocherzhinskiy, V. M. Pan and A. K. Shurin

Through the introduction of new methods of purification, it is now possible to use chromium and its alloys for consturction purposes, particularly as heat-resisting materials. There is consequently, an increase in phase diagrams of metal systems containing chromium, which are indispensable in the selection of new construction materials.

Binary Phase Diagrams

Chromium - Niobium. The chromium-niobium diagram has been investigated in somewhat greater detail than the niobium-vanadium and chromium-vanadium diagrams. Data obtained from the first studies on this question [1, 2] have reen rendered more precise by the most recent investigations [3, 4]. These last two studies give similar overall representations of the chromium-niobium diagram, but they differ with regard to particulars. According to the data supplied, there are present in the diagram two solid solutions, (one based on chromium and one on niobium), one chemical compound $NbCr_2$, and two eutectics. The solubility of niobium in chromium at saturation is 50% by weight [4] or 10 atom percent [3].

The lattice of the chromium-base α-solution is body-centered cubic lattice with a parameter of 2.88 to 2.89 KX units irrespective of composition [3], with a parameter ranging from 2.881 KX in pure chromium to 2.886 KX at maximum saturation [4]. The microhardness of the α-solution is 196 kg/mm^2 at 0% Nb; 290 kg/mm^2 at 1.6% Nb; in the two-phase part of the diagram, it is from 430 to 650 kg/mm^2 [4], or from 220 kg/mm^2 in pure chromium up to 420 kg/mm^2 with 5% Nb.

The β-phase of $NbCr_2$ has a face-entered cubic lattice, a = 6.95 to 6.98 KX [3], and the microhardness is 1560 to 2120 kg/mm^2 [4].

The niobium-base γ-solid solution has a body centered cubic lattice with a parameter of 3.25 KX at 40 to 80 atom percent Nb up to 3.28 KX at 90 atom % Nb [3]; the microhardness is from 590 kg/mm^2 in pure niobium up to 1320 kg/mm^2 [4], or from 505 to 740 kg/mm^2 [3]. The solubility of chromium in niobium is 25% by weight [4] or 20 atom percent [3].

The eutectic α + β is at 1660° and with 31% Nb by weight [4], or at 1660° with 22 atom % Nb [3]. $NbCr_2$ melts at 1750° [4], or at 1680° [3]. The eutectic α + γ is at 1710° with 65% Nb by weight [4], or at 1660° with 40 atom % Nb [3]. The Vickers hardness of the alloy ranges from 200 to 1200 kg/mm^2.

Niobium-vanadium. According to the work described in [5], the system niobium-vanadium represents an interrupted series of solid solutions at temperatures of 650° and more. The fusibility diagram has its minimum at 1810° with 35% Nb by weight. As regards the σ-phase of this system, published material contains contradictory data.

Research [6] detected precipitations along the grain boundaries

in alloys with 30 and 40% Nb. The nature of the precipitation has not been established. The authors study [5] deny the existence of the second phase.

Chromium-vanadium. This system has not been properly studied. Investigations were limited to the changes in the solid solution parameter of specimens annealed at 700° for 240 hours [7]. An uninterrupted series of solid solution was discovered at this temperature and this was confirmed in study [6].

Program Research of Investigations and Materials

Chromium-base alloys, containing up to 50% niobium and up to 10% vanadium both by weight were investigated with a view to plotting the chromium angle of the phase diagram and studying some of the physical properties of the alloys.

The latter were prepared from the following materials:

Electrolytic refined chromium, containing admixtures in %: Pb, Sn, Bi, Sb, Cd $\leqslant$ 0.0003; O, N $\leqslant$ 0.003; S $\leqslant$ 0.001;

Pulverized niobium containing admixtures in %: Fe - 0.34; Ti - 0.23; Si - 0.05; Pb - 0.11; C - 0.18;

Compact vanadium containing admixtures in %: V -95; Al $\leqslant$ 2; Fe $\leqslant$ 0.2; C $\leqslant$ 0.03; Al_2O_3 - 2.12.

Preparation of the Alloys

The chromium and niobium were mixed and compacted prior to smelting. Smelting was carried out in a high-frequency furnace in crucibles made of zirconium oxide, and partly of aluminum oxide; the castings weighed 100 g. Heating up to temperatures around

1200 to 1500° was carried out in vacuum (~ 10^{-4} mm Hg), and further heating, melting and crystallization were carried out in argon at a pressure of 200 to 400 mm Hg. After solidification of the alloy, the combustion space was once more evacuated to ~ 10^{-4} mm Hg. A second cruicible made of magnesite (prepared mechanically from brick) was used to prevent the metal leaking in case the cruicible cracked. Cruicibles made of zirconium oxide usually cracked during melting, and some of the metal hardened in the narrow space between the two cruicibles. When the alloy had hardened, the cruicibles were broken and the pieces of the cruicible which had become welded to the surface were removed from the metal by emergy grinders. All the piglets proved to be brittle (though not to the same degree), and emergy wheels were the only means of cutting them.

Specimens were also cast in the form of rods. Here, after they had been melted and briefly held in the liquid state, argon pressure in the combustion space was raised to atmospheric pressure or somewhat higher; the sight glass was removed and a quartz tube connected to a manual piston pump was inserted into the metal through the upper opening in the quartz retort of the furnace. When the metal had been drawn into the tube, the latter was swiftly removed from the surface; the opening was covered with the glass. The cooling piglet and the evacuation of the combustion space took place at the same time. In spite of the temperature of the liquid metal being higher than the melting point of quartz, it was possible to produce compact rods more than 100-mm long in tubes up to 4 mm in diameter.

The alloy composition (per charge) (Table 1) was selected with a view to an investigation of three cross sections of the diagram (at 0.5 and 10% V).

TABLE 1

Обозначение сплава	Состав по шихте, вес. %			Состав по анализу, вес. %		
	Cr	Nb	V	Cr	Nb	V
1	100	—	—	Анализ не производился		
2—0	98	2	—			
5—0	95	5	—		5,4	
10—0	90	10	—		9.6	
20—0	80	20	—		19,9	
30—0	70	30	—		29,2	
35—0	65	35	—		34,8	
40—0	60	40	—		39,8	
50—0	50	50	—		50,3	
0—5	95	—	5		0	4,8
2—5	93	2	5		2,0	4,8
10—5	85	10	5		9,6	4,8
30—5	65	30	5		29,0	6,1
50—5	45	50	5	45,7		4,2
0—10	90	—	10			10,0
2—10	88	2	10		2,0	9,6
5—10	85	5	10		5,0	9,7
10—10	80	10	10		10,1	11,0
20—10	70	20	10		20,3	10,0
30—10	60	30	10		28,4	10,0
40—10	50	40	10	49,8		9,1
50—10	40	50	10		48.8	10,8

Structure of the Cast Alloys

The specimens were prepared mechanically and given a final polishing with cloth with chromium oxide suspension. They were etched in a boiling 1% solution of H_2SO_4, less frequently, they were etched electrolytically in a solution of oxalic acid, and, lastly, by evaporation in vacuum at a temperature up to 1000° (parallel with measurements of hot hardness). Photographs were taken with a PMT-3 apparatus, using additional attachments for magnifications of × 100 and × 600.

A study of the microstructure of cast, binary chromium-niobium alloys confirmed existing scientific data on the solubility of more

than 2% of niobium in chromium, with the presence of an eutectic at about 30% Nb, and a chemical compound of approximately 50% by weight.

The solubility of niobium in chromium undergoes no significant change when vanadium is added (up to 10% in weight). Judging by the microstructure, the content of niobium in the eutectic alloy (30%) does not depend on the addition of vanadium (up to 10%).

The solubility of vanadium in the intermetallic compound $NbCr_2$ was discovered. Fig. 1 represents the microstructure of alloy 50-10 revealed by vacuum etching (10^{-4} mm Hg, 1000°). It can be seen that only one phase is present in the alloy which is, apparently, the solid solution of vanadium in the intermetalloid compound $NbCr_2$.

GRAPHS NOT REPRODUCIBLE

Fig. 1. Microstructure of alloy. 50-10 (× 600)

Hardness of the Cast Alloys

The hardness of the cast alloy was measured with the Vickers device under a load of 10 kg. The effect of vanadium on the hardness

of alloys is small, whereas that of niobium is significant: from 200 to 250 kg/mm^2 with 0% Nb and up to 550-600 kg/mm^2 with 30% Nb. A further increase in the niobium content hampers the measurements of hardness since the excessive brittleness of the alloys renders indeterminate the results obtained.

Microhardness of Phases in the Cast Alloys

The microhardness was determined with PMT-3 apparatus under a load of 30 g. In alloy No. 1 the microhardness amounted to approximately 220 kg/mm^2. Vanadium increases the hardness of the α-solution up to 350 kg/mm^2 with 10% V. Niobium increases the hardness of the α-solution even beyond the limits of solubility, up to 600 kg/mm^2 in alloy 30-0, and up to 720 kg/mm^2 in alloys 20-10 and 30-5, which indicates the state of nonequilibrium of the alloys. The microhardness of the β-phase of $NbCr_2$, irrespective of the composition of the alloys, r ges from 950 to 1300 kg/mm^2.

Structure of the Annealed Alloys

Annealing at 1170° for 75 hours in an atmosphere of argon does not cause any noticeable changes in the structure, hardness, microhardness, or specific electric resistance of the alloys. In the absence of special equipment, the following device was used for annealing at higher temperatures. A heavy cylindrical ampule of the following dimensions from Armco iron; outer diameter 46 mm, inner diameter 16 mm and length 125 mm. Specimens (ϕ 15 × 5 mm) were placed inside the ampule. The gaps were filled with pulverized aluminum oxide. The ampule was sealed with threaded Armco-iron

plug, heated in a crucible furnace to 1000°, and welded together. The heating during the welding process served to expel the air. The specimens inside were annealed in a TVV-2M furnace in vacuum (10^{-4} mm Hg.) at 1350 to 1450°. The temperature was measured with a TsNIIChM-1* (tungsten-molybdenum alloyed with aluminum). Alloys 1, 2-0, 5-0, 10-0, 20-0, 0-5, 2-5 were annealed at 1350° for 56 hours and alloys 0-10, 2-10, 5-10, 10-10 and 20-10 at 1450° for 30 hours. Figure 2 represents the microstructure of alloy 20-10 when case (a) and after annealing for 30 hours at 1450° (b), and shows the precipitation of the excess phase in grains of the primary α - solution. The change in microhardness of the α - phase in relation to the niobium content is shown in Fig. 3.

GRAPHIC NOT REPRODUCIBLE

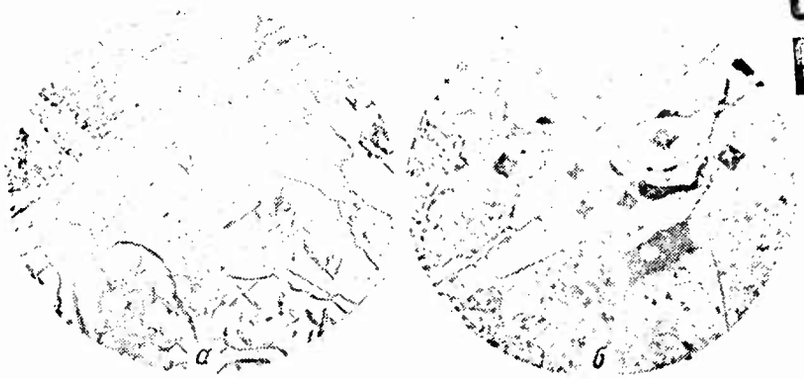

Fig. 2. Microstructure of alloy 20-10 (× 600). Etching in H_2SO_4 (× 600).

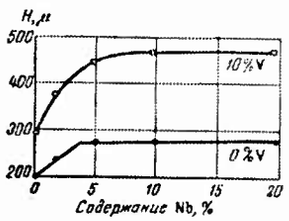

Fig. 3. Influence on alloys composition on microhardness of α-phase

---

* TsNIIChM: Tsentral'nyy Nauchno-Issledovatel'skiy Institute Cherny Metallurgii (Central Scientific Research Instute of Ferrous Metallurgy).

Determination of the Solidus Temperature

A method proposed by the Baykov Institute of Metallurgy of the Academy of Sciences of the USSR was used to determine the temperature of the beginning of fision. In this a rod-shaped specimen of constant cross section is fastened between two-cooled electrodes and is electrically heated. A small cavity is made in the middle of the specimen and the junction of a thermocouple is inserted into it. The unevenness of the temperature along the length of the specimen, which is made much greater by the presence of the cavity, causes the melting to start in the cavity rather than elsewhere. As the experiment shoes, the zone of the melting metal or alloy then spreads while the temperature of the liquid phase remains constant. This is even the case with a single-variant system when, at the point where an ordinary temperature curve passes the solidus line, only a small inflection can be seen. This is evidently caused by the intensity with which the melting metals absorb heat from the liquid phase which does not thereby increase in temperature.

In our experiments the specimens were heated in the structural-investigation chamber of a VIM-1 unit, and a crude (unannealed) TsNIIChM-1 thermocouple was used. The thermocouple was calibrated by the method described above according to the melting points of the pure metals: copper (1083°), nickel (1445°), iron with 0.07% C (1525°), titanium (1660°), chromium (1840°), and zirconium (1860°). The emf of the thermocouple was measured with an indicating millivoltometer with a 17mv scale.

The precision of the method for a non-variant system (for instance, pure metal, a eutectic) amounted to $\pm$ 5° and for a single-variant system $\pm$ 10°.

Cavities of the required shape and depth are drilled in the specimens by the electric spark method, and heating is carried out in an atmosphere of purified argon at a pressure of approximately 100 mm.

In certain cases, after a "shutdown" at the temperature corresponding to the solidus, the increase in current through the specimen led to a rise in temperature right up to the moment when the current was cut off due to the fracture of the specimen. The temperature at this fracture point was taken as the liquidus.

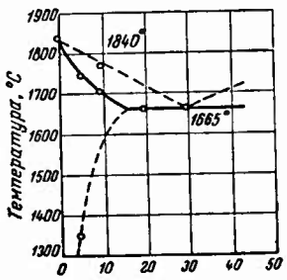

(a)

Content of Nb, % by weight

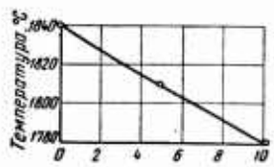

(b)

Content of V, % by weight

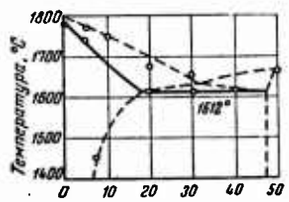

(c)

Content of Nb, % by weight

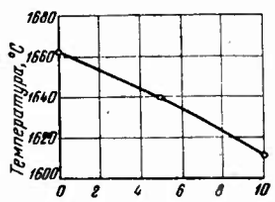

(d)

Content of V, % by weight

Fig. 4. Diagrams of Binary and Ternary Alloys.

The results of the experiments are given in Fig. 4, which shows a diagram of (a) the binary system chromium-niobium ranging from 0 to 50% Nb (b), the binary system chromium-vanadium from 0 to 10% V (c), a vertical cross section at a constant content of 10% V by weight. Figure 4 also illustrates the displacement of the eutectic transformation temperature in chromium-niobium alloys according to the vanadium content (d). A lowering of the melting point from 1840° at 0% Nb to 1665° at 30% Nb by weight is observed in the binary system chromium-niobium. The eutectic level begins at 1665° with 15% Nb.

A decrease in the temperature at the beginning of the melting from 1840° for pure chromium to 1780° at 10% V by weight is apparent in binary alloys of chromium-vanadium. These data correspond to data obtained from microstructural analysis, which establishes the homogeneous solid solution in these alloys. Eutectic transformation was also discovered in the crosssection with 5 and 10% V. The eutectic temperature at 5% V is 1642°, and at 10%, 1612°.

The addition of vanadium to chromium-niobium alloys (at least in the limits of 0 to 10%), seems to broaden somewhat the range of the chromium-base solid solution and to reduce the eutectic temperature.

X-Ray Difraction Analysis

The chromium-niobium-vanadium system was investigated by x-ray diffraction mainly to ascertain the effect of niobium and vanadium on the parameter of the chromium-base solid solution.

The alloys were first annealed at 1350° for56 hours, or at 1450° for 30 hours and then pulverized in a special mortar. Next,

the powder was annealed at 1000° for 2 hours to eliminate any stress originating in the pulverization process.

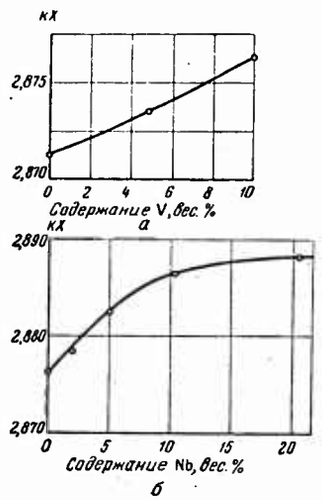

Fig. 5. Influence of admixtures on the lattice parameter.

Photographs were taken in a back-reflection camera using chromium radiation K_{α_1} and K_{α_2}. Pure chromium served as a standard; its parameter being assumed equal to 2.8714 KX [8].

No changes in the solid solution parameter in relation to the niobium content were observed in the binary chromium-niobium alloys. The addition of vanadium to chromium increases the parameter of the crystal lattice from 2.8714 KX at 0% V to 2.8763 KX at 10% V by weight. Here there is a small negative deviation from the law of additivity (Fig. 5a). A change in parameter in the alloy containing 5% V by weight and 2% Nb by weight, in comparison with alloy 5-0, were practically nonexistent. In alloys containing 10% V by weight

there is a definite change in parameters dependant upon the niobium content. The parameter changes from 2.8763 KX at 0% Nb to 2.8880 KX at 20% Nb by weight. As is clear from Fig. 5 b, the solubility of niobium in the α-solution containing 10% V at 1450° is approximately 7%, which also is confirmed by measurements of the microhardness.

X-ray diffraction analysis was also made in the case of the phase composition of the same alloy specimen 20-0 (80% Cr, 20% Nb), one half of which had undergone annealing at 1170° for 75 hours, and the other half of which had been hardened by cooling at a rate of about 200°/sec in a temperature range of 1700 to 600°. Photographs were taken of a strongly etched specimen in a cylindrical chamber 57.3 mm in diameter, using chromium radiation. The identical nature of the diffraction patterns obtained proves that the phase composition is the same in both cases.

Change in the Hardness of the Alloys due to Heating

Hardness during heating was determined on a VIM-1M unit from the indentations left by a diamond square-based indenter under a load of 1 kg. The imprints were measured with a PMT-3 device. Fig. 6 (a) represents the dependence of binary chromium-niobium alloys on temperature. A diagram of the change in the hardness of chromium and Ezh4 steel obtained under similar conditions is also given for comparison. The advantage of chromium over an iron-base alloy is easy to see. The hardness of steel at room temperature is greater than that of chromium, but at temperatures higher than 500° the contrary is true, and at 1000° the hardness of chromium is threefold that of steel. Nevertheless, in terms of the absolute value, the

hardness of chromium at high temperatures is low (about 50 kg/mm^2).

An addition of 2% Nb increases the hardness of chromium throughout the entire temperature range, and considerably more at high temperatures (from 180 to 260, i.e., by 80 units at 20°, from 60 to 190, i.e., by 130 units at 1000°). An increase in the niobium content to 5% increases the hardness at room temperature (up to 380 kg/mm^2) but is practically speaking of no advantage in comparison to 2% Nb at high temperatures. Among the alloys with a higher niobium content the eutectic alloy stands out as having great hardness (600 kg/mm^2) at room-temperature, which it maintains with hardly any change when heated up to 800°). Even 1000° it still maintains 84% of its initial hardness (490 kg/mm^2).

Figure 6b, represents the changes in the hardness of alloys with a 5% V content. The most interesting of these is the binary chromium-vanadium alloy, which at room-temperature has a hardness of 220 kg/mm^2. During heating, its hardness first declines to a minimum at 500° (150 kg/mm^2), and thereafter increases until it regains its initial hardness between 700 and 1000°. This phenomen is reversible. It is apparently not connected with aging, since the hardness of this alloy after heating and recooling to 20° is again equal to 220 to 230 kg/mm^2.

The heat resistance of the alloy containing 2% Nb and 5% V is very high. On heating, its hardness undergoes a slight through uniform decrease over the entire range of temperature studied from 290 kg/mm^2 at 20° to 200 kg/mm^2 at 1000°. Up to 700° the hardness of this alloy is greater than that of the binary chromium-niobium alloy with an equal niobium content. Alloys with a greater niobium content (10%) are either very hard at room temperaute, abruptly

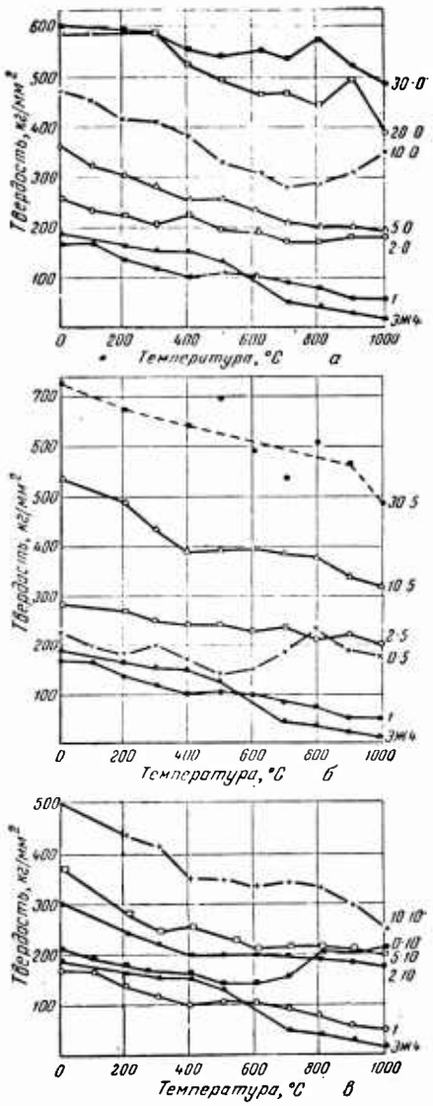

Fig. 6. Dependence of alloy hardness on temperature.

loosing their hardness, however, when heated, or they are brittle (30% Nb) to the extent that considerable scattering is obtained during the measuring.

The hardness of alloys containing 10% V as a function of temperature is given in Fig. 6(b). Here again the particular behavior of the binary chromium-vanadium alloy is confirmed, i.e., maximum harndess at 800° and a hardness at 1000° not inferior to hardness at 20°. Alloy 2-10 is slightly inferior to alloy 2-5. Alloy 5-10 behaves in more or less the same way as the alloy 5-0 and 2-5. The hardness of alloy 10-10 declines more steeply at heating in comparison with 10-0 and 10-5 (from 500 kg/mm^2 at room temperature to 250 kg/mm^2 at 1000°, i.e., by 250 units).

The data obtained enable us to conclude that the preservation of hardness upon heating is guaranteed mainly by adding small quantities of niobium (2-5%) and vanadium (5%). A further increase in the niobium content has the effect of considerably increasing hardness at room temperature rather than at higher temperatures.

Resistance to Scaling at High Temperatures

Specimens of regular geometrical shape (parallelepiped, cylindrical), to allow the magnitude of their surface to be determined were from the alloys. The specimens were placed is small porcelain boats, which had first been annealed to a constant weight. The boats containing the specimens were weighed on analytical scales prior to heating for 5 hours in a furnace at 960°. Figure 7 shows the changes in weight of the specimens per surface unit, depending on their composition.

Binary chromium-niobium alloys proved to be the most stable. At a content of 5 to 20% Nb, their stability is not inferior to that of pure chromium (the increase in weight is 0.01 mg/mm^2). The only alloys to gain slightly more in weight were the alloy

containing 2% Nb (0.047 mg/mm^2) and those with a niobium content greater then 30%. Vanadium sharply reduces stability. Alloys containing 5% vanadium undergo an weight increase 8 to 10 fold greater on the average and maximum oxidizability (0.13 mg/mm^2) observed at 2% V. Alloys containing 10% V oxidize still more intensively; the influence of niobium in these alloys proves to be very great. If the niobium content is stepped up from 0 to 5%, the weight increases rapidly (from 0.13 to 0.735 mg/mm^2); a further addition of niobium causes the weight increase to decline (to 0.096 mg/mm^2 at 40% Nb). For purposes of comparison we should point out that under the same conditions, a weight increase of 0.45 mg/mm^2 was obtained for technical iron. Repeated heating under the same conditions (5 hours at 960°) produced the same weight increase in most cases.

These observations make it clear that alloys containing more than 5% vanadium can not be used in an oxidizing atmosphere at high temperatures.

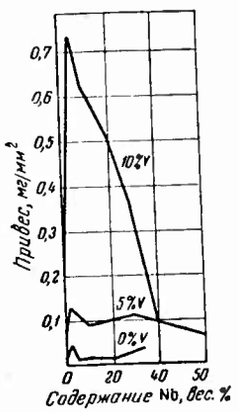

Fig. 7. Resistance of alloys to scaling.

Conclusions

As a result of the study of chromium-base alloys with a niobium content up to 50% by weight and of vanadium up to 10% by weight produced by melting in an induction furnace in an atmosphere of argon, a section of a ternary diagram of phase-equilibriums was plotted within the given concentration ranges. The hardness and resistance to scaling of alloys at temperatures up to 1000° were investigated.

2. At high temperatures, binary chromium-vanadium alloys, the hardness of which at temperatures of 800 to 1000° is not inferior to that at room temperautre, are especially stable from the viewpoint of their hardness. Best among the invesigated alloys with regard to hothardness are those alloys with low contents of both admixtures (niobium, 2 to 5%; vanadium, 5 to 10%), and also the binary alloy containing 30% Nb. However, it is not possible to use alloys containing more than 5% vanadium alloys in an oxidinzing atmosphere. It is therefore the binary and ternary alloys with a small (2 to 5%) content of niobium and vanadium which are of practical value as a base for heat-resistant alloys.

REFERENCES

1. KUBASCHEWSKI, O. and SCHPEIDEL, A. J. Inst. Met., 75, 1949.

2. DUWEZ, N. and MARTENS, P. J. Metal., 4, No. 1, 1952.

3. YELYUTIN, V. P. and FUNKE, V. F. Izv. An SSSR (Acad. Sci. USSR, Tech. Sci. Dept.), No. 3, 1956.

4. YEREMENKO, V. N.; ZUDILOVA, G. V. and GAYEVSKAYA, L. A. Papers of the Conference on the Physicochemical Fundamentals of Steel Production (Trudy soveshchaniya po fiziko-khimicheskim osnovam proizvodstva stali), Izd. AN SSSR (Acad. Sci.of USSR Press), 1956.

5. WILHELM, H. A.; CARLSON, O. N. and DICKINSON, J. N. J. Metal, 6, No. 8, 1954.

6. ROSTOKER, W. and JAMAMOTO, A. Tr. ASM, 46, 1954.

7. MARTENS, H. and DUWEZ, P. Tr. ASM, 44, 1952.

8. UMANSKIY, Ya. S.; FINKEL'SHTEYN, B. N.; BLANTER, M. Ye.; KISHKIN, S. T. FASTOV, N. S. and GORELIK, S. S. Fizicheskoye Metallovedeniye (St. Sci. Press Lit. Ferr. Non-ferr. Met), Metallurgizdat, 1955.

INVESTIGATION OF THE STRUCTURAL CHANGES IN IRON-NICKEL ALLOYS AT THE PHASE TRANSITION $\gamma \rightarrow (\gamma + \alpha)$

M. I. Zakharova and N. A. Khatanova

The aim of our research was to investigate the phase transition $\gamma \rightarrow (\gamma + \alpha)$ in iron-base alloys containing 30 to 32% Ni. It was determined that at a temperature of 400° this transition proceeds extremely slowly. Cold deformation of alloys at room temperature not only speeds up the process $\gamma \rightarrow \alpha$, but the deformation of an alloy subjected to martensitic transformation at -196° helps equally to accelerate the reverse transition $\alpha \rightarrow \gamma$. At temperatures higher than the martensitic point the initial stage of $\gamma \rightarrow \alpha$ transition follows the usual martensitic transition pattern, and the newly formed layers of the α-phase lie parallel to plane (111) of the γ-phase. At the annealing temperature of 400° the coherence of lattices is apparently disrupted during the initial transition stage, and this is what actually decelerates the transition process.

Different kinds of phase transitions are superimposed on one another during the heat treatment of multicomponent alloys, which is why it is so difficult to their individual influencs on the changes in alloy properties. The study of each phase transition by itself will enable us to analyze them correctly taken as a whole.

Extensive literature has been published on the study of the $\gamma \rightarrow \alpha$ transition in ferro-nickle alloys [1]; nevertheless, the extraordinary stability of the nonequilibrium state in these alloys [2] still remains unexplained. It was the polymorphic transition in alloys containing 30% Fe and 32% Ni which were studied in the present work.

Electrolytic iron and nickel were used to prepare alloys containing 30% Fe and 32% Ni. After casting, alloys were homogenized at 1000° for 10 hours, were annelaed for 18 hours at 600°, and were then quenched in water. Single crystals were produced by recrystallization at 1200°. After continuous annealing for 60 hours, the 1 mm thick laminae developed up to 20 mm^2 in area.

X-ray and microscopic analysis of the polycrystalline specimen and x-ray analysis of stationary single crystals were made.

The process of polymorphic transformation was studied during isothermal heating at 400°, at which temperature, according to the Owen and Sully diagram [3], about 27% of the phase should be present in an iron-base alloy with 32% nickel that is in a state of equilibrium.

For x-ray analysis of the polycrystals, powder was obtained from a homogenized specimen by filing the powder was then annealed for 20 hours at 600° and subjected to isothermal annealing at 400°. X-ray pictures were taken by cameras 114 cm in diameter, using iron radiation; the specimens were 0.4 mm in diameter.

After annealing for 100 to 200 hours only γ-phase lines appeared on the x-ray pictures. A very weak α-phase line (110) appeared in the alloy containing 30% Ni after 300 hours, and after 500 hours in an alloy containing 30% Ni. An increase in annealing

time to 500 hours in the case of the 35% Ni alloy, and to 800 hours in the case of the 32% Ni alloy, brought about no appreciable changes, which indicates that the $\gamma \rightarrow (\gamma + \alpha)$ at 400° is very slow.

Cold deformation by filing powder from annealed specimens leads to $\gamma \rightarrow (\gamma + \alpha)$ transition at room temperature, and lines (110) and (112) of the α-phase appear on the x-ray pattern immediately after deformation.

In order to compare the transition rates at 400° and at temperature lower than the martensitic point, the phase composition of the iron alloy containing 32% Ni, under different treatments was determined by the intensity of the corresponding lines.

TABLE 1

Обработка сплава	Количество фаз, %	
	γ	α
Закалка порошка сплава в жидкий азот с 600°	16	84
Закалка образца в жидкий азот с последующей деформацией при 20°	46	54
Закалка образца в жидкий азот, деформация и отжиг при 400°—6 час.	73	27

During the quenching in liquid nitrogen 84% of the γ-phase is transformed into the α-phase; subsequent deformation at room temperature leads to the reverse transition of 30% of the α-phase to the γ-phase. When the alloy was subjected after the deformation to annealing at 400° for 6 hours, 27% of the α-phase appeared in the alloy, which corresponds to the equilibrium state at 400° (Table 1). Consequently, cold deformation of the alloy in which martensitic

transformation has taken place soon leads to a state of equilibrium in the alloy both at 20 and 400° through the reverse transition of the α-phase to the γ-phase, whereas in the case of isothermal annealing (400°) and water quenching the alloy remains far from equilibrium even after an annealing period of 1000 hours

Because of the difference in the specific volumes of the γ- and α-phases the phase transition $\gamma \rightarrow (\gamma + \alpha)$ is accompanied by the formation in the α-phase lattice of elastic stresses which were indeed those investigated in this study with respect to the breadth of the lines and to changes in the correlation of intensities. Because of the slight broadening of the lines, this broadening was related to second-kind stresses only

The second-kind stresses were determined from the width of the γ-phase line (113), using standard specimen Line width (113) was determined as the quotient of the integral intensity divided by the maximum intensity

The true width of the β-line was determined by the method evolved by G. V Kurdyumov and L I Lysak [4]. The width of the line under study was determined from the relationship

$$B = \frac{b\beta}{\int f(x) F(x) dx},$$

where f (x) and F (x) represent the distribution function of densities of the standard line and of the line under study;

b is the width of the standard line

It was assumed that $f(x) = F(x) = \underline{1}^{-\alpha x^2}$, in which case $B^2 = b^2 + \beta^2$ Photometric readings taken from x-ray patterns of the iron-base alloy containing 32% Ni, enabled us to determine that the magnitude of the stress after annealing at 400° for 350 hours

is 10.4 kg/mm^2, and after annealing for 500 hours, 12 kg/mm^2.

A determination of changes in the relationship of the intensity of lines (110), (200) and (113) during the annealing at 400°, disclosed that the rms values for atomic displacement are quantitatively small and that they reach their maximum value of 0.07 A, after tempering for 400 hours.

The low magnitude of second-kind elastic stresses and the low value of rms displacements are determined by the slowness of the phase transition and by the relaxation of stresses due to thermic regression.

A study of the mechanism of the phase transition $\gamma \rightarrow (\gamma + \alpha)$ by x-ray photography of stationary single crystals was made using white Mo radiation. The investigation disclosed that in the process of isothermic annealing at 400° there appeared in the x-ray diffraction effects of a deformation type (in the form of bands passing through the Laue maxima), fragmentations of the Laue maxima, and texturized Debye rings of the γ-phase. In our opinion, all these effects are caused by the formation of very thin layers of the α-phase in γ-phase single crystals during annealing, in which the γ-phase lattice has changed into a α-phase lattice.

The formation of thin α-phase intermediate layers must cause elastic stresses on the boundaries between these layers and the γ-lattice. These stresses most probably exceed in magnitude the elastic limit, which fact led to plastic deformation in the boundary zones. The plastic deformation caused, on the one hand, a disturbance of the coherence between the α-phase lattice layer and the γ-phase lattice, cessation of the regular atomic displacement, and growth of the α-phase layers. On the other hand, part of the

matrix was converted in the boundary zones into a polycrystalline state; this explains the appearance of Debye rings on the x-ray patterns of stationary single crystals The α-phase layers are evidently very small and for this reason do not give rise to a diffraction effect of their own in the Laue diffraction patterns. As has been pointed out, a very feeble α-phase line (110) appeared on Debye powder patterns after 300-500 hours.

The construction of a gnomonic-stereographic projection of the bands appearing in Laue diffraction patterns has shown that they intersect in pole (111), and this fact enables us to conclude that the layers are parallel to plane (111) of the γ-phase. As is known, in the process of martensitic transformation in steels α-phase crystals are oriented by plane (110) parallel to plane (111) of the γ-phase. Consequently, the nuclei of the α-phase also originate by regular atomic rearrangement parallel to plane (111) of the γ-phase of the matrix at temperatures higher than the martensitic point. Through the formation of the α-phase layers the crystal of the matrix breaks up into blocks; this becomes apparent upon transition from continuous maxima in the Laue diffraction pattern to a maximum consisting of lines. An increase in the distance between the lines with an increase in the annealing time to 1500 hours at 400° indicates an increase in the displacement angle of the blocks.

Optical and electron microscopes were used to study the phase transition $\gamma \leftarrow (\gamma + \alpha)$ Microsections were prepared by electrolytic polishing; the electrolyte was composed of the following: 78% H_3PO_4, 10% H_2SO_4, 8% CrO_3, and 4% H_2O. The best surface was obtained at a current density of 50 - 60 amp/dm^2, an electrolyte temperature of 30·- 70°, and a polishing period of 1 to 5 minutes.

As is clear from the figures cited, this electrolyte enables the operating conditions to be varied over a wide range. The specimens were etched in nitric acid and aqua regia.

After quenching, the microstructure of the alloy was composed of polyhedrons of the γ-phase solid solution.

GRAPHIC NOT REPRODUCIBLE

Fig. 1. Substructure of γ-solid solution crystals in an iron nickel alloy after tempering at 400° for 300 Hours.

The investigation of specimens submitted to annealing for periods of 100, 300, 500, and 3500 hours reveals a crystal substructure, on the surface of the microsection; triangular etching patterns parallel to the plane of the section or at an angle to it (Fig. 1) can be seen. Consequently the microstructure of an iron alloy with 32% Ni displays after annealing at 400° the topography of the γ-phase, and shows that crystals of the γ-phase are segregated into blocks. Microscopic analysis brings to light the disorientation of the blocks within several degrees. Slight

displacement of blocks is not visible from the microstructure. The thickness of the blocks in ferrous alloys with 32% Ni is determined microscopically as of the order of 1 micron.

Examination by electron microscope, using quartz-replicas of specimens subjected to annealing at 400° for 100 hours, also discloses a substructure of the matrix similar to that reproduced in Fig. 1. Consequently these data, just as the data obtained by the x-ray analysis of stationary single crystals, are evidence of the fragmentation of matrix crystals during the transition $\gamma \rightarrow (\gamma + \alpha)$. The α-phase layers did not coagulate into larger crystals even after annealing for 3500 hours.

By comparing the data obtained from microscipic and x-ray analysis in the study of the phase transition $\gamma \rightarrow (\gamma + \alpha)$ at temperatures below and above the martensitic point, we can see which features there are in common and which features are different in this. The $\gamma \rightarrow \alpha$ transition at temperatures below the martensitic point, according to the ideas of Kurdyumov, takes place through a regular atomic displacement. Because of the high elastic limit the regions of the solid solution whose lattice is transformed from γ to α are able to attain large dimensions. At temperatures higher than the martensitic point ($\sim$ 400°), the mechanism of creating the nuclei of a new phase by regular atomic displacement is based in our view, on the same principle, but in this case the rearrangement of the lattice extends over a small volume since the elastic deformation of the γ-lattice changes into plastic deformation even when the α-phase nucleis is of small volume. This plastic deformation for its part, leads to the nuclear lattice breaking away from the matrix lattice and to the transition of the adjoining layers of the matrix into a

polycrystalline state. The rearrangement of the lattice takes place without any change in concentration. The process then continues diffusion.

The diffusion growth of nuclei is very slow; even after tempering of the alloy at 400° 3500 hours, α-phase crystals do not acquire large dimensions.

GRAPHIC NOT REPRODUCIBLE

Fig. 2. Deformation zones in γ-crystals of a solid solution near α-nuclei after tempering at 400°.

An increase in the size of the γ-phase nuclei due to the difference in the specific volumes of γ- and α-phases leads to an enlargement of the deformation zone in the γ-phase near the α-phase nucleus. under microscopic examination these deformation zones appear in the form of figures approximating the circle (Fig. 2).The dimensions of the deformation zone appearing on the microsection are determined by the dimensions of α-phase nuclei and by the distance of the nuclei from the plane of the section.

REFERENCES

1. GOLOVCHINER, Ya. M. Problemy Metallurgii i fiziki metallov, (Problems of Metallurgy and Metal Physics), Moscow, 1951.

GOLOVCHINER, Ya. M. and TYAPKIN, Yu. D. DAN SSSR, 93, No. 1, 1953; Burst. Journ. of Met., Sept., 1951. Edmonson. Acta Metal., No. 2, 1954. Compt. Rend., 240, 2, 1955. MACHLIN, E. S. and COHEN, M. J. Metal, 4, No. 5, 1952.

2. BRADLEY, J. Proc. Phys. Soc., 80, Lond., 1940.

3. OWEN and SULLY, Phil. Mag., 27, 1939.

4. KURDYUMOV, G. V. and LYSAK, L. I. ZhTF, Zhurn. Techn. Fiz. 7, No. 9, 1947.

5. EARLY, Allen, J. Iron Steel Inst., 166, 1950.

CHANGES IN FINE CRYSTAL STRUCTURES DURING AGING OF NICKEL-BASE AND NICKEL-IRON ALLOYS

G. V. Kurdyumov, I. A. Bil'dzyukevich,
A. G. Khandros and V. G. Chernyy

The structure and properties of Nimonic-type alloys have been investigated during the postwar period both in the Soviet Union and abroad [1, 2, 3, 4]. The present work gives an account of some of the results obtained from investigation of the changes in fine crystal structures which occur in alloys of this type during aging and after hardening.

The dimensions of mosaic blocks of the basic solid solution and of the α'-phase, as well as the heterogeneity of the parameter $\frac{\Delta a}{a}$, were determined from the width of the x-ray diffraction lines. In addition, changes in the lattice parameters of both phases were also determined.

Four alloys, the composition of which is given in Table 1, were investigated. The last two alloys were of interest in connection with the conclusion reached on the basis of data obtained from diffusion, according to which the partial substitution of nickel by iron need not weaken the bonds of the basic solid-solution lattice. X-ray patterns were taken in Debye cameras with a cylinder diameter of 57.3 and 150 mm. Pictures of the first two alloy specimens were

obtained with copper radiation and, in the case of the last two alloy specimens, with manganese radiation. The use of copper radiation and cameras of large cylinder diameter made it possible to detect even slight broadening of the diffraction lines, since the k_α-doublet of copper was split even on reflections from plane (111) at an angle of 22°3'.

TABLE 1

Сплавы	Содержание элементов, %					
	C	Fe	Cr	Ti	Al	Ni
ЭИ 437	0,035	—	19,55	2,38	0,59	Ост.
То же	0,04	—	19,67	1,60	0,43	»
Fe 20	—	20,45	19,45	2,64	0,47	»
Fe 40	—	40,25	19,45	2,76	0,47	»

Figure 1 shows the change in block dimensions (zones of coherent x-ray scattering) of the basic solid solution of the specimens, quenched in water from 1080°, and then subjected to aging for 4 hours at different temperatures. The dimensions of the mosaic blocks of the basic solid solution undergo no change up to the aging temperature 850° and are of the order of $7 \cdot 10^{-6}$ cm. The high dispersion of the blocks even in the quenched state is caused by the preliminary treatment (cold plastic deformation, and a comparatively low temperature prior to quenching). This treatment was necessary to obtain solid lines in the x-ray patterns.

The inhomogeneity value of the parameter $\frac{\Delta a}{a}$ of the quenched specimen is practically equal to zero. It increases appreciably

after heating and annealing for 4 hours at 500 and 600°, reaching the value $0.8 \cdot 10^{-3}$, and decreases to its initial value at 700°. The increase of $\frac{\Delta a}{a}$ at 500 and 600° is apparently connected with the appearance of inhomogeneous concentration of the solid solution and not with second-kind dislocations, the formation of which is unlikely here. Figure 1 also gives data for the change in hardness in the specimens as a result of similar treatment. The maximum of the hardness curve is found at 700°, at which the ratio $\frac{\Delta a}{a}$ already is practically zero.

Further, the α' phase was electrolytically segregated from specimens subjected to the same kind of thermal treatment, and the dimensions of the blocks were determined from the breadth of the x-ray diffraction lines. Attempts to isolate the α' phase electrolytically after aging at temperatures lower than 700° proved unsuccessful. The particles obtained after aging for 4 hours at 700° were of linear dimensions of the order of 50 A. The amount of α'-phase was very small. Particles increased to 350 A with an increase in the aging temperature (850° at the given soaking, and the amount of α'-phase greatly increased. After this, over the temperature range 850°-910° the dimensions of the particles (blocks) grow smaller, and at still higher temperatures it is not possible to segregate them at all. The amount of α'-phase decreases in this temperature range too. This can be observed by the quantity of powder which it is possible to isolate electrolytically over a certain period of time. The decline in the size of the particles in the narrow temperature range (850-910°) is apparently connected with the fall in the rate at which they grow; this in turn is caused by a lesser degree of super saturation of the solid solution in this

temperature range.

The parameter of the basic solid solution lattice in alloy EI 437, quenched and tempered at different temperatures, was determined in addition. The lattice parameter declines from 700° and reaches its minimum value after tempering at 850°. The lattice parameter of a specimen tempered at 950° approaches the parameter value of a quenched specimen.

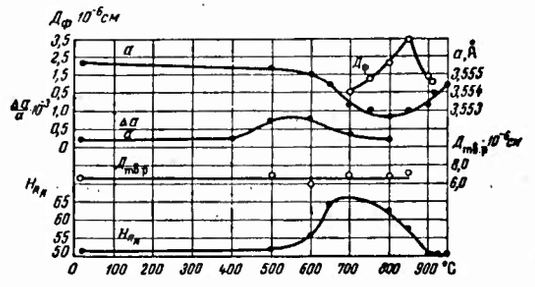

Fig. 1.

By comparing the data obtained one can see that in our case the increase in hardness of an alloy after aging is not accompanied by a noticeable change in the dimensions of the blocks of the basic solid solution. The increase in hardness begins at 600°, that is to say, at the point where attempts to isolate the α'-phase electrolytically are unsuccessful. A broadening of the lines due to the inhomogeneity of the composition $\frac{\Delta a}{a}$ is observed in the same temperature range. It is only possible to obtain small quantities of the α'-phase after aging at 700°. The maximum hardness can be observed at about the same temperature. Further growth of

the particles is accompanied by diminishing hardness. The latter also continues to decline after tempering in the temperature range 850-910°, in which the dispersion of α'-phase particles increases.

Results of the investigation of the second alloy, containing a somewhat lesser amount of titanium, are shown in Fig. 2. In this alloy the maximum hardness after tempering and 4-hours of aging was found at 700°. As with the first alloy, it is possible electrolytically to isolate the α'-phase after aging at this temperature. The linear dimensions of the particles of this phase proved to be approximately 70 A. The dimensions of the particles increase with the increase in aging temperature, and at the same time hardness decreases. The lattice parameter varies within the temperature range over which the hardness changes as in the case of the first alloy. The maximum change, both in the first and second alloys, exceeds three units in the third decimal place.

Let us consider the results of our study of alloys containing iron. These alloys were melted in a high-frequency furnace in vacuum and then annealed at 1150° for 8 hours.

Previous experiments showed that heating to 1080°, following by soaking for two hours, suffices to make the particles of the segregated phase dissolve. Changing the quenching temperature from 1080 to 1200° produces no difference in the lattice parameter. Moreover the second phase is not revealed by anodic dissolution. After quenching from a temperature of 1080° the specimens were subjected to soaking for one hour at temperatures ranging from 400° to 950°.

Figure 3 gives the results of measurement of the hardness of two ferrous alloys and compares them with the hardness curve of the

first alloy (EI437). As in alloy EI 437, the aging of ferrous alloys in the temperature range 600-900° leads to an increase in hardness the maximum of which is to be found at 700-750°. Hardness in this range proved to be the same for both alloys.

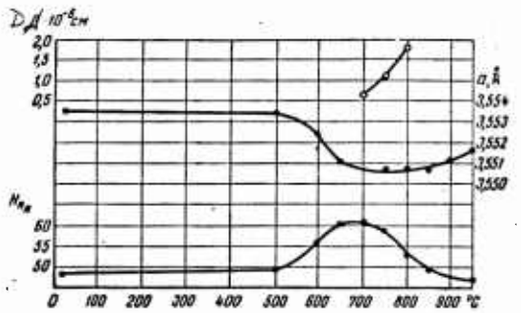

Fig. 2.

The hardness of ferrous alloys, whether in the quenched state or after tempering at any temperature, is lower than that of alloy EI437(not forgetting the difference in the length of aging). Alloy EI437 was tempered for 4 hours, and the ferrous alloys for 1 hour.

It is possible to segregate the phase precipitated during aging by electrolytic dissolution. X-ray patterns of powder from a phase isolated in this way reveal the similarity of this phase to the α'-phase´ of alloy EI437. As in Nimonictype alloys this phase has a face-centered cubic lattice with a parameter slightly larger than that of the basic solid solution.

The lattice parameters of basic solid solutions and of the α'-phases of alloys containing 20% Fe and 40% Fe and of alloy EI437 are given in Table 2. From Table 2 it can be seen that the partial substitution of iron for nickel leads to an increase in the α'-phase lattice parameter, with the parameter increasing together with

an increase in the iron content.

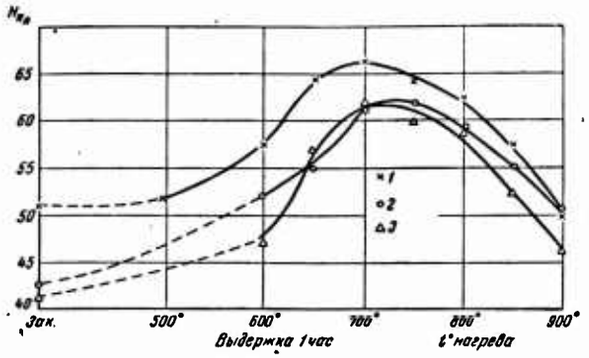

Fig. 3. 1) EI437; 2) Fe 20; 3) Fe 40

The constant of the α'-phase lattice also increases, and the more it does so, the more iron is there present in the alloy. The increase in the α'-phase lattice parameter enables us to conclude that iron is likewise contained in the α'-phase. Nevertheless, the possibility that iron affects the change in the content of the other elements in this phase is not excluded.

Changes in the lattice parameter after aging of the alloy containing 40% Fe are shown in Fig. 4. The minimum parameter value is observed at 800°. A further rise in the aging temperature leads to an increase in the lattice parameter, this is linked with the greater solubility of titanium and aluminum.

The dimensions of α'-phase particles in these alloys were determined by line (311) situated at an angle of 76°. Since the extinction of lines might have been due not only to the small dimensions of the particles but also to the inhomogeneity of the α'-phase composition, the broadening at both small and large angles

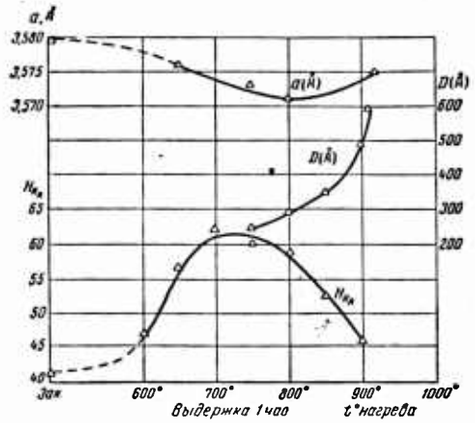

Fig. 4.

was assessed. It appeared that they were proportional to the secant of the reflection angle. Hence the dispersion of the α'-phase particles is responsible for the broadening of the lines in the x-ray patterns.

Data on the linear dimensions of particles of the alloy contaning 20% Fe after various aging temperatures are given in Fig. 5. After tempering for 1 hour at 750°, the mean linear dimensions of the particles was approximately 140 A. An increase in aging temperature results in enlargement of the particles. After tempering for 1 hour at 900°, the particles attained a size of 420 A. Electrolytic segregation of the α'-phase is only possible after tempering at temperatures not below 750°, when maximum hardness is observed. In this case the size of the precipitated particles is at its minimum.

A similar pattern can also be observed in the alloy containing 40% Fe. After aging for 1 hour at 750°, particles were 240 A in dimension. Maximum hardness is observed after aging at the same

TABLE 2

Сплавы	Параметр решетки a, Å		
	твердого раствора закаленного	твердого раствора, отпущенного на 700°	α'-фазы
ЭИ437	3,556	3,553	3,584
Fe 20	3,562	3,559	3,559
Fe 40	3,580	3,578	3,578

temperature. The linear dimensions of particles after soaking for 1 hour at 900° were approximately 600 A. Efforts to isolate the α'-phase at higher aging temperatures proved unsuccessful.

Contrary to the observations made in the case of alloy EI437, we did not succeed in observing a down slope for the dependence dimensions on aging temperatures of the α'-phase particles in alloys both with and without iron but containing a smaller content of titanium. Apparently, the temperature range over which diminution of the particle dimensions can be observed is very narrow.

Other authors have used different methods to determine the dimensions of α'-phase particles in Nimonictype alloys. For example, in [4], after a soaking period of 300 hours at 700°, the linear dimensions of the particles were 300 A. In our case they were 50 A. Bagaryatskiy and Tyapkin found the particle dimension at the maximum value of hardness, to be of the order of 200-400 A. Considering the difference in methods, our data and those obtained by other authors accord reasonably.

In the alloys we investigated distortions of the second type did not occur during the decomposition of the solid solution, which was accompaned by an increase in hardness. In our case, disintegration of α'-phase blocks does not take place in the process of de-

composition. This is apparently due to the small size of the blocks in their initial state.

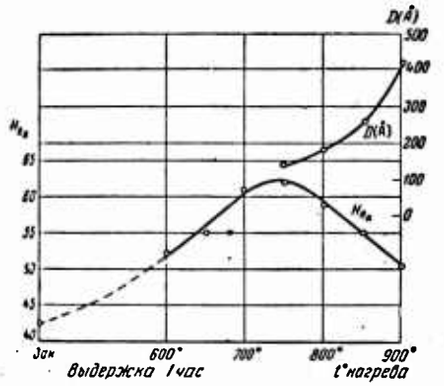

Fig. 5.

Thus the formation of second-phase dispersion particles does not produce any change in the given elements of the fine structure of solid solutions. Increase in the hardness due to the presence of second-phase dispersion particles, is caused, on the one hand, by the reduction of the path along which the beginning of plastic deformation spreads, and, on the other hand, by an increased number of imperfections in the structure at the boundary between the two phases.

REFERENCES

1. BLOK, N. I.; GLAZOVA, A. I.; DUBOVIKOVA, S. T.; KISHKIN, and LASHKO, N. F. Zav. Lab, (Works Laboratory), 20, 8, 1954.

2. KHIMUSHIN, F. F.; TRUSOVA, E. F. and GAVRILYUK, M. I. Struktura i Svoystva Splava EI437 (Structure and Properties of EI437 Steel), Oborongiz, 1955.

3. PFEIL, L. V.; ALLEN, N. P.; and CONWAY, S. G. High-temperature Steels and Alloys for Gasturbines. Special Report, No. 43. The Iron and Steel Inst., London, 37, 1952.

4. BAILLIE, Y and POULINIER, J. Revue de Metallurgie, 51, No. 3, 1954.

5. MANENC, J. Compt. Rend. Acad. Sci., No. 18, 1954.

TEMPERATURE AND TIME-DEPENDENCE OF RESISTANCE TO DEFORMATION IN COPPER AND ITS ALLOYS

M. A. Bol'shanina, M. B. Makogon, and V. Ye. Panin

The ability of heat-resistant alloys to withstand external loads at high temperatures is usually determined from the degree of plastic deformation produced over a certain period of time under conditions of constant stress below the yield point (determined at the normal deformation rate).

A number of facts which have recently come to light indicate that creep is a variant of plastic deformation. V. M. Rovinskiy and L. M. Rybakova [1], and L. M. Rybakova [2], for instance, in comparing structural changes during plastic elongation and creep, came to the conclusion that in principle creep does not differ from elongation. The difference between them is merely quantitative. M. Ya. Fuks, N. V. Slonovskiy, and L. I. Lupilov [3] have demonstrated that the broadening of lines in Debye powder patterns in creep at 500° is the same as in ordinary elongation at the same temperature, except that it is smaller in magnitude in accordance with the lower rate of deformation. The broadening of lines diminishes as the creep rate decreases.

Under these circumstances it is clear that the laws governing creep should derive particularly from the theory of plastic deforma-

tion. Unfortunately, no quantitative theory of plastic deformation has as yet been formulated; hence one must rely on experimental data and qualitative laws of behavior in order to arrive at explanations and descriptions of related phenomena. The qualitative aspect of plastic flow has now been thoroughly studied, and an application to creep of the laws of behavior already discovered would be very fruitful. The phenomena involved in creep and plastic deformation can be linked by studying extremely low rates of plastic flow, since creep should be considered as plastic flow at very low rates. The present work is devoted to a study of the influence of the rate of deformation on mechanical properties under various conditions. It is based on the theory of hardening and relaxation, which has been fully verified in the study of pure metals.

On the basis of available information on the influence of the rate of deformation on mechanical properties and following the theory of hardening and relaxiation, many features of the behavior of metals and alloys at high temperatures and low deformation rates can be predicted, including many of those that apply to creep. In view of this it seemed to be of importance and great topical interest to verify the predictions based on the theory of hardness and relaxation by studying the behavior of single-phase solid solutions at various temperatures and rates of deformation.

Deviations in the crystal lattices that are caused by plastic deformation may vanish through the kinetic processes occurring in solid bodies. A number of experimental findings [4, 5] indicate not only the occurrence of such processes in the course of deformation but also that they are stimulated by external shear stress. The effect of these processes manifestly depends on time and tempera-

ture.

At high rates of deformation the softening process can take place only to a very small degree, and it is this that results in higher strain resistance. The relaxation process at very low rates of deformation causes a considerable lessening of strain resistance. The higher the temperature, the sharper is the difference between resistance to rapid and to slow deformation under equal stress. The rate factor, determined as the ratio of strain resistance at a high rate to resistance at a low rate under equal strain, increases in the case of pure metals with a rise in the test temperatures. Consequently the higher the rate of deformation, the less does the resistance to deformation depend on temperature [6, 7], and conversely, the lower the rate of deformation, the steeper should be the decrease in strain with a rise in temperature. This explains the large measure to which temperature influences the rate of creep.

If the influence of the rate of deformation is explained by the degree to which relaxation has time to take place during the deformation process, then specimens deformed at a lower rate can naturally be expected to display smaller lattice distortions and less strain hardening [8, 3]. In creep, the lattice distortions should be smaller than in conventional elongation at the same temperature, and this is in fact confirmed experimentally [2, 3].

The decline in strain resistance with a temperature rise is caused to a great extent by softening [6]. The temperature coefficient of strain resistance $\Delta\sigma/\sigma \cdot \Delta T$ for pure metals, as well as the time factor, must depend qualitatively on a number of factors. It should especially increase in the case of pure metals with a lower melting point and deformation rate, and experiments confirm

both these dependencies.

Since softening occurs with greater intensity at high temperatures, the temperature coefficient of strain resistance should increase with a higher temperature; in other words, resistance to strain in a temperature range remote from recrystallization temperatures slightly decreases with a rise in temperature (for instance, for copper, it declines by $8 \cdot 10^{-4} \frac{1}{\text{degree}}$, between 20 and 100°, whereas a rapid decline can be observed at high temperatures (i.e., for copper between 500 and 600°, by $46.6 \cdot 10^{-4} \frac{1}{\text{degree}}$).

Inasmuch as the softening process requires time, relaxation should occur to a higher degree when the rate of deformation declines. In this connection the temperature range in which an especially sharp decline in strain resistance is observed decreases with a fall in the deformation rate.

At high temperatures, when metal undergoes total recovery in the course of experimentation, a further increase in temperature is comparatively without effect, and the temperature coefficient, having passed its maximum, begins to drop.

Let us consider single-phase solid solutions. Due to the presence of foreign atoms in the alloy lattice, supplementary static distortions appear in it which contribute to the appearance of strain distortions. Moreover the bond energy may also undergo a change. The behavior of the alloy will be determined by the quantitative ratio between these two factors [10, 11]. In a large group of alloys the influence of static lattice defects prevails over the modification in bond strength at normal temperatures. Resistance to strain in such metals is considerably greater than in the pure metal on which the alloy is based. Experimental data

indicates that in such cases the softening processes are greatly impeded, the rate of deformation is of little influence [12], the effect of temperature on mechanical properties is considerably lessened [12], the recrystallization temperature is higher, and the ratio of $T_{recrystallization}/T_{melt}$ is greater.

The level of diffusion mobility needed in order to allow recrystallization proved to be considerably higher in all the alloys [13]. It is important that recrystallization in various pure metals requires an approximately identical level of diffusion mobility $\sim 10^{-20}$ — 10^{-22}, and in solid-solution alloys, $\sim 10^{-12}$— 10^{-13}. It is natural that here the recyrstallization temperatures of different metals and alloys are not the same but will depend on the bond energy in the lattice.

Hence one should expect a substantial influence on the part of the interatomic bonds in the temperature ranges in which there is a high degree of softening and recrystallization and where the decline in strain resistance with a temperature increase is the greatest.

Let us consider a copper-base alloy system: copper--nickel; copper--aluminum; copper--zinc. The bonds in copper are increased by nickel and weakened by aluminum and zinc. For this reason one should assume that at high temperatures (400--600°) both time and temperature factors will be smaller in the copper-nickel alloy than those of pure copper, i.e., that at elevated temperatures the resistance to strain in the copper-nickel alloy will be less influenced by the deformation rate and by temperature than in copper.

At low temperatures the static distortions resulting from the alloying process in copper-aluminum and copper-zinc alloys are greater

than in the copper-nickel alloy. They impede softening and are responsible for their increased strain resistance. Hence, up to temperatures of 200--300°, the time and temperature factors of copper-aluminum and copper-zinc alloys should be lower than those of copper. However, at high temperatures when the diffusion movility of atoms is of particular significance and the bonds consequently begin to play an important part, the time and temperature factors of copper-aluminum and copper-zinc alloys must increase sharply and may even become higher than those of copper, not to mention the copper-nickel alloy.

Thus the heat softening of alloys is influenced by static distortions resulting from the alloying process as well as by the intensity of the lattice bonds; strongly bonded alloys are more stable with respect to temperature than alloys with weaker bonds, despite the fact that the static distortions may be samller.

At low temperatures, if the bond energy decreases only slightly in the alloying process, the part played by static distortions in hardening becomes decisive. It is these distortions which impede the kinetic processes in alloys and lessen the influence of the temperature and rate of deformation on the mechanical properties. Static distortions have a positive effect in this connection. Nevertheless their hardening effect cannot be relied on, since it falls off sharply as soon as diffusion increases to the extent that the strain distortions of the lattice rapidly begin to vanish.

In order to assess the role of static distortions and that of the bond strengths in the lattice, it is of interest to trace the heat resistance of strain distortions. The presence of static distortions can hardly ensure the stability of strain distortions

during annealing. A strong bond energy, on the other hand, is probably a more reliable guarantee of this stability.

Finally, if we assume that the presence of static distortions resulting from alloying contributes to the occurrence of strain distortions, we can expect to find under equal conditions a more intensive absorption of energy in the deformation of those alloys in which static distortions are stronger. Their resistance to deformation will also be greater.

The experimental material confirming the theoretical assumptions postulated above is as indicated below.

Materials and Methods of Study

The materials used in the investigation were pure copper M1, and its solid-solution alloys: with nickel (5.19; 10.71 and 15.69 atom %). All the material was melted in an Ajax high-frequency furnace. After homogenization the castings were forged into rods, 11--12 mm in diameter, which were then drawn to a diameter of 8 mm. The specimens prepared for reduction (7.00 $\pm$ 0.02 mm in diameter, and 11.00 $\pm$ 0.02 mm in height) were annealed prior to deformation under optimum conditions.

The reduction of the specimens to a deformation of approximately 40% was carried out in a specially constructed device on an Amsler machine and an IM-4a machine at average rates of 6mm/min (v_3), 0.05 mm/min (v_2) and 0.005 mm/min (v_1) and temperatures of 20, 100, 200, 300, 400, 500, and 600°. The reduction of the specimens was carried out in an atmosphere of purified nitrogen at a temperature of 200°, or higher, to prevent oxidation.

The true stress (σ) and relative strain (ϵ) were calculated for every given moment, but the elastic deformation of the specimen and of the components of the device was not taken into consideration. No fewer than 5 specimens were tested under identical conditions (temperature and rate). The divergence of the individual values did not exceed 3-4% at low temperatures, and 8-10% at high temperatures. The stability of strain distortions occuring in pure copper and in alloys with an approximate content of ~ 10 atom % Ni, Al, and Zn after their reduction in area down to 40% at rates v_3 and v_2 and temperatures of 20, 200, 400, and 600° was also determined and accessed qualitatively from the changes in microhardnes (at a load of 200 gr on the indenter) of the deformed specimens after their successive annealings at rising temperatures. We also investigated the internal layers of specimens which, as shown experimentally, reflect more truly the state of the material under conditions of inhomogeneous compressive strain.

The latent strain energy according to known methods [14, 15] at different stages of compression in copper and its aluminum alloys (of all concentrations) was determined.

Experimental Results

Flow Curves of copper alloys under compression at various rates.

In accordane with the theory of hardening and relaxation [15, 16], provided there are no secondary processes (aging, decomposition of solid solutions), the increase in the reduction rate, should result in an increase in the deforming stress as already pointed out above. This effect occurs as a result of the diminishing role of relaxation (removal of strain distortion) when the period of defor-

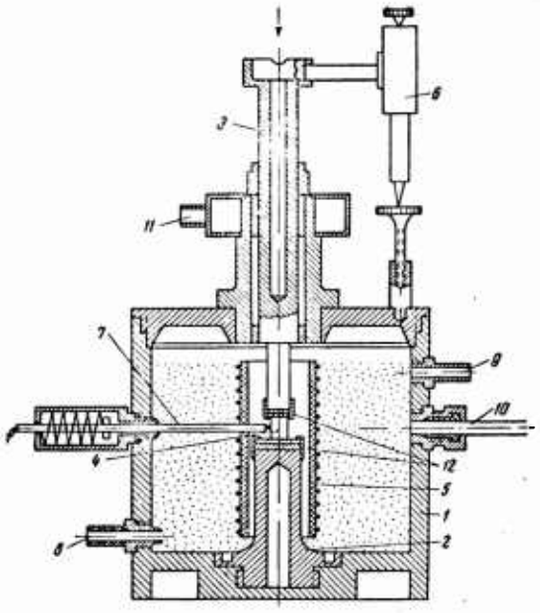

Fig. 1. Device for compressive reduction at high temperatures: 1) frame; 2) stage; 3) piston; 4) specimen; 5) furnace; 6) indicator for measuring reduction; 7) thermocouple; 8) nitrogen inlet; 9) out let of U-gauge; 10) power inlet to furnace; 11) cooling of piston guide brushing; 12) ceramic insulating plates.

mation is shortened. A decrease in the test temperature [6] should also lead to a higher value of the deforming stress. The above statements are fully confirmed by an analysis of the curves showing the flow of the copper alloys investigated. Curves showing the flow of copper alloys containing 5% Zn, at rates v_3, v_2, and v_1, and at temperatures of 20, 400 and 600° are given in Fig. 2. Curves showing the flow of other alloys are, on the whole, of the same nature.

The lower the rate of deformation in an alloy, the smaller are

the deforming stress and the degree of hardening of the material in deformation, and the smaller the angle of slope of the actual flow curve. The same dependence is observed at a higher deformation temperature.

The following characteristics of the resultant flow curves can be pointed out: 1) In undergoing deformation at temperatures higher than 400° beginning from a certain degree of deformation, copper and its alloys exhibit a loss in true compressive strength. The lower the rate and the higher the temperature of deformation, the sooner this decline begins. Thus for the copper alloy with 5%

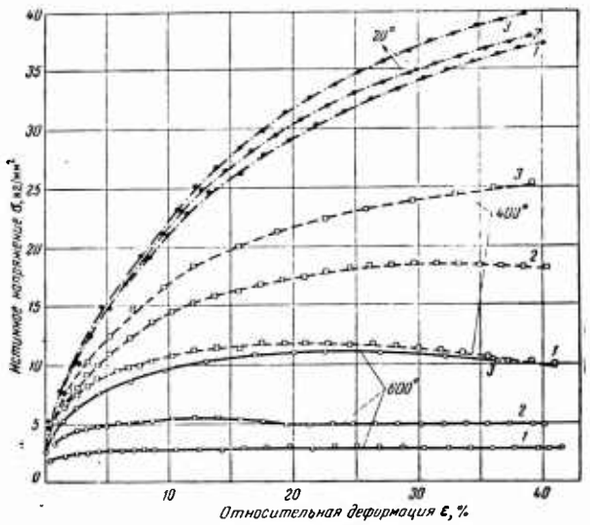

Fig. 2. Curves showing the flow of alloy Cu + 5 atom % Zn at various rates and temperature reduction. Rate (mm/min): 1) $v_1 \cong 0.005$; 2) $v_2 \cong 0.05$; 3) $v_3 \cong 6$

Al no decline in stress is observed on the flow curve at a reduction temperature of 400° and a rate v_3. At a rate v_2, the decline begins at $\epsilon = 32\%$, and with a rate v_1 at $\epsilon = 16\%$. When the test tempera-

ture is raised from 400 to 600° (rate v_1), the decline in stress of the same alloy starts at ϵ = 28, 16 and 14%, respectively.

Comparing different alloys, we can point out that all other conditions being equal this decline in copper-nickel alloys is less noticeable than in alloys of the copper-aluminum group, and still less in the latter than in alloys of the copper-aluminum group, and still less in the latter than in alloys of the copper-zinc group. The decline in stress in alloys of the copper-nickel group can be observed from a temperature of 500°, whereas in copper-aluminum and copper-zinc alloys it is already rather marked at 400°.

The decline in deforming stress can be explained by an intensification of the softening process at high degrees of deformation, when in the process of deformation both distortions resulting from the actual process of deformation as well as those formed at previous stages disappear.

The theory of hardening and relaxation [15] provides the following approximate expression for the curve flow of compression: $\sigma = \sigma_0 (l_0/l)^{b-\frac{a}{v}}$,

where: l_0 is the initial length;

l is the length at each given moment;

v is the rate of deformation;

b is the hardening factor, which depends in the first approximation safely on the nature of the material;

a is the relaxation factor which depends in the given material on the degree of deformation, its rate, the stress and the temperature [17].

σ_0 is a constant coefficient.

From the formula it can be seen that when there is a certain relationship between b, a and v ($a/v > b$), which occurs at a defi-

nite ϵ value (a is a function of ϵ, as has been indicated), σ can diminish with a further rise of l_0/l. It is also evident that the lower the rate of deformation v, or the higher the test temperature a increases with the temperature), the more b-a/v will fall below zero, at increasingly smaller degrees of deformation, and σ will start to decrease accordingly.

It is easy to observe that the above data fully support the conclusion reached on the basis of the theory.

The change in the contour of flow curves, particularly the shift of its maximum to one side or the other during the transition from pure metal to alloy, is naturally a consequence of the change in the hardening and relaxation factors b and a. The given experimental data enable us to conclude that copper-nickel alloys recover to a smaller degree than copper-aluminum and copper-zinc alloys (a decline in true stress on the flow curve in copper-nickel alloys starts to be noticeable at relatively higher temperatures).

As already pointed out, in accordance with the theory of hardening and relaxation recovery is more pronounced in low melting metals and alloys. On this basis, the decline in true stress on the flow curve of these metals should be observed at smaller degrees of strain, at lower temperatures, and at relatively higher rates of deformation. This phenomenon was actually observed by a number of investigators [12, 18] in lead alloys and other low-melting metals at room temperature.

2) at test temperatures of 200-300° a convergence of the flow curves pertaining to various rates of deformation was noticed in almost all the alloys, i.e., the rate effect diminishes. The reason for this phenomenon should be sought in the secondary processes.

It is known [19] that in plastic deformation aging can continue through mounting diffusion until the precipitation of a new phase in equilibrium solid solutions, including copper-zinc and copper-aluminum alloys. Under certain conditions this aging leads to increased resistance to deformation, and the smaller the rate of deformation, the greater is the increase; the result is that the influence of the deformation rate diminishes and may even cease altogether due to this effect. This is apparently what happened in our alloys also.

3) the very slight incline in the flow curves for copper and its alloys at a temperature of 600° and a deformation rate v should likewise be noted. This incline indicates the slight hardening of the alloy at deformation, which accords with the data obtained from x-ray analysis. Composing different alloys under the given conditions of deformation ($T = 600°$, v_1), we can see relatively greater hardening in copper-nickel alloys in comparison with copper-aluminum alloys, and especially with copper-zinc alloys and pure copper. An increase in nickel concentration in copper improves its capacity for cold-working under the given deformation conditions.

Hardening coefficients. The nature and the degree of the influence exerted by an alloying admixture on the mechanical properties of an alloy, as is clear from the above, are determined to a large extent by the temperature and rate of deformation. The same alloying admixture can under certain conditions depending on the temperature and strain rate, exert a positive influence on the properties of an alloy, whereas under different conditions its influence may not be as effective. Hardening coefficients, equal to the ratio of the compressive stress of an alloy to the compressive

stress of pure copper at the same rate, degree, and temperature of deformation were determined in [20] for the purpose of describing this influence.

The values calculated for hardening coefficients at a degree of deformation $\epsilon = 30\%$ are in Table 1. It can be seen from the Table that the raise in test temperature from 20 to 600° for alloys of the copper-nickel group increases the hardening coefficient at all three of the rates studied. This can be explained by the relatively more intensive softening of copper as a result of rising temperature, by comparison with the softening of alloys belonging to the copper-nickel system. A fall in the deformation rate also increases the hardening coefficient of copper-nickel alloys. At a temperature of 600° however during the transition from rate v_2 to rate v_1, copper-nickel alloys of all concentrations display a certain decline in the hardening coefficient rather than an increase. This indicates the beginning of more intensive recovery in the alloy. An increase in the nickel concentration in copper leads naturally to an increase in the hardening factor, and, the higher the temperature of deformation the greater this is.

The values of the hardening coefficients for alloys of the copper-aluminum and copper-zinc system change in a somewhat different manner. First, there should be noted the less intensive increase in the hardening coefficients of these alloys, particularly the copper-zinc system, with a rise in the test temperature. Moreover, in the copper alloy with 10% Zn at a rate v_1 this factor first increases during a change in temperature from 20 to 200° then gradually diminishes. A similar decline can be observed in the copper alloy containing 15% Al, during transition from 400 to 600°

(rate v_3), and from 200 to 400° (rate v_2 and v_1). This behavior by the hardening coefficients of copper-aluminum and copper-zinc alloys as a result of the rise in test temperatures is accounted for by the fact that they soften more intensively at higher temperatures in comparison with alloys of the copper-nickel system.

A similar conclusion follows from an analysis of the changes in the hardening coefficient as a result of a decrease in the rate of deformation. Whereas in alloys of the copper-nickel system this coefficient declines only with transition from rate v_2 to rate v_1 at 600°, in the case of alloys pertaining to the copper-aluminum and copper-zinc systems it declines at transition from rate v_3 to v_2 and still further in transition from rate v_1 at 400°.

A greater concentration of aluminum in an alloy, all other conditions being equal, helps to raise the hardening coefficients, but this increase is scarcely noticeable at 600° (whereas at rate v_1 this is the case even at 400°). Thus at high test temperatures (higher than 400°), and even more so at low deformation rates, an increase in concentration of a copper aluminum alloy has little effect.

It is of interest to compare the absolute value of the hardening coefficients for alloys of different systems. Table 1 shows that at temperatures up to 400° and at a high rate of deformation (v_3), the admixtures studied assume the order Al-Zn-Ni when considered according to their effect on the hardening of copper. The significant extent to which copper is hardened by aluminum at room and relatively low temperatures can probably be explained by the considerable static distortions of the crystal lattice of copper during the formation of a solid solution with aluminum. If we

TABLE 1

Hardening Coefficients ($\eta = \sigma_{alloy}\ \sigma_{copper}$) and its Alloys at Various Temperatures and Deformation Rates $\epsilon = 30\%$

Температура, °С	Концентрация примеси, ат. %							
	5			10			15	
	Cu–Ni	Cu–Al	Cu–Zn	Cu–Ni	Cu–Al	Cu–Zn	Cu–Ni	Cu–Al
	$v_3 = 6$ мм/мин							
20	1,1	1,1	1,1	1,2	1,5	1,1	1,5	2,0
200	1,0	1,1	1,1	1,1	1,6	1,2	1,5	2,1
400	1,1	1,3	1,2	1,3	1,8	1,3	1,8	2,7
600	1,5	1,6	1,2	1,9	1,6	1,6	2,7	1,5
	$v_2 = 0{,}05$ мм/мин							
20	1,1	1,1	1,1	1,1	1,6	1,2	1,5	2,1
200	1,1	1,2	1,2	1,2	1,7	1,3	1,6	2,4
400	1,3	1,4	1,2	1,5	1,6	1,3	2,3	2,0
600	2,0	1,6	1,2	2,8	1,7	1,4	4,2	1,9
	$v_1 = 0{,}005$ мм/мин							
20	1,0	1,1	1,1	1,2	1,6	1,2	1,5	2,1
200	1,1	1,2	1,2	1,2	1,8	1,3	1,7	2,5
400	1,6	1,3	1,0	1,9	1,4	1,2	2,6	1,3
600	1,6	1,5	1,1	2,3	1,6	1,1	2,7	—

proceed from the relationship between the atomic radii of the admixture and of copper, these distortions should be most distinct in aluminum alloys, less so in alloys containing zinc, and still less so in copper-nickel alloys. Static distortions not only increase the critical shear stress but also block the strain distortions of the lattice resulting from plastic deformation. By so doing, they hamper relief of the strains; i.e., they contribute to the intensive increase in strain-forming distortions. On the other hand, at high temperatures, when diffusion is greatly accelerated, static distortions are no longer of great significance; the strain distortions vanich easily and the stress sharply declines. The rise in the in-

tensity of the diffusion-softening process in copper-aluminum and copper-zinc alloys also contributes to the loss of bond strength that occurs in these alloys. But in alloys of the copper-nickel system the diffusion softening is accelerated to a lesser degree when the temperature rises, owing to an increase in bond strength as compared to copper.

The magnitude of the latent strain energy in alloys of the copper-aluminum system indicates the considerable extent of static distortions in copper-aluminum alloys and, more importantly, of the strain distortions blocked by them at low reduction temperatures.

The dependence of the quantity of absorbed energy on the concentration of aluminum in copper at various degrees of deformation is shown in Fig. 3, from which it can be seen that far more energy is absorbed by all the alloys studied than by copper.

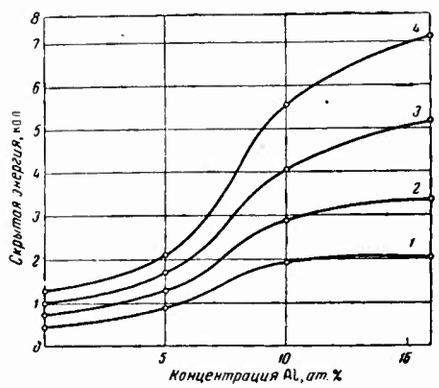

Fig. 3. Latent strain energy of copper-aluminum alloys. ε (%) 1) 15; 2) 20; 3) 40.

A greater aluminum concentration, in the same way as an in-

crease in deformation, contributes to an increase in the energy absorbed.

There should be noted the close correspondence between mechanical properties (resistance to deformation) and the latent strain energy, which is expressed by the identical nature of the dependence of these values on the concentration of the alloy (Figs. 3 and 4). This correspondence shows that the latent energy gives a good indication of the state of the material during deformation.

There is as yet no exact explanation for the inflexion of the curves in Figs. 3 and 4 at a concentration of 5% aluminum in the alloy.

The intensity of the softening in an alloy during deformation can be judged to a certain degree by the stability of the strain distortions appearing in the metal during its plastic deformation. This stability can be determined from the change in the mechanical properties of the deformed material caused by annealing at various temperatures. The greater the stability of the distortions (i.e., the greater the activation energy for their removal), the higher the annealing temperature at which these distortions will disappear, thereby determining the change in mechanical properties.

It resulted that the most intensive disappearance of strain hardening resulting from compression at 20° occurred in the case of copper* in the temperature range 400-450°; in the copper-nickel

---

* It was found that the copper had higher phosphorus content, which was the reason for its high recrystallization temperature.

alloy (10 atom% Ni) at 500-600°; in the copper-zinc alloy (10 atom % Zn) at 350-450°. If the reduction is carried out at 400°, the temperature ranges over which recovery occurs will accordingly be higher, since the most unstable distortions will be removed by the actual process of deformation. In this last instance, the temperature ranges over which the strain distortions disappeared most intensively were for copper 430-500°; for copper-nickel alloys, 550-600°; for copper-zinc alloys 360-450° and for copper-aluminum alloys, 380-450°.

Thus the presence of considerable static distortions in copper-aluminum and copper-zinc alloys does not guarantee the stability of strain distortions during annealing. A higher bond energy (copper-nickel alloys) helps to augnment this stability to a considerably larger degree.

Let us note that the nature of the influence of various factors (temperature, strain rate, alloy concentration, characteristics of the alloying element) on the value of the hardening coefficient, calculated for 15% deformation, remains essentially the same as for the coefficient calculated for $\epsilon = 30\%$. But is should be pointed out that the value of the hardening coefficient itself also increases with increased deformation; i.e., the higher is the deformation, the greater the positive influence of the admixture on the properties of the basic component. The latter fact apparently indicates that the difference in resistance to deformation in pure metals and alloys is determined to a large degree by the difference in hardening and softening during the processes that accompany plastic deformation [12].

Dependence of the compressive strength of copper and its alloys

on temperatures at various rates of deformation. On the basis of curves showing the flow of copper and its alloys, families of curves were plotted representing the dependence of compressive strength on the temperature at various rates of deformation at degrees of reduction of 15 and 30[. The curves for copper and its alloys with 10 atom % Ni (ϵ = 30%) are shown in Fig. 5. In the case of a rise in deformation temperature is accompanied by a monotonic drop in compressive resistance, the intensity of this drop increasing slightly with rise in temperature.

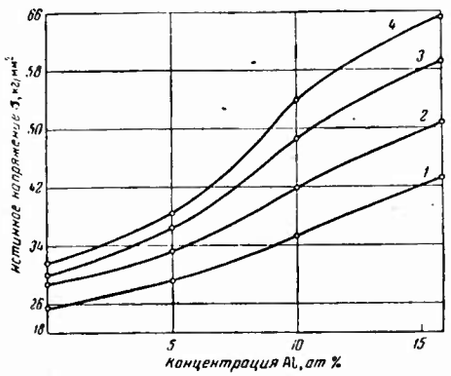

Fig. 4. True compressive stress of copper-aluminum alloys. ϵ (%): 1) 15; 2) 20; 3) 30; 4) 40.

In the case of alloy, these cruves are of a somewhat different character; i.e., with a rise in temperature in the intermediate temperature region a less marked decline is observed in stress, and a sharp fall is seen in the high temperature region. Curves of this type are typical alloys; they are consolidated by the alloying admixture, which shifts intensive thermal softening toward the higher temperature region. In the case of our alloys the addition of nickel

to copper which increases the bond strength, shifts the region of an intense drop in stress toward high temperatures (400-450° for alloy Cu + 15 atom % Ni) to a greater extent than aluminum and zinc (300° for alloy Cu + 15 atom % Al).

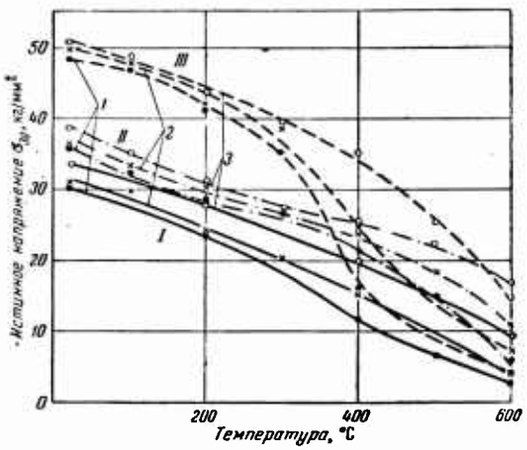

Fig. 5. Influence of the test temperature on the strain-forming stresses of copper and its alloys at various reduction rates (ϵ = 30%).
I) Cu; II) Cu + 10 atom % Ni; III) Cu + 10 atom % Al. Rate (mm/min): 1) $v_1 \cong 0.005$; 2) $v_2 = 0.05$; 3) $v_3 = 6$.

For copper, and also for copper-aluminum and copper-zinc alloys at temperatures of 400-450° and at relatively low reduction rates when stresses are relieved to a considerable degree, an inflection can be observed in the σ - T curves (in this case the intensity of the decline of stress at high temperatures diminishes with a rise in temperature).

The temperature coefficient of resistance $\alpha = \Delta\sigma/\Delta T$ (lowered resistance to deformation at a temperature increase of 1°) is smaller for an alloy with a more highly strengthening admixture (nickel) than in the case of aluminum or zinc admixtures. For instance, in

a temperature range from 300 to 400° and at rate v_1 for the alloys copper + 10% Ni, copper + 10% Zn, and copper + 10% Al, the temperature coefficients are $4.8 \cdot 10^{-2}$; $11.8 \cdot 10^{-2}$, and $18.0 \cdot 10^{-2}$ kg/mm^2 degrees respectively.

With a decline in the strain rate, the region of the intensive decline in stress is shifted toward the lower temperatures owing to the fact that over a longer period of time softening proceeds at an increased rate. It is clear that recovery will be still more intensive during creep, and the temperature at which there is intensive recovery should in this case be lower still. With a decline in the reduction rate the temperature coefficients also increase, which indicates more intensive recovery in the metal at lower strain rates.

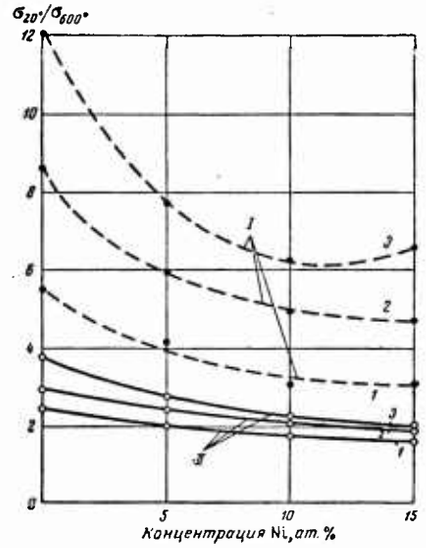

Fig. 6. Change in the ratio of strain-forming stresses at 20 and 600° for copper-nickel alloys at various degrees and rates of reduction. Rate (mm/min): I) $v_1 \cong 0.005$; II) $v_2 \cong 6$. ϵ (%): 1) 5%; 2) 15; 3) 30.

Let us consider the influence of the concentration of the alloying elements on the temperature coefficient. For copper-nickel alloys an increase in concentration helps to strengthen the alloy and causes the temperature coefficient to decline. For copper-zinc and copper-aluminum alloys the strengthening effect of the admixture and the decline in the temperature coefficient with increased concentration occur at comparatively low temperatures (up to 300-400°), and the lower these are, the lower the strain rate. At high temperatures, the greater the concentration, the more these alloys recover. The reason is apparently that when the bond energy is lower than that of copper, the static distortions resulting from the alloying process are unalbe to retard the softening involved in intensive diffusion.

It is of interest to trace the fall in resistance to deformation through out the whole temperature spread from 20 to 600° that was studied. In order to describe this process, we selected the ratio $\sigma_{20°}/\sigma_{600°}$. These data are given in Table 2 and partly in Fig. 6. Here the rise in the strengthening effect of the nickel admixture with the increase in concentration is quite distinct (less decline in stresses with a rise in temperature). This admixture is most effective at low deformation rates where, for instance, at a temperature rise from 20 to 600° the stresses in copper are reduced to one twelfth, whereas in the alloy copper 10 atom % Ni they drop to only one sixth. In the same manner, nickel is more effective at higher degrees of deformation. Thus whereever the conditions of deformation cause intensive softening in copper, the addition of nickel has a very favorable effect since it retards the kinetic processes in the alloys. Additions of aluminum and zinc

TABLE 2

Ratio of Strain-forming Stresses $\frac{\sigma_{20°}}{\sigma_{600°}}$ in Copper and its Alloys at Various Degrees and Rates of Deformation

Скорость деформации	Степень деформации ε, %	Концентрация примеси, ат. %								
		Cu	5			10			15	
			Cu–Ni	Cu–Al	Cu–Zn	Cu–Ni	Cu–Al	Cu–Zn	Cu–Ni	Cu–Al
v_3	5	2,4	2,0	1,8	2,0	1,8	1,5	1,8	1,7	2,1
	15	3,0	2,5	2,2	2,7	2,1	2,1	2,2	1,9	3,0
	30	3,7	2,7	2,7	3,4	2,3	3,3	2,6	2,0	4,8
v_2	5	3,4	2,6	2,4	3,0	2,2	2,5	3,1	2,1	3,3
	15	5,2	3,7	3,7	5,0	3,0	4,2	4,7	2,6	5,0
	30	8,0	4,1	5,6	7,3	3,4	7,4	6,6	2,9	9,1
v_1	5	5,4	4,1	4,2	5,6	3,0	4,5	6,0	3,2	—
	15	8,6	5,9	6,7	9,3	5,0	6,8	9,1	4,8	—
	30	12,1	7,7	9,2	12,2	6,2	12,1	12,6	6,7	—

produce a different effect. They harden copper and maintain the hardness only in cases when the conditions for intensive softening are unfavorable, i.e., at high rates and slight degrees of deformation. But at low rates and high degrees of deformation they soften in the same way as copper, only more so (in spite of the deforming stresses in them always being greater than in copper). Consequently the reliable alloying elements in solid solutions are those which strengthen the interatomic bonds in the lattice. The presence of large static distortions at a low level of bond energy is not a guarantee that the alloy will work well at high temperatures the question of inhomogeneous strengthening is not studied here.

Influence of the strain rate on the mechanical properties of copper and its alloys. As has been shown above, the rate of coefficient Z, equal to the relationship between the deforming stresses at

any two rates but at equal degrees of deformation, may serve as a qualitative characteristic of the intensity of the softening process occuring during deformation. The higher the rate coefficient and the higher the sensitivity of the material to the duration of strain, the more intensive the deformation, all other conditions being equal.

The values of the rate coefficients $Z \equiv \sigma_{V3}/\sigma_{V1}$ at all temperatures for ϵ = 15% and 30%, were determined for all alloys investigated in our work.

As is clear from Fig. 7, an increase in test temperature causes a rise in the value Z, which fact fully accords with the theory of hardening and relaxation. However, the intensity with which this increase occurs differs with the various alloys. The value Z for copper-nickel alloys is at all temperatures smaller than the corresponding values for pure copper. The value of the rate coefficient for copper-aluminum and copper-zinc alloys is only smaller than for pure copper at low temperatures (up to 300-400°). At high temperatures the picture is reversed due to the intensity with which the value Z for the alloys increases in comparison to value Z for copper.

This relationship between the rate coefficients for pure copper and for the copper-aluminum and copper-zinc alloys indicates in all probability greater intensity of softening at high temperatures in alloys as compared to copper, and is especially by comparison with copper-nickel alloys. The observed reduction of the effect produced by alloying copper with aluminum and zinc under conditions of deformation favorableto the relaxation (high temperature, low rate, and high degree of deformation) is therefore natural.

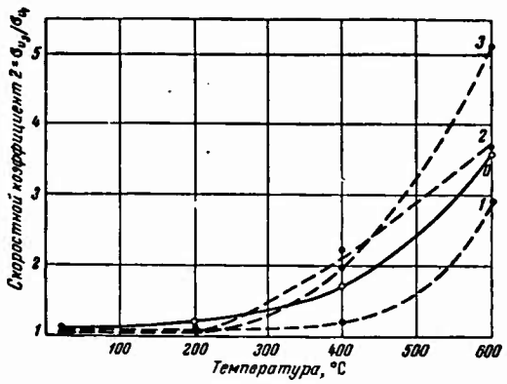

Fig. 7. Rate coefficient for copper and its alloys at different temperatures ($Z = \frac{\sigma v_3}{\sigma v_1}$, ϵ = 30%). 0) Cu; 1) Cu + + 10 atom % Ni; 2) Cu + 10 atom % Al; 3) Cu + 10 atom % Zn.

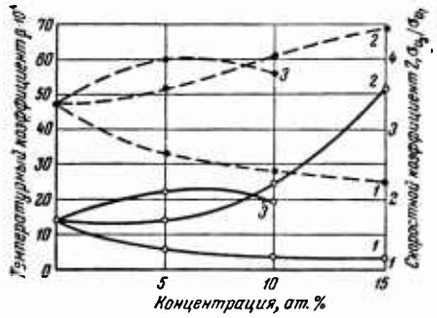

Fig. 8. Dependence of the rate coefficient (solid lines) and the relative temperature coefficient (broken lines) of alloys on concentration (400°, ϵ = 30%). 1) Cu - Ni; 2) Cu - Al; 3) Cu - Zn.

As an example, the dependence of the rate coefficient Z on the alloy concentration at a reduction temperature of 400° is shown in Fig. 8. From Fig. 8 it can be seen that with more nickel in an alloy (in our case up to 15%), this coefficient declines, whereas a greater aluminum and zinc content results in a higher coefficient. This behavior of the curves is not difficult to understand, if it is recalled that the addition of nickel to copper increases the bonds in the lattice and that the adding of aluminum and zinc weakens them. At high deformation temperatures, this should have an effect upon the intensity of the softening process to a significant degree.

Of interest is the coincidence of the contour of the curves relating to the change in the rate coefficient Z and the relative temperature coefficient $\beta = \Delta\sigma/\sigma_1\Delta T$ with the change in the concentration of the alloy, as shown in Fig. 8, for $\epsilon = 30\%$, T = 400° and rate v_1. The qualitative correspondence of these two characteristics was earlier observed in the case of pure metals [12]. This indicates that the same process - relaxation underlies the influence of both the temperature and the strain rate on mechanical properties. Nevertheless, the difference in the nature of the influence of these two factors should not be forgotten. Hence it would be wrong to expect this correspondence under any conditions of deformation whatever. From the results of our work this correspondence can be observed whenever the nature of the changes in stress resulting from higher temperatures is the same for different rates of deformation.

Conclusions

1. The study of the mechanical properties of copper and its nickel, aluminum, and zinc alloys in the field of solid solutions

has shown the full applicability to alloys as well as pure methods of the theory of hardening and relaxation over a broad range of temperatures and rates of deformation.

2. When the temperatures are lower than the temperature of recrystallization and when the strain rates are not too low, the alloying of copper with nickel, aluminum, and zinc results in a decrease in the sensitivity of the alloys to temperature changes and changes in the strain rates (lower rate and temperature coefficients than in copper).

3. A qualitative relationship exists within the same temperature ranges between the rate and temperature coefficients, as well as the hardening coefficients of alloys. The reason for this relationship is that the dependence of mechanical properties on rate and temperature are conditioned by relaxation processes.

4. At high temperatures and very low strain rates the change in the bonds of the lattice during alloying becomes considerable. The admixture renders the alloy more stable if it increases the bond strength.

The same alloying element can bring about a very considerable improvement in mechanical properties an and increase in the stability of alloys with respect to a rise in temperature and a fall in the strain rate, at certain temperatures and strain rates, whereas at higher temperatures and lower strain rates hardening effect is slight.

5. The results obtained are in conformity with the known postulate, according to which static distortions in the lattice play a considerable part in the change of properties resulting from alloying when temperatures are not high, whereas at higher temperatures it

is the bond in the lattice which are of basic importance.

6. There is an analogy between the changes in mechanical properties due to alloying or to change in temperature, as well as the change in the rate of deformation for such high-melting alloys as copper-base alloys, and the laws governing low-melting lead-base alloys. Thus the laws of behavior discovered are common to all solid solutions.

REFERENCES

1. ROVINSKIY, B. M. and RYABAKOVA, L. M. Bulletin of Academy of Science, USSR, Phys. Ser.), 20 , No. 6, 1956.

2. RYBAKOVA, L. M. IZV, AN USSR, Ser Fiz., 20, No. 6, 1956.

3. FUKS, M. Ya.; SLONOVSKIY, N. B. and LUPILOV, L. I. Izv. AN USSR, 20, No. 6, 1956.

4. KARPOV, G. I. Trudy SFTI, Papers of Sci Phys and Tech Inst. No. 24, 1947.

5. STUDENOK, Yu. A. Journ Tech Phys, 20, 1950.

6. BOL'SHANINA, M. A. Papers of SFTI, No. 32, 1953.

7. KLASSEN-NEKLYUDOVA, M. B. and REGEL, V. R. Otchet Institutov AN USSR i dr po probleme zharoprochnosti za 1 pol 1956, Moscow 1956.

8. STUDENOK, Ya. A. Trudy SFTI, Issue 28, 1949.

9. ZHDANOVA, V. N. Trudy SFTI, Issue 28, 1949.

10. KURDYUMOV, G. V. et al. Problemy metallovedeniya is fiziki metallov. Chetvertyy zbornik turdy. Metallurgizdat, 1955.

11. NIKOLAYEYA, S. M. and UMANSKIY, Ya. S. Izv. AN USSR, Ser fiz. 20, No. 6, 1956.

12. MAKOGON, M. B. Diss. Tomsk, 195 . Physics of Metal and Metallurgy.

13. GRUZIN, P. L. and TYUTYUNNIK, A. D. Fizika metallov i metallovedenie, Vol. III Issue 1, 1956.

14. PANIN, V. E. Diss. (thesis) Tomsk, 1955.

15. KUZNETSOV, V. D. Physika tverdogo tela (Solid Body Physics), Vol. II, 1941.

16. BOL'SHANINA, M. A. Izv. AN USSR, Ser fiz., 14, 2, 1950.

17. VASSILIEV, L. I. ZhTF, 20, 5, 1950; 22, 11, 1952; 23, 2 1953; 23, 8, 1953.

18. EGIBERG, V. and SMITH, H. Trans. Amer. Inst. Min. and Met. Eng. Inst. Met. Div. 1929; SCHWARZ, M. and SUMMA, O. Matallkunde, 4, 1933; ODING, I. A. and KULIKOV, F. V. Sb. Trenie i iznos v mashinakh (Friction and Wear and Tear in Machines), 7, AN USSR, 1953.

19. ROVENSKIY, G. M. Trudy VIAM Papers of Acad of All Union Sci Inst. Aviat. Materials, 1946.

20. KORNILOV, I. I. Izv. AN USSR, OTN, 1, 1956.

STUDY OF THE BEHAVIOR OF NICKEL AND THE SOLID SOLUTIONS OF TITANIUM IN NICKEL UNDER HIGH-TEMPERATURE CONDITIONS AT LOW STRAIN RATES

V. M. Rosenberg

The dependence of the durability of a material on temperature and stress within a time interval of 9 to 10 orders of magnitude (from fractions of a second to hundreds of hours) was established by Zhurkov and others [1-3] for a large variety of materials, such as plastics, stratified crystals, and metals.

In these publications it was demonstrated that the relationship between the durability (time to failure) and the amount of applied stress could be expressed by

$$\tau = Al^{-\alpha\sigma}, \qquad (1)$$

where τ is the time to rupture;

σ is the applied stress;

A and α are certain constants which depend on the temperature and on the material.

A study of the heat resistance of nickel and of the solid solutions of titanium in nickel [4] has established that the above relationship is true (although for a considerably shorter period of time) for solid solutions. In publication [2] it was noted that the

TABLE 1

№ сплава	Состав, вес. %										Режим термообработки		Величина зерна, балл
	C	Mn	Cr	Ti	Al	Fe	Co	S	P	Ni	температура, °C	время, час.	
134	0,02	0,04	не обн.	0,08	следы	0,23	следы	0,006	0,002	следы	1200	1	2—3
136	0,02	0,05	» »	3,57	»	0,20	»	0,007	0,001	»	1200	2	2—3
137	0,02	0,05	» »	6,20	»	0,40	»	0,006	0,001	»	1200	3	2—3
138	0,08	0,16	19,80	3,20	0,05	0,53	»	0,004	0,003	»	1200	3	2—3

dependence on stress of the time to failure is a particular instance of a more general rule, since the extreme conditions ($\sigma \to 0$ or $\tau \to 0$) have no physical meaning.

In the present paper the results of tests on nickel and solid solutions of titanium in nickel conducted within the temperature range of 400 to 1100° are described.

Data on the chemical composition and on the conditions of heat treatment of the materials tested are given in Table 1. The tests for long-time strength were conducted in a "Shopper" or MP-3 tensile-testing machine using DP-5 standard specimens.

Study of the Long-Time Strength of Solid Solutions

The results of tests conducted at 900, 1000, and 1100° are given in Fig. 1; sets of isotherms for each material tested are given in Fig. 2. For preparation of the diagram we also used data from tests we had conducted earlier at 600-800°.

As seen from these figures, the relation between the time failure and the initially applied stress at constant temperature is satisfactorily depicted by Eq. 1, and, moreover, the angle of slope of the experimental straight lines depends on both the test temperature (Fig. 2) and the composition of the solid solutions (see Fig. 1).

The higher the test temperature, the lower along the stress axis the experimental curve for a given alloy is situated. It may be seen when individual alloys are compared that at 600-800° [4] as well as at higher temperatures the solid solutions alloyed with titanium and chromium, (i.e., those with higher strength characteristics

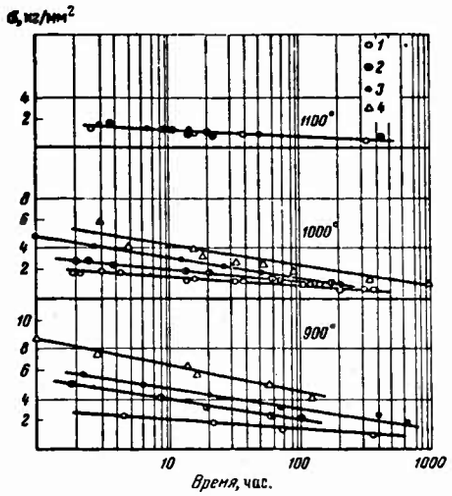

Fig. 1. Dependence of the change in time failure on the applied stress and on the composition of the solid solution at 900, 1100, and 1100°. 1) Ni; 2) Ni + 3.6% Ti; 3) Ni + 6.3% Ti; 4) Ni + 20% Cr + 3.2% Ti.

of the interatomic bonds possess higher heat resistance.

The results obtained confirm the conclusion reached in [4], that the interatomic bonds are of decisive importance for the alloys resistance to failure at high temperatures. However, the differences between solid solutions diminish under the stresses causing rupture in the long run, despite the fact that at a given temperature the binding forces in solid solutions remain unchanged with time. This is expressed by the convergence of the straight lines with variations in temperature and composition. The slope of the experimental straight lines towards the time axis may be defined by the value of the ratio $\frac{\Delta\sigma}{\Delta\tau \ln}$, i.e., by the reciprocal of the parameter α in expression (1).

The fact that the straight lines converge when test tempera-

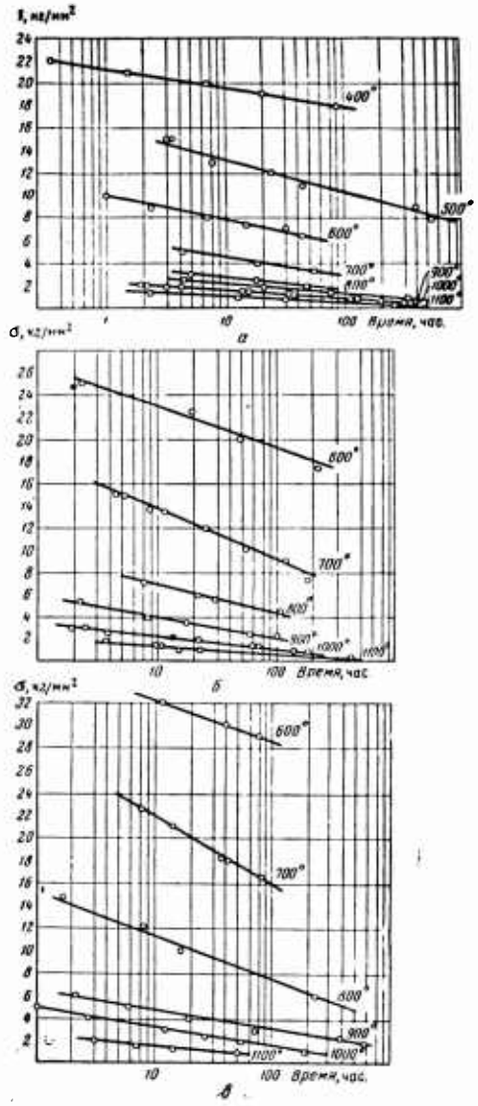

Fig. 2. Dependence of the time failure on the applied stress and on the test temperature. a) Ni; b) Ni alloy with 3.6% Ti c) Ni alloy with 6.2% Ti.

tures are raised was established in [4]. It was linked to the leveling out of the difference in diffusion mobility of the atoms with an increase in temperature for nickel and its solid solutions,

provided that a considerable part of the total deformation was contributed by the diffusion mechanism.

The increased diffusion mobility of the atoms in the crystal lattice of solid solution as compared to the mobility in nickel can result either from the static distortions in them caused by the dissolution of foreign atoms (titanium) [5], or from a more rapid decrease of the interatomic bond strength with a temperature increase in solid solutions than in pure nickel. It is possible that this phenomenon is caused by both the first and second factors.

It can be seen (see Fig. 1-2), when the behavior of each material at different test temperatures is compared, that the higher the temperature, the less the straight lines linking the logarithm of time to failure with the applied stress inclines towards the time axis. This means that equal changes in stress at different temperatures cause greater changes in the time to failure as the test temperatures progressively increase. At high temperatures, slight change in the applied strew s causes a considerable change in the time to failure. This is not altogether common. In this connection we should take a closer look at the results of publications [1, 3], in which it is shown that an increase in the test temperature causes an increase in the angle of slope between the time axis and the straight line $\ln \tau = \varphi(\sigma)$. The angle of slope is insignificant at room temperature. Consequently a slight change in the applied stress (a change not greater than the spread of values in the normal mechanical tests) causes a very considerable change in the time failure. For this particular reason, the rupture stress assumes the nature of a critical value at room temperature. The increase in the angle of slope between the time axis and the straight lines with the increase

in the test temperature permits us to throw more light on the temporary nature of the strength of the material.

The results obtained by us show that the angle of slope of the straight line $\ln \tau = \varphi(\sigma)$ first changes in the same manner as for platinum and aluminum [3] (the slope of the straight line toward the time axis in the case of nickel is greater at 500° than at 400°, whereas for solid solutions it is greater at 700 than 600°) and then decreases; i.e., with the higher temperature it begins to take the direction opposite to that in the case of platinum and aluminum. This can be seen from the data presented in Table 2.

An understanding of this difference should be sought in the fact that the temperature conditions of our tests differed substantially from those used in the research [1-3]. The tests on nickel and nickel-base solid solutions were conducted in our case at temperatures closer to the melting point than those used in the tests on aluminum and platinum. The mechanism of deformation may be essentially changed at relatively high temperatures.

Without going into the details of the rupture mechanism for lack of sufficient experimental data, we may only indicate that in cases where the slope of the straight lines $\ln \tau = \varphi(\sigma)$ becomes greater with an increase in temperature, there occurs some one certain basic process, the development of which is accelerated under load with the increase in temperature. At still higher temperatures when the slope of the straight lines diminishes with the increase in temperature, an other basic process comes into play that even may suppress the influence of the first process. If it is assumed that at lower temperatures the temporary nature of the strength of a material is linked with the development of submicroscopic cracks it

TABLE 2

Variation in Angle Isotope α Toward the Time Axis for a Number of Materials

Температура, C°	Al [3]	Pt [3]	Ni	Ni + 3.6% Ti	Ni + 6.2% Ti
18	0,74	0,54	—	—	—
100	0,96	—	—	—	—
200	1,04	—	—	—	—
300	1,16	1,9	—	—	—
400	—	2,8	1,60	—	—
500	—	3,6	2,80	—	—
600	—	—	2,10	3,75	3,80
700	—	—	1,60	4,55	5,9
800	—	—	1,10	2,50	3,85
900	—	—	0,95	1,80	1,7
1000	—	—	0,80	1,00	1,6
1100	—	—	0,70	0,70	0,70

can be presumed that this development is suppressed by the plastic deformation and the increased diffusion mobility of the atoms in the crystal lattice of the tested material with the increased diffusion mobility of the atoms in the crystal lattice of the tested material with the increase in temperature. The two processes may even result in partial healing of the submicroscopic cracks. It should be noted in this connection that B. Ya. Pines [6], examining the theoretical aspect of the growth of the "embryonic" cracks conditioning toughness in metals, came to the conclusion that the mechanism of rupture through the growth of submicroscopic cracks is disturbed at high temperatures, when there is a considerable increase in the rate of selfdiffusion. Brittle fractures do not occur at this stage, either.

Structural Changes in Nickel and in Solid Solutions of Titanium in Nickel at Temperatures of 700 and 900°.

To verify the assumption that the tendency of nickel and its solid solutions to approach one another in heat resistance with an increase in temperature and a decrease in stress is caused by the change in the mechanism of deformation, a study was made of the changes in their structure during tensile tests. The load selected for the tests was such that the fracture occurred either within a few hours or in a few days.

The tensile test was carried out in a vacuum chamber of the same type as the one described in [7]. Prior to testing, the flat specimens were electrolytically polished and etched to reveal the grain boundaries. The x-ray camera was focused on interference line (420) and the photographs were taken with copper radiation.

Let us present here the more typical changes in structure that are characteristic of the tested materials and note the qualitative differences that occurred at different strain rates.*

As an example of rapid deformation (rupture within several hours), we will consider a specimen of nickel (tensile stress of 5.2 kg/mm^2 at 700°. Figure 3 shows photographs obtained at different stages of tension from which it is clear that deformation of the specimen is mainly due to slip. The specimen ruptured after 35% elongation in 1 1/2 hours.

Figure 4 is a photograph of a specimen of a solid solution (6.3% Ti) elongated at 700° under a tensile stress of 8 kg/mm^2.

---

* The experiments were performed with the participation of L. V. Gradova.

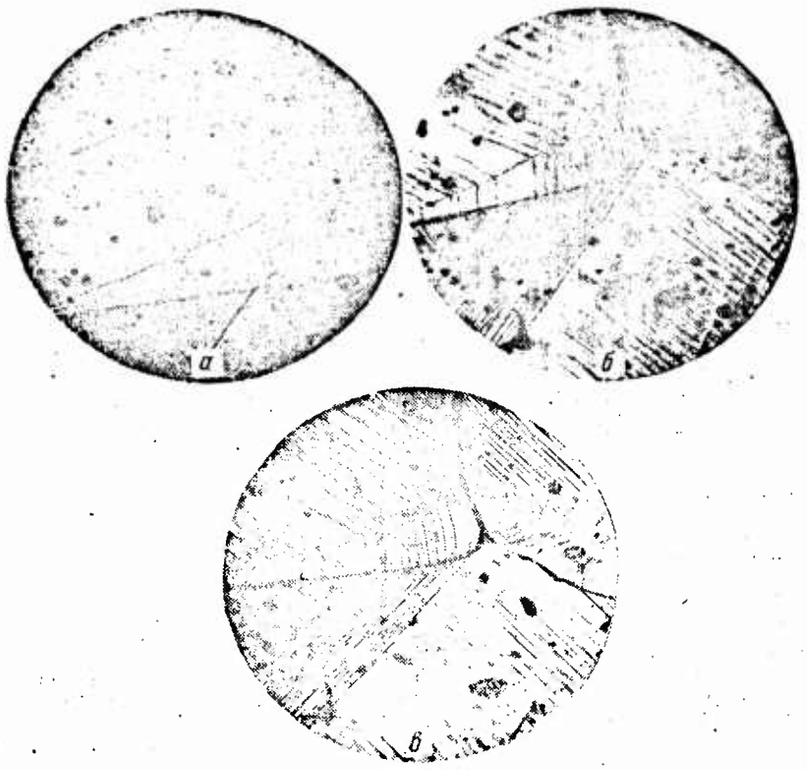

Fig. 3. Microstructure of nickel specimen × 200. a) before deformation; b) after 10.7% deformation; c) after 35% deformation.

The fracture occurred after 2 1/2 hours. Here, too, the deformation was caused by slip.

X-ray photographs of undeformed and stretched specimens show different patterns. The first shows relative perfection of the original grains. The fact that the K_α doublet is not divided indicates that any possible disorientation of the grains prior to the deformation does not exceed 40 min. The diffraction pattern is changed when deformed material is photographed. It appears in the

form of arcs representing sections of the Debye rings with maxima at points corresponding to the original interference spots (Fig. 5). This should be connected with the division of the original grains into sections or fragments by the slip planes, and with a certain degree of rotation of these sections relative to one another.

GRAPHIC NOT REPRODUCIBLE

Fig. 4. Microstructure of nickel alloy with 6.3% Ti. ×200. 18% deformation.

The changes in the microstructure during deformation under a stress that causes rupture in a few days differ from those occurring during rapid deformation and do not basically depend on the stress temperatures selected in this work. Figure 6 shows an example of the microstructure of a nickel specimen containing 6.3% Ti after 4% deformation and with failure following 14.5% elongation after 30 hours at 900° and with a 2 kg/mm² stress. The microstructure in this case differs from the microstructure occuring when the strain rate is relatively high. New boundaries can be observed inside the grain with-

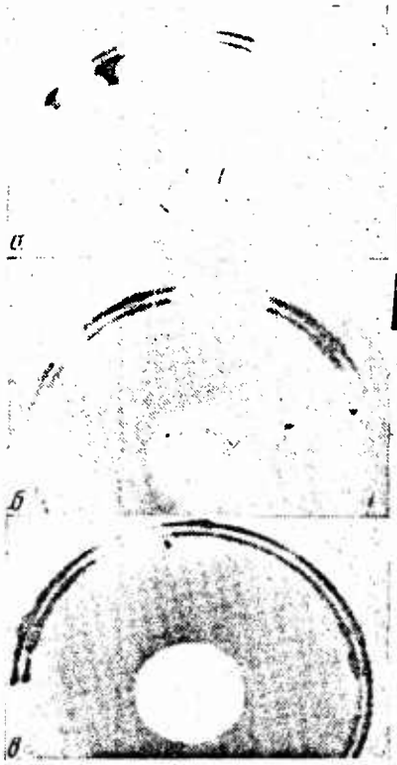

GRAPHIC NOT REPRODUCIBLE

Fig. 5. X-ray photographs of a nickel specimen at different stages of deformation at 700° and a tensile stress of 5.2 kg/mm². Radiation copper, line (420). Deformation: a) 10.7; b) 29%; c) 35%.

in the limits of the old grains. Subboundaries appear in grains in which intensive slip has occurred, as well as in grains in which no slip has been observed (Fig. 6b).

Figures 7 a, b, c, and d show x-ray photographs from which it can be seen that the appearance of the K_α doublet, and the division of the initial spot into a number of smaller spots forming an arc are

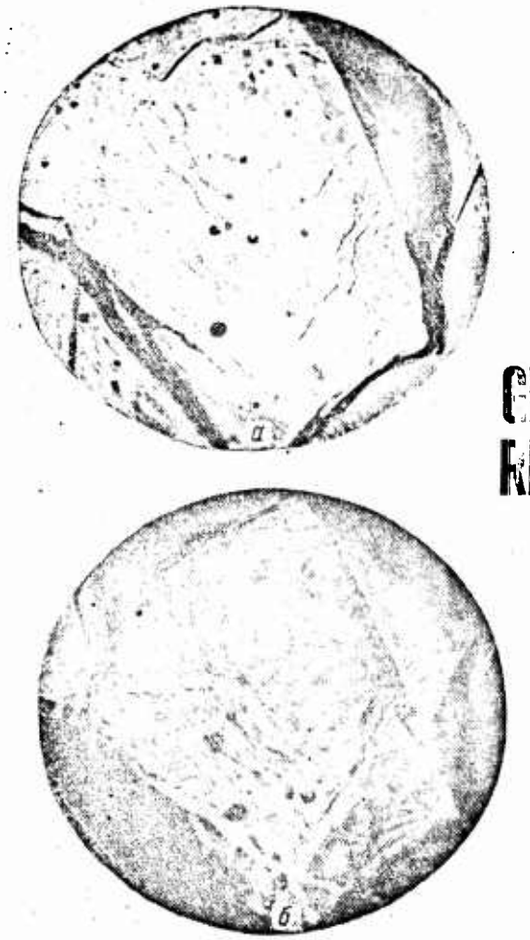

GRAPHIC NOT REPRODUCIBLE

Fig. 6. Microstructure of Ni-specimen with 6.3% Ti. × 200.
Deformation: a) 4%; b) 14.5% after 30 hours.

due to strain. This means that the initial grain has disintegrated into a number os separate smaller fragments whose orientation in relation to the initial grain has slightly changed. This fragmentation of the grains appears to be a special case of polygonization occuring through the simultaneous effect of temperature and stress.

GRAPHIC NOT REPRODUCIBLE

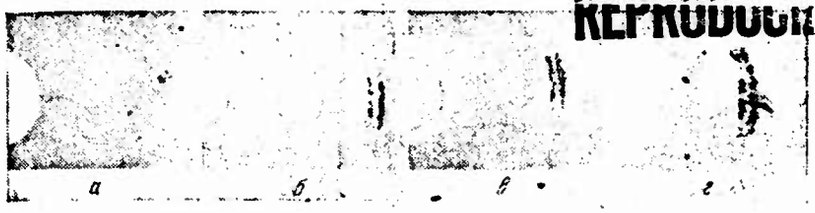

Fig. 7. X-ray photographs of specimens of a solid solution of (6.3%) in nickel at different stages of deformation at 900° and with a tensile stress of 2 kg/mm². Radiation-copper line (420). a) initial state deformation: b) 4%; c) 10%; d) 114.5%.

Grain fragmentation should lead to an increase in the overall diffusion mobility of atoms inside the grain, since the number of shear planes inside the grain grows larger in the process. This, in turn, must necessarily lead to the increased effect of the diffusion mechanism of creep on the total deformation. This may explain the tendency of the values of time to failure in nickel and solid solutions of titanium in nickel to converge at temperature increases.

Conclusions

1) The greater the strength of the interatomic bonds in the crystal lattice of the metal, the greater the time to failure of nickel and its solid solutions, up to temperatures 0.75 or 0.8 of the melting point. At higher temperatures the long-time strength of the metals becomes identical. At high temperatures the slope of the lines linking the logarithm of the time to failure and the degree of the applied stress in the direction of the time axis is less.

2) In slow deformation under conditions of high temperature

fragmentation of the grains occurs in addition to slip. This fragmentation leads to an increase in the diffusion mobility of the atoms in the grain since the number of internal shear planes is thereby increased. This narrowing of the gap between the values of the time to failure for nickel and solid solutions of titanium in nickel under tension and at high temperatures and under relatively slight stress can be explained by the fact that during prolonged tests the diffussion processes of plasticity come into play.

References

1. ZHURKOV, S. N. and NARZULAYEV, B. N. ZhTF, Journ.Techn. Phys. 23, Issue 10, 1953.
2. ZHURKOV, S. N. and TOMASHEVSKIY, E. Ye. ZhTF, Journ. Techn. Phys. 25, Issue 1, 1955.

3. ZHURKOV, S. N. and SANFIROVA, T. P. DAN SSSR, Report of Academy of Science USSR, 101, No. 2, 1955.

4. KAMINSKIY, Ye. Z. and ROZENBURG, V. M. Research on Heat-Resistant Metals, Vol. II, AN SSSR (Academy of Science USSR) 1957.

5. KURDYUMOV, G. V. and TRAVINA, N. T. DAN SSSR, 99, No. 1, 1954.

6. PINES, B. Ya. ZhTF, 25, Issue 8, 1955.

7. LOZINSKIY, M. G. and ANTIPOVA, Ye. I. Metallovedennie termicheskaya obrabotka, No. 5, 1955. Study of Metls and Heat Treatment.

DEFORMATION MECHANISM OF SINGLE CRYSTALS OF ALUMINUM AT VARYING TEST TEMPERATURES

L. I. Vasil'yev, Tsen Ling-Chao, and Yang Ta-Yu

Ludwik [1], and later Hoolomon and Zener [2], claimed that in the plastic deformation of metals the stress was a single-valued function of the instantaneous values of the degrees of deformation, the rate of deformation, and the test temperature. The existence of a mechanical equation of state

$$\sigma = f(\varepsilon, v, T),$$

where σ is the deforming stress;

ϵ is the degree of deformation;

$v = \dot{\epsilon}$ is the strain rate;

T is the test temperature,

was thereby postulated.

The existence of a mechanical equation of state means that at a given value of ϵ σ is not dependent on the temperature and rate of the prior deformation of a metal. This is shown schematically in Fig. 1.

Dorn, Goldberg, and Tietz [3] critized Hollomon's experiments on the deformation of steel at different test temperatures, which he put forward as evidence of the existence of a mechanical equation

of state. The tests conducted by these authors [3] by varying the test temperature during stress and the experiments performed by one of the authors and his assistants [4] at varied rates of plastic elongation with polycrystals of aluminum, copper, tin, brass and stainless steel refuted the mechanical equation of state. Similar results were obtained by Paterson [5], who varied the test temperature from minus 180° to room temperature and vice versa in testing the plastic torsion of polycrystalline copper. F. F. Vitman, N. A. Zlatin, and B. S. Ioffe [6], in studying the dependence of strain resistance on the strain rate in polycrystalline lead, aluminum, copper, duralumin, and soft steel by the cone indentation method, came to the conclusion that over a wide range of strain deformation rates this dependence is not uniform. Wyatt [7], who studied creep in copper in tests wherein there was no instantaneous increase in stress, and Cottrell [8] note that the mechanical equation of state is not fulfilled in creep either, excluding cases of very slight deformation and comparatively low temperatures when the dependence of deformation on time approaches the logarithmic dependence.

Rosi and Mathewson [9] experimented with extremely pure single crystals of aluminum, producing plastic elongation at various temperatures. They found that the flow curve at 205°K for specimens elongated before hand by 0.22% drops even lower at 295°K than the flow curve of specimens deformed only at 205°K (Fig. 2a). Brown [10] cites data obtained by Los [11] when also studying the influence of the test-temperature change (from -180 to 20° and conversely on the flow curve of aluminum single crystals. The results are shown diagramatically in Fig. 2 b, and c. Thus the experiments with single crystals of aluminum, like those with metallic polycrystals, confirm

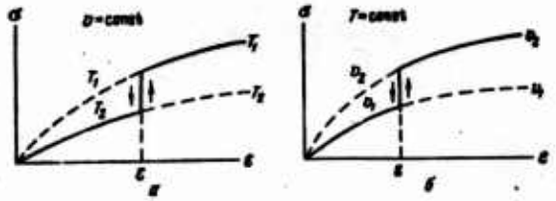

Fig. 1. Influence of variation in test temperature. a) and rate; b) in a case when a mechanical equation of state exists.

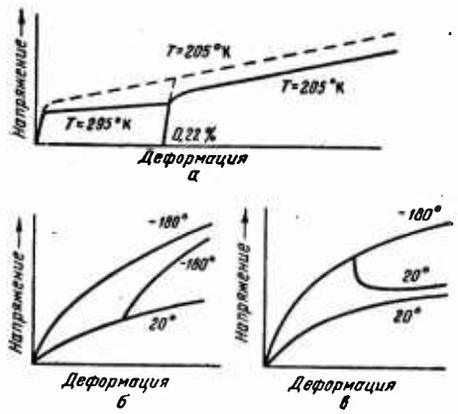

Fig. 2. Influence of variation in test temperature on elongation curves of aluminum. Single crystals. Data: a) obtained by Rosi and Mathewson [9]; b and c) by Brown [10].

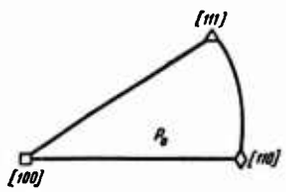

Fig. 3. Initial orientation of the axis of specimens under load.

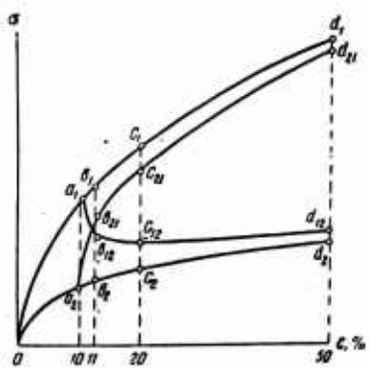

Fig. 4. Elongation curves of single aluminum crystals.

the invalidity of the mechanical equation of state. The question arises as to why the equation of state is not fulfilled. One explanation is that the difference in the conditions of the prior strain (rate, test temperature correspondingly stress) causes a difference in the number and variety of the strain distortions of the lattice on which hardening and other changes in the properties of metals depend [4, 12]. By the term "variety of distortions" we understand here the whole complex of distortions or their groups (dislocations or other types), differing under given conditions in stability, the nature of their volumetric distribution in a metal and their capacity for relocation, the effectiveness of their retarding effect on further deformation, etc. However, a more accurate knowledge of the influence of prior strain conditions requires a more detailed and complete study of the influence of these conditions on the state and mechanism of subsequent deformation.

In the present publication we are considering only one deformation parameter the test temperature. The purpose of this work was to study by metallographic methods and by electron microscopy the structural features and mechanism of deformation in single aluminum crystals with variation in temperature before and after elongation. The degree of correlation between the change in the mechanical properties of crystals in deformation and their structure and contours (the mechanism of plastic deformation) was also clarified.

Specimens and Test Conditions

Aluminum of a high degree of purity (99.99%) was used. Single

crystals of aluminum were grown by gradual crystallization, and specimens 15 x 4 x 1 mm were out from them. In order to be albe to compare all observations of plastic deformation on the surfaces of different specimens, all of the single crystals were prepared with the same orientation, as shown in Fig. 3, in which the point P corresponds to the direction of the axis of the specimens (the direction of stress).

Before deformation the specimens were subjected to electrolytic polishing by the customary method. In view of the fact that after electropolishing cross sections of the specimen were no longer identical throughout its length, the deformation under load might not have been completely uniform, with the result that the overall elongation might not have corresponded exactly to the deformation in its separate sections. In order to determine the precise extent of deformation at close intervals along the length of the specimen's surface. The distance between two adjacent marks served as a measure for calculating the deformation of the section between them. This distance was about 1.2 mm and was approximately equal to the linear dimensions of the part of the surface covered by one micrograph at 20. An enlargement of 450 was used for a more accurate study of slip bands and deformation zones. Moreover, an electron-microscopic examination was made, with the use of oxide replicas and chrome shading.

The specimens were tested under tension either at constant temperatures (20, -80, -180°) or under conditions where the temperature of the preliminary elongation (-180, -80, +20°) differed from those of the subsequent testing (+80, +20, -80, -180°). In the latter case, each specimen scheduled to be subjected to tension a

second time was soaked for a certain period (about 5 min.) in a container of fresh heating (or cooling) liquid before deformation in order to keep the temperature constant. The elongation rate was 0.16 mm/sec, and the degree of prior strain was 10%.

The single crystals used to study the kinetics of their plastic deformation were extended directly on the microscope stage by means of a special device.

Basic Relief Patterns

The curves $oa_1b_1c_1d_1$ and $oa_2b_2c_2d_2$ in Fig. 4, represent schematically the elongation curves of single aluminum crystals at the temperature of liquid air and at room temperature, respectively. The letters a, b, c, and d mark the points at which there is 10, 11, 20 and 50% deformation. The indexes 1 and 2 indicate the test temperatures -180 (T_1 = 180, T_2 = 20°). The curve $oa_2b_{21}c_{21}d_{21}$ is for the extension of a single crystal, initially by 10% at 20° and then, additionally, by 1, 10 and 40% at -180°. Similarly, the curve $oa_1b_{12}c_{12}d_{12}$ reproduces diagramatically the elongation by 10% at -180° and furhter elongation again by 1, 10, and 40% at 20°.

Figure 5 shows micrographs of the surface of single aluminum crystals at different stages of deformation represented by the points on the curves in Fig. 4. The photographs a_1, b_1, c_1, d_1 present a typical deformation pattern for aluminum single cyrstals at a low temperature. The slip traces (bands) are very thin. The deformation bands developing with the elongation of the specimen are clearly visible. The photographs a_2, b_2, c_2, d_2 showing distinct, borad, straight slip bands are characteristic of deformation at room temperature. Photographs a_1 and a_2 of the two series considered

represent specimens extended to a fairly high degree of plastic deformation (10%). The deformation bands and the slip traces (bands) are already well developed at this stage of deformation, and under further extension (up to 50%) no substantial changes in the deformation pattern are observed. It may be noted that at more advanced stages of extension (d_2) neighboring slip bands frequently cross, whereas in a_2 this is almost nonexistent.

The series of photographs b_{21}, c_{21} and d_{21} (Fig. 5) shows the pattern of single crystals extended by 1, 10 and 40% respectively, at -180_o, after a prior deformation of 10% at 20°. The slip bands in photograph b_{21} differ little from those in photographs b_2, showing 11% extension of the crystal at room temperature. The deformation pattern in c_{21} slightly resembles the pattern at a low temperature; thin, uneven slip lines have appeared and the deformation bands are growing (in some sections of the crystals these are comparable to the bands appearing in c_1, i.e., at T = 180° and ϵ = 20%). At the next stage of deformation (d_{21}) the pattern shows the superpositioning of the deformation bands and thin slip lines appearing at room temperature. Although this pattern (d_{21}) resembles d_1, it is actually different.

The typical breaks (b_{12},c_{12}, d_{12}) in the slip bands are a characteristic feature of deformation at room temperature after low-temperature preliminary deformation. It is of interest that distinctive slip lines with breaks even appear at the earlier stages of the secondary deformation. A crystal which has been extended by 10% at 180° has only to be extended an additional 1% at 20° for these slip bands to appear on the surface (b_{12}). The number of slip bands increases under further tension (c_{12}, d_{12}). The newly-appeared slip

bands also have breaks in them. In a number of cases, the slip bands appear to fork near the breaks. Although the deformation patterns d_{12} and d_2 are similar, there is however a difference to it, in the former case, the slip bands with breaks are more frequent, the breaks are more distinct and the bands are thicker.

The pattern in photograph b_{12} differs appreciably from that in photograph b_1. At the same time, as pointed out above, the patterns in the case of b_{21} and b_2 resemble one another closely. This leads us to believe that the influence of low temperature on further strain at room temperature is greater than the influence of the high-temperature deformation on subsequent low-temperature elongation. However, the screening effect of the pattern of prior deformation on the progress of the deformation during subsequent extension should be borne in mind in considering this fact. This is particularly true of the transition from high-temperature prestrain to subsequent low-temperature extension since, in this case, the low-temperature pattern (thin slip lines) emerges on top of a comparatively coarse high-temperature pattern (broad slip bands) which obscures the picture. Hence, the influence of the prior deformation does not appear in its true form. In the case of low-temperature prestrain this fact is not significant.

Influence of Electrolytic Polishing after Prestrain

In order to observe the influence of prior strain on the development of subsequent deformation in its true form, the preliminary pattern deformation was removed by electropolishing before the second extension. The thickness of the removed layer measured about

100 microns, polished so that the surface of the specimen viewed through a microscope was smooth. The electropolishing lasted 5 minutes. The overall time interval between the preliminary and secondary tensile test, including the electropolishing, was about 20 minutes. Since the electropolishing was carried out at a temperature slightly above room temperature, the fact had to be taken into account that in spite of the briefness of the time interval, relaxation might have occurred to some extent in the specimens. If relaxation were nearly complete after 10% deformation, in the subsequent tensile test the deformation would clearly approximate that observed in the case of deformation of the original crystal, experience shows that this does not occur. Thus, the pattern on a crystal extended by 10% at -180°, electropolished, and again extended by 10% at 180° (Fig. 6 c'_1) differs from that of a crystal subjected to one extension of 10% at 180° (Fig. 5 a_1). The number of deformation bands is appreciably higher in the case of the former operation. Consequently, even in the most unfavorable case, when prior extension was carried out at -180°, relaxation during the interval before the secondary extension does not eliminate the effect of the preliminary deformation but merely diminishes it to some extent. This was confirmed by other data. In the case of high-temperature prestrain, the influence of the intervening relaxation will naturally still be less. On the basis of the above we considered it advisable to use electropolishing to remove relief pattern of the prestrain.

Figure 6 reproduces photographs depicting the development of secondary strain for specimens in which the pattern formed by prior deformation was removed by electropolishing.

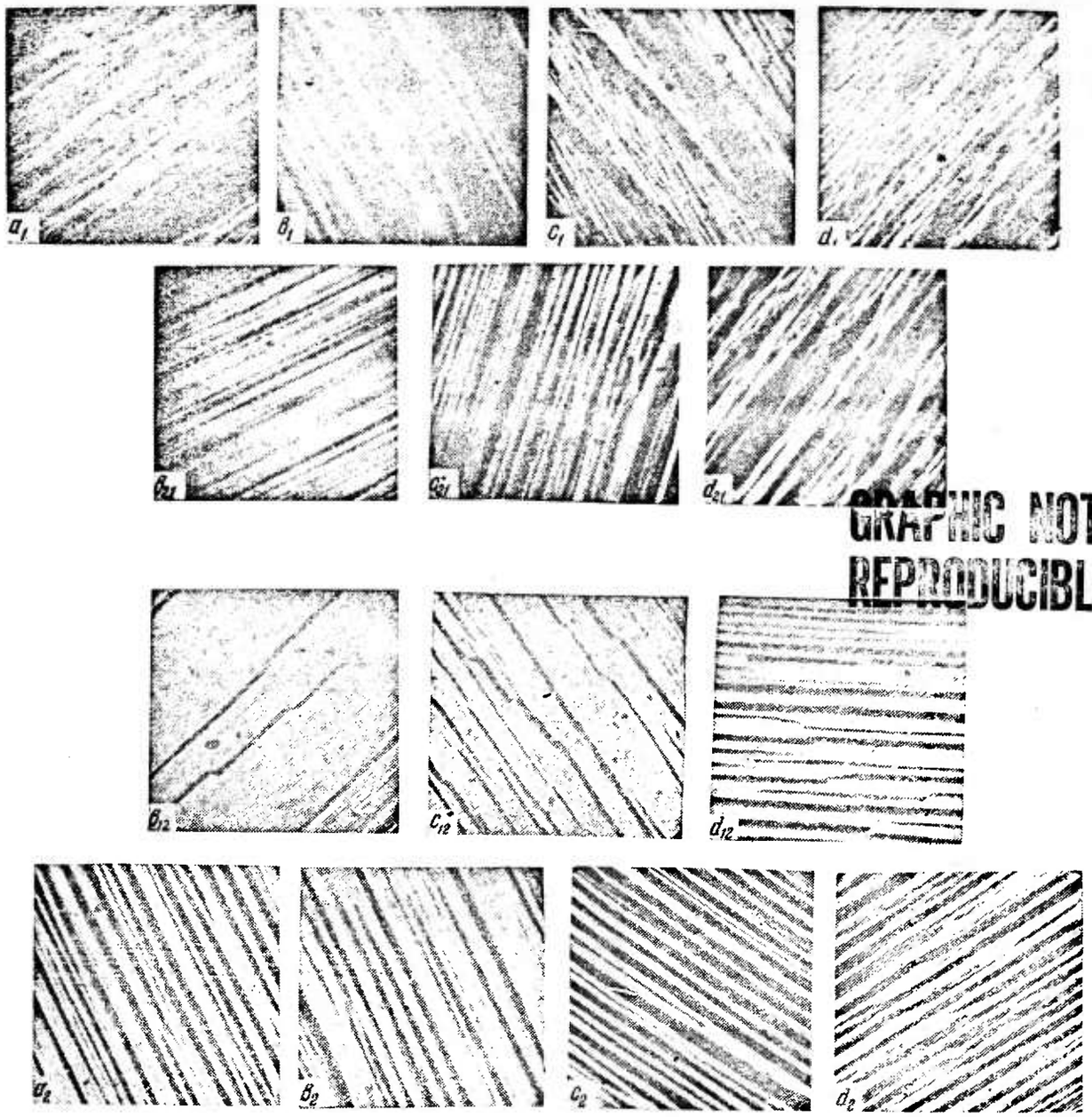

GRAPHIC NOT REPRODUCIBLE

Fig. 5. Micrographs of the surface of single aluminum crystals at different stages of deformation. × 450. Σ (%): a_1, b_1, c_1, d_1 - 10, 11, 20, 50 (-180°); a_2, b_2, c_2, d_2-10, 11, 20, 50, (20°).

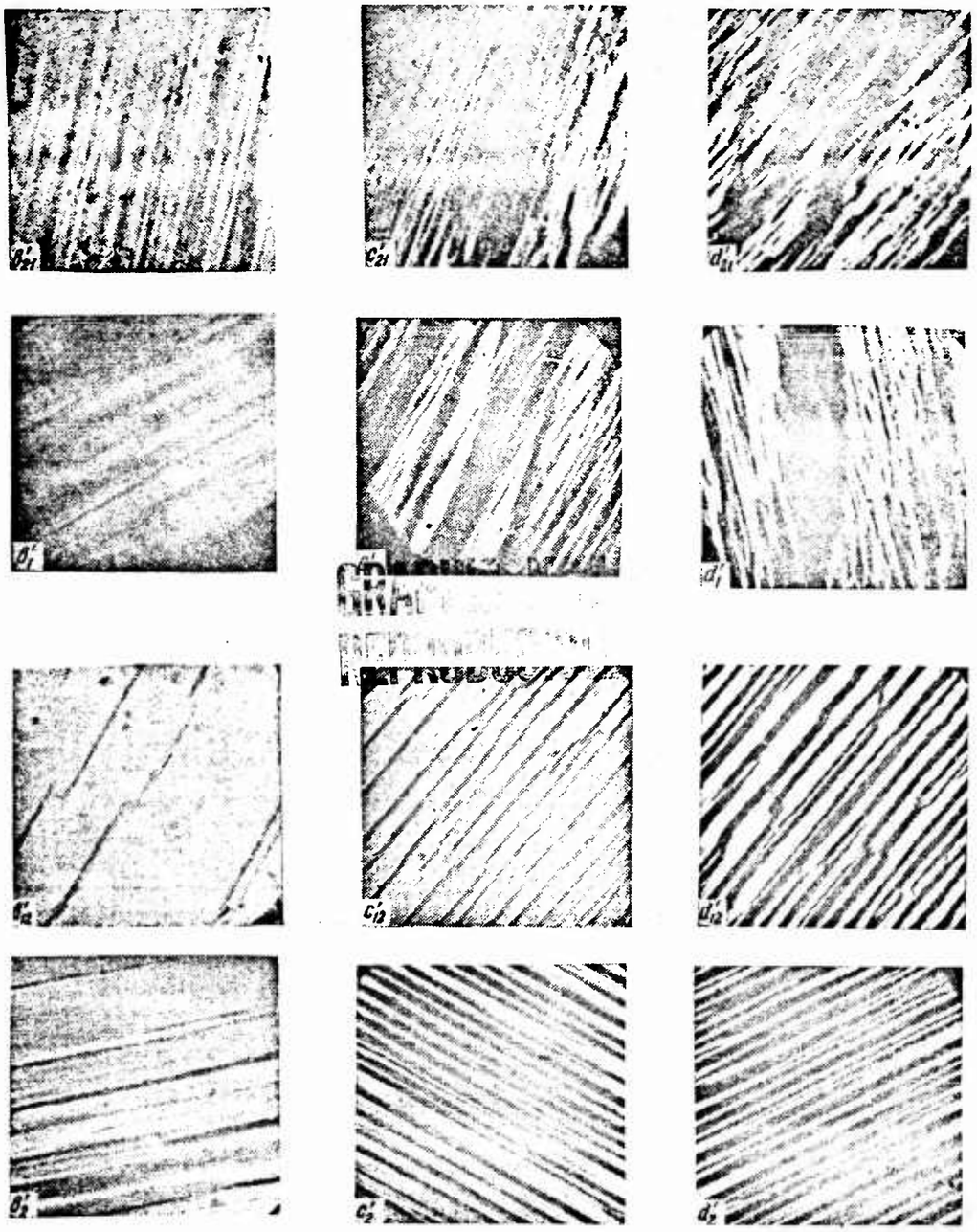

Fig. 6. Micrographs of the surface of single aluminum crystals at different stages of deformation × 450.

Photographs b'_1, c'_1, d'_1 illustrate a case where after 10% prior deformation at -180° and electropolishing (EP) the crystals were further extended at -180° by 1, 10, and 40% respectively. The test conditions for the series b'_2, c'_2, d'_2 were the same, but the preliminary and secondary tensile tests were carried out at 20°. The development of deformation on further extension by 1, 10, and 40% at -180° after 10% prior deformation at 20° and electropolishing is shown in photographs b'_{21}, c'_{21} and d'_{21}. For the series b'_{12}, c'_{12}, and d'_{12} the preliminary 10% extension was done at -180° and further extension by 1, 20, and 40% was respectively performed at 20°.

The similarity of the corresponding micrographs in the series b'_{21}, c'_{21}, d'_{21} and b'_1, c'_1, d'_1, which increases as the secondary extension is increased as might have been expected, is more considerable than in the series b_{21}, c_{21}, d_{21} and b_1, c_1, d_1 (Fig. 5), the overall picture in the latter case being obscured by the pattern of prestrain. Nevertheless, there is still a difference between c'_{21} and c'_1 and especially between b'_{21} and b'_1 (for example, in the number and degree of development of the deformation bands) which is much less noticeable between d'_{21} and d'_1.

A comparison of the other two series of photographs, b'_2, c'_2, d'_2 and b'_{12}, c'_{12}, d'_{12}, shows that the features in the deformation of crystals subjected to low-temperature prestrain (-180°) are the same as when there is no intermediate electropolishing (Fig. 5). These features are the presence of numerous breaks in the slipbands, greater clarity of the lines and greater distance between adjacent bands as compared with the slip bands deformed

at room temperature only. In this respect the pattern of the series b'_{12}, c'_{12}, d'_{12} in comparison with b'_2, c'_2, and d'_2 appears more of a "high-temperature" pattern.

The examination also shows that the photographs of series b'_{12}, c'_{12}, d'_{12} resemble the corresponding photographs of series b'_2, c'_2, d'_2 somewhat more than those of series b_{12}, c_{12}, d_{12} resemble the one in series b_2, c_2, d_2. This is natural and is due to possible partial relaxation during electropolishing of the specimens preliminarily deformed at -180°.

Thus comparative metallographic study of the strain mechanism shows that even if the influence of prior deformation as a result of relaxation during electropolishing is very slight, the effect of prestrain is clear, being especially noticeable in specimens deformed at 20° after a preliminary low-temperature deformation (-180°). The influence of high-temperature (20°) prestrain with subsequent low-temperature extension (-180°) is farily noticeable although less characteristic.

Influence of other Temperatures. Structure of Breaks in Slip Bands

It was pointed out above that the occurrence of clearly-marked slip bands with characteristic breaks is a distinctive feature of the relief pattern of single crystals extended first at -180° and subsequently at 20°. It became evident that this development is of a general nature and also occurs during the transition from other low test temperatures (not only from -180) to other high temperatures (not only to + 20°).

Some of the data obtained from these test are given in Fig. 7.

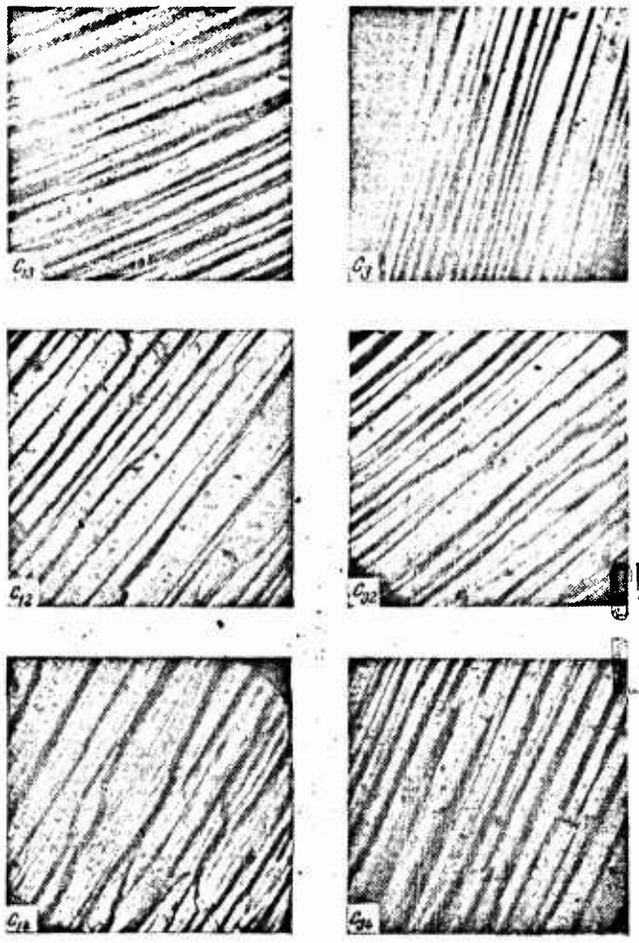

GRAPHIC NOT REPRODUCIBLE

Fig. 7. Micrographs of the surface of single aluminum crystals at different stages of deformation. × 450.

The micrograph c_{13} represents transition from test temperature -180° to temperature -80°, c_{12} from -180 to + 20°, c_{14} from -180 to + 80°, c_{32} from -80 to + 80°, and c_3 relates to the constant test temperature -80°. The degrees of the primary and secdary extensions was kept the same (10%) in all cases. Thus the

total deformation of the single crystals amounted to 20%.*

It can be seen (c_{13}, c_{12}, c_{14}, c_{32}, c_{34}) that at the transition from low elongation temperatures to higher temperatures distinct breaks in the slip bands can always be seen. This applies in particular to transition from -180 to -80°, i.e., to a comparatively low temperature. The higher the temperature of the secondary deformation after prior deformation at the same temperature, the more frequently do we find broken lines.

GRAPHIC NOT REPRODUCIBLE

Fig. 8.

The same trend is apparent as the temperature of the preliminary

---

* The numbers on the micrographs in Fig. 7 correspond to the numbering of the test temperatures: $T_1 = 180°$, $T_2 = +20°$, $T_1 = -80°$, $T_4 = +80°$; the letter c corresponds as before (Fig. 4) to 20% deformation.

elongation decreases when the temperature of the secondary extension is unchanged. This may be observed, for instance, if c_{14} is compared with c_{34} (Fig. 7). The greatest effect is observed in transition from the lowest to the highest test temperature (Fig. 7 c_{14}).

Elongation at -80° without any further change in temperature does not result in noticeable slip bands with breaks (Fig. 7 c_3) as in the test at -180°. The presence of clearer slip bands and less developed deformation bands are features of c_3 not found in c_1. When comparing c_{13} with c_3, we notice that the pattern in c_{13}, has, on the one hand, more of a "low-temperature look" (deformation bands are developed). This is natural because of the prior deformation at -180°. On the other hand, and this is of greater interest, the pattern in this case has also more of a "high-temperature look" (distinct "high-temperature" slip bands with breaks).

An electron microscope was used for a more accurate study of the slip bands with breaks and some of the micrographs taken are reproduced in Fig. 8-12. Figures 8 and 9 show extension $\epsilon = 11\%$ at T = 20°; Fig. 10, $\epsilon = 10\%$ at T = -180° with subsequent elongation by 11% at T = 20°; Fig. 11, $\epsilon = 10\%$ at T = -180° with subsequent exterior by 40% at T = 20°; Figure 12, $\epsilon = 50\%$ at T = 20°. The break in the slip band in Fig. 8 represents a typical cross slip. In other cases, however,(Fig. 10 a, b, d and Fig. 11 and 12) the "bridges", which are places where the breaks in the slip bands occur are more complex in structure. Occasionally (Fig. 11 a and b), they appear as miniature faults. In other cases (Fig. 10 a and b), and this also applies to certain optical observations (Fig. 6_1 b'_{12}), the"bridge" gives the impression of consisting of a bundle of thin

slip lines lying close together, parallel to the slip bands. Figure 9 shows an exceptional stage at which the slip bands are spreading in parallel fashion and apparently toward one another, and at which the "bridges" between them have not formed (or have not yet formed). A similar development is to be observed in Fig. 10, b and c.

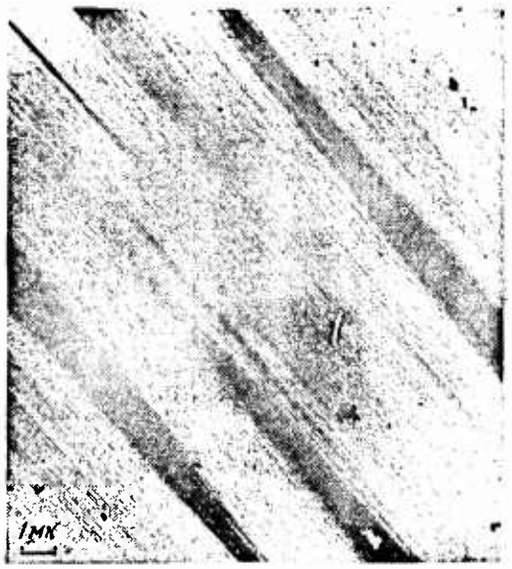

GRAPHIC NOT REPRODUCIBLE

Fig. 9.

Discussion of Results

1. The results obtained testify to the substantial influence of the temperature of prior plastic extension on the surface relief pattern of aluminum crystals subjected to subsequent extension at a different temperature. The surface pattern of such single crystals differs from that of single crystals deformed only at the latter temperature. Consequently, not only from the point of view of

flow stress but also of structure, the state of single crystals is not a single-value function of the test temperature at a given instant, but depends on the temperature of the prior strain.

The difference in the patterns described above, all other conditions being equal, increases at smaller and decreases at higher degrees of secondary extension (Figs. 5 and 6). This is also true in the case of stress-strain curves, some of which are for a constant test temperature (20 or -180°), whereas others relate to extension at the same temperature but after transition from some other temperature (-180 or 20°) (Fig. 2, b and c). In this respect it is possible to speak of a qualitative correspondence between the mechanical properties (flow stress) and the structure of the deformed single crystals (relief pattern). This correspondence is natural, inasmuch as both the change in stress and the change in pattern are in the final analysis, separate manifestations of the single process of a change of state in the lattice during deformation.

2. The effect of the prestrain temperature on the pattern during subsequent extension can be explained by a strengthening of the slip planes through dislocations of the lattice occurring in plastic deformation and by other conditions under which recovery takes place. It is known [10, 13-15] that at low test temperatures there is scarcely any localization of the strain in the form of broad slip bands which can be seen at higher temperatures (e.g., room temperature), and that the slip thus occurs through the body of the crystal, uniformly in the first approximation in the form of thin (up to ~ 200 A) slip lines with slight dislocation, which may reach 10-10A in aluminum [16]. This is also seen from the

GRAPHIC NOT

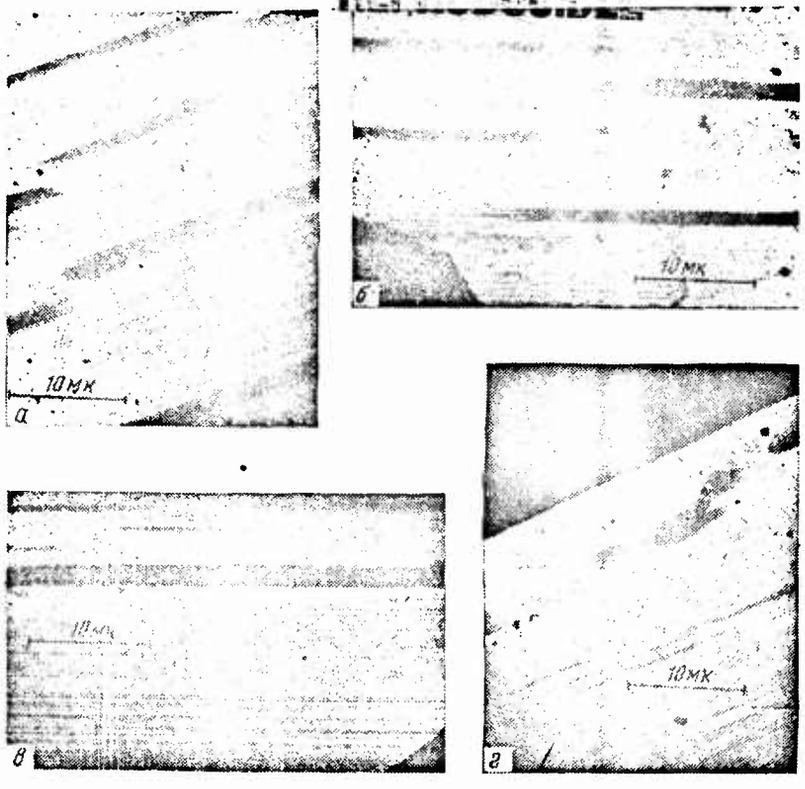

Fig. 10.

data for the extension at -180° (Figs. 5 and 6). It may be assumed [10, 17] that the strong hardening at the affected slip planes is the reason preventing the transformation of the slip lines at low temperature into slip bands at those "weakened" places in the crystal where they might have formed at a higher temperature.

The processes of recovery are intensified during the transition from low-temperature deformation to extension at a comparatively high temperature: the toughening distortions of the lattice, unstable at the new temperature, disappear and redistribute them-

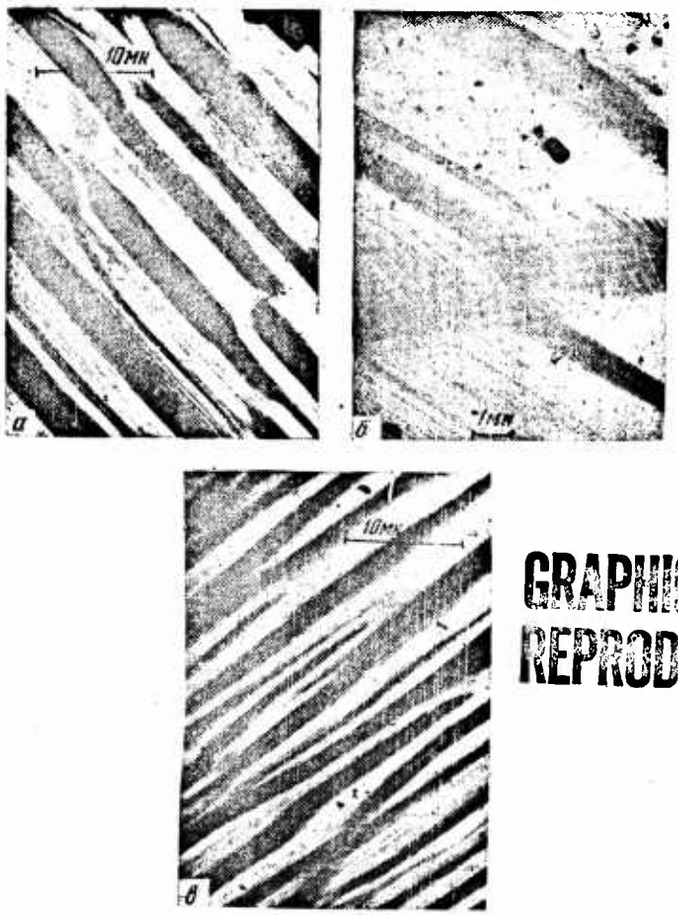

GRAPHIC NOT REPRODUCIBLE

Fig. 11.

selves or become less effective. As a result, the slip bands develop rapidly at corresponding places on the crystal (e.g., Fig. 5 b_{12} and c_{12}, Fig. 6 b'_{12} and c'_{12}).

When the slip bands spread toward each other but in parallel fashion, a "bridge"* may form between them due to the localization

* This word is used to denote normal cross slip and the more complicated forms of contact between slip bands discussed earlier.

GRAPHIC NOT REPRODUCIBLE

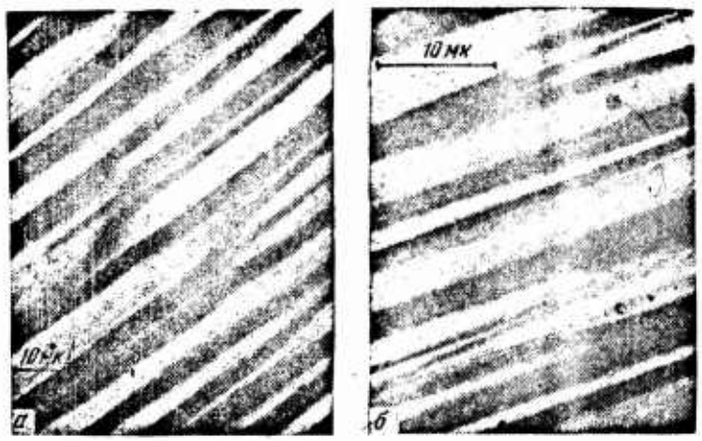

Fig. 12.

of tensions in the zone N-P (Fig. 13), when the edges of the slip bands approach one another (N and P in Fig. 13 Figure 9 and Figure 10 a and b. It may be assumed that local overstressing in the zone N-P, and consequently the probability of the formation of a "bridge", will be greater with the development of slip bands and the narrowing of the distances between them. The formation of a "bridge" may be facilitated by barriers in the N-P zone that prevent the further spread of the slip bands and a change in crystal orientation in this zone.

In this respect, extension at a higher temperature after prior low temperature deformation is more likely to produce "bridge" than extension without prior deformation. As already noted, the slip bands in the first instance appear more developed. Furthermore, slip bands develop more often in nearest neighboring bundles of slip

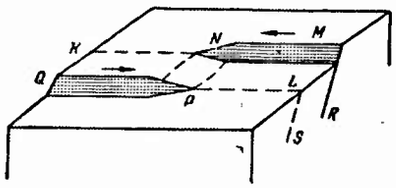

Fig. 13. Diagram of development of slip bands. RMNK and QPIS are slip planes; MN and QP are slip bands; NP is the zone in which a "bridge" between slip bands may form.

planes rather than in the same bundle (i.e., Fig. 10 b and c).* We believe that this results from the fact that recovery does not progress to the same degree along each slip plane which was blocked. The secotrs of planes that contained low-temperature distortions and which are less stable and effective at the new, elevated temperature will be unblocked first. The formation of "bridges" is also facilitated by the structural distortions of the deformation band type that appear in great numbers at low temperature deformation

---

* We should point out that although the slip bands appearing at very high temperature deformation, generally speaking, are comparatively dense in their arrangement (e.g., Fig. 5 b); those that appear and newly develop are located at considerably greater distances from each other (Fig. 6 b'_2).

and remain at high temperature (Fig. 14 b_1, c_1, b_{12}, c_{12}). By crossing the active slip planes (for example, in the direction NP in Fig. 13), they prevent the slip bands from spreading in the same direction and, because of the change in crystallographic orientation, may also stimulate the formation of a"bridge". This statement is reinforced, for example, by the fact that in many cases the ends of the blocked slip bands and the "bridges" appear to be contained within the limits of a certain band that crosses the active slip planes (Fig. 9; Fig 10 a and b; Fig. 11 a and c; Fig 12 a).

Fig. 15 shows the formation of breaks in the slip bands at points of intersection where there is visible uneveness in the relief. It should be noted that the formation of a break may also occur where a deformation band is intersected by one slip band, not necessarily by two bands spreading toward each other.

To substantiate our views (in particular the diagram in Fig. 13) of the formation of the relief pattern of a single crystal during a change in the test temperature from -180 to 20°, experiments were made on the kinetics of structural changes. Single crystals which had been previously extended by 10% at -180° on a special apparatus were extended at 20° on the stage of horizontal microscope. Successive micrographs of the same section of the crystal were taken for each 0.3% deformation.

Some of the frames obtained are reproduced in Fig. 16. Frame 1 corresponds to approximately 1% deformation at 20° and frame 37 to 11% deformation. The complete set demonstrates the gradual development and spreading of the slip bands on the base of the fine slip lines. The "bridges" form in accordance with the diagram in Fig. 13. The formation of the breaks was also visually observed

during spreading of single slip bands (in this case, the development resembled that observed by Chen and Pond in their work [18]. In this was, the concepts regarding the formation of slip bands and breaks were experimentally confirmed.

3. The results obtained from varied test temperatures may also be accounted for by the above considerations. In the case shown in Fig. 7 c_{13}, however, we must assume that at least some of the distortions of the lattice at -180° become less effective and less stable even at a comparatively low test temperature (-80°). In paper [19], which deals with the study of the influence of repeated variation of the test temperature on the original sections of the respective extension curves for pure single aluminum crystals, was shown that the transition from deformation at -183° to deformation at -77° is actually accompanied by an appreciable softening of the crystal.

As regards the appearance of "bridges" with a more complex structure than that observed in common cases of cross slip, the possibility of their formation apparently depends on a combination at their point of formation, of such factors as sufficiently high overstress, a complex state of tension, and possible structural (orientational) distortion of the lattice.

4. In view of the concepts postulated in paragraph 2, the increase in the number of breaks in the slip bands with the higher degree of deformation in tests conducted at higher (20°) temperatures (Fig. 5 b_2, c_2, d_2; Fig. 12 a and b) is to some degree understandable. Indeed, the inhomogeneity of the lattice distortions increases with an increase in the degree of deformation and so too do the inhomogeniety and intensity of recovery, which fact augments

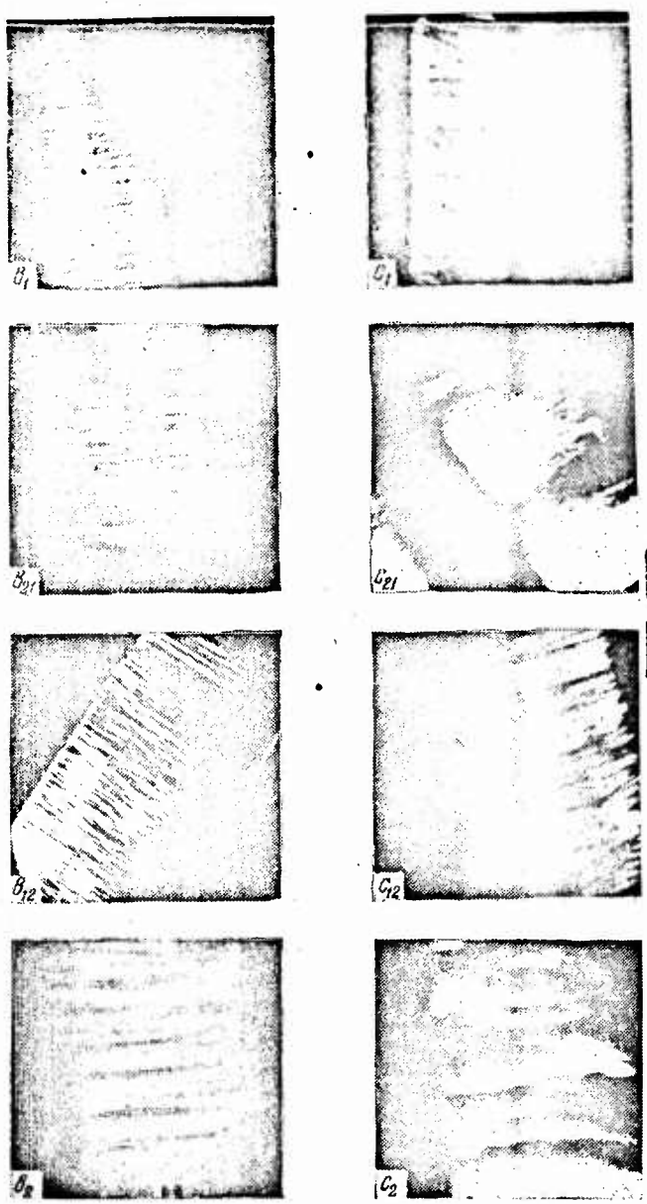

GRAPHIC NOT REPRODUCIBLE

Fig. 14. Structure of single crystals of aluminum after various stages of deformation. b_1 - Σ = 11% (-180°); c_1 - Σ = 20% (-180°); b_{21} - Σ = 10% (20°) + 1% (-180°); c_{21} - Σ = 10% (20°) + 10% (-180°); b_{12} - Σ = 10% (-180°) + + 1% (20°); c_{12} - Σ = 10% (-180°) + 10% (20°); b_2 - Σ = = 11% (20°); b_2 - Σ = 11% (20°); c_2 - Σ = 20% (20°).

GRAPHIC NOT
REPRODUCIBLE

Fig. 15. Breaks of slip bands at points with visible unevenness of relief. × 250.
ϵ = 18% (-180) + 2% (20°).

the possibility of forming well-developed slip bands, not in one but in two neighboring parallel bundles of slip planes (this also takes place in the case of comparatively small degrees of deformation, Fig. 9). The number of distortions of the deformation-band type increases their presence, as already mentioned, also being a prior condition for the formation of the slip band fractures. The third prerequisite is the progressive development of the slip bands, i.e., their degree of dislocation (Fig. 5, a_2, b_2, c_2, and d_2; Fig. 6 b'_2, c'_2 and d'_2). The fourth prerequisite consists in an increase in flow stress. This gives rise, first, to a greater probability that a spreading slip will break through the

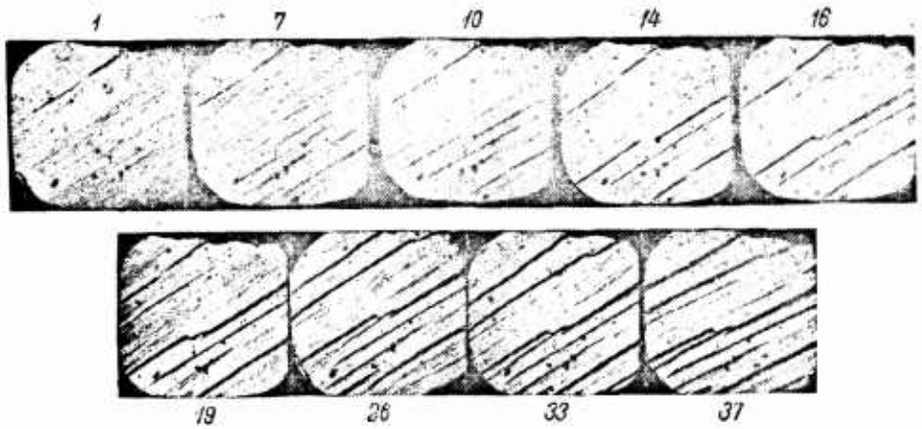

Fig. 16. Micrograph of a section of crystal showing gradual development and spread of slip bands and formation of "bridges". ϵ = 10% (-180°C), subsequent extension at 20°.

orientation barriers of the deformation band type and, second, to a greater probability of considerable overstress in the N-P type zones (Fig. 13) between the ends of the blocked slip bands.

5. As already noted, the effect of prior high-temperature extension (20°) is manifested to a comparatively slight degree (Fig. 6) during subsequent low-temperature (-180) tests. Here however it should be borne in mind that in the present case of extension, with intermediate electropolishing to remove the relief pattern established by prior extension, the second low-temperature deformation (180°) is obtained through the fine slip lines. Development of the normal slip bands appears impossible (due to considerable hardening).

The structural difference between single crystals extended at

-180°, with and without prestrain at 20°, is clearly seen from a study of their rough relief pattern (Fig. 14). In the latter case, a great number of deformation bands lying close to each other (Fig. 14 b_1 and c_1) appear on the surface of the specimen. In the former case, they are fewer in number and more distant from each other; moreover, a more distinct deformation bands further away from each other (i.e., traces of prestrain at 20°) are also observed (Fig. 14 b_{21} and c_{21}).

6. It is of interest to note that the slip bands originating in high-temperature tests after prior low-temperature deformation (Fig. 6 b'_{12} and c'_{12}) closely resemble those appearing near scratches made on the surface of single crystals of aluminum. The distinctness of the slip bands in both cases is most characteristic of this resemblance. The question arises whether this is not a manifestation of the similarity of normal changes in the crystal structure, produced (in the area of the scratch) by scratching or low-temperature extension.

7. The absence of a mechanical equation of state for single crystals during plastic deformation was shown by data on the influence of varied test temperatures and test rates on the shape of the elongation curves. The same conclusion was drawn from our study of the influence of varied test temperatures on the flow curves of single crystals (in particular on their initial sections [19], and on data from x-ray analysis in the case of polycrystals [5]. In the present study this has been shown to be the case for single crystals by metallographic analysis of the influence of varied test temperatures. Finally, in a study conducted under the supervision of one of the authors by a team of canidates at Peking

University, the same conclusion was reached in a study of the influence of varied rates of extension on the metallographic pattern of the structure of single crystals and on their flow curves. Consequently it may be concluded that the invalidity of the mechanical equation of state has been proved reasonably well.

Conclusions

1. The structure of deformed single crystals, like the flow stress, is not a single-value function of temperature at the moment of testing. A considerable part is played by the prestrain temperature.

2. Prior low-temperature extension with subsequent high-temperature deformation produces a number of characteristic structural changes in the single crystal (numerous breaks in the slip bands, the dispersed nature of these bands, greater density of the deformation bands, etc.). The influence of prior high-temperature deformation is mainly revealed, in the course of subsequent low-temperature tests, in the typical rough relief pattern (number and appearance of deformation bands).

3. The results obtained may be explained by the difference in the effectiveness and stability of the strain distortions of the crystal lattice responsible for hardening during both preliminary and subsequent deformations. In this case the structure of the crystals at the moment of completion of the preliminary deformation is taken into consideration.

4. A qualitative correspondence was observed to exist between the effects of temperature variations on the change in mechanical properties (flow stress) and on the relief pattern (deformation

mechanism) of the crystal during the course of extension.

REFERENCES

1. LUDWIK, P. Elemente der Technologischen Mechanik, Berlin, 1909.

2. HOLLOMON, J. H. Trans. AIME, 162, 1945; 171, 1947. ZENER, C. and HOLLOMON. J. Appl. Phys., 17, 1946; HOLLOMON, J. N. and LUBAHN, J. D. Gen Elec Rev Feb., April, 1947.

3. DORN, J. E.; GOLDBERG, A. and TIETZ, T. E. Metals Technology, 15, 6, 1, 1948.

4. VASIL'YEV, L. I. ZhTF, 22, 11, 1952. (Journ Techn Phys), VASIL'YEV, L. I. ; BYLINA, A. S. and ZAGREBENNIKOVA. DAN SSSR, (Reports of Acad Sci USSR) 90, 5, 1953. VASIL'YEV, L. I. and YEREMINA, L. I. DAN SSSR, 93, 1953. VASIL'YEV, L. I. ZhTF, 23, 8, 1953.

5. PATERSON, M. S. Acta Metallurgica, 2, 6, 1954.

6. VITMAN, F. F.; ZLATIN, N. A. and IOFFE, B. S. ZhTF, 19, 3, 1949. VITMAN, F. F. and ZLATIN, N. A. ZhTF, 19, 3, 1949.

7. WYATT, O. H. Nature (Lond), 167, 1951.

8. COTTRELL, A. H. Progress in Metal Physics (Ed. B. Chalmers), IV, 1953.

9. ROSI, F. D. and MATHEWSON, C. H. Trans. AIME, 188, September, 1950.

10. BROWN, A. F. Inst Metals, 80, 3, 1951.

11. LOS. J. Abs. Dissert Univ Cambridge, 1947-1948.

12. VASIL'YEV, L. I. Trudy SibFTI, (Papers of Sib Inst. Phys Techn) volume 26, 1948.

13. KURNOSOV, D. G.; TRONINA, N. M.; and YAKUTOVICH, M. V. ZhTF, 18, 2, 1948. YAKUTOVICH, M. V. Trudy IFM UFAN, 12, 1949. YAKUTOVICH, M. V.; YAKOVLEVA, E. S.; LERINMAN, R. M. and BUYOV, N. N. Symposium dedicated to 70th anniversary of Acad Ioffe, A. F., 1950; Bulletin of Acad Sci of USSR, Phys. Ser., 15, 3, 1951. Sbornik posvyashchennyy 70-letiyu akad. BUYNOV, N. N. FMM, 2, 3, 1956, Phys. Met and Metallurgy.

14. BROWN, A. F. Advances in Physics, 1, 4, 1952.

15. TSEN LIN-CHAO and HUO SHOU-AN. Data on influence of temperature contained in a report given by L. I. Vasil'yev at the plenary

session of Fifth All-union Conference on Use of x-rays. (June 1955, Leningrad); Acta Physica Sinica, 12, No. 6, 1956.

16. WILSDORF, H. and KUHLMANN-WILSDORF, D. Naturwiss., 38, 1951 Z. angew. Physik. 4, 10, 1952; 4, 11, 1952.

17. VASIL'YEV, L. I. Reports given at North-Eastern Peoples University (November 25, 1955) and at Naking University (March 3, 1956).

18. CHEN, N. K. and POND, R. B. J. of Metals., 4, 10, 1952.

19. COTTRELL, A. H. and STOKES, R. J. Proc. Roy. Soc. A232, 1192, 17, 1955 - 1956.

HARDENING AND SOFTENING MECHANISM

A. M. Yuferov

The difference between the theoretical and actual strengths of a crystalline substance is considered by the majority of research workers to be due to the fact that, in practice, a crystal does not correspond to the ideal concept envisaged in the theory. In an actual crystal there are always defects of different kinds, with the result that prevent destruction of the atomic bonds throughout the whole cross section under an external load does not occur instantly and simultaneously, but gradually. As a result, the true yield strength of an actual crystal is considerably lower than that calculated theoretically for the ideal crystal lattice [1, 2, 3].

This explanation of the low value of the actual strength of a crystal, despite the fact that it is very logical and resonable, contradicts what is actually observed in the strengthening of alloys. Practice shows that the greatest strength is found in alloys which have acquired a particular metastable state with a less perfect lattice [4] as a result of plastic deformation, thermal treatment, or alloying.

On the one hand, elimination of defects of various kinds in the structure of the lattice definitely helps to strengthen the

crystals, but on the other hand the strengthening of crystals is always accompanied by increased distortion of their lattice. Both statements are correct and yet obviously contradict each another. In our opinion, this contradiction in the theory and practice of strengthening and softening stems from the fact that the existing concepts of the strength of the ideally perfect lattice take into account the atomic interaction only in the lattice proper, considered abstractly and disregarding the interaction between atoms of the lattice and those of the ambient medium [2]. It is the efforst which have been made(solely on the basis of changes in the crystal lattice proper and disregarding the changes in the interaction between the atoms of the lattice and those of the surrounding medium),the reasons for the low strength of crystals in practice and the reasons for changes in strength with different method of processing, which have led to the above controversy.

In our opinion, local forces are generated on the boundaries of the structural elements through the interaction of atoms in differently-oriented boundary lattices, and these forces cause mutual elastic deformation of the abutting lattices. The cause of the origin and distribution of the local forces can be explained by the general law of the dependence of the interatomic forces on the distance between particles. This law directly provides the condition required for a balanced-state system consisting of two identical atoms (a two-atom molecule), characteristic of which is the resultant of the interaction of the particles $j = \frac{du}{dr} = 0$. Here, the free energy level of the system U has a minimum value. The distance between the particles in the case of F = 0 is usually given the symbol r_o.

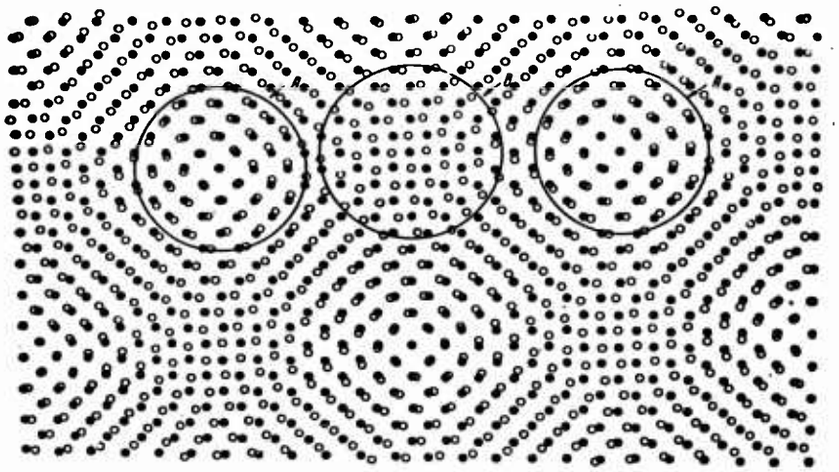

Fig. 1. Zones A and B on the border of conjugation along the planes of the cube of differently orientated lattices.

Let us take the simplest case of boundary conditions. When two face centered lattices adjoin by means of the planes of a cube, the location of the points of the bordering lattices relative to each other depending on their degree of disorientation, can be determined by superposing the lattice in accordance with A. V. Shubnikov's method [5].

The arrangement of the atoms in one lattice relative to the atoms in another lattice is govered by the following features (Fig. 1).

At some sites on the boundary plane the atoms of both lattices lie almost along the same straight line normal to the boundary plane; at other sites, the atoms of one lattice are exactly opposite the spaces between the atoms of the other lattice. It is as if the entire plane of union of the two bordering lattice would consist of

separate areas or zones (dislocations) [6]; in the center of the A zones the atoms are opposite one another, while in the center of the B zones they are opposite the interstitial spaces.

The areas or zones having a similar disopsition of atoms are regularly distributed in the boundary plane and alternate with each other in such a way that a pattern is formed which corresponds to the distribution of the atoms in the crystallographic planes, but on a larger scale.

The sizes of the areas or zones and the frequency of their repetition depend on the rotation angle of the bordering lattices or of of the superimposed planes relative to one another. With an increase in the rotation angle up to 45° the A and B zones are reduced.

The dependence of this increase in the angle of the relative rotation of the lattices α is expressed as follows:

$$\frac{a'}{a} = \frac{1}{2\sin\frac{\alpha}{2}};$$

if we take a as the distance between the atoms in the crystallographic plain, and a' as the distance between the zones A and B formed in the boundary plane.

V. I. Arkharov [6] points out that a similar regularity in the arrangement of atoms in the boundary plain of two crystal lattices should take place in all cases of lattice abutment by any crystallographic plain. This regularity must also take place in the boundary between a crystalline substance and an intercrystalline substance, a liquid phase, and even a gaseous phase.

To obtain an idea of the stresses arising in bordering lattices let us examine the distribution of forces interacting between the atoms of two lattices in a plain perpendicular to their border.

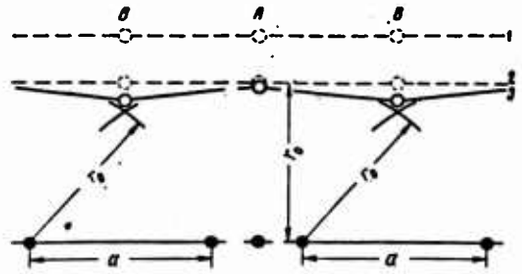

Fig. 2. Diagram of local forces causing elastic deformation of bordering lattices in A and B zones.

When the distance between the lattices is r_o (Fig. 2, position 2), the atoms of one lattice will only be this far away from the atoms of the other lattice in the center of the A zones, since these atoms lie on a straight line normal to the boundary plane. The distance between the atoms in zones B at that instant is greater than r_o. Forces of atomic attraction will prevail between these atoms, and bordering lattices will approach each other. When the lattices approach still closer, the distance between the atoms in the A zones becomes less than r_o; the forces of repulsion will prevail and prevent further drawing together of the lattice.

Equilibrium will be established when the resultant of the interaction of all atoms on the boundary between two lattices is zero. This means that when there is equilibrium on the boundary between adjacent lattices, the distance between the atoms of both lattices in the A zones will be less than r_o and greater than r_o in the B zones (Fig. 2, position 3). If the state of both lattices is the same, both bordering lattices will be elastically compressed by the repulsive forces in the A zones, and they will be extended

in the B zones by the forces of attraction.

It follows from the relative position of the atoms in both lattices that the interacting forces between atoms asymmetrically positioned with respect to each other will be directed at an angle to the boundary plane. The action of these forces may therefore be represented as the action of two components, one of which is perpendicular to the boundary, while the other is tangential to the boundary plane.

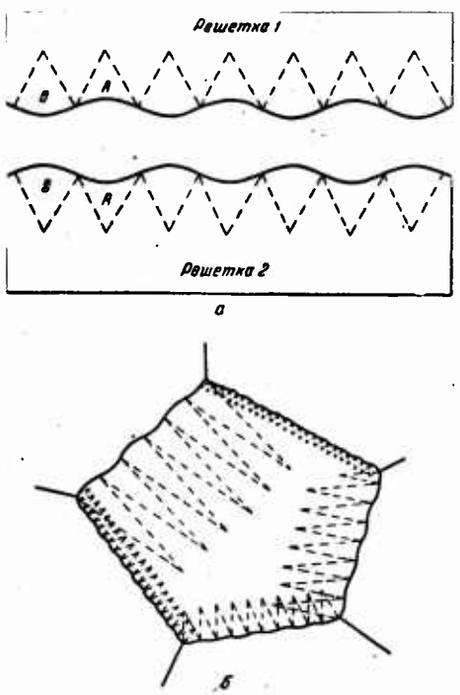

Fig. 3 a and b. Diagram of distribution of elastic, compressive, and tensile strain on grain boundaries.

The tangents, which are components of the interatomic forces in each zone, produce a moment of force about an axis passing through the center of the zones perpendicular to the boundary. Not only,

therefore, is there elastic, compressive, and tensile strain in the lattices, but also deformation by lateral dislocation of the atoms due to the moment of force in each zone.

The elastic strain of the lattices in both the A and B zones will spread to a certain depth into the center of the grain. In this way we obtain an ideal of differently deformed structures in the zone between adjacent lattices, which are shaped like wedges and alternate in regular fashion (Fig. 3 a and b). Henceforth, these structures will be marked, in the same way as the zones in the boundary by the letters A and B. It should be borne in mind that whenever zone A or B is mentioned, this means the arrangement of atoms in the boundary and whenever structure A or B is mentioned this means the elastically deformed sections of the lattices adjacent to the respective zones on the grain boundaries.

The local stresses and elastic deformation of the adjacent lattices must depend on a number of factors, namely:

1) The size of the zones A and B. The larger these zones, i.e., the less the lattices are disoriented, the greater the local froces are and, consequently, the greater also the elastic deformation of the lattices in A and B zones.

2) The elastic properties of the bordering lattices proper and their orientation, to the extent that the lattices are anisotropic.

3) The effect of the external loads. Stresses brought about by external loads should combine with the local tensions on the grain boundaries, thereby influencing elastic deformation in zones A andB. However, this cannot change the general pattern of distribution of the elastic deformations on the grain boundaries.

4. The presence of solute atoms of other elements in adjoining

lattices should also influence elastic deformation in zones A and B. This follows from our current thinking on the inter-connection of elastic deformation and the diffusion of the atoms [7, 8] established by S. T. Konobeyevskiy:

$$D' \frac{\partial^2 c}{\partial x^2} = D'' \frac{\partial^2 \varepsilon}{\partial x^2},$$

where D' and D'' are the coefficients of decreasing and mounting diffusions;

$\frac{\partial^2 c}{\partial x^2}$, $\frac{\partial^2 \varepsilon}{\partial x^2}$ are gradients of the concentrations and stresses respectively.

The elastic deformation of adjoining lattices should be reduced through the occurrence of mounting diffusion between the elastically deformed structures A and B.

5) The elastic deformation of adjoining lattices in zones A and B should to increase with a decrease in temperature. This is shown first by the fact, established in tests by G. V. Kurdyumov and N. T. Travina, that the inhomogeneity of composition inside the grains of a solid solution increases with a fall in temperature [9], and, second, by the fact that intercrystalline failure at high temperature and transcrystalline failure of metals at low temperature can also be considered as a result of an increase in the local forces on the grain boundaries at a lower temperature.

From the above concepts of an equilibrium state on the grain boundaries of a polycrystalline substance it follows that inside the grains of pure metals there are statically fixed structures with an inhomogeneous density of atoms, whereas in alloy polycrystals these structures contain different atomic concentrations of alloy components.

This concept of the boundaries between the structural components of polycrystals in metals and alloys corresponds to data obtained experimentally on coherent areas and dislocations [9, 10, 11, 12].

It can be considered that the elastically deformed structures on the grain boundaries of a polycrystal are, first, a site for the formation of nuclei of the new phase in the recrystallication process in metals and alloys; second, they are a focus for the formation of primitive crystal particles in the course of recrystallization; third, by weakening the adjoining lattices, they are a site for dislocations in plastic deformation and of failure in transcrystalline brittle fracture of the polycrystal.

The hardening and softening mechanism in metals and alloys can be partly explained on the basis of the concepts expressed above.

The variation in strength of pure metals due to thermal treatment, plastic deformation, and recrystallization cannot be explained by a change in the strength of the lattice proper, since in all cases the atomic bond strength in the lattice should be nearly identical at the same temperature this derives from the constant value of the modulus of elasticity. Consequently the variation in strength in all cases results from a change in the magnitudes of the local forces on the boundaries of the structural components.

A change in magnitude of local forces in pure metals is only possible as a result of change in the disorientation of lattices between adjoining structural elements. In all cases the disorientation of the lattices at their boundaries increases with a reduction in size of the structural elements and this causes a reduction in size of the zones A and B and consequently reduces the local

forces and increases the strength.

The process of plastic deformation amounts to division of the crystals into parts which in principle are related crystallographically in the same way as the adjoining grains in the original metal, with the only difference being that the disorientation of the adjoining lattices among the emerging structural elements is greater than that on the grain boundaries before deformation. At a certain stage in plastic deformation the polycrystal is usually fractured; this indicates that the process of strengthening cannot continue any further. In our opinion, further plastic deformation is not possible because of insufficient strength of the boundaries between the structural components.

In an undeformed polycrystal fracture by shearing separation does not occur along the grain boundaries but across the grain-not because the boundaries are stronger but because the local forces on the boundaries weaken the adjoining lattices so much that their resistance to an external load becomes lower than the resistance to shearing in the boundary. A decrease in local stresses under plastic deformation results in an increase in the strength of polycrystals only until the resulting stresses exceed the resistance to shear in the boundary plane between the structural components. In other words, the process of plastic deformation (the hardening process) is limited by the strength of the boundaries between structual components. This motion completely accords with observations of the initial stage of failure [14].

The softening of a deformed metal on recrystallization should take place as a result of greater local forces. This can only occur if the disorientation of the lattices on the grain boundaries is reduced.

This is exactly what the process of recrystallization is believed to amount to from the standpoint of hardness. A greater disorientation on the boundaries of the structural elements is observed when the latter grow in size; hence softening on recrystallization should be considered the result of a growth of the structural elements.

The mechanism of grain growth, in our opinion, is as follows:

Grain growth with an increase in temperature first occurs on those boundaries where the A and B zones are smallest in size and where the lattices are disoriented most. On the grain boundaries where the A and B zones are larger in size, the growth of the grains occurs at a still higher temperature.

Grain growth is determined by the mutual orientation of the adjoining lattices. Not only can larger grains grow at the expense of smaller grains, but smaller grains can also grow at the expense of larger ones. It may be assumed, in view of the fact that the lattices of adjacent grains in a polycrystal are differently oriented that a grain can grow along its boundary with another grain, and at the same time, on its boundary with a different grain, it can become smaller.

Grain growth at a given temperature continues until the relative orientation of the lattices on all boundaries is such that zones A and B exceed a certain size. Further growth of the grains is then only possible with a rise in temperature, after a reduction in the elastic deformation in the zones A and B.

An increase in temperature, speeds up grain growth, since a larger number of boundaries are therby displaced.

The minimum temperature at which grain growth begins and the

rate of grain growth depend on the degree of disorientation in the adjoining lattices. The greater the disorientation, the lower the temperature at which the growth begins.

The growth of the neighboring blocks inside the grains is only possible at a farily high temperature, near the critical temperature of recrystallization, since the disorientation of the lattice blocks is slight.

The great strength of single-phase solid solutions in comparison with pure metals likewise cannot be explained solely by an increase in the strength of the crystal lattice proper. This is supported by the fact that a small amount of impurities in a metal cause no apprecaible change in the modulus of elasticity. The great strength of single-phase solid solutions is the result of the lower magnitude of the local forces on the grain boundaries.

A decrease in local forces on the grain boundaries in solid solutions can occur not only as the results of an increase in the disorientation of adjoining lattices, as in pure metals, but also as a result of the redistribtution of the atomic concentrations of a solute component among differently deformed grains of adjoining lattices through mounting diffusion. This redistribution should result in a reduction in the local stresses. This view is in conformity with the phenomena of hardening and softening observed during the heat treatment of single-phase solutions [7, 13].

The hardening observed during plastic deformation of single-phase solid solutions, as in the case of pure metals is due to a reduction in local forces on the boundaries of the structural components resulting from the increasing disorientation of adjacent lattices. The increase in strength of the deformed single-phase solid solutions

at low heating is caused by the decrease in local tensions due to redistribution of the concentration among the differently deformed grains.

The recrystallization process in a deformed solid solution begins to occur as the annealing temperature is further increased (in principle, this process should be the same as in pure metals), resulting in a lower degree of disorientation in the neighboring lattices and in greater local forces. As a result the yield point is lowered.

In supersaturated solid solutions, as in pure metals, the increase in strength that occurs when the structure becomes finer should depend solely on a modification of the boundary structure, since the structure and composition of the phase components during slow cooling are identical in both fine-grained and coarse-grained alloys.

The change in grain-boundary structure with a reduction in size of the structural elements consists in an increase in the disorientation of neighboring lattices at the boundaries of structural components, causing a reduction of the zones in which there is similar deformation of the lattices and consequently reducing the local forces therby increasing the strength.

The hardening of super-saturated solid solutions in plastic deformation is also caused by a decrease in local forces at the boundaries of the structural components: first because of an increase in the disorientation of neighboring lattices as in pure metals; second because of the redistribution of the concentration, as in single- phase solutions; third, because of the precipitation of excess phases, on the boundaries of which there is then greater

lattice than that existing on the grain boundaries of the super-saturated solid solution before precipitation.

On the basis of what has been explained above, the general conclusions can be drawn that in all cases, both for pure metals as for alloys, hardening and recovery are the result of either a change in bond strength between the atoms in the lattice proper or a change in the strength of the local forces at the boundary of the structural components. The first case occurs with a change in temperature and in the atomic concentration of the phase components. The second case results from a change in the disorientation of the neighboring lattices of the structural components (as a result of heat treatment or plastic deformation) and from redistribution of the atomic concentration of the components among differently-deformed lattice grains.

The hardening and softening of steel with different types of processing should not differ in principle from this process in heteorphase alloys and super-saturated solid solutions. These views can be used to explain the hardening and softening mechanism of steel in relation to its structure and the effect of an external load, for instance the mechansims of fatigue, relaxation, creep, etc.

The foregoing views on the mechanism of hardening and softening during plastic deformation, thermal processing, and alloying lead us to the conclusion that the basic reason for the hardening which can be achieved in practice is a decrease in local forces at the boundaries between the structural components, whereas the reason for softening is an increase in those forces. This conclusion, at first glance, may appear to contradict the existing view that hardening is always connected with an increase in the lattice dis-

tortions in metals and alloys. But there is actually no contradiction here, as we shall explain below.

The existing belief that lattice distortion causes hardening is mainly based on the existence of increased diffuseness and intensity of the interference lines. The diffuseness of the latter is expressed in angular units by the formula

$$\Delta\theta = \operatorname{tg}\theta\left(\frac{\Delta a}{a}\right)_{max}.$$

It is not usually possible to determine the experimental value for $(\frac{\Delta a}{a})_{max}$ since the presence of a background on an x-ray photograph obscures the contour of the curves at their base. Therefore, $(\frac{\Delta a}{a})_{max}$ is calculated theoretically on the assumption of a number of conditions.

In practice, the diffuseness of the interference lines is quantitatively defined by the line width of B measured at half the height of the photometric curve

$$B = 4\left(\frac{\Delta a}{a}\right)\operatorname{tg}\theta,$$

where $(\frac{\Delta a}{a})$ is the mean of the absolute values for the deformation of the lattice.

In view of the generally accepted view that a mean value is not dependent on the maximum and minimum deviations of particular values, it is evident that the width of the lines B and the mean of the absolute values for lattice deformation $(\frac{\Delta a}{a})$ cannot give an accurate idea of the absolute value of maximum distortions of the lattice $(\frac{\Delta a}{a})_{max}$.

But the ideas postulated by the author of this paper that an increase in resistance to shearing and an extension of the elastic limit result from a decrease in the absolute value of the maximum local distortions of the lattice do not exclude the possibility

of an increase in the absolute value of the average distortion of the crystal lattice in the hardening of metals and alloys.

The above can be stated in this manner. The lattice in an undeformed metal is distorted most at the grain boundaries and the distortion values of the lattice parameter decrease toward the center of the grain with a large number of the lattice cells in the center of the grain remaining undeformed. The local forces appear after deformation in the shear planes, their magnitude being lower however than in the undeformed metal but the number of their zones of activity is higher. The lattice distortion is probably at its maximum at the boundaries of slip bundles and decreases towards the center of the bundles. Since the thickness of the slip bundles as compared with the size of undeformed grains is very small, the lattice, despite the decrease in local forces, is distorted almost over its entire structure, the average value of the distortion of the lattice increasing in spite of the lower absolute values of the maximum distortions. It is these changes in a metal, occurring when the structural components change in size, which are shown by the photometric curves obtained in x-ray structural analysis of the lattice state.

Hence the degree of disorientation of neighboring lattices at the boundaries of the structural elements of a polycrystal is the principal structural element responsible for changes in the structurally sensitive properties of a polycrystal caused by a change in its structure.

REFERENCES

1. KUZNETSOV, V. D. Crystals and Crystallization (Kristally i kristallizatsiya), Moscow, 1954.

2. FRENEKL', Ya. I. Introduction to the Theory of Metals (Vvedeniye v teoriyu metallov), Moscow-Leningrad, 1950.

3. KONOBEYEVSKIY, S. T. Physical Basis of Strength of Metals (Fizicheskiye osnovy prochnosti metallov), Vestn. AN SSSR (Herald of Acad Sci. USSR), 25, No. 7, 1955.

4. MIRKIN, I. L. Metallurgy and Metal Treatment (Metallovedeniye i obrabotka metallov), No. 1. 1955.

5. SHUBNIKOV, A. V. ZhTF (Journ Techn Phys), 22, No 12, 1952.

6. ARKHAROV, V. I. Concerning the Nature of Intercrystalline Coupling in Polycrystalline Bodies (O prirode mezhkristallicheskogo sochleneniya v polikristallicheskikh telak), Trudy Instituta fiziki metallov, Papers of Institute of Metal Phys. No. 16, 1951.

7. KONOBEYEVSKIY, S. P. Collection of Reports Submitted to Metallurgy and Thermal Processing Section of All-Union Metallurgical Research Society (Sbornik dokladov sektsii metallovedeniya i termicheskoy obrabotki VNITO metallurgov), Moscow, 1940.

8. KONOBEYEVSKIY, S. T. ZhTF Journal of Experimental and Theoret Physics (ZhETF), 13, No 11 and 12, 1943.

9. KURDYUMOV, G. V. and TRAVINA, N. T. ZhETF, 25, No. 2, 1955.

10. KURDYUMOV, G. V. Concerning the Hardness of Tempered Steel, Collection 4. Problems of Metallurgy and Metal Physics, O prirode tverdosti zakalyonnoi stali, 4 sbornik. Problemy metallovedeniya i fizika metallov, Metallurgizdat, 1955. St. Sc. Press. Lit on Ferr and Non-Ferr Met.

11. IOFFE, A. E. Fizika Kristallov (Physics of Crystal) Gosizdat, State Press, Moscow-Leningrad.

12. RID, V. T. Dislokatsii v kristallakh (Dislocations in Crystals) Moscow, 1957.

13. LASHKO, N. F.; SERGEYEV, Ya. and CHICHAGOV, V. V. Influence of Deformation on Recovery in Duralumin, Vliyaniye deformatsii na effekt vozvrata v dyuralyuminii, Trudy VVIA im. Zhukovskogo (Papers of Zhukovskiy Aviat. Eng. Acad.) No. 153, 1945.

14. LASHKO, N. F. Uprocheniye i razrusheniye metallov i nekotorye predel'nye mekhanicheskiye svoystva metallov (Strengthening and Failure in Metals and Certain Limiting Chancial Properties of Metals Oborongiz, 1951. St. Press of Def. Industry.

L_{β_6} and L_{γ_5} LINES IN THE SPECTRA OF COPPER AND ZINC

M. I. Korsunskiy and I. A. Rumyantsev

In most of the research work on changes in the x-ray spectra of compounds and alloys, study has been made of the lines of the K series. The transition of the valence electrons (the energy states of which naturally undergo very intensive changes) have also been considered in this work. The use of apparatus with adequate resolving power in order to detect slight energy changes of the order of fractions of eV is essential in such studies.

Since energy dispersion increases as the wavelength increases, study of the L-series for elements with middle-range atomic numbers (from Mn^{25} to Mo^{42}) is more convenient than study of the K series (the lines of the L-series in these elements are located in the range of 5-20A, which is within the possibility of measurement).

For a more accurate study of the changes in chemical compounds and alloys it is desirable to observe also the transitions of the valence electrons in the L-series. However, for a number of elements with middle-range atomic numbers, unfortunately, these lines have not yet been discovered in the L-spectra. This applies in particular to the elements Cu^{29} and Zn^{30}. These transitions in the elements Ge^{32}, as shown in the research of G. P. Borovikovaya and M. I. Korsunskiy [1] actually take place, and the corresponding lines are marked by

great intensity. Before studying the spectra of copper and zinc alloys, therefore, the L-spectra of pure copper and zinc elements were examined in order to discover the lines connected with the transitions of valence electrons and also in order to through light on conditions under which the lines appear. The present article gives an account of the preliminary results of these studies.

Our study of the spectra was conducted with a vacuum illuminating x-ray spectrograph [1] which used a curved mica crystal and a photo-recording system. An anode of electrolytic copper was prepared for the study of the copper, while the zinc was made into plates, 2 mm thick, and fastened on the copper anode; the zinc used was chemically pure.

The use of an x-ray tube which had a comparatively large focus (about 4 cm^2) enabled us to eliminate intensive local heating of the surface of the specimen; this was vitally important in obtaining the spectra of pure elements. The temperature of the anode did not exceed 350° (measured by a copper-constantan thermocouple at 5-7 kv and 10-15 ma.

The spectrographic photographs were taken on Isopan F film. The cassette window was covered with aluminum foil about 2 microns thick to prevent the penetration of visible light. The exposure time was 5-6 hours for copper and 2-6 hours for zinc; the photographs were measured with an MF-4 recording microphotometer.

Photoelectric examination of the first 20 spectrograms for the L-spectra of copper and zinc made it possible to establish a number of regular developments common to all the photographs.

Lines $L_{\alpha_{1,2}}$ and L_{β_i} for the spectra of both copper (Fig. 1) and zinc (Fig. 2) appeared to be double. The wavelength of the short-

wave components of those lines differs from that of the basic line by approximately 65 X-units. In wavelengths, those components are close to the satellites of the basic lines ($L_{\alpha''}$ and $L_{\beta''}$), but, the intensity of the lines we found greatly exceeds that of the satellites described in [2, 3, 4].

The great intensity of our lines which in some pictures even exceeds that of the basic lines, justifies the statement that they are not satellites. We identified them as lines L_{β_6} and L_{γ_5}.

It is of interest to note that the intensity of the L_{β_6} and L_{γ_5} lines in the Zn spectrum largely depends on the photographic procedure. As seen in Fig. 2 and 3, the relative intensity of L_{β} compared with $L_{\alpha_{1,2}}$ noticeably diminishes with an increase in exposure time. This results from gradual oxidation of the zinc plate during exposure. A similar change in the zinc spectrum occurs even with a short exposure when the vacuum is low (of the order of 10^{-4} mm Hg.).

A difference in wave-length between the lines L_{β_6} and $L_{\alpha_{1,2}}$ and between the lines L_{γ_5} and L_{β_1} correspond to an energy interval approximately equal to 4.6 eV for copper and 5.6 eV.

The dispersion in the L-series photographs for copper was 22-24 X/mm (1.5 eV/mm) and for zinc, 25-27 X/mm (2.1 eV/mm), i.e., it was at least double the dispersion for the L-series of copper and zinc given in earlier papers.

The possibility of finding the lines L_{β_6} and L_{γ_5} is to a considerable degree bound up with the oxidation of the specimen's surface. In an oxide those lines are almost entirely absent. According to Borovikovaya, a similar change in the intensity of the lines L_{β_6} and L_{γ_5} takes place with helium in the transition from pure metal to an oxide.

Fig. 1. Lines $L_{\alpha_{1,2}}$ and L_{β_6} in Cu spectrum. Scale 2 : 1.

Fig. 2. Lines $L_{\alpha_{1,2}}$ and L_{β_6} in Zn spectrum. Scale 4 : 1, 3 exposure time = = 3 hours.

Consequently the use of a high-dispersion spectrograph, a high vacuum (not less than $2 \cdot 10^5$ Hg), and comparatively weak currents in the tube to reduce the heating of the surface of the specimen are essential conditions for the discovery and study of the lines L_{β_6} and L_{γ_5} in copper and zinc.

It can be observed from the table of x-ray emission spectra that L_{β_6} and L_{γ_5} lines have been discovered for all elements, beginning with Rb^{37}. Since these lines refer to the respective dipole transitions $L_{III} - N_I$ and $L_{II} - N_I$ and copper and since copper and zinc possess electrons at these levels, it was not clear why these lines had not been discovered in copper and zinc spectra. Since the difference in wavelength between L_{β_6} and $L_{\alpha_{1,2}}$ is determined by the energy interval between $M_{IV,V}$ and N_I, we examined the dependence of the value for this interval on the atomic number. It was shown by extrapolation of the curve obtained for the elements $Ag^{47} - Rb^{37}$ to elements with lower atomic numbers that this interval for the elements $Ge^{32} - Cu^{29}$ amounts to several eV, i.e., the lines L_{β_6} and L_{γ_5} should be located respectively near the lines $L_{\alpha_{1,2}}$ and L_{β_1}

(since the curve showing the dependence of the energy interval $M_{IV} - N_I$ on Z can also be extrapolated for the lines L_{γ_5} and L_{β_1}).

In our case, the energy interval is 4.6 eV for copper and 5.6 eV for zinc, which fully confirms the existence of the lines L_{β_6} and L_{γ_5} in the copper and zinc spectra which were analyzed.

On the strength of this we can conclude that the published data on L-spectra of copper and zinc do not refer to pure elements.

CONCLUSIONS

1. The lines discovered in the copper and zinc spectra are lines L_{β_6} and L_{γ_5} and relate to the transitions $L_{III} - N_I$ and L_{III}- $-N_I$.

2. The distances of these lines from $L_{\alpha_{1,2}}$ and L_{β_1} were measured.

3. It was established that the proper conditions are essential in recording these lines photographically.

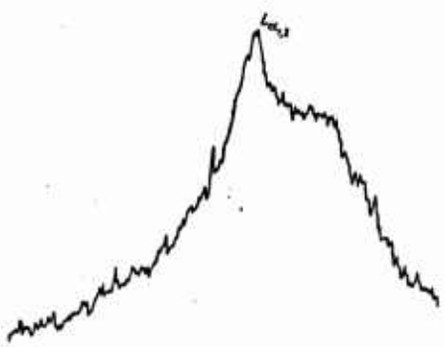

Fig. 3. Lines $L_{\alpha_{1,2}}$ and L_{β_6} in Zn spectrum.
Scale 4 : 1; 6 hour exposure.

REFERENCES

1. BOROVIKOV, G. P. and KORSUNSKIY, M. I. Concerning the L-Series of Germanium (Ob L-serii germaniya) Otchet KhPI, 1957.

2. GWINNER. Zschr. f. Phys., 108, 1938.

3. CAUCOIS. Phil. mag., 44, 1953.

4. LANDOLT. Bernstein, 1955.

INFLUENCE OF THE CONCENTRATION OF COMPONENTS IN IRON-CHROMIUM ALLOYS ON THE STRUCTURE OF THE ENERGY SPECTRUM OF THE CHROMIUM AND IRON CONDUCTIVITY ZONE AT HIGH TEMPERATURES

N. D. Borisov, V. V. Nemoshkalenko and A. M. Fefer

The present article is a direct continuation of earlier research [1] and is aimed at studying characteristic changes in the structure of the energy spectrum of chromium and iron electrons under the influence of the concentration of alloy components in an iron-chromium system and the transition (along the axis of composition) of the γ-solid solution into the α-solid solution.

For our investigation we studied the K_{β_5} - lines of chromium and iron produced by transition of electrons from the 3d subshell to the K-level, and K_{β_1} - lines of the same elements, produced by the transition of electrons from the 3p-subshell to the K-level combined with the longwave $K_{\beta'}$ - satellite.

The distribution of electrons through the energy levels of free chromium and iron atoms is given in Table 1.

The spectrum lines shown are those of pure chromium and iron and of iron-chromium alloys Nos 1, 2, 3, 4, 5, and 6 containing 4, 8, 20, 30, 45, and 50% chromium by weight, respectively. The spectral lines of the chromium K_β - group were not recorded for alloys Nos 1, 2, and 3 because of their weak intensity.

Electrolytic chromium and iron of high purity were used as test metals. All the test metals were made into special plates, which were then attached to the primary anticathode in the x-ray tube.

Equipment and Method of Work

The high-voltage apparatus used was a four-kenotron unit based on the Grätz layout. A ferromagnetic resonance stabilizer maintained a constant output of primary voltage with an error factor of 0.5%. For all the x-ray spectrograms of the pure metals and alloys we used an x-ray tube which we had constructed ourselves and which was designed to obtain flourescent spectra at high temperatures. After replacement of the electrodes the tube could be used for obtaining x-ray spectra by the primary excitation method. The tube was evacuated by an oil initial-vacuum pump, a mercury diffusion pump and a MM-40 high-vacuum vapor-oil pump, connected in series. The vacuum was obtained was 2 to $3 \cdot 10^{-5}$ mm Hg and it was regulated by HG-200 and VI-3 ionization gages. A fast nonvacuum x-ray spectrograph, in which the radius of curvature of the crystal was 500 mm [4], was used as the diffraction apparatus. A quartz crystal (prism face 1010) was used to break up the radiation from the specimen.

As distinct from previous studies, all the spectra were obtained from a crystal oscillating through 2°. This was essential in measuring the fine structure of x-ray bands produced by the primary excitation method because of the difficulties in subtracting the background (retarding spectrum). The latter, as is known, superposes its own pattern on top of the intensity of the x-ray bands under study. The linear orifice of the crystal was set by a blade (diaphragm) and did not exceed 1.5 mm.

The conditions for recording the x-ray spectra of the specimens were selected after measuring the latter's temperature with a Pt-PtRh thermocouple, the hot junction of which was welded directly onto the focal point which had been set beforehand, the position of the tube filament remaining unchanged. To reduce the temperature gradient along the diameter of the focal point, the length of the diameter did not exceed 1 mm and was regulated by the focusing cup of the cathode. A Kent thermorecorder was used to register the temperature of the radiating specimens. The filament was a tungsten spiral made of wire 0.25 mm in diameter. The life of the spiral was about 500-700 hours.

The target, a metal plate 3 mm thick cut into the shape of a truncated trapezium with sloping sides, was tightly inserted into the corresponding hollow ("swallow tail") in the copper cap of the anticathode. All spectra were taken on single-sided Agfa film and were developed for 5 minutes in a thermally-controlled chamber at 18°, with fresh Metol-hydroquinone developer in constant concentration being used in each instance. In selecting the exposure time, we sought to obtain the photodensities of the spectral lines in the rectilinear section of the sensitometric curve of the given film. The optimum time exposure was selected on the basis of the following equation [7],

$$t_{\text{опт}} = \frac{\lg \frac{S_n}{S_\Phi}}{S_n - S_\Phi} t, \qquad (1)$$

where S_{pk} and S_{bg} are the photodensities of the peak of the time and the background obtained during exposure time t. Given this condition, the optimum values for photodensities S_{bg} and S_{pk} will be

respectively:

$$S_{\Phi} = \frac{\lg(x+1)}{x}, \tag{2}$$

$$S_{\Pi} = \frac{x+1}{x}\lg(x+1), \tag{3}$$

TABLE 1

Элемент	Уровень						
	K	L_{I}	$L_{II, III}$	M_{I}	$M_{II, III}$	$M_{IV, V}$	N_{I}
	$1S$	$2S$	$2p$	$3S$	$3p$	$3d$	$4S$
Cr 24	2	2	6	2	6	5	1
Fe 26	2	2	6	2	6	6	2

where x is the ratio of the intensity of the line to the intensity of the background.

The maximum contrast of the faint spectral lines is obtained by exposing the background up to a photodensity of between 0.2 and 0.4.

The photometry of the spectrograms was done with a MF-4 recording microphotometer with a magnification of X7, an X20 extension, and a 0.7 X 14 mm slit. The rate of progress of the photographic plate was 60 mm/min. A single preliminary microphotogram was made up on one film plate from six microphotograms of sections of the K_{β_5} band of differing heights, before the measurement of each duplicated spectrogram. This method made it possible to see the structure of the whole line with respect to height and enabled the researcher to avoid possible errors.

Experimental Data

FeK_{β_5} and $FeK_{\beta_1\beta_1}$ lines of the fourth order of reflection were obtained at 1000° from pure iron and from iron-chromium alloys containing 4, 8, 20, 30, 45 and 50% chromium.

The experimental conditions under which the duplicated spectrograms were obtained are given in Table 2.

TABLE 2

Объект исследований	Температура образца, °С	Символ линии	Режим съемки		
			напряжение, кв	ток, ма	амп. час.
Хром	1000	Cr $K_{\beta', \beta_1, \beta_5}$ III	35	6,0	50
Сплав № 4 (30% Cr)	1000	Cr $K_{\beta', \beta_1, \beta_5}$ III	35	4,5	100
Сплав № 5 (45% Cr)	1000	Cr $K_{\beta', \beta_1, \beta_5}$ III	35	4,4	115
Сплав № 6 (50% Cr)	1000	Cr $K_{\beta', \beta_1, \beta_5}$ III	35	4,5	100
Железо γ	1000	Fe $K_{\beta', \beta_1, \beta_5}$ IV	35	6,4	60
Сплав № 1 (4% Cr)	1000	Fe $K_{\beta', \beta_1, \beta_5}$ IV	35	5,0	60
Сплав № 2 (8% Cr)	1000	Fe $K_{\beta', \beta_1, \beta_5}$ IV	35	4,6	60
Сплав № 3 (20% Cr)	1000	Fe $K_{\beta', \beta_1, \beta_5}$ IV	35	4,5	80
Сплав № 4 (30% Cr)	1000	Fe $K_{\beta', \beta_1, \beta_5}$ IV	35	4,5	90
Сплав № 5 (45% Cr)	1000	Fe $K_{\beta', \beta_1, \beta_5}$ IV	35	4,4	115
Сплав № 6 (50% Cr)	1000	Fe $K_{\beta', \beta_1, \beta_5}$ IV	35	4,5	120

Analysis of Spectrograms

For calculation of the wavelengths of the spectral lines we used the equation

$$\lambda_x = \frac{2d_n}{n} \sin \varphi_x = \frac{2d_n}{n} \sin\left[(l_0 \pm \Delta l)\frac{90}{\pi r}\right], \qquad (4)$$

where d_n is the constant of the crystal lattice with an n-order of reflection;

l_0 is the calculated distance from the center of the crystal to the standard spectral line;

Δl is the measured distance from the unknown line to the standard line, mm;

$\frac{90}{\pi r}$ is the constant.

The value of the constant was determined by the equation

$$l_1 - l_2 = \frac{\pi r}{90}(\varphi_1 - \varphi_2), \qquad (5)$$

where: $(l_1 - l_2)$ is the measured distance between the known standard spectral lines registered on the film, mm;

φ_1, φ_2 are the calculated Wulf-Bragg angles for the same lines.

The distance Δl between the lines $CrK_{\alpha I\ III}$ - (λ = 2285.0 XE) and $FeK_{\beta I\ IV}$ - (λ = 1752.99 XE) established by photometric measurement of the spectrograms was in our case 16.01 mm.

Substituting this value and the corresponding values of the Bragg angles for the lines $CrK_{\alpha\ I\ III} = FeK_{\beta I\ IV}$ in Eq. (5), we find

$$\frac{90}{\pi r} = \frac{\Delta\varphi}{\Delta l} = \frac{55,66188 - 53,82805}{16,01} = \frac{1,83383}{16,01} = 0,11456 \text{ град/мм.}$$

The constancy of this value was checked throughout our work at fixed intervals.

The lines $CuK_{\alpha I\ IV}$ and $CrK_{\alpha\ I\ III}$ respectively, were taken as standard spectral lines in calculating the spectrograms of chromium and iron.

In computing the l_0 distances of the chromium and copper K_{α_1} lines from the crystal center, the wavelengths were taken from published data [9]

$$\lambda = 2285,00\ XE,$$
$$\lambda = 1537,40\ XE.$$

l_0 was calculated from the formula

$$l_0 = \frac{\pi r}{90} \varphi_0,$$

where φ_0 was found from the relationship

$$\sin \varphi_0 = \frac{\lambda_{отр}}{2d_n} \qquad (7)$$

In our case the l_0 distances from the crystal center to the K_{α_1} lines of chromium and copper were respectively 469.864 and 405. 026 mm.

Further calculations of the location of the maxima for the K_{β_1} and K_{β_2} lines of chromium and iron were made, using Eq. (4).

TABLE 3

Символ линий	$\Delta\lambda/\Delta l$, XE/мм	$\Delta\nu/\Delta l$, эВ/мм	$\Delta\nu/R/\Delta l$, ν/R/мм
Cr $K\beta_{5\ III}$	4,144	11,195	0,826
Fe $K\beta_{5\ IV}$	2,430	9,917	0,732

Other quantities related to the derived wavelength were calculated according to the equations:

$$\lg(\nu/R) = 5{,}9596486 - \lg\lambda, \qquad (8)$$

$$\lg\nu = 7{,}0911491 - \lg\lambda, \qquad (9)$$

where the value for λ is given in XE.

Table 3 gives data on the dispersion in the K_{β_5}-line region for chromium and iron, calculated according to the equations:

$$\Delta\lambda/\Delta l = \frac{2d_n}{nR}\cos\varphi \ \text{XE/мм}, \qquad (10)$$

$$\Delta\nu/\Delta l = \frac{\operatorname{cotg}(n\lambda)}{8{,}09R\lambda}10^8 \ \text{эл.-в/мм}, \qquad (11)$$

$$\Delta\nu/R/\Delta l = \frac{\operatorname{cotg}(n\lambda)\,9{,}1245}{R\lambda}\nu R/\text{мм}. \qquad (12)$$

TABLE 4

№ спектрограммы	Объект исследования	Температура образца, °С	Стандартная линия	Δl/Cr $K_{\alpha_1\,III}$ — Fe $K_{\beta_1\,IV}$, мм	Δl/Cr $K_{\alpha_1\,III}$ — Fe $K_{\beta_5\,IV}$, мм
112/56	γ-железо	1000	Cr $K_{\alpha_1\,III}$	15,98	10,78
113/56	γ-железо	1000	Cr $K_{\alpha_1\,III}$	15,97	10,78
				Ср. = 15,975	Ср. = 10,78
124/56	Сплав № 1	1000	Cr $K_{\alpha_1\,III}$	15,96	10,77
125/56	То же	1000	Cr $K_{\alpha_1\,III}$	15,94	10,78
				Ср. = 15,950	Ср. = 10,775
136/56	Сплав № 2	1000	Cr $K_{\alpha_1\,III}$	15,97	10,78
137/56	То же	1000	Cr $K_{\alpha_1\,III}$	15,98	10,77
				Ср. = 15,975	Ср. = 10,775
138/56	Сплав № 3	1000	Cr $K_{\alpha_1\,III}$	15,99	10,79
139/56	То же	1000	Cr $K_{\alpha_1\,III}$	15,96	10,78
				Ср. = 15,975	Ср. = 10,785
132/56	Сплав № 4	1000	Cr $K_{\alpha_1\,III}$	15,98	10,78
134/56	То же	1000	Cr $K_{\alpha_1\,III}$	15,97	10,78
				Ср. = 15,975	Ср. = 10,780
119/56	Сплав № 5	1000	Cr $K_{\alpha_1\,III}$	15,98	10,78
120/56	То же	1000	Cr $K_{\alpha_1\,III}$	—	—
				15,980	10,780
115/56	Сплав № 6	1000	Cr $K_{\alpha_1\,III}$	15,99	10,79
118/56	То же	1000	Cr $K_{\alpha_1\,III}$	15,98	10,78
				Ср. = 15,985	Ср. = 10,785

Tables 4 and 5 give the initial data for computating the spectrograms obtained for chromium and iron, and Table 6 contains summarized data for calculations of the wavelengths of the K_{β_1}, K_{β_5} lines and the energy for the $M_{II,III}$ and $M_{IV,\,V}$ levels of chromium and iron, expressed in Rydberg constants and compiled from measurements of the corresponding spectrograms. The figures given in Table 6 show that only in the CrK_{β_5} line is there observed a considerable displacement of the maximum toward longwaves with an increasing concentration of iron in alloys of the iron-chromium system. The position

of the maxima of the other lines in all cases remain constant, within the limits of errors in measurements.

TABLE 5

№ спектрограмм	Объект исследования	Температура образца, °С	Стандартная линия	Δl/Cu $K_{\alpha_1\ IV}$ — Cr $K_{\beta_1\ III}$, мм	Δl/Cu $K_{\alpha_1\ IV}$ — Cr $K_{\beta_5\ III}$, мм
127/56	Хром	1000	Cu $K_{\alpha_1\ IV}$	7,92	4,29
128/56	То же	1000	Cu $K_{\alpha_1\ IV}$	7,91	4,28
				Ср. = 7,915	Ср. = 4,285
116/56	Сплав № 6	1000	Cu $K_{\alpha_1\ IV}$	7,87	4,32
117,56	То же	1000	Cu $K_{\alpha_1\ IV}$	7,88	4,34
				Ср. = 7,875	Ср. = 4,330
122/56	Сплав № 5	1000	Cu $K_{\alpha_1\ IV}$	7,87	4,38
123/56	То же	1000	Cu $K_{\alpha_1\ IV}$	—	—
				7,870	4,380
129/56	Сплав № 4	1000	Cu $K_{\alpha_1\ IV}$	7,90	4,41
135/56	То же	1000	Cu $K_{\alpha_1\ IV}$	7,90	4,49
				Ср. = 7,900	Ср. = 4,450

Photometric Analysis of Spectrograms

Figures 1 through reproduce some of the microphotograms of the duplicated spectrograms K_{β_5} lines for chromium and iron obtained from the pure metals and iron-chromium alloy at 1000°. From these it follows that it is only in the CrK_{β_5} - band that the shortwave branch is not obscured by the $K_{\beta III}$ satellite is clearly superimposed on the shortwave branch of the K_{β_5} band, and is simple in shape. The microphotograms show that in studying the shape and the breadth of the FeK_{β_5} line it is essential to break up the line into its components parts.

TABLE 6

Объект исследования	Символ линии	Источники данных	λ			ν/R III, V	ν/R III, V	Ошибки измерения		
			XE	V	ν/R			XE	ва	ν/R
Железо	Fe K_{β_1}	Таблич-ные	1752,99	—	519,84	4,1	—	—	—	—
	Fe K_{β_3}		1740,54	—	523,56	—	0,29	—	—	—
Железо и сплавы железо—хром № 1, 2, 3, 4, 5, 6	Fe K_{β_1}	Экспери-ментальные	1752,99	7042,25	519,84	4,06	—	—	—	—
	Fe K_{β_3}		1740,43	7093,06	523,59	—	0,31	±024	±099	±007
Хром	Cr K_{β_1}	Таблич-ные	2080,60	—	437,98	3,1	—	—	—	—
	Cr K_{β_3}		2066,53	—	440,97	—	0,14	—	—	—
Хром и сплавы железо—хром № 4, 5, 6	Cr K_{β_1}	Экспери-ментальные	2080,48	5933,73	438,01	3,09	—	—	—	—
Хром	Cr K_{β_3}	То же	2066,53	5973,77	440,97	—	0,13	±041	±0112	±008
Сплав № 6	Cr K_{β_3}	»	2066,69	5973,32	440,93	—	0,17	±041	±0112	±008
Сплав № 5	Cr K_{β_3}	»	2066,88	5972,77	440,89	—	0,21	±041	±0112	±008
Сплав № 4	Cr K_{β_3}	»	2067,16	5971,96	440,83	—	0,27	±041	±0112	±008

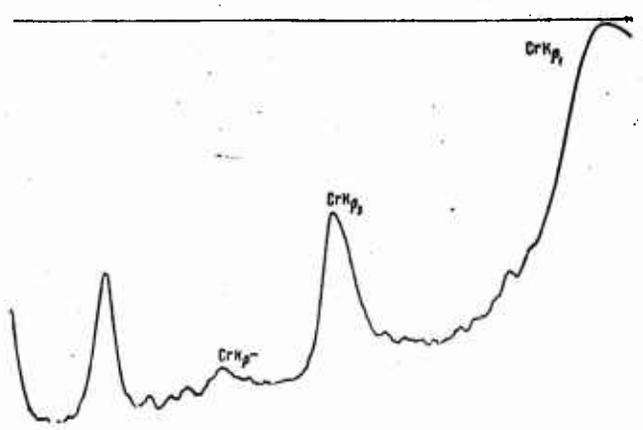

Fig. 1. CrK$_{\beta_5}$ line for chromium.

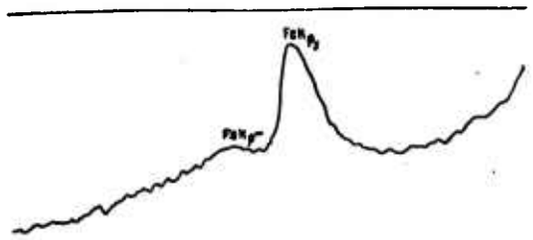

Fig. 2. FeK$_{\beta_5}$ line for Iron.

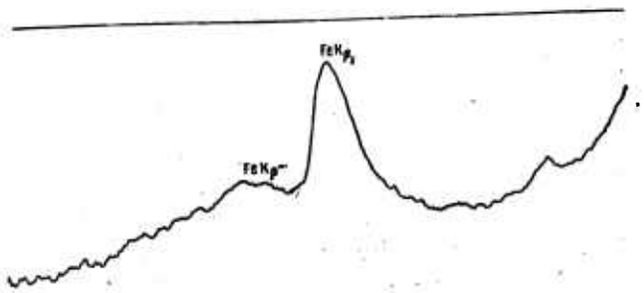

Fig. 3. FeK$_{\beta_5}$ line for Alloy No 6 (50% Cr).

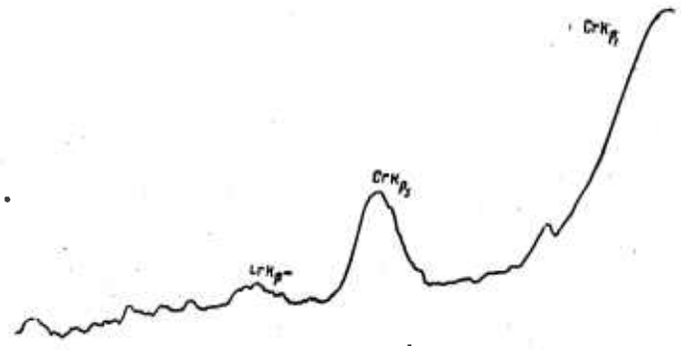

Fig 4. CrK$_{\beta_5}$ line for alloy No 6 (50% Cr).

Treatment of Microphotograms

The treatment of the microphotograms is briefly this [1].

On the assumption that the change in the magnitude of the background within a short section of the spectrum is a linear function, a straight line is drawn tangentially to the two branches of the K_{β_5} band. Through the points of minimum density of the background a straight line is drawn parallel to the dark line recorded on the microphotogram, which was taken as the fog line. The whole of the microphotogram is divided into equal sections of 1.5 mm by vertical lines, corresponding to 0.075 mm on the film, at a magnification of 20. Each point where the vertical lines interject with the contour of the band, the photodensities of the $S_{c'}$ contour are calculated without the background by the equation

$$S_{\kappa'} = S_{\kappa} - S_{\phi} = \lg \frac{i_{\phi}}{i_{\kappa}}, \tag{13}$$

where i_{bg} and i_c are the distances from the dark line to the corresponding points of the background and of the band contour measured in the microphotogram. For the values for $S_{c'}$, we calculated the values of the $i_{c'}$ distances from the dark line to the corresponding points on the band contour, reduced to a common fog value, according to the equation

$$\lg i_{\kappa'} = \lg i_{v'} - S_{\kappa'}, \tag{14}$$

where $i_{v'}$ is the distance from the dark line to fog.

The contour of the K_{β_5} band without the background, reduced to the common fog value, is then plotted, from the values of $i_{c'}$.

The breakdown of the composite contour of the FeK_{β_5} band into components is done by the method of successive subtraction at each point on the K_{β_5}-band contour of the photodensities of the $K_{\beta'''}$ satellite. Considering the symmetry of the resolved $CrK_{\beta'''}$ satellite, it is assumed that the $FeK_{\beta'''}$ satellite also preserves this form.

The computation kinetic energy of the electrons in the conductivity band $T_{max} = (E_{max} - E_o)$ is calculated by Eq. (10):

$$T_{\text{макс}} = \frac{\gamma_n}{1 - \frac{1}{n^{1/2}}}, \qquad (15)$$

where γ_n is the breadth of the K_{β_5} band measured at different cross sections of its contour with

$$n = \frac{I_{\text{макс}}}{I_n} = \frac{S_{\text{макс}}}{S_n}.$$

Table 7 gives the computation of a microphotogram where i_n is the distance from the dark line to the point of the band contour that corresponds to the given n.

Table 8 gives composite figures for T_{max}, the kinetic energy of electrons, and similar figures for the n-number of the "outer" electrons per atom in the conductivity band. The value of n is found by Eq. (7):

$$n = 0{,}00453 V_a T_{\text{макс}}^{3/2}, \qquad (16)$$

As can be seen in Table 7, Eq. (15) shows the path of the long-wave branch of the K_{β_5} -band with sufficient accuracy only in its center section.

TABLE 7

Calculation of Microphotogram No. 12. Spectrogram No. 118/56 (FeK_{β_5} of Alloy No. 6)

n	$1-\frac{1}{n^{1/3}}$	S_n	lg t_n	t_n	$\frac{y}{мм}\times 20$.	y, мм	y, ев	$T_{макс}$
1,00	0,00000	0,19691	1,84448	69,9	0,0	0,000	0,000	—
1,25	0,13823	0,15752	1,88387	76,5	5,7	0,285	2,825	20,436
1,50	0,23686	0,13127	1,91012	81,3	7,4	0,370	3,668	15,485
2,00	0,37004	0,09845	1,94294	87,7	10,0	0,500	4,956	13,393
3,00	0,51926	0,06563	1,97576	94,6	14,1	0,705	6,989	13,459
5,00	0,65801	0,03938	2,00201	100,5	17,9	0,895	8,872	13,483
7,00	0,72672	0,02813	2,01326	103,1	20,6	1,030	10,210	14,049
9,00	0,76888	0,02188	2,01951	104,6	22,3	1,110	11,003	14,345
12,00	0,80920	0,01641	2,02498	105,7	24,0	1,200	11,896	14,700
15,00	0,83548	0,01313	2,02826	106,7	25,8	1,290	12,788	15,206

$T_{макс.\ ср}$ $(n = 2, 3, 5, 7) = 13,596$

TABLE 8

Объект исследования	Состав, %		№ спектра		$T_{макс}$, ев		$T_{макс.\ ср.}$ ев.		V_a Å³		n	
	Fe	Cr	Fe	Cr	Fe K_{β_5}	Cr K_{β_5}	Fe K_{β_5}	Cr K_{β_5}	Fe	Cr	Fe	Cr
Fe α	100	0	141/56	—	16,34	—	16,2	—	12,07	—	3,57	—
			144/56	—	16,08	—						
Fe γ	100	0	112/56	—	15,49	—	15,48	—	12,25	—	3,38	—
			113/56	—	15,47	—						
Сплав № 1	96	4	124/56	—	15,45	—	15,38	—	—	—	—	—
			125/56	—	15,32	—						
Сплав № 2	92	8	136/56	—	15,21	—	15,16	—	12,236	—	3,27	—
			137/56	—	15,10	—						
Сплав № 3	80	20	138/56	—	14,76	—	14,83	—	11,932	—	3,09	—
			139/56	—	14,90	—						
Сплав № 4	70	30	132/56	129/56	14,59	16,12	14,48	15,96	11,904	11,904	2,97	3,44
			134/56	135/56	14,38	15,80						
Сплав № 5	55	45	119/56	122/56	13,63	15,22	13,76	15,39	11,857	11,857	2,74	3,24
			120/56	123/56	13,88	15,56						
Сплав № 6	50	50	115/56	116/56	13,61	15,29	13,60	15,31	11,857	11,857	2,70	3,22
			118/56	117/56	13,60	15,33						
Cr	0	100	—	127/56	—	12,91	—	12,99	—	12,47	—	2,65
			—	128/56	—	13,07						

where V_a is the atomic volume expressed in cubic angstroms.

A correlation of the values of the lattice constants of Cr, Fe_α, F_γ and of iron-chromium alloys for a temperature of 1000° was made, with account taken of the coefficients of linear expansion obtained from the dilatometric curves.

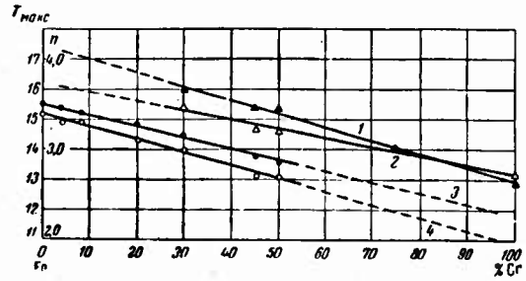

Fig. 5. Dependence of T_{Cr} (1), n_{Cr} (2), T_{Fe} (3), n_{Fe} (4) in the iron-chromium system.

Figure 5 shows a graph of the dependence of T_{max} and the number n plotted from the data in Fig. 8 and illustrates the linear dependence of these quantities on the concentration of the alloy components. Of special interest is the path of these straight lines in the region of low concentration.

Conclusions

1. Using a spectrograph with a high-ratio aperture (radius of crystal curvature 500 mm) and with a tube suited to high temperature spectography, we obtained emissivity lines of the K group from pure chromium and iron and from iron-chromium alloys containing 4, 8, 20, 30, 45, and 50% Cr by the primary excitation method at 1000° with an oscillating crystal.

2. The transition of chromium and iron into an iron-chromium alloy within the range of concentration studied and also the transition of the γ-phase into the α-solid solution have no effect on the position of the maxima of the FeK_{β_1}, FeK_{β_5}, and CrK_{β_1} lines, within the limits of errors in measurement (Table 6.).

3. The position of the maximum of the CrK_{β_5} band is displaced toward the longwaves as the concentration of iron in iron-chromium alloys increases; this is connected with an increase in the value (absolute) of the energy of the 3d-shell of the chromium atoms (Table 6).

4. The breadth of the conductivity band and the number n of "outer" electrons per atom, in all cases examined are different for chromium and iron, decreasing for iron with a greater chromium concentration in iron-chromium alloys and, conversely, increasing for chromium with a greater concentration of iron (Table 8).

5. Within the range of concentration of the components of iron-chromium alloys studied we observed a linear dependence on the concentration of the components in iron-chromium alloys of the value for T_{max} (the kinetic energy of electrons) and the number n the "outer" electrons per atom in the conductivity band of chromium and iron (Fig. 5).

6. The differences found in the energy states of the chromium and iron atoms in the α solid solution of iron-chromium alloys at 1000°, within the range of concentrations studied, require additional thorough study of the fine structure of the x-ray bands in order to determine the nature of the influence of individual factors on that structure.

References

1. BORISOV, N. D. and FEFER, A. M. Spectroscopy of the solid state of metals and alloys as a method of studying the electronic structure of their conductivity zone. (Spektroskopiya tverdogo stanu metaliv ta splaviv yak metod vyvchenya elektronnoi strukturi ikh zoni providnosti). Ukrains'kiy fizichniy zhurnal, AN SSSR, 1956. (Ukrainian Journal of Physics, Acad. Sci. USSR).

2. SKINNER, H. W. Phil. Trans. Roy. Soc., A239, 95, 1940.

3. BORISOV, N. D. and FOGEL', Y. M. Journ. Techn. Phys, 7, No. 12, 1946.

4. BORISOV, N. D. and FOGEL', Y. M. ZhTF, 7, No. 2, 1937.

5. BORISOV, N. D. ZhTF Journ. Exp. Theor. Phys.), 6, No. 5, 1936.

6. BORISOV, N. D. Trudy Instituta Chernoy Metallurgii AN USSR Papers of Ferrous Metallurgical Institute of Acad Sci USSR, Vol. VI, 1953.

7. BLOKHIN, M. A. Fizika rentgenovshikh luchey, x-ray physics, Moscow, 1953.

8. BORISOV, N. D. K voprosu vybora optimal'nykh usloviy syemki i fotografirovaniya rentgenovskikh polos, (Concerning the choice of optimum conditions for recording and photography of x-ray bands. Fizika metallov i metallovedeniye, AN SSSR, 1957. Physics of Metals and Metallurgy, Acad Sci USSR.

9. VAYNSHTEYn, E. Y. and KOKHANA, M. M. Spravochnye tablitsy rentgenovskoy spektroskopii (x-ray Spectrographic Tables), Izd. AN SSSR, Acad. Sci. USSR Press, Moscow, 1953.

10. VAYNSHTEYN, E. Y. Rentgenovskiye spektry atomov v molekulakh khimicheskikh soyedineniy i splavakh (x-ray spectra of atoms in molecules of chemical compounds and alloys, Moscow-Leningrad 1950.

THE THEORY OF DILUTE SOLID SOLUTIONS

I. B. Borovskiy and K. P. Gurov

Sound theoretical concepts of the alloying mechanism in heat-resistant alloys are essential if the problem of alloying these is to be effectively solved. Owing to the complexity of the question, it is possible at the present time to make only a rough, qualitative, and theoretical study which to a large degree is semi-empirical in nature.

Most of the properties of solid solutions are determined by their atomic and electronic structure, which it is possible to study with adequate thoroughness only if the whole range of available physico-chemical methods of analysis are applied. Such was our purpose in investigating x-ray spectra [1], self-diffusion [3], and the coefficient of linear expansion [11] in solid solutions.

Much of the available experimental data gives direct evidence of the tremendous effect of small quantities of admixtures on the physical properties of condensed systems. The meaning of the term "small quantity of admixture" varies quantitatively in systems with different properties. A small admixture in the transition metals is an addition of the order of 10^{-1} to 10^{-3} atom %. Hence the problem of purity in a base metal acquires considerable importance.

We studied the change in the characteristics of x-ray spectra of chromium as a function of its purity; the materials used were hydrogenized, electrolytic, and iodized chromium. We then studied the

influence of molybden admixtures on the characteristics of the electrolytic chromium x-ray spectrum.

The characteristics studied were the following: its position on the energy scale, the shape of the chromium emissivity lines (K_{B_1}, K_{B_5}), the K absorption edge and the index of unsymmetry of the $K_{d,de}$ lines. Special attention was paid in the work to the question of methods of eliminating the possible influence of the excitation potential on the indices of unsymmetry of the "last spectral lines" (with regard to the absorption of radiation by the anode) and on the thickness of absorbers on the line structure of the basic absorption edge 1.

The results of the x-ray spectragraphic studied are given in Table I and Fig. 1.

An approximate evaluation of the influence of the atomic concentration of admixtures and temperature was made, using lead-tin alloys in the temperature range − 190 to + 300° from the L_{III} absorption spectra of lead. Despite the fact that in previous studies of the change in the fine structure of absorption spectra caused by temperature the latter was considered only in respect to its influence on the scattering (the change in the fine structure on the shortwave side of the basic absorption edge 2), it physically seemed clear to us that the vibration of the atoms in the lattice of metals and alloys, reaching 10-15% of the interatomic distance at temperatures close to the melting point must also exert substantial influence on the whole electron energy spectrum of the crystal. The question of the influence of admixtures on the "melting away" of the fine structure of the absorption spectrum was raised for the first time in connection with the idealized conceptions which we have recently been developing

regarding the theory of regarding dilute solid solutions [3].

L_{III} absorption spectra of lead in lead metal and lead-tin alloys containing 0.2, 0.5, 2.0, 10% tin were studied in a spectrograph with a bent crystal, using the "pass-through" method (the linear dispersion was 4 XE/mm).

The structure of the alloys was determined from the results of the x-ray structural studies which confirmed the fact that all alloys are solid solutions (the 10% tin alloy was prepared by quenching from 200°). The absorption spectra were obtained at four or five temperatures in the range from -190 to 300°. The photographs were taken in a special vacuum camera (1.10^{-5} mm Hg.). The absence of oxidation at higher temperatures in the operation was verified by photographs the same specimen at a high temperature and then at room temperature. L_{III} absorption spectra of lead in PbO and PbO_2 were specially photographed for additional control.

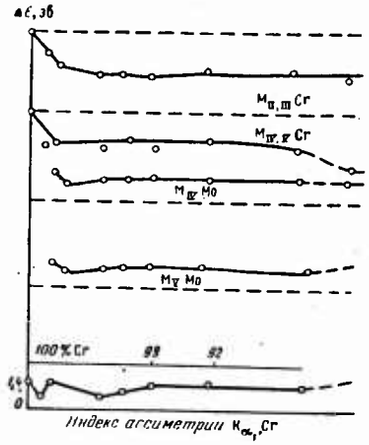

Fig. 1. Changes in relative values of $M_{II,III}$ and $M_{IV,V}$ energy levels of chromium of M_{II}, III and $M_{IV,V}$ energy levels of molybdenum, and the unsymmetry index of the K_{α_1} line of chromium in chromium-molybdenum alloys.

TABLE 1

Вид хрома	K_{β_1}, XE эв	K_{β_2}	K-край	K_{α_1}
Иодидный № 1	2080,41±0,04 5946,1±0,1	2066,45±0,03 5986,3±0,1	2065,76±0,08 5988,3±0,3	1,30±0,06
Электролитический № 2	2080,61±0,05 5945,5±0,1	2066,59±0,03 5986,0±0,1	2066,03±0,06 5987,5±0,2	1,40+0,06
Гидридный № 3	2080,79±0,04 5945,0±0,1	2066,73±0,03 5985,5±0,1	2066,1±0,1 5987,5±0,3	1,20±0,04

The absorption spectra, averaged for all the microphotograms, obtained are represented by the curves in Fig. 2 (each curve is an average for 4 or 5 spectrograms), and Table 2 gives the wavelengths of the characteristic points on the L_{III} edge.

An analysis of the results obtained enables the following conclusions:

1. A change in parameters of the $K_{\ 1}$, $K_{\ }$, $K_{\ 5}$ of the spectrum for all three specimens of chromium metal of varying purity is firmly established experimentally (we should recall that two of these lines, $K_{\ 1}$, and K_{d_1} originate theory transitions between deep atomic levels 1s 2p, 1s - 3p.

As the impurity content diminishes in the chromium form hydrogenized to iodized chromium $K_{\ 1}$ and $K_{\ 5}$ lines are displaced towards the shortwave side. The unsymmetry index for the $K_{\ }$, line changes sharply. The position of the K absorption edge and the path of the absorption coefficient remain unchanged.

2. As an indicator of the relative behavior of the electron energy spectrum in the transition from pure metals to alloys, we can take the absolute value of the energy-level change with respect to the energy of the corresponding levels of pure chromium and molybdenum. It is assumed in this comparative evaluation that the (1s) energy level for atoms in a pure metal or in an alloy remains constant. The energy of the $M_{II,III}$ Cr level increases in absolute value during the transition from electrolytic chromium to alloys with an admixture of 0.14 to 1% (remaining further unchanged up to 31% molybdenum). A similar displacement occurs for the $M_{IV,V}$ level of chromium.

However, having undergone appreciable displacement in the region of low impurities content, this level retains a constant displacement in absolute value in relation to pure chromium, up to alloys containing 2.50% molybdenum.

TABLE 1

Вид хрома	K_{β_1}, XE / эв	K_{β_2}	K-край	K_{α_1}
Иодидный № 1	2080,41±0,04 5946,1±0,1	2066,45±0,03 5986,3±0,1	2065,76±0,08 5988,3±0,3	1,30±0,06
Электролитический № 2	2080,61±0,05 5945,5±0,1	2066,59±0,03 5986,0±0,1	2066,03±0,06 5987,5±0,2	1,40+0,06
Гидридный № 3	2080,79±0,04 5945,0±0,1	2066,73±0,03 5985,5±0,1	2066,1±0,1 5987,5±0,3	1,20±0,04

The absorption spectra, averaged for all the microphotograms, obtained are represented by the curves in Fig. 2 (each curve is an average for 4 or 5 spectrograms), and Table 2 gives the wavelengths of the characteristic points on the L_{III} edge.

An analysis of the results obtained enables the following conclusions:

1. A change in parameters of the K_{1}, $K_{}$, K_{5} of the spectrum for all three specimens of chromium metal of varying purity is firmly established experimentally (we should recall that two of these lines, K_{1}, and K_{d_1} originate theory transitions between deep atomic levels 1s 2p, 1s - 3p.

As the impurity content diminishes in the chromium form hydrogenized to iodized chromium K_{1} and K_{5} lines are displaced towards the shortwave side. The unsymmetry index for the $K_{}$, line changes sharply. The position of the K absorption edge and the path of the absorption coefficient remain unchanged.

2. As an indicator of the relative behavior of the electron energy spectrum in the transition from pure metals to alloys, we can take the absolute value of the energy-level change with respect to the energy of the corresponding levels of pure chromium and molybdenum. It is assumed in this comparative evaluation that the (1s) energy level for atoms in a pure metal or in an alloy remains constant. The energy of the $M_{II,III}$ Cr level increases in absolute value during the transition from electrolytic chromium to alloys with an admixture of 0.14 to 1% (remaining further unchanged up to 31% molybdenum). A similar displacement occurs for the $M_{IV,V}$ level of chromium.

However, having undergone appreciable displacement in the region of low impurities content, this level retains a constant displacement in absolute value in relation to pure chromium, up to alloys containing 2.50% molybdenum.

TABLE 2

Position of the Maximum and Minimum Fluctuations of L_{III} Absorption Spectra of Lead in the Energy Scale

Температура, °С	№№	Pb					
		1		2		3	
		max	min	max	min	max	min
300							
200	Энергии, эв	—	—	—	—	—	—
20		13046	13048	13060	13071	13084	—
—190		13046	13050	13057	13071	13078	13102

Температура, °С	№№	PbSn (0.2% Sn)						PbSn (0.5% Sn)					
		1		2		3		1		2		3	
		max	min	max	min	max	min	max	min	max	min	max	min
300	Энергии, эв	13048	13050	—	—	—	—						
200		13047	13050	13061	13072	13088	—	13049	13050	13062	13069	—	—
20		13046	13048	13060	13072	13083	—	13047	13050	13060	13070	13084	—
—190		13048	13050	13062	13072	13088	13103	13047	13050	13060	13069	13083	13102

Температура, °С	№№	PbSn (2% Sn)						PbSn (10% Sn)					
		1		2		3		1		2		3	
		max	min	max	min	max	min	max	min	max	min	max	min
300	Энергии, эв	—	—	—	—	—	—						
200		13048	13050	13064	13072	—	—	—	—	—	—	—	—
20		13045	13048	13060	13070	13082	—	13046	13047	13060	13067	13078	—
—190		13046	13050	13062	13071	13086	13102	13046	13050	13060	13072	13086	13098

In alloys with a higher concentration of molybdenum a further increase in absolute value for energy of the $M_{VI, V}$ level of chromium

is observed*.

From our viewpoint, the practically constant value of the unsymmetry index of the K_{α_1, α_2} Cr lines in all the alloys studied (excluding the 0.07 %) is experimental confirmation of our original assumption of the constancy of K-level energy in chromium atoms in alloys.

---

* Examination of the behaviour of the $M_{IV, V}$ and $N_{IV, V}$ levels of molybdenum in alloys shows that the energy of these levels increases in absolute value when the chromium content in molybdenum is small (up to 1%). A further increase in chromium concentration reduces the absolute value of these energies. Here the $M_{IV,V}$ levels nearly retain their absolute energy value, with a tendency toward a slight decrease in alloys with a higher chromium content. Initially there is a characteristic sharp decrease in the absolute energy value of the $N_{IV, V}$ levels, proves that the latter acqures a surplus positive charge as compared with their charge in pure metal, whereas the decrease in the absolute value of the energy levels indicates a reduction in the effective charge of the nucleus.

Consideration of the experimental results from this stand point leads to the assumption that in chromium-molybdenum (as an admixture) carries surplus negative charge, whereas chromium (as the base), carries a positive charge relative to its charge in a pure state. However, the change in sign has no effect on the shape of the K_{β_5} Cr and L_{β_2} Mo lines since, as an average (per atom) it is small.

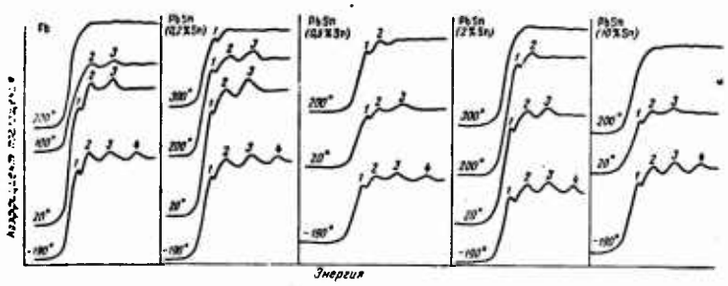

Fig. 2. Fine structure of L_{III} absorption edge for lead-tin alloys at different temperatures and concentration of Sn.

Figure 3 gives the results of the study of the change in the self-diffusion coefficient for α iron and its alloys with chromium, molybdenum, and tungsten as a function of their concentrations and temperature. A method developed for this particular purpose [4] enabled us to determine the values of the self-diffusion coefficients with a very low error factor 7 to 9%. Let us note the principle result of the data which is the minima of self-diffusion coefficients for small concentrations of admixtures of an order of 10^{-1}%.

The following general conclusions can be drawn from the above:

A small admixture changes the whole electron energy spectrum of an alloy when the atoms of the alloys base are those of the elements of the transition groups or of the elements with virtually un-

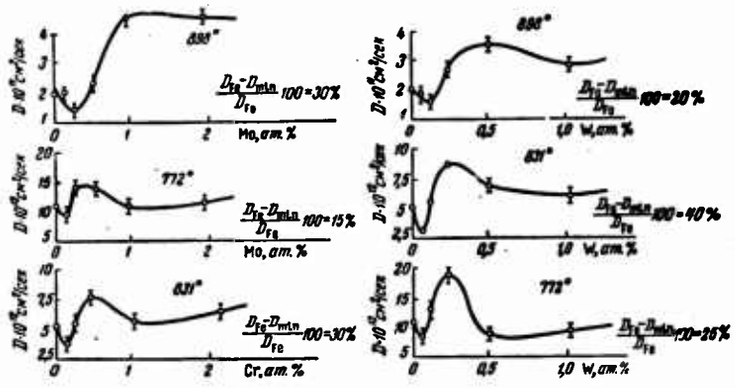

Fig. 3. Change in the self-diffusion coefficient for α Fe depending on concentrations of tungsten, molybdenum, and chromium admixtures.

filled inner levels (5f, Pb);

When an interatomic bond is formed in alloys, the distribution of the energy states is changed at outer valence levels as well as at rather deep levels;

An evaluation of the relative charge of atoms in alloys on the basis of data from x-ray spectral analysis indicates that molybdenum, as an admixture, carries a surplus negative charge, as compared with chromium;

Thermal vibration of atoms not only greatly influences scattering but also affects the entire electron energy spectrum, including the signs of the atoms of the base;

The presence of small amounts of admixtures changes the mobility of the atoms of the base and minimizes the mobility of the atoms of the base and minimizes the mobility of atoms of the transition elements. The change in mobility due to temperature depends on the

sign of the surplus charge of the atoms of the admixture.

These experimental facts, as well as an analysis of the papers [5, 6], led us to develop an idealized concept of the forming of "atomic blocks" in dilute solid solutions based on transition metals. In so doing, we assumed that this is the principal development in the mechanism of alloying transition metals with small additions of admixtures.

Generally speaking, alloying is a very complex phenomenon depending on a great many active factors, such as structure, composition, defects, temperature, and method of processing. Theoretical views therefore, can only be developed by an idealized approach, namely by first considering only one of the factors and then in turn making allowances for the others in the results obtained. An ideal crystalline structure (without defects) at absolute zero temperature was chosen as the original model, i.e., we are considering ideal static conditions.

It was assumed that the atoms of the admixture did not correlate with one another (infinitely dilute solid solution; one atom of the admixture in the metal as the limit). Under these conditions the ideas wer are developing can be summed up in the following fashion.

An admixture (substitutional or interstitial) introduced into a metal transmits its outer electrons to the common conductivity band of the electron spectrum of the base and assumes a charge that in general differs from that of the atomic framework of the base-metal. The number of lost electrons depends on the relative position (on the energy scale) of the electron levels in the admixture atom and on the electron spectrum of the metal base. The excess charge (both signs are possible) of the admixture is considered as a perturbance

causing deformation of both the conductivity band and the other bands of the electron energy spectrum of the base. This disturbing potential is of short duration. Hence the deformation of the electron spectrum is of a local nature and results in a special redistribution of the conductivity electrons (leveling their energies to the Fermi level). This redistribution also affects the electrons of the unfilled inner shells of the atomic framework of the base, and, as a consequence, the charge of the atomic framework of the matrix in the region of the effective disturbing potential is somewhat changed; "induced" admixtures appear, with excess charges opposite in sign to the excess charge of the base alloy. It should be noted that the displacement of the electron energy levels is negligible and only increases as a linear function of the concentration of the admixture in an infinitely diluted solid solution. Consequently this development will not directly affect the fine structure of the x-ray spectra in the zone of small concentrations. However, as has been noted the effective charge of the atomic framework of the base metal is changed in the local zone surrounding the admixture. A positive excess charge of the admixture will result in a decrease in the effective charge of the neighboring atomic frameworks, whereas a negative charge will lead to an increase. This effect can be identified by studying the fine structure of x-ray spectra at finite, though small, concentrations of the admixture. Theoretically the change in the effective charge of the atomic framework of the base can be viewed as the appearance of "induced" admixtures at the corresponding points. The sign of the excess charge of these admixtures is always the opposite of that of the alloy base. Therefore, between the base and the "induced" admixtures, an addi-

tional bond appears, i.e., stable blocks are formed (short range order). When the active zones of the disturbing potentials of the base admixtures overlap interferential effects occur which weaken the additional bonds in the blocks. When there is complete overlapping and the basic admixtures start interacting, the blocks disappear and the normal alloys bonds are established. Consequently there is an optimum concentration of admixtures at which the activity of the blocks is most effective and a maximum concentration at which they occur. This is shown by the path of the curve of the dependence of the self-diffusion coefficient on the concentration of the admixture; the minimum of the curve in the zone of small concentrations, according to our view, corresponds to the optimum zone of concentration of the admixtures.

The active zone of the atomic blocks can only be evaluated theoretically if the density of the energy levels of (n - 1) d, the bands near the Fermi boundary of the electron spectrum of the basic metal, is known from experimental data.

An approximate semi-empiric of the active zone of the blocks can be made from the experimental results for the change in the self-diffusion coefficient (Fig. 3). If we compare the minimum of the self-diffusion coefficient curve with the "close packing" (without overlapping) of the active zones of blocks, a formula for evaluation of the effective radius of the action of an admixture can be derived in a simple way

$$R_{эф} = a\left(\frac{23,9}{x}\cdot C_{min}^{-1}\right)^{1/3},$$

where a is the lattice constant;

x is the number of atoms per elementary lattice cell;

C_{min} is the concentration in atom % corresponding to the minimum

coefficient of diffusion.

Evaluated in this way, the effective radius of action of an admixture was found to be of the order of 10^{-8} cm.

These were theoretically examined in greater detail in an approximation of the so-called "right band", used for the first time in [7]. On this point research [8] has shown that the basic formula $\Delta E = eW(r)$ (ΔE is the change in energy of any level of the electron spectrum, e is the charge on the electron, and W (r) the disturbing potential of the admixture) cannot be derived for this approximation from the general theory of perturbance. However, an approximation of the rigid band can be obtained by approximating the Block function by means of the atomic functions that comply with the rigid conditions of localization.

It should be taken into consideration, in going from an infinitely dilute solid solution to a solid solution in which the added second component is small but finite in content, that in the latter case changes occur in the constants of the elementary lattice cell of the alloy (these changes as a rule do not obey Vegard's law; see,for instance, [9]).

With a change in the lattice parameters, the whole electron spectrum obviously changes. In particular, there is a displacement of the Fermi level E_f. This displacement can be roughly evaluated in the approximation for free electrons from the formula

$$\Delta E_{\Phi} = -\frac{2}{3}\frac{\hbar^2}{2m}(3\pi^2 n)^{1/3} v_0^{-1/3}\Delta v_0,$$

where n is the number of conductivity electrons per atom;

v_0 is the volume per atom.

It is obvious that the bonds in a metal are likewise changed

in this process, so that this rival development should be taken into account.

It is essential to know whether or not the suggested ideal picture of the formation of strengthening blocks obtained at absolute zero (static conditions) is still valid at high temperatures, if we are to apply the results obtained to the problem of heat resistance.

The data obtained for self-diffusion (the occurrence of zones with lower atomic mobility) and the "retarding" of the "melting away", increase in temperature, of the fine structure of lead through small additions of an admixture justify the statement that the block effect is also manifested at high temperatures, although at this point of course thermal effects which destroy the short-range order start to play a considerable role.

Consequently the question becomes one of evaluating two rival effects. At the present time, only qualitative views may be expressed regarding this problem.

The increase in temperature causes a thermal dispersion of the electron energy near the Fermi level (of the Fermi boundary). This development apparently plays the major part in the "melting away" of the first maximum of the fine structure of the absorption edge in the x-ray spectrum for lead.

Moreover, the change in lattice parameters due to temperature must influence the electron structure. As noted above, this results in the displacement of the Fermi level [10]. However, this displacement will not be the same in the conductivity band and in the band corresponding to the electrons with an unfilled shell; the displacement in the latter will be less, resulting in an electron

flow from this band into the conductivity band to bring their energies up to the new Fermi level. This effect signifies a change in the charge of the atomic framework of the base with an increase in temperature.

It is evident that two cases are possible in the local deformation of the energy levels due to the disturbing action of the admixture. In the first case the direction of the local dislocation of the levels coincides with the direction of the displacement of the Fermi level; in the second the displacements occur in opposite directions. In the first instance the effect of forming the induced admixtures around the basic admixture will be weakened, whereas in the second it will be strengthened; the first case is that of an admixture with an excess positive charge, whereas the second case is that of an admixture with a negative charge.

It can be expected, therefore, that an admixture with an excess negative charge maintains its alloying properties at high temperatures whereas an admixture with an excess positive charge lacks this ability. The excess charges of an admixture with respect to the base can be determined, for instance, by experimental electrolysis of solid solutions.

Consequently the conclusions can be drawn from our calculations and observations that in the alloying of transition metals with small amounts of admixtures there is an optimum zone at admixture concentrations of the order of 0.05-0.1 atom %; this zone can be best determined by studying self-diffusion. At high temperatures only a certain class of admixtures (those with excess negative charge with respect to that of the atom framework of the metal base) retain their alloying properties.

REFERENCES

1. BOROVSKIY, I. B.; GUROV, K. P.; DITSMAN, S. A.; BATYREV, B. A.; and LOBANOVA, N. D. Izv. AN SSSR, Fiz. ser., (Bull. Acad. Sci., USSR, Phys. Ser.) No. 10, 1957; BOROVSKIY, I. B. and RONAMI, G, Ibid.

2. HANOWALT, G. Ztschr. f. Phys., 70, 1931.

3. BOROVSKIY, I. B. and GUROV, K. P. Kodl. AN SSSR (Reports of Acad. Sci. USSR) 118, No. 2, 1958.

4. BOROVSKIY, I. B. and MILLER, Yu. G. Research on the Heat-resistant alloys (Issledovaniya po zharoprochnym splavam), Vol. II Izd. AN SSSR, 1957.

5. MOTT, N. and JOHNES, H. The Theory of the Properties of Metals and Alloys. Oxford, 1945.

6. SKINNER, and JOHNSTON. Proc. Camb. Phil. Soc., 34, 1938.

7. FRIEDEL. Advances in Physics, 3, No. 12, 1954.

8. BOROVSKIY, I. B.; GUROV, K. P.; DITSMAN, S. A. and BATYREV, V. A. Research on Heat-Resistant Alloys Vol. II. Izd. AN SSSR, 1957.

9. SUTTON, HUM-ROSERY. Phil. Mag. 46, No. 383. 1955.

10. SKINNER. Nature, 187, 1937.

11. MILLER, Y. G. Dokl. AN SSR, 119, No. 3, 1958.

INFLUENCE OF THE THERMAL VIBRATION OF ATOMS ON THE ELECTRON SPECTRUM OF METALS AND ALLOYS

I. B. Borovskiy and G. N. Ronami

Study of the distribution of the intensity J (ω) through the frequencies in the x-ray emission and absorption spectra enables us to obtain a very important characteristic of solid bodies, such as the distribution of the electron states N (ω) through the energies. The following relationship exists between the characteristics J (ω), N (ω), and the probability of transitions between f (ω) states [1]:

$$J(\omega)=\frac{e^2\hbar^3\omega^2N_0\omega_0G^2}{6\pi^3m^2c^3}\int\int\left\{\left(\frac{\partial E}{\partial k_0}\right)^{-1}\int|\psi_kV\psi_0d\tau|^2\right\}\cdot dk_2dk_3=AN(\omega)f(\omega).$$

The calculation of the values of N (ω) and f (ω) can only be reduced to numerical results in rough approximations for completely free electrons or those with strong bonds at absolute zero [2, 3].

In [4] an attempt has been made to estimate the effect of the vibration of electrons at changing temperatures in solid bodies on the so-called fine structure of the absorption spectra on the short-wave side of the basic edge, and on the structure of the emission bands (in the ultralongwave zone of the x-ray spectrum) [5, 6].

In papers [4, 5] the interaction of an electron ejected during absorption from an atom in the lattice with the photon field of the lattice is considered a minor perturbance. As a consequence of this theoretical reasoning the prediction appeared of the disappearance or "melting away", of the fine structure in the absorption spectrum on the shortwave side of the basic edge with an increase in the temperature of a solid body, (in paper [5], for copper this temperature was estimated from experimental data to be 800°).

The study conducted by us was aimed first at a thorough verification of the conclusions reached in previous theoretical and experimental studies [4, 6], since physically it appeared clear that the vibration of atoms in the lattices of metals and alloys, whose amplitude at high temperatures (near melting points) reach 15-20% of the interatomic distances, must influence more than the mere process of dispersion and should not be considered minor perturbances. Second, we were particularly interested in determining the influence of "small" admixtures on the "melting away" of the fine structure of the absorption spectra in connection with the recently advanced ideas (7) on the formation in dilute solid solutions of "atomic blocks" with reduced mobility among the atoms located in their zone of action.

The L_{III} absorption spectra of lead in lead metal and in lead-tin alloys containing 0.2, 0.5, 2.0, and 10% tin were studied with a bent spectrograph crystal by the "passage" through method. The linear dispersion was 4 XE/mm; the photographic factors: 21.5 kv, 20 ma, exposure time to to 12 hours.

The crystalline structure of the alloys was determined from the results of x-ray structural analysis, which confirmed that all

alloys were solid solutions. The absorption spectra were obtained at four to five different temperatures ranging from -190° to + 300°. The photographs were taken in a special vacuum camera ($1 \cdot 10^{-5}$ mm Hg.).

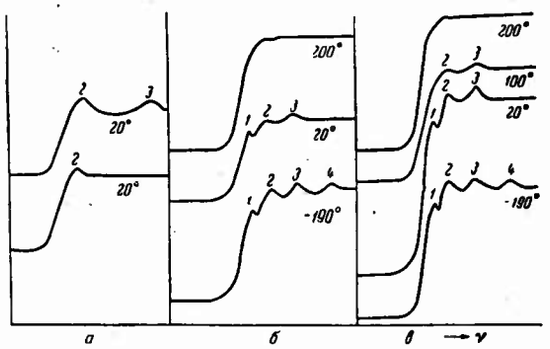

Fig. 1. L_{III} absorption spectra for lead.

a) for compounds of lead with oxygen (PbO and PbO_2);
b) for alloy with 10% Sn; c) for lead metal.

The absence of oxidation during the photography at increased temperature was checked by recording the same specimen at a high temperature and at room temperature. For additional verification special photographs were taken of the L-spectra of PbO and PbO_2.

The absorption spectra averaged for all the microphotograms obtained (each curve being the average for 4 to 5 spectrograms) are shown in Figs. 1 and 2. The wavelengths for characteristic points of L-absorption spectra of lead in the metals and alloys are given in Fig. 1.

An analysis of the results obtained experimentally permits the following conclusions:

1. Besides the well-known phenomenon of "melting away" of the

TABLE 1

Wavelengths in the fine structure of the L_{III} edge

(a) Длина волн для тонкой

Температура, °C		Pb				
		1	2	3	4	1
300	λ_{XE} $E_{эв}$					948 13048
200	λ_{XE} $E_{эв}$	— —	— —	— —	— —	948,1 13047
100	λ_{XE} $E_{эв}$	— —	947,3 13059	945,3 13086	— —	
20	λ_{XE} $E_{эв}$	948,2 13046	947,2 13060	945,4 13084	— —	948,2 13046
—190	λ_{XE} $E_{эв}$	948,2 13046	947,4 13057	945,8 13078	943,3 13112	948 13048

Температура, °C		PbSn (2% Sn)				PbSn (10% Sn)		
		1	2	3	4	1	2	3
300	λ_{XE} $E_{эв}$	— —	— —	— —	— —			
200	λ_{XE} $E_{эв}$	948 13048	947 13064	— —	— —	— —	— —	— —
100	λ_{XE} $E_{эв}$							
20	λ_{XE} $E_{эв}$	948,3 13045	947,2 13060	945,6 13082	— —	948,2 13046	947,2 13068	945,8 13078
—190	λ_{XE} $E_{эв}$	948,3 13046	947 13062	945,3 13086	943,3 13112	948,2 13046	947,2 13060	945,3 13086

Длины волн для

	Pb	Pb Sn (0,2% Sn)	Pb Sn (0,5% Sn)
λ_{XE} $E_{эв}$	948,8 13038	948,8 13038	948,8 13038

TABLE 1

(continued)

(в) Таблица 1

структуры L_{III}-края

PbSn (0.2% Sn)			PbSn (0.5% Sn)			
2	3	4	1	2	3	4
—	—	—				
—	—	—				
946,9 13064	945,2 13088	— —	948 13049	947 13062	— —	— —
947,2 13060	945,5 13083	— —	948,1 13047	947,2 13060	945,4 13084	— —
947 13062	945,2 13088	943,3 13114	948,1 13047	947,2 13060	945,5 13083	943,2 13116

	PbO				PbO_2			
4	1	2	3	4	1	2	3	4
—								
—								
—	—	947,4	—	—	—	947	942,9	—
—	—	13057	—	—	—	13062	13120	—
943,2 13116								

(b)

TABLE 1

(continued)

Wavelengths in the basic L_{III} edge

основного L_{III}-края

PbSn (2% Sn)	PbSn (10% Sn)	PbO	PbO_2
948,8 13038	948,8 13038	948,6 13042	948,4 13044

(c)

fine structure on the shortwave side of the basic absorption edge, a change in the structure and in the basic absorption edge itself also takes place with an increase in temperature. Consequently the frequencies and amplitudes of the vibrations not only influence the processes of dispersion (minor perturbance) but also the whole energy spectrum of the crystal lattice of a metal.

2. The intensity of the "melting away" of the fine structure of the absorption spectrum and the basic absorption edge itself in lead and in lead-tin alloys during an increase in temperature greatly depends on the percentage of "alloying" element. Thus in the case of pure lead and a lead alloy with 10% Sn the whole structure of the absorption spectrum vanishes completely at temperatures below 200°, whereas for an alloy with 0.2-0.5% Sn the structure of the basic absorption edge is retained up to 300° (i.e., even up to the melting point).

Similar studies of Pb alloys with Tl and Sb confirmed the results obtained for the alloys with Sn. The strongest influence of "admixtures", however, was observed when their content differed. The maximum effect of "stabilization" of the basic L_{III} absorption

for Pb is achieved when the content is 0.1% Sb and ~0.5% Tl.

Thus the presence of "small" admixtures below 1% essentailly changes the frequencies and the amplitudes of atomic vibration with an increase in temperature, compared with the respective values in a pure metal. Consequently the presence of an "admixture" in a metal will influence the dispersion process (for instance, the known dependence of residual resistivity at low temperatures, of the specific heat, etc., on "admixtures") as well as the whole energy spectrum of an alloy.

A rough estimate of the influence of the amplitude of the vibration of atoms at a given temperature on the distortion of the interaction potential of atoms in a pure metal makes it possible to state that this distortion might be the reason for the blurring of the levels at the Fermi border, which is what causes the disappearance of the structure of the basic absorption edge.

The monotonically delining influence of an "admixture" with the increase in its content finds its explanation in the previously developed theory of "atomic blocks".

REFERENCES

1. DIRAK, P. Osnovy kvantovoy mekhaniki (Fundamentals of Quantum Mechanics), Moscow-Leningrad, 1937; GEYTLER, V. Kvantovaya teoriya izlucheniya, M-K 1956.

2. JONES, MOTT. Theory of the Properties of Metals and Alloys Oxford, 1936.

3. WILSON. (Quantum Theory of Metals) Kvantovaya Teoriya Metallov, Moscow Leningrad, 1939.

4. BETE and ZOMMERFELD. Elektronnaya Teoriya Metallov (Electron Theory of Metals), Moscow-Leningrad 1938; KOSTAREV, A. I. Journ. Exp. Theor. Phys. ZhETF, 20, 1950.

5. KOSTAREV, A. I. Journ. Exp. Theor Thesis, 1953, ZhETF, 21, 1951.
6. SKINNER, W. Phil. Trans. Royal Soc. Br. 239, 95, 1940; Serpe Y. C. R. T., 202, 1936.

7. BOROVSKIY, I. B. and GUROV, K. P. Physics of Metals and Metallurgy (Fizika metallov i metallovedeniye), No. 1. 1957.

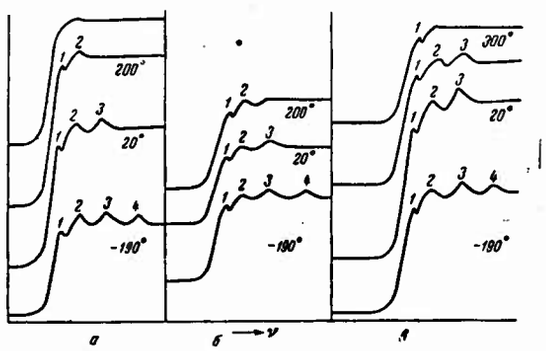

Fig. 2. L_{III}-absorption spectra of lead in lead-tin alloys. a) 2%, b) 0.5% and c) 0.2% Sn.

X-RAY SPECTROSCOPIC STUDIES OF FERRO-MOLYBDENUM AND FERRO-ALUMINUM ALLOYS

S. A. Nemnonov, V. A. Trapeznikov and K. M. Kolobova

The crystalline and electronic structures of solid bodies are basic factors predetermining their various physical and chemical properties. These two factors closely depend on one another and depend in turn on the structure of the electron shells of the atoms of the elements in a given alloy. At the present time, the most widely developed field of experimental research is that dealing with the determination of the crystalline structure of various substances. As regards the study of the electronic structure of solid bodies and the assessment of the type and strength of the interatomic bonds, research has been conducted on a comparatively small scale. However, a knowledge of these factors as applied to alloys and other technologically important materials together with structural data, is vital in substantiating and understanding various physical and chemical properties of the materials under study. X-ray spectroscopy and x-ray structural analysis are the principal methods for solving these problems.

X-ray spectra reproduce not only the distribution of electrons in the energies of the inner electron shells but also the condition of the outermost valence electrons (emission spectra) as well as the distribution in the energies of the unfilled states (absorption spectra). Hence the x-ray spectra may provide direct experimental data on the sum total of the energy characteristics of the electron structure for different classes of solid bodies.

In a number of studies on x-ray spectroscopy [1, 2, 3] it has been established that the so-called fine structure of the absorption spectra, (i.e., the alternation of clearly defined maxima and minima of absorption coefficients μ/ρ for certain pure elements, such as iron) begins to fade gradually with an increase in the temperature of the absorbent, the fading starts on the shortwave side of the edge and spreads, with a rise in temperature, over the whole edge. According to one of the existing theories [4, 5] and on the basis of research work [7], this uniform leveling of the maxima and the minima of the fine structure of the absorption spectra of solid substances is related to an increase in the amplitude of the thermal vibration of the atoms in the lattice. In view of this it was natural to assume that the thermal stability of the fine structure of the absorption spectra of solid substances should increase with the strengthening of the interatomic bonds, through the reduction of the root-mean-square deviations of the atoms from their equilibrium positions. Consequently it seemed advisable to utilize and to widen the opportunities afforded by x-ray spectroscopy by applying them to a particular factor in heat-resistant materials, namely, the strength of the interatomic bonds. Moreover, x-ray spectroscopy is not only suited to this purpose but also enables us to study the

nature and pattern of these bonds, the distribution of the outer valence electrons among the energies, and other aspects or characteristic features of the electron structure of metals and alloys.

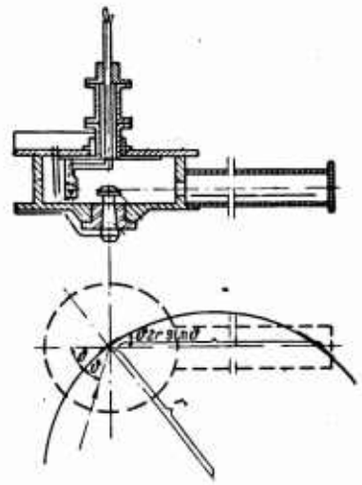

Fig. 1. Cross-section of vacuum spectrograph.

In view of this, we undertook an x-ray spectroscopic study of ferro-molybdenum and ferro-aluminum alloys. The present paper gives some of the results of the part of the study dealing with the x-ray spectra of one of the components of the alloy iron. The effectiveness and high accuracy of x-ray spectroscopic studies on different aspects of the electron structure of solid, and is some cases also liquid, bodies made it necessary to construct a vacuum spectrograph of a new type with greater linear and angular dispersion. A schematic cross-section of this apparatus [6] and an inside view of it are shown in Figs. 1 and 2. The advantages of this apparatus are: a single vacuum system for the path of the x-rays from the source to the crystal and from the latter to the recorder, which makes it possible to study the spectra in the soft longwave band (up to 19 A), when mica is used as an analyzer.

GRAPHIC NOT REPRODUCIBLE

Fig. 2. Interior of vacuum spectrograph.

The use of various crystals with different radii of curvature (the latter can be varied for a given crystal and a given crystallographic plane from 50 to 2000 mm); the possibility of using Johann's method at angles up to 83° as well as Cauchoix's* method in view of the complete circular rotation of the tube and the crystal; the availability of a considerable amount of unoccupied space inside the apparatus in which additional equipment can be housed for instance, an oven for heating foil(up to 900°), an arrangement for cooling it to temperatures of liquid nitrogen by the absorption method, a second anode when using the fluorescent method; the possi-

---

* transliteration is Koshua.

bility of recording x-rays both photographically and by ionization; the latter is ensured by the available rotating x-ray tube and sinus mechanism.

With this spectrograph K-absorption spectra and emission spectra for iron contained in ferro-molybdenum alloys (0, 0.5, 1.0, 2.0, 4.0, 10.0, 15.0, 25.0, 46, and 52% of Mo) and the ferro aluminum alloys of stoichiometric composition Fe_3Al, FeAl and $FeAl_3$ were studied. In addition, some ferro-zinc alloys were studied for comparison. For the K-spectra of iron we used a single quartz crystal with a reflecting plane (1340, Johann's method). The linear dispersion in the region of the K-absorption edge and the emission lines of the K_β group for iron was about 2.5 XE/mm.

As is known, the K absorption edge, i.e., the sudden jump in the x-ray absorption coefficient, occurs when ever the quantum energy x-ray suffices to remove one of the electrons of the K-shell of an atom of a given element beyond the Fermi surface of the lattice in a metal or alloy. The characteristic features of the fine structure of the basic edge and of the entire absorption edge of an element contained in a certain substance, like the fine structure of the emission spectra, depend basically on four factors, namely:

The structure of the outer electron shells of the absorbing atom;

The atoms which are nearest-neighbors of the absorbing atom, i.e., the atoms constituting short-range order;

The nature or type of the interatomic bonds between the absorbing atom and the surrounding atoms; and

The type of crystal lattice in the given alloy.

Consequently these four factors predetermined all the character-

istic features of the electron structure of various types of solid bodies. Moreover, they basically predetermine the physical-chemical and mechanical properties of materials. Hence the study of the diverse x-ray characteristics of both the absorption and the emission spectra of various solid bodies, including heat-resistant alloys, assumes a great scientific and practical importance. The present work is only a beginning in research of this kind which is now being conducted at the Institute of Physical Metallurgy of the Ural Branch of the Academy of Science of the USSR.

Study of Ferro-Molybdenum Alloys

The fine structure of the K-absorption spectra of iron was studied from the standpoint of both the concentration of molybdenum in a ferro-molybdenum solid solution (0.5; 1.0; 2.0 weight % Mo) and temperature (20, 600, 700, and 800°). Figure 3 shows the K-absorption edge of pure iron and the fine structure of the edge. As is seen from this figure, after the initial jump in absorption there is a clearly defined alternation of the maxima and the minima of the absorption coefficient, the so-called fine structure of the absorption spectrum, the features and extension of which in the direction of the shortwave depend on the nearest surrounding atoms [7], as has already been noted, the intensity of the maxima begins to decrease with a rise in temperature, with the influence of the thermal vibration of the lattice atoms on the reduction of this intensity increasing with the distance of the maxima from the basic edge (an effect similar to that observed in Debye lines with an increase in the angle of reflection.

A quantitative estimate of the change in the degree of contrast

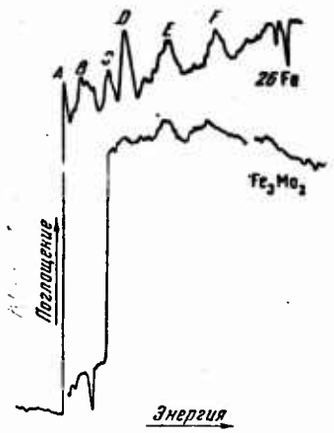

Fig. 3. Fine Structure of K absorption edges of iron for Fe_3Mo_2 and pure iron.

of the fine structure of the absorption edges was made from the relative change in the intensity of the fourth (D) and first (A) fluctuations. This estimate based on the ratio of the relative amplitudes of $\frac{F_D}{F_A}$ fluctuations within each spectrogram, was made according to the following equation:

$$\frac{\Phi_D}{\Phi_A} = \frac{\frac{t_{4\text{макс}} - t_{4\text{мин}}}{t_{4\text{макс}} - t_{4\text{фон}}}}{\frac{t_{1\text{макс}} - t_{1\text{мин}}}{t_{1\text{макс}} - t_{1\text{фон}}}}, \qquad (1)$$

where t_{4max} and t_{1max} are the maximum absorption coefficients of the fourth and first fluctuations;

t_{4min} and t_{1min} the respective minima of absorption; and

$t_{4background}$ $t_{1background}$ are the absorption coefficients corresponding to the values of the background from the longwave side of the edge extrapolated for the zone of the first and fourth fluctuations. The ratios of the amplitudes of fluctuation were taken for each spectrogram, while for several spectrograms together

the result was obtained as the arithmetic mean of the individual spectrograms, the relative error in measurement being not greater than 5%.

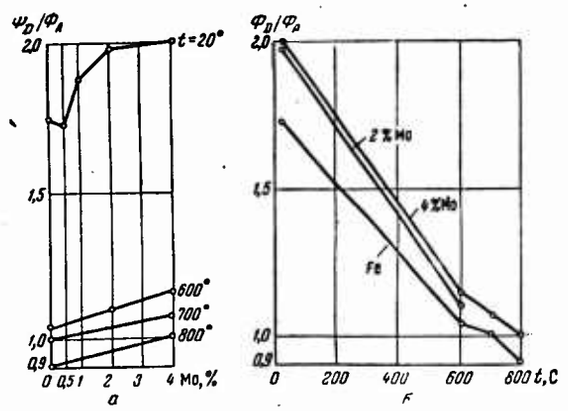

Fig. 4. Variation in the relative stability of the amplitude of fluctuations of the absorption coefficient dependent on the molybdenum concentration (a) and on temperature (b).

The results of the measurements [7], taken at room temperature and depending on the molybdenum concentration in a solid solution, are given in Fig. 4a and in Table 1.

Apart from the ratios of the amplitudes of the fluctuations of the fine structure of the absorption edges for iron in the respective solid solutions, obtained at different temperatures, Table 1 also gives data for the positions of the maxima of fluctuations at 20°. Figure 4a shows that the relative value of the intensity of the fourth maximum, which is more readily affected by the thermal movement of atoms than the first maximum, increases with a greater molybdenum content in ferro-molybdenum solid solutions excluding the alloy containing 0.5% Mo for which this value is within the limits of the experimental error. This increase in the degree of contrast or

stability of the fine structure of the K-absorption edge for iron with the increase of molybdenum content points to a fall in the amplitude of the thermal vibration of the lattice atoms (the various alloys were investigated at the same temperature).

We can conclude from this that the strength of the interatomic bonds in iron alloyed with 1, 2, and 4% Mo correspondingly increases, rising sharply between 0.5 and 2% Mo and very slightly between 2 and 4%. These conclusions accord with the data from radiographic determination of the characteristic temperature θ (θ = 430°K for pure iron and θ = 500°K for Fe + 1.8 atom% Mo), the x-ray spectroscopic characteristics of an alloy, unlike those obtained by radiographic methods, directly reproduce the changes in the electron energy spectrum of the lattice and the nature of the bond strength between atoms. However, the experimental data on the nature of atomic interaction in alloys studied at room temperature can not be extrapolated in advance for the increased temperature zone. Hence the necessity of studying these alloys at higher temperatures is thoroughly evident.

We studied the absorption spectra of the same alloys at 600, 700 and 800°. Figure 4b gives curves showing the course of the changes in the relative stability of the amplitudes of the previously discussed fluctuations of the absorption coefficient that are dependent on temperature. It can be seen from Fig. 4b and Table 1 that compared with pure iron the effect of molybdenum on strengthening the interatomic bonds in a solid solution lattice was also maintained at higher temperatures. From Fig. 4b it can also be seen that the slope $\frac{F_D}{F_A}(t)$ of the curves showing the dependence on temperature of the ratio of the fluctuation amplitudes is manifested more strongly for solid solutions than for pure iron. These data

apparently indicate that in solid solutions the relationship between the dynamic and the static distortions of the lattice changes with the temperature of the alloy under study. The changes in the relationship between these distortions in solid solutions may result from different degrees of inhomogeneity in the total concentration of molybdenum in the lattice of the solvent, which establish an equilibrium at a given temperature and at a given concentration of molybdenum. Establishment of the short-range order with redistribution of the molybdenum concentrations in the lattice of iron, and the stability of this inhomogeneity will depend on two conflicting factors namely the strength of the bonds between heterogeneous atoms and the energy of thermal motion i.e., temperature).

The fullest and most productive manifestation of the interatomic bond strengths of iron and molybdenum inherent in a given solid solution can best be achieved if sections of the lattice are molybdenum-enriched, i.e., if local differences in concentration are possible at the given temperature. The effect of the inhomogeneity of concentration on the fine structure of the absorption spectra is discussed in paper [9]. This uneven distribution of molybdenum in the lattice of a solid solution will evidently correspond to stronger interatomic bonds and the least static distortion of the alloy lattice. However, this nonuniformity in concentration will be destroyed at higher temperatures by the increased thermal motion of atoms, which in fact turn results in additional weakening of the bond strength depending solely on the redistribution of concentrations of atoms in the alloying element.

In order to reach a conclusion on the changes in the nature of the interatomic bond strength in iron when alloyed with molyb-

denum, we studied various x-ray spectroscopic characteristics of iron in the intermetallic compound Fe_3Mo_2. The results of these studies and, for purposes of comparison, similar data for pure iron and its oxides are given in Table 2.

An analysis of the data given in Table 2 shows that in the intermetallic compound Fe_3Mo_2, along with the metallic type, a covalent type of interatomic band strength is apparent to a considerable degree. This follows from a number of x-ray spectroscopic characteristics (namely: the K absorption edge of iron in Fe_3Mo_2 as seen in Fig. 5) shifts towards the shortwave section by 0.8 ev, the position of the K_{β_5} emission band remaining unchanged; the shortwave border of the liberated $K_{\beta'}$ satellite shifts in the opposite direction, i.e., towards the longwave section, by the same amount (0.7 ev) as the absorption edge. Moreover, we observe a sudden narrowing (by 4.1 ev) of the basic edge without the zone of initial absorption and a great decrease in the index of asymmetry of the $K_{\alpha'}$ line (from 1.53 to 1.28).

TABLE 1

Mo, wt. %	Ratio of fluctuation amplitudes $\frac{\Phi_D}{\Phi_A}$ at various temperatures, °C				Position of maxima, ev			
	20	600	700	800	A	B	C	D
Armco iron	1,75 ±0,09	1,04	1,00 ±0,05	0,91 ±0,04	7129,0	7154,1	7193,7	7219,0
0,5	1,73 ±0,05	—	—	—	—	—	—	—
1,0	1,88 ±0,08	—	—	—	—	—	—	—
2,0	1,98 ±0,09	1,10	—	—	—	—	—	—
4,0	2,0 ±0,05	1,15	1,07 ±0,05	1,00 ±0,05	7129,2	7152,1	7190,8	7216,8

TABLE 2

Material	position of line K_{β_1} ± 0.3 ev	position of line $K_{\beta_1'}$ ± 0.3 ev	$\Delta E = \beta_1 - \beta_{1'}$ ± ± 0.5 ev	position of line K_{β_5} ± 0.3 ev	Asymmetry K_{β_5} ± 0.2	$\Delta E = K_{\beta_5}$ - K_{β_5} abs., ev	$\Delta E = K_{\beta_5}$ Fe_3Mo_2 - K_{β_5} Fe ev	Asymmetry of line K_{α_1}
Fe	7056.7	-	0.8	7107.1	2.05	0.25	0.8	1.53
Fe_3Mo_2	7056.6	7044.7	1.5	7106.9	1.75	1.15		1.28
Fe_2O_3	7056.6	7042.9	2.0	7104.4	1.80	1.6		

TABLE 3

Материал	Асимметрия	Материал	Асимметрия	Материал	Асимметрия
Железо Ф	1,56	2% Mo_2	1,56	46% Mo	1,35
Железо	1,53	4% Mo	1,5	53% Mo_1 Ф	1,31
0,5% Mo	1,53	10% Mo	1,53	53% Mo_1	1,28
1% Mo	1,53	15% Mo	1,5	53% Mo_2	1,32
2% Mo_1	1,53	25% Mo	1,5		

In Table 3 is given data on the asymmetry of K_{α_1} for iron in ferro-molybdenum alloys. The relative error does not exceed 3% (Ф denotes the secondary spectra; the indices 1 and 2 alloys from different meltings.

The pattern and extent of the fine structure of the K-absorption spectrum of iron in Fe_3Mo_2 (see Fig. 3) are not those of ionic compounds, which also indicates the considerable degree of covalency of the intercrystalline bonds. Increased brittleness and great electrical resistivity (the latter, according to the low-temperature laboratory of the Institute of Physical Metallurgy increases 50-100 times as opposed to pure iron) also indicate a deterioration of the metallic

properties. If we take it that an intermetallic compound possesses a covalent type of bond besides a metallic one, it is quite natural to expect this change in the nature of the band strength to begin to show up even in solid solutions, since the transition of the metallic type bond into the covalent type is not abrupt. On the strength of this, it may be assumed that the increase in the strength of the interatomic bands in ferro-molybdenum solid solutions with an increase in their molybdenum concentration is due to an increase in the covalent component of the atomic interaction and that the manifestation of the covalence of the band strengths also requires a corresponding coordination of atoms, i.e., of molybdenum-enriched local zones in the lattice of the solvent.

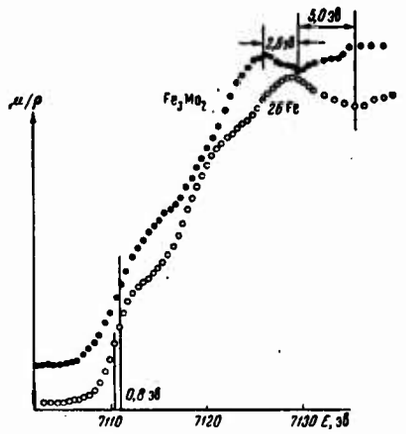

Fig. 5. Basic k-absorption edges of iron for Fe_3Mo_2 and for pure iron.

Study of Certain Ferro-Aluminum Alloys

X-ray spectroscopy acquires great importance in the study of the electron structure of the transition elements (titanium, vanadium, chromium, iron, cobalt, nickel, columbium, molybdenum, tantalum, tungsten, and others) and the alloys based on them. These metals and

their alloys with the other elements are the basic ingredient of extremely important industrial materials (ferromagnetic materials, ferrites, heat-resistant and oxidation-resistant alloys). The specific nature of these metals and their alloys with other elements is connected with the incompleteness of nd electron shells, and the extent to which the electrons in these shells are active in producing interatomic bonds differing in type and strength depends on the nature of the other elements composing either simple or complex alloys. The formation of such strong intermetallic compounds as carbides, borides, silicides, and a number of other alloys on transition elements is also explained by this peculiarity of their electronic structure.

It is known from x-ray spectroscopic studies that there are a number of anomalies in both the absorption and the emission spectra for the transition metals of the first long period. It is known, for instance that the asymmetry of some spectral lines, with the rise in the atomic number of the element, first increases, reaching its maximum in the case of iron, and then decreases again to nearly zero in copper [10]. A similar dependence is also observed for the value of the magnetic moment of atoms, or more exactly, the divalent ions of these elements [11]. It is thought that both dependences are linked with the number of unpaid electrons in the 3d shell.

The degree of incompleteness of the 3d electron shells for atoms of titanium. chromium, iron, and nickel is different, decreasing from titanium to nickel. Nonetheless, it is precisely this feature which determines the specific nature of the various properties of these metals and their alloys with other elements. At the same time very little is known about the influence of this feature on the pattern of the energy spectrum of the transition elements and their alloys. As a

result of this redistribution of electrons, for instance, strong interatomic bonds are established in titanium carbides or in some of the nickel-aluminum alloys. Also, uncertain are the degrees of participation of the valent electrons of various elements in the interatomic bonds and the change in the nature of the bond strengths in transition-element alloys, with nontransition elements, the number of valent electrons in which varies (for instance, in such systems as iron-zinc, iron-aluminum, iron-silicon, and iron-sulfur). Hence it is vital to the principal laws governing the changes in the electronic structure and in the strength and nature of the interatomic bonds according to the physicochemical nature of the alloyed elements. It is advisable in so doing to make of such x-ray spectra characteristics of the transition elements of the iron group as the degree of asymmetry of some of the spectral lines, the features of the fine structure of the absorption spectra of these metals and other characteristics.

In order to establish such laws and to theorize on the basis of experimental data, a study must be made of alloys of different systems over a rather wide range of concentrations and temperatures. With this in mind, we made x-ray spectroscopic studies of ferro-aluminum alloys with comparatively high concentrations of a nontransition element (Fe_3Al, FeAl, and $FeAl_3$). Some ferro-zinc alloys were also studied and the k-absorption spectra of iron, the asymmetry K_α at altitude K_{α_2}, the emission lines and K_β bands of the iron group were examined in these cases. For comparison, the K_α asymmetry of iron and ferro-zinc alloys of approximately the same composition as that of ferro-aluminum alloys was studied. The studies were carried out with a spectrograph of the same design and the same order of linear dispersion as the one used for ferro-molybdenum alloys. The dependence of the value of the asymmetry of the K_α and K_{β_5} lines for iron on the

atomic concentration of aluminum, zinc, and molybdenum in the corresponding alloys with iron were determined from a study (Fig. 6 and Table 4). From the diagram we can see that the asymmetry of the K_{α_1} spectrum line for iron decreases markedly with an increase in the aluminum concentration in the alloy, this decrease being a rectilinear function. The slope of the straight line is less marked for ferro-zinc alloys than for ferro-aluminum alloys.

As has been noted, the asymmetry of a given line is conditioned by the number of unpaired electrons in the 3d shell of the iron atoms, i.e., by the number of electrons capable of participating in the formation of a certain type of interatomic bonds.

But the degree to which these electrons are involved in interatomic bonds will depend on the number of valent electrons in the atoms of the nontransition elements alloyed with the iron, as well as on the concentration of those elements. Experimental data permit us to establish the following dependence of the change in the asymmetry of the K_{α_1} line of pure iron a_{Fe} on the atomic concentration $\underline{c}$ and on the valence $\underline{n}$ of the solute element:

$$a_{alloy} = a_{Fe} - kcn \qquad (2)$$

where a_{alloy} is the asymmetry of the K_{α_1} line of iron in the alloy and $\underline{k}$ is the proportionality coefficient found by calculation to equal $1.51 \cdot 10^{-3}$.

atomic concentration of aluminum, zinc, and molybdenum in the corresponding alloys with iron were determined from a study (Fig. 6 and Table 4). From the diagram we can see that the asymmetry of the K_{α_1} spectrum line for iron decreases markedly with an increase in the aluminum concentration in the alloy, this decrease being a rectilinear function. The slope of the straight line is less marked for ferro-zinc alloys than for ferro-aluminum alloys.

As has been noted, the asymmetry of a given line is conditioned by the number of unpaired electrons in the 3d shell of the iron atoms, i.e., by the number of electrons capable of participating in the formation of a certain type of interatomic bonds.

But the degree to which these electrons are involved in interatomic bonds will depend on the number of valent electrons in the atoms of the nontransition elements alloyed with the iron, as well as on the concentration of those elements. Experimental data permit us to establish the following dependence of the change in the asymmetry of the K_{α_1} line of pure iron a_{Fe} on the atomic concentration $\underline{c}$ and on the valence $\underline{n}$ of the solute element:

$$a_{alloy} = a_{Fe} - kcn \qquad (2)$$

where a_{alloy} is the asymmetry of the K_{α_1} line of iron in the alloy and $\underline{k}$ is the proportionality coefficient found by calculation to equal $1.51 \cdot 10^{-3}$.

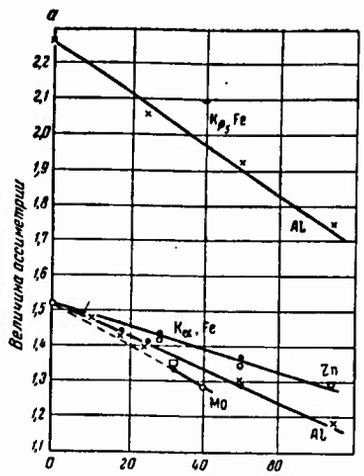

Fig. 6. Dependence of value and of unsymmetry of K_{α_1} and K_{β_5} line of iron on atom concentration of alloying components.

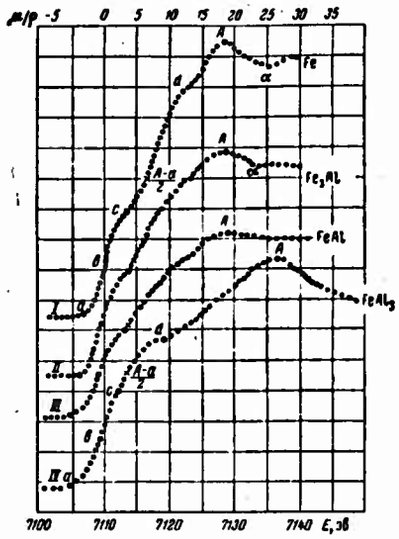

Fig. 7. K absorption edge of iron for Fe, Fe_3Al, and $FeAl_3$.

By using this formula it is possible, in particular, to determine the values of the asymmetry of the K_{α_1} line of iron for those ferro-aluminum and ferro-zinc alloys for which they were found experimentally. These values, given in Table 4, fully accord with experimental data and fall readily on the relevant straight lines (marked by dots).

The change in assymetry over the range of concentration where there is a mixture of two phases, is caused by the combination of lines of both phases with different asymmetries; in this particular case the value of the asymmetry is determined by the relationship between the two phases, as in the case of ferro-zinc alloys with 28 and 50% concentrations of zinc and in ferro-zlimunium alloys with concentrations of aluminum from 50 to 75%. This development is similar to that defined by an equation previously evolved by Sadron [12] covering the dependence of the mean magnetic moment of saturation in an alloy on the concentration and valence of a nontransition element in nickel.

The physical significance of the dependence expressed by Eq. (2) lies in the fact that the spins of the valent s and p electrons of aluminum atoms are oriented towards the 3d uncompensated electrons of the iron atoms and thereby compensating them and "extinguishing" the magnetic moment of the iron atoms by a corresponding amount. This extinction is proportional to the number of valent electrons of the atoms of the alloying elements. The compensation of the 3d unpaired electrons in the iron atoms thereby reduces the interaction of the 3d electrons with their own 2p electrons and, as a consequence, also reduces the asymmetry of the K_{β_5} emission line. Figure 6 also shows that the change in the asymmetry of the K_{β_5} band of iron in the same ferro-aluminum alloys is identical with that of the K_{α_1} line.

TABLE 4

Concentration of alloying element in atom	Valence of alloying element	Index of asymmetry of K_{α_1} line (exper)	Index of asymmetry calculated from Eq. 2
0	-	1.52 ± 0.03	-
25 Al (Fe_3Al)	3	1.40 ± 0.04	1.41
50 Al (FeAl)	3	1.30 ± 0.04	1.29
75 Al ($FeAl_3$)	3	1.18 ± 0.03	1.18
25 Zn	2	1.41 ± 0.02	1.43
50 Zn	2	1.35 ± 0.02	1.37
75 Zn	2	1.29 ± 0.02	1.29

TABLE 5

Aluminum concentration in alloys in atom %	0	25 Al(Fe_3Al)	50 Al(FeAl)	75 Al($FeAl_3$)
Index of asymmetry of K_{β_5} line for iron	2.26 ± 0.14	2.06 ± 0.12	1.92 ± 0.04	1.74 ± 0.06

K_{β_5} band originates from transitions of 3d electrons to the excitation level of the iron atoms. Hence, the change in the asymmetry of the K_{β_5} band of iron with an increase in the concentration of the alloying element (in this aluminum) also shows that the 3d electrons are compensated and that as a result this electron shell is, as it were, "completed." Thus, a study of the asymmetry of certain spectrum lines of the transition metals of this period gives a good indication

of the nature of the atomic interaction in alloys based on transition metals. However, from a study of the asymmetry of the spectrum lines we cannot indentify the class of interatomic bonds in these alloys since the compensation of the 3d electrons of the iron atoms may not only result from the presence of covalent bond strength, but also from the easily detachable valent electrons of the zinc and aluminum atoms by the 3d shell. We need to study the absorption spectra of iron in the same alloys.

In Fig. 7 is shown the K absorption edges of iron in Fe, Fe_3Al, FeAl and $FeAl_3$. Analysis of the fine structures of these edges indicates that the initial part of the K absorption edge originating from the x-ray electrons into the generalized 3d and 4s band shifts with an increase in the concentration of aluminum in the alloy towards the longwave side; this shift is 0.8 ev for Fe_3Al and 1.0 ev for FeAl (compared with pure iron). With regard to the FeAl alloy the fine structure of the basic edge of the iron becomes clearly distinct by comparison with Fe, Fe_3Al and FeAl; the features of the 3d and 4s absorption band disappear almost completely, and furthermore, the crystalline structure of this phase is very complex. The shift of this part of the absorption edge in the ferro-aluminum alloys Fe_3Al and FeAl appears to be the opposite of that found in Fe_3Mo_2. This difference is probably connected with the appearance of various types of bonds. In the case of Fe_3Mo_2, covalent bonds, as was already noted, appear to a considerable degree, along with the metallic bonds, while for Fe_3Al, FeAl and $FeAl_3$, the ionic nature of the interatomic bonds becomes more evident with an increase in aluminum content. The K absorption edges of iron in Fe_3Al, FeAl and $FeAl_3$ alloys also indicate that the first inflection of the basic edge caused by the generalized 3d and 4s band and by the incompleteness of the 3d electron

shell gradually disappears with an increase in aluminum content and vanishes almost completely in $FeAl_3$. This apparently also indicates that the valent electrons of the aluminum atoms are captured by the 3d unfilled shell of the iron atoms. The most convincing evidence of the ionic nature of the bonds manifested to a considerably greater degree in the $FeAl_3$ alloy is the great difference between pure iron and the iron in $FeAl_3$ in the pattern and the extent of the fine structure of the absorption spectrum.

The fine structure of the K absorption edge of pure iron covers several hundred electronvolts (six maxima are well marked) whereas for $FeAl_3$ there are only two clearly defined maxima, the first of them being so high and narrow in intensity that it can be called a selective line with full justification. This maximum is shifted 8 ev towards the shortwave side in comparison with the first maximum pf pure iron. The occurrence of one or two clearly marked selective lines is a characteristic of ionic crystals.

It should be pointed out that the nature of atomic interaction in alloys may change continuously, depending on their composition and the test temperature, and as a rule, bonds of different kind coexist and act simultaneously in the process. Hence, when the interatomic bonds are subdivided into their basic types (metallic, covalent and ionic) not only should the arbitrary character of this division be emphasized, but also the degree to which a certain type of bond is expressed. For instance, the presence of covalent bonds but which have been polarized to a certain degree can be assumed in the case of ferro-aluminum alloys. Consequently, in this case, there are indications of the presence of both covalent and ionic bonds, along with the metalic properties; the degree of polarization of the

covalent bonds, apparently increasing with an increase in the aluminum content. This signifies that the electron density of a pair of electrons forming a covalent bond shifts more and more towards one of the atoms (in our case, towards the iron atoms.

REFERENCES

1. J. Hanawalt. Z. F. Phys., 70, 1931.

2. W. Sjoerdsma. Physica, 4, 29, 1937.

3. D. Coster and H. Levi. Physica, 6, 44, 1939.

4. A. I. Kostarev, ZhETF (Journal of Experimental and Theoretical Physics), 11, 60, 1941.

5. A. I. Kostarev, ZhETF, 20, 811, 1950.

6. V. A. Trapeznikov and S. A. Nemnonov, FMM (Physics of Met. and Metallurgy) 1, number 3, 1955.

7. V. A. Trapeznikov and S. A. Nemnonov, FMM 3, number 2, 1956.

8. V. V. Ilyina and V. K. Kritskaya. Problems of Metallurgy and Metals. Moscow, 1955.

9. S. A. Nemnonov and V. A. Trapeznikov. Papera of the Institute of Metal Physics, Number 16, 1955.

10. E. Ye. Vaynshtein, DAN SSSR (Report of Academy of Science USSR) 40, Number 3, 1943.

11. M. A. Blokhin. Physics of X-Rays. Moscow, 1953.

12. Sadron. Ann. de Phys., 17, 1932.

K. P. ROMADIN

ELECTRODISPLACEMENT IN METALLIC SOLID SOLUTIONS

All processes in the thermal and thermochemical treatment of metal alloys are based entirely on the phenomenon of redistribution of the composing elements. However, the relationship between mobility and structure in metal systems has not yet been sufficiently explored.

The present study is devoted to the question of the movement of the solute substnace in a metal solid solution under the influence of direct electric current.

Fig. 1. Microstructure of steel wire containing 1.2% C in its initial state, after migration at 980° for 50 hours at a current density of 28.6 amx/mm² (X 100).
At the anode - ferrite; in the middle - ferrite with perlite; at the cathode - perlite, cementite, and a certain amount of graphite.

We carried out experiments on the migration of atoms (ions) in metal solid solutions with alloys of the iron – carbon system containing 0.65 and 1.2% C, a number of binary alloys of nickel and chromium, nickel and aluminum, nickel and iron, and nickel and titanium, and with a complex eight-component alloy based on nickel. The alloys to be studied were prepared in an induction furnace and were pumped in a fluid state into small porcelain tubes with an inner diameter of 2 mm. In this way,

the cross section of the specimens acted on by direct current turned out to be 3.14 mm^2 instead of 0.283 mm^2, as previously assumed.

After homogenization at 1100° for 24 hours, platinum electrodes were welded to the ends of the specimens 40 mm long. Direct current (35-45 amp) was then passed through the specimens in a vacuum using a VUP-2 apparatus, and they were heated to 1000°. Next, the specimens were examined under a microscope, their electroresistivity and microhardness were measured and a spectrum analysis made. The results of all the methods used in our research were in agreement.

Figure 1 shows the microstructure of a steel wire which contained 1.2% C in its initial state, and in Fig. 2 the microstructure of a specimen prepared from a nickel-aluminum system which contained 18% Al in its initial state. The photographs make it clear that the ions of the solute substance migrated in the tests.

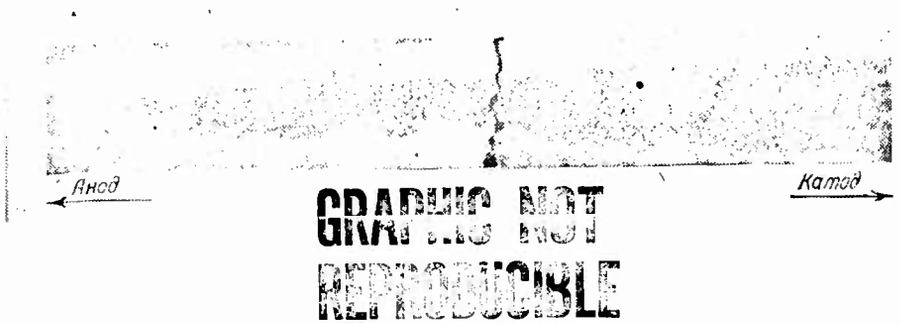

GRAPHIC NOT
REPRODUCIBLE

Fig. 2. Microstructure of specimen prepared from nickel-aluminum alloy containing 18% Al in its initial state after electro displacement at 1000° for 50 hours at current density of 14.3 amp/mm^2 (X 150).

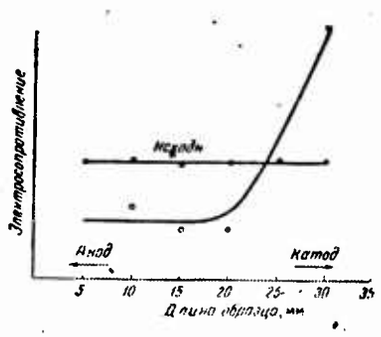

Fig. 3. Variation in electroresistivity along the length of specimen prepared from an alloy of nickel-chromium system containing 40% Cr in its initial state after migration at 1000° for 100 hours at current density at 14.7 amp/mm^2.

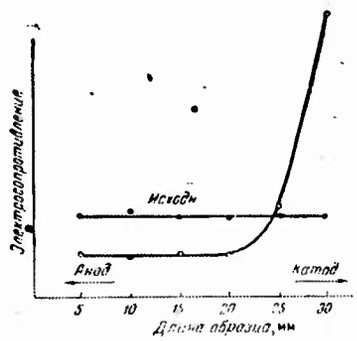

Fig. 4. Variation in electroresistivity along the length of specimen prepared from a complex 8-component alloy with a nickel base after migration at 1000° for 100 hours at current density of 14.2 amp/mm^2.

Figure 3 gives the results of measurements of the electroresistivity along the length of a specimen at 5 mm intervals which was prepared from a nickel-chromium system containing 40% Cr in its initial state. Figure 4 gives the sound data for a specimen prepared from a complex 8-component alloy with a nickel base. The curves show considerable increase in resistivity at the cathode and a decrease at the anode as compared with the original resistivity of the alloys.

Thus, the measurements of resistivity along the length of the specimens also indicate that the migration of the ions of a substance dissolved in a metal solid solution when a direct current is applied to it takes place both in simple and complex alloys.

It should be noted during these tests that a decrease in the temperature of the specimens was observed a certain time after they were started (1-2 hours) and that the current had to be stepped up.

All the specimens showed a drop in temperature. The current was stepped up at the beginning of the test by 1-2 amp and this was continued for 10-15 hours, depending on the alloy, up to a total of 8-10 amp. These changes in temperature were caused by the change in composition of the alloy along the length of the specimen, brought about by electromigration. It follows from this that migration is a common occurrence in metal solid solutions.

Let us now examine the nature of the active forces of diffusion responsible for leveling out concentrations of a solute element in a homogeneous medium. The kinetic energy of the movement of the elementary particles in the active force during diffusion in gaseous and liquid media. In the dissociation of the diffusing particles during diffusion in gases and liquids, electric forces are also active. But with regard to diffusion in a solid, the energy of vibration of the particles cannot cause oriented movement. Not only the lattice forces but also the interparticle electric forces in the solute substance are active here. Consequently, diffusion in a solid should not be considered movement of the neutral noninteracting particles (molecules and atoms) but rather diffusion of their dissociation products, the ions.

On the other hand, the theory of electroconductivity states that conductivity in metals is due to the fact that a certain number of highly mobile electrons are separated from each atom and that this mobility brings about high conductivity. Hence ions with a definite valence are to be found at the lattice points of metals.

From our investigation of migration, it follows that the metal with the higher electroconductivity moves to the cathode. For instance, during migration in liquid metals of the tin-bismuth, cadmium-tin and copper-tin systems, the former are more conductive

than the latter, and move to the cathode.

The experiments also indicate that if the diffusing atoms differ little from the atoms of the base metal in size, chemical composition, and other characteristics, diffusion proceeds through an interchange of positions. Duringthis process their mutual solubility increases, very frequently to an unlimited degree; this is due to the freedom of action in the formation of a uniform lattice (substitution solid solutions). But when the diffusing atoms differ considerably in their properties, particularly in size, from the atoms of the metal base, their solubility in the metal base decreases, which is evidently determined to a considerable degree by the presence of unoccupied sites in the interatomic space. In this case the solid solution is formed through the filling of the interatomic gaps (interstitial solid solutions).

Conclusion

1. Migration of the components of alloys takes place when a direct current is passed through a metal solid solution. This migration is a common feature in metal solid solutions.

2. Disturbance of the balanced state of a system by passing direct current through it causes a movement of the components of alloy, the ion with the greater charge density moving to the cathode.

3. On the basis of the theory of the metallic state the processes of diffusion in metal solid solutions should be viewed as processes conducted with phenomenon of dissociation. The diffusion flow should be considered a flow of ions rather than of atoms.

4. The migration of ions in metal solutions can be used in practice for the most varied purposes; for instance, refining alloys in a liquid state, obtaining pure metals in a solid state by

removing impurities, etc.

REFERENCES

1. KHEVESHI, Movement of Matter in Solids (Peremeshcheniye Materii v Tverdykh Telakh). Z. F. Elektrochemie, No. 39, 1933.

2. KHEVESHI, Self-Diffusion in Solids (Samodiffuziya v Tverdykh Telakh). Trans. Faraday Soc., No. 34, 1938.

3. YOST and LINKE, Studies of Electrolysis of Solid Alloys (Opyty Elektroliza Tverdykh Splavov). Z. F. Physikalische Chemie, No. 29, 1935.

4. KREMAN, ORTNER and MARKL'. Electrolysis of Alloys of Antimony and Zinc. Monatshefte Chemie, No. 44, 1924.

5. ZEIT and ETZOLD, Diffusion in Metals. Z. F. Elektrochemie, No. 6, 1934.

6. ZEIT and ETZOLD, Mobility of Gold in Solid Lead. Z. F. Elektrochemie, No. 12, 1934.

7. ZEIT and KUBASHEVSKI, Electrolytic Movement of Carbon in Solid Steel, Z. F. Elektrochemie, No. 41, 1935.

8. SKAUPI, Conductivity in Metals. Verh. D. Deutsch. Physikal, Ges. No. 16, 1914.

9. SCHWARZ, Movement of Matter and Current Flow in Liquid Alloys. Z.F. Elektrochemie, No. 39, 1933.

10. SCHWARZ, Concerning the theory of Electrolytic Effects in Solid Metals. Z. F. Elektrochemie, No. 43, 1937.

11. SCHWARZ and STOCKERT, Electrolytic movement of Gold in a Solid Alloy of Gold and Lead. Z. F. elektrochemie, No. 45, 1939.

12. V. PROSVIRIN, Concerning Ionic Diffusion in Metals (K Voprosu ob Ionnoy Diffusii v Metallakh), "Vestnik Metallopromyshlennosti" (Herald of Metal Industry), No. 12, 1937.

13. T. LEBEDEV, Fundamentals of New Theory of Ferro-Carbon Alloys (Osnovnye Polozheniya Novoy Teorii Zhelesouglerodistykh Splavov) Leningradskiy Institut Usovershenstvovaniya Inzhenerov NKTP) Leningrad Institute of Higher Engineering Studies of Peop. Comm. of Heavy Mach. Institute.

14. O. YESIN and P. GELD, Concerning the State of Metalloids Dissolved in Metals (O Formakh Sushchestvovaniya Metalloidov Rastvorennykh v Metalle) Advances in Chemistry, No. 1, 22, 1954.

15. N. AGEYEV, Nature of Chemical Bond in Metallic Alloys (Priroda Khimicheskoy Svyazi v Metallicheskikh Splavakh) Izd. AN SSSR (Academy of Science, USSR Press), 1947.

16. I. FRANTSEVICH and D. KALINOVICH, Study of Migration in Solid Metallic Solutions (Issledovaniye Elektroperenosa v Tverdykh Metallicheskikh Rastvorakh), Izd. AN SSSR, 1957.

17. K. ROMADIN, Electrolytic Migration in Liquid and Solid Solutions of Metals (Elektroliticheskiy Perenos v Metallicheskikh Zhidkikh i Tverdykh Rastvorakh) Papers of Zhukovsky Aviat. Eng. Inst.) No. 167, 1947.

18. S. DRAKIN. Migration and Distribution of Components of Metallic Alloys in the Electric Field (Perenos i Raspredeleniye Komponentov Metallicheskikh Splavov v Elektricheskom Pole) Journal of Physical Chemistry, No. 10, 27, 1953.

ON THE POSSIBILITY OF RADIOAUTOGRAPHIC DETECTION OF INHOMOGENEITIES IN CONCENTRATIONS OF ADSORPTION ORIGIN

V. I. Arkharov, et al

A great number of papers are available at the present time on the radioautographic study of inhomogeneous distribution of alloy components by means of radioactive indicators. The majority of these papers deal with the unevenness in concentration originating either from segregation [1, 2, 3] or from the decomposition of solid solutions and the precipitation of new phases [4]. In all these papers the uneven distribution of the alloy components was detected by adding radioactive indicators to the alloy or by activation of the alloy followed by radioautographic recording of the labeled component.

The study of the uneven distribution of an alloy component of segregation or phase origin by micro-radioautography proved possible, essentially for two basic reasons:

the size of the zones with a modified concentration is macroscopic;

the ratio of concentrations reached a great magnitude (of the order of 10^2).

Given these conditions and the use of emitters with a rather low radiation, the contrast of the radioautograms is quite pronounced.

Research has shown that the response of the radioautographic method depends greatly on the type of radiation, its degree of scattering and absorption in the specimen and in the emulsion, and on the closeness of contact between the specimen and the photoemulsion. In view of this, extra precautions had to be taken when studying gross inhomogeneity in concentration in order to obtain sufficient response and to solve the problem correctly. The use of specimens with a thickness considerably less than the maximum electron path in the given substance and the use of one-sided films coated with an emulsion a few microns thick made it possible to reduce the influence of radiation scattering on the quality of the picture.

Papers [5, 6] have shown that there is a stable (balanced) unevenness of concentration connected with the structural inhomogeneities, particularly in intercrystalline transition zones, considerably decreases when these inhomogeneities are enriched by one of the components of the alloy. This decrease in surplus energy due to differences in concentration in the alloy (internal adsorption) creates very small domains with a modified concentration (100-1000 A) and the change in concentration in these domains can apparently reach 1-2 orders, compared to the average composition of the alloy [7]. This internal adsorption occurs at very small admixture contents compared to the maximum solubility. Until now, this phenomenon has been studied mainly by various indirect methods which made it possible to bring to light certain laws governing internal adsorption.

Our own purpose was to confirm, ny the most direct method possible, the data on the adsorptive activity of certain small admixtures in the alloys based on copper and aluminum which had been previously obtained in the laboratory.

Studies of the copper-antimony and aluminum-silver systems [8, 9, 10] showed that the silver and antimony in these alloys are adsorption-active elements. However, the radiographic examination of the distribution of antimony labeled with isotope Sb^{124} in an alloy of copper with 0.4% antimony, and the distribution of silver marked by isotope Ag^{110} in an alloy of aluminum with 0.1% silver failed to detect any irregular distribution of these admixtures.

The tests were carried out in the following manner. A coarse grain of the order of 1 mm was grown in the specimens in order to widen the distance between the domains with a modified concentration. The specimens were subjected to a series of prolonged annealings (about 100-200 hours) at maximum solubility temperatures for the admixture in the alloy to bring about complete redistribution of the admixture between the grains and the intercrystalline transitional zones.

Thin, 50-micron plates were prepared from the specimens after the heat treatment. The radioautographing was carried out on MR NIKFI film. The films were subjected to standard processing after exposure. The absence of any changes in density on the radioautograms with respect to the microstructure of the specimen indicated that the radioautographic method was most suitable for our purpose.

Our results gave rise to doubt regarding the possibility in principle of radioautographic detection of adsorption in the selected systems, and also with regard to establishing the experimental conditions necessary for the detection of this kind of unevenness of concentration as a whole.

Considerable difficulties are encountered in the experimental solution of the problem. The preparation of the superfine specimens

1 micron thick, and of the applied emulsions and special selection of the systems tested make an empirical method of solving the problem practically unacceptable. In this connection an a priori evaluation of the possibility of detecting a fine degree of unevenness of concentration of this order requires a knowledge of the dependence of the distribution of emission electrons over the surface of the

specimen on its thickness and on the radiation energy.

We attempted to calculate theoretically the distribution of β-radiation on the surface of the specimen, taking into account its adsorption through repeated scattering. Let us deal briefly with the diffusion theory of the repeated dispersion of electrons. As early as 1929 Bothe [11] drew attention to the fact that one of the principal reasons for the reduction in the radiation of electrons in matter was repeated scattering. A strict theory of this phenomenon was developed in a number of studies in the following years [12, 13]. In a well-known paper by Bethe, Rose and Smith [14], it was stated that the theory of the repeated scattering of electrons, generally speaking, can be reduced to a question of diffusion when the electrons are emitted in all directions from a radioactive source or when the majority of the electrons constituting a narrow beam lose their initial direction owing to dispersion. We give the equation formulated by Bethe, Rose, and Smith in the following formula:*

$$\frac{\partial F(x,y,z,\tau)}{\partial \tau} = \Delta F(x,y,z,\tau) + s(x,y,z)\,\delta(\tau). \qquad (1)$$

Here F (x, y, z, τ) is the full density of the electrons (irrespective of the direction of movement) near a given point in the space (x, y, z) characterized by parameter τ;

Δ is the Laplace operator;

s (x, y, z) is the density of electrons near the points (x, y, z) emitted by the source;

δ is Dirac's delta function.

* In the original text of [14] misprints occurred in Eqs. (27), (28) and (31).

Let us call parameter τ "symbolic age," as is done in the theory of neutron age [16]. The symbolic age depends on the complete path of the electron covered by it from the moment of emanation. The path, in turn is a single valued function of the energy loss of the electron. Soncequently, the symbolic age is determined by the energy E of the electron and its initial energy E_o.

In the theoretical treatment of our experimental data, it appeared quite natural to adopt the following simplified model. Let us assume that the specimen under study is a plane-parallel plate with a finite thickness b in the direction of the axis y and that it expands infinitely in the direction of x and z axes. Further, let the intercrystalline zone be approximate to the section of the plane $x = 0$ bounded by the surfaces of the plate. It is presumed that other intercrystalline zones are distant enough to be able to discount their influence.

Let us also take into account that the concentration of the radioactive atoms of antimony (Sb^{124}) or silver (Ag^{110}) measures only 0.1% in the main body of the specimen and 10% in the intercrystalline zone. Then in the adopted model, it is entirely quite logical in the first approximation to disregard completely, the radioactive atoms of antimony or silver in the main body of the specimen and to consider the intercrystalline zone a plane source with a uniform distribution of antimony and silver atoms, producing isotropic radiation in all directions.

The density of the electron radiation from such a source close to the surface of the specimen depends on the energy of the electrons, distance from the source along the x axis, and on the thickness of the specimen. The problem is to deduce an explicit expression for

this electron density close to the surfaces of the specimen based on the above assumptions.

Let us proceed from the diffusion equation (1). Here, the term containing the source is given as

$$s_0\delta(x)\,\delta(\tau),$$

where s_0 is the number of electrons emitted by each square centimeter of the source.

Let us take into account that the electron density remains unchanged in the direction z, i.e., that Eq. (1) is reduced to a two-dimensional equation. In this case we obtain the equation

$$\frac{\partial F(x,y,\tau)}{\partial \tau} = \frac{\partial^2 F(x,y,\tau)}{\partial x^2} + \frac{\partial^2 F(x,y,\tau)}{\partial y^2} + s_0\delta(x)\,\delta(\tau). \qquad (2)$$

We will select boundary conditions for the problem in full accordance with the manner adopted for similar problems in the theory of heat conductivity [17] and diffusion [18], namely: we will assume that the gradient of the electron density over the surface of the specimen in the direction of the outer normal is proportional to the electron density close to the surface:

$$-\frac{\partial F(x,y,\tau)}{\partial y} + hF(x,y,\tau) = 0 \text{ at } y = 0 \qquad (3)$$

$$\frac{\partial F(x,y,\tau)}{\partial y} + hF(x,y,\tau) = 0 \text{ at } y = b, \qquad (4)$$

where the proportionality coefficient h is assumed to be constant.

We will now introduce the Fourier transform with respect to the variable x of the electron density:

$$F(\xi,y,\tau) = \frac{1}{\sqrt{2\pi}}\int_{-\infty}^{\infty} F(x,y,\tau)\,e^{i\xi x}dx. \qquad (5)$$

Then taking into account the behavior of the electron density

at infinity, we obtain instead of Eqs. (2) and (4)

$$\frac{\partial F(\xi,y,\tau)}{\partial \tau} = \frac{\partial^2 F(\xi,y,\tau)}{\partial y^2} - \xi^2 F(\xi,y,\tau) + \frac{s_0}{\sqrt{2\pi}}\delta(\tau) \tag{6}$$

and

$$-\frac{\partial F(\xi,y,\tau)}{\partial y} + hF(\xi,y,\tau) = 0 \text{ at } y = 0, \tag{7}$$

$$\frac{\partial F(\xi,y,\tau)}{\partial y} + hF(\xi,y,\tau) = 0 \text{ at } y = b. \tag{8}$$

By substituting

$$F(\xi,y,\tau) = G(y,\tau)e^{-\xi^2\tau} \tag{9}$$

the Eqs. (6) and (8) are further reduced to the form

$$\frac{\partial G(y,\tau)}{\partial y} = \frac{\partial^2 G(y,\tau)}{\partial y^2} + \frac{s_0}{\sqrt{2\pi}}\delta(\tau) \tag{10}$$

and

$$-\frac{\partial G(y,\tau)}{\partial y} + hG(y,\tau) = 0 \text{ at } y = 0, \tag{11}$$

$$\frac{\partial G(y,\tau)}{\partial y} + hG(y,\tau) = 0 \text{ at } y = b. \tag{12}$$

The solution of the Eq. (10) with boundary conditions (11) and (12) is equivalent to that of the problem of heat transfer in a limited rod, at the termini of which there is a heat exchange with a medium of zero temperature, provided the initial temperature of the rod is constant and there is no heat exchange on the lateral surface [17].

Consequently, we have for the function G (y, τ)

$$G(y,\tau) = 4\frac{s_0 h}{\sqrt{2\pi}}\sum_{r=0}^{\infty} exp\left(-\alpha_{2r+1}^2\tau\right)\frac{\cos\alpha_{2r+1}y + \frac{h}{\alpha_{2r+1}}\sin\alpha_{2r+1}y}{(\alpha_{2r+1}^2 + h^2)b + 2h}, \tag{13}$$

where α_{2r+1} is the (2r + 1) root of the transcendental equation

$$\operatorname{tg}\frac{\alpha_{2r+1}b}{2}=\frac{h}{\alpha_{2r+1}} \quad \text{at} \quad 2r\frac{\pi}{2}<\frac{\alpha_{2r+1}b}{2}<(2r+1)\frac{\pi}{2}. \tag{14}$$

Knowing G (y, τ) from Eq. (9), we find F (ξ, y, τ) and substituting for the inverse Fourier transform, we obtain

$$F(x,y,\tau)=\frac{2hs_0}{\sqrt{\pi\tau}}e^{-\frac{x^2}{4\tau}}\sum_{r=0}^{\infty}e^{-\alpha_{2r+1}^2\tau}\frac{\cos\alpha_{2r+1}y+\frac{h}{\alpha_{2r+1}}\sin\alpha_{2r+1}y}{(\alpha_{2r+1}^2+h^2)b+2h}, \tag{15}$$

where α_{2r+1} is determined by Eq. (14).

At y = 0 and y = b, i.e., on the boundaries of the specimen

$$F(x,0,\tau)=F(x,b,\tau)=\frac{s_0}{\sqrt{\pi\tau}}e^{-\frac{x^2}{4\tau}}\sum_{r=0}^{\infty}e^{-\alpha_{2r+1}^2\tau}\frac{\sin\alpha_{2r+1}b}{\alpha_{2r+1}b+\sin\alpha_{2r+1}b}. \tag{16}$$

The roots of the transcendental equation (14) are equal to the abscissae of the intersection points of the curves

$$\eta=\operatorname{tg}\xi \quad \text{и} \quad \eta=\frac{p}{\xi}, \tag{17}$$

where

$$\xi=\frac{\alpha_{2r+1}b}{2} \quad \text{и} \quad p=\frac{hb}{2}.$$

More specifically, for $\alpha_1 b < \pi$ ($\xi < \frac{\pi}{2}$) we obtain

$$(\alpha_1 b)^2\simeq 2hb\ll\pi^2\left(p\simeq\xi^2\ll\frac{\pi^2}{4}\right), \tag{18}$$

according to which the thickness b of the specimen must comply with inequality

$$b \ll \frac{\pi^2}{2h}. \tag{19}$$

All other roots are determined by the equality

$$\alpha_{2r+1}b\simeq(2r+1)\pi \quad \text{at} \quad r = 1, 2, \ldots \tag{20}$$

Using the relationships (18) and (20) we can find an expression for the density of electrons near the surface of the specimen,

$$F(x, b, \tau) = F_0(\tau) \frac{1}{\sqrt{2\tau}\sqrt{2\pi}} e^{-\frac{x^2}{2(\sqrt{2\tau})^2}}, \tag{21}$$

where

$$F_0(\tau) = s_0 e^{-\frac{2h\tau}{b}}. \tag{22}$$

The Eqs. (16), (21), and (22) give the final solution of the problem stated above. These formulas were derived on the assumption that the number of radioactive atoms in the main body of the specimen is small compared with the intercrystalline zone; that is why in the first approximation they generally were not taken into account at all. It would have been more consistent to allow for the presence of these atoms in the main body of the specimen from the very beginning, but nevertheless we can still estimate this effect without making that calculation. Indeed, if it is assumed that the radioactive atoms are distributed uniformly with a volume density v_0, in the main body of the specimen and that there is no intercrystalline zone at all, the determination of the density $F'(y, \tau)$ of electrons close to the surface of the specimen is reduced to the solution of one-dimensional diffusion equation

$$\frac{\partial F'(y,\tau)}{\partial \tau} = \frac{\partial^2 F'(y,\tau)}{\partial y^2} + v_0 \delta(\tau); \tag{23}$$

given the additional conditions

$$-\frac{\partial F'(y,\tau)}{\partial y} + h' F'(y,\tau) = 0 \text{ at } y = 0, \tag{24}$$

$$\frac{\partial F'(y,\tau)}{\partial y} + h' F'(y,\tau) = 0 \text{ at } y = b. \tag{25}$$

Here, instead of expression (16) we will have

$$F'(0,\tau) = F'(b,\tau) = \frac{2v_0}{\sqrt{2\pi}} \sum_{r=0}^{\infty} e^{-\alpha_{2r+1}^2 \tau} \frac{\sin \alpha_{2r+1} b}{\alpha_{2r+1} b + \sin \alpha_{2r+1} b}, \tag{26}$$

specifically, for $b \ll \frac{\pi^2}{2h'}$,

$$F'(b,\tau) = \frac{v_0}{\sqrt{2\pi}} e^{-\frac{2h'\tau}{b}}. \tag{27}$$

From Eqs. (16) and (26) we obtain the ratio (at h = h')

$$\frac{F(0,b,\tau)}{F'(b,\tau)} = \frac{s_0}{v_0} \frac{1}{\sqrt{2\tau}}. \tag{28}$$

In appraising the results obtained, we will first take into account Eq. (16) which is valid for any thickness of the specimen. According to this formula for the electrons reaching the surface (which is the section of interest to us) the normal law of distribution along the x axis, with $\sigma^2 = 2\tau$ dispersion, is valid. The maximum distribution is x = 0. With an increase in σ^2 the maximum of the distribution decreases and its breadth increases.

The ratio of this electron density at the maximum point to the electron density at the same point, but calculated on the assumption of uniform distribution of radiation sources in the main body of the specimen and the absence of the intercrystalline zone, is, according to Eq. (28), a quantity that depends on the electron energy (through τ) and does not depend on the thickness of the specimen. A clear form of this dependence can be found, but it requires additional calculation. Without going into this, we will merely point out that the symbolic age τ increases with the increase in the electron energy so that the above ratio of the maximum electron density to the background value will be reduced.

The approximate Eqs. (21), (22), and (27) are only valid for thin specimens, i.e., when $b \ll \frac{\pi^2}{2h}$. A direct evaluation of the

thickness of the specimen b satisfying this inequality is possible when the constant quantity h is known. The latter, can apparently be determined by comparing the theory with the experiment as is done in the theory of heat conductivity [17].

This theoretical study provides an expression for the distribution of the intensity of β-radiation at the surface of a specimen, i.e., an expression determining the degree of contrast of the radioautographic picture.

To obtain a numerical value for the degree to which the maximum density of the electron radiation exceeds the background, further study to determine the theoretical parameters would be needed as well as a more accurate formulation of the theory itself for the transition from the simplified model to real conditions.

REFERENCES

1. A. KOHN, Rev. Metallurgie, No. 2, 50, 1953.

2. S. Z. BOKSHTEYN, G. I. GUDKOVA, S. G. KISHKIN and L. M. MOROZ Zav. Lab. (Fact. Lab), No. 4, 1955.

3. M. E. DRITS, Z. A. SVIDERSKAYA, E. S. KADANER Zav. Lab. No. 7, 1955.

4. S. F. YURYEV, V. I. BRUK DAN SSSR, (Report of Academy of Science, USSR), No. 4, 104, 1955.

5. V. I. ARKHAROV, Trudy IFM UFAN, (Papers of Institute of Physics of Metals, Urals Branch) No. 8, 1946.

6. V. I. ARKHAROV, Trudy IFM UFAN, No. 14, 1954.

7. V. I. ARKHAROV, N. N. SKORNYAKOV. DAN SSSR, No. 5, 89, 1953.

8. V. I. ARKHAROV, T. YU. GOLDSHTEIN, DAN SSSR, No. 6, 66, 1949.

9. V. I. ARKHAROV, N. N. SKORNYAKOV, Trudy IFM UFAN, No. 16.

10. V. I. ARKHAROV, A. F. GERASIMOV, and P. L. GRUZIN, Physics of Metals and Metallurgy (Fizika Metallov i Metallovedeniye), No. 2, 2, 1956.

11. W. BOTHE, Zeits. F. Phys., 54, 1929.

12. M. C. WANG and E. GUTH, Phys. Rev., 84, 1951.

13. L. V. SPENCER and U. FANO, Phys. Rev., 93, 1953.

14. H. E. BETHE, M. E. ROSE and L. P. SMITH, Proc. Amer. Phil. Soc., 78, 1938.

15. R. E. MARSHAK, Rev. Mod. Phys., 19, 1947.

16. I. SNEDDON, Fourier Transforms (Preobrazovaniya Furiye), IL, (Foreign Language Press), Moscow, 1955.

17. G. S. KARSLOU, Theory of Heat Conductivity (Teoriya Teploprovodnosti), GITTL, (St. Press for Tech. Theor. Lit.), 1947.

18. R. BARRER, Diffusion in Solids (Diffusiya v Tverdykh Telakh) IL, Moscow, 1948.

EFFECT OF THE DISTRIBUTION OF ALLOYING ELEMENTS ON THE BEHAVIOR OF ALLOYS AT ELEVATED TEMPERATURES

M. Ye. Drits, et al

Modern concepts regarding the strength of metallic materials indicate that the structure of the alloy, i.e., its micro- and submicroscopic inhomogeneity, plays an important part in the behavior of the material at normal and especially at elevated temperatures.

The uneven distribution of elements and admixtures in the structure of true metals and alloys depends on the characteristic features of the process of forming a ploycrystalline material. Direct contact between differently oriented crystals occurs via the transition zones, in which the alloying elements and admixtures are concentrated in addition to defects of various kinds (vacancies and lattice distortions, etc.). Besides uneven distribution at the boundaries of crystals, intercrystalline inhomogeneity is also observed in true metals and alloys, caused by a disturbance of the equilibrium during solidification. This type of inhomogeneity is clearly evident in solid-solution alloys.

The condition of the internal interfaces is of great importance in heat heat-resistant materials, since at elevated temperatures the

deformation and failure of metallic materials begin at the grain boundary zones where the diffusion process develops more intensively than in the body of the grain. In this connection the distribution pattern of the alloying components and the admixtures, as well as the composition of the phases on the internal interfaces, determines to a considerable degree the diffusion rate and, consequently, the heat resistance and strength of the alloys as well.

The development of the methods of using labeled atoms (radioautography) affords new possibilities in the study of the local distribution of alloying elements and admixtures in the structure of alloys. Of particularly great importance is the method of quantitative radioautography, which enables us to evaluate the scope of the intradendtitic nonuniformity of alloys in relation to the casting conditions and their subsequent treatment.

We tried to establish the relationship between the degree of inhomogeneity of cast alloys which occurs during their crystallization and the behavior of alloys at elevated temperatures. To determine the heterogeneity of the structure we used the method of quantitative radioautography [1, 2] which is based on the calculation of the content of elements in the microstructures of the alloy by photometric measurement of the blackening density of the radioautograms.

The microradiograms were measured on an MF-2 microphotometer with a square 1 mm^2 slit at X24 magnification. A section of the radiogram with the most characteristic structure, 4-5 mm in length, was examined, its blackening density being measured at intervals of 0.01 mm, i.e., at 400-500 points.

Curves were plotted showing the change in blackening density along the length of the measured section. The data obtained were treated statistically and presented as frequency distribution curves, the character of which makes it possible to determine the deviations in the concentration of the element from its average content in the alloy. It is clear that the higher the maximum of the frequency curve and the smaller the distance between the branches of the curve on the abscissa axis, the less marked the intracrystalline inhomogeneity of the structure of the alloy (Fig. 1).

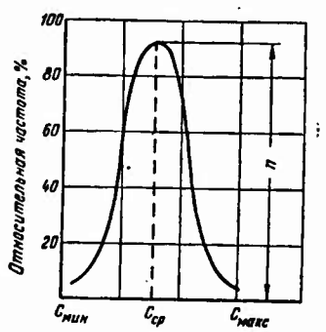

Fig. 1. Frequency distribution curve.

For a clearer and more complete generalization of the data obtained, we suggested two coefficients, K and C. The former is calculated from the formula $K = \frac{100 - n}{100}$, where 100 is taken as the total number of microstructures in which the content of the element was measured and n is the maximum of the frequency curve and

represents the number of microstructures of average concentration in the alloy. Consequently, the coefficient of the inhomogeneity K shows the total number of deviations from the average content in the section of the structure examined.

The coefficient C gives an idea of the magnitude of possible deviations in individual microstructures of the alloy and is calculated as the ratio between the maximum and minimum concentrations of calcium in the examined section of the structure ($C = \frac{C_{max}}{C_{min}}$). A combined use of these coefficients makes possible a quantitative estimate of the degree of inhomogeneity in the alloy.

The relationship between the lack of homogeneity resulting from the preferred nature of the crystallization of alloys and their heat resistance under different cooling conditions during solidification was one of the subjects of our study.

It is known that the rate of crystallization is one of the basic factors influencing the structure of a cast metal. D. K. Chernov [3], even in his time, pointed out that during high grade casting the properties of an alloy could approximate those of a metal processed under pressure. Indeed, the introduction into technology of the most efficient casting process, continuous casting, ensures the rapid crystallization of alloys, enables us to obtain castings that are not inferior in quality to deformed material. According to V. I. Dobatkin [4], the additional strengthening of duralumin alloys by acceleration of the rate of crystallization may reach 10-15 kg/mm^2. Research carried out by B. B. Gulyayev, [5], has also shown the considerable improvement in ultimate strength of steel castings when the hardening rate is quickened.

However, the data available on the influence of the rate of crystallization of alloys on their properties mainly concern tests

at normal temperatures, without direct relation to the degree of inhomogeneity of the alloys. We made a study of the relationship between the rate of crystallization and the nonuniformity of alloys by quantitative radioautography, using the radioactive isotope Ca^{45}. It should be noted that a study of the map of distribution of calcium in alloys of this system is of some interest, since it was shown earlier that a positive influence has small additions of calcium on the strength of these alloys at elevated temperatures.

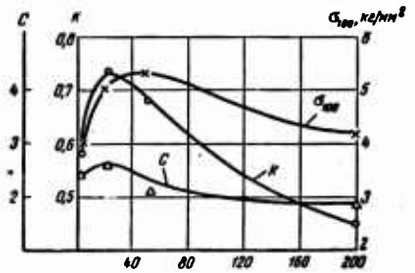

Fig. 2. Influence of cooling rate on the microinhomogeneity and heat resistance of magnesium-manganese-aluminum-calcium alloys.

Variations of cooling rate in our tests was effected by changing the diameter of the earthen mold (from 11 to 80 mm). Specimens were prepared from the castings for microradiographic study.

Under similar conditions, specimens were cast for long-time strength tests for the purpose of determining the ultimate long-time strength of the alloy at 250° for 100 hours. The results of the tests are given in Table 1 and Fig. 2, together with the curves defining the variation in microinhomogeneity of alloys cast at different rates of crystallization.

TABLE 1

Cooling rate °C/min	Coefficient of inhomogeneity		Ultimate long time strength σ_{100}^{250}, kg/mm^2
	K	C	
200	0.45	1.7	4.2
45	0.68	2.2	5.0
22	0.73	3.2	5.2
4	0.58	2.9	4.0

The comparative microradiograms are given in Fig. 3.

As seen from the given curves the relationship between the inhomogeneity and the rate of crystallization is expressed by a curve with a maximum. The inhomogeneity of the alloy is at a minimum at both a high and low rate of cooling, i.e., the distribution of the calcium in the structure is more uniform (Fig. 3a and 3b); the highest degree of inhomogeneity is found at medium rates of cooling, which is demonstrated by a structure with clearly worked distribution of the calcium in the indentritic spaces (Fig. 3b). Such a pattern of this kind in the influence of the crystallization rate on the progress of intradentritic inhomogeneity can be explained by the different diffusion rates in liquid and solid phases under varying casting conditions. For instance, very rapid cooling creates conditions under which the primary diffusion in the liquid phase responsible for the segragation effects is suppressed, and dendritic crystallization does not develop to any appreciable degree. The diffusion processes are facilitated at certain medium rates of cooling, and as a result, the difference in composition of the solid and liquid solutions

increases, intracrystalline heterogeneity reaching its maximum in this case. A further decrease in the cooling rate facilitates the processes of secondary diffusion in a solidified metal, which results in a certain leveling out of the inhomogeneities in the alloy structure.

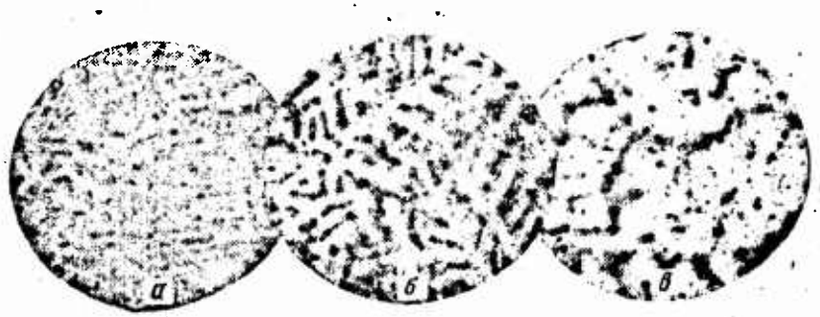

Fig. 3. Microradiograms of magnesium-manganese-aluminum-calcium alloys. Rate of cooling (°C/min): a) 200; b) 45; c) 4.

GRAPHS NOT REPRODUCIBLE

With a change in the cooling rate, the heat resistance of an alloy is modified in such a manner that the highest values of ultimate long-term strength are obtained at medium crystallization rates, i.e., at the highest values of the coefficients of inhomogeneity and, consequently, at the most marked degree of nonuniformity in the distribution of calcium (Fig. 3b). It may be assumed that at higher cooling rates as also in very slow cooling a more uniform distribution of calcium facilitates the diffusion processes and, to a certain degree, reduces heat resistance (see Fig. 3a and 3b).

Besides the degree of heterogeneity in the cast structure of a solid solution caused by the presence of calcium, a number of other factors, for instance grain size, the extent and manner of precipitation of the strengthening phases as well as the pattern of distribution of other alloying elements, can influence the long-time strength

of these alloys. It should be noted in this connection that the quantity of the second phase was very small in the alloys studied and was only detachable under great magnifications (× 1000); further, if impurities are rather fine in rapid cooling, they become coarser at medium and low cooling rates, even though their quantity remains about the same. As regards grain sizes a slight trend toward an increase of the grain is observed, but the extent of these changes is not comparable to that of the intracrystalline structure of the grain, i.e., nature of the distribution of calcium.

It is known that the structural changes occurring in alloys during heat treatment greatly influence their properties at both room and elevated temperatures. The stability of the properties of an alloy at elevated temperatures largely depends on the stability of the original structure. In view of this, the study of the kinetics of the redistribution of elements in the structure of alloys under the influence of heating acquires great practical importance.

The development of radiographic methods for investigating the structure of alloys has given rise to the possibility of the quantitative characteristics of this process. We investigated the influence of the nature of the redistribution of certain elements in the structure of magnesium and aluminum alloys under heat treatment. For this we studied complex and binary alloys of magnesium and calcium as well as alloys of aluminum and iron with the use of the radioactive isotopes Ca^{45} and Fe^{59}. The kinetics of the redistribution of these elements in the alloy structures was studied during the homogenization at a temperature 50° below solidus, the specimens being kept in the furnace for periods up to 100 hours.

Our experiments showed that given identical conditions of casting

and heat treatment, the intracrystalline heterogeneity of the structure occurring during solidification may vary to a large extent in different alloys.

The nonuniformity of structure of complex magnesium alloys composed of magnesium-manganese-aluminum-calcium remains stable even if the annealing is of relatively long duration. Along side this, the redistribution processes in the binary magnesium-calcium alloys develop at a rather rapid rate, and a leveling out of the calcium concentration in the body of the grain is already observed after eight hours of annealing. Further, alloying of magnesium-calcium alloys with manganese and aluminum evidently results in a marked decrease in the diffusion which may be of positive significance in influencing the heat-resistance characteristics of alloys.

TABLE 2

Composition	State	Coefficient of inhomogeneity		Hardness H_B, kg/mm^2; P = 100 kg D_{III} = 10 mm					
		K	C	30 sec	1 min	15 min	30 min	60 min	120 min
Mg + 0.2% Ca	Cast	0.697	2.2	14.3	13.8	9.7	10.1	10.1	8.5
	Annealing at 565°, 24 hours	0.107	1.75	13.8	11.4	8.9	8.2	7.6	7.6
Al + 0.2% Fe	Cast	0.66	4.0	8.8	7.5	6.6	5.8	5.9	5.6
	Annealing at 605°, 24 hours	0.59	3.0	8.7	8.7	6.4	5.9	6.5	6.5

The study of the kinetics of the redistribution of iron in binary alloys with aluminum showed that the dendritic character of the structure is well preserved notwithstanding prolonged annealing. The data we obtained on the stability of the inhomogeneous cast structure

brought about by crystallization in the presence of iron evidently conform with published data [6] which indicate the positive role of iron in the heat resistance of aluminum.

The greater the stability of the structure of a casting should also produce increased stability of its properties during heating. We carried out as a preliminary experiment a study of the inhomogeneity of simple binary magnesium-calcium and aluminum-iron alloys in connection with the behavior of these alloys at elevated temperatures. The data on the inhomogeneity of alloys and the results of hardness tests at elevated temperatures are given in Table 2.

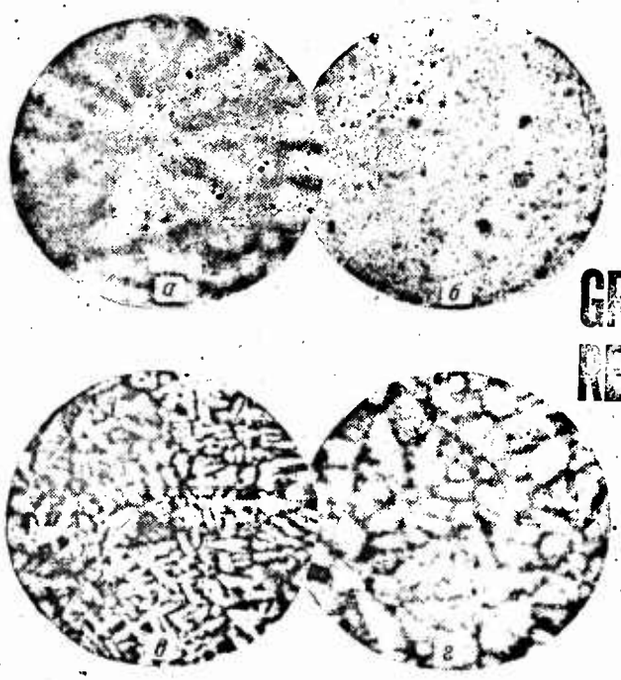

GRAPHIC NOT REPRODUCIBLE

Fig. 4. Microradiograms of alloys (× 25). a) Mg + 0.2% Ca, cast; b) Mg + 0.2% Ca, annealing at 565° for 24 hrs; c) Al + 0.2% Fe, cast; d) Al + 0.2% Fe, annealing at 605° for 24 hrs.

The microradiograms of the examined alloys as cast and after heat-treating are given in Fig. 4. In the case of the Mg-Ca alloys

(Fig. 4a and 4b), considerable changes in the distribution of calcium occurred under the influence of annealing; the coarse cast dendritic structure is transformed into a structure with a fairly uniform distribution of calcium with the exception of conglomerations at certain points. The coefficient of inhomogeneity K changes with particular abruptness and is reduced to one seventh of its original value as a result of annealing. Under the same conditions of heating, scarcely any changes in the structure of the aluminum-iron alloy are observed (Fig. 4b and 4c). The dendritic character of the structure is completely retained, the only difference being an increase in size of the dendritic cells; the coefficient of inhomogeneity K remains practically unchanged (0.66-0.59).

In Fig. 5 a graph of hardness against test-duration is shown and shows the results of comparative creep-tests of the same alloys performed by the lasting-hardness method. The path of the curves shows that in the case of aluminum-iron alloys, the variation in hardness with time at 250° is equal, both in the cast state and after homogenization. This accords well with the absence of appreciable changes in the degree of dendritic inhomogeneity, as can be seen in Fig. 4c and 4d. In the case of the magnesium-calcium alloys, the hardness values of the annealed alloy are appreciably lower than those of the cast alloy, thereby indicating intensification of the creep process as a result of the heat treatment. At the same time there is a noticeable redistribution of calcium tending toward reduction of the intracrystalline heterogeneity (Fig. 4a and 4b). The values of the K and C coefficients are lower after homogenization than in the cast state. Thus the changes in the structure of the alloys are likewise responsible for their difference in behavior at elevated temperature.

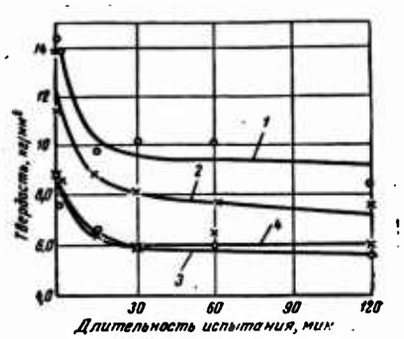

Fig. 5. Influence of length of test on the hardness of alloys. t = 250°; P = 100 kg; D_{III} = 10 mm: 1) Mg + 0.2% Ca, cast; 2) Mg + 0.2% Ca, annealed; 3) Al + 0.2% Fe, cast; 4) Al + 0.2% Fe, annealed.

REFERENCES

1. M. A. STUDNITS and O. T. MALYUCHKOV, Autoradiographic Study of Metals and Alloys by Means of Radioactive Isotopes (Avtoradiograficheskiy Metod Issledovaniya Metallov i Splavov s Pomoshchyu Radioaktivnykh Izitopov), Metallovedeniye i Obrabotka Metallov, (Metallurgy and Metal Treatment), No. 6, 1955.

2. Z. A. SVIDERSKAYA, M. Ye. DRITS, and E. S. KADANER, Influence of the Rate of Crystallization on Nonuniformity of Magnesium Alloys Metallurgy and Treatment of Metals, No. 5, 1957.

3. D. K. CHERNOV and the Science of Metals, St. Sc. Press for Lit. on Ferr. and Nonferr. Mets., 1954.

4. V. I. DOBATKIN, Continuous Casting and Casting Properties of Alloys, 1948.

5. B. B. GULYAYEV, Solidification and Nonuniformity of Steel, 1950.

6. A. A. BOVCHAR, Z. A. SVIDERSKAYA, and L. M. KYCHAKOVA,(Bull. A. Sci. USSR, Tech. Sci. Dept.), No. 2, 1954.

INFLUENCE OF ALLOYING ADDITIONS ON THE TEMPERATURE DEPENDENCE OF THE MODULI OF ELASTICITY IN NICKEL AND NICHROME ALLOYS

I. G. Polotskiy, T. Ya. Beniyeva and Z. L. Khodov

The elastic properties of metals and alloys are determined to a considerable degree by the strength of the interatomic bonds and can be considered one of their fundamental properties. A combination of important physical and technological properties of alloys depends on the strength of the interatomic bonds in the crystal lattices. Hence a study of the elastic constants and of the factors affecting them is of interest in the study of heat-resistant alloys. The present paper deals with Young's modulus, the shear modulus of elasticity and the internal friction in test alloys with a nickel and nichrome base.

Dependence of Young's Modulus on Concentrations and Temperature in Nickel-Base Alloys*

There have been a number of studies on the dependence of Young's modulus on concentration in binary alloys. Among these are the

* Research performed by T. Ya. Beniyeva.

studies made by Koester and Rauscher [4] and by Smith [5], in which they establish laws governing the change in Young's modulus with a varying concentration in numerous binary alloys and are of great interest. In addition to this, Smith studied the influence of valence and atomic size size on Young's modulus in binary alloys. He showed that Young's modulus decreases with the increase in concentration of the additive in many solid solutions, the decrease becoming more rapid with the increase in valence of the alloying additions. The decrease in Young's modulus in alloying does not, however, obey any laws (in fact, an increase is frequently observed). For instance, it was established that there is a strengthening of the interatomic bond in iron when alloyed with gold. A number of studies [6-10] have dealt also with the dependence of Young's modulus on temperature in metals and alloys.

A study of the influence of alloying additives on the moduli of elasticity and their dependence on temperature was considered to be of interest. It is known that chromium, molybdenum, titanium and aluminum increase the heat resistance of nickel-base alloys. Our intention was to investigate the dependence of Young's modulus on concentration and temperature in binary solid solution of nickel-molybdenum, nickel-chromium, and nickel-titanium alloys, and also in nichrome alloys with additions of titanium and aluminum. The dependence of the modulus of elasticity on temperature in the chemically pure nickel which was used as the base for these alloys was likewise investigated. To determine Young's modulus in alloys we used the acoustical method. This method [11], unlike those described by other authors [12-14], enabled us to measure Young's modulus at higher temperatures ranging up to 1200°.

Material and Preparation of Specimens

The nickel-molybdenum, nickel-chromium, and nickel-titanium test alloys were melted in a high-frequency furnace in an argon atmosphere, while the nichrome-aluminum and nichrome-titanium alloys were fused in air. As starting materials we used 99.99% Ni, 99.93% Mo, and 99.95% Al and also 98.5% aluminothermic Cr and 99.6% Ti. The chemical composition of the nickel alloys is given in Table 1.

TABLE 1

Alloy	Content of elements in weight %				
	Mo	Cr	Ti	Al	Ni
Nickel	-	-	-	-	99.99
1	4.98	-	-	-	remainder
2	9.85	-	-	-	" "
3	14.90	-	-	-	" "
4	19.48	-	-	-	" "
5	-	9.40	-	-	" "
6	-	21.36	-	-	" "
7	-	25.75	-	-	" "
8	-	-	4.32	-	" "
9	-	-	8.37	-	" "
10	-	-	10.45	-	" "
11	-	19.78	-	0.82	" "
12	-	19.78	-	2.20	" "
13	-	19.58	2.5	-	" "

Each alloy was prepared from one melting and was cast as an ingot. The ingots of all the alloys, excluding nickel with 12.5 atom % Ti, were then forged into rods with a cross-sectional diameter of 10 mm. Polished rod-shaped specimens, 7 mm in diameter and 200 mm long, were prepared for determination of Young's modulus. All the alloys were studied in the annealed state. During the heat treatment the specimens were soldered into an evacuated quartz tube (a vacuum of 10^{-3}mm Hg). The alloys of nickel, with the exception of nickel-molybdenum alloys, were heat-treated up to 900° for 5 hours and cooled in air. For the purpose of comparing the experimental data on the elastic constants of the nickel-molybdenum alloys with the results of the study on the self-diffusion of the same alloys, the latter were subjected to diffusion annealing. The specimens were soldered into a quartz tube (10^{-3}mm Hg) and heated to 1200° for 48 hours. In studying the dependence of Young'd modulus on temperature, the measurements were made in an argon atmosphere to eliminate the loss of molybdenum in the nickel-alloys and to preserve their chemical composition. The modulus of elasticity of two specimens from the same melting, the characteristic frequency of each alloy being determined twice over the entire temperature range.

Experimental Results and Discussion

The data obtained from thr study of the dependence of Young's modulus on concentrations and temperature in nickel and nickel-molybdenum alloys are given in Figs. 1-4.

As seen from Fig. 1, Young's modulus of the nickel-molybdenum alloys increased with an increase in molybdenum concentration for all alloys, with the exception of that containing 3.13 atom %. The

abnormal change in the modulus of elasticity for this alloy is due to the fact that magnetic alloys show a considerable decrease in Young's modulus. The maximum modulus of elasticity was established for the nickel alloy containing 12.89 atom % Mo. Young's modulus for this alloy is greater than for pure nickel by 6%. The modulus of elasticity of nonmagnetic nickel-chromium alloys also increases with an increase in concentrations of chromium up to 23.46 atom %. The change in the modulus in nickel-titanium alloys is related to the fact that the alloy containing 5.24 atom % Ti is magnetic, but with an increase in titanium content to 10.06 atom %, the modulus decreases.

Consequently molybdenum and chromium strengthen the interatomic bonds in binary nonmagnetic nickel-molybdenum and nickel-chromium alloys. The results coincide with studies made by G. V. Kurdyumov and N. T. Travina [15], who established that additions of chromium to nickel strengthen the interatomic bonds, It is known that even in alloys containing only one transition element, the unfilled d-shell strongly influences the bonds. An explanation of the observed growth of Young's modulus for the nickel-molybdenum and nickel-chromium alloys should therefore be sought in the fact that the vacancies in the d-shell tend to be filled by the atoms of nickel combined with those of molybdenum and chromium during the formation of the alloys.

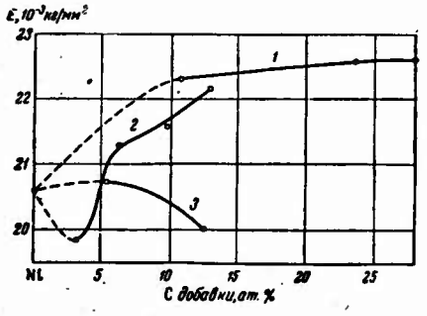

Fig. 1. Dependence of Young's modulus on concentrations in alloys. 1) Ni-Cr; 2) Ni-Mo; 3) Ni-Ti.

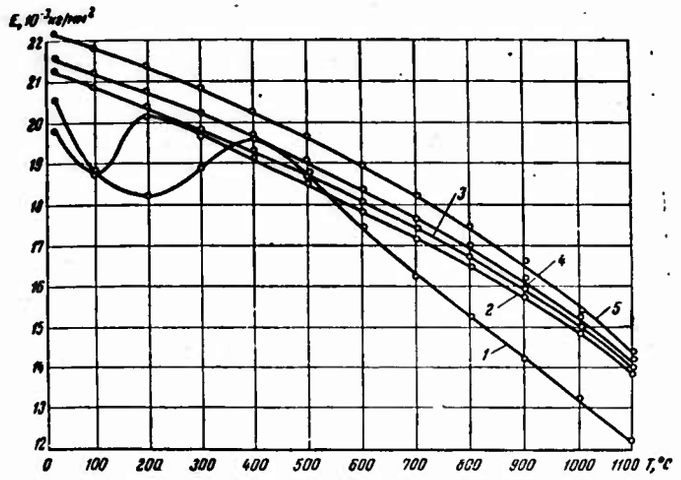

Fig. 2. Dependence of Young's modulus on temperature for nickel and nickel-molybdenum alloys with molybdenum concentration atom %: 1) 0; 2) 3.13; 3) 6.27; 4) 9.68; 5) 12.89.

The dependence of Young's modulus on temperature in nickel reaches a minimum at 200°, and this is connected with its ferromagnetic state [16] (Fig. 2). The dependence on temperature above the Curie point takes the form of an uninterrupted curve. The curve of Young's modulus for the binary solid solution containing 3.13 atom % Mo within the ferromagnetic temperature range is similar to that of pure nickel, but its minimum value shifts into the region of 100°. It should be pointed out that the alloys within the ferromagnetic temperature region showed an additional reduction of Young's modulus along with the temperature, until the Curie point was reached; this is caused by their ferromagnetism.

The change in Young's modulus in nonmagnetic nickel-molybdenum alloys containing from 6.27 to 12.89 atom % Mo is up to 700° practically a linear function, whereas at higher temperatures there is an

accelerated reduction of the modulus. The temperature curves of the modulus for the nickel-molybdenum alloys are situated considerably higher than those for pure nickel. The absolute value of the modulus of elasticity increases and its higher values are maintained in the temperature range from 20° to 1100°, as the molybdenum concentration in the alloys increases.

Young's modulus in solid solutions with 10.48 atom % Cr is greater over the whole temperature range studied (Fig. 3) than in pure nickel. The temperature curve of Young's modulus for the nickel-base alloy containing 23.46 atom % Cr is located somewhat higher than for the alloy with 10.48 atom % Cr. A noteworthy fact is that in the solid solution with an increase in the concentration of Cr up to 28.13 atom %, Young's modulus does not increase and its absolute value at both low and high temperatures is about the same as for the alloy with 23.46 atom % Cr. The data given show that for nickel-chromium alloys a sharp increase occurs in Young's modulus in the 800-900° zone.

In the case of nickel-titanium alloys containing from 5.24 to 12.51 atom % Ti, the higher values of the modulus for temperatures up to 1100° are observed in the alloys with a lower titanium concentration.

Young's modulus for the nickel-chromium-aluminum alloy with 0.82% Al in the temperature range from room temperature to 600° is about the same as for the binary solid solution (Fig. 4). A further increase in temperature causes a considerable decrease in the modulus of elasticity for nichrome whereas the modulus for the nickel-chromium-aluminum alloy is greater than for the nickel-chromium binary solid solution. Consequently, the combined influence of chromium and aluminum causes a considerably higher modulus for the ternary nickel-

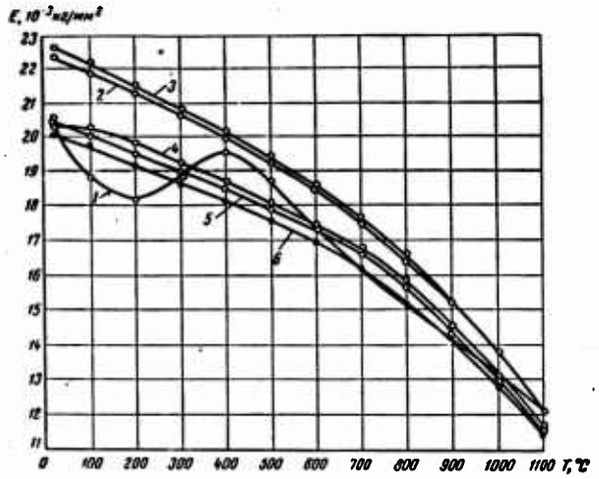

Fig. 3. Dependence of Young's modulus on temperature for nickel, nickel-chromium, and nickel-titanium alloys with chromium titanium concentrations (atom %): 1) Ni; 2) Ni + 10.48 Cr; 3) Ni + 23.46 Cr; 4) Ni + 5.24 Ti; 5) Ni + 10.0 Ti; 6) Ni + + 12.51 Ti.

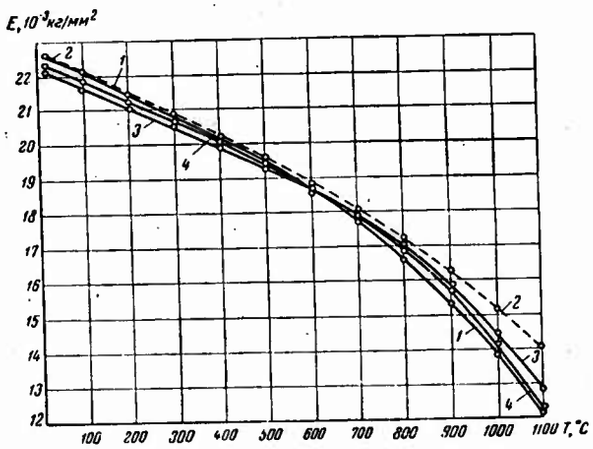

Fig. 4. Dependence of Young's modulus on temperature for nichrome with additions of aluminum and titanium (weight %): 1) Nichrome; 2) Nichrome + 0.82 Al; 3) Nichrome + 2.2 Al; 4) Nichrome + 2.5 Ti.

TABLE 2

Temperature °C	Temperature coefficient of modulus of elasticity of nickel and nickel-molybdenum alloys $\frac{\Delta E}{\Delta TET} \cdot 10^{-4}$ 1/degree				
	Ni	Ni+3.13 atom % Mo	Ni+6.27 atom % Mo	Ni+9.68 atom % Mo	Ni+12.89 atom % Mo
100	-	-	2.542	2.207	2.002
200	-	-	2.705	2.530	2.338
300	-	3.165	2.909	2.843	2.765
400	-	3.393	3.252	3.182	3.086
500	6.283	3.514	3.487	3.427	3.308
600	7.020	3.922	3.740	3.684	3.562
700	6.770	4.228	4.023	3.967	3.836
800	6.415	4.407	4.646	4.720	4.871
900	7.050	5.096	5.346	5.418	5.891
1000	7.580	6.073	6.342	6.394	7.491

chromium-aluminum alloy at elevated temperatures, as compared with nichrome. Young's modulus for the nickel-chromium-aluminum alloy decreases with an increase in the aluminum concentration from 0.82% to 2.2%, but in the ~ 700° zone the temperature curve of the modulus of this alloy intersects with that of nichrome and is located higher than the latter when the temperature is raised to 1100°. The temperature curve for the nickel-chromium-titanium alloy is located lower than that of nickel-chromium at temperatures ranging from 20 to 500°, and with an increase in temperature the difference in the values for the modulus decreases, with the curves approaching each other.

On the basis of these values we determined the temperature coefficients of the moduli (Table 2). The temperature coefficients of the modulus of elasticity for nickel at temperatures ranging from 100 to 200° and for the nickel alloy containing 13.13 atom % Mo at 100-200° were not determined since at that temperature range the dependence of the modulus of elasticity on temperature takes an abnormal course. The temperature coefficient for nickel increases with the temperature, a sharp climb being observed at temperatures ranging from 700-800°. In the nickel-molybdenum nonmagnetic alloys, Young's modulus increases with an increase in the molybdenum concentration, whereas the temperature coefficient of the modulus of elasticity falls at temperatures up to 700°. It should be noted that although the temperature coefficient of the modulus rises with the increase in molybdenum content, the absolute value for Young's modulus up to 1100° is the greatest in alloys with a high molybdenum content.

For the nichrome, nickel-chromium-aluminum, and the nickel-chromium-titanium alloys the temperature coefficients of the moduli of elasticity increase evenly with an increase in temperatures up to

700°, their values at corresponding temperatures being approximately equal. The temperature coefficients of the moduli of these alloys rises steeply at temperatures ranging from 800-1000°. It should be noted that the values of the temperature coefficients of the moduli for the nickel-chromium-titanium alloy at temperatures ranging from 800-1000° are greater than those for the nichrome and nickel-chromium-aluminum alloys. This indicates that in the given temperature range the nickel-chromium-titanium alloy shows the most intensive softening.

Since the temperature coefficient of the modulus of elasticity increases when the interatomic bonds are weakened to any great extent, the coefficients we determined give an idea of the softening of the nickel alloys and of their behavior patterns over a certain temperature range.

Influence of Heat Treatment on Young's Modulus of Nickel-Chromium and Nickel-Chromium-Titanium-Aluminum Alloys

An anomalous change in electric resistivity with temperature variations was observed during the study of certain alloys of nickel. Thomas [17] believes that this is connected with the occurrence of the K state observed in alloys containing at least one element with an unfilled d-shell. There are different views on the nature of this state. G. V. Kurdyumov [18] established that after a hardened nickel-chromium-titanium-aluminum alloy is heated at temperatures at which the single-phase state of the alloy is still preserved, an increase in the interatomic bond strength was observed. The author assumes that this increase results from a distribution of the atoms in a way that causes an increase in the number of paired atoms with the strongest bonds; i.e., the influence of the chemical bonds is greater.

Yu. S. Avramov [19] studied the mechanism and kinetics of the structural transformations in the Kh20N80 and EI437 alloys. He showed that the K state originates in these alloys and interprets it as the formation of short-range-order segregation.

For our study of the changes in the state of nickel-chromium and nickel-chromium-titanium-aluminum alloys we determined Young's modulus under different heat treatments. The study was conducted on a special device which enabled us to determine the modulus of elasticity with great accuracy. The specimens of the nickel alloy with 23.46 atom % Cr were subjected to the following treatment: heating to 1000° for 5 hours and annealing at 400° for 4, 16, 36, 90, and 144 hours. In the investigation of Young's modulus for the EI437b alloy during aging, the annealed temperature was 1080° and the duration 8 hours. The aging was carried out at 500, 600, 700, and 800° for 4 hours. In all instances the specimens subjected to heat treatment were cooled in air. The results of the study of the influence of heat treatment on Young's modulus for the Kh20N80 and EI437b alloys are given in Table 3. The data obtained show an increase in Young's modulus in the Kh20N80 alloy after annealing at 400°. During the first 4 hours of treatment, a rapid increase in the modulus was observed, which slowed down appreciably during further treatment; the modulus, however, steadily increased when heating was maintained up to 90 hours. Consequently, the increase in the modulus for the Kh20N80 alloy proceeds at a rather high rate in the initial stage of the transformation.

Young's modulus for the EI437b alloy, aged at 500 and 600°, is greater than that in the annealed alloy, despite the fact that the alloy is still single-phase at these temperatures. The established pattern of the change in Young's modulus during aging of the nickel-

chromium-titanium-aluminum alloy indicates that the increase in the modulus continues until the decomposition of the solid solution begins and the α' phase is precipitated which confirms G. V. Kurdyumov's observations [18] concerning the increase of the bond strengths even before decomposition of the solid solution begins.

TABLE 3

	Heating 900°	Annealing at 400°C, hrs.				
		4	16	36	90	144
Kh20N80	100%	100.29	100.38	100.67	100.95	100.98
	Hardening 1080°	Aging for 4 hours				
		500°	600°	700°	800°	
EI437b	100%	101.3	101.7	100.5	100.5	

Study of the Temperature Dependence of the Shear Modulus of Elasticity and Internal Friction in Nickel-Molybdenum Alloys and Nichrome with Additions of Titanium and Aluminum

In recent years a number of publications have appeared on the study of the temperature-dependence of the shear modulus and of internal friction in metals and alloys. Of great interest are the studies made by T. Kê [20], A. S. Novik [21], B. N. Finkel'shteyn [22], V. S. Postnikov [23], and others. We studied the temperature-dependence of the shear modulus for nickel-molybdenum alloys and for nichrome with additions of aluminum and titanium for which Young's

modulus had already been determined (see Table 1, alloys 1,2,3,12,13). Measurements of the internal friction for these alloys were also made.

To measure shear modulus and internal friction in the alloys, the torsional-vibrations method was used. The difference between our procedure and that described by other authors [22, 23] is that we used an electronic counter to measure the period of the torsional vibrations.

A beam of light from a source passes through a narrow slit and falls on a mirror which reflects it onto a screen covering the photocell. A voltage pulse is created on the screen at the input of the triggering circuit when the beam passes through the slit. The triggering circuit is set up in such a manner that it functions for four periods of torsional vibrations. During this time the electronic counter counts the number of vibrations of the quartz oscillator working at a frequency of 2.5 kilocycles. This enables us to obtain values for the period of the torsional vibrations, accurate to several tenths of a millisecond.

The absolute value for the shear modulus was determined at room temperature and the relative change in this value was determined under heating. The absolute value at the given temperature was then calculated from the latter value.

The reciprocal of the quality for the material was taken as a measuring unit of the internal friction:

$$Q^{-1} = \frac{\delta}{\pi},$$

where δ is the logarithmic damping ratio, or

$$Q^{-1} = 0.2062 \frac{T}{\tau},$$

where T is the period of torsional vibrations;

τ is the time during which the vibration amplitude decreases by half its value.

In order to obtain τ, the photocell was covered with a screen on which the zero-position of the beam was marked and in which there were two slits. The first slit was located midway between the second slit and the zero mark. The pulse was fed from the photocell into an oscillograph for scanning. The first slit was covered until disappearance of the signal from the screen. The length of time the pulse appeared on the screen with the first slit open was the value required. All measurements were made in vacuum.

The heat treatment of the wire specimens were done in the same way as for the specimens used in the determination of Young's modulus. The results of the study of the temperature-dependence of the shear modulus and internal friction of nickel-base alloys are given in Figs. 5 and 6. The upper limit of the range of the temperature measurements was set by intensive damping of the oscillations which prevented any accurate calculation of the shear modulus.

The shear modulus nickel-molybdenum alloys increases with an increase in the molybdenum concentration (Fig. 5). The variation in the modulus for nickel-molybdenum in the middle temperature range is practically a linear function, whereas at higher temperatures an accelerated decrease is observed. For alloys with a lower molybdenum content, there is a deviation from the linear change at lower temperatures. The dependence of the shear modulus on concentration and temperature established by us for nickel-molybdenum alloys is similar to that established earlier in our study of Young's modulus for the same alloys.

The curves of the dependence of internal friction on temperature

for nickel alloys with different molybdenum contents take the same form. The internal friction in these alloys is practically the same at temperatures ranging from room temperature to 400°, scarcely changing with the increase in internal friction. This increase begins at a lower temperature in the alloys with a smaller molybdenum content. It should be noted that the increase in internal friction and the deviation from linearity of the temperature-dependence of the shear modulus occurs at approximately the same temperature. This may be considered as the result of elastic slip along the grain boundaries in the nickel-molybdenum alloys.

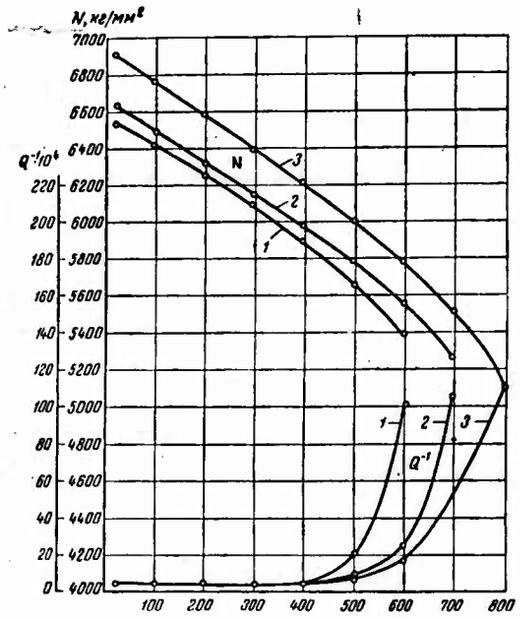

Fig. 5. Temperature dependence of the shear modulus and internal friction of nickel-molybdenum alloys with molybdenum content (atom %) 1) 3.13; 2) 6.27; 3) 9.68.

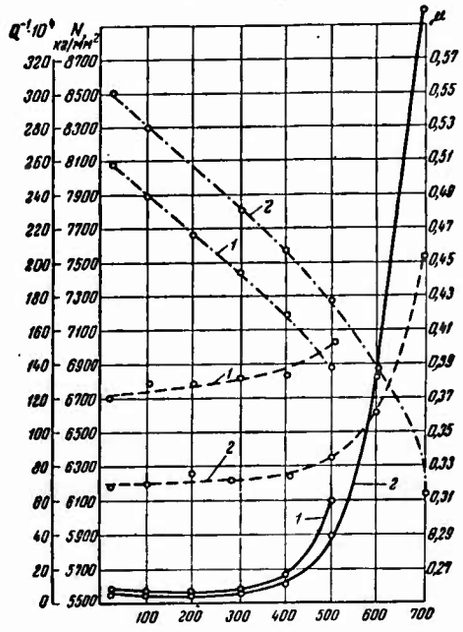

Fig. 6. Temperature dependence of the modulus, internal friction, and Poisson's ratio for nichrome with additions of aluminum and titanium (atom %) 1) 2.2 Al; 2) 2.5 Ti.

The results of our study of the dependence of the shear modulus, internal friction, and Poisson's ratio on temperature for nichrome alloys with additions of aluminum and titanium are given in Fig. 6. The temperature curve of the shear modulus for nichrome + 2.5% titanium is located higher than that for nichrome + 2.2% aluminum, the curves tending to approach one another with an increase in temperature. The shear modulus of these alloys, for all practical purposes, decreases as a linear function up to about 400°, and on a further increase in temperature this decrease becomes rapid.

As in the case of the nickel-molybdenum alloys, the internal friction scarcely changes at all with an increase in temperature over the range in which the path of the temperature dependence of the shear modulus is observed to be linear. In the temperature range within which there is a rapid increase in the internal friction, a deviation from linearity of the temperature dependence of the shear modulus is also observed. The more rapid decrease observed in the modulus with an increase in temperature is probably brought about by the occurrence of imperfections in elasticity and primarily by elastic slip along the grain boundaries.

Poisson's ratio for the whole range of temperatures studied was calculated on the basis of the data obtained for Young's modulus and the shear modulus of the nichrome alloys (see Fig. 6). The calculation was made according to the formula

$$\mu = \frac{E}{2N} - 1,$$

where E is Young's modulus and N the shear modulus.

In accordance with the above results for the elastic constants, an appreciable change in Poisson's ratio starts to occur at 400-500°. Poisson's ratio for nichrome with the addition of titanium reaches

0.45, which can be interpreted as a significant increase in the plasticity of this alloy.

Ultrasonic Pulse Device for Determining the Elastic Constants of Metals and Alloys*

In recent years ultrasonic pulse methods have been introduced for the study of the elastic constants of various types of crystals. Lazarus [24] determined the elastic constants of single crystals of β brass, and investigations [25-32], using the ultrasonic method, have determined the elastic constants of certain pure metals and alloys. Ultrasonic methods make it possible to determine Young's modulus and the shear modulus in the same specimen, affording great opportunities for studying the elastic constants of experimental alloys and establishing the relationship between the moduli and other characteristics of atomic interaction. We constructed an ultrasonic pulse device for the purpose of determining Young's modulus and the shear modulus in single and polycrystals of metals and alloys. Our procedure differed from that described by other authors in that we were able to determine the elastic constants with great accuracy in specimens 25 mm long and 15-20 mm in diameter and to measure the modulus in those metals in which the ultrasonic frequencies experience intensive damping, making it impossible to obtain a large number of "reflected" pulses.

* Study made by T. Ye. Stefanovich, aided by V. V. Chaplenko.

Working Principle of the Device

Our device enables us to determine the speed of propagation of high-frequency ultrasonic waves by a method similar to that used in radar (Fig. 7). By means of an electroacoustic transducer the oscillation pulse generates ultrasonic waves in the specimen which, having passed through the specimen and been reflected from its opposite side, return to the transducer and there generate an "answering" pulse. The time interval between the two pulses is measured in a special electronic device. From the distance traveled by the waves and the time taken to complete the round trip we calculated the speed of propagation of the transverse and longitudinal oscillations of the ultrasonic waves and then from these the speed of propagation of Young's modulus, the shear modulus, and Poisson's ratio in the given metal.

The Poisson ratio is

$$\mu = \frac{v^2_{long} - 2v^2_{tran}}{2v^2_{long} - 2v^2_{tran}} \qquad (1)$$

where v_{long} is the longitudinal wave velocity;

v_{tran} is the transverse wave velocity.

Young's modulus is

$$E = \rho v^2_{long} \frac{(3v^2_{long} - 4v^2_{tran})}{(v^2_{long} - v^2_{tran})}, \qquad (2)$$

where Young's modulus is expressed in dynes/cm^2;

ρ is the density in g/cm^3;

μ is Poisson's ratio.

The shear modulus (N) is determined by the formula

$$N = v_{tran}^2 \rho, \qquad (3)$$

which gives the shear modulus in dynes/cm^2.

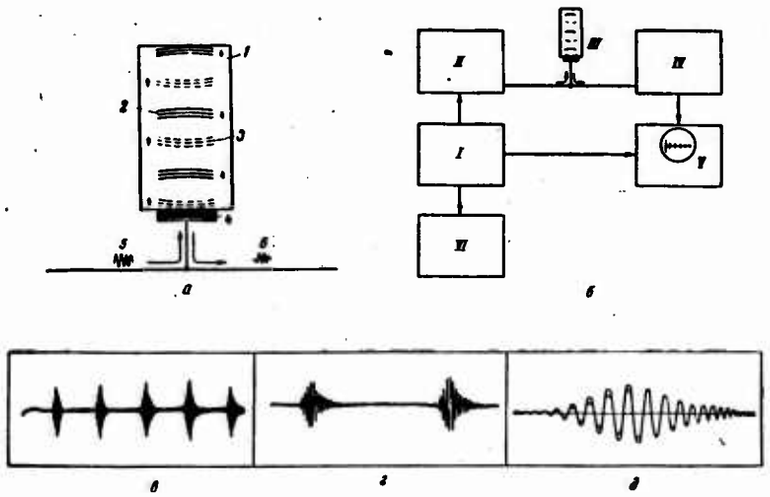

Fig. 7. The working principle of (a) and a block diagram (b) of the ultrasonic pulse device. 1) specimen; 2) initial wave; 3) reflected wave; 4) transducer; 5) generating pulse; 6) reflected pulse.

The ultrasonic device, a block diagram of which is shown in Fig. 7, works in the following way. Under the influence of triggering pulses produced in the timer I, the oscillator II, periodically generates short high-frequency oscillations which are fed into the transducer III. The repetitive rate of the triggering pulses may be selected within the limits of 2-10 kilocycles, the duration of the high-frequency oscillations is about 1 μsec and the frequency is 1-6 megacycles. The electromechanical transducer consists of a piezoquartz plate attached to the specimen with wax or mineral oil. X-cut quartz plates and Y-cut plates are used to generate the longitudinal waves and the transverse waves. The oscillations induced in

the transducer by the reflected pulses are amplified by a receiver IV and fed into a responder V. The receiver is a wide-band amplifier with a pass band at up to 6 megacycles, and a IO-4 oscillograph with minor adjustments is used as a responder.

The ultrasonic waves generated in the specimen undergo multiple reflection and are recorded by the responder each time they reach the transducer. An image of several pulses following one another at equal time intervals, by the length of the specimen, appears on the screen of the responder (Fig. 7c). For measurement of the time interval between pulses, two pulses only are reproduced on the screen (by means of an oscillator in the timer) which delay the scanning, as shown in Fig. 7d. Then without changing the time during which the pulses appear on the screenm the oscillograph scanning is replaced by sinusoidal scanning from the sinusoidal sweep oscillator located in the timer. If the period of sinusoidal scanning is made equal to that of the time between the pulses, the latter will be superposed on each other (Fig. 7e). The frequency of the sinusoidal scanning oscillator is measured with great accuracy by the calibrator VI, which is a type 528 heterodyne wavemeter. The speed of propagation of the ultrasonic waves is calculated by the formula

$$v = 2lf,$$

where v is the speed in cm/sec;

l is the length of the specimen in cm;

f is the frequency in cps determined by the calibrator.

The tests showed that this ultrasonic pulse device is reliable in performance and enables one to measure ultrasonic wave velocities with an accuracy of $\pm$ 0.2% in specimens 25 mm long. The accuracy of the measurements increases in proportion to the increase in the length of the specimen.

Apparatus for Determining Young's Modulus and Damping Factor at Elevated Temperatures*

Acoustic methods are widelt used for measuring the elastic constants of metals and alloys. Various apparatuses for measuring temperature changes in Young's modulus and in the damping factor are described in the published papers [12-14].

In view of the present necessity for great accuracy in measuring Young's modulus and the damping decrement in studying transformations in nickel alloys, we constructed an experimental device that differs considerably from other types in its use of a quartz oscillator and an electronic counter for determining the characteristic oscillation frequency of the examined specimen; this enabled us to reduce the error factor of our measurements to 0.02%. The damping decrement is measured by means of the electronic counter, which counts the number of free oscillations when their amplitude is reduced to half. In order to eliminate the influence of the suspension clips on the resonance frequency of the oscillations and the damping decrement, the specimen was suspended at the nodal points of the oscillation. Since air exercises a damping effect and causes error in determining the extent of damping, the measurements were carried out in a vacuum. Our device used electrostatic excitation, and the recording of the oscillations was effected through frequency modulation of a high-frequency generator.

The block diagram of the device for determining Young's modulus and the damping factor at elevated temperatures is shown in Fig. 8.

* Study made by V. F. Taborov, aided by G. I. Levina.

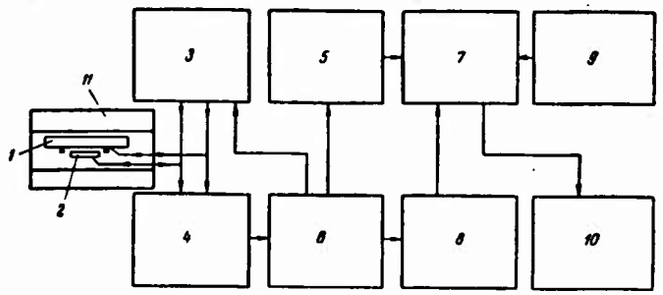

Fig. 8. Block diagram of device for determining Young's modulus and the damping factor.

The specimen 1 and the electrode 2 are simultaneously connected to the audio-oscillator 3 and the oscillatory circuit of the high-frequency generator 4. The output of the audio-oscillator has a polarized alternating voltage

$$U = U_o (1 + \sin 2\pi ft).$$

The electrostatic forces of this voltage produce the maximum amplitude of oscillations when the specimen has resonance frequency. This produces frequency modulation in the high-frequency generator 4 the oscillations of which are received by a standard frequency modulation signal receiver 6. By means of the quartz oscillator 9 the cut-in circuit 7 connects the receiver output to the counter 10 every 20 seconds for 10 seconds. In the case of the specimens with a characteristic frequency of about 800 cps, the counter registers ~ 8000 periods. The readings are reproduced with an error factor of $\pm$ 0.02%. In determining the decrement, the counter, by means of the discriminators 5 and 8, records the oscillations of the specimen when the amplitude of free oscillations is reduced by half. The discriminators switch the counter on and off when the potential at the

receiver input changes by a factor of 2. The damping factor is determined by the formula

$$\delta = \frac{1}{n} \ln 2,$$

where n is the number of oscillations when the amplitude of oscillations is reduced by half.

As a preliminary test the device was used to measure Young's modulus and the damping factor was determined for the Kh20N80 and EI437b alloys. The results showed that it could be used for measuring Young's modulus at temperatures ranging from room temperature to 1000° and for measuring the damping decrement at temperatures up to 800°.

Conclusions

1. The increase in Young's modulus when molybdenum or chromium are added to nickel indicates that the latter strengthen the interatomic bonds in binary nonmagnetic nickel-chromium and nickel-molybdenum alloys.

2. In the case of nonmagnetic alloys containing 6.27 to 12.89 atom % Mo or 10.48 to 23.46 atom % Cr, a higher value is observed for Young's modulus over the whole range of temperatures investigated in alloys with higher concentration of these elements. Young's modulus is observed to be higher up to 1100° in nickel-titanium alloys with a smaller titanium content.

3. An increase in Young's modulus during the aging of the alloy EI437b up to the point where decomposition of the solid solution begins, and an increase likewise in this modulus in the annealed Kh20N80 alloy indicate the occurrence of low-temperature transformation in nickel alloys, leading to the strengthening of the interatomic

bonds.

4. The deviation from linearity of the temperature dependence of the shear modulus occurs within the same temperature region within which internal friction abruptly increases; this is probably caused by the presence of elastic imperfections and primarily by elastic slip along the grain boundaries.

5. Poisson's ratio for nichrome with an addition of 2.5% Ti begins to show a marked increase at 400-500°; this is possibly due to a considerable increase in the plasticity of this alloy.

REFERENCES

1. W. Koester. Z. Metallkunde, 39, 1948.

2. K. Fuchs and H. Peng. Proc. Royal Soc., 983, 1942.

3. I. Frantsevich. Voprosy Poroshkovoy Metallurgii i Prochnosti Materialov, No. 3, 1956.

4. W. Koester and W. Rauscher. Z. Metallkunde, 39, 1948.

5. A. Smith. Journal Inst. of Metals, 9, 1952.

6. W. Koester. Z. Metallkunde, 39, 1948.

7. W. Koester. Z. Metallkunde, 39, 1948.

8. G. T. Harris and M. T. Watkins. Spec. Report, No. 43, 1952.

9. P. Sutton. Phys., 4, 1953.

10. W. Koester. Z. Metallkunde, 39, 1948.

11. T. Ya. Beniyeva. Voprosy Fiziki Metallov i Metallovedeniya AN SSSR, 1957.

12. F. Foerster. Z. Metallkunde, 29, 1937.

13. V. A. Zhuravlev. Zav. Lab., Fact. Lab., No. 4, 1949.

14. A. S. Matveyev, L. S. Freiman and Ye. Kh. Rapp. Zav. Lab., Fact. Lab., No. 5, 1952.

15. G. V. Kurdyumov and N. T. Travina. Problems of Metallurgy

and the Physics of Metals, 4, 1955.

16. W. Koester. Z. Metallkunde, 35, 1943.

17. H. Thomas. Zs. F. Phys., 129, 1951.

18. G. V. Kurdyumov and N. T. Travina. Problems of Metallurgy and Physics of Metals, 4, 1955.

19. Yu. S. Avramov. Investigation of the Mechanism and Kinetics of Structural Transformations in a Nickel-Base Alloy, Abstract from Thesis, 1955.

20. T. Ke. Elasticity and Anelasticity of Metals, IL (Lenin's Inst., Moscow), 1954.

21. A. S. Novik. Advances in Metal Physics, 1st collection of publications, 1956.

22. B. N. Finkelshtein and A. I. Yamshchikova. (Reports of Acad. Sci., USSRO, 98, 1955; I. S. Rysina and B. N. Finkelshtein. Ib., 1954.

23. V. S. Postnikov. Reports of Acad. Sci., USSR, 91, 1955.

24. D. Lazarus. Phys. Rev., 74, 1948.

25. J. R. Frederick. Journ. Acoust. Soc. Amer., 20, 1948.

26. H. J. McSkimin. Journ. Appl. Phys., 24, 1953.

27. H. J. McSkimin, W. L. Bond, E. Buehler, and J. K. Teal. Phys. Rev., 83, 1951.

28. W. L. Bond, W. P. Mason, H. J. McSkimin, K. M. Olsen, and G. K. Teal. Phys., Rev., 78, 1950.

29. J. R. Neighbours and F. W. Bratten. Ch. S. Smith Journ., Appl. Phys., 23, 1952.

30. W. P. Mason, R. M. Bozorth, H. J. McSkimin, and J. C. Walker. Phys. Rev., 76, 1949.

31. R. Neighbours and Ch. S. Smith. Acta Metallurgica, 2, 1954.

32. Ch. S. Smith and W. E. Wallace. J. Chem. Phys., 21, 1953.

LAWS GOVERNING THE MECHANICAL STRENGTH OF MATERIALS OBTAINED BY SINTERING OF METAL POWDERS

B. Ya. Pines, A. F. Sirenko and N. I. Sukhinin

Single and multicomponent powder metal specimens, sintered at the same temperature but soaked for different periods, show a decline in the so-called "transient" mechanical strength with an increase in porosity, which obeys a linear law. The tensile strength of solid specimens may be found by means of linear extrapolation with respect to zero porosity; this value coincides in the case of single-component compacts with the actual value of the strength of cast metals. In multicomponent powder mixtures, including those which form solutions and intermetallic phases, the strength values, extrapolated with respect to zero porosity, are a quadratic function of the concentration. The existence of this function was verified experimentally for two and three-component powder metal specimens of the following mixtures: copper-iron, copper-molybdenum, copper-tungsten, copper-nickel, molybdenum-chromium, chromium-tungsten, nickel-tungsten, copper-nickel-iron, titanium-nickel, and titanium-chromium; this was confirmed in tests at room and at elevated temperatures (up to 1000°).

The sintering of powder metal compacts is usually studied with the use of a high-temperature dilatometer, which either checks the amount of shrinkage (or the corresponding variation in porosity) after the specimens have been soaked at a high temperature, or

registers the shrinkage during the entire sintering process.

However, the phenomenon of sintering is not limited to the shrinkage effect and the accompanying increase in density. As to the features of the phenomenon itself, the changes in the mechanical properties of the materials, particularly in mechanical strength, which takes place during the sintering process, are of considerable interest.

While the laws of shrinkage during sintering (at least in single-phase systems) have been studied in fairly detailed fashion as being dependent on many parameters and a certain theoretical understanding of the phenomenon has been gained [1], the results of investigations into the change in mechanical properties during sintering are still inadequate. Only fragmentary data on this problem have been published; no firmly established general laws of the change in mechanical properties during sintering have been formulated, nor has there been even an approximate quantitative interpretation of the effects obtained. It is also noteworthy that a theory or mechanical properties of materials has scarcely been developed at all up to the present time. In particular, no quantitative connection between the structure of materials and their mechanical characteristics has yet been established. This gap could be partially filled by an experimental study of the properties of materials of different prescribed structure (structural inhomogeneity). The simplest way of producing such materials is apparently by the methods used in powder metallurgy. However, the difficulty of doing so consists in the as-yet unclarified quantitative change in mechanical properties caused by the presence of porosity and shrinkage voids in the powder compacts. In this connection, it is important to establish and interpret the basic laws of mechanical properties of substances produced by sintering powder compacts.

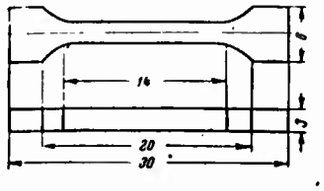

Fig. 1. Specimen for tensile strength test.

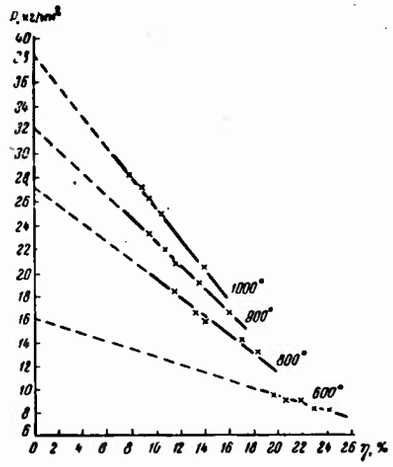

Fig. 2. Dependence of mechanical strength (transient) at room temperature on porosity of compacted powder metal copper specimens sintered at different temperatures.

The present work is an attempt to make a systematic study of the laws governing the mechanical strength of single and multicomponent powder metal mixtures subjected to sintering. Copper was selected as the basic material to simplify evaluation of the results and to avoid complications caused by the redistribution of stresses appearing in heterogeneous brittle substances (the so-called "notch" effect).

Test specimens (Fig. 1) were pressed from powder mixtures and were subjected to sintering for various periods at varying temperatures. The shrinkage)porosity) was determined and then the specimens were tested for tensile strength on a PM-500 machine; ultimate tensile strength and the total elongation to rupture was calculated. The specimens were narrowed down in their central portion to ensure the rupture always taking place in that area. The pressure at which powders were compacted was selected on the basis of preliminary tests which showed that high pressure retards sintering due to the pressure of the gas trapped in the closed pores being formed [2].

Figure 2 reproduces the curves showing the dependence of mechanical strength on the final porosity "eta" in copper specimens sintered at different temperatures. All the specimens were prepared from an electrolytic powder passed through a screen with a mesh 50 microns in diameter. The pressure was ~ 3.5 t/cm^2 and the initial porosity ρ amounted to 26-28%. The difference in porosity of specimens sintered at the same temperature, shown on the same straight line in Fig. 2, was obtained by varying the sintering times. It can be observed that in specimens sintered at the same temperature the mechanical strength S decreases when the porosity η increases, within the range of values under study, on what is approximately a linear pattern.* Given the same porosity, the strength value is found to depend also on the sintering temperature. Thus the porosity of a specimen is not an exhaustive criterion of its state and properties.

* A linear dependence of strength on porosity (for Fe specimens) was also observed in the research described in [3].

We obtained the strength of a nonporous substance by extrapolating the S value to the point $\eta = 0$. If the extrapolation is done along a straight line corresponding to sintering temperatures of 1000°C, we will obtain a strength value of 38.5 kg/mm^2, which is close to that for solid copper. The equation for this straight line can therefore be written as

$$S = S_0 (1 - \mu\eta). \qquad (1)$$

On the other hand, the straight lines showing the dependence of S on η after sintering at other lower temperatures, may be presented analytically by the formula

$$S = S_{rel} (1 - \mu_T\eta), \qquad (2)$$

where $S_{rel} < S_0$ and $\mu_T < \mu_0$ (Fig. 2).

To explain the drop in S with the increase in η, one must first take into consideration the weakening of the cross section of the specimen due to the presence of pores. Let us first assume, for the sake of simplicity, that all the pores in the specimen are spherical, have the same radius r, and are uniformly distributed.

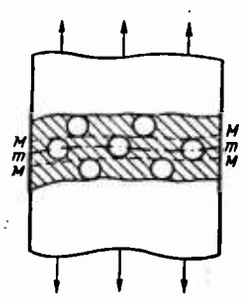

Fig. 3. Diagram showing the influence of porosity on tensile strength.

Let mm (Fig. 3) be the plane along which cleavage of the specimen occurs. Then the layer MM, 2r in thickness, which is adjacent to this plane wiol have, per cm^2 of cross section a pore volume equal to 2r and, consequently, a number of pores $\frac{2r\eta}{\frac{4\pi}{3}r^3} = \frac{3\eta}{2\pi r^2}$. The area occupied by the pores per cm^2 of cross section will be $a = \frac{3\eta\pi r^2}{2\pi r^2} = \frac{3}{2}\eta$. This is the quantity by which a cross section of 1 cm^2 will be reduced, and hence the ultimate tensile strength will decrease accordingly. In addition to the pores which are cut through by the cleavage plane and which thus directly weaken the cross section, the pores situated in the neighboring layers 2r thick will also cause a decrease in strength. Indeed, a distortion in the distribution of stresses caused by the individual spherical pores should, according to the well-known principle of St. Venant, spread to a depth of the order of their diameter. Consequently, the sections of the MM layer which are adjacent to the pores contained in the neighboring layers 2r thick will be subjected to a diminished stress [the area of the sections per unit of cross section will be $2a(1 - a)$]. Taking the weakening factor as s, we shall find that the overall effective decrease in the cross section, and with it, in the strength, is expressed by the value

$$(1 - a)1 - 2s) = 1 - a(1 + 2s) + 2sa^2$$

The experimental data presented in Fig. 2 are not for particularly high values of η. In view of this, we can neglect addends of the order $\eta 2$ in their interpretation and can write:

$$P = P_0[1 - a(1 + 2s)] = P_0\left[1 - \frac{3}{2}\eta(1 + 2s)\right]. \quad (3)$$

For this expression to coincide with Eq. (1) it is required that

$$\mu_0 = \frac{3}{2}(1 + 2\underline{s}).$$

The value μ_0 for specimens sintered at 1000° is ~ 3.45, which according to Eq. (3a) leads to the value $\underline{s} \sim \frac{2}{3}$, which is of the correct order of magnitude.

Let us note that if $\underline{s} = \frac{2}{3}$ the full formula for the dependence of S on η can be written as

$$P = P_0(1 - 3{,}45\eta + 3\eta^2). \quad (3a)$$

As previously mentioned, values for the strength $\underline{S}$rel that are considerably lower than S0 will be obtained if we extrapolate the value $\underline{S}$ with respect to $\mu = 0$ for samples sintered at lower temperatures. In this connection we may suppose that in these specimens there remain elusive areas of loose contact between grains when the porosity changes. The relative extent of such areas in the cross section should be taken equal to

$$\underline{b} = 1 - \frac{Srel}{S0} \quad ,$$

provided that there are no other effects than a decrease in the actual cross section.

Figure 4 shows curves for the dependence of mechanical strength on porosity in specimens sintered at 1000° with different soaking periods; the specimens were made of copper powder of varying initial porosity (μinit) according to the pressure under which they were compacted. The strength values for all the specimens, except those for which η = 8 and 14%, can be plotted on one curve, which even for the greatest values obtained (η = 40%) scarcely differ from the curve calculated according to Eq. (3a).

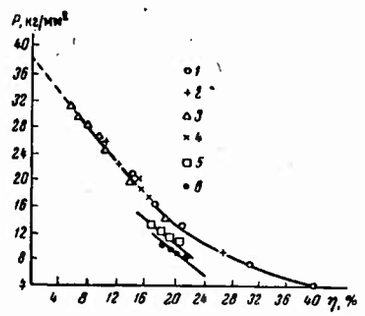

Fig. 4. Dependence of the strength on porosity in copper powder metal specimens with initial porosity ηinit %: (1) 60; (2) 40; (3) 26; (4) 18; (5) 14; (6) 8.

Thus even up to 40% the decrease in the strength of the porous specimens (plastic metals) can be adequately explained by a weakening of the cross section through porosity. With regard to specimens for which ηinit = 8 and 14%, the sintering [2] is not followed by shrinkage but by "growth" of the specimens due to gas pressure in the trapped pores. It is possible that the specimens showing this growth, as well as those sintered at low temperature, have open areas of loose contact which are not detectable in measurements of porosity, and their actual decrease in strength is greater than that calculated from their volumetric porosity.

The dependence of strengths on η arises, according to Fig. 4, when the granulometry of the powder used for compacting the specimens remains constant. If the granular size is changed, other conditions remaining unchanged, a certain increase in strength can be observed along with greater dispersion of the powder granules.

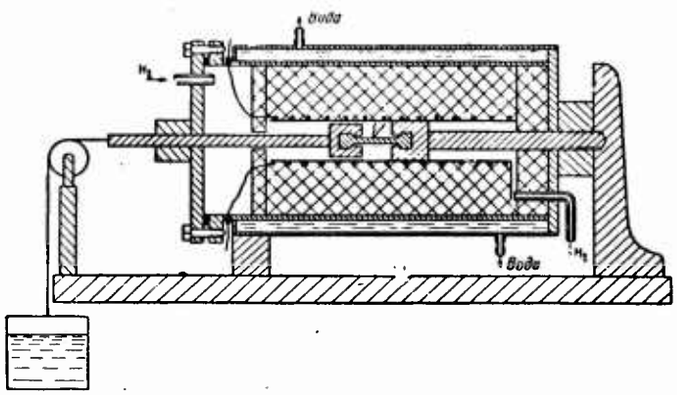

Fig. 5. Schematic diagram of the apparatus used for mechanical tests at elevated temperatures.

The dependence of $\underline{S}$ on η described above leads us to conclude that this law must be valid not only at room but also at higher temperatures. This conclusion was verified by testing powder metal specimens at higher temperature, mainly at 900°, in an H_2 atmosphere. The apparatus shown schematically in Fig. 5 was used for these tests. One of the ends of the specimen was attached to the wall of a metal container, while the other was connected to a cylindrical rod moving through a tightly fitted bushing and protruding through the opposite side. After the specimen was fixed in position, the lid of the apparatus was screwed on with a rubber gasket ensuring a tight fit. Dry hydrogen from an electrolyser was continuously circulated through the apparatus.

The specimen was subjected to stress by means of a tank filled with water attached to a cable passing over a pulley and fastened to the rod protruding from the end of the container. Different loads were achieved by varying the quantity of water in the tank.

The test specimens were prepared by compacting and sintering the powder, and were of the same shape and size as those tested at room temperature (Fig. 1). Prior to the test, the specimens were subjected to sintering of different durations at 1000°.

First of all we examined the dependence of high-temperature strength on the porosity for pure cooper. Various porosity samples were obtained by sintering at different durations at one and the same temperature (1000°). The results of the investigation of the dependence of strength on porosity at various load rates (from $8 \cdot 10^{-3}$ to 1.07 kg/min per mm^2) are presented in Fig. 6a. For a given load rate, with an increase of porosity, the strength drops off linearly. The strength values appeared much lower than at room

temperature. Certain tests conducted at various temperatures (with one and the same load rate ~ 1 kg/min per mm^2) allowed us to determine the curve of temperature dependence S (Fig. 6b). It is, of course, extrapolated to the value S = 0 at the melting point of copper.

If using the data presented in 6b, the dependence S on load rate is established, then the values $S = S_o$ extrapolated to $\eta = 0$ and also the values corresponding to the other η = const, appear to increase linearly with the logarithm of load rate. This result fully accords with the data obtained by Zhurkov [4] in his work on the law governing the dependence of durability on stress.

The linear dependence of the tensile strength S on the porosity η (Fig. 6a) can be obtained by applying a constant loading rate. This method makes it possible to find the strength of specimens with zero porosity by extrapolation according to a linear law.

Let us consider the data on strength ratios in binary mixtures. In the beginning, tests were made with mixtures of noninteracting substances. Figure 7 shows curves for the dependence of strength on porosity at room temperature for copper specimens containing an addition of tungsten and for some containing molybdenum, sintered for different lengths of time at 1000°. Both the admixed powder and the copper powder were screened through a 50-micron mesh.

In the mixtures of powders of a given composition, as in the case of pure copper, a decrease in S with η is observed which more or less obeys a linear law. The strength also decreases with an increase in the additive, since a noninteracting additive merely separates the copper granules and acts in a way similar to the sections with loose contact in the low-sintered compacts of pure copper mentioned above. This influence of the additive becomes particularly clear if we extrapolate the S value with respect to $\eta = 0$,

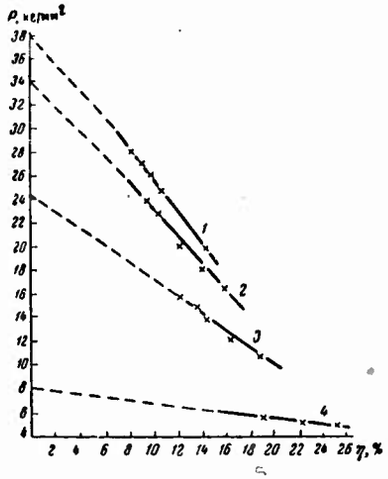

Fig. 7. Tensile strength S at room temperature depending on the porosity η of specimens: 1) Cu; 2) Cu + 5% W (Mo); 3) Cu + 20% W (Mo); 4) Cu + 35% W (Mo).

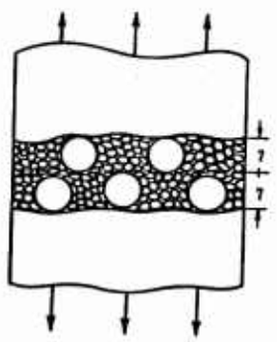

Fig. 8. Diagramatic distribution of components near the surface of the rupture.

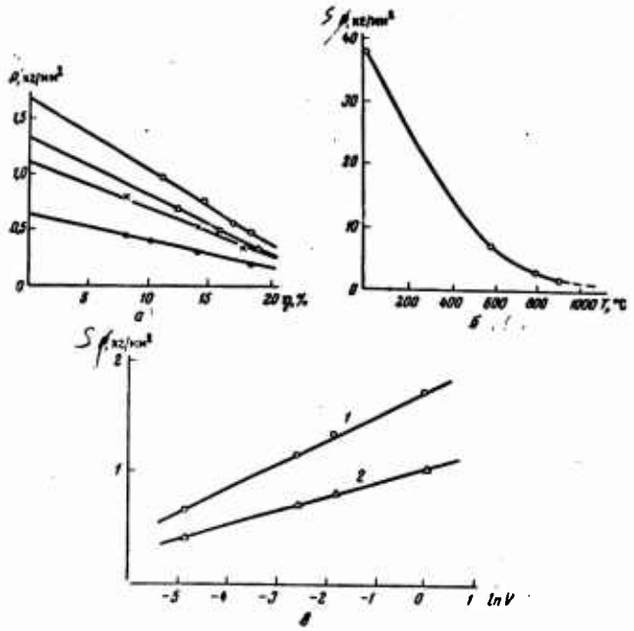

Fig. 6. Dependence of tensile strength of copper specimens. a) on porosity η at different loading rates (t = 900°); ○) 1.07; △) 0.15; ×) 0.08; 4) 0.008 kg/min mm^2; ●) on temperature; c) on the logarithm of the loading rate where η is equal (%) to: 1) 0; 2) 10.

since the extrapolated values are already free from the influence of η. The quantity of the additive is known in this particular case, so that an evaluation of the expected decline in strength can be made (from the decrease in the contact area). For the sake of simplicity let us assume that each metal powder is a collection of isomeric and identical particles having a linear dimension L (different for each powder: L_1 and L_2), while the compact is a close-packed system formed by such particles.

Let us consider the true surface (plane) of fracture of the material and the adjacent two layers of a thickness L on either side, L being the greater of the dimension L_1 and L_2 (Fig. 8.) In both layers the part of the volume w_1 and $w_2 = 1 - w_1$, occupied by each of the components, will be equal to the average volumetric concentration of the components which we shall designate by $1 - x$ and $\underline{x}$. The portions of surface occupied in each layer by the particles of components 1 and 2 will be expressed by the same values. In the case of a disordered and random grain arrangement of the components in each layer, it will be found that the areas Ω_{ik}, occupied on the cleavage surface by points of contact between like and unlike grains, amounts to:

$$\Omega_{11} = w_1 \frac{w_1}{w_1 + w_2} = w_1^2;$$

$$\Omega_{22} = w_1 \frac{w_2}{w_2 + w_1} = w_2^2;$$

$$\Omega_{12} = w_1 \frac{w_2}{w_1 + w_2} + w_2 \frac{w_1}{w_1 + w_2} = 2w_1 w_2,$$

and since

$w_1 = 1 - x$, $w_2 = x$, then $\Omega_{11} = (1 - x)^2$; $\Omega_{22} = x^2$; $\Omega_{12} = 2x(1 - x)$.

Let us assume that during cleavage along the rupture point

1 – 1 a resistance S_1 is overcome; along the contact point 2 – 2, a resistance S_2; and along the contact point 1 – 2, a resistance S_{12}. In this case, if the rupture means the simultaneous overcoming in each section of its "own" critical stress, the ultimate strength of the composite material must be equal to:

$$S = S_1 (1 - x)^2 + S_2 x^2 + 2S_{12} x (1 - x). \qquad (5)$$

In applying Eq. (5) to the data in Fig. 7 we must take into consideration the fact that after sintering at 1000° only the copper grains coalesce, as is clear from the data on shrinkage of specimens [5]; the molybdenum (tungsten) grains, on the other hand, neither fuse with each other, nor with the copper. This means that if we compare the experimental results shown in Fig. 6 with Eq. (6), we must take $S_2 = 0$ and $S_{12} = 0$; i.e., we must assume the dependence of S on $\underline{x}$ to be

$$S = S_1 (1 - x)^2.$$

Diagrams (a) and (b) in Fig. 9 show the values of the ultimate strength S at room temperature, depending on the $\underline{x}$ volumetric concentration in the two series of sintered specimens of copper and iron powder mixtures. The specimens of both series were made from electrolytic copper powder screened through a 50-micron mesh. The iron powder in one of the series was of the "whirled" type; i.e., it was pulverized in a whirl mill,* while in the other it was reduced from carbonyl. The carbonyl powder had a grain size of 2-5 microns, while the whirled powder had a coarser grain since it had been screened through a 50-micron mesh. All the specimens were sintered at 1000° in an atmosphere of H_2, with two soakings of 15 min and 4 hr respec-

* Translator's note: apparently a form of micro-atomizer.

tively. The value of the strength S for a solid specimen was obtained by linear extrapolation along a straight line where $\eta = 0$. The validity and reliability of linear extrapolation based on η were verified by additional experiments, which confirmed the soundness of this method of eliminating the porosity effect.

Equation (5) demonstrates its validity well for the given mixtures, as indicated by the curves shown in Fig. 9a and 9b for the dependence of the extrapolated S values on the concentration. The values $\Delta S = S - S_1(1 - x)^2 - S_2x^2$ fully accord with the magnitudes expected from Eq. (5) and coincide with the curve $2S_{12}x\ (1 - x)$.

The magnitude S_{12} of the strength of the localized welds between copper and iron is found in Cu + carbonyl Fe alloys to be 72 kg/mm^2, and for Cu + Fe of the "whirled" type it is 46 kg/mm^2. The first value is greater than the second, and this accords with the high value of η_{12} = shrinkage in the inhomogeneous point-bonds occurring in alloys with carbonyl iron [5].

After sintering at 1000°, compacts made from Cu + Fe (whirled-type) were tested for tensile strength similarly at 900° and at a loading rate of 0.1 $\frac{kg}{min/mm}2$. The dependence of strength on porosity (when reduced porosity was achieved by longer sintering at the same temperature) was found to be linear in this case as well. The S values extrapolated with respect to $\eta = 0$ also satisfied Eq. (5) when tested at 900°, as indicated by the data shown in Fig. 9c for the dependence on concentration of the values for $\Delta S = S - S_1\ (1 - x)^2 - - S_2x^2$, which easily fall on a curve of the $x\ (1 - x)$ type. According to Fig. 9c we have at a temperature of 900° (kg/mm^2)

$$S_{Cu} = 1.2,\ S_{Fe} = 3.4,\ S_{Fe\text{-}Cu} = 3.2.$$

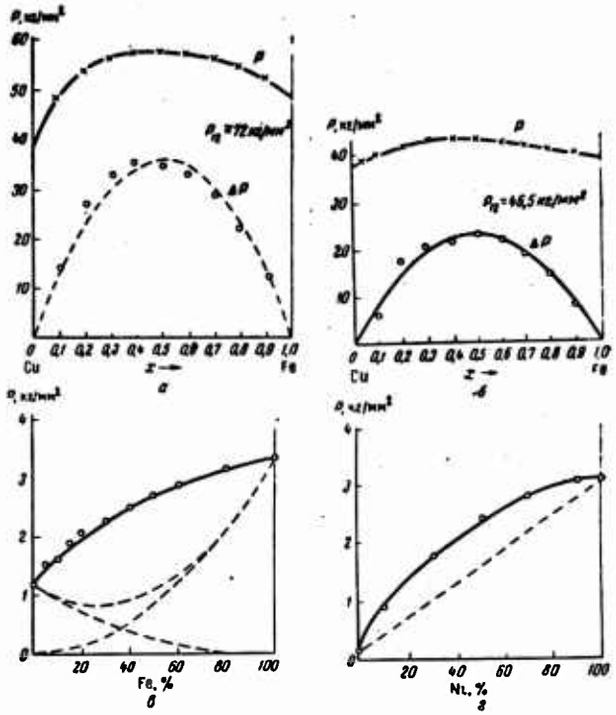

Fig. 9. Values of S = S(x). a) for a mixture Cu + Fe (carbonyl-type at room temperature); b) for Cu + Fe (whirled-type at room temperature); c) for Cu + Fe (whirled-type at 900°); d) for Cu + Ni at 900° (heating rate 0.1 kg/min mm^2).

Similar tests on powder metal specimens prepared from copper-nickel powders have shown that in these mixtures there is a linear dependence of strength on porosity. Notwithstanding the complex structure of these specimens, which were not completely homogeneous solid solutions [6], the experiments showed the dependence of the extrapolated strength values on the concentration, also satisfying the Eq. (5). According to Fig. 9d, we have in kg/mm^2

In the present research we also studied the dependence of the strength values on concentration, extrapolated with respect to $\eta = 0$, in sintered specimens of powder mixtures of chromium-molybdenum, chromium-tungsten, and nickel-tungsten.

The chromium-molybdenum specimens were sintered at temperatures of 1400 and 1500°, the chromium-tungsten at 1500°, and the nickel-tungsten* at 1250°. All the tests were made at 1000° in an H_2 atmosphere. In all cases the sintering period was varied at each selected temperature. This permitted the obtaining of specimens with different porosities, and the results of the tests made it possible to find the S values extrapolated with respect to $\eta = 0$. The dependence of the S values on the concentration in the above-mentioned mixtures satisfied Eq. (5), despite the fact that solid solutions form in these systems at high temperatures, i.e., unlimited solid solutions in the systems chromium-molybdenum and chromium-tungsten, and limited in the system nickel-tungsten.

The quadratic dependence of the S values (strength extrapolated with respect to zero porosity) on the concentration must apply to three-phase systems, i.e.,

---

* Tests were of short duration. This proved to be essential for tests with specimens containing chromium. Under our conditions, heating of specimens up to 1000° lasted about 10 min., the test took less than 5 min., and the cooling about 7 min. The total time that the samples were subjected to high temperatures did not exceed 20 min.

$$P = P_1x^2 + P_2y^2 + P_3z^2 + 2P_{12}xy + 2P_{13}xz + 2P_{23}yz, \quad (6)$$

where x, y and z are the volumetric concentrations of the components

$$x + y = 1; \quad (6a)$$

S_1, S_2 and S_3 are the quantities of tensile strength for pure components. S_{12}, S_{13} and S_{23} are the quantities which can be interpreted as tensile strength of bond contacts between different metals.

This conclusion was verified by an investigation of the ratios of mechanical strength in sintered specimens of the three-phase copper-iron-nickel powder mixture. The specimens were sintered at 1000° and tested at room temperature (using a PM-500 machine).

The data obtained from the study of the three binary systems, enabled us to determine the constants S_{ik} by means of which we found the estimated strength values for the ternary alloys. These values were compared with the experimentally derived quantities for three-phase specimens, the compositions of which corresponded to two cross sections of a ternary system: a) with an iron-copper catio of 2.3 (with a nickel concentration of 0 to 1)and b) with a nickel ratio of 2.3 (with a copper content of 0 to 1).

The calculated and the experimental values closely coincided. Thus Eq. (6) was confirmed, although there was still an inhomogeneous concentration of the solid solution in the specimens.

It should be noted that a quadratic dependence of strength on concentration both at room and at higher temperatures was eveolved in all cases tested parallel with a like quadratic dependence of shrinkage η on concentration [5]. To the systems in which a quadratic dependence of strength on concentration is observed belong not only those mixtures in which solid solutions (limited or unlimited)

are formed, but also such mixtures in which new intermetallic phases originate at high temperatures as a result of interaction. Specifically, according to our data, a similar dependence is observable in specimens of titanium-chromium powders after sintering at 1300°, and of titanium-nickel powders after sintering at 900°. However, if low-melting eutectics are formed in the system, and a liquid phase appears at the sintering temperature or below it, the dependence of strength on concentration according to Eqs. (5) amd (6) is no longer valid. In this respect, the laws governing strength are similar to those governing shrinkage.

TABLE 1

System	Sintering Temperature	Temperature and atmosphere of test, °C	Constants, strength		
			S_1	S_2	S_{12}
Titanium-chromium	1300	1000, vacuum*	6	13	17.2
Nickel-titanium	900	900, vacuum*	3.7	7	12
Chromium-molybdenum	1500	1000, H_2	15	21.5	35.2
	1400	1000, H_2	14.2	13	22
Chromium-tungsten	1500	1000, H_2	15	22	29.6
Nickel-tungsten	1250	1000, H_2	3.2	17	24
Copper-nickel	1000	900, H_2	1.2	4.2	2.4
Copper-iron (carbonyl type)	1000	room temperature	38	48	72
Copper-iron (whirled type)	1000	room temperature	38	39	46.5
	1000	900	1.2	3.4	3.2
Nickel-iron (reduced from ore)	1000	room temperature	41	47	74
Copper-nickel	1000	room temperature	38	41	57
Copper-iron (reduced from ore)	1000	room temperature	38	47	62

* Tests were carried out with the help of a vacuum apparatus similar to the one shown in Fig.5.

The sharpest deviation from the laws described above was observed in an investigation of copper specimens with low-melting additions of lead, tin, cadmium, bismuth, antimony, and zinc; here, an "abnormal" dependence of strength on concentration was observed. In a number of cases, an increase in strength was observed parallel with an increase in prorosity. This is explained by the appearance of an increased number of trapped pores due to the eutectic composition of the liquid flow between the grain boundaries when low-melting additives are present. Hence, together with the growth of contacts through diffusion, which increases the strength, there is an increase in porosity due to the gas pressure in the trapped pores; this results in a simultaneous increase in both strength and porosity. Similar effects were discovered in the nickel-aluminum system.

A peculiar dependence of strength on concentration was found to exist in powder mixtures of Mo + SiC, sintered in a vacuum at 1800° for one hour. In this system a reaction takes place in the solid phase at the indicated temperature, probably resulting in the formation of molybdenum silicide and carbide. The eutectic of a multicomponent system encompassing the reaction products and the original components is very near this temperature. When the reaction products are formed, a liquid phase seemingly also appears in some elements of the structure and spreads along the grain boundaries. This leads to a peak on the curve of the dependence of shrinkage on concentration [5] and an analogous peak on the curve of the dependence of strength on concentration. It is probable that the spreading of the eutectic at medium concentrations is associated with an increased number of stronger bonds between unlike grains cemented together by the reaction products in the solid phase and the eutectic.

The values of the strength constants in powder metal specimens prepared from binary mixtures of metallic powders are given in Table 1. This table only contains those systems in which a quadratic dependence of strength on concentration was observed, i.e., when no liquid phase is present at sintering temperatures. The constants refer to strength values extrapolated with respect to zero porosity.

Conclusions

1. It has been established that the tensile strength in a short-time test (i.e., "transient" strength) decreases according to a linear law with an increase in porosity in porous single and multi-component powder metal specimens (provided that the porosity η is not very great: $\eta < 25\%$). This dependence is only invalid if a liquid phase is formed in the specimens during sintering (i.e., if there are low-melting eutectics present whose temperature is below that of the sintering). The linear dependence of tensile strength on porosity is maintained in tests at higher temperatures. The variation of "transient" strength with porosity, according to a linear law in the case of low porosity and quadratically in the case of increased porosity, is explained by the weakening effect in cross section produced by the pores.

2. The tensile strength of the solid specimens can be found by linear extrapolation with respect to zero porosity, which in the single-phase compacts, coincides with the actual strength of the cast metals. The strength values of multi phase powder mixtures, extrapolated with respect to zero porosity, are a quadratic function of the concentration. This is true of powder mixtures in whose system both unlimited and limited solid solutions, as well as intermetallic phases,

are formed. This result is invalid only if a liquid phase appears in the specimens at the sintering temperature or below it.

3. It was proved experimentally that strength is a quadratic function of concentration in specimens of binary powder mixtures: copper-iron, copper-nickel, iron-nickel, nickel-tungsten, tungsten-chromium, chromium-molybdenum, nickel-titanium, titanium-chromium, and also in the ternary system: iron-copper-nickel.

REFERENCES

1. B. Ya. Pines. Progress of Phys. Sci., 52, 1954.

2. B. Ya. Pines, A. F. Sirenko and N. I. Sukhinin. Journ. Theor. Phys., 27, No. 9, 1957.

3. V. Mikryukov and N. Pozdnyak. Collection "Powder Metallurgy", (St. Sc. Press for Lit. on Ferr. and Nonferr. Met.) Moscow, 1954.

4. S. N. Zhurkov and B. N. Narzullayev. Journ. Theor. Phys., 23, 1953.

5. B. Ya. Pines, A. F. Sirenko and N. I. Sukhinin. Sintering and Coalescence of Multiphase Materials, Journ. Theor. Phys., No. 4, 1957.

6. B. Ya. Pines and A. F. Sirenko. Journ. Theor. Phys., 26, 1956.

CERTAIN PROBLEMS RELATIVE TO THE THEORY OF HEAT RESISTANCE

M. Yu. Bal'shin

The theory of resistance to elevated temperatures is one of the most important and, at the the same time, least studied sections of the general theory of creep resistance.

A very important event in the theory of thermostability was the recent publication of the work of Academicians A. A. Bochvar, S. G. Konobeyevskiy, et al., on the study of directional deformation in a number of metals and alloys, as a result of cyclic heat treatment [1,2,3]. The expansion of materials in some directions, accompanied by contraction in others, during cyclic heat treatment was established and a series of important laws governing this deformation were brought to light by this research. Unfortunately, the volumetric deformation of the specimens during cyclic heat treatment was not dealt with. The published data indicate an increase in volume of the specimens as a result of cyclic heat treatment, although it is difficult to obtain a quantitative idea of this because of the warping of the specimens and their deviation from a regular geometrical shape. The volumetric variation in refractories after cyclic heat treatment was the problem which was dealt with most thoroughly. A great deal of the research

done shows that cyclic heat treatment of refractories is accompanied by a considerable volumetric expansion, in a number of cases exceeding 10%, which leads to cracking and failure of the objects. The experiments on refractories were carried out under conditions which prevented a chemical reaction with the atmosphere. Besides volumetric expansion, cyclic heat treatment also causes a diminished contact surface between the grains of the material, resulting in a considerable loss of strength. Table 1 shows the decrease in strength of metals after heat-resistance tests at 1000° (quenching in water). It should be pointed out that the reduction of the contact surface and the strength is a much more sensitive characteristic than the increase in volume since a change in density of 1% corresponds to a 3-15% change in strength. According to our data, cyclic heat treatment tests also result in an increase in volume for heat resistance.

Thus it can be taken as established that cyclic heat treatment is accompanied by deformation, resulting in a greater volume, a decrease in contact between the structural elements of the material, and in time, its failure.

The majority of researchers consider that deformation after cyclic heat treatment is caused by internal stresses. However, as is known, the sum of the tensile and compressinve internal stresses is always equal to zero. In view of this fact, it should be established why a cyclic heat treatment leads, in this case, to an increase in volume and a decrease in contact area and strength.

TABLE 1

DECREASE IN BENDING STRENGTH AFTER THERMOSTABILITY TESTS [10]

Material	Strength loss in %	Material	Strength loss in %
Fe — Al_2O_3	95.8	Ni — Al_2O_3	99.14
Fe — MgO	88.1	Ni — MgO	97.1
Cr — Al_2O_3	96.6	Co — Al_2O_3	94.0
Cr — MgO	97.8	Co — MgO	93.2

The principle has been advanced [4, 5, 6], that tensile stresses cause very much greater deformation of a solid material than compressive stresses during heat treatment. This principle is substantiated as follows:

1. In the process of extension the nonuniformity in the distribution of the stresses increases, causing the extension to take place at an accelerating rate; for instance, if a cross section of the material is weakened by a defect, it will be subject to a greater stress than other sections and will be deformed more rapidly. This stress differential and the rate of deformation will constantly increase. Conversely, in the process of contraction, there occurs a leveling-out of the stresses and deformation rate. Thus, if one cross section is weakened and deformed under compression at a higher rate, the defect will be eliminated, the cross section will increase up to its mean value, and the stresses and rates will be equalized.

2. Extension results in a greater number of mobile atoms due to an increase in defects, while contraction leads to a decrease in

their number. In this connection creep takes place at an accelera.. rate during extension.

3. Admixtures and oxide films considerably reduce tensile strength, which in this case, is determined by the strength of the admixture but do not lower compressive strength, which is determined by the strength of the basic material.

Let us consider the experimental confirmation of this principle. Mong [7], who investigated the creep rate in a number of refractories, has shown that the creep rate under tension is greater by about one order than under compression. The creep rate under both tension and compression in metals was only studied for molybdenum alloys, and no particular difference in its rate has been detected. This does not disprove Mong's data, however, as the comparison was made under different atmospheric conditions-compression in a vacuum and tension in air. Moreover the difference in the creep rate must be considerably less in thermostable alloys of molybdenum than in the thermally unstable refractories, which do not stand up very well to cyclic heat treatment. The distribution of stresses is especially inhomogeneous in nonheat-conducting and brittle refractories; hence the difference in the effect of tensile and compressive stresses is particularly characteristic of these. Nevertheless, a certain nonuniformity in the distribution of stresses can be found even in the most plastic and heat-conducting metals; therefore, in these metals there must have been at least some difference in the tensile and compressive stresses which can occur after a considerable number of heat changes.

A more indirect argument in favor of this is the difference between the tensile and compressive strengths, and especially between the hardness and true strength at failure point S_k, both at room and

at elevated temperatures. This difference is especially marked in brittle materials which are not thermostable. For instance, silicon carbide has a ratio of $\frac{\sigma_b}{H_B}$ equal to a few tenths of one percent, due to which silicon carbide without admixtures is thermally unstable.

An indirect argument in support of the difference between the action of tensile and compressive stresses lies in the different laws governing creep under tension and in contact deformation. In both cases the creep can be described by the exponential law:

$$\frac{dl}{ldt} = K\,\sigma^n, \qquad (1)$$

where $\frac{dl}{ldt}$ is the creep rate;

σ is the stress;

n is the exponent.

However, in cases of contact deformation, when we determine the hot hardness taking place under hydrostatic nonuniform pressure, the exponent n = 2; in conformity with which there is a dependence of the indentation diagonal y on time t:

$$y \sim (t_0 + t)^4,$$

where t_0 corresponds to the time interval required to obtain creep deformation equal to the initial plastic deformation [5].

There is also a law of flow proportional to the square of stress for the increase in the area of contact between two particles during sintering. For sintering under pressure [5,8], given equal porosity the rate is proportional to the square of the pressure, which means that here too the law of the proportionality of the creep rate to the square of the pressure is obeyed. For creep under load $n \neq$ const, and only very seldom is it near 2, it is usually greater. The experimental data mentioned earlier on the increase in volume and

decrease in strength after cyclic heat treatment also confirm the principle which we have advanced. It is oikewise confirmed by data for the increase in volume when compacts of great density are sintered under high pressures. Figure 1 shows a typical case of the sintering of copper compacts of different density. At a density of 86% there is an increase in linear dimensions in the direction of the pressure as well as an over-all increase in volume. It is generally accepted at present that this increase is caused by relaxation of the residual stresses remaining after compacting. But sine the sum of the tensile and compressive residual stresses in compacting is equal to zero, these data confirm the conclusion that the tensile stresses are predominant.

The phenomena of volume increase and strength decrease under cyclic heat treatment could be explained in a different way. As is known, when the temperature rises there is an increase in the balanced concentration of vacancies, which may not have time to diminish under rapid cooling. As a result of this process, a further accumulation and coagulation of vacancies takes place during subsequent cycles. However, it is difficult to conceive of a tremendous accumulation of vacancies many times greater than the balanced concentration and their massive coagulation, without the action of stress. The variation in the balanced concentration cannot by itself explain why the increase proceeds in one direction and the contraction in another, nor can it explain the influence of size on heat resistance and several other phenomena. It is more correct, therefore, to explain the phenomena of heat treatment by the principle of the dominant influence of tensile stresses. We should, however, emphasize the fact that creep under stress is brought about in the first place by the most mobile

atoms at imperfection sites, and that this principle does not by any means exclude the decisive influence of vacancies and of other defects on the process of deformation in cyclic heat treatment.

Thus the principle advanced implies the inevitability of the failure of the material if the conditions of the cyclic heat treatment are severe enough and it is sufficiently prolonged. But at the same time it indicates the method of increasing thermostability to magnitudes needed in practice.

As is known, the tensile stress acts most harmfully with an evident orientation of particles since in that case it is easier for rupture to occur. As an effective measure to prevent harmful orientation, we can recommend preliminary granulation of the starting powders. Figure 2 shows how granulation reduces the harmful effect of tensile stress during sintering of extruded pieces from copper powder with flat particles.

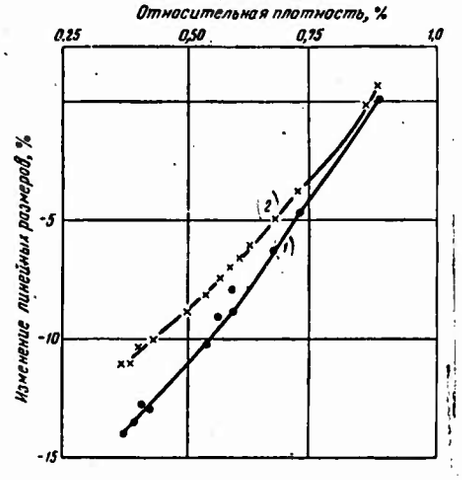

Fig. 1. Changes in dimensions of copper compact after sintering at 800°: 1) in the direction of compacting; 2) in a direction perpendicular to this pressure.

We see frm Fig. 2, after sintering of extruded pieces from nongranulated powder a significant increase in volume (15.2%) is observed. Preliminary sintering powder into granules of 140 and 100 mesh significantly decreases growth but sintering into granules of 60 mesh absolutely stops growth and is accompanied by a certain shrinkage (3.2%).

The practice of powder metallurgy also yields the answer to the question whether tensile stresses are always harmful. In such cases when external pressure is applied, the presence of tensile stresses can be beneficial by helping to relieve deformation. For instance, vibrational settling always creates both tensile and compressive stresses in equal quantities. When the powder is settling under the action of its whole weight and also during compacting, the vibrations greatly increase the density. The hot reduction of sintered powder metal materials without a die followed by rolling, which ensures lateral expansion, eliminates residual porosity more fully than hot compacting in closed molds.

The presence of small pores, which cause the formation of compressive stresses in powder metals, has a similar effect to external pressure. For instance, the standard process of sintering powder materials under capillary pressure, which reduces the volume of the pores, is equivalent to an external pressure on the order of 2-10 kg/cm^2.

It should be pointed out that two conditions are essential for the cyclic heat treatment to be effective, namely, the absence of directional orientation of the structural elements and sufficient fineness of the pores. The data in Table 3 shows that in the cyclic sintering of copper an initial density of 60% gives better results than one of 88%.

In the latter case the orientation of the particles has a markedly harmful effect.

TABLE 2

Influence of Granulation at an 80% Relative Density of the Extruded Pieces on Sintering During 1 Hour at 800°

Mesh Fraction	Volume Change in %
Starting powders — 200	+15.2
Granules — 140	+2.8
Granules — 100	+1.1
Granules — 60	-3.2

TABLE 3

Sintering of Copper Depending on Initial Porosity

Initial Density %	Volumetric change, %		
	Isothermic sintering at 800°		Cyclic sintering at 800°
	1 hr	4 hr	4 x 1 hr
60	− 9.6	− 11.9	− 14.2
88	+ 2.3	+ 1.4	+ 4.8

In this connection, porous ceramic and powder metal materials are generally more thermostable than less porous ones (Table 4).

A comparison of the data on the porosity, modulus, and heat resistance gives reason to suppose that the sharp decrease in thermostability parallel with the comparatively slight decrease in porosity is probably caused by much greater directional orientation in connection with a considerable increase in the modulus.

It is only possible to alimited extent to increase thermostability by increasing porosity, since in the process there is a decrease in strength and heat resistance. It is much more advantageous to increase thermostability by eliminating the harmful effect of orientation.

TABLE 4

Brick Brand	Modulus of elasticity E, kg/mm^2	Porosity %	Number of heat cycles, 850° - water	
			Beginning of weight loss	20% loss
B-2	958	25.0	22	28
	1290	23.5	17	31
	1810	22.3	6	16
KP-3	1900	20.6	10	19
	2810	18.1	8	29
	4270	17.4	4	9

TABLE 5

Initial granules size in mm	Number of heat cycles at 1200° -quenching in water	
	Strong granules	Weak granules
Ungranulated powder up to 0.01	1.0	1.0
Granules 0.4	11.2	5.0
Granules 3	8.3	4.25
30% Granules 0.4	11.3	4.0
70% Granules 3		

The effect of grain size on thermostability is also related to what has been described above. A small grain structure, can, on the one hand, increase thermostability dur to greater strength and smaller flaws, and on the other, decreases it by facilitating the formation of intergranular fissures.

Granulated powder is the most favorable structure for the starting mixture. Granulation ensures strong materials with fine residual porosity and an absence of orientation. This results in greater thermostability of material prepared from powders preliminarily sintered into granules of different strength (Table 5).

It can be seen (from Table 5) that the thermostability of a material sintered into stronger granules is greater by one order than for ungranulated material. The thermal stability of a material agglomerated into weak granules is also 4 to 5 times greater. The final size of the granules depends on the size of the specimen to be made. For instance, if the linear dimensions of the specimen are 10 mm and the size of the granules is also 10 mm, manufacturing the specimen from the latter is almost equivalent to making it from ungranulated powder.

Thus the methods used in powder metallurgy make it possible to considerably increase the thermal stability of heat resistant materials.

The principle of the dominant influence of tensile stress may be applied to explain the behavior of solid materials both under cyclic heat treatment and also under any other kind of treatment which sets up internal stresses, as for instance, exposure to radiation.

Conclusions

1. The volumetric increase and cracking of specimens during

cyclic termal treatment can be explained by a difference in principles in the magnitude and rate of deformation under tensile and compressive stresses.

2. The principle of the dominant influence of the tensile stresses, explains the dependence of thermal stability on structure and porosity, as well as the detrimental influence of preferred orientation.

3. The principle of the dominant influence of tensile stresses can be used to produce the most thermally stable macrostructures by preliminary sintering of powders into granules and other agglomerations.

REFERENCES

1. S. T. Konobevskiy. Reports by Soviet scientists at the International Conference for Peaceful Use of Atomic Energy, Metalurgizdat, 1956.

2. Foot. Reports by foreign scientists at the International Conference on the Peaceful Use of Atomic Energy, Metallurgizdat, 1956.

3. Chizunk, Kelman. Idem.

4. M. Yu. Bal'shin. Powder Metallurgy, Metallurgizdat, 1948.

5. M. Yu. Bal'shin. Research on Heat-Resistant Alloys, Vol. II, Izd. AN SSSR, p. 359, 1957.

6. M Yu. Bal'shin. Metalloceramics, 1938.

7. Mong. Journ. of Research, November 1947.

8. Williams. In the book "Symposium on Powder Metallurgy," London, 1956.

9. Z. I. Veselova and N. I. Nevredimova. Refractories, No. 3, 1956.

10. A. E. S. White, F. K. Earp, T. H. Blackely, and J. Werker. In the book "Symposium on Powder Metallurgy, London, 1956.

BRITTLENESS DURING CREEP

N. Ye. Karskiy

Brittle fracture in metals working under conditions of creep limits the service life of a great deal of the machinery used in power plants. For instance, the increase in the diameter of high pressure steam pipes should not exceed 1%, due to the low plasticity of steel in creep. On the other hand, it is known that metal which has been working for a long time shows high rather than low plasticity during subsequent short-time tests. This applies equally to the ultimate stage of failure by creep; at this stage, a considerable distension of the grains and failure in the body of the grain is often observed, while deformation at the beginning of failure at the boundaries is slight. The opposite effect has also been observed; a metal which is brittle during static tests or which has a low impact strength can only be fractured during creep after considerable residual deformation — for instance, the creep rate of cast iron may be greater than that of steel. Similar behavior is characteristic of many cast alloys with an iron or nickel base, having a shell of excess phases at the grain boundaries and in the interdendritic space. Consequently, brittleness at high deformation rates and brittle fracture as a

result of prolonged creep are not linked by any one cause, but rather are caused in different ways.

A qualitative coincidence of the behavior of undamaged metal in short-time and long-time tests could be expected only if the deformation mechanism remained the same in both cases, i.e., if the deformation is not by nature an athermic shear*. The latter, however, is not typical of slow creep at high temperatures and low stresses.

There are two points of view with regard to brittle fracture in metals during creep.

---

* Relaxation, which eliminates the hardening due to shear at high temperatures, can only facilitate further shear deformation but does not change its mechanism. Crystallographic shear occurs only at terminal values of shearing stress; these values change relatively slightly with a rise in temperature and, according to data obtained by E. I. Shmid and V. Boas [1], do not become zero even up to the melting point of the metal.

According to the first and most popular view, the metal acquires brittleness in the process of creep as a new property which did not have in its original state (prior to creep). Among the diverse causes of embrittlement and weakening of the metal in creep are sometimes cited the diffusion processes accompanying creep, such as aging. At present one of the most probable causes is considered to be latent imperfections, or the formation and development of cracks, in a number of cases even at an early stage of deformation [2,3]. A number of hypotheses have been advanced on the micromechanism of the genesis of these cracks [4].

According to the second point of view, first expressed by Jeffries as early as 1919, there exists an equicohesive temperature at which the strength of the boundaries becomes equal to the strength of the grain, while at a higher temperature it declines. This explains the transition from intragranular to intergranular failure. The concept of the equicohesive temperature has been investigated in greater detail, and this temperature is no longer considered constant but dependent on the stress, the duration of the stress applied to the metal, and on the creep rate [5]. According to the second point of view in its original version, brittleness (intergranular failure) is a natural property of a metal and not one acquired during creep.

This elaboration of the concept as well as various hypotheses proposed by some investigators on the different behavior of the grain and the boundaries at high and low creep rates narrow the gap between the two theories. The possibility that a unified theory of the failure of metal at high temperatures will later be formulated on this basis is not excluded.

Types of Deformation and Failure During Creep

ATHERMIC SHEAR

Deformation can be divided into athermic and thermic (diffusional) types. The athermic types include shearing and twinning. The latter is typical of deformation at low temperatures is apparently not very active in creep. Shear should therefore be considered as a basic form of athermic plasticity at high temperatures.

It has been established that shear begins when the shearing stress reaches a certain (critical) value, which depends comparatively little on the temperature and the deformation rate. Shear is accompanied by greater strength. In contrast to the critical shearing stress, the strength decreases sharply with a rise in temperature. This is explained by relaxation in the crystals, i.e., the elimination of distortions in the crystal lattice caused by the shear. In the range of temperatures having a great effect on the strengthening, the latter increases considerably with an increase in the deformation rate.

In single crystals or in the separate grains of a polycrystals, the dislocations are localized in thin bundles, between which are located the crystal bodies which are only elastically deformed. Dislocation bundles moving in the same direction divide into crystal bands, while dislocations which are not parallel to the above break up the bands into blocks. The formation of dislocations is accompanied by the appearance of "deflection" lines, which according to N. F. Lashko [6], help the crystal to stay in one piece during plastic deformation.

The plastic deformation of a polycrystal is very much impeded and is nonuniform in different grains as a result of interaction between neighboring grains. The point-bounds between three grains show the greatest resistance to plastic deformation in the grain; deformation is minimal in their vicinity and tensile stresses are therefore especially great and lead to local ruptures [7]. A diagram showing how cracks form at the bond contacts of three grains according to Zener, is given in Fig. 1b.

Traces of slip both in single crystals and in polycrystals become more pronounced as the temperature rises and the deformation rate decreases. At the same time the number of dislocation bundles decreases and the crystal (grain) is sharply divided into large single blocks. This "degeneration" of shear deformation is described in detail by Wilms and Wood [8]. Under very small loads, when the shearing stress does not reach a critical value, athermic shear does not take place even at temperatures near the melting point [1].

In accordance with the views of I. A. Oding [9], the speed of sustained creep is directly proportional to the intensity (rate) of recovery and is in inverse proportion to the intensity of hardening. This conception satisfactorily explains shearing creep. It can explain in particular, the damping of the creep rate at the beginning of the process. It is sufficient here to keep in mind that the deformation in the individual grains of a polycrystal and in different parts of a grain is not uniform and is accompanied by the appearance of peaks of stress. Hence, alongside nonstrengthened or poorly strengthened areas, there will also be considerably strengthened sections. The

relaxation of the latter, and consequently* also their recovery, progresses at an accelerated rate, which apparently causes a higher creep rate immediately after loading. In the course of time the initial peaks of stress and intensive hardening are gradually smoothed out, recovery is slowed down, and the creep rate decreases. A similar point of view has been expressed by L. P. Nikitina [10].

Shearing creep, as it is known, is dominant at moderate temperatures and high degrees of stress and deformation rates. The grain boundaries resist deformation under these conditions. Due to the imperfections of the actual crystals in the dislocation bundles, a loosening effect takes place as the degree of deformation increases. According to contemporary thinking [4], vacancies accumulate here, uniting to form pores; these are the basis of subsequent cracks gradually leading to the final failure in the body of the grain. Failure is preceded by "necking" and a considerable degree of deformation. A. Salli [5] points out that single metal crystals are subject to this type of failure at all temperatures and test rates.

Viscous Flow of Grain Boundaries

At high temperatures, low stresses, and low creep rates, when

---

* Recovery through relaxation means here relaxation of the critical shearing stress in a cold-hardened metal.

athermic shear is basically supressed thermic (diffusional) plasticity comes to the fore. The diffusional deformation rate under a given stress is determined by the thermal mobility of the atoms. It is well-known that the latter is greater on the boundaries than inside the grain [11] and that it assumes an appreciable magnitude on the boundaries at lower temperatures than in the grain. This is explained by the presence of a transition layer on the boundaries, in which the arrangement of the atoms is an intermediate one as compared to that in the neighboring grains. Moreover in industrial alloys, there may be an accumulation of low-melting admixtures, additionally stimulating thermal mobility. Disturbance of the crystallographic pattern renders the properties of the boundary more similar to those of amorphous bodies, apparently, of the hard-glass type.

It follows from the theory of amorphous substances [12] that the probability of the group mechanism of the displacement of molecules in hard glass is infinitely small and that diffusion takes place only by elementary jumps without disturbing the arrangement of the neighboring molecules. The viscous flow in amorphous bodies is built up from jumps of this kind.

As is known, under the prolonged action of stress plastic deformation may occur in substances having great viscosity. At the same time, sudden impact loads prevent the development of a noticeable relaxation even in low-viscosity systems, and they react to an external force as elastic bodies.

Ke Tin-Sui [13] points out that the grain boundaries in metal behave like a viscous substance, with the viscosity coefficient decreasing as the temperature increases. This easily explains why the boundaries behave as if they were areas of great resistance to

deformation of the metal at a low temperature and higher deformation rate, and low resistance at a higher temperature a low deformation rate. On this ground Ke Tin-Sui proposes that a polycrystalline metal should be considered a two-component system. One of its components behaves as a viscous component and obeys the equation

$$\dot{S} = a\sigma + b\sigma,$$

where $\dot{S}$ is the total rate of deformation;

a is the coefficient, inversely proportional to the coefficient of internal friction;

b is the coefficient inversely proportional to the shear modulus.

The other component is of a purely elastic nature and obeys Hook's law. For a certain limited range of temperatures and stresses this model is very near to real conditions. Ke Tin-Sui showed convincingly the presence of viscous behavior of the boundaries of metal grains by methods of measuring the non-elastic phenomena.

Displacement on the grain boundaries in aluminum during creep was noticed by Fazan, Sherby and Dorn [14] in the course of metallographic observations. It is characteristic that considerable local deformation, concentrated on the boundary, correspond to total deformation of only 0.07%. From this it follows the important conclusion that viscous flow of the grain boundaries without appreciable grain deformation cannot ensure a highe degree of deformation in creep, since the volume of metal on the boundaries is an infinitely small part of the volume of the whole polycrystal. This is the cause of brittle fracture in metals under low stress, at high temperatures, and low creep rates, when grain deformation is almost suppressed and when viscous flow and failure is centered at the boundaries. A similar idea has been expressed by K. Zener [13] and M. Ya. L'vovskiy.

Thus, viscous flow on the grain boundaries is not the reserve plasticity of the alloy under conditions of creep. The sooner it begins with respect to grain deformation and the fewer impediments it encounters in its development, the sooner failure will start along the boundaries, continuing until the metal accumulates even slight residual deformation.

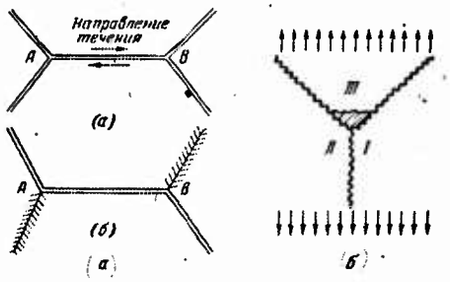

Fig. 1. Diagram of crack formation. a) on boundaries with low tangential stresses; b) at bond contacts of three grains (I, II, III).

GRAPHIC NOT REPRODUCIBLE

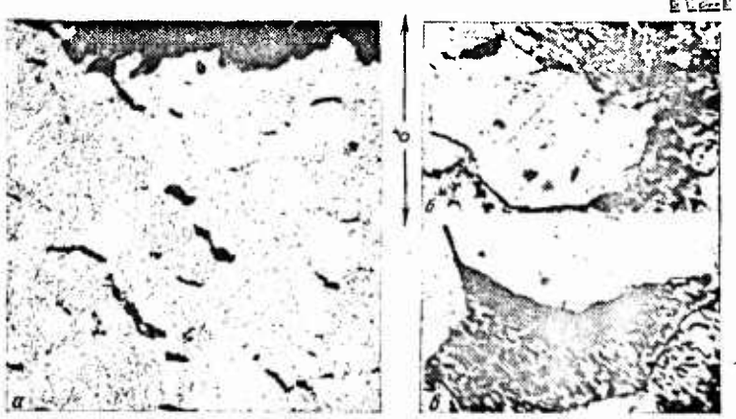

Fig. 2. Fracture sites during creep in pearlite steel. a) boundary rupture ($t - 630^{\circ}$, $\sigma - 12$ kg/mm^2, θ_k = = 123 hours, ε_k = 3.85%, ψ = 13.8%; steel 15KhIMIFL) (× 100); b) beginning of failure on grain boundaries ($t - 540^{\circ}$, $\sigma - 25$ kg/mm^2, θ_k = 1430 hours, ε_k = 7.5%, ψ = 19.6%; steel 20KhMFL) (× 2000).

In the case of absence of deformation in the grain the viscous flow of the boundaries is inevitably accompanied by failure. Only the displacement of a single grain with respect to another along a limited section of a flat boundary is possible without disrupting continuity. The boundaries in actual polycrystals are irregular. Moreover, in practice there are boundary sections in every grain that are not parallel to the direction of force of the maximum tangential stresses. Hence, in polycrystals there are always sections of the grain boundaries where displacement is difficult and where peaks of normal stresses are observed. This has been shown diagramatically by Salli (Fig. 1a).

In boundaries perpendicular to the direction of the maximum normal stresses, the latter are particularly great. It is natural to assume that the bond contacts of three grains are the places where failure starts and continues until the boundaries prevent the formation of displacement. From the moment that the grain becomes a zone of impeded deformation, the fracture sites become localized on the boundaries perpendicular to the direction of the maximum normal stresses. It is precisely here that boundary rupture cracks originate for the most part.

The extent of viscous displacement of groups of grains is greatest in those sections of the polycrystal where the boundaries of neighboring grains coincide in direction, at least approximately, and are oriented parallel to the maximum tangential stresses. These chain boundaries are points at which viscous shear occurs most easily. They break the metal up into macroblocks. At the points along the chain where separate grains or grain protrusions are encountered, peaks of tangential stresses may appear during the

creep and deformation may occur in the grain itself. Therefore, crystallographic grain orientation also influences the progress of boundary deformation.

In those links of the chain where the tangential stresses are low and the normal stresses are high, boundary rupture takes place. This case is shown in Fig. 2a. Thus, a chain of favorably oriented boundaries (and grains) is at the same time a chain of fracture sites. Microphotographs of the beginning of fracture on the grain boundaries are shown in Fig. 2a and 2b.

The cup-like, nearly equiaxial shape of the sites of fracture (Fig.2b) contradicts the idea of a purely mechanical rupture and accords with the notion of the accumulation of vacancies.

Viscous Flow in Grains

With an increase in temperature, a decrease in stress and an increase in the duration of creep, the shear deformation of the grain degenerates,the role of diffusive plasticity of the boundaries becomes greater, and a decline in plasticity is observed at the moment of fracture. However, we know of cases of a gradual increase in plasticity over a very long period of creep after minimum value of the deformation accumulated by the moment of fracture has been passed [14]. From our viewpoint, this is possible only under conditions where there is an increase in grain deformation, since the displacement along the boundaries takes place in an infinitely small volume and cannot ensure substantial deformation without disrupting the continuity of the metal. The theory proposed by Ke Tin-Sui, according to which the grain is considered a purely elastic body, discounts such a possibility. By keeping to this theory we ignore the

diffusional mobility of the atoms of the grain as a source of residual deformation. But in actual fact, the higher the temperature and the longer the duration of creep, the greater the part played by this mobility. Many facts which will be mentioned below, suggest that viscous ("shear-less") flow in the grain is actually possible. It proceeds more slowly than on the boundaries, but it develops in a greater volume of metal, and in sum may cause a considerable residual deformation.

The viscous flow of the grain generally remains unnoticed since the service temperatures and comparable test temperatures of metals are too low and the test period is limited. Moreover, it is often difficult to distinguish viscous flow from other forms of crystal deformation. Nevertheless, a number of factors which can be observed confirms the reality of this phenomenon in the grain body. Hanson and Wheeler [5] showed that deformation in polycrystals at high temperature may proceed without any visible slip. Observing very great elongations of up to 4% at the initial stage of creep, they measured the deformation of the individual crystals at the end of this stage and found that the crystals were extended in the direction of the stress and were compressed in the direction perpendicular to it, to the same extent as for the specimen as a whole. A comparison of all observations made clearly showed that deformation of the individual crystals may take place under conditions of a slow elongation without any signs of slip. Commenting on the results of the Hanson and Wheeler tests, Salli pointed out that the high degree of deformation observed during the initial stage of the process, cannot be accounted for solely by the displacement of grain boundaries.

Herring [15], referring to Nabarro* points out that self-

* Translator's note: "Nabarrd" is a transliteration.

diffusion within a polycrystal grain may cause flow in the solid body under shearing stresses. In Nabarro's opinion, the displacement caused by diffusional flow, spreads out from the boundaries where there is pressure, to the boundaries where tensile stresses act on the grain. The result of this is that the polycrystalline body becomes similar to a viscous liquid. Herring expresses the view that the given phenomenon is the main cause of creep at very high temperatures and under very low stress, as distinct from creep observed under normal conditions. Gich [16] refers to the creep tests carried out by Alexander, Kuchinski and Dawson with gold wire (diameter 0.254 mm) at 970°. These investigators obtained a linear dependence of the deformation rate on stress in the section of steady-state creep.

It was found that at the initial deformation rate, viscous flow takes place at a stress of less than 7 kg/mm^2 and that the coefficient of viscosity amounts to $1.4 \cdot 10^{12}$ poise. At stresses greater than this, the initial deformation rate again depends linearly on stress but increases faster; in this case, the coefficient of viscosity is equal to $1.5 \cdot 10^{12}$ poise. Gich assumes that viscous flow is produced under low stress by Frenkel's migration of vacancies, while the deformation rate under greater stress obeys the law formulated by Nabarro, relating the deformation rate to the size of the block in the mosaic structure or in another zone of coherence of the lattice. Furthermore, Gich refers to the results of the study of creep in gold wire (diameter 0.028 mm) at 920-1020°, in which Alexander, Dawson and Kling also found a linear dependence of the creep rate on the stresses, i.e., viscous flow. Gich comes to the conclusion that the volumetric diffusion of vacancies within blocks of the mosaic

structure may cause viscous flow and equates the two processes.

Ya. B. Fridman [17] points out that thermal plasticity is observed to some degree in all materials, including brittle intermetallic compounds, given a sufficient increase in temperature. It is known that recrystallization during creep accelerates this plasticity. When the process of recrystallization terminates, the creep rate declines. It is characteristic that, according to Salli, failure seldom takes place during this process. Phase transitions [18, 19] affect the acceleration of creep in the same was as recrystallization. Viscous flow of the grain does not exclude failure on the grain boundaries but it does apparently smooth out to some extent the stress peaks at the fracture sites.

It is therefore easy to conclude that with a higher temperature and a longer period of creep, we should expect a decline in plasticity to be followed by an increase in viscous flow on the grain boundaries as a result of viscous flow in the grain itself. Structural and phase variations are important only so far as they change the relationship between the resistance to deformation of the grain and that of its boundaries. Alloying, heat treatment, the processes of smelting and pressure treatment, cold hardening etc., have a similar effect.

All the factors which increase resistance to deformation in the grain as compared to resistance to deformation on the boundaries, must increase the intergranular brittleness of the metal during creep. This view enables us to understand certain facts which are at first sight paradoxical. For example, accretions of a thermally and mechanically strong excess phase on the grain boundaries block the boundaries and prevent the displacement of grains relative to each other. An alloy with this kind of structure generally has low

plasticity and low impact strength but does not decline in plasticity during prolonged creep (e.g., heat-resisting cast alloys with a nickel base and cast austenitic steel with accretions of carbides or intermetallic compounds on the boundaries). The example cited gives us reason to assume that the viscous flow of the boundaries may be reduced not only by raising the coefficient of internal friction but also by their "mechanical blocking."

This point of view underlies our approach to the evaluation of a number of phenomena that take place in the metal during creep and provides a basis for the solution of certain problems of practical importance. One of these problems is the increase in plasticity during creep. Attempts are often made to retard aging for this purpose, but this approach does not seem to us to be always correct. It is obviously more important to suppress the viscous flow on the boundaries, thereby eliminating "premature" intergranular fracture, and to compensate if necessary for the degeneration of athermic shear by moderate viscous flow in the grain.

In the majority of cases pure metals (and also other polycrystalline bodies) are not subject to this requirement: the viscosity on the boundaries is, as a rule, much lower than the viscosity in the grains, and it is very difficult to reverse this ratio. Hence polycrystals, in contrast to single crystals, must be considered to be brittle by nature when there is slow creep due to the inevitable development of cracks on the grain boundaries. The task thus is reduced to strengthening the boundaries in every way in relation to the grain.

Similarly, in the alloying of heat-resistant alloys viscous flow on the boundaries and in the grains of the metal is seldom taken into account and the mistake is often made of obtaining a

grain which is much too hard in relation to the boundaries, which did not receive enough attention in this respect. "Premature" fracture on the boundaries makes an alloy of this kind brittle and precludes the possibility of utilizing the heat resistance of its grain.

Attempts to evaluate the tendency of an alloy to become brittle during creep by aging it without stress cannot be justified either. Thermal brittleness and structural stability may be disclosed in this way, but not the tendency toward brittleness during creep. Instead, the relationship between the athermic shearing strength and the breaking strength of the grain changes in aging without stress, while the tendency toward brittle fracture during creep is, in the first place, determined by viscous flow on the grain boundaries and the formation of fracture sites near the boundaries.

The nature of these two forms of brittleness is entirely different. Therefore, especially when using the term "embrittlement" in connection with metals in creep, we must decide whether it means the effects of aging, detectable by short-time testing or the brittleness due to cracking of the metal as a result of viscous flow on the boundaries.

Henceforth, we will take "embrittlement" to mean the transition from intragranular to intergranular fracture, and the corresponding decline in plasticity in long-time strength tests or in the long-time use of a metal which has failed as a result of creep.

Certain Laws Governing the Embrittlement of Steel During Prolonged Creep

The following section gives an analysis of the dependence of residual deformation on temperature and time to fracture during creep in 12 MKh steel (which was investigated in detail by the author, L. P. Trusov [20] and L. P. Nikitina), in EI275 steel, and in certain other types.

In order to represent the test results graphically, we used the parametric dependence [22, 23] resulting from the exponential law:

$$\theta_k = Ae^{\frac{Q}{RT}},$$

where θ_k is the time to fracture;

A is a coefficient;

Q is the variation in the activation heat;

R is the gas constant;

T is the absolute temperature.

For σ = const, the exponential law gives an equal parameter for different temperatures:

$$T_1(C + \lg \theta_k) = T_2(C + \lg \theta_{k_1}).$$

$$T_1 (C + \log \theta_k) = T_2 (C + \log \theta_{k_2}).$$

The coefficient C was taken to be equal to 20; i.e., the parameter T $(20 + \log \theta_k)$ was used. The advantage of the parameter is that it encompasses both factors (temperature and time) on which the rupture stress and the deformation rate during creep depend.

The relative elongation* ε_{cr} caused by creep was chosen as the characteristic of plasticity:

$$\varepsilon_{cr} = \varepsilon_k - \varepsilon_0,$$

where ε_{cr} is the elongation due to creep;

ε_k is the general elongation at the moment of fracture;

ε_0 is the elongation under load.

Long-Time Strength and Embrittlement of Pearlite 12MKh Steel

The results of long-time strength tests on 12MKh steel are summarized in Table 1, and Fig. 3 shows the dependence between the initial stress and the temperature-time parameter of fracture $(20 + \log \theta_k)$ and the dependence of the creep deformation $\varepsilon_{cr} = \varepsilon_k = \varepsilon_0$ on this parameter. It can be seen from the graph that at temperatures up to 600° inclusive, the dependence of the stress on the parameter may be expressed by a general straight line from which only the results of tests under greater stress deviate to the left. For each test temperature there is a corresponding left-hand branch

* The relative contraction in this case (extension) gives way to the relative elongation, since it often characterizes fundamentally the rapidly developing final stage of fracture. Moreover, the great quantity of scale forming at high testing temperatures distorts the measurements of the contraction.

and the higher the temperature, the lower this branch is situated. Thus, the general straight line exists only on the right of the "break." A check showed that the results of tests with specimens which fractured along the grain boundaries without "necking" for which the initial and actual stress at the moment of fracture are almost the same, can be satisfactorily plotted on the general straight line. The branches deviating to the left correspond to specimens with a neck, which fractured in the grain.

The results of tests conducted at 650° deviate from the results obtained at lower temperatures. The reason for this is the failure of all specimens with great residual deformation. The specimens tested under great stress produced a local neck, whereas under low stress (5 kg/mm^2) and less they produced more uniform contraction and elongation. Considerable uniform contraction without a marked local neck is characteristic of fracture in amorphous bodies. This confirms our view of viscous flow in metal at high temperatures.

In all the tests at 650° the stress greatly increased toward the moment of fracture and several times exceeded the initial stress. However, the results obtained in tests at 650° were distorted because of considerable scaling, particularly in specimens tested under low stress and subjected to the prolinged action of high temperature. Examination of the dependence of creep deformation on the parameter (with a decrease of the initial stress) shows how the creep deformation at first increases with the rise in the parameter and then begins to decline sharply. The higher the temperature in long-time strength, the greater the parameter at which plasticity begins to decline. This decline occurs at any temperature up to a certain minimum value, which we call the physical limit of embrittlement or

simply the limit of embrittlement. After that, ε_{cr} shows a tendency to increase, which can be seen from the results of testing at 540 and 600°.

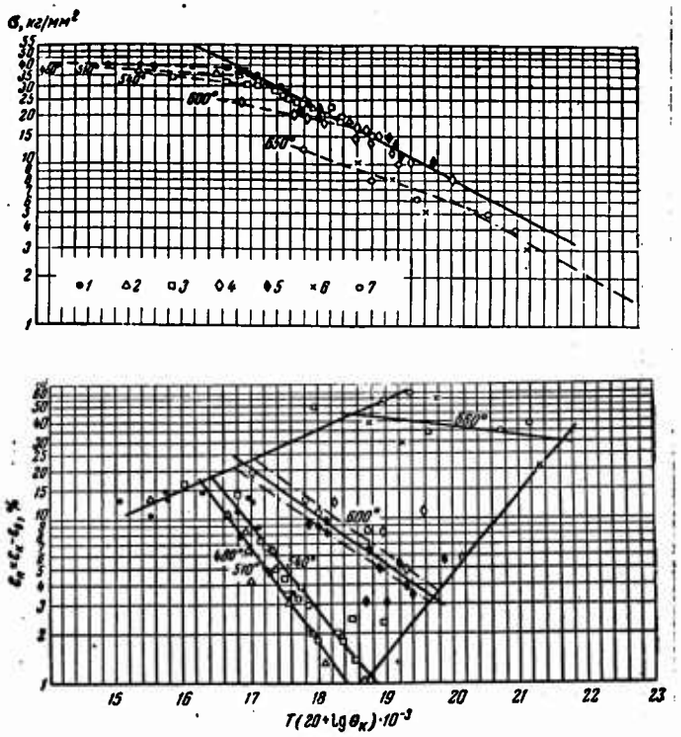

Fig. 3. Results of long-time strength tests on 12MKh steel at temperatures of (°C): 1) 480; 2) 510; 3) 540; 4) 500; 5) 600; 6) 650; 7) 650 (particularly even load).

For each parameter there are several minimum and maximum plasticities. The maximum and minimum plasticity increases with the rise in the parameter; the maximum plasticity increases less intensively with the rise in the parameter.

TABLE 1

Results of Long-Time Strength Tests on 12MKh Steel

t, °C	σ, kg/mm^2	θ_k, hours	ε_0, %	ε_k, %	ε_{cr}, %	ψ, %	Remarks
480	30	2245	0.9	4.4	3.5	1.5	Series I of specimen *
	34	686	1.9	7.4	5.5	2.4	
	35	856	2.5	7.6	5.1	5.4	
	36	320	4.2	17.4	13.2	35.8	
	36	505	3.7	12.6	8.9	18.3	
	36	376	4.2	16.3	12.1	30.4	
	38	204	4.2	15.2	11.0	45.1	
	38	214	3.5	11.2	7.7	18.6	
	38.5	9	5.7	18.9	13.2	69.5	
	39	44	4.8	19.4	14.6	57.5	
	39	8	5.3	19.7	14.4	68.4	
	40	5.25	7.75	17.9	10.1	69.2	
	40	1.15	5.7	19.0	13.3	66.1	
510	18	6466	0.19	1.2	1.01	69.2	
	22	1252	0.40	1.7	1.3	11.4	
	24	674	0.60	2.6	2.0	7.6	
	25	807	0.60	2.5	1.9	3.9	
	28	260	1.0	4.3	3.3	7.6	
	30	145	1.7	6.6	4.9	12.0	
	32	121	2.1	8.3	6.2	17.3	
	34	53.5	2.5	6.6	4.1	11.4	
	35	21.5	3.2	13.6	10.4	37.8	
	35	50	2.5	8.9	6.4	13.9	
	35	41	2.9	11.3	8.4	22.1	
	36	4.3	4.6	18.5	13.9	66.5	
540	15	2293	0.12	2.4	2.28	4.6	
	18	696	0.2	1.5	1.3	7.3	
	19	588	0.2	2.6	2.4	0.6	
	20	320	0.25	2.2	2.0	4.2	
	22	396	0.5	2.2	1.7	1.5	
	24	93	0.5	3.4	2.9	7.1	
	24	136	0.4	2.2	1.8	7.3	
	25	67	0.8	4.6	3.8	11.3	
	26	53.5	0.6	3.7	3.1	9.2	
	28	40	1.2	4.6	3.4	10.5	
	28	34.5	1.3	5.6	4.3	11.6	
	30	15.3	1.6	8.2	7.6	20.4	
	30	18	1.5	7.8	6.3	13.1	
	31	5.5	2.2	16.0	13.8	47.6	
	32	0.6	4.5	20.7	16.2	71.8	
600	8	1203	0.06	5.5	5.44	15.6	
	10	228	0.06	12.0	11.04	20.8	
	12	123	0.07	4.8	4.73	14.6	
	13	55	0.07	8.3	8.23	16.2	
	14	30	0.10	8.2	8.1	17.0	
	16	46	0.13	5.1	4.97	11.2	
	17	8.7	0.2	13.0	12.8	25.2	
	19	4.25	0.25	11.2	10.95	24.0	

* The specimens of series II differed from those of series I by somewhat greater long-time strength and lower plasticity.

TABLE 1 (CONT'D)

t, °C	σ, кг/мм²	θ_k, час.	ε_e, %	ε_k, %	$\varepsilon_п$, %	ψ, %	Примечание
	13	55	0,07	8,3	8,23	16,2	
	14	30	0,10	8,2	8,1	17,0	
	16	46	0,13	5,1	4,97	11,2	
	17	8,7	0,2	13,0	12,8	25,2	
	19	4,25	0,25	11,2	10,95	24,0	
	20	2,5	0,36	13,4	13,04	30,8	
	24	0,3	1,58	20,8	18,22	62,4	
600	10	578	0,06	5,6	5,54	16,9	II серия образцов **
	11	185	0,07	3,5	3,43	15,2	
	13	131	0,09	4,0	3,91	19,8	
	14	102	0,10	5,3	5,2	11,6	
	15	59	0,12	3,1	2,98	12,8	
	17	26,5	0,19	6,5	6,31	17,1	
	18	28	0,15	3,2	3,05	15,3	
	18,5	6,5	0,20	9,5	9,30	22,4	
	21	3,0	0,35	9,4	9,05	25,8	
	22	5,8	0,30	8,4	8,10	14,6	
	23	4,9	0,40	9,0	8,60	22,2	
650	3	1308	0,02	20,2	20,18	75,8	
	4**	845	0,03	37,05	37,02	76,7	
	5	27	0,07	54,3	54,23	90,9	
	5**	309	0,03	34,8	34,77	69,7	
	6**	20	0,10	34,0	33,9	84,3	
	8	8	0,07	28,3	28,23	92,1	
	8**	3,75	0,24	51,7	51,46	85,4	
	10	2,3	0,20	37,6	37,4	91,8	
	10**	10,1	0,125	59,2	59,1	90,0	
	12**	0,3	1,33	48,4	48,07	78,5	

** Particularly even loading.

The physical meaning of these laws is made clear by examination of the three complexing forms of deformation, viz., athermic shear, viscous flow on the boundaries, and viscous flow in the grain. The straight line showing the increase in maximum plasticity corresponds to an increase in shear deformation with rise in the parameter (i.e., with an increase in the temperature and testing time). This variation is the shear plasticity is entirely regular, since the increase in the parameter is equivalent to the progress of recovery and the shearing process. This increase in plasticity is then arrested by intergranular fracture, due to viscous flow on the boundaries, and is replaced by a decline in plasticity — embrittlement starts. At high parameter values (corresponding to high temperatures, long test

periods and low stress), plasticity again starts to increase owing to viscous flow in the grain.

The straight lines showing the increase in shear and viscous plasticity are determined on a single-value basis by the parameter, whereas the straight line relating to embrittlement is determined on a multi-value basis. Each temperature has its own straight line for embrittlement. With an increase in temperature the slope of this line decreases.

The design of embrittlement of metals during creep (Fig. 4) represents the principle described. The straight line (1) basically characterizes the increase in shear plasticity when viscous flow is almost completely suppressed. The straight line (3) shows primarily the increase in plasticity following viscous flow in the grain, when shear is practically suppressed. The straight line (2) (line of embrittlement) depicts the plastic deformation which has accumulated, mainly in the grain, by the moment of fracture. With the higher parameter, the role of the utilized athermic shear ε_b decreases, and the role of viscous flow ε_a increases in the over-all creep deformation ε_{cr}:

$$\varepsilon_{cr} = \varepsilon_a + \varepsilon_b.$$

Complete utilization of the shear would be possible in the absence of embrittlement due to intergranular fracture. The greatest possible elongation would increase constantly with a rise in the parameter and would amount to $\varepsilon_{cr} = \varepsilon_a + \varepsilon_b + \varepsilon_c$ (or $\varepsilon_{cr} = \varepsilon_a + \varepsilon_c$ to the right of point B, Fig. 4).

This accords with the fundamental tenets of the theory of equilibrium between hardening and fracture during creep [9]. At the same time, it shows the inconsistency of the objection to this theory

raised by a number of metallurgists [5], who see a lack of conformity between the expected increase in plasticity and the decrease actually observed when the length of the process is increased. We have known that an increase in athermic plasticity actually takes place together whith the rise in the parameter. This increase is interrupted by intergranular fracture which is not directly connected with shear deformation in the grain.

Figure 5 shows the dependence of plasticity (calculated for 12MKh steel from the parametric graph and firectly measured by Glen) on the time to fracture. Our curves are qualitatively identical with Glen's curve [14] and to the curves obtained from direct experimental findings [24] during long-time strength tests.

Figure 6 shows the rapid increase of the limit of embrittlement with the rise in temperature and the correspondingly simultaneous sharp decline in stress. The first value tends toward infinity, and the second toward zero at a temperature near 670°. We explain this by the fact that embrittlement gradually disappears with a considerable increase in temperature because of the highly developed viscous flow in the grain.

The tendency of plasticity toward infinity under very low stress is equivalent to the prevention of fracture until the moment the specimen stretches out into a monatomic (or monomolecular) filament. The deformation of amorphous bodies in effect approximates this extreme case under reduced stress.

The ascending straight line (see Figs. 3 and 4), which we attribute to viscous flow in the grain, could not be explained with exhaustive conclusiveness in our experiments because of the shortness of the tests. The existence of this straight line, which is common to

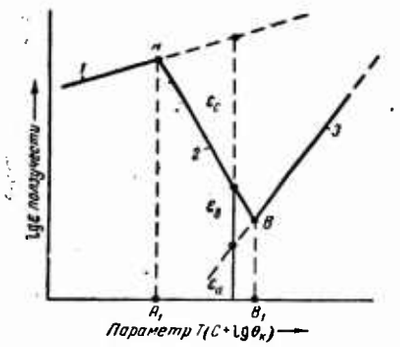

Fig. 4. Schematic drawing of tensile strength of metals during creeping.

various temperatures, is confirmed by the results of the greatly prolonged tests made by Glen.

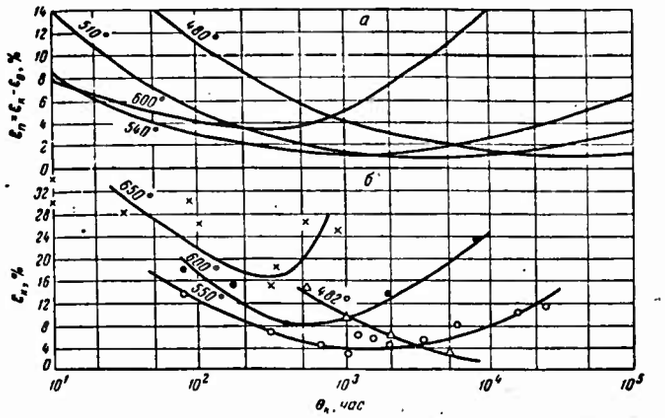

Fig. 5. Dependence of plasticity on time to fracture: a) 12MKh steel; b) 15M steel (Glen).

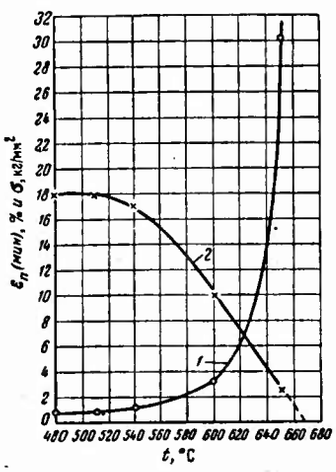

Fig. 6. Dependence of $\varepsilon_{cr(min)}$ (1) and σ (2) on temperature for 12MKh steel.

Long-Term Strength and Embrittlement of Austenitic EI257 Steel

The results of long-term strength tests with EI257 steel are given in Table 2. During the process of loading under high initial stresses, EI257 steel undergoes a very great residual elongation ε_0 rising in percentage to several decimals. Under these conditions, steel previously cold-hardened is subjected to creep. The initial residual deformation diminishes with the decrease in the prescribed stress, i.e., the cold hardening decreases; moreover, the time to fracture increases with the decrease in stress, and this helps to remove the cold hardening during creep. Thus, under low stress the metal being tested for long-term strength, for all practical purposes is not cold-hardened. This makes it understandable why the dependence between plasticity and initial stress, as well as the nature of embrittlement of austenitic EI257 steel, is more complex than in perlite 12MKh steel, in which the role of cold-hardening is small.

We should point out that when speaking of the strengthening of the steel through cold-hardening we must not ignore the processes of aging. If the latter are particularly active during loading or at the very beginning of creep, they may produce an additional resistance to shear in the grain in the later stages, thus preventing, along with the cold-hardening, the accumulation of residual deformation by the moment of fracture on the boundaries.

The parameter dependence of the long-term strength of EI257 steel (Fig. 7) indicates a slight break in the straight line: the slope of the left-hand branches differs little from the slope of the right-hand straight line (cpmmon to all temperatures). The dependence of the elongation $\varepsilon_{cr} = \varepsilon_k - \varepsilon_0$ on the parameter, shown in the same figure,

differs from the similar dependence for 12MKh steel (Fig. 3) only in cases where there is cold-hardening, i.e., at temperatures of 580 and 650°. The clearly defined minimum of plasticity at 580° revealed by the tests and the less clearly marked minimum at 650° must not be considered the limit of embrittlement. In the given instance the ascending straight lines (for 580 and 650°) characterize the transition from the low plasticity of the cold-hardened metal to a higher plasticity in the noncold-hardened metal.

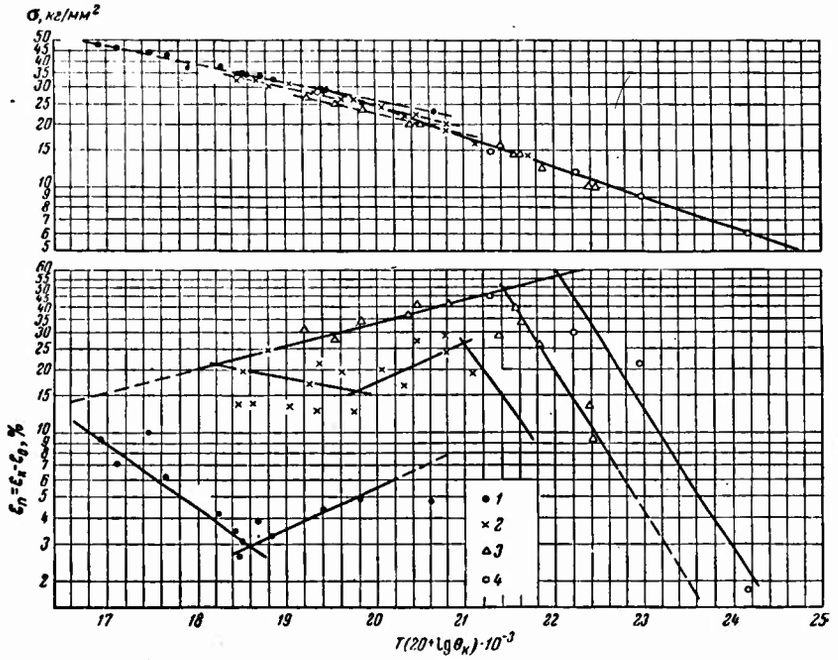

Fig. 7. Results of long-term strength tests on EI257 steel at temperatures of (°C): 1) 580; 2) 650; 3) 700; 4) 800.

The embrittlement of the cold-hardened metal is characterized by an independent set of straight lines, which are located to the right at higher parameter values. The straight lines for the embrittlement of EI257 steel have approximately the same slope at various temperatures up to 800°.

TABLE 2

Results of Long-Term Strength Tests on EI257 Steel

t, °C	σ, kg/mm²	θ_k, hours	ε_0,%	ε_k, %	ε_{cr},%	ψ, %	Remarks
650	14	2604	0,20	14,90	14,70	22,2	
	16	666	0,30	18,90	18,60	40,2	
	18	320,5	0,60	24,0	23,40	47,7	
	20	329	1,70	30,30	28,60	35,7	
	22	93,7	2,70	18,80	16,10	22,2	
	22	130,35	2,43	29,00	26,57	48,1	
	24	51,7	3,55	23,10	19,55	34,1	
	26	15,8	4,05	22,80	18,75	35,9	
	26	22,25	4,57	17,20	12,63	36,5	
	28	8,5	6,90	19,40	12,50	18,8	
	28	8,15	4,89	30,60	25,71	32,0	
	29	7,5	5,81	22,60	16,79	26,3	
	30	4,15	6,87	19,70	12,83	30,1	
	30	2,35	6,33	30,90	24,57	34,2	
	32	1,05	10,63	24,00	13,37	29,1	ε_0
	32	1,7	10,33	23,60	13,27	34,2	graphically
	33	1,2	(11,5)	26,80	15,30	44,3	
580	23	11113	2,55	7,20	4,65	17,1	
	25	1375	3,25	7,00	4,75	11,6	
	28	493	5,30	9,70	4,40	24,2	
	32	112	7,40	10,60	3,20	15,2	
	34	72,5	8,40	12,20	3,80	17,0	
	34	45,5	9,45	12,50	3,05	16,6	
	35	41	10,06	13,50	3,44	18,6	
	35	41,5	10,10	12,60	2,50	—	
	37	22,75	11,60	15,70	4,10	18,6	
	42	5	17,25	23,50	6,25	27,7	
	44	3,05	(19,6)	29,6	10,0	35,1	
	46	1,15	25,40	32,50	7,10	40,3	
	47	0,65	25,70	35,00	9,30	50,8	
700	10	932	0,09	13,80	13,71	26,0	
	10	1003	0,07	9,50	9,43	16,6	
	12	247,5	0,10	25,90	25,80	41,8	
	14	132	0,16	40,00	39,84	53,6	
	14	141,5	0,21	33,80	33,59	54,8	ε_0
	16	81,25	0,90	29,10	28,20	43,5	graphically
	18	20,15	1,29	43,00	41,71	65,0	
	20	8,6	1,30	42,10	40,80	56,3	
	20	7,75	1,40	36,40	36,00	57,5	
	23	2,2	3,60	38,00	34,40	49,7	
	25	1,0	4,50	31,50	27,00	47,9	
	27	0,5	6,50	37,30	30,80	45,0	
800	6	287	0,03	1,80	1,77	7,5	
	9	20	0,08	6,50	6,42	20,6	
	12	3,8	0,30	30,10	29,80	49,4	
	15	0,5	1,98	47,00	45,02	67,5	

The character of the embrittlement of EI257 steel at 800° justifies the view that its limits amount to a fraction of one percent at operating temperatures (580-650°) and stresses but may be attained at high parameter values corresponding upwards of 100,000 hours in the case of the steel casts under consideration. Thus the danger of embrittlement during service is, in the given instance, particularly great only in cold-hardened metal. In our opinion, shear deformation causes cold-hardening of the grain and increases its resistance to shear. At the same time, cold-hardening produces structural instability and stimulates diffusion processes, including viscous flow on the boundaries. As was mentioned earlier, an increase in the resistance of deformation in the grain, compared to the resistance to deformation on the boundaries, must cause an intensification of the embrittlement which is exactly what happened during cold-hardening.

Method for Evaluating Embrittlement

It follows from the parametric graph (Fig. 3) and from the diagram showing the embrittlement of metals during creep (Fig. 4) that to find the limit of embrittlement it is essential to determine reliably the point of intersection of the straight line of embrittlement (line 2 in Fig. 4) and that of viscous flow in the grain (line 3 in Fig. 4). The line of embrittlement may be found in many cases from the results of long-term strength tests on a piece of equipment at service temperature, using current methods. In order to obtain a straight line for viscous flow, tests will be needed at a higher series of temperatures than is usual at present. Hence, a straight line for viscous flow in the grain is, on the whole, unknown.

The hypothetical plasticity, however, can be determined on the

service parameter that corresponds to the given time and temperature. For this purpose we must extrapolate the straight line for embrittlement relative to a given temperature with respect to the service parameter.

The plasticity ε_{cr} at the service parameter, determined by the method indicated, may be said to be the arbitrary limit of embrittlement. In cases where the arbitrary limit of embrittlement is sufficiently high, satisfactory plasticity in the metal may be guaranteed during creep fracture (at a given temperature) since the arbitrary limit of embrittlement characterizes the lowest possible plasticity up to termination of a prescribed service life of the part or machinery used in the power plant. The arbitrary limit of embrittlement may be higher than the physical limit only on condition that the parameter of the latter is higher than the service parameter.

It should be pointed out that the data on the measurement of creep deformation show a great deal of incoherence. A great amount of testing, therefore, lincluding tests with long periods of time to fracture, are necessary to determing the physical and arbitrary limit of embrittlement.

Conclusions

1. Creep in metallic polycrystals is a combination of three components of residual deformation; athermic shear in the grain, viscous diffusional flow in the grain boundaries, and viscous (diffusional) flow in the grain.

Athermic shear is the main component at low temperatures, high stresses, and short time to fracture, whereas viscous flow in the grain is the main component at high temperatures, low stresses, and

long time to fracture. Viscous flow on the boundaries starts at more moderate temperatures than viscous flow in the grain.

2. A considerable residual deformation during creep without disturbing the micro- and macro-continuity of the metal, may only be obtained by grain deformation, i.e., through athermic shear of viscous flow in the grain itself. Viscous flow on the boundaries takes place in a small volume of the metal and cannot cause appreciable deformation of the whole polycrystal.

3. Viscous flow on the grain boundaries is the cause of intergranular fracture and embrittlement during creep. All the factors that increase the grain's resistance to deformation as against the resistance to deformation of the boundaries, intensify embrittlement.

4. The special features of embrittlement during creep in the case of pearlite 12MKh steel and austenitic EI257 steel were clarified. The embrittling effect of cold-hardening, which strengthens the grain and softens the boundaries, was demonstrated.

5. The notion of "physical limit of embrittlement" or simply "limit of embrittlement" was proposed, i.e., minimum plasticity as the moment of creep rupture at a given temperature is approached. It has been shown from the example of pearlitic steel that the limit of embrittlement increases with a rise in temperature.

6. The notion of an "arbitrary" limit of embrittlement has been proposed; that is the plasticity due to creep at a given temperature, obtained by extrapolation of the straight line of embrittlement with respect to the parameter $T(C + \log \theta_k)$ of the endurance limit. The arbitrary limit of embrittlement is below the physical limit if the parameter of the latter is less than the former, and vice versa.

REFERENCES

1. Ye. I. Schmidt and V. Boas. Plasticity of Crystals, 1938.

2. S. T. Kishkin. DAN SSSR, KhSu, No. 4, 1954.

3. Ya. B. Friedman and B. A. Drozdovskiy. DAN SSSR, KhSu, No. 4, 1954.

4. V. S. Ivanova. Metallurgy, Metallovedeniye, No. 1, 1955.

5. A. Salli. Creep in Metals. Oborongiz, 1953.

6. N. F. Lashko. Strengthening and Failure of Metals. Oborongiz, 1951.

7. T. I. Gudkova, N. Ye. Karskiy and G. I. Sobolev. Zav. Lab., No. 7, 1949.

8. G. R. Wilms and W. A. Wood. J. of the Inst. of Metals, April 1949.

9. I. A. Oding. Trudy TsNIITMASh (Papers of Sc. Res. Inst. Technol and Mach.), Vol. 71, 1955.

10. L. P. Nikitina. Trudy TsNIITMASh, Vol. 71, 1955.

11. W. Seith. Diffusion in Metallen, 1939.

12. P. P. Kobeko. Amorphous Substances, Metallurgizdat, 1952.

13. Symposium "Elasticity and Non-Elasticity of Metals," 1954.

14. J. Glen. Journ. Iron and Steel Inst., 179, p. 4, April 1955.

15. C. Herring. Jounr. Appl. Phys., 21, No. 5, 1950.

16. Gich. Theory of Sintering. Coll. "Achievements in Physics of Metals," Vol. 1, 1956.

17. Ya. B. Friedman. Mechanical Properties of Metals. Oborongiz, 1952.

18. G. Wasserman. Arch. Eis., 6, 1932/33.

19. N. Ye. Karskiy and G. I. Sobolev. Zav. Lab., Factory Lab., No. 11, 1949.

20. L. P. Trusov. Works of the TsNIITMASh, Vol. 171, 1955.

21. L. P. Nikitina. Works of the TsNIITMASh, Vol. 79, 1956.

22. Lorson and Miller. TASMEm 74, No. 5, 1952.

23. L. Ya. Lieberman. Zav. Lab., No. 2, 1955.

24. Symp. on Strength and Duality of Met. at Elev. Temp. ASTM, June 1952.

A THEORY OF THE BINDING ENERGY OF OXIDES OF TRANSITION METALS

A. N. Men' and A. N. Orlov

Calculation of the binding energy of multicomponent oxides containing ions of transition metals by strict quantum mechanical methods involves sizable mathematical difficulties. The use, therefore, of quasi-classical methods for the solution of this problem is of value. If the lattice is a pure ion lattice, the calculation of the basic role of binding energy is reduced to computation of the Madelung constant. There are no simple methods of evaluating the binding energy if partially covalent bonds are involved. Specifically, in the case of multicomponent oxides which form during the oxidation of complex alloys, it is impossible to determine how the ions are distributed among the various types of interstices.

On the basis of quantum chemical considerations, Goodenough and Loeb [1] examined the question of the arrangement of various transition metal ions in octahedral and tetrahedral interstices of a spinel-type lattice.* They proposed qualitative evaluation of the variation in the energy of the penetration of transition metal ions

* For the sake of brevity, henceforth we shall call the octahedral and tetrahedral interstices "O- and T-" points.

into the O- and T- points as a function of the number of d-electrons n_d. The results of their work [1] may be formulated mathematically and made more complete by taking entropy into account. This enables us to obtain an approximate expression for the free energy F of the oxide lattice. The derivation and investigation of this expression for F is presented in the present work.

Goodenough and Loeb evaluate the binding energy of the ions in the O- and T- points, U_O and U_T on the basis of a four-point scale and limit themselves to examination of the most probable combined electron orbits of three types, sp^3, sp^3d^2, and sp^2d, having tetrahedral, octahedral and quadratic symmetry, rwspectively. The quadratic orbits contain atoms located in the O- points (they cause tetrahedral distortion of the lattice). If we designate the binding energy with the participation of a quadratic irbit by U_Q, (then all other conditions being equal) the sign of the difference $U_T - U_O$ (or $U_T - U_Q$) will determine which point will be occupied by an ion of type M.*

If we assume for the sake of simplicity that the four graduations of the scale are of equal weight A [1], then the established dependence of U on n_d can be expressed graphically as shown in Fig. 1. This graph may be approximated by the equations (dotted lines):

$$U_T = 3\,[0{,}16\,|n-5|\,(5-|n-5|)-1]\;A.$$
$$U_O = \{0{,}4\,|n-4|\,(5-|n-4|)-4\}\;A. \qquad (1)$$
$$\Delta = U_T - U_O = \{1+0{,}4\,[6\,|n-5|-5\,|n-4|-0{,}2n^2+4n-14]\}\,A. \qquad (2)$$

* Henceforth, U_O shall be taken to mean the maximum (U_O, U_Q).

Let us consider an oxide in which the oxygen ions form a framework with a face-centered cubic structure. In order to obtain an approximate expression for the free energy of such a lattice let us postulate the following for purposes of simplification:

a) the energy of the framework of oxygen ions does not depend on the oxide composition;

b) the energy of thermal oscillations does not vary with the oxide composition either.

The mutual interaction between the metal ions is not taken into account. The number of O- and T- points which may be occupied by the metal ions in the given structure is set.*

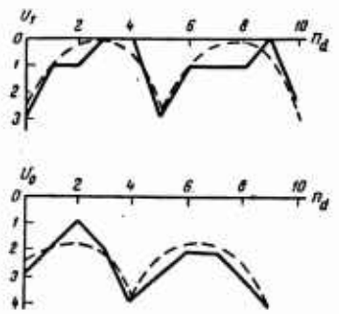

Fig. 1. Dependence of the energy of an ion in a tetrahedral (U_T) and in an octahedral (U_O) interstice on the number of d-electrons.

Hence, in the entropy S only the configurational part depends on the oxide composition. Then

$$F = U - TS + F_O, \qquad (3)$$

* We could consider a more general variant of the theory, in in which these numbers, and consequently the type of structure, are obtained automatically from the condition of a minimum of free energy. However, this requires a more accurate knowledge of the forces of atomic interaction and then given in the work [1], on which we are basing ourselves here.

where F_0 is the amount of free energy that does not depend on the composition and arrangement of the ions at the points;

U is the energy of the interaction of the metal ions with the surrounding oxygen ions, determined by Eq. (1);

S is the entropy of configuration.

In determining the explicit form of the dependence of F on the oxide composition and the arrangement of the ions at the points, we will for the sake of simplicity only deal with a fairly general and not very complex case. Let us consider a lattice at whose T- and O-points there are located metal ions of only two types A and B, of which the A ions may be in two states having the integer valencies P_{A_1} and P_{A_2} while the B ions have a constant valence* P_B. Let us designate the number of different ions in 1 cm^3 by n_j^i, in which i indicates the type of point and j the type of ion; n_k designates the number of oxygen ions which, by agreement, is equal to the number of points in the lattice of the oxygen "framework." Then,

$$\begin{gathered} n_{A_1}^{T} + n_{A_2}^{T} + n_{A_1}^{O} + n_{A_2}^{O} = n_A, \\ n_B^{T} + n_B^{O} = n_B, \\ p_B n_B + p_{A_1} n_{A_1} + p_{A_2} n_{A_2} = 2n_k. \end{gathered} \tag{4}$$

Let us find the equilibrated values of n_j^i from the condition of minimum free energy, satisfying the conditions of (4). Let us designate the following equalities:

$$\begin{gathered} n_1 = n_{A_1}^{T};\ n_2 = n_{A_2}^{T};\ \ n_3 = n_{A_1}^{O};\ \ n_4 = n_{A_2}^{O};\ \ n_5 = n_B^{T};\ \ n_6 = n_B^{O}; \\ U_1 = U_{A_1}^{T};\ \ U_2 = U_{A_2}^{T};\ \ U_3 = U_{A_1}^{O};\ \ U_4 = U_{A_2}^{O};\ \ U_5 = U_B^{T};\ \ U_6 = U_B^{O}; \end{gathered} \tag{5}$$

$$P_1 = P_3 = P_{A_1};\ P_2 = P_4 = P_{A_2};\ \ P_5 = P_6 = P_B;$$

* The latter assumption implies that with a prescribed oxide composition the lattice neutrality (the last equation in (4) determines the ratio P_{A_1}/P_{A_2} as a single value.

then

$$U = \sum_{i=1}^{6} n_i U_i; \tag{6}$$

$$S = \ln W = \ln \frac{m_O!}{n_{A_1}^O! \, n_{A_2}^O! \, n_B^O!} \frac{m_T!}{n_{A_1}^T! \, n_{A_2}^T! \, n_B^T!} \simeq m_O (\ln m_O - 1) + \\ + m_T (\ln m_T - 1) - \sum_{i=1}^{6} n_i (\ln n_i - 1), \tag{7}$$

where m_O and m_T are the whole number of O- and T- points which may be occupied by metal ions in the given structure. The values of m_O and m_T corresponding to 32 ions in certain cubic oxides are given in Table 1. In conformity with the conditions of (4), let us introduce the Lagrange factors λ_1, λ_2, λ_3; the task is then reduced to determining nine unknown items from Eq. (4) and from the System (8) below:

$$\frac{\partial \Phi}{\partial n_i} = 0 \ (i = 1, 2, \ldots, 6), \tag{8}$$

where

$$\Phi = F + \lambda_1 \left[n \bar{\lambda} \sum_{i=1}^{4} n_i \right] + \lambda_2 [n_B - n_5 - n_6] + \\ + \lambda_3 \left[n_k - \sum_{i=1}^{6} n_i p_i \right], \tag{9}$$

$$F = \sum_{i=1}^{6} n_i U_i - kT [m_O (\ln m_O - 1) + m_T (\ln m_T - 1) - \\ - \sum_{i=1}^{6} n_i (\ln n_i - 1)]. \tag{10}$$

TABLE 1

Type of lattice	m_O	m_T
NaCl	32	0
Spinel	16	8
$\gamma - Fe_2O_3$	16	16/3
ZnS	0	32

The solution of the system of equations (4) and (8) leads to the following results:

$$n_{A_1}^{T}=\frac{n_A p_{A_2}+n_B p_B-2n_k}{(p_{A_2}-p_{A_1})D_{-1}},\qquad n_{A_1}^{O}=\frac{n_A p_{A_2}+n_B p_B-2n_k}{(p_{A_2}-p_{A_1})D_1},$$

$$n_{A_2}^{T}=\frac{2n_k-n_B p_B-n_A p_{A_1}}{(p_{A_2}-p_{A_1})D_{-2}},\qquad n_{A_2}^{O}=\frac{2n_k-n_B p_B-n_A p_{A_1}}{(p_{A_2}-p_{A_1})D_2} \tag{11}$$

$$n_B^{T}=\frac{n_B}{\left[1+e^{-\frac{U_B^{O}-U_B^{T}}{kT}}\right]},\qquad n_B^{O}=\frac{n_B}{\left[1+e^{\frac{U_B^{O}-U_B^{T}}{kT}}\right]},$$

where

$$D_{\pm i}=1+\exp\left\{\pm\frac{U_{A_i}^{O}-U_{A_i}^{T}}{kT}\right\}. \tag{12}$$

The substitution of Expression (11) in (10) gives the equation for free energy at the prescribed values of U_{i_1}, n_A, n_B, P_{A_1}, P_{A_2}, and P_B.

A number of consequences follow from Expressions (10) and (11).

The temperature-dependence of the numbers n_1, which determine the arrangement of the ions at points of various types, may be presented by the following general formula

$$n_i=\frac{\beta}{1+e^{-\Delta/kT}}, \tag{13}$$

when Δ and β are constants, and $\beta > 0$.

The curve $n_1(T)$ is shown schematically in Fig. 2. The point of inflection is found from the condition

$$\frac{2kT'}{\Delta}=th\frac{\Delta}{2kT'}. \tag{14}$$

We obtained a particular expression for Eq. (13) in [2](Eq.(10)), but the question of the relative magnitude of the energy U, i.e., of the sign Δ, was not solved in a single-value manner. Within the

framework of the theory under consideration this sign is determined by Eq. (2).

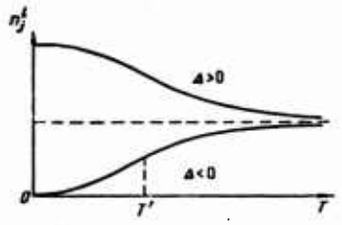

Fig. 2. Temperature dependence of the equilibrated number of ions of j type in i type interstices.

Effect of admixtures on the quantity of equilibrated vacancies. Equation (10) makes it possible to evaluate the manner in which additions to the oxidized metal affect the equilibrated quantity of vacant interstices in the oxide. Let us consider this problem in the particular case when an oxide of spinel structure is formed with the composition

$$A_{3-c-x}B_cO_4. \tag{15}$$

The B atoms play the part of the admixture. For the sake of simplicity we shall consider that they enter into the lattice soley in the form of divalent ions, whereas the A type ions may be both di- and tri-valent. In this case the free energy is a function of the concentration of the admixture c and the vacancies x. The condition

$$\partial F/\partial x = 0 \tag{16}$$

determines the equilibrated number of vacancies $x^0(c)$. Let us determine the form of this function.

In the notations of the structural formula (15) the equilibrated values of the numbers of ions (11) are equal to

$$n_{A_1}^{T}=\frac{3(3-c-x)+2c-8}{D_{-1}},\quad n_{A_1}^{O}=\frac{3(3-c-x)+2c-8}{D_1},$$
$$n_{A_2}^{T}=\frac{8-2c-2(3-c-x)}{D_{-2}},\quad n_{A_2}^{O}=\frac{8-2c-2(3-c-x)}{D_2}. \tag{17}$$

By substituting (17) in (10) and by differentiating with respect to x, we obtain

$$\frac{\partial F}{\partial x}=C_1+C_2-3kT\ln[3(3-c-x)+2c-8]\left[\frac{1}{D_{-1}}+\frac{1}{D_1}\right]+$$
$$+2kT\ln[8-2c-2(3-c-x)]\left[\frac{1}{D_{-2}}+\frac{1}{D_2}\right]=0, \tag{18}$$

in which the constants

$$C_1=-3\left[\frac{U_{A_1}^{T}}{D_{-1}}+\frac{U_{A_1}^{O}}{D_1}\right]+2\left[\frac{U_{A_2}^{T}}{D_{-2}}+\frac{U_{A_2}^{O}}{D_2}\right],$$
$$C_2=kT\left\{3\left[\frac{\ln D_{-1}}{D_{-1}}+\frac{\ln D_1}{D_1}\right]-2\left[\frac{\ln D_{-2}}{D_{-2}}+\frac{\ln D_2}{D_2}\right]\right\}$$

do not depend on c and x. Solving Eq. (18) with respect to c, we find

$$c=1-3x^0-C_3[2(1+x^0)]^{3/5}, \tag{19}$$

where

$$C_3=\exp\left\{-\frac{C_1+C_2}{kT}\right\} \tag{20}$$

and it is taken into account that

$$\frac{1}{D_{-i}}+\frac{1}{D_i}=1. \tag{21}$$

It can be seen from Expression (19) that in the case under consideration the equilibrated number of vacancies x^0 decreases with an increase in c. We may expect that if the composition of $x \neq x^0$ occurs as a result of the actual kinetic characteristics of the formation of the given oxide, the addition of admixtures will then

affect the number of vacancies in the same way.

If, however, the B type ions are also present in the oxide in divalent states, the tendency of the number of vacancies to decline as c increases will appear if the B atoms are less inclined to form trivalent ions than the A atoms.

Since the diffusion rate is determined to a considerable extent by the presence of vacant points in the lattice, we may expect that the addition to the oxidized alloy of B atoms, which do not tend to form trivalent ions, will lead to a decline in the rate of formation of an oxide film with a spinel structure.

A similar investigation can also be made for other, more complex oxides.

Non-stoichiometric combinations. It follows from Eq. (10) that a situation is possible where the free energy of a crystal of a non-stoichiometric composition is lower than that of a stoichiometric oxide. This can be taken to explain the existence of oxides of variable composition over a comparatively wide range of concentration.

Let us illustrate this, using the simplest example of a single-component oxide in which the metal ions may be in divalent states. FeO is a representative of this type of system. We shall consider concentrations close to the composition of FeO with the general formula $Fe_{1-x}O$ ($x < 1$). At $x \ll 1$, the majority of Fe ions will be divalent. Since they each have d-electrons, they prefer O- points, according to Fig. 1, so that from the structures given in Table 1 the one formed is the NaCl type. When there is deviation from stoichiometric composition, there appear O- points and the number of Fe^{3+} ions is doubled.

The complete structural formula (calculated per O atom) takes the form:

$$Fe^{2+}_{1-3x}Fe^{3+}_{2x}\otimes_x O^{\circ}, \tag{22}$$

where $\otimes$ is the vacant octahedral point.

Since experimental data indicates that not only divalent but apparently also trivalent ions do not occupy T- points, we may consider that in all cases $n^T_{A_1} = n^T_{A_2} = 0$ and, consequently that D_1 and $D_2 \gg 1$, and that D_1 and D_2 are of the order of 2. Then the free energy per mole of oxide (22), is, according to (10) equal to:

$$\begin{gathered} F = -(1-3x)(1-\alpha_1)|U^O_{A_1}| - 2x(1-\alpha_2)|U^O_{A_2}| - kT\{m_0(\ln m_0 - 1) + \\ + m_T(\ln m_T - 1) - (1-3x)[\ln(1-3x) - 1] - 2x(\ln 2x - 1) + \\ + \alpha_1(1-3x) + 2x\alpha_2\}, \\ \alpha_i = e^{-\frac{\Delta i}{kT}},\ \Delta i = U^T_{A_i} - U^O_{A_i} \quad (i = 1, 2). \end{gathered} \tag{23}$$

Let us investigate the form of the dependence F(x). For this purpose we find

$$\begin{gathered} \frac{\partial F}{\partial x} = 3|U^O_{A_1}|(1-\alpha_1) - 2|U^O_{A_2}|(1-\alpha_2) + kT\{-3\ln(1-3x) + \\ + 2\ln 2x + 3\alpha_1 - 2\alpha_2\}. \end{gathered} \tag{24}$$

$$\text{If } \frac{\partial F}{\partial x} = 0, \text{ then } \frac{2x}{(1-3x)^{3/2}} = e^{\frac{-3|U^O_{A_1}| + 2|U^O_{A_2}|}{2kT}} e^{\frac{3|U^O_{A_1}|\alpha_1 - 2|U^O_{A_2}|\alpha_2}{2kT}} e^{-\frac{3\alpha_1 - 2\alpha_2}{2}}. \tag{25}$$

Since it follows from Formula (23) that $x < \frac{1}{3}$, then

$$\frac{\partial^2 F}{\partial x^2} = kT\left(\frac{9}{1-3x} + \frac{2}{x}\right) > 0, \tag{26}$$

so that the convexity of the curve F(x) is directed downwards. It is easy to show that the equation $\partial F/\partial x$ has a single radical in the interval $0 < x < \frac{1}{3}$, which according to Eq. (26) corresponds to a minimum of energy. Let us note that $x = 0$ cannot be the radical x_0 of the equation $\partial F/\partial x = 0$ when $T \neq 0$.

Whether or not the given phase actually occurs depends on the magnitude of the free energy of the neighboring phases, pure iron and magnetite.* If, in the diagram of F(x), the tangent to the F(x) curves of the two neighboring phases lies throughout its course below the F(x) curve of the phase under consideration, the latter will not take place. But if a phase with an almost stoichiometric composition is engendered, we may as a rule expect a single-phase zone of finite width near this composition. Tests have shown that the structure of a non-stoichiometric composition with a NaCl-type lattice actually exists in the FeO system; it encompasses a relatively wide single-phase zone, of which the FeO composition is not a part. Knowing the nature of the dependence $n_1(T)$, determined by Eq. (12), it is possible in a number of cases to establish the type of the $x_0(T)$ curve. In particular, in the FeO system under consideration, x_0 is determined by Eq. (25), in which $U^0_{A_1}$ has to be replaced by $U^0_{(n_d)}$ from Eq. (1), and $U^0_{A_2}$ by the quality $U^0_{(n_d-1)}$, in which n_d is the number of d-electrons in the ion under reference. The following relationship is then found:

$$\frac{2x}{(1-3x)^{3/2}} = e^{\frac{-3|U^0_{(n_d)}|+2|U^0_{(n_d-1)}|}{2kT}} e^{\frac{3|U^0_{(n_d)}|x_1-2|U^0_{(n_d-1)}|x_2}{2kT}} e^{-\frac{3x_1-2x_2}{2}}. \qquad (27)$$

However, this equation is not convenient for practical investigation and it is simpler to determine the nature of the $x_0(T)$ curve for specific values of n_d, using the points in Fig. 1.

* The theory does not include the possibility also of other phases in this interval.

When $\underline{x}$ is small, it is easy to find x_0 by expanding $(1 - 3x)^{3/2}$ into a series with accuracy as far as the linear terms. Then,

$$x_0 = \frac{2}{9 + 4\gamma^{-1}}, \tag{28}$$

where

$$\gamma = e^{\frac{-3\left|U^0_{(nd)}\right| + 2\left|U^0_{(n_d-1)}\right|}{2kT}} e^{\frac{3\left|U^0_{(n_d)}\right|\alpha_1 - 2\left|U^0_{(n_d-1)}\right|\alpha_2}{2kT}} e^{-\frac{3\alpha_1 - 2\alpha_2}{2}}.$$

The results of examining Eq. (28) at different values of $U^0_{(n_d)}$ and $U^0_{(n_d-1)}$ are schematically shown in Fig. 3. Curves (1) and (2) were obtained by assuming that $\alpha_1 = \alpha_2 = 0$, which means that (29) the energies of the ions at the T- points are very great. Depending on the relative magnitude of $U^0_{(n_d)}$ and $U^0_{(n_d-1)}$, we obtain, at T = 0, $x_0 = 0$ or $x_0 = 2/9$. However, if we take into account the final value of the constants α_1 and α_2, curve (2) will be displaced upwards, whereas curve (1) will be displaced upwards if $\left|\frac{U^0(n_d)}{U^0(n_d-1)}\right| > \frac{2}{3}$ (curve 4), and downwards if $\left|\frac{U^0(n_d)}{U^0(n_d-1)}\right| > 1$ (curve 5). Thus, if $\left|\frac{U^0(n_d)}{U^0(n_d-1)}\right| < 1$, a rise in temperature will contribute to the deviation of the composition from its stoichiometric form

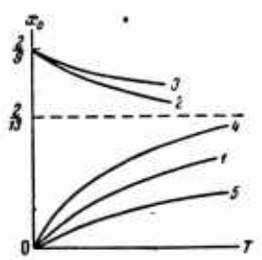

Fig. 3. Types of temperature dependence of the equilibrated concentration of a non-stoichiometric oxide.

and to the formation of vacancies, but if $\left|\frac{U^0(n_d)}{U^0(n_d-1)}\right| > 1$, the equilibrated number of vacancies increases with an increase in T, although more slowly than in the case of $\alpha_1 = \alpha_2 = 0$. In the case of the oxide $Fe_{1-x}O$, according to Fig. 1, $|U^0_{2+}(6)| \simeq 2$, $|U^0_{3+}| = 3$. Since the four graduations on the energy scale in Fig. 1 encompass the range of all possible values of U^0, we must assume that the scale varies more rapidly on the U axis than if it were subject to a linear law. The relationship $\left|\frac{U^0(n_d)}{U^0(n_d-1)}\right| < \frac{2}{3}$ is therefore satisfied, and the $x_0(T)$ curve must be of type (2) or (3), approximating at high temperatures the limit value $x_0 = 2/13 \simeq 0.15$. This point is not far removed from the zone in which the $Fe_{1-x}O$ phase exists; but as regards the dependence of x_0 on temperature, there are apparently no direct experimental data, and even data on the temperature dependence of the limits of the homogeneity of the $Fe_{1-x}O$ phase are contradictory.

Let us note that the proposed system for calculating the free energy could be made more accurate by taking into account the interaction of the metal ions. To this end, use may be made of the methods applied in the theory of metal solid solutions [3]. However, there is hardly any point in further elaborating the theory until more accurate expressions for the energy of U_0 and U_T are obtained by direct computation on the basis of quantum mechanics.

Conclusions

1. An approximated analytical formulation of the results of quantum mechanical evaluations of the binding energy of ions of transition metals in octahedral and tetrahedral interstices (O- and T-points) in oxide lattices with a cubic structure has been advanced.

2. An approximated expression for the free energy was obtained and a form of the temperature-dependence of the equilibrated number of ions of various types and valencies in the O- and T- points was found.

3. As an illustration of the general results obtained, the dependence of the equilibrated number of vacancies on the concentration of an admixture of another metal was investigated in a spinel-type lattice, and an explanation was supplied for the existence of a non-stoichiometric oxide of $Fe_{1-x}O$ composition in a lattice of the rock-salt type.

REFERENCES

1. J. B. Goodenough and A. L. Loeb. 98, 1955.

2. A. N. Men' and A. N. Orlov. FMM (Phys. Met. and Metallurg.) 1, 1955.

3. M. A. Krivoglaz and A. A. Smirnov. FMM, 1, 1955.

ELECTRO-DIFFRACTION STUDY OF PHASE CHANGES IN THIN METAL AND OXIDE FILMS

D. V. Ignatov

The study of phase changes in thin films is of great importance in elucidating the mechanism of the interaction between the various contiguous phases, as a function of temperature and heating time. Such phases may be metal with metal, oxide with oxide, or metal with oxide and other chemical compounds.

Interactions of this kind take place during sintering and oxidation and also occur between the base (a metal or other substance) and the material applied to it in the form of a thin layer of different composition.

The present paper deals with the results of an electron-diffraction study of phase changes relative to temperature and length of heating which take place in oxide films on aluminum, in an iron-aluminum system, and in the oxide systems $NiO - Cr_2O_3$ and $NiO - Al_2O_3$.

Thin metallic films (400-500 Å thick) obtained by evaporation and condensation in a vacuum were used as specimens. The thickness of the films was determined by the gravimetric method. The thin films of iron and aluminum were obtained either by simultaneous

evaporation of the metals or by consecutive evaporation from two points. By regulating the rates of simultaneous evaporation from two centers it is possible to obtain metallic systems in the form of films of any desired composition.

It is particularly easy to obtain chemical (intermetallic) compounds of metals by this method. Conversely, as shown by S. A. Vekshinsky [1], when the rates of simultaneous evaporation of different metals from the corresponding centers are constant and when the lining on which the metallic vapor condenses is reheated, it is possible to obtain a film whose composition corresponds to the full diagram of state.

Thin films were prepared from the oxides as follows. First, thin films of aluminum and chromium were obtained by evaporation and condensation in a vacuum. Mica foil was used as a base, and the metallic films were peeled off by immersion in distilled water. The pieces of thin film were recovered from the surface of the water on small platinum-sheet frames 10 mm long, 5 mm wide, and 0.3 mm thick. The frames had from 2 to 4 perforations, 0.6-0.8 mm in diameter, which when they were removed from the surface of the water, were covered by the thin aluminum or chromium films.

The specimens thus obtained were completely oxidized in heating in air for 20-30 minutes, at 600° for aluminum and 400° for chromium. Next, nickel vapor was allowed to condense on them in a vacuum and as a result two-layer films were obtained, consisting of a layer of oxide γ-Al_2O_3 or α-Cr_2O_3 and a layer of nickel.

By heating these specimens in air for 30 minutes at a temperature of 400° we obtained two-layer films of the oxides NiO and γ-Al_2O_3 in the first case, and the oxides NiO and α-Cr_2O_3 in the second.

The thickness of the nickel-aliminum and nickel-chromium metallic films was selected in such a way that the oxides produced corresponded in quantity to the stoichiometric composition of the $NiAl_2O_4$ and $NiCr_2O_4$. The thin films of metal were obtained in a vacuum ($2 \cdot 10^{-6}$ mm Hg) in the device shown in Fig. 1.

The specimens were next heated in air in the following temperature ranges:

Aluminum - from 300 to 1300°;

Iron-Aluminum - from 100 to 900°;

$NiO-Cr_2O_3$ - from 400 to 800°;

$NiO-Al_2O_3$ - from 600 to 1300°.

Electron diffraction by the "passage through" method was used as the basic method for determining the phase originating in relation to the time and temperature of heating.

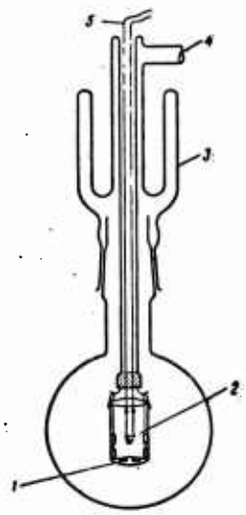

Fig. 1. Device for obtaining thin layers of metal in a vacuum: 1) protective cylinder and specimen (linings) holder; 2) evaporator in form of small tungsten wire baskets; 3) trap for freezing out lubricant vapors (flooded with liquid air or nitrogen; 4) outlet to vacuum installation; 5) wires supplying evaporator with current.

Figure 2 shows the electron diffraction patterns of a thin film of aluminum (with spectral purity), heated in air at 300° for 5 hours, and at 400, 450, 500, 600, and 700° for 10 minutes at each temperature. It follows from these electron diffraction patterns that an oxide modification of γ'-Al_2O_3 already starts to form at 300° and exists together with the metal up to 600°. At 600°, γ'-Al_2O_3 turns into the oxide modification γ-Al_2O_3; this phase

is stable up to 1300°. At 1300° it turns into the oxide modification α-Al_2O_3 in 5 hours.

Thus our results do not confirm the claim made by O. Kubashevsky and B. Hopkins [2] that oxide films on aluminum are amorphous while being heated in the temperature range of 300-500°. The amorphous oxide film which forms at room temperature on polycrystalline aluminum only exists up to 300°.

Figure 3 shows the electron diffraction patterns of an iron and aluminum film (both metals were evaporated simultaneously from two centers), for the same specimen heated in air in the temperature range 20 to 900°. The specimen was heated for 10 minutes after every 100°.

Analysis of the electron diffraction pattern 4a showed that the film consists of a mixture of iron and aluminum. The considerable increase in intensity of the second diffraction ring in this pattern is caused by the exact coincidence of this aluminum ring with the first and strongest iron ring.

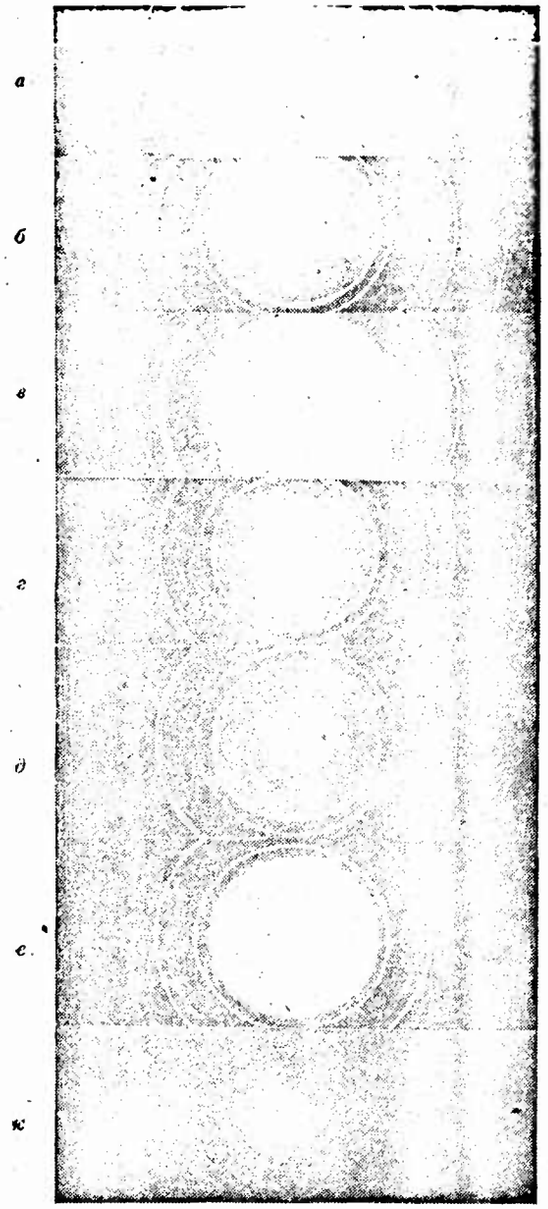

GRAPHIC NOT REPRODUCIBLE

Fig. 2. Electron diffraction patterns of a thin film of aluminum, heated at the temperatures (°C) of: a) 300; b) 400; c) 450; d) 500; e) 600; f) 700; g) 1300 (5 hours).

As can be seen from patterns 3b and 3c, the diffraction picture of this specimen, heated at 100 and 200°, does not change; i.e., the iron and aluminum mixture continues to exist. Pattern 3d includes, besides the iron and aluminum lines, very strong Fe_3O_4 lines, whose low intensity indicates the presence of a small quantity of the Fe_3O_4 phase in the film.

Heating the specimen at 400° leads to a sharp change in the diffraction picture, which is clearly visible from pattern 3e. Analysis of this electron-diffraction pattern showed that the lines of reflection correspond mainly to the chemical compound Fe_2Al_5.

Besides the Fe_2Al_5 lines there are also Fe_3O_4 but, as in the previous case, their intensity is very low. Further heating up to 500 and 600° does not change the diffraction pattern.

An analysis of the electron-diffraction patterns 3g, 3h, 3i of a specimen heated at 700, 800 and 900° showed the presence of the following phases: Fe_2Al_5, FeAl and γ-Al_2O_3 at 700°; FeAl and $FeAl_2O_4$ at 800°, and $FeAl_2O_4$ at 900°.

Thus the phase Fe_2Al_5 gradually decomposed from 700° onwards and the phase $FeAl_2O_4$ formed in its place.

In connection with these results we should point out that the phase Fe_2Al_5 is more resistant to oxidation than iron and aluminum taken separately. Films of this thickness oxidize completely in 10 minutes, at 400° in the case of iron and at 700° in the case of aluminum. A film of Fe_2Al_5 however, only oxidizes completely at 900°. The protective properties of thin aluminum coatings on steels (without the addition of chromium) can apparently be explained by the formation of the Fe_2Al_5 phase in the surface layer, as well as by the subsequent formation during heating of an oxide film consist-

ing mainly of $FeAl_2O_4$.

We should point out that in the case of simultaneous evaporation of iron and aluminum or nickel and aluminum from two closely located centers (metal spheres of 1 mm size) and condensation of their vapors on cold linings (up to 100°), the products of condensation were always metal mixtures. However, in the case of evaporation of these metals on other bases (glass, mica, et al.) heated to 400°, the products of condensation were always chemical compounds (Fe_3Al, Fe_2Al_5, NiAl etc.). these compounds were also obtained on a cold base provided the compounds themselves were used as the evaporating substance.

Figs. 4 and 5 show the electron-diffraction patterns of specimens in the form of two-layer films composed of $NiO - Cr_2O_3$ (Fig. 4) and $NiO - Al_2O_3$ (Fig. 5). The results of the analysis of these diffraction patterns are given in Table 1.

It follows from Table 1 that in the system $NiO - Cr_2O_3$ a chemical compound with a spinel-type structure begins to form in an appreciable quantity at 700° and ceases at 800°. The specimens were destroyed at 900° (probably because of recrystallization), and it was thus impossible to determine the products of decomposition of the spinel $NiCr_2O_4$ in specimens of this type. We then resorted to heating the sepcimens of $NiCr_2O_4$ in a vacuum (~ 10^{-6} mm Hg). For this purpose we prepared specimens in the shape of cylinders 10 mm long, 3 mm in diameter and with a wall thickness of 0.8-1 mm by compacting and sintering fine $NiCr_2O_4$ powder. A spiral 4 mm in diameter made of tungsten wire with a section of 0.2 mm was used as a heater. The temperature was measured by a platinum and platinum-rhodium thermocouple, the bulb of which was placed inside the cylinder. In this case as in the previous case the temperature was determined with an accuracy of $\pm$ 10°.

The products of decomposition of the spinel $NiCr_2O_4$ (i.e., the products of its evaporation) were condensed on mica foil (or laminae of NaCl). They then peeled off the mica when immersed in water and were recovered on platinum frames in the form of a film.

An analysis of the electron-diffraction pattern obtained from them showed that the products of evaporation contain Ni, NiO and α-Cr_2O_3 in about the same proportion corresponding to the spinel $NiCr_2O_4$. This conclusion was made in view of the fact that after the films were heated in air at 800° the spinel $NiCr_2O_4$ reappeared.

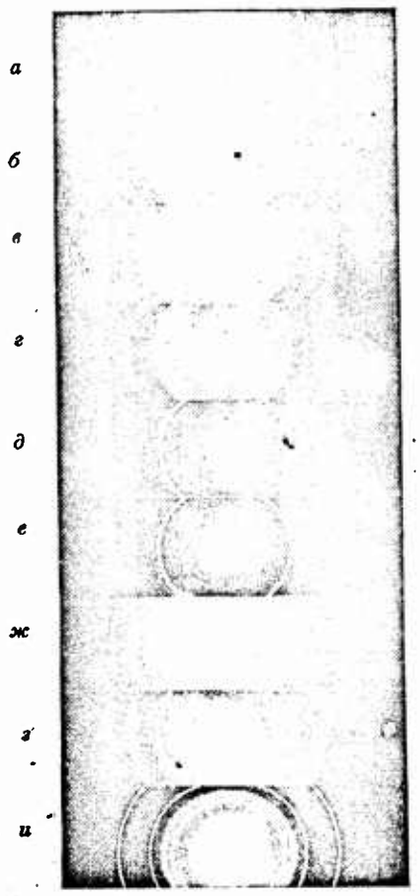

GRAPHIC NOT REPRODUCIBLE

Fig. 3. Electron-diffraction patterns of an iron-aluminum specimen, heated at the temperatures (°C) of: a) 20; b) 100; c) 200; d) 300; e) 400; f) 500 and 600; g) 700; h) 800; i) 900.

GRAPHIC NOT REPRODUCIBLE

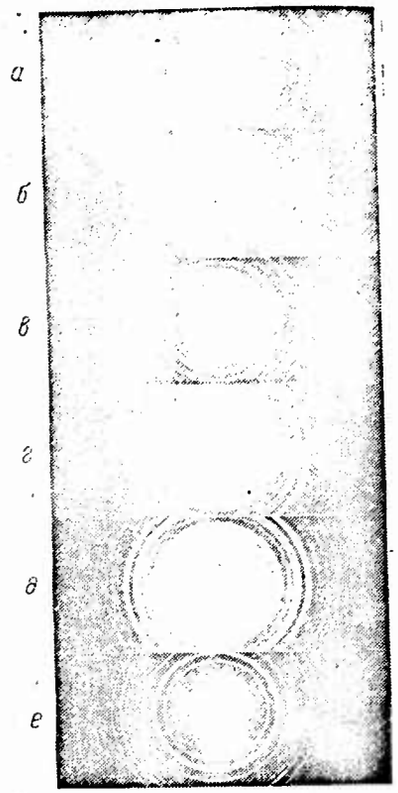

Fig. 4. Electron-diffraction patterns of a NiO - Cr_2O_3 specimen heated at the temperatures (°C): a) 400 (5 hours); b) 600 (5 hours); c) 600 (10 hours); d) 600 (15 hours); e) 700 (15 hours); f) 800 (15 hours).

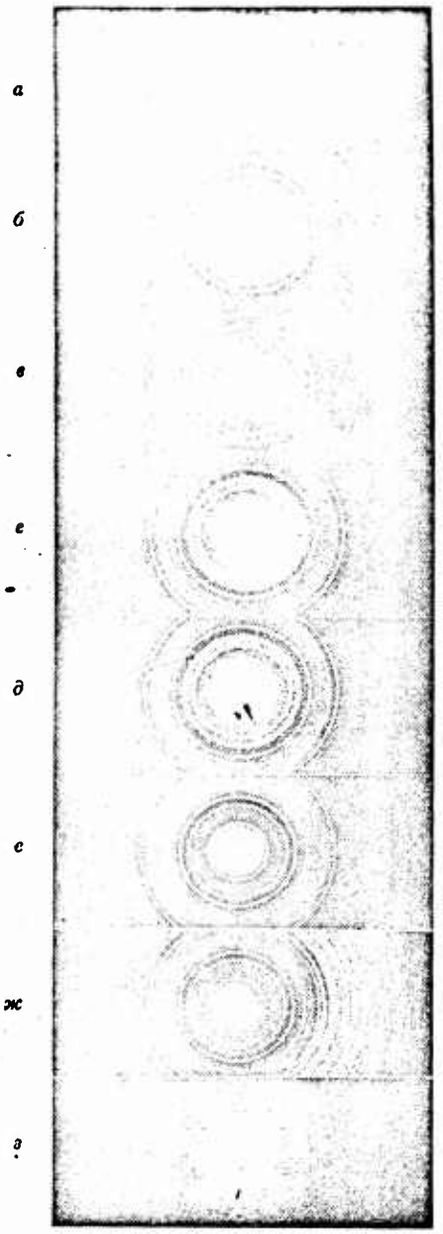

Fig. 5. Electron-diffraction patterns of a NiO - Al_2O_3 specimen heated at the temperatures (°C): a) 600 (5 hours); b) 800 (5 hours); c) 800 (10 hours); d) 800 (15 hours); e) 900 (10 hours); f) 100-1200 (15 hours); g) 1300 (1 hours); h) 1300 (5 hours).

TABLE 1

Change in the Phase Composition Relative to Temperature in the Systems NiO - Cr_2O_3 and NiO - Al_2O_3 (heating time 15 hours)

Temperature °C	NiO - Cr_2O_3	NiO - Al_2O_3
	Phases	Phases
400	Mixture α-Cr_2O_3 + NiO	Mixture γ-Al_2O_3 + NiO
500	same	same
600	primarily the same mixture with traces of phase $NiCr_2O_4$	same
700	α-Cr_2O_3 + NiO and an appreciable quantity of phase $NiCr_2O_4$	same
800	primarily phase $NiCr_2O_4$ and traces of the oxides NiO and Cr_2O_3	γ-Al_2O_3 + NiO and an appreciable quantity of phase $NiAl_2O_4$
900	Specimens were destroyed	primarily phase $NiAl_2O_4$ and traces of the oxides NiO and γ-Al_2O_3
1000		$NiAl_2O_4$
1200		$NiAl_2O_4$
1300		α-Al_2O_3 and traces of $NiAl_2O_4$

Appreciable evaporation of the above-mentioned specimens was observed after two or three hours in a vacuum at 1100°. When the same specimens were heated in air, appreciable evaporation was observed at 1100° after 50 hours and at 1200° after 20 hours. The product of evaporation in this case was the phase α-Cr_2O_3.

As it follows from Table 1, the system NiO-γ-Al_2O_3 exists in the form of the mixture NiO + γ-Al_2O_3 upon heating in air over the temperature range 400 to 800°. The formation of the phase $NiAl_2O_3$ in

an appreciable quantity is observed after 15 hours of heating at 800° (this phase forms in a small quantity after 5 hours). The almost complete formation of phase $NiAl_2O_4$ in the case of thin films (thickness 800-900 A) terminates after 15 hours of heating in air at 900°. This phase is stable up to 1300°, and we did not detect any other chemical compounds except the spinel $NiAl_2O_4$ over the temperature range from 900 to 1300°.

After 1 hour of heating at 1300° in air the decomposition of the said spinel into $NiAl_2O_3$ is to a great extent recrystallized, as is visible from the electronic-diffraction pattern (Fig. 5g).

Heating for 5 hours at this temperature resulted in almost complete decomposition of the spinel $NiAl_2O_4$, and the diffraction lines in the pattern for this specimen corresponded mainly to the phase α-Al_2O_3, which in this case had also highly recrystallized; this fact is attributed to the deterioration of the diffractional rings into point-like reflections (see the electron-diffraction pattern in Fig. 5h). The NiO phase is not detected in the pattern for this specimen. We may conclude therefore that the spinel $NiAl_2O_4$ decomposes at 1300° through evaporation of the NiO phase. This conclusion was confirmed by heating the $NiAl_2O_4$ specimens in a vacuum in the same way as was done with specimens of $NiCr_2O_4$.

After the $NiAl_2O_4$ specimens had been heated in vacuum for 20-30 minutes at 1100°, a change from the blue spinel color to white occurred which is characteristic of sintered specimens of pure aluminum oxide. Electron-diffraction analysis of the products of evaporation and condensation showed that they consisted of Ni and NiO. In a vacuum of 10^{-6} mmH_2, the NiO phase partially dissociates into nickel and oxygen and the oxygen is then evacuated. Thus the spinel $NiAl_2O_4$

decomposes into NiO and α-Al_2O_3 at a temperature of 1300° during which the NiO evaporates, while the α-Al_2O_3 phase is highly recrystallized. It is interesting to note that after 5 hours at 1300° γ-Al_2O_3 also turns into α-Al_2O_3, which is also highly recrystallized, as can be seen from the electron-diffraction pattern (Fig. 2g).

Regarding the results obtained from our study of the interaction between oxides relative to temperature and heating time, certain conjections may be formulated which differ from those put forward by K. Hauffe and K. Pschera [3]. These authors investigated the formation of the spinels $NiCr_2O_4$, $ZnCr_2O_4$, $NiAl_2O_4$, and $ZnAl_2O_4$ during the interaction of specimens made from the original oxides in the form of sintered tablets and heated in air at 1100 and 1200°. As a result of this study they came to the conclusion that the formation of spinels is faciliated to a considerable degree by the evaporation phase of the more volatile component (oxide) in the spinel, for example ZnO in the systems ZnO - Cr_2O_3 and ZnO - Al_2O_3 or α-Cr_2O_3 in the system NiO - Cr_2O_3.

According to S. Wagner's theory [4], spinels (for example $MgAl_2O_4$ in contact with specimens of the oxides MgO and Al_2O_3) are formed as a result of diffusion of the bivalent (Mg^{+2}) and also the trivalent (Al^{+3}) metal ions. Proceeding from our experimental data on the decomposition of spinels and taking into account the heat of formation of the oxides NiO, Cr_2O_3 and Al_2O_3, we can assume that the spinel $NiCr_2O_4$ is formed by diffusion of the Ni^{+2} as well as of the Cr^{+3} ions.

In our opinion, the spinel $NiAl_2O_4$ forms mainly as a result of diffusion of the nickel ions Ni^{+2}. The evaporation factor could not have played any great role in our case since the spinels formed over

the temperature range 700-900°. On the contrary, the evaporation rate played a negative part, since the spinels decomposed as a result of evaporation of the oxides α-Cr_2O_3 or NiO.

The data which we obtained on the thermal stability of the spinels $NiCr_2O_4$ are of great practical importance since these oxide compounds compose the major part of scaling on alloys of the type nickel-chromium and nickel-chromium-aluminum containing various inclusions. Moreover, the composition nickel-chromium-aluminum is often used for coating steel and certain heat resistant molybdenum-base alloys. The oxides α-Cr_2O_3 and α-Al_2O_3 are themselves very often used as the basic components in oxide or enamel coatings.

The three examples of the use of the electron-diffraction method in research which we have considered manifestly show that this method can be successfully applied to the study of phase transitions in thin free films of complex composition, in surface films on metals and alloys and along interphase boundaries, in the same way as the X-ray method is used to study phase transitions within the body of the substances concerned.

REFERENCES

1. S. A. Vekshinskiy. A New Method of Metallographic Investigation of Alloys. Gostekhizdat, M., 1944.

2. O. Kubashevsky and B. Hopkins. Oxidation of Metals and Alloys. IL, M., 1955.

3. K. Hauffe and K. Pschera. Zs. f. anorg. Chem., 262, 147, 1950.

4. S. Wagner. Zs. phys. Chem., 1334, 1936.

APPARATUS FOR STUDYING THE KINETICS OF OXIDATION IN METALS

P. M. Arzhanyi and N. N. Velichenko

The existing methods for studying the kinetics of oxidation in metals and alloys, which are based on short-time heating and weighing have great disadvantages and do not provide an accurate picture of the process. In this respect it is more convenient to conduct the study by subjecting the specimens to continuous heating and automatically recording the results of oxidation while they are still in the furnace. But there is almost no apparatus of this kind in use. A number of designs for balances can be found in scientific literature, which fall into two main groups:

Those with back coupling (continuous resetting of the balance to the position of zero equilibrium), and

Those without back coupling.

An example of the first type is the solenoid balance; and of the second group, a balance which records on photographic paper by means of a pen or spark.

We have constructed an apparatus for studying the kinetics of oxidation in metals with automatic recording of weight variations

(Fig. 1). It consists of three major parts: the heating surface, a balance containing a photoelement, and the automatic recording instruments. The design is based on an ADV 200 analytical balance mounted on a welded metal base, in the lower part of which we installed a ShP-1 type heating furnace. The left pan of the balance was removed and replaced by a platinum hanger with a platinum crucible which fitted the combustion space of the furnace. In order to eliminate the influence of the furnace heat on the balance and to reduce convection currents, asbestos and testolite shields were placed between the platform of the balance and the furnace; the shields contained a small aperture through which the platinum hanger passed. An STsV photoelement fixed to the upright of the balance was used as a feeler to transform the swing of the balance beam into an electic signal.

A small flag made of aluminum foil was fixed to the pointer carrying the balance dial to act as an interrupter of the beam of light produced by the source whenever the dial moved. The photoelement was connected to the input of a DC amplifier and was supplied with a stabilized voltage from a rectifier-amplifier. In order to keep the light beam stable and to eliminate the possibility of any change in the illumination of the photoelement, the light source was fed from a low-voltage stabilized rectifier of the BN-1 type. An EPP-09 recording instrument which registered the current fluctuation of the photoelement was connected to the output of the DC amplifier.

The furnace is equipped with a self-registering heat regulator of the EPD-17 type, making it possible to record the temperature in the combustion space

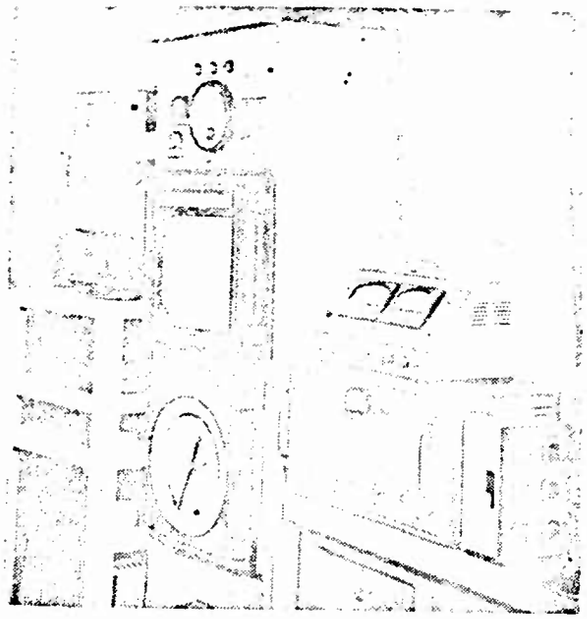

GRAPHIC NOT
REPRODUCIBLE

Fig. 1. External view of the apparatus used to study the kinetics of oxidation in metals.

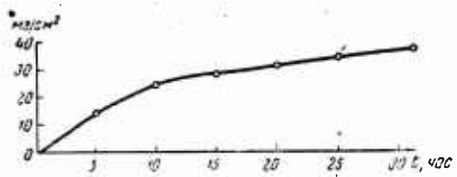

Fig. 2. Oxidation curve of Armco iron.

The tests were carried out in the following order. First, the specimen is suspended from the left-hand side of the arm and the balance is set at equilibrium. The furnace is heated and the light source, amplifier and recorders are switched on. When the furnace reaches the prescribed temperature, the specimen which is inside the platinum crucible is lowered into the furnace and the balance moves out of equilibrium. If the specimen's weight alters during oxidation, the balance beam and the small flag fixed to the pointer swing from the zero position, which results in a change in the beam of light.

This causes a change in the current passing through the photo-element which is transmitted to the self-registering potentiometer and causes the recorder needle to move to an extent proportional to the swing of the balance beam. The direct weight variation within testing time is thereby recorded on the dial of the potentiometer with the margin of error not exceeding 0.2 mg.

The results of the research are illustrated by a curve showing the oxidation of Armco iron at a temperature of 700° over a period of 30 hours (Fig. 2).

THE INFLUENCE OF CHROMIUM ON LONG-TIME STRENGTH OF CHROMIUM-MOLYBDENUM STEEL

O. A. Bannych and I. F. Zudin

The study of the influence of chromium concentration on long-time strength and creep in heat-resistant steel is of obvious practical interest, since chromium is one of the basic alloying components of the overwhelming majority of heat-resistant types of pearlitic steel produced so far.

A great deal of the numerical data compiled from the results of tests made by 17 firms in the USA until 1953 is contained in a symposium by W. Simmons and H. Cross*. The symposium contains data on 52 steel compositions.

Six compositions, differeing in their chromium content but very similar in their content of other alloying elements, were selected for our analysis of the influence of chromium on long-time strength of chromium-molybdenum steel (see page 30).

The long-time strength values obtained from treatment of the

---

* W. F. Simmons and H. C. Cross. The Elevated-temperature properties of chromium-molybdenum steels; spec. Tech. Publ., No. 151, ASTM, 1953.

experimental data in a dual logarithmic system of coordinates log σ — log τ are given in Table 1.

An examination of the relative variation in long-time ultimate strength relative to time and temperature reveals some interesting laws of behavior.

By expressing the values for long-time ultimate strength after 1000, 10,000, and 100,000 hours in percentages of the strength value after 100 hours, we can show the susceptibility of the steel to a decline in long-time strength with an increase in time. Figures showing this decline in relation to time are given in Table 2 as percentages of the 100-hour values.

he less chromium there is in the steel, the greater the relative decline in the magnitude of the long-time strength. This dependence is most clearly evident at a temperature of 593° (Fig. 1). At 538° an abnormally small relative decrease in the ultimate strength from 100 to 1000 hours is observed in the steel from melts Nos. 3 and 4 (0.97 and 1.24% cr. respectively). At 649° the curve for steel without any chromium (No. 1) is located somewhat higher than that for steel containing 0.97% Cr (No. 3).

A clear idea of the nature of the dependence on time of the relative variation in the value of long-time strength is given by the curves plotted as relative variation in long-time strength against chromium content (Fig. 2). The curves in Fig. 2 show a sharp

TABLE 1

melt no.	test temperature °C	long-time strength kg/mm²			
		100 hours	1000 hours	10,000 hours	100,000 hours
1	538	28,0	16,0	8,7	4,75
	593	11,9	5,5	3,5	2,2
	649	5,9	3,5	2,2	1,3
3	538	39,6	27,3	15,7	9,1
	593	16,8	9,7	5,5	3,15
	649	7,1	3,9	2,2	1,2
4	538	33,2	26,6	17,5	11,2
	593	17,5	11,2	7,5	4,9
	649	8,4	5,6	2,9	1,4
5	538	21,3	15,0	10,5	1,4
	593	12,2	8,7	6,2	4,5
	649	7,4	4,9	3,2	2,1
6	538	16,8	14,1	12,0	10,1
	593	10,5	8,1	6,2	4,7
	649	6,65	5,0	3,3	2,1
7	538	—	—	—	—
	593	12,2	9,6	7,5	5,9
	649	7,0	5,0	3,6	2,5

TABLE 2

Melting No.

Time, hours	1			3			4		
	538°	593°	649°	538°	593°	649°	538°	593°	649°
100	100	100	100	100	100	100	100	100	100
1000	57,2	46,2	59,4	81,3	57,7	55,0	80,3	64,0	66,6
10000	31,1	29,3	37,3	46,7	32,5	31,0	52,7	42,8	34,5
100000	17,0	18,5	22,2	27,1	18,8	16,9	33,7	28,0	16,7

TABLE 2 (continued)

Melt No.

Time, hours	5			6			7		
	538°	593°	649°	538°	593°	649°	538°	593°	649°
100	100	100	100	100	100	100	100	100	100
1000	70,4	71,2	66,2	84,0	77,1	75,2	—	78,6	71,4
10000	49,4	50,8	43,2	71,4	59,2	49,6	—	61,4	51,4
100000	34,7	36,8	28,4	60,1	44,7	31,6	—	48,3	35,6

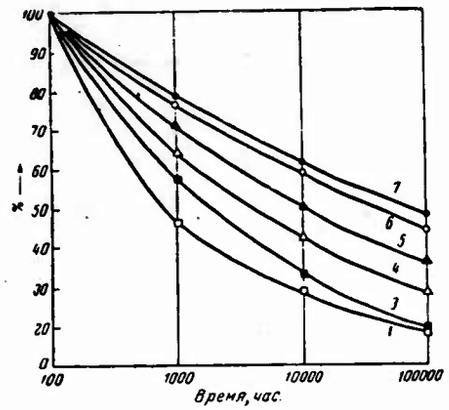

Fig. 1. Relative variation in the ultimate long-time strength on time (t = 593°).

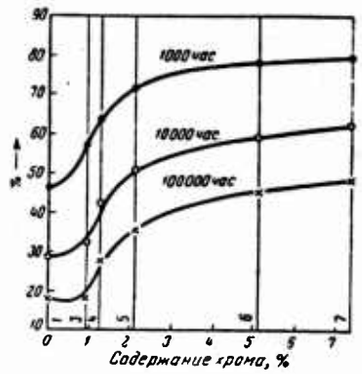

Fig. 2. Relative variation in the long-time strength of steel, depending on the chromium content (t = 593°).

rise in the area where the chromium content is 0-2.08% and a slight rise at higher concentrations (up to 7.33%).

Taking the value of the long-time strength at 538° as 100% and expressing the values of the ultimate long-time strength at 593 and 649° in percentages of that value, we can determine the susceptibility of the long-time strength of steel to variation in temperature (Table 3).

With an increase in the chromium content the temperature variation in the interval under consideration has less effect on the relative change in the ultimate strength after 100 and 1000 hours (Fig. 3). This dependence is less pronounced for the 10,000 and 100,000 hour ranges, which is probably due to the fact that the respective values of the ultimate long-time strength, obtained by extrapolation are less reliable.

TABLE 3

Time, hour	Melt No.														
	1			3			4			5			6		
	538°	593°	649°	538°	593°	649°	538°	593°	649°	538°	593°	649°	538°	593°	649°
100	100	42.3	21.1	100	50.0	21.2	100	52.7	25.3	100	57.3	34.3	100	62.4	39.5
1000	100	34.1	21.7	100	35.5	14.3	100	42.1	21.0	100	58.0	32.7	100	57.4	35.4
10,000	100	40.2	25.3	100	35.0	14.0	100	42.7	16.4	100	59.1	30.4	100	51.6	27.4
100,000	100	46.1	27.4	100	34.6	13.2	100	43.7	12.5	100	60.7	28.4	100	46.5	20.8

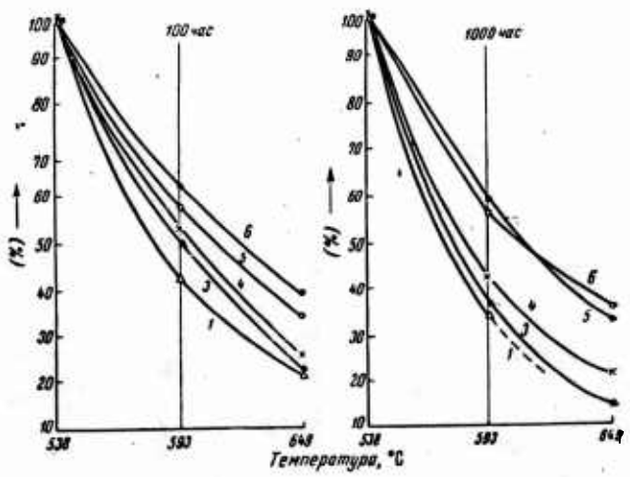

Fig. 3. Relative variation in ultimate long-time strength as a function of temperature.

Conclusions

When steel is treated in order to ensure a stable structure (annealing), the slope of the straight line σ - log τ or log σ - log τ decreases as the chromium content increases.

The existence of a clear time-dependence of the relative variation in the value of the ultimate long-time strength is an advantage under conditions where the steel is working under stresses higher than the prescribed maxima. Consequently, whenever there is instability in the service stresses the ultimate long-time strength over 100,000 hours, being equal, steel with a lower chromium content should be more reliable in service.

The sharp temperature-dependence of the relative variation in the value of the ultimate long-time strength, observed in steel with a low chromium content, is a disadvantage when the service conditions of the steel involve the possibility of temperature variation in time. The higher the chromium content in steel, the less effect overheating will have on the level of the long-time strength. The latter factor is important when the steel is intended for the manufacture of steam superheaters in boiler plants, for example, in which overheating is inevitable while in service.

INVESTIGATION OF THE RESISTANCE TO PLASTIC DEFORMATION IN ALLOYS OF THE NICKEL-IRON SYSTEM

K. A. Osipov and Ye. M. Miroshkina

The present paper presents the results of a study, by the use of hot-hardness tests, of the resistance of a number of alloys of the nickel-iron system to plastic deformation as a function of composition, temperature, and duration of loading.

The alloys, whose chemical composition is given in Table 1, were fused from electrolytic iron and nickel with repeated remelting in a vacuum.

TABLE 1

Chemical Composition of the Nickel-Iron Alloys Studied

Alloy No.	Ni wt.%	Ni atom%
1	31.40	30.36
2	46.45	45.2
3	55.25	54.44
4	59.79	58.61
5	79.18	78.36

The hardness of the alloys was determined by the diamond indentation method. The diamond used was in the form of square-based pyramid and the angle of the point was 136°. Prior to testing, the specimens were annealed in a vacuum for 50 hours at a temperature of 1200°. The load on the indenter amounted to 1 kg and the deformation time was 1 to 20 minutes. The tests were carried out at temperatures of 850 and 1000°.

The study established that the variation in the indentation diagonal, satisfactorily obeys, in time, the well-known dependence

$$d = a \cdot t^b \qquad (1)$$

where d is the indentation diagonal;

t is the deformation time;

a and b are parameters depending on the alloy concentration and temperature.

The values of d for various alloys relative to the deformation time at 850 and 1000° are shown in Tables 2 and 3.

TABLE 2

Values of the Indentation Diagonal at 850°

Alloy No.	Ni atom %	Deformation time (min) and values of the indentation diagonal (mm)					
		1	2	3	5	10	20
1	30.36	0.277	0.286	0.284	0.2943	0.305	0.316
2	45.20	0.220	0.234	0.241	0.151	0.267	0.286
3	54.44	0.225	0.240	0.245	0.259	0.277	0.286
4	58.61	0.213	0.224	0.240	0.243	0.268	0.264
5	78.36	0.246	0.260	0.256	0.262	0.286	0.306

TABLE 3

Values of the Indentation Diagonal at 1000°

Alloy No.	Ni, atom %	Deformation time (min) and the values of the indentation diagonal (mm)					
		1	2	3	5	10	20
1	30.36	0.339	0.352	0.366	0.377	0.439	0.481
2	45.20	0.248	0.270	0.276	0.291	0.341	0.370
3	54.44	0.244	0.263	0.280	0.299	0.309	0.424
4	58.61	0.301	0.299	0.328	0.327	0.356	0.391
5	78.36	0.222	0.247	0.252	0.250	0.296	0.381

TABLE 4

Values of Parameters a and b and the Rate of Deformation ($v_{10\ min}$) at 850°

Alloy No.	Ni, atom %	a, mm · min $^{-b}$	b	$v_{10\ min} \cdot 10^3$ mm · min^{-1}
1	30.36	0.275	0.04	1.21
2	45.20	0.22	0.08	2.12
3	54.44	0.22	0.08	2.12
4	58.61	0.216	0.07	1.78
5	78.36	0.24	0.07	1.98
pure nickel	100	0.356	0.04	1.39

TABLE 5

Values of the Parameters a and b and the Rate of Deformation ($v_{10\ min}$) at 1000°

Alloy No.	Ni atom %	a, mm · min^{-b}	b	$v_{10\ min} \cdot 10^3$ mm · min^{-1}
1	30.36	0.325	0.12	4.99
2	45.20	0.243	0.13	4.52
3	54.44	0.236	0.16	5.52
4	58.61	0.240	0.18	6.74
5	78.36	0.216	0.17	5.52

The data of these tables are represented in Figs. 1 and 2 by a graph of the logarithm of time against the logarithm of the indentation diagonal.

The values of the coefficients a and b in Eq. (1), calculated for temperatures of 850 and 1000° on the basis of the primary data given in Tables 2 and 3, are shown in Tables 4 and 5, which give additionally the values of the deformation rate of the alloys, corresponding to the moment of testing time t = 10 min.

Figures 3 and 4 show the dependence of the coefficients a and b on the nickel content in the solid solution.

A comparison of the values of the parameters a and b at 850 and 1000° leads us to the conclusion that a depends but little on temperature, whereas parameter b increases very sharply with a rise in temperature: the increase in the latter from 850 to 1000° produced an increase in parameter b of about one order.

It follows from Eq. (1) that the rate of plastic deformation may be expressed by the relationship

$$v = abt^{b-1} \qquad (2)$$

from which it can be seen that the deformation rate is a function of the deformation time.

The values of the rate, calculated from Eq. (2) and corresponding to the moment of test time t = 10 min, given in Tables 4 and 5, are shown by the graph in Figs. 5 and 6. As is seen from these data at 850° those alloys which by their composition are located in the central part of the diagram of state have the highest creep rate; at a temperature of 1000° these alloys containing 60-70 atom % Ni apparently have the highest creep rate.

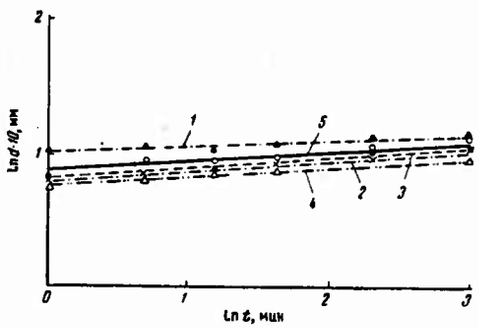

Fig. 1. Variation in the logarithm of the indentation diagonal as a function of the logarithm deformation time (t = 850°) for alloys with a nickel content (wt %). 1) 31; 2) 46; 3) 55; 4) 60; 5) 79.

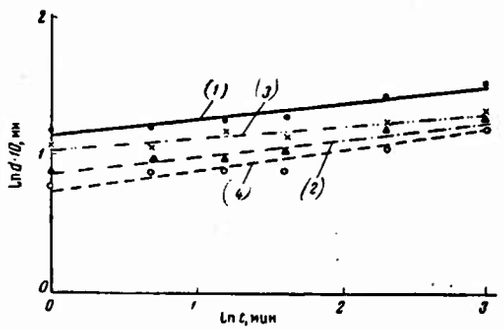

Fig. 2. Variation in the logarithm of the indentation diagonal as a function of the logarithm of deformation time (t = 1000°) for alloys with a nickel content (wt %). 1) 31; 2) 46; 3) 60; 4) 79.

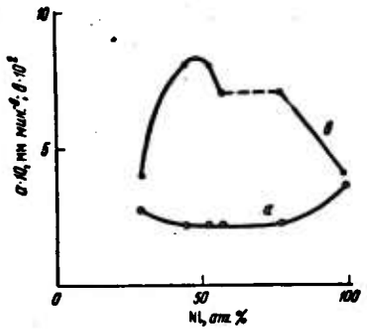

Fig. 3. Dependence on concentration of the parameters a and b for iron-nickel alloys at a temperature of 850°.

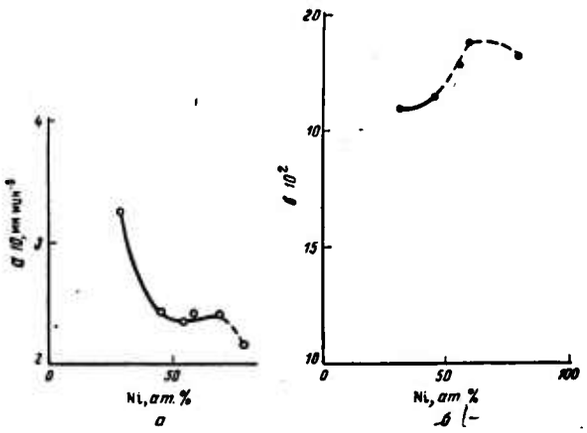

Fig. 4. Dependence of parameters a (Fig. 4a) and b (Fig. 4b) on concentration in iron-nickel alloys at 1000°.

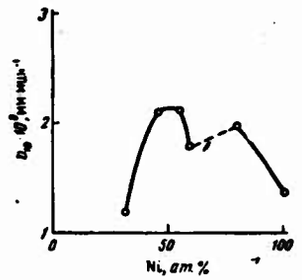

Fig. 5. Dependence of the creep rate on concentration at the moment of time t = 10 min for iron-nickel alloys at 850°.

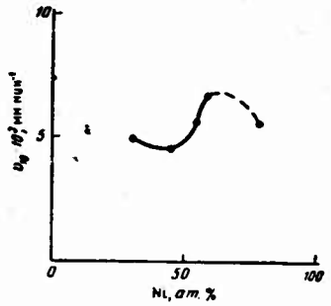

Fig. 6. Dependence of the creep rate on concentration at the moment of time t = 10 min for nickel-iron alloys at 1000°.

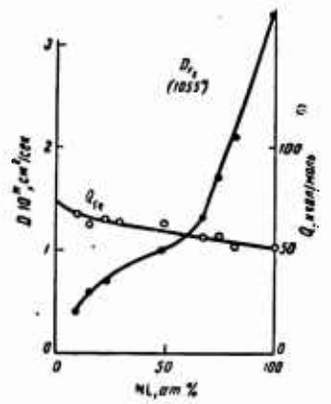

Fig. 7. Dependence on concentration of the activation energy and the coefficient of self-diffusion of iron in iron-nickel solid solutions.

Figure 7 shows data obtained by A. Ya. Shinyayev (from his thesis 1954) on the self-diffusion of iron in the solid solution of an iron-nickel system relative to a temperature of 1055°. By comparing Figs. 5, 6, and 7, we can conclude that the concentration dependence of the activation energy of self-diffusion of iron in solid solutions of iron-nickel is essentially different from the dependence on concentration of the rate of plastic deformation in alloys at temperatures

of 850 and 1000°. No close similarity is observed either between the dependence on concentration of the deformation rate at a temperature of 1000° and the coefficient of self-diffusion of iron at a temperature of 1055°. Our previous statement that diffusion parameters determined for an unstressed state cannot be considered as criteria for the heat resistance of solid solutions is apparently confirmed.

Conclusions

1. The resistance to plastic deformation of solid solutions of the iron-nickel system was studied by the hot-hardness method at temperatures of 850 and 1000°. It was established that those solid solutions which by their composition correspond to the central part of the diagram of state have the greatest creep rate at these temperatures.

2. It was further shown that no well-defined conclusion concerning the heat resistance of alloys can be made on the basis of the parameters of self-diffusion of iron in iron-nickel solid solutions obtained for an unstressed state in the absence of plastic deformation of the alloy. We reached a similar conclusion in a study of alloys of the nickel-copper and nickel-chromium systems.

HEAT RESISTANCE AND HOT-HARDNESS OF ALLOYS OF BINARY SYSTEMS OF NICKEL WITH CHROMIUM, MOLYBDENUM, AND TUNGSTEN

I. I. Kornilov and N. T. Domotenko

The application of physicochemical analysis, first developed by N. S. Kurnakov, to the study of the properties of metal systems at high temperatures makes it possible to establish a dependence between the measurable properties and the chemical composition of systems in equilibrium, i.e., to plot composition-property diagrams.

The present work deals with the results of study of the influence of chromium, tungsten and molybdenum on the heat resistance of nickel.

Preparation of Alloys and Their Heat Treatment

The alloys used for the study of heat resistance of nickel solid solutions (and also their neighboring zones) were prepared from chromium, tungsten, and molybdenum; their compositions are given in Table 1.

The stated compositions were selected in accordance with the data of the diagrams of state of the corresponding binary systems.

TABLE 1

Alloying Element	Content, %												
Chromium	20	25	27	30	34	35	36	38	40	42	45		50
Tungsten	5	10	15	24.6	29.6	35	37.3	40.9					
Molybdenum	5	10	15	20	22.8	25	26	27.8	29.8	30	35	37	42.2

The melting was effected in a high-frequency furnace in "corundiz" crucibles under a layer of base slag. The tests pieces were obtained by pumping the melt into heated porcelain tubes, using the method of N. I. Stepanov [14].

Before testing, the alloys of the nickel-chromium system were homogenized in an atmosphere of commercial argon at a temperature of 1150° for 6 hours and were then slowly sooled, together with the furnace. The nickel-tungsten and nickel-molybdenum alloys were subjected to homogenization annealing under the following conditions: at 1200° for 120 hours, at 1000° for 100 hours, and subsequent quenching in water. The alloys which were to be tested below the temperature of peritectoid reactions were further annealed at the test temperature for 200 hours.

The heat resistance of the alloys was studied in bending by the centrifugal method [1]. The time taken by the specimens to reach a prescribed flexure reading was made the criterion of heat resistance.

Relationship Between Stress and Heat Resistance

In [2-9] the study of heat resistance in alloys and the plotting of a composition — heat-resistance diagram were carried out (for a given test temperature) at the same initial stress. The effect of a variation in stress on the heat resistance of the alloys was not studied. The present work, however, deals with using the example of nickel-chromium alloys and the effect on the maximum heat resistance caused by variation in stress when the test temperature is kept constant. An analysis of the results of the tests, which were carried out at a temperature of 800° and at stresses of 10, 12.3, 14.3 and 15.8 kg/mm^2, shows the following.

Those alloys whose composition is in the transition zone from a solid solution to heterophase alloys (35-42% Cr) are the most heat resistant, regardless of the magnitude of the stress.

As the stress increases, there is a slight shift of the maximum heat resistance into the zone of the less supersaturated solid solutions. It may be assumed that this shift is caused by a more rapid coagulation of the excess phase in the supersaturated solid solutions, due to acceleration of the diffusion processes taking place in the direction of the stress gradient [12].

Heat Resistance of Nickel-Chromium Alloys

For the study of the relationship between composition, temperature and heat resistance, the alloys were tested at temperatures of 600, 700, and 750° and under a stress of 15.8 kg/mm^2, and also at temperatures of 800, 900, 1000, and 1100° at stresses of 8, 7.2, 2.7, and 2.15 kg/mm^2, respectively.

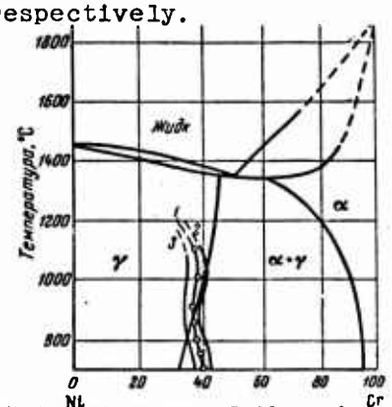

Fig. 1. State diagram of the nickel-chromium system and polythermic composition heat-resistance diagram.

On the basis of the tests "Composition heat-resistance" diagrams were plotted, making it possible to determine the alloy zones with maximum heat-resistance.

Figure 1 gives a state diagram of the nickel-chromium system with a superposed polythermic composition heat-resistance diagram. The curve (1) is for alloy compositions with the maximum heat resistance at the given test temperature. The curves (2) and (3) delimit the zones of alloys of this system with a greater heat resistance.

From the results of our investigations and data obtained by other workers [3, 13] it can be stated that the maximum heat resistance is shifted into the zone of homogeneous solid solutions as the test temperature increases on alloys of the nickel-chromium system as well as in

alloys of other systems [4, 6, 8]. At low temperatures (600-700°), when the diffusion processes during creep are not very active, those alloys in which the second phase was in a finely dispersed state had the greatest heat resistance. At 800-900°, the alloys in the transition zone had increased heat resistance, while at 1000-1100° the homogeneous solid solutions became most heat resistant. At still higher temperatures the melting point becomes the deciding factor and it may happen that a pure metal is more resistant than alloys based on it (as was the case in alloys of the aluminum-magnesium system [6]).

Heat Resistance of Nickel-Tungsten and Nickel-Molybdenum Alloys

The heat resistance of nickel-molybdenum alloys was studied at a temperature of 800° and at stresses of 10, 12.3 and 15.8 kg/mm^2, and also at a temperature of 900° and a stress of 10 kg/mm^2.

The nickel-tungsten alloys were studied at temperatures of 700, 900, and 1000° and under stresses of 10, 8 and 2.7 kg/mm^2, respectively.

The composition-heat resistance diagrams given in Figs. 2 and 3 were either plotted according to the time taken by the specimens to attain the prescribed flexure reading (3-5)mm or else the time to failure.

The following points ensue from the test results; i.e., an increase in the molybdenum and tungsten content in the solid solution of nickel results in an increase in the heat resistance of the alloys; the maximum heat resistance of the alloys is interconnected with the phase transitions which take place in the system during an increase in temperature; at test temperatures below the peritectoid reactions the path of the curves in the composition-heat resistance diagram

changes at the boundary of the saturation limit of the solid solution and for nickel-molybdenum alloys in the zone of the β-phase (Ni_4Mo).

It follows from an analysis of the curves given in Fig.2 that the alloys containing 22-24% and 28-30% Mo are most heat resistant at the temperature of 800°. The tests at stresses of 12.3 and 15.8 kg/mm^2 also confirmed the high heat resistance of these alloys. For example, the alloy containing 29.8% Mo showed a flexure reading of 5.5 mm when tested for 100 hours at a temperature of 800° and a stress of 15.8 kg/mm^2, while the other alloys either failed or showed a flexure reading of more than 20 mm. Moreover, subsequent testing for 20 hours under stress of 23 kg/mm^2 increased the reading by only 1 mm.

In the temperature range of 850-900°, peritectoid reactions take place in the nickel-molybdenum alloys with the disappearance of the β- and γ-phases. The maximum heat resistance which existed at a temperature of 800° in the β-phase zone, also disappears.

It is clear from the graphs in Fig. 2 that at a temperature of 900° the heat resistance of the alloys rises as the molybdenum content is increased.

Figure 3 shows the dependence of heat resistance on composition in nickel-tungsten alloys for the isotherms 700, 900, and 1000°. The path of the curves showing the dependence of variation in heat resistance of the alloys on composition shows that the time required to reach a prescribed flexure reading increases with an increase in tungsten content, attaining a maximum in the zone of the saturation limit of the solid solution. As the quantity of the second phase increases, the heat resistance of the alloy decreases. A dependence of a similar kind was obtained in study [7] on the heat resistance of alloys of this system at a temperature of 800°.

Peritectoid reactions take place in the system at 970°, and this is also shown by the nature of the "composition-heat-resistance" diagram.

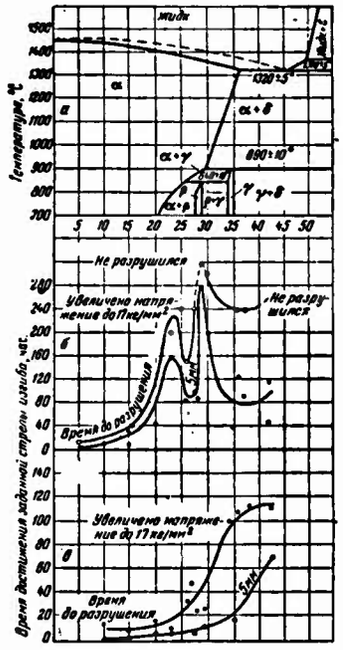

Fig. 2. State diagram of a nickel-molybdenum system (a) and composition-heat resistance diagram at test temperatures (10 kg/mm²) of: (b) 800; (c) 900°.

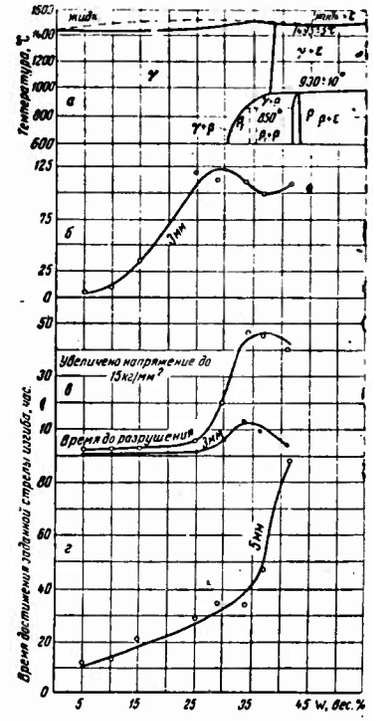

Fig. 3. State diagram of a nickel-tungsten system (a) and composition-heat-resistance diagram at test temperatures and a stress (kg/mm²) of: (b) 700°-10; (c) 900°-8; (d) 1000°-2.7.

It can be seen from Fig. 3 that the heat resistance of the alloys increases at a temperature of 1000° as the tungsten content is increased.

Hardness of Alloys at High Temperatures

The alloys of the compositions given in Table 2 were prepared for the study of hardness (hot-hardness) at high temperatures.

TABLE 2

Alloying Element	Composition, %								
Chromium	20	25	30	33.1	35.5	40	43.5	47.3	50
Molybdenum	5	15.4	20	21.5	25.8	28.8	30	31	35.5 40
Tungsten	3	16.8	17.7	28.8	31	33	35	39.4	41.1

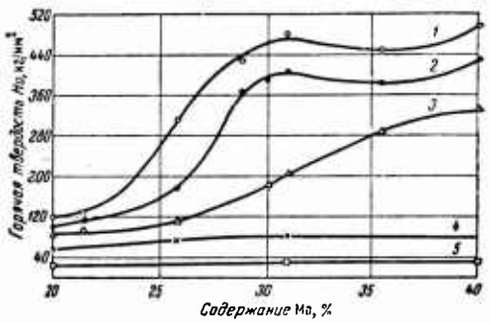

Fig. 4. Influence of composition on the hardness of nickel-molybdenum alloys at temperatures (°C): 1) 700; 2) 800; 3) 900; 4) 1000; 5) 1100.

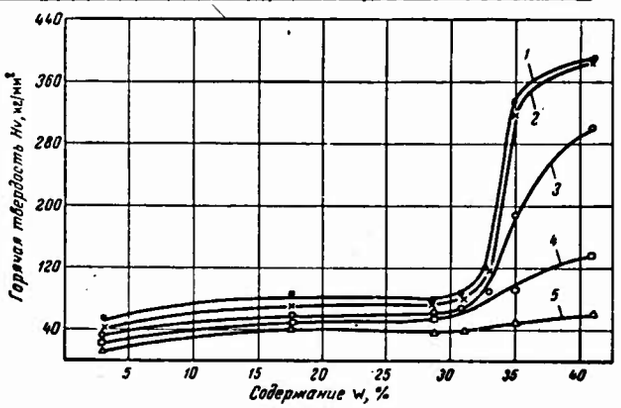

Fig. 5. Influence of composition on the hardness of nickel-tungsten alloys at temperatures (°C): 1) 700; 2) 800; 3) 900; 4) 1000; 5) 1100.

Cast specimens 15 mm in diameter and 5 mm in height underwent the following heat treatment:

nickel-chromium alloys, homogenization annealing at a temperature of 1150° for 6 hours;

nickel-tungsten and nickel-molybdenum alloys underwent two variants of the heat treatment: 1) homogenization annealing in quartz ampoules at a temperature of 1150° for 120 hours with subsequent water quenching; 2) gradual annealing from 1150 to 450° for 1600 hours.

The hardness of the alloys was determined at room temperature as well as at 600, 700, 800, 900, 1000, and 1100° on a VIM-1m hardness tester.

The results of the tests are given in Figs. 4 and 5 and suggest the following:

an increase in the concentration of the alloying element in the solid solution of nickel results in an increase in the hot-hardness of the alloys; a considerable increase in hot-hardness is observed during the transition from single- to two-phase alloys;

at a temperature of 1100° an increase in the alloying element does not lead to an increase in the hot-hardness of the alloys for all practical purposes.

It follows from this that at high temperatures the second phase does not play a great part in strengthening the alloy. The strength of the alloy at these test temperatures will be characterized by the properties of the alloy base — the nickel solid solution.

DEPENDENCE BETWEEN HEAT RESISTANCE AND HOT HARDNESS OF ALLOYS

The academician A. A. Bochvar, in his study of the dependence of heat resistance of aluminum alloys on composition and structure [11], recommends the method of lengthy hardness testing at high temperatures and points to the correspondence found to exist between the results of these tests and the results of ordinary creep tests. I. L. Mirkin and D. Ye. Livshits [15], while studying the hardness of metals and alloys at high temperatures (up to 850°), came to the conclusion that there is a correlation between hot hardness and long-time strength, which is even linear in nature in a certain type of alloy.

In the present work the dependence between heat resistance and hot hardness was studied on the basis of nickel-chromium alloys. Combined diagrams on composition, heat resistance and composition, and hot hardness for the isotherms 800, 1000, 1100° are reproduced in Fig. 6. Analysis of these data indicates that an increase in the concentration of chromium in the nickel solid solution results in an increase in both heat resistance and hot hardness.

A considerable increase in both properties takes place in the transition zone from a solid solution to heterophase alloys and

reaches a maximum at a certain concentration of the alloying element. A dependence of this kind must exist for all aloys which have increased plasticity at high test temperatures. If, however, the alloys are brittle at high test temperatures, they may fail at small degrees of plastic deformation. In this case, the normal link between strength and hardness breaks down. Nevertheless, the hot hardness testing method may be used for a preliminary evaluation of heat resistance in cases where the metals or alloys under investigation are undergoing intense oxidation, when long-time strength and creep tests using the centrifugal method present considerable difficulties under ordinary conditions.

Conclusions

1. An increase in concentration of the elements in the solid solution of nickel results in an increase in the heat resistance and hot hardness of the alloys.

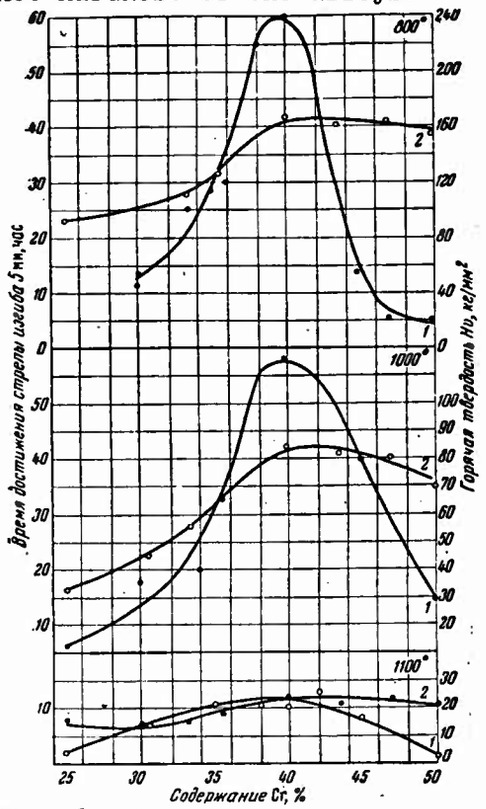

Fig. 6. Composition – heat-resistance (1) and composition hot hardness (2) diagrams of alloys of the nickel-chromium system.

2. There is a direct connection between the chemical composition of alloys, the nature of the phases, and heat resistance in the temperature range under study.

3. The zone in which alloys with highest heat resistance exist depends on these phase transitions which take place in the system during temperature variation.

4 There are two maxima in the composition – heat-resistance diagram of the nickel-molyodenum system; one of them corresponds to the zone of saturated nickel solid solutions, and the other to the β-phase zone based on the compound Ni_4Mo.

5. The maxima on the curves for hot hardness at the investigated temperatures are less clearly marked than in the composition – heat-resistance diagrams.

REFERENCES

1. I. I. Kornilov. A New Method for Investigating Bending Strength of Metallic Systems at High Temperatures. (Novgg metod issledovaniye upochas cti na izgib metallichestcikh sistem por vypkikh temperatur aktn) Izv. SFKhA, (Bult. Lector of Phys. Chem. Anal.) 72, 1949.

2. Ibid. Concerning the Theory of Heat Resistance of Solid Solutions of Metals. (K teorii zhovo prochn osti tverdykh rastvovov metallov) DAN SSSR (Reports of Asi. USSR , 67, no. 6, 1949.

3. Ibid., L. I. Pryakhina, T. F. Chuyko. Composition-Heat Resistance Diagrams of Certain Metallic Systems. (Diagrammy Sostav-zhovo Krochnsyt' nekotorznh metallicheskike sistem)

4. I. I. Kornilov, F. M. Titov. Relation Between Composition, Temperature and Heat Resistance. (Svotno sheniye mezhon sostavom, temperaturvy i zhoppoprochnosti) Izv. AN SSSR, OTN, (Bull. ASc. USSR, Tech. Sci. Dept.), No. 10, 1956.

5. I. I. Kornilov, R. S. Mints and S. D. Onopriyenko. Composition-heat Resistance Diagram of Alloys of the Nickel-Aluminium System. (Diagramma sostav-zhavoprochnost' splavov sistemy nickel'-aluminiy)

6. I. I. Kornilov, L. I. Pryakhina. Relations Between Composition, Temperature and Strength of Alloys of the Aluminium-Magnesium System, (Svotinosheniyn mezhdn sostavom, temperotupoz i zharopmoch u ost'yu splavov sistemy eluminiy-magniy). Izv. AN SSSR, OTN, No. 9, 1954.

7. I. I. Kornilov, P. B. Budberg. Composition-heat Resistance Diagram of Alloys of the Binary System Nickel-Tungsten, (Diagramma sostav-zhavoprochnost' splavov sistemy nikel'-vol'tram.) DAN SSSR, 100, No. 1, 1955.

8. I. I. Kornilov, V. V. Kosmodem'yanskiy. Relation Between Composition, Temperature and Heat Resistance. Izv. AN SSSR, OTN, No. 2, 1955.

9. I. I. Kornilov, and L. I. Pryakhina. Composition-Heat Resistance Diagram of Alloys of the Ternary System Nickel-Chromium-Titanium (Diagramma Sostav-zharoprochnost' speavov troyuoy sistemy nikel-khrom-titan., Izv. AN SSSR, OTN, No. 7, 1956.

10. M. V. Zakharov. Izv. AN SSSR, OTN, No. 1, 1949.

11. A. A. Bochvar. Dependence of Heat Resistance of Aluminium Alloys on Their Composition and Structure Zavisinost' zharoprochnosti splavov ot itch sostava i stroyeniya) Izv. AN SSSR; OTN, No. 10, 1947.

12. S. T. Konobeyevskiy. Concerning the Theory of Phase Transitions. (K teorii fazovykt prevrashcheriy) ZhTEF, (Journ. Theor. Exp. Phys.) No. 13, 1943.

13. K. A. Osipov. Concerning the Plasticity of Homogenous Metallic Alloys at High Temperatures. O mekhan i zme plostichuosti gomogenuykh metallichevkikh splavov upi vysokikh temperaturakt. Izv. AN SSSR, OTN, No. 9, 1949.

14. N. I. Stepanov. Concerning the Electrical Conductivity of Metallic Alloys. ZhRFKhO, 40, 1908.

15. I. L. Mirkin and D. Ye. Livshits. Method for Testing Hardness at High Temperatures. Metod ispztaniya tverodosti por vysokikh (Journ. Russ Phys. Chem. Soc.) Zav. lab, (Factory tal.) No. 9, 1949.

THE ROLE OF NITROGEN IN HIGH-TEMPERATURE OXIDATION OF CHROMIUM IN AIR

V. I. Arkharov, V. N. Konev, I. Sh. Trakhtenberg, S. V. Shumila

The process of oxidation of chromium represents an extensive class of phenomena involved in heterophase reaction diffusion [1]. These phenomena are based on the same mechanism but differ from each other in a number of details. In order to evolve a general theory of heterophase diffusion, particularly one on high-temperature oxidation of metals, the greatest possible number of specific cases must be investigated in order to obtain detailed experimental data on these processes.

Chromium is of special interest because it belongs to a category of metals which are comparatively stable under high-temperature chemical action and is one of the most important components of chemically stable alloys of practical significance.

During their operational service, parts made of low-alloy chromium and of high-chromium steel are affected by air at high temperatures. In order to study the mechanism of this effect and the role of the composition of the atmosphere in which the parts are used, it is first necessary to study the oxidation of pure chromium in media containing nitrogen and oxygen (air).

The investigations made by Miyake [2], Gulbransen [3, 4], V. I. Arkharov [5], and others, enable one to conclude that the scale forming on chromium when oxidized in oxygen as well as in air consists of the rhombohedral oxide Cr_2O_3. In some of these papers [2,3,5], on the strength of indirect evidence, the existence of a γ - Cr_2O_3 phase was surmised, but it was not directly detected. The effect of atmospheric nitrogen on oxidation has not been accounted for in any research with which we are familiar.

However, in principle, the direct influence of atmospheric nitrogen on chromium at high temperatures is also possible. It has been found [9] that in the nitriding of chromium a nitride is formed which produces in radiographs a diffraction pattern (diatropic maximum) similar to the one which was interpreted in [5] as an indication of the presence of a γ - Cr_2O_3 phase. With a view to further clarifying this mechanism, we investigated chromium oxidation in air and in oxygen. A study was made at different temperatures of the kinetics of the process of scaling (from the increase in weight of the specimens), the phase composition and texture of the layers of incipient scale, and the microstructure of the layers.

Method of Experimentation

Our starting material was electrolytic chromium obtained by precipitation from an electrolyte composed of 150 g CrO_3 and 1.5 g H_2SO_4 per liter of water, the conditions of the electrolysis being varied to produce two essentially different types of chromium precipitate-bright and dull. As was previously established by one of the investigators [6], these two types of precipitate differ with respect to the crystallographic character of the texture and the degree of its perfection: in bright precipitates there is a highly perfect chromium texture in which plane (111) Cr is parallel to the outer surface; in "dull" precipitates, the plane (100) Cr is parallel to the surface, but (and this is important for the evaluation of the test results) the degree here of perfection of the texture is very low here.

The chromium was precipitated onto the outer surface of copper tubes 8 mm in diameter and 20 mm long. When a chromium layer of a thickness of 0.5-0.8 mm had been deposited, the specimens were placed in nitric acid to dissolve the copper base; by this means the chromium specimens were obtained in the form of hollow cylinders. Oxidation in air was carried out in a vertical electric furnace. The specimen was suspended by Nichrome wire from one of the pans of an analytical balance above the furnace. The increase in the weight of the specimens was measured without their removal from the hot part of the furnace. The oxidizing in oxygen was carried out in a closed vertical quartz tube in a tubular electric furnace. The specimen was suspended in the quartz tube on Nichrome wire in such a way that it was possible to move it by means of a cantilever, which could be rotated through

a lateral port in the side of the tube near the top, without disturbing the atmosphere in the tube. At the beginning of the test, the specimen was located in the upper, cold part of the reaction tube; the air was then pumped out of the tube and replaced by dry oxygen at a pressure of 160 mm Hg. The furnace was heated to the test temperature and the specimen was then lowered into the center of the furnace. After soaking at this temperature, it was quickly raised to the upper, cold part of the furnace, where it cooled, and thereafter removed from the quartz tube. The specimens were weighed before and after oxidation with an error factor of $\pm$ 0.1 mg to discover the increase in weight during the experiment.

In order to determine the phase composition of the scale, the specimens were prepared from remelted chromium in the form of laminae. The photographs were taken in cameras of the Ivensen type with K-Cr rays, using the flat microsection method.

The textures were photographed in K-Mo radiation and interpreted by the method described in [7].

Polished transverse sections of oxidized specimens were prepared for the metallographic analysis in the following way: a solution of Bakelite in alcohol was poured over the specimen in a special mold, and it was then heated to 150-160° and soaked for 2-3 hours; the Bakelite was polymerized in the process, thereby consolidating the layer of scale, after which the polished section was prepared.

Results of the Experiments

Oxidizine in oxygen was carried out at temperatures of 700, 800 and 1000°. The layer of scale forming on the chromium is a thin crust, black or dark gray in color, which is comparatively easy to peel off the oxidized specimen; it is very brittle and easy to

pulverize (when being pulverized in a mortar, the powder takes on the green color that is characteristic of ordinary chromium oxides).

In the radiographs of the outer surface of the scale on highly oxidized specimens, Debye lines are observed which conform wholly to the system of lines for normal chromium oxides (rhombohedral lattice with an elementary cell edge a = 5.35 A and $\alpha = 55^{\circ}09$). The characteristic (most intensive) lines of this phase are also present in radiographs of the outer surface of the scale on slightly oxidized specimens, along with lines of the chromium metal lying under the scale. No preferred orientation was detected in the outer surface of the scale, either at the outset or in the later stages of oxidation.

Microscopic investigation confirmed the presence of a single phase in the scale (Fig. 1a). Figure 2 gives graphs for the dependence of the weight increase in the specimen (calculated per unit of area) on the oxidizing time at temperatures of 700 and 1000°.

Oxidizing in room atmosphere was also carried out at temperatures of 700, 880, and 1000°. The outward appearance of the scale is the same as in specimens oxidized in oxygen.

In the radiographs of slightly oxidized specimens of bright chromium, a diffraction reflection of relatively high intensity in the form of a diatropic maximum density (d = 1.37 A) was obtained in addition to the lines of normal (rhombohedral) chromium oxides and chromium metal as in [5]. This additional maximum is not observed in radiographs of the outer surface of scale on highly oxidized specimens of bright chromium, when the thickness of the scale is so great that no Debye lines are obtained for the chromium itself. Nor is this maximum observed in radiographs of slightly or highly oxidized

specimens of dull chromium.

The additional maximum was always present when the surface of a specimen of oxidized bright chromium was radiographed after removal of the surface layer of scale.

We can conclude from these observations that the additional diatropic maximum is produced by the inner layer located between the metal and the surface layer of the rhombohedral chromium oxide. The Debye lines for rhombohedral chromium oxide are continuous and do not show any signs of grain-oriented maxima in any of the radiographs, of either bright or dull chromium specimens.

Lines in full conformity with the corresponding oxide Cr_2O_3 are observed in the Debye powder diagrams obtained from the outer surface of oxidized chromium specimens with K-Cr radiation. In particular, it should be pointed out that the Debye lines of Cr_2O_3 are appreciably "displaced" toward small reflection angles with respect to the lines in radiographs of Cr_2O_3 obtained from chromium oxidized in oxygen. This indicates an increase in the parameters of the Cr_2O_3 crystal lattice which formed in the chromium when oxidized in air.

The Debye pattern obtained by the same means from the layer remaining on the metal after removal of the surface layer of scale is different from the system of lines for rhombohedral Cr_2O_3 and chromium metal (with a body-centered lattice). In radiographs of the outer surface of slightly oxidized specimens, lines of both this new phase and chromium metal are observed.

Metallographic investigation of the specimens confirmed the presence of two phases, or layers, in the scale on chromium oxidized in air; i.e.,

a surface layer of dark color, consisting of the rhombohedral

oxide Cr_2O_3 according to x-ray data;

an inner layer similar in color and grain size to the base chromium metal, but producing a diffraction pattern different from that of chromium.

The Debye pattern of this layer conforms well to the data for hexagonal chromium nitride Cr_2N [8]. The diatropic maximum (d = = 1.37 A) appearing in the patterns also originate from Cr_2N. Its presence in the grain-oriented patterns of oxidized specimens of bright chromium and its absence in those of dull precipitates is thoroughly in agreement with our results for the nitriding of chromium [9] in which the process of its origin is examined in detail.

The weight increase of the specimens during oxidation in air at temperatures of 700, 880, and 1000° and its dependence on the duration of oxidation is shown by the graphs in Fig. 2b.

The fact that the parameter of the Cr_2O_3 forming on chromium in air, is greater compared to the parameter of the same phase forming in oxygen shows that the nitrogen in the air partially dissolves in the chromium oxide and diffuses through its lattice into the metal.

The absence of any sign of grain orientation in the outer layer of the Cr_2O_3 scale at all test temperatures and during prolonged oxidation in both oxygen and air indicates that a diffusion of chromium through the oxide phase Cr_2O_3 does not take place to any appreciable extent. From this we can draw the following conclusion:

reaction diffusion in the chromium-oxygen system is brought about by the diffusion of oxygen atoms through the chromium oxide layer into the metal at the boundary of which the growth of the Cr_2O_3 layer takes place (the basic front of the reaction is located at the boundary Cr/Cr_2O_3). This oxidation mechanism in chromium was previously suggested by one of the authors [5];

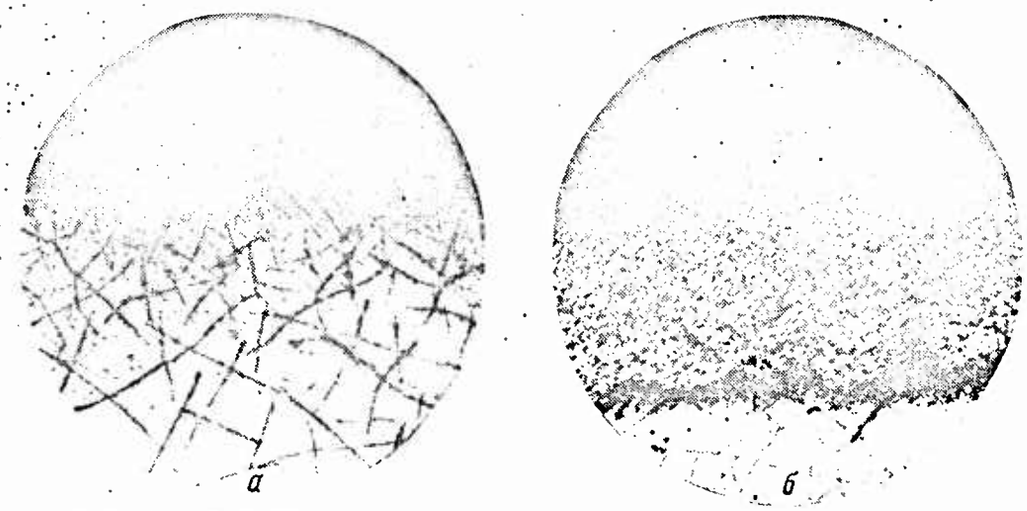

Fig. 1. Microsection of chromium (× 190) oxidized: a) in oxygen; b) in air.

COPY MADE NOT REPRODUCIBLE

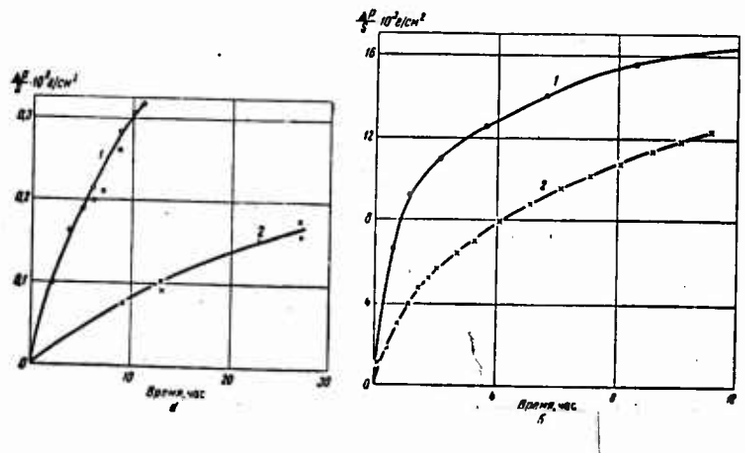

Fig. 2. Kinetic curves of chromium oxidizing at temperatures of 700° (a) and 1000° (b): 1) in oxygen; 2) in air.

reaction diffusion in the chromium-air system takes place because of the diffusion of nitrogen and oxygen atoms into the metal through the newly-formed layers. Since the diffusion mobility of nitrogen atoms is greater than that of oxygen, the front along which the nitrogen reacts with the chromium (having entered the metal) is ahead of the reaction front along which the oxygen and chromium react*

The reaction between nitrogen and chromium takes place on the boundary Cr_2N/Cr, and the reaction between oxygen and chromium on the boundary Cr_2N/Cr_2O_3 through the elimination of the chromium from the Cr_2N layer by the oxide.

During the nitride reaction on the boundary Cr/Cr_2N , a correspondence in orientation and size is established, through which the nitride on well-oriented bright chromium is also oriented, while the nitride on the dull chromium with highly imperfect orientation is not grain-oriented.

During the reaction involving the oxide formation on the boundary of the metal (during oxidation in oxygen) and also on the chromium nitride boundary (during oxidation in air), no correspondence in such orientation and size is observed, obviously in view of the power conditions for the bonding of crystal lattices.

It follows from the kinetic curves that the weight increase in the specimens is greater in oxygen than in air (we must take into account here the fact that nitrogen is included in the weight increase of the specimens oxidized in air so that only a part of the total weight increase relates to oxygen). The retardation of the oxidation of chromium in air is obviously caused by the fact that oxygen

* The fact that two layers are formed with a phase boundary between them is a result of the limited solubility of the chromium oxide and nitride.

diffuses with difficuly through the Cr_2O_3 which contains dissolved nitrogen.

Conclusions

1. The scale forming on chromium during oxidation in oxygen at 700-1000° is composed of the normal oxide α-Cr_2O_3; no other phase is detected in the scale by x-ray analysis.

The scale on chromium oxidized in air in the temperature range 700-1000° has two layers:

a) an outer layer consisting of the rhombohedral oxide α-Cr_2O_3 with a parameter greater than the normal value;

b) an inner layer consisting of the hexagonal chromium nitride Cr_2N.

2. The greater value of the Cr_2O_3 lattice parameter in the scale on chromium oxidized in air can be explained by the fact that the nitrogen dissolves in the chromium oxide.

3. Reaction diffusion in the chromium-air system occurs because of the diffusion of nitrogen and oxygen atoms through the newly-formed layer into the metal, while the front along which the nitrogen reacts with the chromium (on the boundary Cr/Cr_2N) is ahead of the front along which the oxygen reacts with the chromium (on the boundary Cr_2N/Cr_2O_3).

4. The scaling rate on chromium in air is lower than in oxygen (160 mm Hg). The retardation of oxidation of chromium in air is obviously caused by the difficulty with which oxygen diffuses through Cr_2O_3 containing dissolved nitrogen.

REFERENCES

1. V. I. Arkharov. Trudy (Works of Inst. Phys. Met. Ukr. Branch ASC, USSR), No. 12, 94, 1949.

2. O. Kubashevskiy and B. Hopkins. Oxidation of Metals and Alloys. IL, (For. Lang. Press), M, 1955.

3. E. Gulbransen and Hickman. Trans. AJME, 171, 1947.

4. E. Gulbransen and K. Andrew. J. Electrochem. Soc., 99, 1952.

5. V. I. Arkharov. Trudy (Works of Inst. Phys. Met. Ukr. Branch ASC, USSR) No. 11, 1950.

6. V. I. Arkharov. ZhTF, (Journ. Techn. Phys.), 6, No. 10, 1936.

7. V. I. Arkharov. ZhTF, 6, No. 10, 1936.

8. R. Blix. Zs. Phys. Chem., B3, 1929.

9. V. I. Arkharov, V. N. Konev, and A. Z. Men'shikov. Investigation of reactional diffusion in a chromium-nitrogen system (article in the present symposium, p. 408).

STUDY OF REACTION DIFFUSION IN A CHROMIUM-NITROGEN SYSTEM

V. I. Arkharov, V. N. Konev and A. Z. Men'shikov

The present research was part of a series of investigations of reaction diffusion in binary systems of solid metals and chemically active gas [1-10]. The theoretical importance of such research lies in the accumulation of experimental data in order to explain the physical mechanism of reaction diffusion as a whole. Its importance in practice lies in the need to study the processes encountered in technology including the effect of gases on solid phases, particularly gas corrosion and the chemical heat treatment of alloys. Among other things the reaction diffusion in a chromium-nitrogen system is of interest in view of the fact that air and other media containing nitrogen affect high-chromium alloys undergoing heat treatment and also metal parts made from these alloys when used at high temperatures. In order to study this effect, it is first necessary to investigate the simpler chromium-nitrogen system. Reaction diffusion in this system is also interesting from the viewpoint of developing new methods of chemical heat treatment, for example, the method of carbidizing electrolytic chromium platings [11-12] using nitrogen as a

carrier gas.

This system, among others, has certain distinctive features connected with the very small size of the nitrogen atoms compared to that of chromium atoms.

The dpecial nature of the phases entering into the chromium-nitrogen system and the difference in the diffusion mobility of chromium and nitrogen in these phases is also related to this fact. On the basis of the investigations made by Valensi [13], Tammann [14], Blix [15], and by V. S. Mozgovoy and A M. Samaris as well [16], it can be concluded that phases form in the chromium-nitrogen system, Cr_2N and CrN; the latter is only stable at temperatures below 950° and at pressures below 190 mm Hg. According to Blix's data [15], the phase Cr_2N (zone of homogeneity 11.3-11.9% N) has the most close-packed hexagonal lattice, with parameters increasing with the chromium content: a = 2.747-2.770 A, c = 4.439-4.474 A and the phase CrN has a lattice of the NaCl type with a parameter a = 4.140 A.

We made an investigation of the nitriding of chromium in an atmosphere of ammonia gas. We studied the rate of this process at various temperatures (from weight increase of the specimens), the phase composition and grain orientation in the layers of the nascent nitrides (by x-ray analysis), and the microstructure of the layers (metallographically).

Method Employed

The chromium was electrolytically precipitated on hollow copper cylinders with an external diameter of 7 mm and a length of 16-17 mm. The tank contained 150 g CrO_3 and 1,5 g H_2SO_4 per liter of water. The conditions of the electrolysis (for the basic series of bright deposits)

were: tank temperature 50°, current density 40 amp/dm^2, duration of precipitation 10-20 hours (during which deposits 0.3-0.8 mm thick were obtained). In some cases the precipitation was carried out at room temperature (gray deposits). When the deposition of the chromium was complete, the copper base was dissolved in nitric acid, producing chromium specimens in the form of cylinders with thin walls of the above-mentioned dimensions.

The nitriding was carried out according to the method described on page .

The Debye diagrams for phase analysis were obtained by the method (developed by Yevin'sh) of placing the film asymmetrically in K-Cr rays.

For the metallographic study the chromium was deposited on steel cylinders on which flat sections had been previously filed along the generatrix; after nitriding, microsections were prepared from these flat sections by oblique cutting. Small hollow chromium cylinders (insulated from the living) were also studied metallographically; in this case, after nitriding, a polished section of the end plane was prepared, i.e., perpendicular to the axis.

Results of the Experiments

At a nitriding temperature of 600°, no weight increase was detected in the specimen, even after prolonged soaking. The weight increase at temperatures of 800, 850, 900, 1000, 1100, 1160, and 1200° is shown in Fig. 1 in the form of graphs showing the dependence on the duration of nitriding of the square of the weight increase (calculated per unit of area of the specimen's surface). As can be seen from the linear nature of these graphs, the diffusion in all experiments obeys

a parabolic time law.

Figure 2 shows the temperature-dependence of the angle of slope of the kinetic straight lines reproduced in Fig. 1 (plotted as $\log \tan\alpha - \frac{1}{T}$).

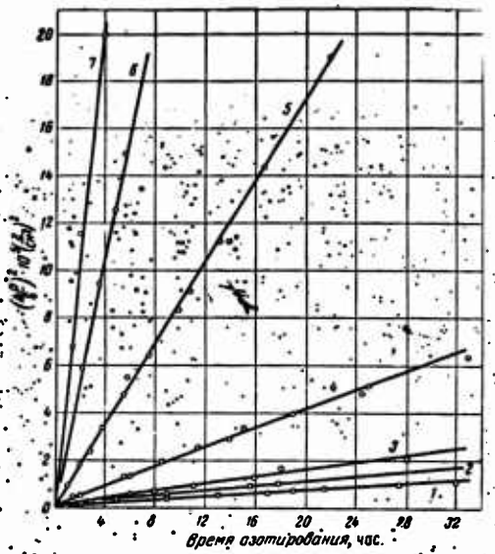

Fig. 1. Kinetic curves of nitriding of chromium at temperatures (°C) of: 1) 800; 2) 850; 3) 900; 4) 1000; 5) 1100; 6) 1160; 7) 1200.

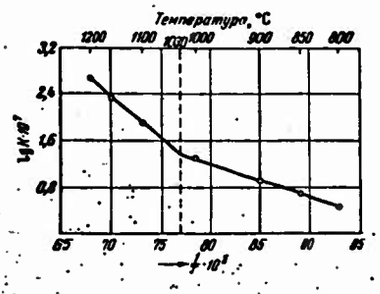

Fig. 2. Temperature dependence of the angle of slope of the kinetic curves shown in Fig. 1.

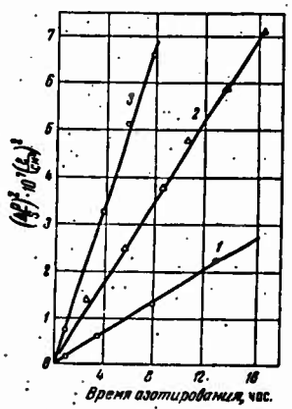

Fig. 3. Kinetic curves of nitriding of Cr_2N at temperatures (°C) of: 1) 800; 2) 900; 3) 1000.

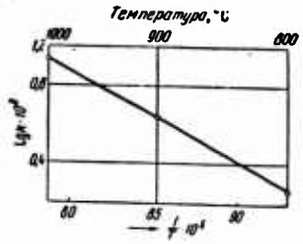

Fig. 4. Temperature dependence of angle of slope of the kinetic curves shown in Fig. 3.

The tangential values of this angle express, as we know, the diffusion coefficient. The graph in Fig. 2 is a broken line consisting of two linear sections; the break occurs at 1030°. It is important to point out that the specimens are a dark violet, almost black, color below this temperature and a metallic luster above it, almost as in pure electrolytic chromium.

A qualitative x-ray phase analysis showed that there were two layers, differing in phase, on the chromium specimens nitrided at temperatures below 1030°, CrN on the surface and Cr_2N underneath. The Debye patterns of the layers are well in accord with Blix [15] for these phases. There is only one layer of Cr_2N on chromium specimens nitrided at temperatures above 1030°.

Grain-orientation radiographs showed that signs of a well-defined orientation of the type

$$(110)\ Cr_2N \parallel OS^* \qquad (1)$$

are detectable in the Cr_2N layer from the very beginning of its formation on the specimens of bright chromium after nitriding.

After nitriding at a temperature below 1030°, a diatropic maximum appears first. When nitriding time is increased, other lines with grain-oriented maxima appear alongside the increase in intensity of the diatropic maximum; the position of these maxima calculated by the

---

* OS = outer surface

method stated in research [17], accords well with the texture of type (1). The degree of perfection of the texture is fairly high (the angle of scattering is of the order of 2°). With a further increase in the duration of nitriding in the zone below 1030°, CrN lines appear and become stronger, alongside the x-ray pattern of the textured phase Cr_2N. Above 1030°, the pattern of the phase Cr_2N with a texture of the same type (1) is alone visible in the texture photographs. The dot-like character of the Debye lines indicates a grain growth.

Texture photographs of specimens of gray (low-temperature, untextured) electrolytic chromium nitrided at 1000° do not show any signs of texture in the nitride layers, which is in sharp contrast with similar specimens of bright chromium. Since the latter, as opposed to untextured gray chromium, has a well-defined texture of the type

$$(111)\,Cr \parallel HII, \qquad (2)$$

it may be concluded from a comparison of these results that texture (1) in the Cr_2N layer is the outcome of correspondence in orientation and size between the chromium metal with texture (2) and the Cr_2N phase forming on its surface (by chemical reaction). In other words, texture (1) is the texture which corresponds in its orientation. It originates at the very beginning of the Cr_2N nitride layer with a very high degree of perfection, and is preserved up to the last stages of nitriding.

Metallographic investigations confirmed that as a result of nitriding below 1030° two nitride layers are formed, but above 1030° only one; the latter is similar in color and grain size to the layer which forms underneath at temperatures below 1030°. This observation is in conformity with the results of x-ray studies.

We should mention in particular the metallographic pattern of a cross section of the chromium specimen fully nitrided (until cessation of weight increase) at 1200°. Only two layers are visible in this pattern; they are identical in appearance and are interlocked along a clear-cut boundary without any sign of friability or roughness (let us recall that the nitriding took place from both the outer and inner surfaces of the thin-walled cylindrical specimen). In addition to the described tests, we also studied the nitriding chromium nitride Cr_2N, which was obtained by transverse nitriding of bright chromium at 1100°. These specimens were further subjected to nitriding at 800, 900, and 1000°. As shown by x-ray phase analysis, a second surface layer of CrN nitride formed in this case. Here the weight increase followed a parabolic time law, as can be seen from the graphs in Fig. 3, plotted in the same way as in Fig. 1.

The dependence of the tangent of the angle of slope of the straight lines 3 is shown in Fig. 4 (plotted as log $\tan\alpha - \frac{1}{T}$). This linear dependence is disrupted above 1000°, since C and N does not form after this point. If a specimen consisting of Cr_2N is nitrided at a temperature below 1030°, then, as already mentioned, it gains in weight and a layer of CrN grows on its surface; but if it is further exposed to a temperature above 1030° in a stream of amonia, it loses weight down to its initial value when it consisted of Cr_2N alone. The outward appearance of the specimen changes in accordance with these variations. Its surface in the initial state (Cr_2N) has a metallic luster; after the nitriding soaking (1030°) it acquires a dark violet color (CrN), and after further soaking above 1030° in a stream of amonia, it again takes on the metallic luster. These conclusions were directly confirmed by x-ray phase analysis.

Analysis of the Results Obtained

The absence of grain-orientation in the Cr_2N layer forming on untextured (gray) chromium shows that the texture (1) is one of orientational correspondences. It is preserved for a long time while the nitriding continues, i.e., as the layer thickens. This indicates a good dimensional congruence between the textures of the initial chromium (2) and that of the nascent Cr_2N layer (1), and consequently, the absence of distortions in the abutment of these orientations and of stresses in the Cr_2N layer.*

*The best correspondence in orientational dimension between the lattice of Cr_2N and Cr, requiring only slight displacement of the chromium atoms in the rearrangement and producing only slight deformation in the plane of abutment (and, consequently, also low stresses), is obtained if the plane (110) of the Cr_2N is situated at a small angle (8°) to the plane of the chromium orientation (111); this relationship may be written as follows

$$\begin{matrix}(110)\ Cr_2N \parallel (332)\ Cr, \\ [001]\ Cr_2N \parallel [110]\ Cr.\end{matrix} \qquad (3)$$

This texture is very close to the texture of type (1) and corresponds to a theoretically calculated texture pattern in which, instead of the Cr_2N diatropic maximum (110) there must be two short maxima very close to each other in the equatorial (central) line of the texture pattern. If the texture is imperfect, which is fully possible, even though it be only slightly so, these two maxima merge into one common maximum extended in small peaks on both sides of the central line of the texture pattern.

(footnote continued on bottom of next page)

If this fact is contrasted with the absence of growth texture in the outer CrN layer and also the absence of porosity and separation in the abutment zone of the chromium metal and the inner nitride layer, the conclusion may be reached that reaction diffusion in the chromium-nitrogen system is brought about by the nitrogen atoms diffusing through the layers of nitrides into the metal, at the boundary of which the growth of the Cr_2N layer takes place (the basic front of the reaction is on the boundary Cr_2N/Cr).

The CrN layer (in nitriding below 1030°) grows on the boundary CrN/Cr_2N at the expense of the Cr_2N layer. The conditions with respect to orientation and dimension for the abutting of the nitride phases are obviously unfavorable, and no preferred orientation takes place in the CrN layer at any stage of its formation.

Apparently there is no diffusion of chromium through the nitride layers; in any case, it does not play any appreciable part at all in the structural pattern of the nitriding of chromium; in this respect, reaction diffusion in the chromium-nitrogen system is similar to diffusion in an iron-nitrogen system [9].

The variation in the increase of the diffusion rate relative to temperature, beginning at 1030°, is linked up with the fact that below this temperature at which the curve breaks, nitrogen diffuses through two layers (CrN and Cr_2N), and above it through one layer (Cr_2N). We should point out that in dealing with these characteristics we should

*(Continued from previous page). The textural maxima on other Debye rings will, in the case of prefered orientation (3) have positions similar to the texture (1), within the limits of azimuthal scattering due to the slight imperfection of the texture.

Further tests using a more accurate method are necessary to discover which type of texture is found in the Cr_2N layer on bright chromium deposits, i.e., type (1) or (3), which is very close to it.

not only evaluate the apparent activation energy from the slope of the corresponding linear sections in Fig. 2, but should also take into account the circumstances considered in [18] which complicate the investigation.

Conclusions

1. Reaction diffusion in the chromium-nitrogen system takes place at an appreciable rate at 700° and obeys a parabolic time law over the whole temperature studied, up to 1200°.

2. When the temperature rises, the diffusion rate in the chromium-nitrogen system at first slowly increases (below 1030°), and then (above 1030°) it becomes rapid. At 1030° the sharp increase in the acceleration of diffusion with a temperature rise amounts to 3.34 times.

3. Below 1030° nitriding produces two layers on the chromium, different in their phases — an inner, thicker layer of Cr_2N and an outer, thinner layer of CrN, which is detected only after it becomes sufficiently thick in the process of nitriding. Above 1030° only one layer of Cr_2N forms; the CrN phase is unstable above 1030° in an atmosphere of ammonia and does not re-form, while the CrN phase forming below 1030° is rearranged into Cr_2N above 1030°. The variation in the increase in the diffusion rate at a temperature in the zone above 1030°, as compared to the zone below 1030°, is apparently related to the change in the phase nature of the diffusion layers.

4. During the formation of the Cr_2N layer, a texture with a correspondence in orientation and dimension originates on the grain-oriented chromium at all temperatures of the type (110) Cr_2N ∥ (111) Cr ∥ НП or possibly $\begin{matrix}(110)\ Cr_2N \parallel (332)\ Cr,\\ [001]\ Cr_2N \parallel [110]\ Cr\end{matrix}$. The Cr_2N layer has no preferred orientation on untextured chromium.

5. Texture is absent in the surface layer of CrN (forming below 1030°); consequently, no texture forms in the growth on the external surface during the nitriding of chromium.

6. No porosity, loosening, or separation is observed on the boundary between the Cr_2N layer and the chromium metal. In effect, if the specimen is subjected to transverse nitriding from two directions, the Cr_2N layers interlock and closely adhere along a sharply defined boundary without any gap between them.

7. All the structural characteristics of nitride layers indicate that during reaction diffusion in the chromium-nitrogen system, the nitrogen diffuses into the metal from the outside through the nitride layers and that there is no diffusion at all appreciable of the metal in the opposite direction.

REFERENCES

1. V. I. Arkharov. Oxidation of Metals. Metallurgizdat, 1945.

2. V. I. Arkharov and S. Mardeshev. Vest. AN KazSSR, 11, No. 5, 122, 1955.

3. V. I. Arkharov and S. Mardeshev. DAN SSSR, 103, 1955. See also FMM, 1, 1955.

4. V. I. Arkharov. Symposium "Physicochemical Bases of the Blast Process," Metallurgizdat, Sverdlovsk, 1956.

5. V. I. Arkharov and Z. P. Kichigina. FFM, 3, 1956.

6. V. I. Arkharov and G. P. Luchkin. DAN SSSR, 83, 1952.

7. V. I. Arkharov. Trudy IFM UFAN SSSR, No. 11, 1950.

8. V. I. Arkharov and Z. P. Kichigina. Ibid.

9. V. I. Arkharov and Z. P. Kichigina. Ibid.

10. V. I. Arkharov, V. N. Konev, I. Sh. Trachtenberg, and S. V. Shumilina. Article in the present symposium, page 402.

11. V. I. Arkhov and V. N. Konev. Vestnik mashinostroyeniya, (Engineering Herald), 35, No. 11, 1955.

12. V. I. Arkhov and V. N. Konev. Physics of metals and metallurgy (Fizika metallov i metallovedeniye urals branch, Asc., USSR), UFAN SSSR, 6, No. 3, 1958.

13. G. Valensi. Journ. de chimie phisique, 26, 1929.

14. G. Tammann. Zs. Anorg. allg. Chem., 188, 1930.

15. R. Blix. Zs. phys. Chem. (13), 3, 1929.

16. V. S. Mozgovoy and A. M. Samarin. Izv. AN SSSR, OTN, (Bull. ASc., USSR, Tech. Sc. Dept.), No. 10, 1950.

17. V. I. Arkharov. ZhTF, 5, No. 10, 1936.

18. V. I. Arkharov. ZhTF, 16, 1955. See also Trudy IFM UFAN SSSR, No. 16, 1955.

Inst. Phys. Met., Urals Branch,
ASc, USSR

STRUCTURE AND PROPERTIES OF CARBONITRIDED CHROMIUM

V. N. Konev

As has been shown in the preceding studies of reaction diffusion in a chromium-carbon system and the properties of carbidized chromium plating on steels and molybdenum [1, 2, 3], carbidized chromium plating has high corrosion and wear resistance at high temperatures which gives reason to consider them suitable for the protection of thermally unstable metals and alloys against gaseous corrosion and wear in the range of service temperatures up to 1000° inclusive.

The present study deals with the results of investigations of the structure and properties of carbidized chromium platings obtained by methods described in the studies, using nitrogen as a carrier gas in the carbidizing treatment.

Method of Experimentation

Steel 3 was used as the base material to be coated by electrolytic chromium. The conditions under which the chromium was precipitated were the same as in the study [3].

The specimens for the study of the kinetics carbidization process

were prepared from remelted chromium in the form of a film. After chromium plating the specimens underwent gaseous carbidization in a flowing atmosphere of a mixture of benzine vapor and nitrogen, in a vertical tubular electric furnace. The composition of the atmosphere was determined by the temperature of the thermostat which contained a benzine saturated, through which oxygen-free nitrogen was supplied from a cylinder at a rate of 10 liters per hour. The specimen was placed in a closed quartz tube on a nichrome suspension and could be moved by means of a side port (cantilever) in the upper part of the tube. At the beginning of the experiment the specimen was placed in the upper part of the tube, the air was pumped out; the reaction tube was then washed with nitrogen and finally, the mixture of nitrogen and benzine vapors was released into it. The furnace was heated to the test temperature and the specimen lowered into the center of the furnace. When the soaking was complete, the specimen was raised again into the upper, cold part of the apparatus and allowed to cool.

The investigation was carried out at temperatures of 700, 900, 1000, and 1100°. The Debye powder diagrams for determination of the phase composition were photographed according to the method in which the film is placed asymmetrically under K-Cr radiation. The textural radiograms were taken with K-Mo radiation and were interpreted by the method described in research [4].

The chromium deposits were prepared for metallographic examination on small steel cylinders, on which flat areas had previously been ground; after carbidization, polished sections were cut transversely from these areas.

Results of the Experiments

Structure of the Platings. The stratified structure is clearly

visible in the microstructure of the carbonitrided platings. There are three successive layers in the outer part of the plating (Fig. 1).

GRAPHIC NOT REPRODUCIBLE

Fig. 1. Micrograph of section of specimen carbonitrided at 1100° for 3 hours (× 86).

On the strength of data from an x-ray structural phase analysis confirming the presence of three phases, the layers may be considered to be in the following order:

an outer, comparatively thin layer of higher (rhombic) chromium carbide Cr_3C_2;

an intermediate, very thick layer of hexagonal chromium carbide Cr_7C_3;

an inner, thin layer of hexagonal nitride Cr_2N.

This order of phase arrangement in carbonitrided chromium plating is confirmed by x-ray phase analysis at various stages of carbonitriding. Besides chromium metal the only other lines in the radiograms of the slightly carbonitrided chromium specimens are those of hexagonal chromium carbide Cr_7C_3 and hexagonal nitride Cr_2N. With an increase in the carbonitriding time, lines corresponding to the rhombic carbide Cr_3C_2 appear and the intensity of the Cr_7C3 and Cr_2N

lines gradually diminishes. With a further increase in the duration of carbonitriding time the Cr_2N and Cr_7C_3 lines disappear due to absorption of the x-rays by the upper layers, with Cr_2N lines disappearing first.

Texture radiograms showed that there are signs of a well defined orientation of the Cr_2N || OS* type (110) in the Cr_2N layer from the very beginning of its formation on the slightly carbonitrided specimens. With an increase in the carbonitriding time the intensity of the diatropic maximum (d = 1.37 A) pertaining to the Cr_2N phase and and characterizing the given type of texture decreases, while the intensity of the Debye rings for Cr_7C_3 and Cr_3C_2 increases. In the texture radiograms, carbonitrided specimens of gray (untextured) electrolytic chromium did not show any sign of a texture in the layers of carbides and nitride, in sharp contrast to similar specimens of bright chromium. As has been established [5], deposits of bright chromium, as opposed to untextured gray chromium, have a well defined orientation of the type

(111) Cr || OS

It may be concluded from this comparison that the texture in the Cr_2N layer is a texture which corresponds in orientation. No texture was detected in the external layer consisting of chromium carbide Cr_3C_2. In particular, it should be pointed out that the lattice parameters of the Cr_7C_3 phase are lower than those in the same phase obtained from chromium carbidization in the absence of nitrogen.

Figure 2 shows the curves of the dependence of the weight increase of the chromium specimens on the duration of the carbidization (1), carbonitriding (2) and nitriding (3).

* OS = outer surface of the specimen.

Properties of carbonitrided platings. Tests for acid resistance were carried out by the method described in research [2] to establish the solidity of the platings. As the results of the tests show, carbonitrided, like carbidized plating, has a high degree of solidity.

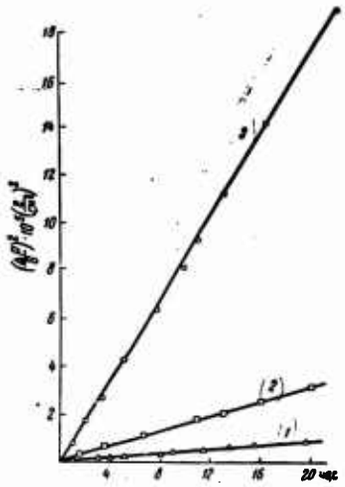

Fig. 2. Dependence of the weight increase of specimens at 1100° on the duration of the process of chromium saturation.

Wear resistance tests showed that carbonitrided chromium platings are highly wear-resistant. Quantitative data on wear (determined by the method explained in [2]) endorse our results on the wear of carbidized chromium platings [2, 3]. This gives us reason to hope that carbonitrided chromium platings may be used to protect machine parts from wear at high temperatures.

Heat-resistance tests of the platings in air at 1000° are illustrated in Fig. 3 by the curve of the dependence of the weight increase specimen (calculated per unit of surface area) on the soaking time at the test temperature.

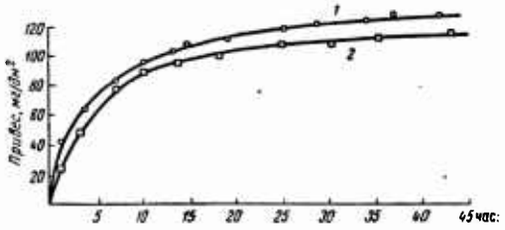

Fig. 3. Weight increase in specimen dependent on soaking time in air at 1000°. 1) Carbidized platings in a nitrogen-free atmosphere [3]; 2) Carbonitrided platings in a mixture of benzene vapor and nitrogen.

Analysis of Results

The absence of texture in the outer layer of carbonitrided chromium specimens indicates the predominant diffusion of nitrogen and carbon toward the metal through the layers forming during the reaction. There is apparently no diffusion of chromium through these layers; at any rate, it was not found to be present to any appreciable degree.

Assuming that the diffusion mobility of nitrogen atoms is greater than that of carbon atoms, which could be expected from comparison of their atomic radii, the front along which the nitrogen and chromium react must spread through the metal more rapidly than that along which the carbon reacts with the chromium. In fact, as indicated above, a layer of nitride forms under the carbide layers. A similar phenomen is observed during the oxidation of chromium in air; where during the simultaneous diffusion of nitrogen and the oxygen in the air in chromium, the front along which the nitrogen and chromium react outstrips the oxygen and chromium reaction front, forming a layer of nitride Cr_2N below the chromium oxide layer.

The mechanism of the simultaneous diffusion of nitrogen-carbon in chromium can be reduced to the following: the reaction between the nitrogen and chromium takes place on the phase boundary $Cr\text{-}Cr_2N$; the reaction between the carbon and chromium takes place on the phase boundary $Cr_2N\text{-}Cr_7C_3$, where the chromium is obtained from the Cr_2N phase. The physical process of the rearrangement of the phase lattices on the boundaries of the latter type has still to be examined in greater detail, and this will require experimental investigation of the mechanism of reaction diffusion in systems of the type Me-X,Y

and MeX-Y in which Me is a solid metal and X and Y are chemically active gases. From the practical point of view, this is necessary for a clearer understanding of the mechanism of gas corrosion as a whole and chemical heat treatment of metals in particular.

It was established that the parameters of the carbide Cr_7C_3 forming during carbidization in an atmosphere containing nitrogen are lower than the lattice parameters of the same phase forming during carbidization in the absence of nitrogen. This gives ground to assume that the nitrogen diffuses in the direction of the metal through the lattices of the newly-formed carbides, replacing the carbon atoms in them.

As can be seen from the path of the curves in Fig. 2, reaction diffusion in a chromium-nitrogen-carbon system at 1100° obeys a parabolic time law, as do the systems chromium-nitrogen [6] and chromium-carbon. The rate of the simultaneous saturation of chromium with nitrogen and carbon is lower than the nitriding rate, but higher than that of carbidization.

It follows from a comparison of the properties of carbidized chromium platings [2, 3] with those of carbonitrided chromium plating, that the platings of both types have the same properties (heat-resistance, resistance to wear, and acid resistance). This affinity was to be expected considering that in both cases the surface layers consist of the same phases, i.e., rhombic and hexagonal chromium carbide. It is these surface layers that determine the above-mentioned properties of the plating. In acid-resistance and heat-resistance tests, the surface layers of the plating are first allowed to interact with the external active agents of the corroding medium. In tests for wear resistance it is also the outer layer, the layer of

rhombic chromium carbide Cr_3C_2 that is subjected to abrasion.

Conclusion

1. It was established that during the carbidization of chromium plating in an atmosphere containing nitrogen, three different layers were formed; i.e.,

an outer layer of rhombic chromium carbide Cr_3C_2;

an intermediate layer of hexagonal chromium carbide Cr_7C_3;

an inner layer of hexagonal chromium nitride Cr_2N.

2. During formation of the Cr_2N layer, a texture corresponding in orientation and size to the textured chromium can be detected at all temperatures. The crystallographic character of the rearrangement of the chromium lattice into the nitride lattice is the same as in the case of nitriding chromium in ammonia. The layer of Cr_2N on untextured chromium has no texture.

3. Reaction diffusion in a chromium-nitrogen-carbon system is brought about through the diffusion of nitrogen and carbon atoms into the metal through the nascent layer.

4. The front along which the reaction between the nitrogen and chromium takes place is located on the interphase boundary Cr — Cr_2N, while the front of the reaction between the carbon-chromium is on the interphase boundary Cr_2N — Cr_7C_3.

5. The presence of an interphase boundary between Cr_2N and Cr_7C_3 points to the limited mutual solubility of these phases.

6. The acid resistance, heat resistance and wear resistance of carbonitrided chromium plating are not lower than in carbidized chromium plating. This warrants the use of nitrogen as a carrier gas in the gaseous carbidization of electrolytic chromium plating in

order to increase its protective properties.

REFERENCES

1. V. I. Arkharov and S. A. Nemonov. Izv. AN SSSR, (Bull. ASc. USSR), No. 9-10, 1943.

2. V. I. Arkharov and V. N. Konev. Vestnik Mashinostroyeniya (Engineering Herald), No. 11, 1955.

3. V. I. Arkharov and V. N. Konev. Research on Heat-Resisting Alloys, Izd. AN SSSR, Vol. II, 1957.

4. V. I. Arkharov. ZhTF, (Journal Tech. Phys.) 6, 1936.

5. V. I. Arkharov. ZhTF (Journal Tech. Phys.) 6, 1936.

6. V. I. Arkharov, V. N. Konev and A. Z. Men'shikov. Article in the present symposium, p. 408.

THERMAL AND ELECTRICAL PROPERTIES OF COPPER, SILVER, GOLD, ALUMINUM, AND ALLOYS WITH A COPPER BASE

V. Ye. Mikryukov

The study of the influence of admixtures of various elements in the periodic table on the thermal and electrical properties of a substance is one of the problems of the theory of solids and is of great practical importance. The theoretical investigation of this influence is related to the band theory of solids and is based in practice on a model of typical metals or semi-conductors. The influence of admixtures in metals and semi-conductors on their thermal and electric properties is substantially different; in metals, admixtures reduce electrical conductivity as well as thermal conductivity, whereas, in semi-conductors, on the contrary, they increase these parameters. There is at present strict theory of the metallic state of substances.

The kinetic coefficients (thermal conductivity, electrical conductivity, the Hall effect, thermo-emf and the Wiedemann-Franz law) are theoretically obtained by means of an approximate theory (the band theory), using the Fermi-Dirac statistics and taking into account the weak interactions of the conduction electrons with the thermal

vibrations of the metal lattice.

When the current carriers are of the same sign, the constant of the Hall effect and the therom-emf do not depend on mobility and have the value

$$R = \frac{A}{Ce^n} \quad \text{and} \quad \alpha = \pm \frac{K}{e}\left[B + \ln \frac{2(2\pi kTm^*)^{3/2}}{h^3 n}\right],$$

where R is the Hall constant;

α is the thermo-emf;

A and B are constants;

n is the number of current carriers;

K is the Boltzmann constant;

C is the velocity of light;

m*is the effective mass;

T is the absolute temperature.

The temperature dependence of thermal and electrical conductivity was calculated for two approximations, high and low temperatures. At temperatures above the Debye temperature electrical conductivity is inversely proportional to the absolute value of the temperature ($\varkappa = \frac{B}{T}$), while the thermal conductivity does not depend on it all (λ = const). In this case the Wiedemann-Franz ration, obtained for high temperatures above the Debye temperature, takes the form

$$\frac{\lambda_n}{\varkappa T} = \frac{\pi^2}{3}\left(\frac{k}{e}\right)^2 = 2.45 \cdot 10^{-8} \frac{\text{watt} \cdot \text{ohm}}{\text{deg}^2}.$$

In explaining the dependence of the Wiedemann-Franz ratio and the thermal conductivity of metals, it is assumed that the conductivity of heat and electricity is brought about solely by electrons. Thermal conductivity through the metal lattice is not taken into account.

At low temperatures (below the Debye temperature), the electrical conductivity is $\varkappa \sim T^{-5}$, and the heat conductivity is $\lambda \sim T^{-2}$. It follows that from this the theoretical Wiedemann-Franz ratio is not valid in this case. This is also confirmed experimentally.

The lack of a strict theory of the metallic state of substances prevents us from determining theoretically the limits of applicability of the band theory.

It follows from what has been said that the question of current carriers and their mobility is a fundamental one in the investigation of conductivity in electron conductors. Hence, if the investigator is to gain a deeper understanding of the nature of conductivity of heat and electricity in metals and alloys, he is confronted with the task of making complex studies of a whole series of kinetic coefficients on the same specimens rather than studying the separate kinematic coefficients.

In the first place, the simultaneous investigation of thermal and electrical conductivity, the Hall effect, the thermo-emf and the Wiedemann-Franz ratio on the same specimens, given current carriers of equal signs provides the possibility of determining the degree of concentration of the carriers n, their mobility u and effective mass m*, i.e., the quantities which determine the electronic mechanism of conductivity in the above-mentioned macroscopic kinetic coefficients. In the second place, by comparing the experimental and theoretical values of the kinetic coefficients obtained, it is possible to reach certain conclusions concerning the internal concordance or nonconcordance of the theoretical notions. Furthermore, experimental investigation of the kinetic coefficients, irrespective of their theoretical importance, is of independent interest since they are

widely used in practice.

Method of Experimentation

For the investigation of thermal and electrical conductivity in metals and alloys, a method must be used which would enable us to determine these quantities with a sufficient degree of accuracy over a wide temperature range. This specification was met by the apparatus designed by the author at the Molecular Physics Department of Moscow University, which operates according to the Kohlrausch method. The chief advantages of the method are the following:

the measurement of the quantity of heat is linked to the the measurement of the current and the drop in voltage in the working sector; as is known these electrical quantities can be determined by the compensation method with great accuracy (up to 10^{-8}a and 10^{-6}b respectively);

the ratio between thermal and electrical conductivity can be determined without knowing any other quantities except the current, the temperature at three points on the specimen, and the voltage drop in the working sector; measuring $\frac{\lambda}{\nu}$ makes it possible to compare the results obtained with the theoretical values;

the thermal and electrical conductivity of metals and alloys can be determined by this method.

The error in measurement in this apparatus does not exceed 3% for thermal conductivity and 1-1.5% for electrical conductivity. This degree of accuracy can be achieved since the measurements of the current in the circuit, the voltage drop in the working sector and the temperature of the specimen are performed by the compensation method on a PPTN-1 type compensator. As is known the compensation method is the most accurate method of measurement now in use. The theory of the method and a description of the apparatus and of the experiments conducted are set forth in detail in research [1, 2, 3].

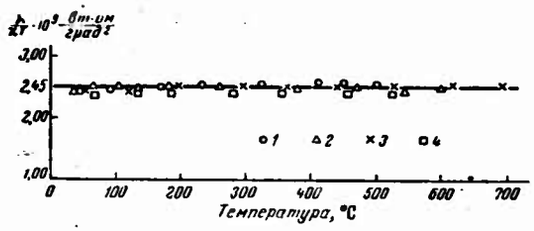

Fig. 1. Temperature dependence $\frac{\lambda}{\nu T} - T$ in pure metals. 1) Cu; 2) Ag; 3) Au; 4) Al.

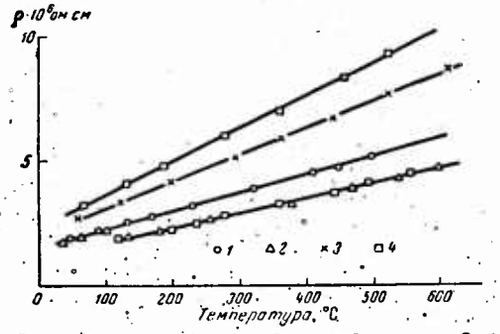

Fig. 2. Temperature dependence of the specific electrical resistance in pure metals (for symbols see Fig. 1).

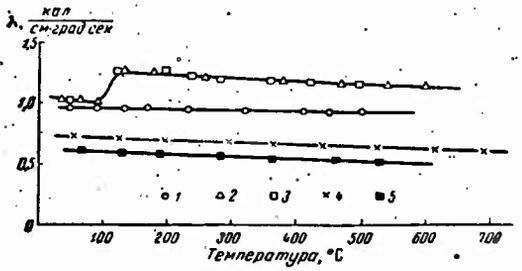

Fig. 3. Temperature dependence of heat conductivity in pure metals. 1) Cu; 2) Ag (1st measurement); 3) Ag (2nd measurement); 4) Au; 5) Al.

Measurement of Copper, Silver, Gold, and Aluminum Polycrystals

Copper, silver, and gold are metals in which the free atoms contain one valence electron in addition to a filled group of 18 electrons. These metals have a face-centered cubic lattice and differ from each other only in the lattice constant. The assumption that there is one valence electron per atom in copper, silver and gold is confirmed by measurement of the Hall effect.

According to the band theory of solids and taking into account the Pauli principle, the first Brillouin zone should only be half-occupied by electrons. In this case the Fermi surface is a slightly distorted sphere which does not touch the surface of the zone. Consequently, along with the occupied states, there are also free states in all directions. Under these conditions the theoretical explanation of the conductivity of heat and electricity will be similar to the simple theory of free electrons, according to which the Wiedemann-Franz law will be closely obeyed in the above-mentioned metals (if the temperature is above the Debye temperature), while the temperature dependence of the specific electrical resistivity must follow a linear law. It is interesting therefore, to compare the experimental results with respect to thermal conductivity, the Wiedemann-Franz ratio and electrical resistivity of these metals with the calculated dependence.

In effect, it turns out that the experimental value of the Wiedemann-Franz ratio for copper, silver, gold and aluminum is in close agreement with the theoretical dependence:

$$\frac{\lambda_e}{} = 2.45 \cdot 10^{-8} \frac{\text{watt} \cdot \text{ohm}}{\text{deg}^2}$$

The temperature dependence of the experimental ratio is shown in Fig. 1, where the bulk of experimental points are located on the theoretical straight line, shown as continuous and corresponding to 2,45. Some of the experimental points differ from the theoretical value by $\pm$ 3%, which is within the limits of our error of measurement.

The temperature dependence of the specific electrical resistivity of copper, silver, gold and aluminum follows the theoretical dependence; i.e., it varies linearly with an increase in temperature (Fig. 2).

In the metals considered above, the thermal conductivity is performed by electrons. In this case

$$\lambda_e = 2.45 \cdot 10^{-8} \varkappa T \frac{\text{watt}}{\text{cm} \cdot \text{deg}}$$

Consequently the temperature dependence of heat conductivity depends on the product $\varkappa T$. Experience shows that with copper, silver, gold, and aluminum this product slowly decreases with an increase in temperature, causing in turn a decline in heat conductivity (Fig. 3).

Thermal and Electrical Properties of Heat-Resistant Precipitation-Hardening Alloys with a Copper Base

Proceeding from the foregoing theoretical concepts, we may expect that the influence of small additions in copper alloys of beryllium, nickel, chromium, zirconium, titanium, aluminum, molybdenum, iron, tantalum, cobalt, tin, manganese, silicon and phosphor (which we investigated) on the thermal and electrical properties of copper should not change substantially the number of current carriers, as compared to pure copper. The mobility of the current carriers should alone differ, compared to the mobility of pure copper, since in the crystal lattice of alloys there develops additional centers from which the electron waves will be scattered. If this assumption is correct, the

the observed and calculated values of the Wiedemann-Franz ratio must coincide in copper alloys with small admixtures and any number of components, as well as in pure copper.

The temperature dependence of the kinetic coefficients (thermal conductivity, electrical conductivity, and the Wiedemann-Franz ratio) was investigated in the following alloy systems: copper-nickel-beryllium, copper-chromium-zirconium, copper-beryllium-cobalt and copper-nickel-beryllium-zirconium. These alloys are precipitation-hardening and heat resistant; i.e., they are heterogeneous systems in which the chemical compounds were NiBe, Cr_2Zr and CoBe, respectively.

It transpired that the experimental and theoretical values of the Wiedemann-Franz ratio in the above-mentioned alloys, as well as in pure copper, coincide. Consequently, the heat and electricity are here transmitted chiefly by electrons.

The alloys investigated have a high degree of heat and electrical conductivity. These parameters may be divided, according to magnitude, into two groups. The first group contains alloys in which the ratio of thermal and electrical conductivity to pure copper attains 75-90% at 600°. The second group comprises the remainder in which these values, at the same temperature, reach 60-75%. Only a few of the alloys investigated are dealt with here; the results of the other measurements have already been published [4, 5].

Measurement of the Temperature Dependence of Heat Conductivity, Electrical Resistivity and the Weidemann-Franz Ratio in the Alloys: Copper-Cobalt-Beryllium-Silver, Copper-Zirconium-Molybdenum-Cobalt, Copper-Cobalt-Zirconium-Iron, Copper-Cobalt-Beryllium-Nickel, Copper-Cobalt-Zirconium-Aluminum, Copper-Cobalt-Zirconium, Copper-Nickel-Zirconium-Phospher, and Copper-Nickel-Zirconium-Tin

Specific electrical resistivity. Examination of the microstructure showed that all of the above-mentioned alloys represent solid solutions of the alloy components and a finely dispersed strengthening agent in the form of a chemical compound.

The electrical conductivity of the alloys Cu + 1.7% Co + 0.15% Be + 1.0% Ag, and Cu + 0.27% Zr + 0.30% Co + 0.14% Mo differs little up to 500° and have the same temperature dependence of resistivity has a lower temperature coefficient. The latter fact is to be explained by the change in the mobility of the electrons in the alloys compared to pure metals. Cu + 0.10% Zr + 0.30% CO + 0.03% Fe has the lowest resistivity of all the given alloys. The electrical resistivity increases with an increase in temperature, following a linear law. The alloys Cu + 0.60% Ni + 0.27% Zr + 0.1% P, Cu + 0.30% Co + 0.30% Zr, and Cu + 0.60% Ni + 0.26% Zr + 0.15% Sn have low resistivity compared to copper.

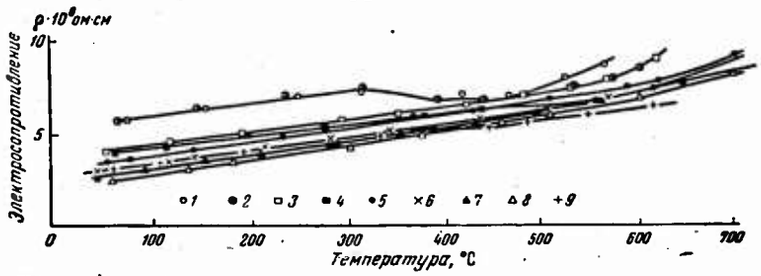

Fig. 4. temperature dependence of the specific electrical resistance in alloys of the systems: Cu plus: 1) 1.7% Co + 0.15% Be + 1.0% Ag; 2) 0.27% Zr + 0.3% Co + 0.14% Mo; 3) 0.1% Zr + 0.3% Co + + 0.03% Fe; 4) 0.7% Ni + 0.1% Be + 0.15% Co; 5) 0.29% Zr + 0.25% Co + 0.2% Al; 6) 0.3% Zr + 0.3% Co%; 7) 0.6% Ni + 0.27% Zr + 0.1% P; 8) 0.5% Be + + 2.2% Co; 9) 0.6% Ni + 0.26% Zr + 0.15% Sn.

It increases up to 400° with an increase in temperature, according to a linear law; i.e., it follows the theoretical dependence. Above 400° the resistivity of some alloys decreases, while it increases in others.

The deviation of the specific resistivity in the copper base alloys investigated from the linear dependence, is caused by decomposition of the solid solution with an increase in temperature and by precipitation of the chemical compound. The electrical conductivity of the latter is higher than that of the solid solution; the electrical conductivity of the alloy, therefore, increases and the resistivity decreases, which can be seen from Fig. 4.

The alloys Cu + 1.7% Co + 0.15% Be + 1.0% Ag and Cu + 0.27% Zr + + 0.30% Co + 0.14% Mo, have the highest electricial resistivity. The temperature dependence of electrical resistivity varies according to a linear law up to 300°, decreases up to 500° and then increases above 500°.

Heat Conductivity and the Wiedemann-Franz Ratio

The method of investigation which we developed makes it possible to determine simultaneously the temperature dependence of the relationship between thermal and electrical conductivity and the electrical conductivity itself on the same specimen.

If the ratio between thermal and electrical conductivity is divided by the absolute temperature, the temperature dependence of the Wiedemann-Franz ratio $\frac{\lambda}{\varkappa T}$ is obtained. It transpired that the observed values of the Wiedemann-Franz ratio for the above-mentioned alloys, in effect, agree closely with the theoretical dependence

$$\frac{\lambda e}{\varkappa T} = 2.45 \cdot 10^{-8} \ \frac{\text{watt} \cdot \text{ohm}}{\text{deg}^2}$$

The temperature dependence of the Wiedemann-Franz ratio obtained experimentally, is shown in Fig. 5 where the bulk of the experimental points are situated along the theoretical straight line, which is shown here as continuous and corresponding to 2.45. A few of these points differ from the calculated values by ± 2-3%, which is within the error in measurement.

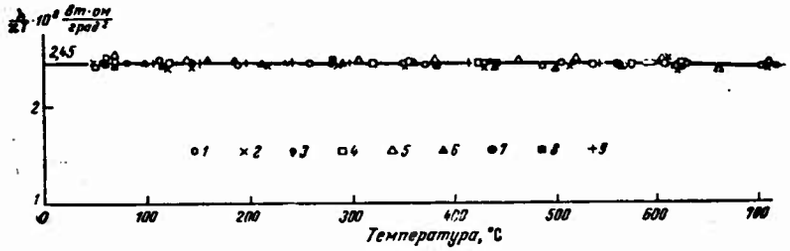

Fig. 5. Temperature dependence of the Wiedemann-Franz ratio for various alloys (for symbols, see Fig. 4).

It has been shown above that the electron theory, which is based on the assumption that heat and electricity are transmitted in metals solely by electrons, follows the Wiedemann-Franz law. Since the copper and its alloys with small soluble admixtures and finely dispersed strengthening agents in the form of a chemical compound under investigation obey this law, it can be stated that thermal conductivity in alloys is also performed by electrons. In this case

$$\lambda_э = 2{,}45 \cdot 10^{-8} \times T \ \frac{вт}{см \cdot град}.$$

Consequently the temperature dependence of thermal conductivity and its absolute value will be determined by the product $\varkappa T$. Experience shows that this product increases in the given alloys with an increase in temperature, causing in turn an increase in heat conductivity (Fig. 6).

The increase in heat conductivity with an increase in temperature in alloys of solid solutions and with a finely dispersed strengthening agent in the form of a chemical compound with a copper base, is caused by the fact that the experimental and theoretical values of the Wiedemann-Franz ratio coincide. It follows from this that the heat conductivity is determined by the product $\varkappa T$. If the latter increases the heat conductivity must as a result also increase, which is precisely what is observed in experiments (Fig. 6).

Thus, the experimental value of heat conductivity in electroconductive alloys and its temperature dependence may be calculated theoretically, irrespective of the number of components, on the basis of the Wiedemann-Franz law and the experimental values of the temperature dependence of electrical conductivity.

The Wiedemann-Franz law is obeyed by specimens with a normalized state as well as a tempered state following hardening, and also in a cold-worked state. This fact is of great practical importance since it enables us to calculate theoretically the heat conductivity of specimens in any state of heat treatment or cold-working from the electric conductivity, measured in the state in which the specimen is used in practice.

Heat is transmitted in metals and alloys by two mechanisms: electron and lattice conductivity. The investigated metals and alloys belong to those which are good conductors of electricity. Therefore, the heat conductivity of the lattice is a small quantity as compared to electron heat conductivity. The experimental value of the Wiedemann-Franz ratio agrees in such alloys with the theoretical values since the heat conductivity of the lattice will be within the limits of error in measurement. If the alloy is a poor conductor of electricity, compared to copper, the heat conductivity of the lattice

compared to the electron heat conductivity, will be of some magnitude, while the experimental value of the Wiedemann-Franz ratio will differ from the theoretical value by the value of the heat conductivity of the lattice, divided by the product $\varkappa T$, i.e.,

$$\frac{\lambda_{\text{наб}}}{\varkappa T} = \frac{\lambda_{\text{э}} + \lambda_{\text{реш}}}{\varkappa T},$$

in which λ_e is the electron heat conductivity;

λ_{lat} the heat conductivity of the lattice.

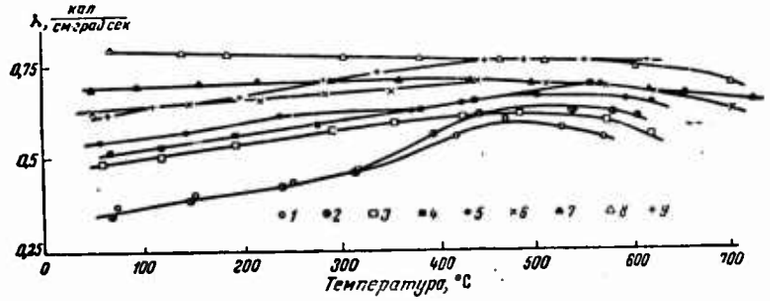

Fig. 6. Temperature dependence of heat conductivity in various alloys (for symbols see Fig. 4).

Consequently the observed deviations from the Wiedemann-Franz law are explained by the fact that the heat conductivity of the alloy cannot be calculated theoretically from the electrical conductivity. Consequently, the Wiedemann-Franz law is only applicable to good electrical conductors in which the heat and electricity are transmitted by electrons.

It has been shown experimentally that if the electrical conductivity of metals and alloys amounts to 25-30% in relation to the electrical conductivity of copper, they are classed as good electrical conductors. In these metals and alloys, the thermal conductivity of the lattice

will be a small quantity compared to the electron heat conductivity. The experimental value of the Wiedemann-Franz ratio will in this case coincide with its theoretical value, since the value of the heat conductivity of the lattice will be within the error of measurement.

If the metals and alloys have an electrical conductivity of less than 25%, the heat conductivity of the lattice compared to the electronic heat conductivity will be an appreciable quantity, and the experimental value of the Wiedemann-Franz ratio will be different from the theoretical value.

Conclusion

1. For temperatures above the Debye temperature the modern electron theory, in essence, correctly explains the electronic mechanism of the conductivity of heat and electricity in metals and alloys of solid solutions.

The Wiedemann-Franz law for electronic conductivity is apparently a more general law than follows from the Sommerfeld-Bloch theory (λ = const, $\varkappa = \frac{B}{T}$ for pure metals, $\rho = \rho_o + \rho_T$ for alloys). Investigations of copper alloys show that both λ and $\varkappa$ deviate from the theoretical values, while the Wiedemann-Franz law remains valid.

Therefore if heat and electricity in metals and alloys are transmitted by electrons, holes, or through mixed conductivity (electrons and holes together), the experimental value of the Wiedemann-Franz ratio will coincide with the theoretical value.

2. Heat is transmitted in metals, alloys, and semi-conductors by two processes: those of electronic and lattice conductivity. Since the investigated metals (copper, silver, gold, aluminum, and alloys with a copper base) are rated as good electrical conductors, their lattice heat conductivity is a small quantity compared to the electronic conductivity. The observed value of the Wiedemann-Franz ratio agrees in this case with the calculated value, since the heat conductivity of the lattice of these metals and alloys is within the error of measurement.

In alloys, which are good conductors, the Wiedemann-Franz ratio does not depend on the state of heat treatment or cold working of the specimen. This enables us to calculate the thermal conductivity theoretically from the measurement of the electrical conductivity in any state. The heat conductivity and electrical conductivity will depend on the heat treatment and cold working of the specimen.

REFERENCES

1. V. Ye. Mikryukov and S. N. Rabotnov. Investigation of heat conductivity and electric conductivity of mono- and polycrystals from 100° up to melting point. (Issledovaniye teplorovodnosti i electro provodnosti monô- i polikristallov ot 100° do temperatury plavleniya). Uch. zap. MGU, No. 74, 1944.

2. V. Ye. Mikryukov. Method of investigating the heat conductivity, the electrical conductivity, and the heat capacity of metals and alloys up to melting point. Zav. lab. (Factory Lab.) No. 6, 1951.

3. V. Ye. Mikryukov and N. Z. Posdnyak. Heat conductivity, electrical conductivity and mechanical properties of porous iron-graphite alloys. Powder metallurgy. Metallurgizdat, 1954.

4. V. Ye. Mikryukov. Thermal and electric properties of copper and its alloys, Part I-II (Moscow University Bulletin, phys.-math. series), No. 2, 1956.

5. V. Ye. Mikryukov. Thermal and mechanical properties of copper alloys, Part III, (Moscow University Bulletin, phys.-math series) No. 2, 1957.

DISTRIBUTION LIST

DEPARTMENT OF DEFENSE	Nr. Copies
HEADQUARTERS USAF	
AFCIN-3D2	1
ARL (ARB)	1
OTHER AGENCIES	
CIA	1
NSA	6
DIA	9
AID	2
OTS	2
AEC	2
PWS	1
NASA	1
ARMY (FSTC)	3
NAVY	3
NAFEC	1
RAND	1
AFCRL (CRXLR)	1

MAJOR AIR COMMANDS	Nr. Copies
AFSC	
SCFDD	1
DDC	25
TDBTL	5
TDBDP	2
TDEWT (Mangio)	1
AEDC (AEY)	1
AFFTC (FTY)	1
AFWL (WLF)	1
ASD (ASYIM)	2
ESD (ESY)	1

UNCLASSIFIED

UNCLASSIFIED